Institute of Sound
and Vibration Research

UNIVERSITY OF
Southampton

UNIVERSITY OF SOUTHAMPTON

FACULTY OF ENGINEERING AND THE ENVIRONMENT

INSTITUTE OF SOUND AND VIBRATION RESEARCH

Effects of sitting posture and seat backrest on the biodynamic response of the human body and prediction of spinal forces during vertical whole-body vibration

by

Mingming Yang

Thesis for the degree of Doctor of Philosophy

December 2016

UNIVERSITY OF SOUTHAMPTON

ABSTRACT

FACULTY OF ENGINEERING AND THE ENVIRONMENT

Institute of Sound and Vibration Research

Doctor of philosophy

EFFECTS OF SITTING POSTURE AND SEAT BACKREST ON THE BIODYNAMIC RESPONSE OF THE HUMAN BODY AND PREDICTION OF SPINAL FORCES DURING VERTICAL WHOLE-BODY VIBRATION

by Mingming Yang

Biodynamic models have been developed to predict the dynamic spinal forces induced by whole-body vibration but the effects of sitting posture and backrest conditions on these forces are unclear. The main objectives of the research reported in thesis were to advance understanding of: (i) how sitting posture and contact with a backrest affect the biodynamic responses of the human body, and (ii) the effects of sitting posture and backrests on spinal forces during exposure to vertical whole-body vibration.

Experimental measurements found that the apparent mass of the body and transmissibilities to the spine (to the pelvis, L5, L3, and T5) are affected by the presence of a vertical backrest or an inclined backrest (inclined by 10º, 20º, and 30º). An inclined backrest induced a broad peak, or even two peaks, around 4 to 8 Hz in the vertical apparent mass at the seat pan, probably because the backrest separated the body modes contributing to the principal resonance around 5 Hz evident when sitting with no backrest. Sitting with either vertical or inclined backrests increased vertical motions of the pelvis and the spine.

Leaning forward in an ‘anterior leaning’ sitting posture increased the frequency of the principal resonance in the vertical apparent mass at the seat, possibly due to increased tension in back muscles. Leaning forward in ‘anterior leaning’ or ‘kyphotic leaning’ postures induced a resonance around 2.5 Hz in the vertical apparent mass at the seat pan, due to excitation of body modes at frequencies less than 5 Hz associated with fore-and-aft motions of the pelvis and the spine.

Changing sitting posture changes muscle activity. Tensing muscles in the lower body (including the lower lumbar spine, pelvis, and thighs), or tensing muscles in the whole body (the lower and upper torso), produces similar increases in the frequency of the principal resonance in the vertical apparent mass at the seat around 5 Hz. This suggests tensing muscles in the lower body causes a greater increase in the frequency of the principal resonance than tensing muscles in upper body.

Biodynamic models of the seated human body that included forces from muscles were developed to fit the measured responses of the body (apparent mass and transmissibilities) in the various sitting conditions (normal and leaning forward, vertical and inclined backrests). The spinal forces in the vertical and fore-and-aft directions at the L5/S1 intervertebral disc were estimated from the sum of the predicted static and dynamic forces in both directions. In each sitting condition, a linear model was used to predict the frequency-dependent transfer function between the vertical seat acceleration and the dynamic forces in the spine. For the sitting conditions studied in this research, the contributions from the muscles to static spinal forces were comparable to the forces from gravity of the body mass supported on the intervertebral disc. Dynamic muscle forces were predicted to contribute significant dynamic spinal forces in the vertical and fore-and-aft directions during vertical whole-body vibration.

Varying the sitting conditions varied the spinal forces predicted by the models, both with and without exposure to vibration. Transfer functions between vertical seat acceleration and dynamic spinal forces showed one or two resonances around 4 to 8 Hz. The resonance frequency in the transfer function between vertical seat acceleration and dynamic vertical spinal force increased with increasing inclination of a backrest, similar to the effect of backrest inclination on the vertical apparent mass at the seat pan. Compared to a normal sitting posture, sitting with 20º-inclined backrest increased the predicted static and dynamic spinal forces in the spine in the vertical and fore-and-aft directions, due to increased forces at the backrest and increased motion of the spine in both directions. Forward leaning sitting postures increased the fore-and-aft motions of the spine and increased the fore-and-aft dynamic spinal forces predicted by the model.

It is concluded that sitting posture and contact with vertical or inclined backrests alter the biodynamic responses of the seated human body. The changes arise from several mechanisms including the backrest supporting some of the body mass, changes in static muscle activity, changes in dynamic muscle activity, and changes in the modes of vibration in the body. These mechanisms are also responsible for predicted changes in the forces in the spine during vertical whole-body vibration.

Table of Contents

List of Tables

List of Figures

List of Symbols

a	acceleration (m/s^2)
a_w	weighted acceleration
c	damping coefficient (Ns/m)
c_r	rotational damping coefficient (Nms)
C	coherency function
d	vertical distance between the two accelerometers mounted on the wooden block used to measure the accelerations at the spine, equal to 30 mm.
d_{mz}	horizontal distance from the vertical muscle force at T7 to the centre of the intervertebral disc L2/L3
d_{mx}	vertical distance from the vertical muscle force at T7 to the centre of the intervertebral disc L2/L3
f	frequency (Hz)
F	force (N)
F_{zs}	vertical force at the human-seat pan interface
F_{xs}	fore-and-aft force at the human-seat pan interface
F_n	force at the human-backrest interface in the direction normal to the backrest surface
F_p	force at the human-backrest interface in the direction parallel to the backrest surface in the sagittal plane
$F_{L5/S1\_z}$	vertical spinal force at L5/S1
$F_{L5/S1\_x}$	fore-and-aft spinal force at L5/S1
F_{mx}	fore-and-aft muscle force
F_{mz}	vertical muscle force
g	gravity constant, g =9.81 m/s^2
H	transfer function in Chapter 2

I	Moment of inertia of the body segments in the multi-body models shown in Chapter 4, 5, 7 and 10.
k	spring stiffness (N/m)
k_r	rotational spring stiffness (Nm)
l	horizontal distance from the centre of gravity of the mass of the body segments to the centre of the intervertebral disc L2/L3; It was used in the lever-arm system in Chapters 4, 5, 7 and 10
m	mass (kg)
M_o	moment applied at the intervertebral disc due to the non-concentric compression of the disc
M	Apparent mass (kg) predicted from the model
r	rotational joint in the multi-body model used to connect the body segments
t	time (s)
T	transfer function between the acceleration and other variable, could be transmissibility to the spine, and transfer function between accelerations and dynamic forces
T_{pz}	pitch transmissibility to the spine
$T_{L5/S1\_z}$	transfer function from the vertical seat acceleration to the vertical spinal force at L5/S1
$T_{L5/S1\_x}$	transfer function from the vertical seat acceleration to the fore-and-aft spinal force at L5/S1
w	weightings in the error function defined for optimisation process in Chapters 4, 7 and 10
α	angle between two adjacent vertebra
β	inclination angle of the muscle attached from T7 to S1 with respect to the vertical direction (Chapter 5)
γ	inclination angle of the backrest (used in Chapter 6)
θ	pitching angle of the vertebral body (rad)

φ the inclined angle of the skin surface with respect to the vertical direction

ξ damping ratio estimated from the frequency response of the skin-tissue system

subscript with spinal force and muscle force

$_d$ dynamic spinal force or muscle force

$_s$ static spinal force or muscle force

subscript used with transfer functions, including M, T or F:

$_{xz}$ apparent mass or transmissibility, or force in the fore-and-aft direction

$_{zz}$ apparent mass or transmissibility, or force in the vertical direction

$_m$ modulus of the apparent mass or body transmissibility

$_{ph}$ phase of the apparent mass or body transmissibility

$_e$ indicating the apparent mass or transmissibility is measured from experiment (Chapters 4, 7 and 10)

DECLARATION OF AUTHORSHIP

I, MINGMING YANG.....

declare that the thesis entitled and the work presented in it are my own and has been generated by me as the result of my own original research.

Effects of sitting posture and seat backrest on the biodynamic response of the human body and prediction of spinal forces during vertical whole-body vibration

I confirm that:

1. This work was done wholly or mainly while in candidature for a research degree at this University;

2. Where any part of this thesis has previously been submitted for a degree or any other qualification at this University or any other institution, this has been clearly stated;

3. Where I have consulted the published work of others, this is always clearly attributed;

4. Where I have quoted from the work of others, the source is always given. With the exception of such quotations, this thesis is entirely my own work;

5. I have acknowledged all main sources of help;

6. Where the thesis is based on work done by myself jointly with others, I have made clear exactly what was done by others and what I have contributed myself;

7. Parts of this work have been published as:

Yang M, Qiu Y and Griffin MJ (2013) Developing a simple mathematical model of the seated human body to predict spinal forces caused by vertical vibration. The 48th UK conference on Human Response to Vibration, Ascot.

Yang M, Qiu Y and Griffin MJ (2014) Biodynamic modelling of spinal forces caused by vertical vibration in three sitting postures, 49th UK conference on human response to vibration, Buxton, UK, 9th – 11th September.

Yang M, Qiu Y and Griffin MJ (2015) Effect of backrest inclination on apparent mass at the seat and the backrest during vertical whole-body vibration, Presented at the 50th UK Conference on Human Responses to Vibration, Southampton, UK, 9th - 10th September.

Yang M, Qiu Y and Griffin MJ (2016) Effect of muscle activity on the apparent masses of the human body when exposed to vertical whole-body vibration, Presented at the 51st UK conference on Human Responses to Vibration, INM, Gosport, 14-15 September.

Signed: .....

Date: .....

Acknowledgements

It is never easy to write something with such a long length. By writing these hundreds of pages, I would like to thank those who helped and supported me for finishing a Ph.D.

Firstly, I would like to thank my supervisors: Dr Yi Qiu and Professor Mike Griffin for offering me the opportunity to study and enjoy the life in Southampton. They have offered me professional guidance and enormous patience in doing the project.

Secondly, I would like to thank Gary, Peter, and Weidong for helping me during my experimental studies. I would like to thank the colleagues in the Human Factors Research Unit in helping and teaching me about the knowledge in the field of human vibration.

I also appreciated the time I spent with the members in the unit and all the friends in University of Southampton. I will miss the time I spent with you guys in Southampton.

Finally, I would like to thank my family for supporting me financially and spiritually. I love you, my parents and my grandma and my wife. Thank you, Lin, my wife. Without your support, I will never finish the degree.

In addition, this work was undertaken on contract ROD – HQ SG 34/02/08/05 in association with the Institute of Naval Medicine. The support and advice of Dr G.S. Paddan is gratefully acknowledged.

Chapter 1. INTRODUCTION

People are exposed to whole-body vibration in various means of transport during daily life, such as driving a vehicle or riding on a high-speed marine craft. The vibration to which the human body is exposed may cause discomfort and even be harmful to the body. Long-term exposure to whole-body vibration may increase the risks of low-back pain, which is believed to be associated with the forces in the spine. Due to practical and ethical problems, the forces in the spine during whole-body vibration cannot be measured in-vivo but biodynamic models can be developed to predict the spinal forces.

This thesis reviews studies of spinal forces so as to identify what factors affect the forces in the spine and consider how the forces might be predicted by models. From this information the advantages and disadvantages of current models can be identified and improved models for predicting spinal forces can be investigated.

Sitting posture and support for the back while seated play crucial roles in determining the forces in the spine when there is no vibration. It is reasonable to assume that sitting posture and backrest contact may also affect spinal forces during whole-body vibration. However, most biodynamic models and the current standard (ISO 2631-5:2003) provide no useful prediction of the effects of posture and backrest contact. Due to the complexity of the human body it remains to be identified what structures of the body are required in models predicting spinal forces during whole-body vibration. The alternative methods that can be used to calculate spinal forces also merit investigation.

Biodynamic responses of the human body (i.e., apparent mass and body transmissibilities) indicate how vibration is transmitted to and through the human body. Changes in body posture and backrest contact have been shown to affect the apparent mass of the seated human body but the effects of posture and sitting with inclined backrest on the transmissibilities of the body have not been studied systematically. Knowledge of the transmissibility of the body to various locations along the spine will advance understanding of the mechanisms associated with the effects of body posture and backrest contact and assist the development of biodynamic models for predicting their effects on forces in the spine.

The main objectives of the research in this thesis are: 1) to advance understanding of how sitting posture and backrest support affect biodynamic responses of the body (i.e., apparent mass and transmissibilities), and 2) to develop biodynamic models that predict the effects of sitting posture and backrest support on spinal forces during vertical whole-body vibration.

The thesis consists of 12 chapters:

Chapter 1 introduces the scope of the research.

Chapter 2 reviews the biodynamic response (including the apparent mass and body transmissibilities) of the seated human body in different sitting postures. The advantages and limitations of the previously developed models for predicting spinal forces are discussed. The mechanisms generating forces in the spine are also studied. The review shows the current stage of

knowledge in the fields of biodynamic response and prediction of spinal forces. Research questions to be answered by this study are presented at the end of the review.

Chapter 3 describes the main experimental apparatus and the data analysis methods.

Chapter 4 introduces a simple multi-body mathematical model for predicting spinal forces in the human body sitting in a normal upright posture. The necessary structure of such a model is discussed.

Chapter 5 describes a modified version of the multi-body model with the addition of a muscle model to reflect the contribution of muscles to the spinal forces. Normal, erect, and slouched sitting postures are also modelled to investigate whether the model can reflect the effects of variations in posture.

Chapter 6 describes an experimental study about the effect of vertical and inclined backrests on the apparent mass and transmissibility of the seated human body.

Chapter 7 describes a series of multi-body models developed to reflect the effects of vertical and inclined backrests on the biodynamic responses and predict the forces in the lumbar spine exposed to vertical whole-body vibration. The multi-body models are developed from the model previously developed in Chapter 5 so as to predict more appropriate static and dynamic spinal forces.

Chapter 8 presents an experimental study of the effects of forward leaning sitting postures on the apparent mass and transmissibility of the seated human body. The postures include ‘kyphotic leaning’ and ‘anterior leaning’ sitting postures.

Chapter 9 presents an experimental study. It investigates the effects of tensing the muscles in the upper body and the lower body on the apparent mass of the seated human body.

Chapter 10 presents a modelling study. The multi-body model developed in Chapter 7 is further adjusted for the forward leaning sitting postures studied in Chapter 8. The effect of the forward leaning sitting posture on the spinal forces is investigated.

Chapter 11 presents a general discussion of the findings from both the experimental and the modelling studies.

Chapter 12 presents the main conclusions of this thesis and offers recommendations for future studies.

Chapter 2. Literature Review

2.1 Introduction

2.1.1 Fundaments of vibrations

Human beings are exposed to vibration everywhere. One of the main sources of vibration is various means of transportation, including vehicles, trains, aircraft, marine craft, and motor bikes. Vibration is defined as oscillatory motion containing magnitude and frequency. The magnitude indicates the extent of oscillation and the frequency describes the repetition rate of cycles of oscillation. The human body is exposed to vibration of various waveforms, including sinusoidal vibration, multi-sinusoidal, transient, shock, random and the combination of these waveforms. The vibration to which the human body is exposed can be represented by displacements, velocities or accelerations, but acceleration is commonly used for the evaluation of the effects of vibration on human comfort. To specify the severity of vibration to human body, the magnitude of a vibration acceleration is usually expressed in terms of either the root-mean-square (r.m.s.) value or the vibration dose value (VDV). The root-mean-square value is defined as the square root of the average value of the square of the acceleration (Equation 2.1).

$$r.m.s.. = \left[\frac{1}{T} \int_0^T a_w^2(t)dt \right]^{1/2} \tag{2.1}$$

When the vibration contains high magnitude shocks, vibrations with same r.m.s. values may induce obviously different responses regarding human discomfort (Griffin, 1990). In this case, the VDV is suggested. The VDV is calculated as the fourth power of the frequency-weighted acceleration ($a_\omega(t)$), which emphasises the greater acceleration arising from shock motions (Equation 2.2):

$$VDV = \left[\int_0^T a_w^4(t)dt \right]^{1/4} \tag{2.2}$$

The VDV provides a convenient measure of total severity and has been found to correlate well with human response to vibration containing shocks (Griffin, 1990). The crest factor is sometimes calculated to determine whether to use the root-mean-square (r.m.s.) or VDV, and it is calculated as the ratio between the peak acceleration and the r.m.s. acceleration. In some standards, when the crest factor is lower than 6, the root-mean-square (r.m.s.) value is considered suitable, otherwise, the VDV is more appropriate.

2.1.2 Biodynamic response of the human body to vibration

The vibration transmitted to and through human body in various kinds of transport causes discomfort of drivers and passengers (Griffin, 1990). Consensus standards have been published to suggest the vibration evaluation methods for predicting the discomfort or the risks to the health of the human body when exposed to vibration and/or mechanical shocks (e.g., British Standard 6841; ISO 2631–1 and ISO 2631-5). Apart from studies of subjective human responses to vibration (e.g. subject feelings of discomfort), objective studies of how vibration is transmitted to and through

human body can assist understanding of the mechanical movements of the human body and identify how to control the adverse effects on the human body. The objective study of the dynamic movements of the human body is within the area of biodynamics.

Biodynamics is the science of physical, biological and mechanical responses of human body to applied force or motion (Griffin, 1990). Transfer functions are used to evaluate the dynamic responses of the human body, and they can be divided into two categories: transmissibility and mechanical impedance (Griffin, 1990). Both transfer functions are functions of frequency and can be represented either by complex numbers or by the modulus and phase.

The transmissibility is determined by the ratio of vibration at two different points. It describes the amount of motion transferred from one point to another. The transmissibility of the human body exposed to whole-body vibration might be determined from the seat surface to the head, to the spine, or to other positions of interest.

The mechanical impedance helps to understand where the biodynamic responses have mass-like, spring-like, or damper-like characteristics and gives information that allows the dynamic interaction of the body with other systems to be predicted. The biodynamic response can be represented by driving point mechanical impedance (in Nsm^{-1}) or driving point apparent mass (in kg). The driving point mechanical impedance of a system is defined as the complex ratio of the force acting on the system to the resulting velocity measured at the same point in the system, while the driving point apparent mass is defined as the ratio of force acting on a system to the acceleration at the same point.

The biodynamic response of human body has been studied widely when exposed whole-body vibration in different directions, including either single (vertical, fore-and-aft) or multi-axis. Both apparent mass and body transmissibility are affected by many factors, including sitting postures (e.g., Kitazaki, 1994; Wang *et al.*, 2004), contact with a backrest (e.g., Griffin *et al.*, 1979; Paddan and Griffin, 1988; Nawayseh and Griffin, 2004; Toward and Griffin, 2009), footrest or steering wheel (e.g., Toward and Griffin, 2010a; M-Pranesh *et al.* 2010), inter-subject variability (e.g., Fairley and Griffin, 1989; Boileau and Rakheja, 1998; Toward and Griffin, 2011), and the magnitude of vibration(e.g., Hinz and Seidel, 1987; Fairley and Griffin, 1989; Qiu and Griffin, 2010). The effects of the above factors on biodynamic responses (i.e., apparent mass and body transmissibility) are reviewed below.

Biodynamic models have been developed to represent the above biodynamic responses of the human body exposed to vertical whole-body vibration excitation. The relevant modelling techniques are also reviewed in this chapter.

This chapter also reviews the relevant standards and the modelling techniques used to predict the risks from spinal loads during exposure to whole-body vibration and shock.

2.2 APPARENT MASS OF A SEATED PERSON DURING VERTICAL EXCITATION

2.2.1 Introduction

The apparent mass is calculated as the complex ratio of force to acceleration measured at the same point (Equation 2.3).

$$M(f) = \frac{F(f)}{a(f)} \tag{2.3}$$

where $M(f)$ is the apparent mass at a frequency f, $F(f)$ is the driving force at the seat-human body interface, and $a(f)$ is the acceleration measured at the same position.

The apparent mass can be obtained from the time-histories of signals from accelerometers and force transducers placed at the interface between the human body and a rigid seat. When the measured force and acceleration are in the same direction, then their ratio is called the 'inline apparent mass'; when the force is measured in a direction perpendicular to the vibration excitation, their ratio is called the 'cross-axis apparent mass'.

The modulus of the apparent mass can be determined from the transfer function between a(f) and $F(f)$ with either the cross spectral density (CSD) method (Equation 2.4) or the power spectral density (PSD) method (Equation 2.5) (Griffin, 1990).

$$\text{CSD: } H(f) = \frac{G_{io}(f)}{G_{ii}(f)} \tag{2.4}$$

$$\text{PSD: } H(f) = \left[\frac{G_{oo}(f)}{G_{ii}(f)}\right]^{1/2} \tag{2.5}$$

The CSD method gives both the magnitude and the phase of the transfer function, whereas the PSD method only gives the magnitude (Griffin, 1990). The CSD method is preferred by many researches as both phase and magnitude of the response are generated, and the effects of noise in the measurement are reduced (Shin and Hammond, 2008). The calculation of transfer function using CSD method in this thesis is based on H1 estimation (Soyal and Semlyen, 1993). The PSD and the CSD of the time-history accelerations are averaged with overlap.

The coherence function is a statistical indicator of the linear association between input and output signals (Jenkins and Watts, 1968; Shin and Hammond, 2008). The coherence function between the input and output signals is defined as:

$$coherency(f)^2 = \frac{\left|G_{io}(f)\right|^2}{G_{ii}(f)G_{oo}(f)} \tag{2.6}$$

The coherence function is unity if the input and output signals are linearly related. If the coherence function is zero, then the two signals are uncorrelated (i.e., two signals are independent). If the coherence function is greater than zero but less than one, then two signals are partially linearly related. Possible reasons could be: (1) the noise is included in the measurements of either input or

output signals; (2) the two signals would have nonlinear relationship; and (3) the output is not only due to the input signal but also due to other inputs (Shin and Hammond, 2008).

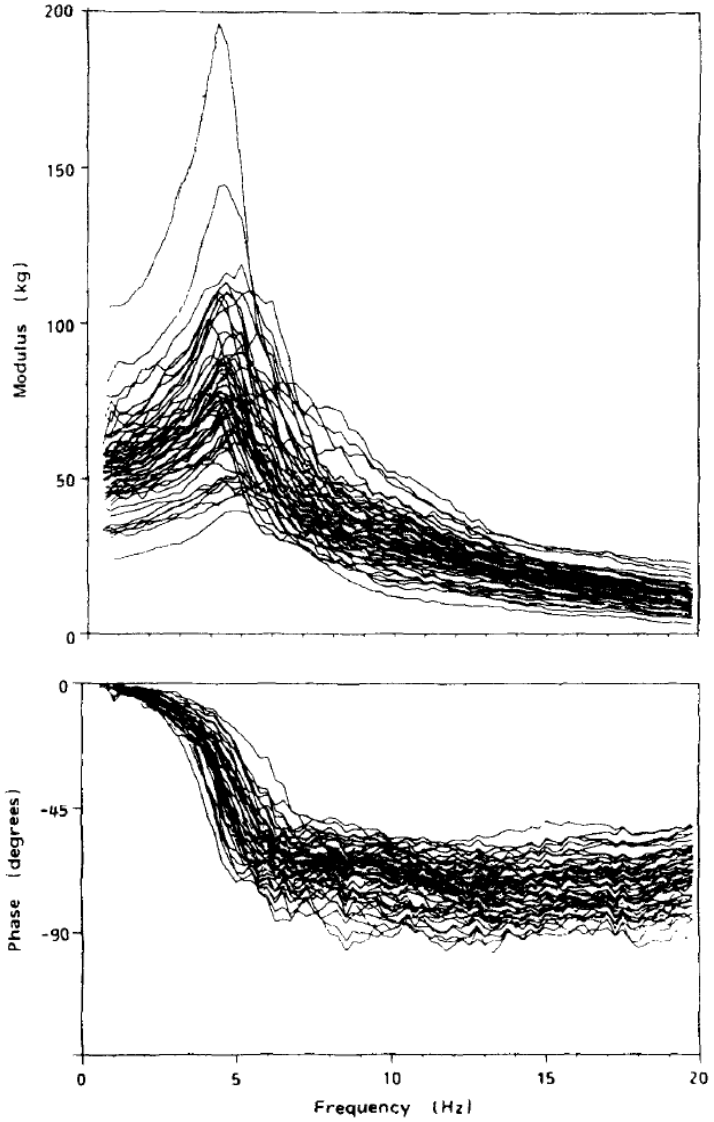

Figure.2.1 Vertical in-line apparent masses of 60 subjects (Fairley and Griffin, 1989)

Both vertical in-line apparent masses and fore-and-aft cross-axis apparent masses of the human body exposed to vertical whole-body vibration have been measured in various conditions, including different sitting postures, with vibration magnitudes and different contact conditions.

An example measurement of the apparent mass (modulus and phase) is shown in Figure 2.1, where the vertical in-line apparent masses of 60 subjects (12 children, 24 men and 24 women) sitting on a rigid seat without backrest but with a footrest were measured with vertical vibration excitation (Fairley and Griffin, 1989). It can be seen from the results that the apparent mass varies from subject to subject. There is a general phenomenon for each subject that, at low frequencies (less than 2 Hz), the apparent mass equals the sitting weight, roughly. Over the frequency range from low to high, the modulus of the apparent mass of the human body increases to a peak, the resonance (at a frequency close to 5 Hz), and then decreases as the frequency increases. Each

subject has a principal resonance frequency around 5 Hz, and some subjects have a significant second resonance frequency around 10 Hz. Similar findings have been reported by many other researchers (e.g. Kitazaki and Griffin, 1998; Mansfield and Griffin, 2000; Matsumoto and Griffin, 2002a; Matsumoto and Griffin, 2002b; Nawayseh and Griffin, 2003; Qiu and Griffin, 2010).

The difference in apparent mass among subjects is called inter-subject variability, which includes effects of body mass, gender, age, standing height, sitting height, body mass index, etc. The apparent mass of a seated subject is not only affected by inter-subject variability, but also influenced by intra-subject variability. The intra-subject variability indicates those factors that cause a change in biodynamic response within a subject, such as changes of posture, muscle tension, body support (e.g., backrest, footrest and steering wheel). How these factors affect apparent mass will be discussed in the following sub-sections.

2.2.2 Effect of gender and anthropometric effects (e.g., mass, age, BMI, etc.)

Among the influencing factors, the body mass causes the majority of variability from subject to subject and had a dominant influence on the apparent mass at resonance frequency (e.g., Fairley and Griffin, 1989; Toward and Griffin, 2011).

To reduce the variability caused by subject sitting weight, each curve can be normalized by dividing the modulus of the apparent mass at each frequency by the apparent mass at 0.5 Hz (static weight supported on the platform) (Fairley and Griffin, 1989). For the apparent masses shown in Figure.2.2, normalisation reduces the variance among the subjects, indicating the large effect of body mass on inter-subject variability.

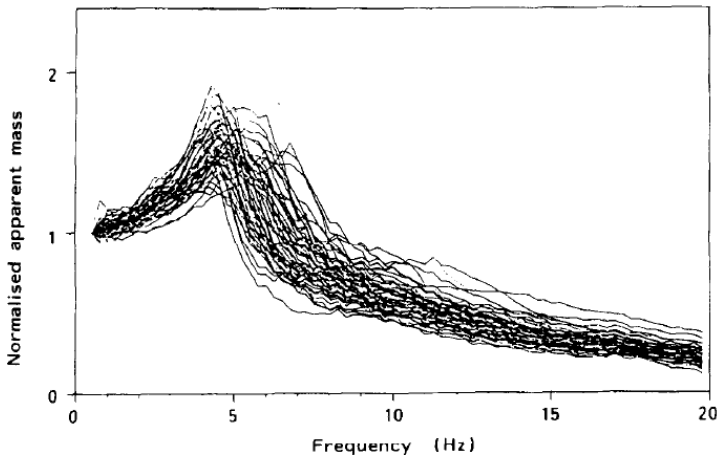

Figure.2.2 Normalized apparent masses of 60 subjects (Fairley and Griffin, 1989)

The BMI (body mass index) and age also appear to have an influence on the vertical apparent mass at the seat pan. The age factor may influence the normalized apparent mass at 20 Hz (Fairley and Griffin, 1989) and may increase the principal resonance frequency with increasing age (i.e., increase up to 1.7 Hz with age increasing from 18 to 65 years old; Toward and Griffin, 2011). Increasing BMI from 18 to 34 kg/m^2 may cause the resonance frequency to decrease by up to 1.7 Hz (Toward and Griffin, 2011). Some studies found that gender would have an effect on apparent mass, for example, female subjects have been reported to have a greater normalized apparent

mass than male subjects at frequencies between 15 Hz and 40 Hz (Wang *et al.*, 2004). The frequency of the principal resonance in the vertical apparent mass of males has been reported to be greater than that of females (Dewangan *et al.*, 2013). The effect of gender found in the above two studies could be due to the absence of control of BMI and age during the statistical analysis. After adjusting for BMI and age, males may have greater principal resonance frequency in the apparent mass and greater apparent mass at the resonance frequency than females, but only when sitting with a reclined backrest (Toward and Griffin, 2011). Gender and BMI are suggested to be significant predictors of the resonance frequency, particularly with a reclined rigid backrest (e.g., Toward and Griffin, 2011).

2.2.3 Effects of posture and muscle tension

A change in sitting posture would induce a change in the body geometry and the muscle tension used to maintain body stability. Studies about the effects of posture and muscle tension were usually combined together.

Increased muscle tension was found to increase the principal resonance frequency of the apparent masses of 8 subjects sitting in four conditions with different muscle tensions (Fairley and Griffin, 1989). It was found that the resonance frequency increased by around 1.5 Hz and the resonance peak became broader as the sitting posture changed from ‘slouched’ to ‘very erect’ (Figure.2.3).

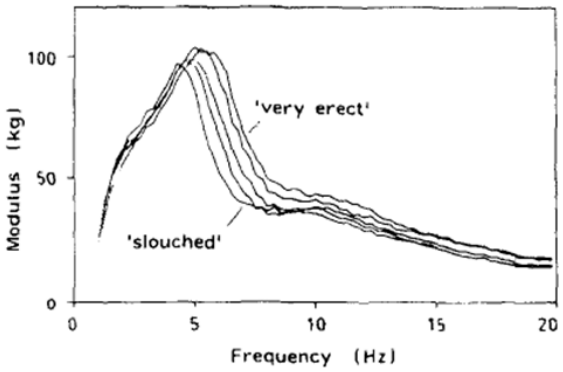

Figure.2.3 Effect of posture on the vertical in-line apparent mass of one person: ‘slouched’, normal, ‘slightly erect’, ‘erect’, ‘very erect’ posture (Fairley and Griffin, 1989)

Similarly, Kitazaki and Griffin (1998) measured the vertical in-line apparent masses of 8 subjects sitting in ‘slouched’, ‘normal’, and ‘erect’ postures. It was found that both the modulus and resonance frequency of the mean normalized apparent mass changed (see Figure.2.4), illustrating a stiffening phenomenon in the erect posture.

From ‘slouched’ posture to ‘erect’ posture, subjects tend to increase the tension of muscles in the upper body, and it was suggested that increasing muscle tension could have a stiffening effect on the biodynamic response of the body (Fairley and Griffin, 1989), resulting in the increase in the frequency of the principal resonance in the vertical in-line apparent mass measured at the seat. However, the change in sitting posture also involved a change of body geometry (i.e., spinal curvature). Hence, the trend described above could be due to either changes in the spinal

curvature, increased muscle activity, or the changes in the buttock tissues. However, changing only the spinal curvature has been suggested to have little significant effect on the vertical apparent mass at seat (Huang, 2008). Based on the modal analysis of human resonance behaviour (Kitazaki and Griffin, 1997 and 1998), it was suggested a change from 'erect' to 'slouched' sitting posture would decrease the natural frequencies of the entire body mode, resulting in a decrease of principal resonance frequency. The causes include that when changing from 'erect' to normal, and to 'slouched' sitting posture, the effective contact area between the buttocks and the seat pan increase, probably resulting in a decrease in the axial stiffness of the buttocks tissues. The decrease in the axial stiffness of the buttocks tissues further decreases the frequency of the principal resonance in the vertical apparent mass at the seat pan. The shear stiffness in the buttock tissues may increase at the same time, probably causing an increase in the resonance frequency of the fore-and-aft cross-axis apparent mass, but the fore-and-aft apparent masses in the three sitting postures (normal, 'erect' and 'slouched') have not been compared in the previous studies.

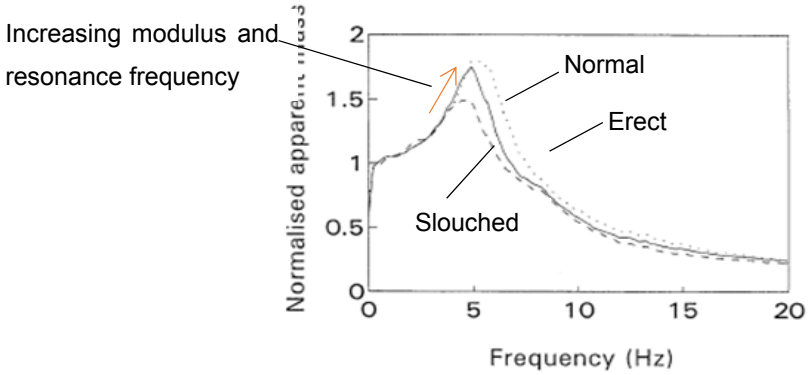

Figure.2.4 Mean normalised apparent mass of 8 subjects sitting in an 'erect' posture (….), normal posture (–), and 'slouched' posture (---) (Kitazaki and Griffin, 1998).

Regarding the effect of sitting posture on vertical in-line apparent mass at the seat, a study involved 12 male subjects sitting in nine different postures: 'upright', 'anterior lean', 'posterior lean', 'kyphotic', 'back-on', 'pelvis support', 'inverted SIT-BAR', 'bead cushion', and 'belt' (Mansfield and Griffin, 2002; Figure 2.5).

Among the investigated sitting postures, 'anterior lean', 'back-on' and 'inverted SIT-BAR' postures showed the greatest inter-subject variability. A secondary resonance at around 8 Hz was observed more clearly in the 'anterior lean sitting posture than in the other sitting postures, including 'kyphotic'. However, no significant difference was found between the vertical apparent masses measured in these nine sitting postures. Possible reasons could be the inter-subject variabilities among the subjects, or the control of subject posture during the experiment.

Many studies of the effects of muscle tension have involved 'erect', 'slouched', or normal sitting postures, with the muscles in the body tensed in different patterns depending on the spinal curvature. However, the roles of muscle tension and spinal curvature have not been elucidated from these studies. Apart from investigating muscle tension by changing posture, the voluntary control of muscle tension has also been found to influence apparent mass. The effects of three muscle tension conditions (i.e., normal upright, buttocks muscles tensed, abdominal muscles

tensed) on the nonlinearity of the apparent mass (decrease in principal resonance frequency with increasing in vibration magnitude, as discussed in Section 2.2.6) were investigated by Matsumoto and Griffin (2002a). It was found that in the two conditions with buttocks muscles tensed and abdominal muscles tensed, the principal resonance frequency of the apparent mass decreased slightly, and the extent of decrease of the principal resonance frequency of the apparent mass with increasing vibration magnitudes was less than with the normal upright sitting posture, suggesting involuntary changes in muscles tension during vibration may contribute to the nonlinear behaviour of human biodynamic response.

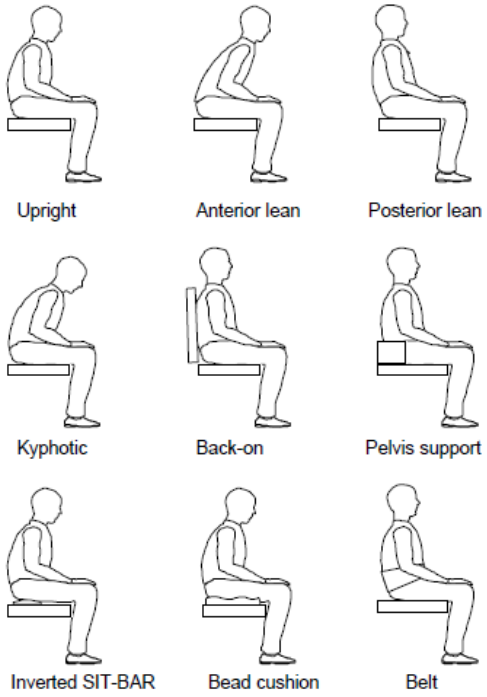

Figure.2.5 Nine sitting postures used in experiment of Mansfield and Griffin (2002).

Muscle activity can be divided into tonic activity (used to maintain static postural stability) and phasic activity (which changes in response to vibration). In the majority biodynamic studies considering muscle activity, in the postures involving greater muscle activity a group of muscles have been tensed to increase mainly the tonic activity, but the changes in muscle activity (both tonic and phasic) is not known and the relative contributions of tonic and phasic activity is unknown. A more comprehensive understanding of how tonic and phasic muscle activity affects biodynamic response is needed.

The effect of phasic activity on the apparent masses of sitting subjects has been studied with voluntary periodic muscular activity induced by a pattern of body motions (Huang and Griffin, 2006). It was suggested that the nonlinearity of the human body (extent of decrease of principal resonance frequency of vertical apparent mass at the seat with increasing vibration magnitudes) could be significantly reduced with suitable voluntary periodic muscular activity. The voluntary

control of muscles (in the upper body) would alter the equivalent overall body stiffness, especially when exposed to low magnitude of vibration.

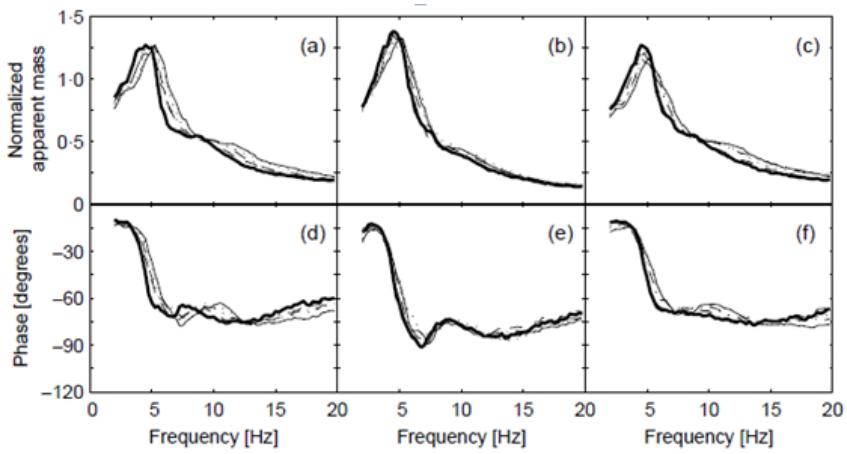

Figure 2.6 Median normalized apparent mass and phases of eight subjects measured with random vibration at five vibration magnitudes with three postures. (a and d) comfortable upright, (b and e) buttocks muscles tensed, (c and f) abdominal muscles tensed. , — 0.35 ms^{-2} r.m.s.; ···· 0.5 ms^{-2} r.m.s.; –·–· 0.7 ms^{-2} r.m.s.; ––– 1.0 ms^{-2} r.m.s.; —— 1.4 ms^{-2} r.m.s. (Matsumoto and Griffin, 2002a)

2.2.4 Effect of backrest

Body supports include the use of a backrest, footrest, and steering wheel, and their effects on the vertical apparent mass at the seat pan have been investigated. The resonance frequency of a subject with a backrest tended to be higher than the subject without a backrest under same vibration magnitude (e.g., Fairley and Griffin, 1989; Mansfield and Griffin, 2002; Nawayseh and Griffin, 2004; Toward and Griffin, 2009; Qiu and Griffin, 2012). It was also found that the backrest tended to decrease the vertical apparent mass at frequency lower than resonance frequency and increase the vertical apparent mass at frequency higher than resonance frequency (e.g., Qiu and Griffin, 2012, Figure.2.7).

The causes could be due to a part of body mass supported on the backrest, resulting in the slight increase in the principal resonance frequency (Fairley and Griffin, 1989; Toward and Griffin, 2009). Another possible reason would be that contact with a backrest changes the curvature of the spine and, therefore, the dynamic response of the body (Griffin, 1990). With increasing inclinations of a backrest without foam, the resonance frequency of the vertical apparent mass at the seat pan tended to increase gradually (Toward and Griffin, 2009). It was found that when contacting a backrest with foam, the resonance frequency in the vertical apparent mass at the seat decreased with increasing inclination of the backrest, opposite to the trend measured without foam.

A footrest and steering wheel will affect the posture and mass distribution of the human body, thereby influencing the apparent mass (Wang *et al.*, 2004; Nawayseh and Griffin, 2003; Toward and Griffin, 2010a). For example, when sitting against inclined backrest, a ‘hands in lap’ sitting posture yields a greater principal resonance frequency of the vertical apparent mass at the seat

and induces greater apparent mass at the principal resonance frequency than a 'hands on steering wheel' posture (Wang *et al.*, 2004). The height of a footrest changes the contact area between the thighs and a seat. A minimum thigh contact (high footrest) was found to reduce the extent of nonlinearity of human body compared to feet hanging, maximum thigh contact, and average thigh contact (Nawayseh and Griffin, 2003), However, the principal resonance frequency of the vertical apparent mass at the seat showed no statistical significant difference between the four postures with different thigh contact (Nawayseh and Griffin, 2003).

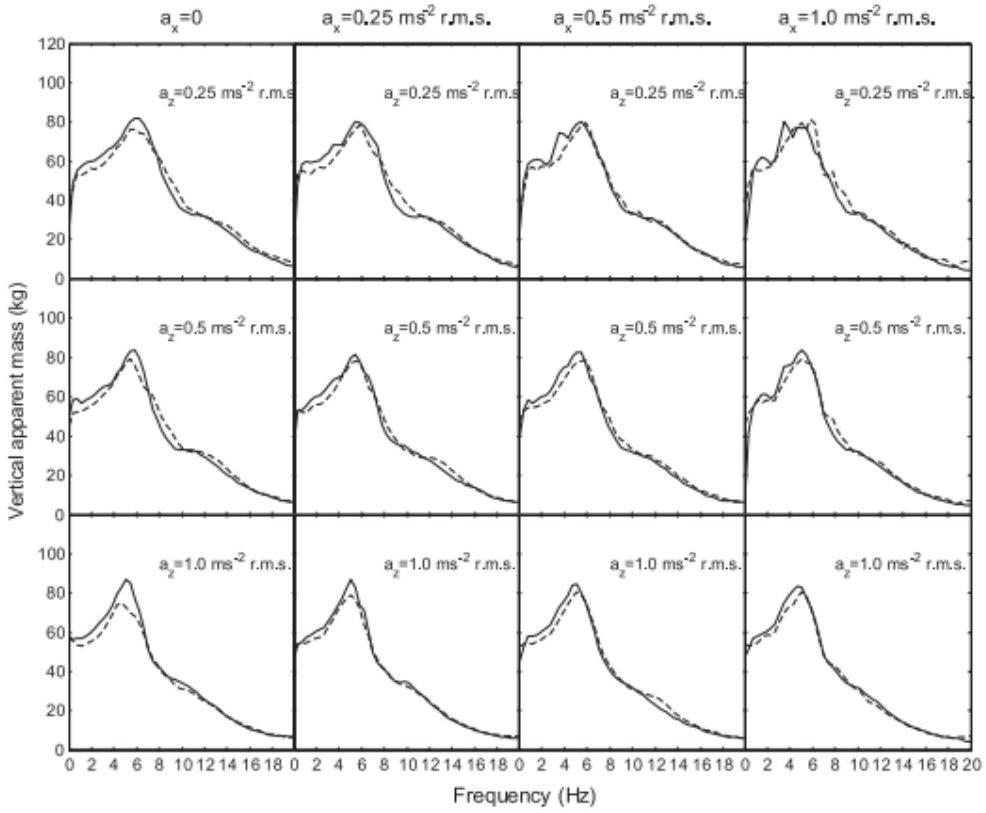

Figure.2.7 Vertical apparent mass with backrest (---) and without backrest (–) (Qiu and Griffin, 2012)

Sitting with a backrest induces considerable fore-and-aft dynamic forces on both the seat pan and the backrest (e.g., Nawayseh and Griffin, 2004; Qiu and Griffin, 2012). The fore-and aft cross-axis apparent mass is also affected by contact with a vertical backrest and whether the feet are supported (e.g., Nawayseh and Griffin, 2004). When sitting supported by a vertical backrest, the resonance frequency in the fore-and-aft cross-axis apparent mass seems to be correlated with the resonance frequency in the vertical in-line apparent mass (e.g., Nawayseh and Griffin, 2004; Qiu and Griffin, 2012). The fore-and-aft cross-axis apparent mass at the seat has not been reported with inclined backrests.

2.2.5 Effect of excitation type (shock)

Exposure to shocks may be associated with greater health risk to the human body than continuous exposure to vibration (Griffin, 1990). With subjects exposed to specific exposure conditions with

and without shocks, the principal resonance frequency of the vertical apparent mass at the seat tended to increase when exposed to vibration containing shocks compared to exposure without shocks (Mansfield *et al.,* 2001). Possible explanation could be that a shock excitation has a stiffening effect on the human body and increases the equivalent overall body stiffness. Besides, the nonlinear behaviour of the human body was observed for exposure either to continuous vibration or to vibration containing shocks. It was suggested that a stiffness effect during exposure to shocks and a softening effect with increasing vibration magnitudes would operate simultaneously during vibration.

2.2.6 Nonlinear behaviour of human body: effect of excitation magnitude

Vibration magnitude in working vehicles varies between the vehicle types (e.g., saloon car on flat road; working environment for off-road vehicles like excavator) and working conditions (i.e., different roughness of the road) (e.g., Griffin, 1990; Paddan and Griffin, 2002). With increasing vibration magnitudes, the resonance frequency of the apparent mass (or transmissibility) decreases, and is referred to as the 'nonlinearity' of the human body.

Examples of apparent mass measurements are shown in Figure.2.8 (Fairley and Griffin, 1989), where the principle resonance frequency of the individual vertical apparent mass at the seat decreases with increasing vibration magnitude from 0.25 m/s^2 to 2.0 m/s^2. For the subjects showing a clear second resonance frequency, the second resonance frequency also decreases with increasing vibration magnitude.

Similar results are presented elsewhere, for example, Mansfield and Griffin (2000) reported that the principal resonance frequency of the median normalized apparent mass decreased from 6 Hz to 5 Hz with increasing vibration magnitude (Figure 2.9). It was also suggested that decreases in the resonance frequency were greater with lower magnitudes (0.25−1.5 ms^{-2} r.m.s.) compared to higher magnitudes (1.5−2.5 ms^{-2} r.m.s.).

The nonlinear behaviour of human body has been widely reported and has been observed with sitting postures (e.g., Mansfield and Griffin, 2002) and standing postures (Matsumoto and Griffin, 1998b). Different postures alter the dynamic properties of the body parts that would contribute to the nonlinearity of human body (e.g., buttock tissues), resulting in a decrease or increase in the extent of nonlinearity (as discussed in Section 2.2.3).

Apart from the nonlinear response in the vertical in-line apparent mass, a 'softening' characteristic is also observed in the fore-and-after cross-axis apparent mass (e.g., Nawayseh and Griffin, 2003; Mansfield *et al.*, 2006; Qiu and Griffin, 2010; Mandapuram *et al.*, 2011).

Although the 'softening' characteristic, or non-linearity, in the human biodynamic response has been studied and reported by many researchers, comprehensive and convinced causes of the non-linearity have not yet been established. The reasons behind the 'softening' characteristic within human body have been explored. Possible causes may include posture changes, geometry of the body, muscle activity changes, and mechanical properties of the soft tissues. For example, Fairley and Griffin (1989) suggested that the stiffness of the muscular-skeletal structure of the body would reduce with the increase of vibration magnitude. This kind of loosening effect is consistent with

'thixotropic' behaviour of human body (Huang, 2008). It has also been suggested that the non-linearity in the human body biodynamic response may be related to the geometry of the body, combining the effect of other factors including tissue beneath the ischial tuberosities, the bending or buckling of spine and muscle activity (Mansfield and Griffin, 2000). Based on the modelling studies, it was suggested that the geometry of the body had only a minor effect on the non-linearity (e.g., Huang and Griffin, 2006).No model has been developed to reflect the nonlinear behaviour of the human body with only a change in the body geometry (Kitazaki and Griffin, 1997; Matsumoto and Griffin, 2001; Huang and Griffin, 2008).

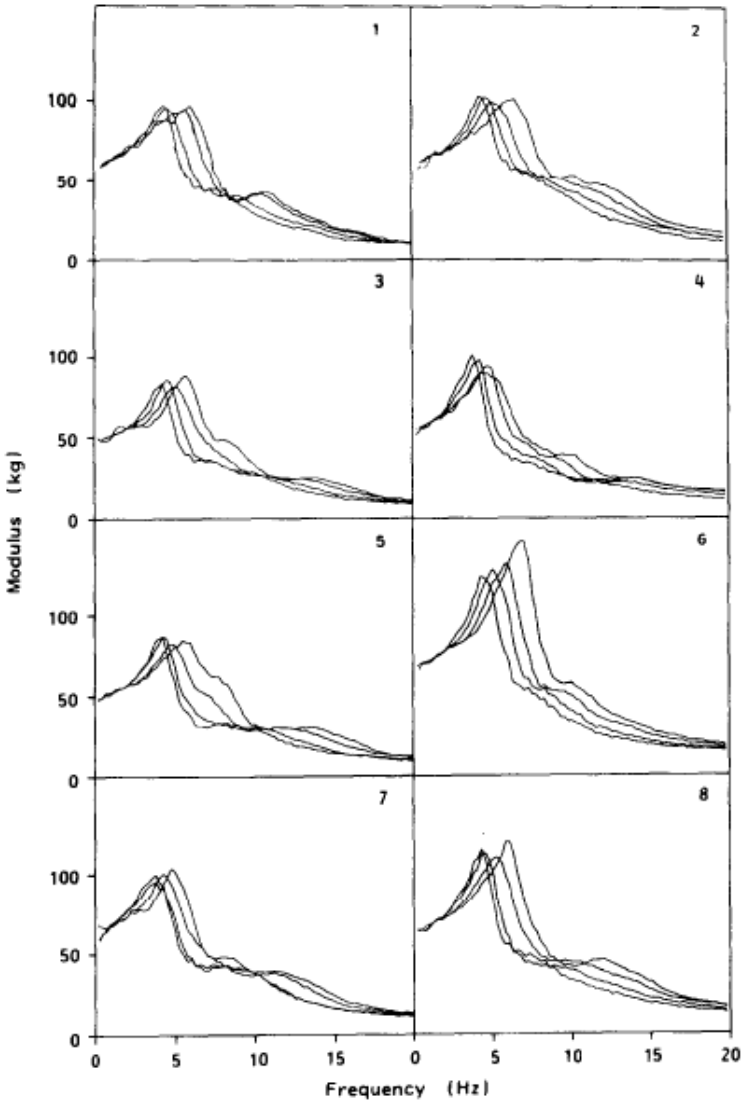

Figure.2.8 Vertical apparent mass of 8 seated subjects exposed to 4 vibration magnitudes (0.25, 0.5, 1.0, 2.0 ms^{-2} r.m.s.). (Fairley and Griffin, 1989)

Muscle tension has also been suggested to affect the nonlinear behaviour of human body (Matsumoto and Griffin, 2002a). It was found that with increase of muscle tension in the buttocks and the abdomen, the body showed less non-linearity. While tensing buttocks muscles during vibration, the nonlinearity decreased with increased muscle tension, which implied that the buttocks

tissues may be partly responsible for the non-linearity. Similar suggestions were made by Nawayseh and Griffin (2003), where a decrease in the extent of contact between thigh and seat tended to decrease the extent of nonlinearity represented by a decrease in the principal resonance frequency of the vertical apparent mass. This was explained as compression of the tissue beneath the ischial tuberosities increasing the tissue stiffness and reducing non-linearity, which was consistent with the results from Matsumoto and Griffin (2002a) about the effect of tensing tissues in the buttocks. The results also suggest that thigh stiffness had little effect on non-linearity, but that the tissues of the buttocks affect the non-linearity to a greater extent.

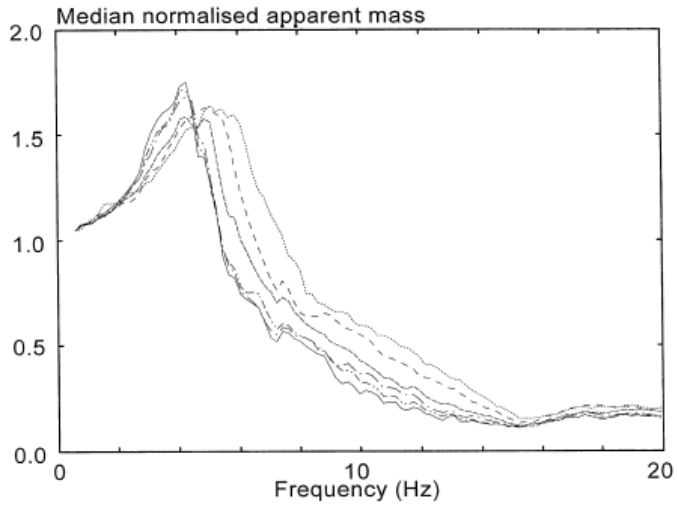

Figure.2.9 Median normalised apparent mass of 12 subjects measured at 6 magnitudes (Mansfield and Griffin, 2000).

2.3 Transmissibility of the human body exposed to vertical whole-body vibration

2.3.1 Introduction

Body transmissibility reflects the amount of vibration transmitted from seat to various body locations, including head, spine, abdomen, and pelvis. The body transmissibility is calculated as the transfer function from seat acceleration to the accelerations at various body locations. Understanding of body transmissibility will help understand the discomfort and potential for injury at different body parts, and it will further help investigate the body moving mechanism combined with apparent mass measurements.

Seat-to-head transmissibility has usually been measured with one of two alternative methods: a ‘helmet’ or a ‘bite-bar’ with transducers installed on them (Griffin, 1990). The use of a ‘helmet’ may provide inaccurate results as relative motions may be observed between helmet and head (Matsumoto, 1999). The use of a ‘bite-bar’ (as shown in the Figure 2.10, Paddan and Griffin, 1988) is recommended when measuring head motion as the teeth are regarded as rigidly connected to the skull within the frequency range of interest. Six miniature single-axis accelerometers were

installed on the bite bar, allowing the measurement of head motion in three translational axes and three rotational directions. The effects of various factors (including sitting posture, muscle tension, inter-subject variability, and vibration magnitude) on seat-to-head transmissibility have been investigated, and are reviewed below.

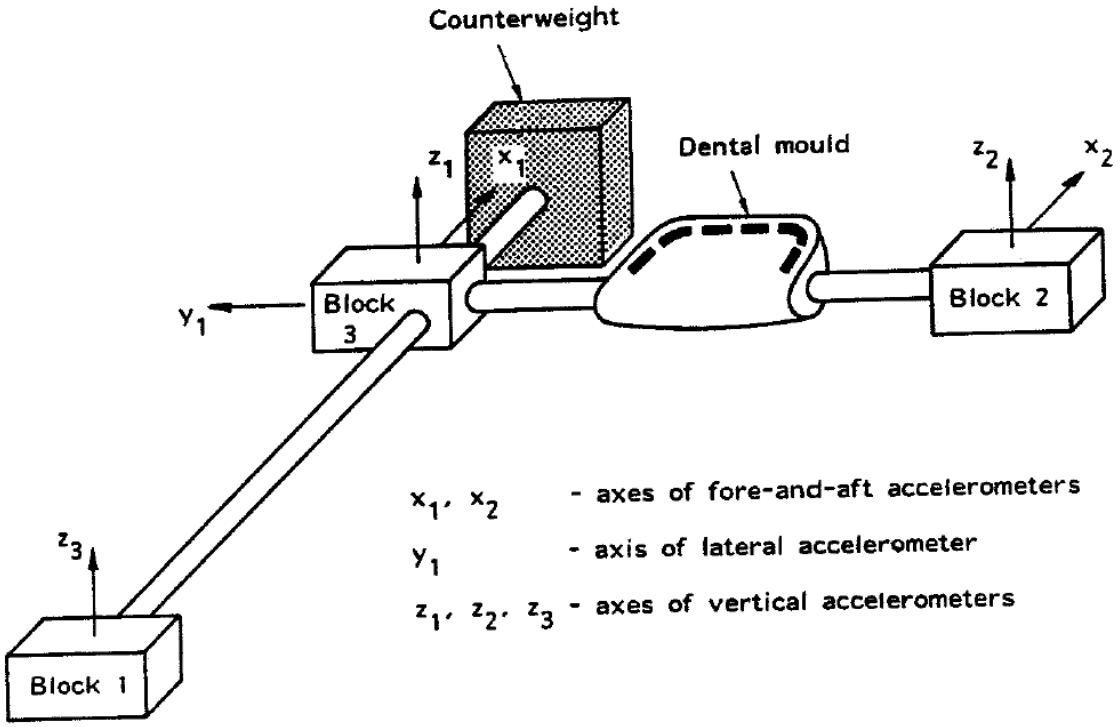

Figure 2.10 Bite-bar with relative positions of the accelerometers, mounting blocks and a counterweight from Paddan and Griffin (1988).

Transmissibilities to the spine could be used to understand the vibration modes of the body exposed to whole-body vibration. For example, the body motions corresponding to the principal resonance frequency of the vertical apparent mass at the seat (5 Hz) could be investigated with information of transmissibilities to various spinal levels. The transmissibility from seat to various body locations could also improve understanding of spinal forces, which are suggested to be the cause of low back pain associated with long-term exposure to whole-body vibration (e.g., ISO2631-5; Pankoke *et al.*, 1998). Forces at the intervertebral discs are related to the motions of spinal segments, and they would be further affected by the motion of other body parts including the pelvis, lumbar spine, thoracic spine, head, and even viscera (Figure 2.11) as suggested by the modelling studies of spinal forces (introduced in Section 2.6.3). The transmissibilities from the seat to these locations in the vertical, fore-and-aft, and pitch directions might be of interest within the investigation into spinal forces.

The acceleration at the spine may be measured with either invasive or non-invasive methods. The invasive method is a direct method in which accelerometers are mounted to a thin pin (K-wire) and inserted into the spinous processes (e.g., Pope *et al.*, 1986). However, because of the practical and ethical problems, many researchers prefer the non-invasive method, which is carried out by

taping accelerometers on the skin surface of each spinous process. The transmissibility to the vertebral body is then corrected with the skin-tissue correction method introduced by Kitazaki and Griffin (1995), which can reduce the influence of the skin and tissue system between the transducer and the bone. Details about the skin-tissue correction method are described in Chapter 6.

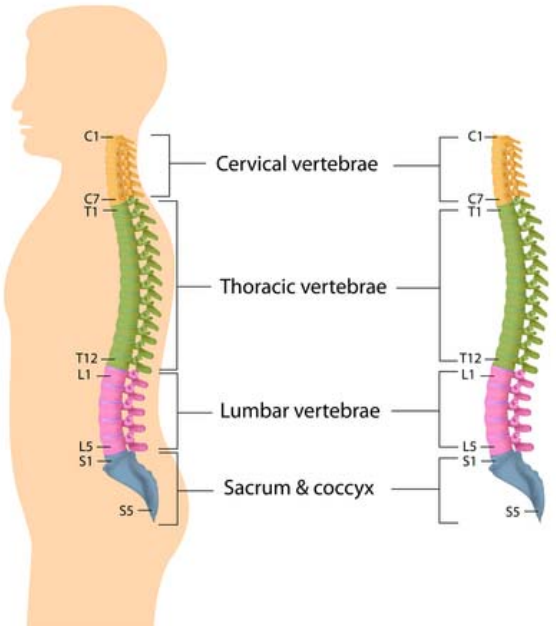

Figure 2.11 Human spine anatomy, including the pelvis, lumbar, thoracic and cervical spine (from Spinehealth.com, available online).

Similar to the study of apparent mass, the effect of inter-subject variability, backrest contact, sitting postures, muscle tension, and vibration magnitudes on the transmissibility from the seat to head and there spine are reviewed.

2.3.2 Transmissibility to the head and the spine in the normal sitting posture

In the normal upright sitting posture, the vertical in-line seat-to-head transmissibility shows a principal resonance at 4 to 5 Hz, close to the principal resonance frequency in the vertical in-line apparent mass at the seat (e.g., Griffin *et al.*, 1979, Figure 2.12; Paddan and Griffin, 1988, Figure 2.13; Kitazaki, 1994; Matsumoto and Griffin, 1998a and 2002a). A secondary resonance at around 10 to15 Hz is also observed in the vertical in-line seat-to-head transmissibility (e.g., Figures 2.12 and 2.13). The seat-to-head transmissibility at the resonance frequency shows large inter-subject variability, partly due to the characteristics of subjects, including weight, height, gender, body size (e.g., Griffin *et al.*, 1979; Paddan and Griffin, 1988). For example, the subject weight may have a negative effect on the seat-to-head transmissibility (Griffin *et al.*, 1979), and females may have greater transmissibility at frequencies from 8 to 100 Hz than males (Figure 2.12). The intra-subject subject variability (i.e., repeatability) was usually small compared to inter-subject variability (e.g., Paddan and Griffin, 1988).

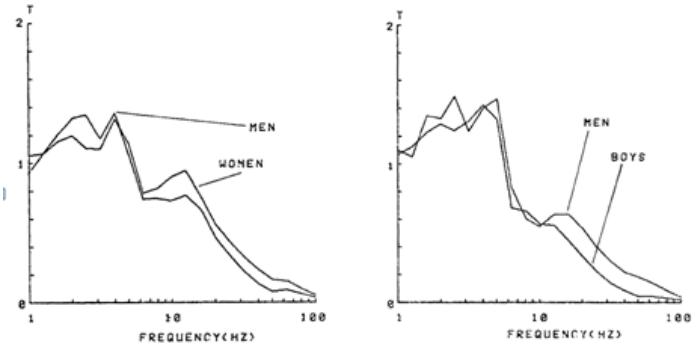

Figure 2.12 Mean seat-to-head transmissibilities of 18 men and 18 women (left) and 18 men and 12 boys (right) (Griffin *et al.*, 1979).

Seat-to-head transmissibilities in all six directions (i.e., *x*, *y*, *z*, pitch, roll and yaw) when exposed to vertical whole-body vibration have been measured (e.g., Paddan and Griffin, 1988; 1998). A principal resonance at around 5 Hz is observed for transmissibilities in all six directions. A great inter-subject variability is observed in the vertical seat to fore-and-aft head transmissibility (e.g., Paddan and Griffin, 1988; Matsumoto and Griffin, 1998), possibly due to the same causes for the inter-subject variability in the vertical seat-to-head transmissibility. Head motions occur principally in the fore-and-aft, vertical, and pitch axes of the head when the body is exposed to vertical whole-body vibration, while the motions in the other axes are relatively small.

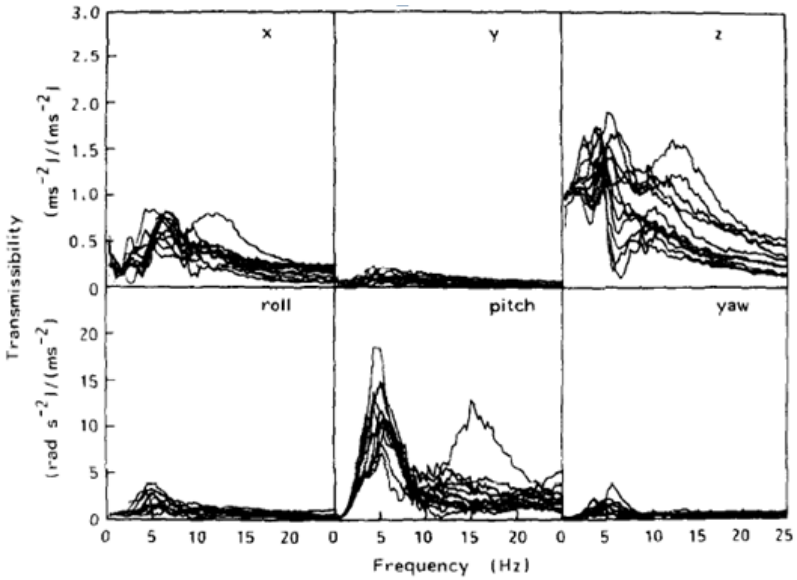

Figure 2.13 Seat-to-head transmissibilities in six directions of 12 subjects in a 'back-off' sitting posture when exposed to vertical whole-body vibration (Paddan and Griffin, 1988).

Great inter-subject variability has also been found in the vertical, fore-and-aft, and pitch transmissibilities at all spinal levels (e.g., Kitazaki, 1994; Matsumoto and Griffin, 1998; Mansfield and Griffin, 2000; Zheng, 2011). Knowledge of transmissibilities to the spine is required to improve understanding of body motions at the principal resonance frequency of the vertical apparent mass at the seat (around 5 Hz). For example, transmissibilities from seat to various spinal levels of subjects sitting in the normal upright posture and exposed to vertical random vibration of 1.7 ms^{-2}

r.m.s. from 0.5 to 30 Hz were measured by Kitazaki (1994), and the median transmissibilities are shown in Figure 2.14. The vertical transmissibilities from seat to most locations along the spine show a principal resonance at around 5 Hz (e.g., to L3, T11, T6 and T1), and some locations show a secondary resonance at around 8 Hz (e.g., to L3 and T1). The vertical seat-to-S2 transmissibility showed a resonance at 8 Hz, and the transmissibility at this peak (around 8 Hz) is greater than the transmissibility at 5 Hz. The fore-and-aft transmissibilities from seat to T1, T6 and T11 show distinct peaks at 5 Hz, but such a peak is not clearly shown in the fore-and-aft seat-to-L3 transmissibility. At frequencies greater than 5 Hz, the fore-and-aft seat-to-T11 and seat-to-L3 transmissibilities show an increasing trend with increasing frequency, but the fore-and-aft seat-to-T1 and seat-to-T6 transmissibilities show a decreasing trend. Both the fore-and-aft seat-to-S2 transmissibility and the vertical seat-to-S2 transmissibility show one resonance at 5 Hz and another resonance at 8 Hz.

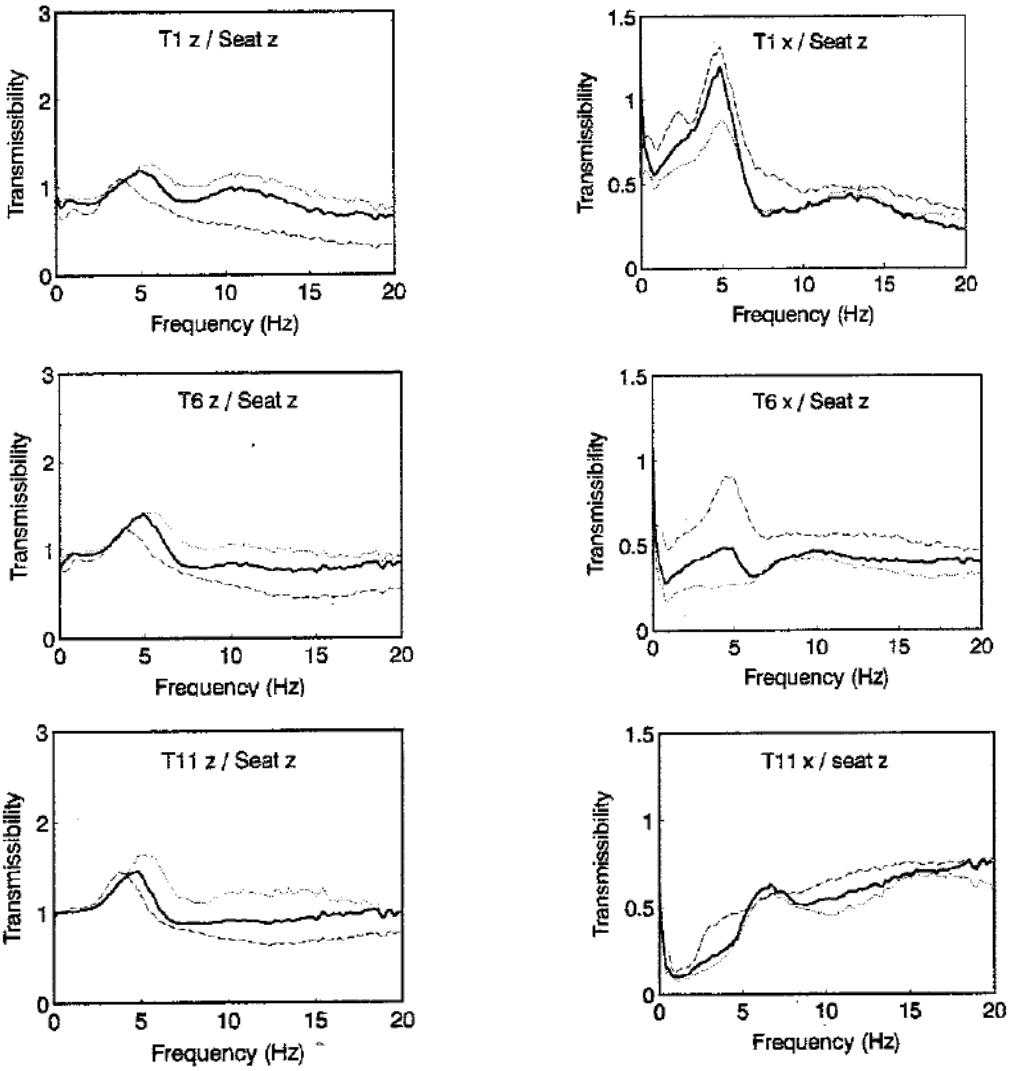

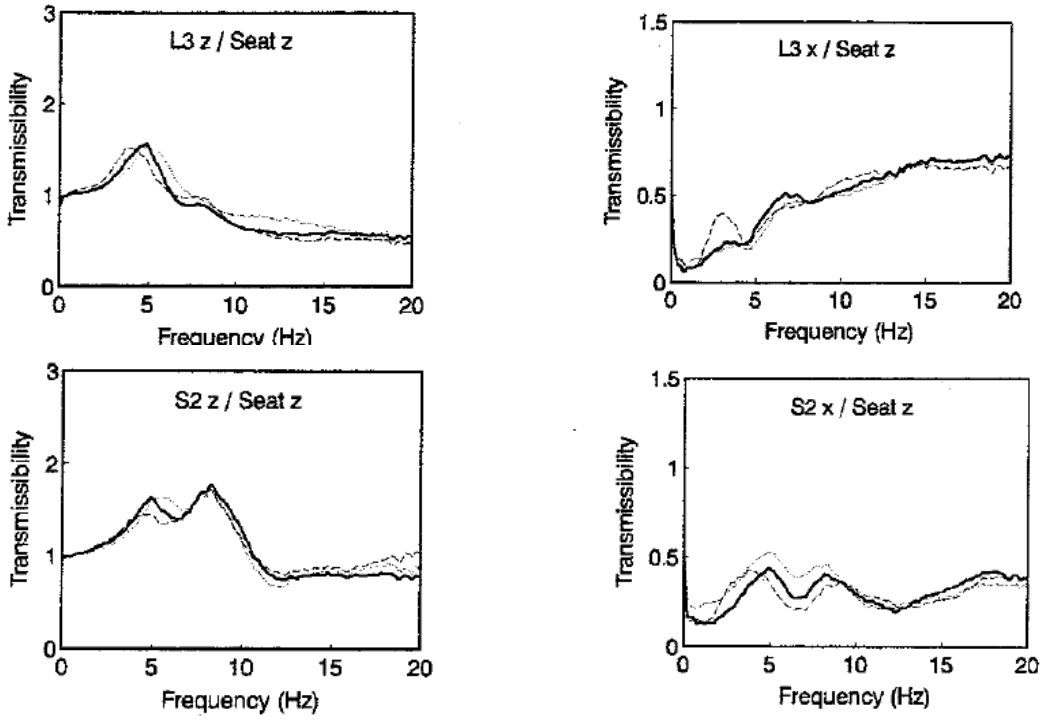

Figure 2.14 Mean transmissibilities from seat to various spinal levels of the seated human body exposed to vertical whole-body vibration in three sitting postures: '— normal upright' '— erect' '--- slouched' (Kitazaki, 1994).

The transmissibilities from vertical seat acceleration to vertical, fore-and-aft and pitch accelerations at the head, six spine levels (T1, T5, T10, L1, L3 and L5), and the pelvis in the normal upright sitting posture when exposed to vertical whole-body vibration were measured by Matsumoto and Griffin (1998) (Figures 2.22, 2.23 and 2.24). The vertical, fore-and-aft and pitch transmissibilities to the spine varied with the different measurement locations along the spine. The vertical seat-to-spine transmissibility at the principal resonance frequency (around 5 Hz) tended to decrease at higher spinal locations except for T1. The fore-and-aft transmissibilities from seat to all spinal locations (except for head and T1) were much smaller than the corresponding transmissibilities in the vertical direction. The fore-and-aft transmissibilities to the spine tended to increase at higher spinal levels. Pitch transmissibility was greater to the head than to the spine at frequencies less than 10 Hz, and the pitch transmissibilities to most spinal levels were small at frequencies less than 4 Hz. The pitch seat-to-head and seat-to-T1 transmissibilities both showed a resonance at 5 to 7 Hz. Some other studies have reported similar results for body transmissibilities (e.g., Zheng, 2011).

Statistical correlation analysis has been conducted between the principal resonance frequency of the vertical in-line apparent mass and resonance frequencies of the body transmissibilities (e.g., Kitazaki and Griffin, 1997; Matsumoto and Griffin, 1998; Zheng, 2011). The statistical results have suggested that bending or pitching motions of the spine are dominant at the principal resonance frequency (around 5 Hz) in the vertical apparent mass at the seat pan (e.g., Kitazaki and Griffin, 1997; Matsumoto and Griffin, 1998; Zheng, 2011). The bending motion of the lumbar spine is more significant than the bending motion of the upper spine, due to the rib cage restricting bending of the upper spine. A pitch motion of the pelvis occurs together with bending of the lumbar spine and may contribute to the principal resonance around 5 Hz in the vertical apparent mass at the seat.

2.3.3 Effect of backrest on the transmissibility to head and spine

When sitting on a rigid seat the addition of a vertical backrest has been found to increase the vibration transmitted from seat to head (e.g., Paddan and Griffin, 1988; Hinz *et al.*, 2002). For example, Paddan and Griffin (1988) found that contact with a vertical backrest significantly increased the transmission of vibration to the head in the vertical, fore-and-aft, and pitch directions at 5 Hz (i.e., principal resonance frequency) and at frequencies greater than 5 Hz (Figures 2.13 and 2.15). A vertical backrest tended to increase the principal resonance frequency of the seat-to-head transmissibilities in all directions, and make the peaks more distinct. The effect of a vertical backrest on seat-to-head transmissibility is similar to the effect of a vertical backrest on the vertical apparent mass at the seat. Contact with a vertical backrest seems to provide a stiffening effect to the human body (i.e., increased equivalent overall body stiffness).

There are few studies investigating the effects of vertical and inclined backrests on the vibration transmitted to the spine, probably due to the difficulty in measuring the motions of spine when contacting with a backrest.

The studies of the effects of a backrest on seat-to-spine transmissibilities show contrary results. For example, Magnusson *et al.* (1993) measured the seat-to-L3 transmissibility of three female subjects using K-wires, and found that backrest contact had an insignificant effect on the body transmissibility, with minor attenuation of vibration to the lumbar spine from 4 to 6 Hz. However, several other biodynamic studies (e.g., Mansfield and Griffin, 2002; M-Pranesh *et al.*, 2010) found a backrest had an effect on the transmissibility from seat to the spine.

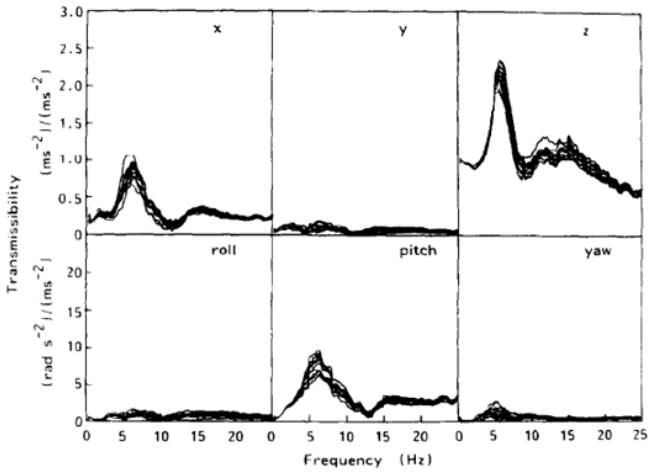

Figure 2.15 Seat-to-head transmissibilities in six directions of one subject sitting in a 'back-on' posture during vertical whole-body vibration (Paddan and Griffin, 1988).

A vertical backrest has been found to increase the rotational seat-to-pelvis transmissibility, and a distinct resonance at around 10 Hz has been observed when sitting with vertical backrest (Mansfield and Griffin, 2002; Figure 2.16).

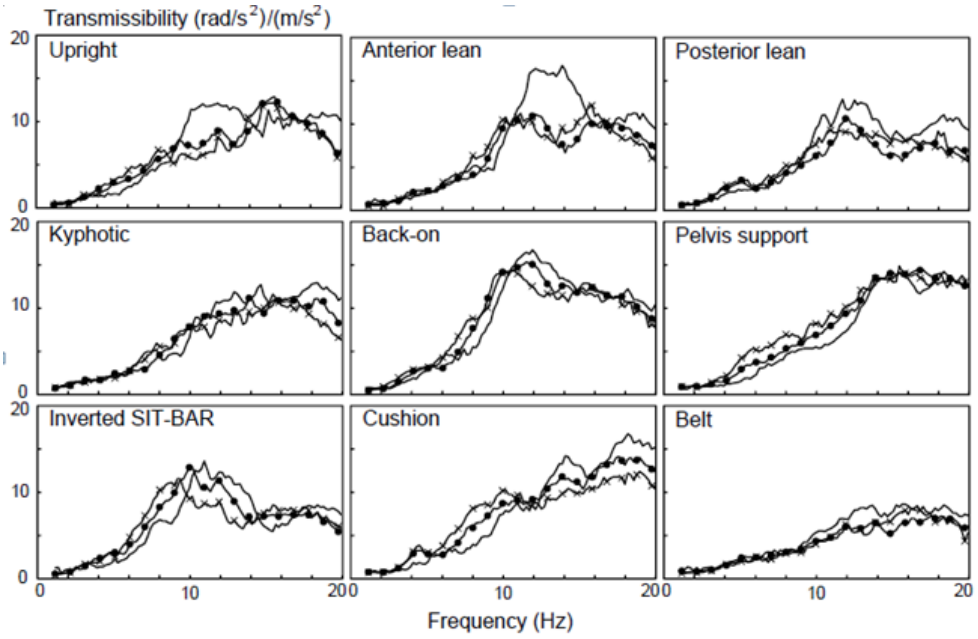

Figure 2.16 Median seat-to-pelvis rotation transmissibility for 12 subjects sitting in nine postures at 0.2, 1.0 and 2.0 ms^{-2} r.m.s. when exposed to vertical whole-body vibration: —, 0.2; —●—, 1.0; — x —, 2.0. (Mansfield and Griffin, 2002).

Transmissibilities from a seat pan to various spinal levels when sitting with a vertical backrest has been measured by M-Pranesh *et al.* (2010). A vertical back support significantly attenuated the vibration transmitted to all spinal levels in the vertical direction but increased the fore-and-aft vibration at C7 and T5 (Figure 2.17). The backrest support tended to decrease the fore-and-aft transmissibilities to lower spinal levels, T12, L3 and L5 at frequencies from 0 to 5 Hz, but marginally increase them from 5 to 10 Hz. A hand support has been reported to have a relatively small influence compared to a back support, but it may increase the fore-and-aft transmissibility to C7 and vertical transmissibility to L5 at their principal resonance frequencies (M-Pranesh et al., 2012). Possible reasons include the additional input of vertical acceleration to the body from the hand support and also support to the upper body from the hands.

In summary, contact with a vertical backrest tends to decrease vertical transmissibilities to the lumbar and thoracic spine at frequencies less than 5 Hz, and increase them at frequencies greater than 5 Hz, similar to the effect of a backrest on the vertical apparent mass at the seat pan. The inconsistent findings in the above studies (e.g., results from Magnusson *et al.* (1993) and M-Pranesh *et al.* (2010)) could be due to the small numbers of subjects being tested, the lack of control of the postures adopted by the subject when sitting again the backrest, and also differences in the measurement methods (i.e., K-wires or accelerometers attached at the skin surface). It seems reasonable to conclude that further investigation of the effect of vertical and inclined backrests on the motion of the lumbar and thoracic spine are required.

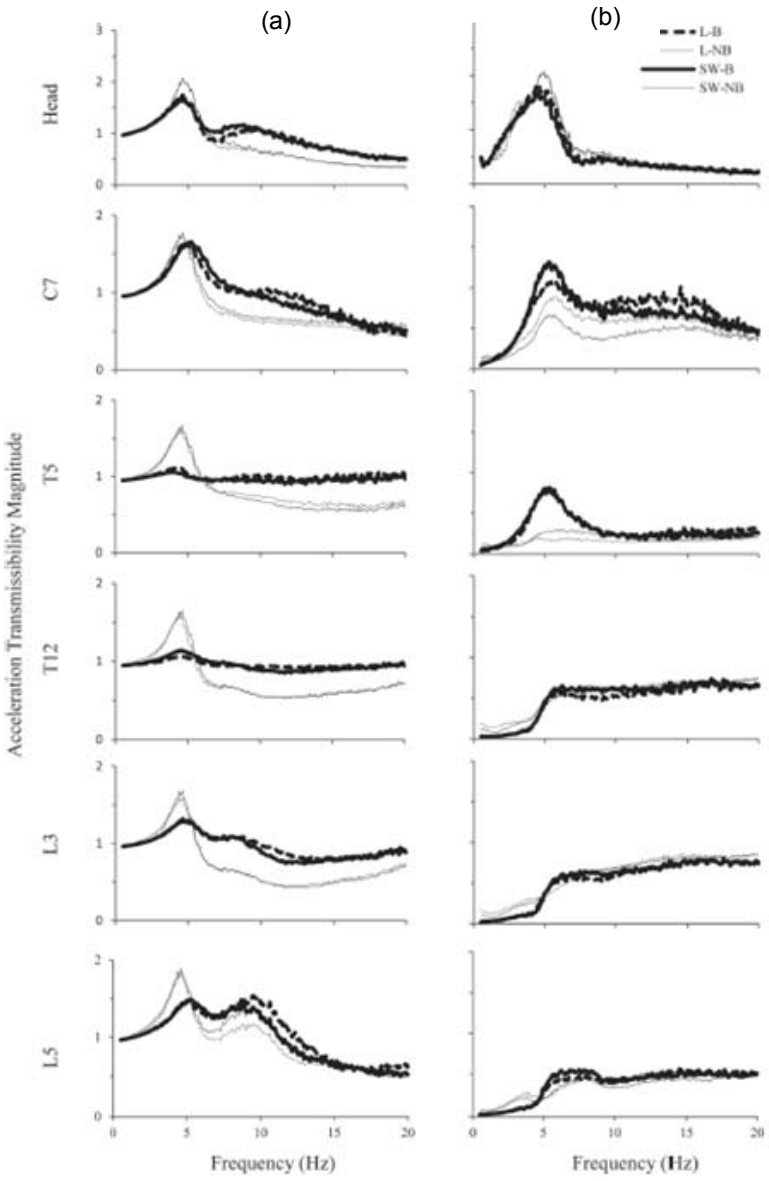

Figure 2.17 Mean responses of the body segments with different support conditions when exposed to 1.0 m/s^2 r.m.s. vertical random whole-body vibration. Left column (a): vertical transmissibilities; Right column (b): fore-and-aft transmissibilities. (M-Pranesh *et al.*, 2010).

2.3.4 Effect of posture and muscle tension on transmissibility to head and spine

Variations in sitting postures can affect transmission of vibration to the head (e.g. Griffin *et al.*, 1979; Messenger, 1987; Kitazaki and Griffin, 1994). For example, Griffin *et al.* (1979, Figure 2.18) found that a 'stiff' sitting posture would decrease the vertical seat-to-head transmissibility at frequencies less than 6 Hz, and would increase the vertical seat-to-head transmissibility at frequencies greater than 6 Hz, compared to a 'normal' sitting posture. A 'relaxed' sitting posture tended to decrease the vertical seat-to-head transmissibility at frequencies greater than 5 Hz. Consistent findings were observed by Kitazaki (1994) when measuring the seat-to-head transmissibility in 'normal', 'erect', and 'slouched' sitting postures (Figure 2.19). An 'erect' posture

tended to increase the vertical seat-to-head transmissibility at frequencies greater than 6 Hz and a 'slouched' posture tended to decrease the seat-to-head transmissibility at frequencies greater than 6 Hz. No significant differences were found in the resonance frequencies of the vertical seat-to-head transmissibility between the three sitting postures.

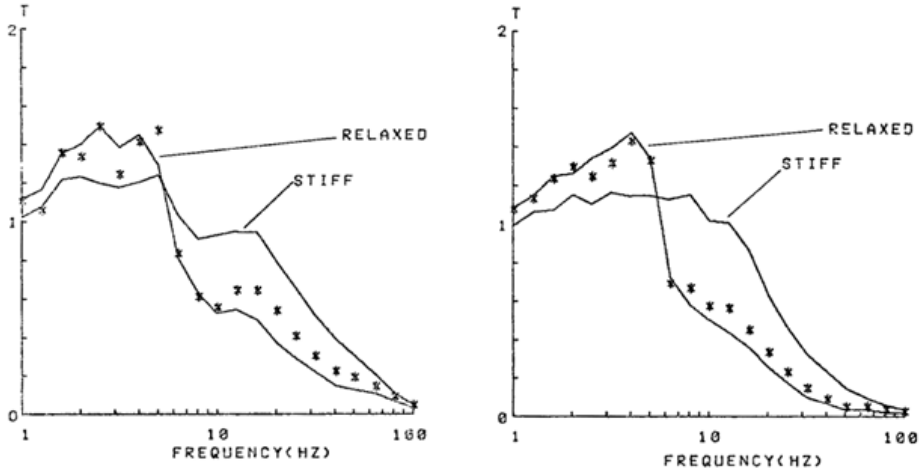

Figure 2.18 Effect of posture on the mean seat-to-head transmissibility of 18 men (left) and 12 boys (right). "Normal upright posture" is shown as asterisks; "stiff" and "relaxed" postures as continuous lines. (Griffin *et al.*, 1979).

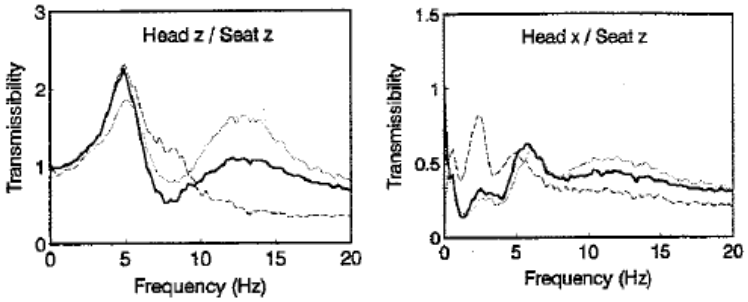

Figure 2.19 Mean transmissibility to head in vertical and fore-and-aft directions in three sitting postures: '**—':** 'normal'; '⋯': 'erect'; '---': 'slouched' (Kitazaki, 1994)

Sitting posture also has an effect on fore-and-aft seat-to-head transmissibility (Kitazaki, 1994). A 'slouched' sitting posture has been found to increase the fore-and-aft seat-to-head transmissibility at frequencies less than 5 Hz, compared to a 'normal' and an 'erect' sitting posture. An 'erect' and a 'normal' sitting posture may have similar fore-and-aft seat-to-head transmissibility (Figure 2.19).

The effects of sitting posture on seat-to-head head transmissibility might be due to changes in muscle tension and spinal curvature. An increase in the tension of muscles would be expected to increase the overall body stiffness. A change in the spinal curvature would alter the mass distribution of the body and affect the transmission route for vibration to the head. For example, a 'slouched' sitting posture may have different angles between the head and neck compared to an 'erect' sitting posture, which may further affect head motion during vibration. The dynamic properties of buttocks tissues (stiffness and damping coefficient) may also be affected by sitting posture (e.g., Kitazaki and Griffin, 1997), resulting in different seat-to-head transmissibilities. For

example, a forward tilt of the pelvic region from 105º to 85º has been found to increase the vertical seat-to-head transmissibility at frequencies greater than 6 Hz (Messenger and Griffin, 1989; Figure 2.20). Possible reasons may include the tension of buttocks tissues increasing in a forward tilted posture increasing the motion transmitted to the body.

Posture has been reported to have a significant influence on the transmission of vibration to the spine (e.g., Kitazaki, 1994; Mansfield and Griffin, 2002). Similar to the study of apparent mass, 'erect', 'normal' and 'slouched' sitting postures have been used to investigate the effect of posture on transmissibility to the spine (e.g., Kitazaki, 1994). For example, Kitazaki (1994) found that the resonance frequency of the vertical transmissibility to various spinal levels increased from about 4 Hz in a 'slouched' posture to 5 Hz in a 'normal' sitting posture, and then increased further to 6 Hz in an 'erect' posture (Kitazaki, 1994). The fore-and-aft and vertical transmissibility to T1, T6, and T11 at the resonance frequency increased from a 'slouched' sitting posture to a 'normal' sitting posture and then to an 'erect' sitting posture. The vertical and fore-and-aft transmissibilities to L3 and S2 in the three postures only varied slightly at the peak. The transmissibilities to some locations (e.g., T1, T6, L3, and S2) at the second resonance frequency around 8 Hz were not affected by posture.

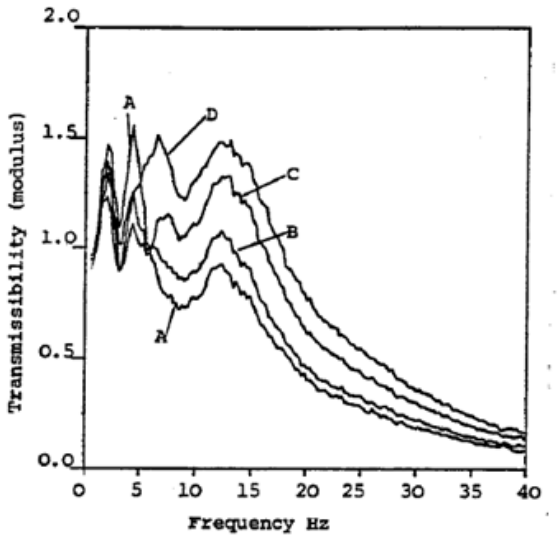

Figure 2.20 Mean vertical seat-to-head transmissibility measured with four initial pelvis angles. (A: pelvic angle of 105°; B: normal upright posture; C: pelvic angle of 95°; D: pelvic angle of 85°) (Messenger and Griffin, 1989).

The transmissibility from vertical seat acceleration to pelvis rotation has also been found to be affected by sitting posture, including 'upright', 'anterior lean', 'posterior lean', 'kyphotic, 'pelvis support', 'inverted sit-bar', 'cushion', 'back-on' and 'belt' sitting postures (Mansfield and Griffin, 2002; Figure 2.16). The 'back-on' and 'cushion' sitting postures induced the greatest individual transmissibilities. The majority subjects showed the greatest transmissibility in the frequency range 10-18 Hz. Two peaks were observed in the transmissibilities in the majority postures, including a broad peak at around 10-15 Hz and a smaller peak around 5 Hz. The 'pelvis support' posture tended to have the greatest resonance frequency in the transmissibility, and an 'inverted SIT-BAR' sitting posture tended to have the smallest resonance frequency in the transmissibility. The increase of resonance frequency of the pelvis rotation transmissibility in the 'pelvis support' sitting

posture may be due to contact between pelvis and pelvis support increasing the stiffness of the pelvis.

In summary, the transmissibility to head or spine is affected by variations in sitting postures, and possibly due to the differences in muscle tension or the dynamic properties of tissues (e.g., buttock tissues). Transmissibilities along the spine would help to understand how each part of the body moves in different postures that may assist the prediction of risks to health during whole-body vibration (e.g., spinal injury).

2.3.5 Effect of vibration magnitude on transmissibility to head and spine

A nonlinear behaviour has also been observed in seat-to-head transmissibility (including vertical in-line, pitch, and fore-and-aft cross-axis transmissibilities), referring to a decrease in the principal resonance frequency with increasing vibration magnitude (e.g., Griffin, 1975; Hinz and Seidel, 1987; Matsumoto and Griffin, 2002). For example, Matsumoto and Griffin (2002) found that with vibration magnitudes increasing from 0.123 m/s^2 r.m.s. to 2.0 m/s^2 r.m.s., the principal resonance frequency in the seat-to-head transmissibility decreased (from about 7 Hz to 5 Hz) in all three directions (vertical, fore-and-aft and pitch). The transmissibility at frequencies greater than 5 Hz also decreased with increasing vibration magnitude (Figures 2.22, 2.23, and 2.24). However, the effect of vibration magnitude on the seat-to-head transmissibility was suggested to be less than the variability associated with inter-subject variability (e.g., Griffin, 1975; Figure 2.21).

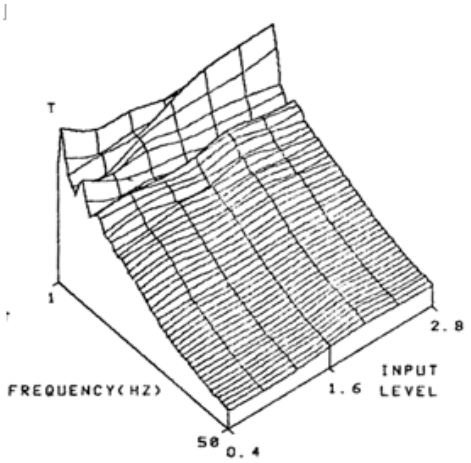

Figure 2.21 The vertical seat-to-head transmissibility from 1 to 50 Hz of a single subject exposed to 7 vibration levels during vertical whole-body vibration (0.4, 0.8, 1.2, 1.6, 2.0, 2.4 and 2.8 m/s^2 r.m.s.). (Griffin, 1975).

A nonlinear behaviour has also been observed in the vertical, fore-and-aft and pitch transmissibilities to various locations at the spine when exposed to vertical whole-body vibration in the normal upright sitting posture (e.g., Matsumoto and Griffin, 2002b, Figures 2.22 – 2.24; M-Pranesh *et al.,* 2010; Zheng, 2011) and other sitting postures (e.g., nine postures tested by Mansfield and Griffin, 2002, Figure 2.16). For example, with increasing vibration magnitude, the resonance frequency at around 10-15 Hz in the seat-to-pelvis pitch transmissibility has been found to decrease in all nine sitting postures (see Section 2.3.4) except for the 'pelvis support' posture (Mansfield and Griffin, 2002). Similar to the findings about the nonlinearity in the vertical apparent

mass at the seat, reductions in the resonance frequency of seat-to-pelvis pitch transmissibility were more significant with changes at low magnitudes (e.g., 0.2 to 0.5 m/s^2 r.m.s.) than with changes at high magnitudes (e.g., 1.0 to 2.0 m/s^2 r.m.s.) (Mansfield and Griffin, 2002).

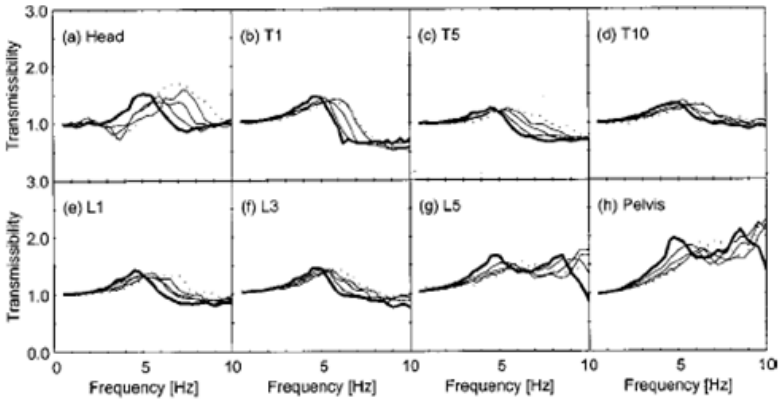

Figure 2.22 Median transmissibilities from vertical seat acceleration to vertical acceleration at each measurement location along the spine at five magnitudes of vibration: '…': lowest magnitude (0.125 m/s^2 r.m.s.); '—': greatest magnitude (2.0 m/s^2 r.m.s.). (Matsumoto and Griffin, 2002b).

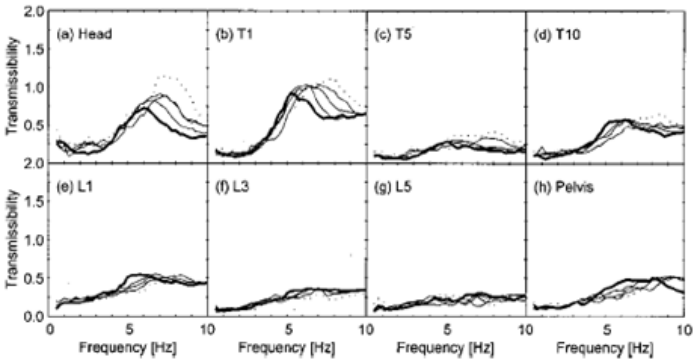

Figure 2.23 Median transmissibilities from vertical seat acceleration to fore-and-aft acceleration at each measurement location at five magnitudes of vibration: '…': lowest magnitude (0.125 m/s^2 r.m.s.); '—': greatest magnitude (2.0 m/s^2 r.m.s.). (Matsumoto and Griffin, 2002b).

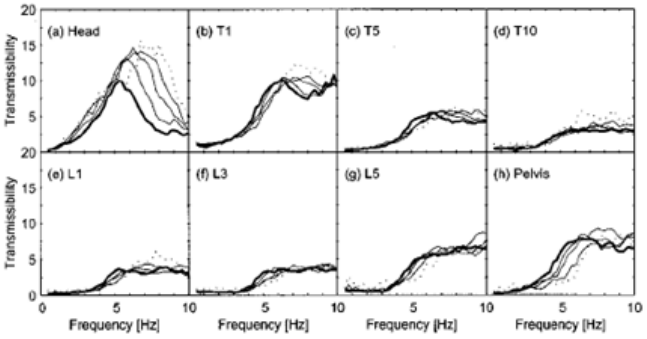

Figure 2.24 Median transmissibilities from vertical seat acceleration to pitch acceleration at each measurement location at five magnitudes of vibration: '…': lowest magnitude (0.125 m/s^2 r.m.s.); '—':greatest magnitude (2.0 m/s^2 r.m.s.). (Matsumoto and Griffin, 2002b).

The alteration of the principal resonance frequency of body transmissibility with the effect of vibration magnitude may be less significant than the effect of backrest support (M-Pranesh *et al.,* 2010).

The causes of the nonlinearity shown in the vertical apparent mass at the seat may also contribute to the nonlinear behaviour in the body transmissibilities. Possible causes include the dynamic properties of the tissues in the buttocks or muscle behaviour in the body.

Although it is desired to have a biodynamic model with the capability of reflecting the nonlinearity of human body, no such model has been developed. Possible reasons include the lack of understanding of the underlying causes of the nonlinearity and not enough information on the dynamic behaviour of body tissues (e.g., muscle behaviour during whole-body vibration). The biodynamic model developed with biodynamic response measured at one vibration magnitude requires justification for application to other vibration magnitudes.

2.3.6 Vibration modes of the seated human body

The investigation of the transmissibility of the body has always been motivated by a desire to improve understanding of the resonance behaviour in the vertical apparent mass at the seat or the causes of the nonlinearity (e.g., Kitazaki and Griffin, 1997 and 1998; Matsumoto and Griffin, 1998; 2002). The mode shapes of seated human body in three sitting postures ('erect', 'slouched' and 'normal') have been extracted with transmissibility measurements along spine (T1, T6, T11 and L3, head, and pelvis) by Kitazaki and Griffin (1998). Eight modes have been extracted below 10 Hz using the mean transfer function for the human body in the 'normal' sitting posture (Figure 2.25). The principal resonance around 5 Hz has been found to be correlated with the fourth and fifth modes which both consisted of motion of the entire body. The fourth mode at 4.9 Hz corresponds to the principal resonance of the vertical apparent mass. It consists of an entire body mode, in which the head, spine and trunk moved vertically due to shear and axial deformation of the buttock tissue, in phase with a vertical visceral mode, a bending mode of upper trunk and cervical spine. The fifth mode contains the bending of lumbar spine and the lower thoracic spine, and it occurs at a frequency (5.6 Hz) close to the fourth mode. The heavy damping of body may merge the fourth and fifth body modes together, contributing to the principal resonance of the vertical apparent mass at around 5 Hz. The secondary resonance at about 8 Hz has been found to be correlated with sixth, seventh and eighth modes, which include the pitch motion of pelvis and vertical motion of viscera. The vibration modes in the same posture have also been extracted from the analysis of a two-dimensional finite element model (Kitazaki and Griffin, 1997, reviewed in Section 2.4.4), which showed good agreement with the measured mode shapes, especially for the modes contributed to the principal (5 Hz) and secondary (8 Hz) resonances of the vertical apparent mass.

With biodynamic models, Matsumoto and Griffin (2001) extracted the mode shapes of the seated human body at the principal resonance frequency around 5 Hz. It was found that the principal resonance could be attributed to a body mode at 5.66 Hz, and this mode consisted of a combination of deformation of buttocks tissues, vertical motion of viscera and bending motion of the spine. The findings were consistent with the findings from Kitazaki and Griffin (1998).

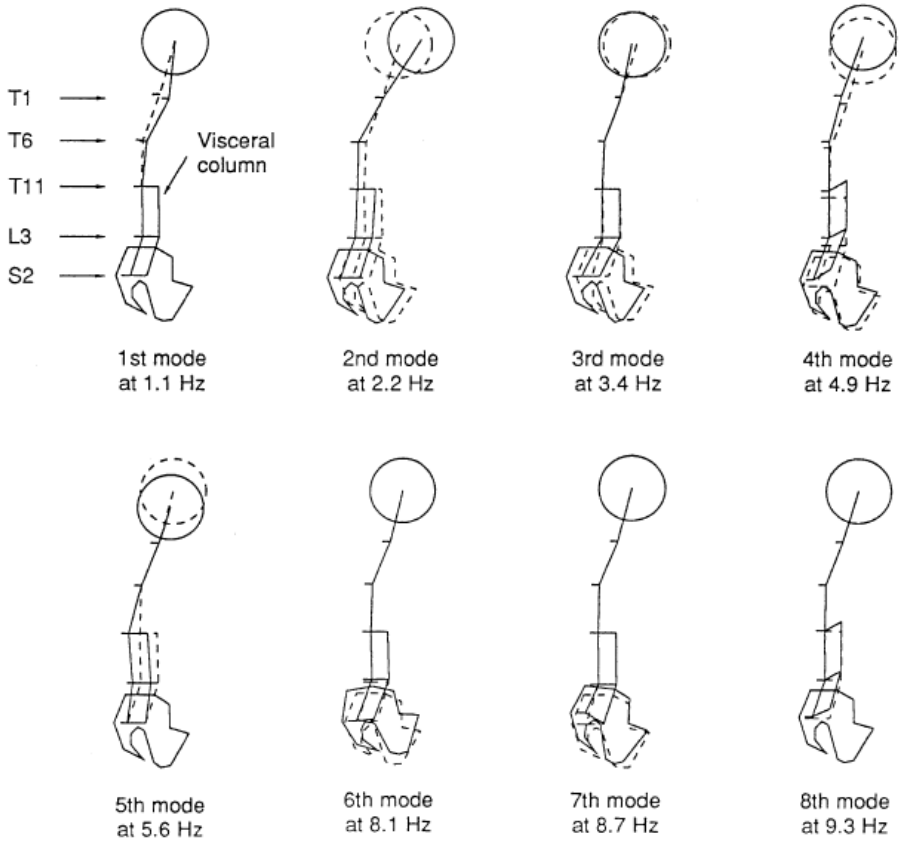

Figure 2.25 Measured mode shapes below 10 Hz in the normal sitting posture (Kitazaki and Griffin, 1998).

As discussed above, the response of the human body to whole-body vibration is complex and the motions of body segments are affected by each other. A bending motion of the spine may contribute to the principal resonance of the vertical apparent mass at the seat, and may induce great risk to health (e.g., spinal injury). The complex body motions suggest that the biodynamic models aimed at predicting the spinal forces should reflect appropriate body motions (both overall biodynamic responses and motions of the spine) and the effects of changes in body posture (Kitazaki and Griffin, 1998).

2.4 Biodynamic modelling

2.4.1 Introduction

Biodynamic models are used to predict the movement or force of body structures exposed to vibration. Biodynamic models are developed for various applications, including understanding the nature of body movements or predicting the influence of variables affecting the biodynamic response (Griffin, 2001).

Biodynamic models may be divided into three categories based on what kind of information the model tries to explain and predict (Griffin, 2001): (i) ‘quantitative model’, which is used to predict the relationship between input and output; (ii) ‘mechanistic model’, which explains how the body

moves; (iii) ‘effect model’, which predicts the probability of some specified response to an input, like risk to health and discomfort.

A ‘quantitative model’ is also called the ‘input-output’ model, which is developed to match the measured relationship between input and output. It can be used to describe the biodynamic response of human body, including apparent mass and body transmissibility (e.g., Wei and Griffin, 1998a; Wei and Griffin, 1998b; Qiu and Griffin, 2011b). But such a model has no predictive power, a large variability of data is required for a wide range of applications (Griffin, 2001).

A ‘mechanistic model’ generally reflects the mechanisms associated with the biodynamic response of human body, and it represents the current knowledge of a defined mechanism. A ‘mechanistic model’ can be in the form of combined lumped parameters (i.e., mass, spring and damper), which can predict the apparent mass or transmissibility in multiple directions or to various locations (e.g., Matsumoto and Griffin, 2001). It can also be a finite element model which is more complex, and is used to describe the body moving mechanism, such as the vibration modes of the body (e.g., Kitazaki and Griffin, 1997).

An ‘effect model’ focuses on the relationship between causes (motions or shock) and effects, and gives indications of the effects of body motion on human health or comfort or performance (Griffin, 2001). An ‘effect model’ could be numerical values indicating the probability of a specific degree of a specific injury for a specific input or equations and models representing or predicting such values. For example, the equations described in International Standard (ISO 2631-5: 2003) to evaluate the risk of health of the spine based on the predicted values of spinal loads is an ‘effects model’.

In general, there are three kinds of model development methods for biodynamic modelling of the human body, referring to the lumped parameters technique, multi-body approach, and finite element method. The complexity increases among these three kinds of model and their ranges of applications differ.

2.4.2 Lumped parameters model

A lumped parameter model is used in both ‘quantitative models’ and ‘mechanistic models’, and it has the advantage of simplifying and quantifying the complex biodynamic responses of the human body with a small number of parameters. Various lumped parameters models have been developed to reflect the required characteristics of the biodynamic responses measured in experiments (e.g., Fairley and Griffin, 1989; Wei and Griffin, 1998a). A lumped parameter model represents the human body by combinations of masses, springs, and dampers, without representation of the anatomic structures of the human body.

The lumped parameter models can predict the vertical apparent mass at the seat of seated human body, including the modulus and phase, either by a single degree-of-freedom model (e.g., Wei and Griffin, 1998) or a two degree-of-freedom model (e.g., Wei and Griffin, 1998, Figure 2.26), or more complex models (e.g., Fairley and Griffin, 1989; ISO 5982, 2001). The effects of various factors (e.g., muscle tension, backrest contact, inter-subject variability, vibration magnitudes etc.) on the vertical apparent mass at the seat can be reflected by changing some of the parameters in the lumped parameters model (e.g., Toward and Griffin, 2010b), but the corresponding experimental

data are required. Without a representation of human anatomy, the lumped parameter -models have rarely been used to predict body transmissibilities or the forces in the lumbar spine.

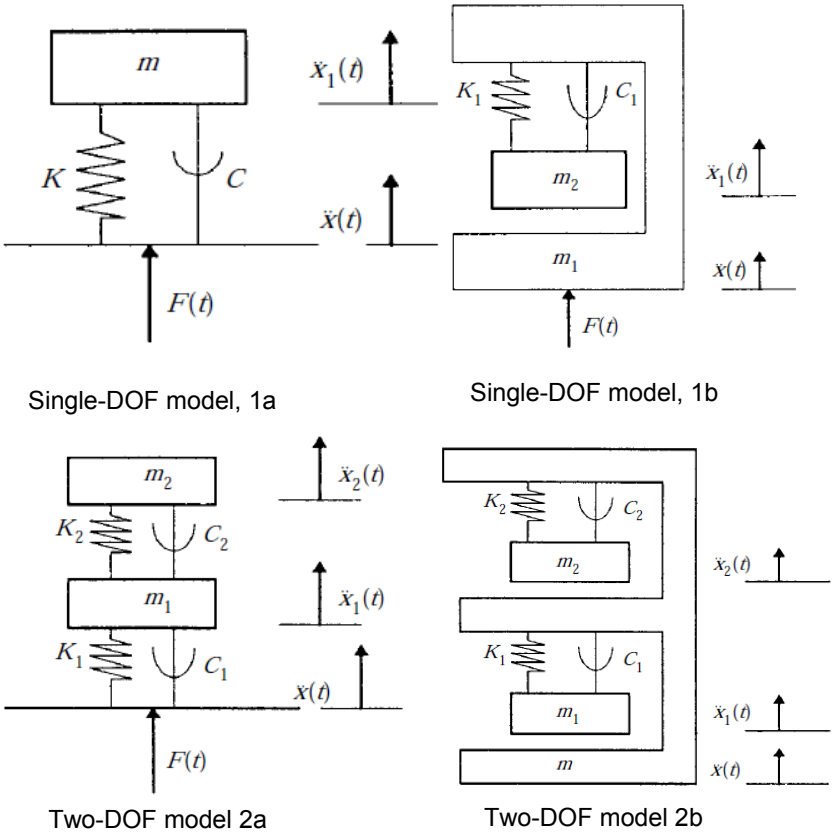

Figure.2.26 Two single degree-of-freedom lumped parameters models (top two models) and two two degree-of-freedom models (bottom two models) (Wei and Griffin, 1998)

2.4.3 Multi-body model

A multi-body dynamic model usually treats the body segments as rigid bodies interconnected by joints and force elements. This type of model is capable of representing the gross anatomy of the body and predicting the motion of each segment when exposed to vibration.

A multi-body model is usually developed when representing the biodynamic response of the human body in multiple directions. For example, the vertical and fore-and-aft apparent mass at the seat and the vertical and fore-and-after transmissibilities of the various spinal levels of a seated human body exposed to vertical whole-body vibration have been predicted by various multi-body models (e.g., Matsumoto and Griffin, 2001; Nawayseh and Griffin, 2009; Zheng *et al.*, 2011). In such models, a rotational joint with stiffness and damping coefficient is commonly adopted to connect the body segments. The positions of body segments, the positions of the connection joints, and the inertial and mass properties of body segments are determined based on the anthropometry of the human body.

A multi-body model developed with appropriate elements can help to understand the body moving mechanisms. A typical multi-body model is shown in Figure 2.27. A five-degree-of-freedom model was developed by Matsumoto and Griffin (2001; Figure 2.27) to investigate the movement of the body at the resonance frequency of the vertical apparent mass. Masses 1, 2 and 4 represent the legs, and masses 3 and 5 represent the upper body. The elements underneath mass 1 are used to model the deformation of tissues beneath the pelvis and thighs (buttock tissues). The rotation of the pelvis and bending of the spine are represented by the rotational elements used to connect the masses. The movements of masses 1 and 4 are restricted to the vertical direction for simplification. A modal analysis of this model suggests that the principal resonance frequency around 5 Hz in the vertical apparent mass at the seat is mainly contributed by vertical motion caused by deformation of buttocks tissues and vertical motion of viscera, while the contribution from the bending motion of the spine is small. The use of rotational joints enables the model to reflect both vertical and fore-and-aft motions of the upper body, and similar structures have been adopted in other models (e.g., Nawayseh and Griffin, 2009).

As stated before (Section 2.2.3 and 2.3.4), biodynamic responses of the human body are affected by various factors, including change of posture, effects of body support. Such effects could be achieved by suitable adjustments made to the multi-body model, including adjustments in the body geometry based on postures and adding the representation of backrest.

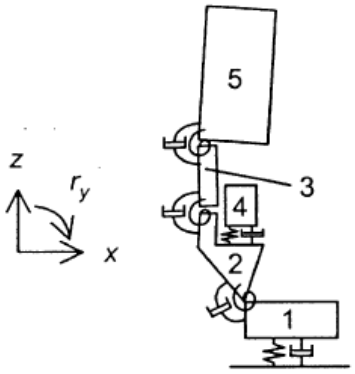

Figure.2.27 A multi-body model representing the seated human body exposed to vertical whole-body vibration (Matsumoto and Griffin, 2001).

The effects of a backrest on the biodynamic responses of the seated human body have been investigated with a two dimension multi-body model (Zheng *et al*., 2011). This model comprises five body segments: the upper body, middle body, pelvis, thighs, and legs. Both translational and rotational movements of each segment have been considered. The contact between the body and backrest is represented with two pairs of translational springs and dampers in the vertical and fore-and-aft directions. The model can reflect appropriate apparent masses at the backrest in the vertical and fore-and-aft directions similar to the apparent masses measured by Nawayseh and Griffin (2004). Contact with a vertical backrest at the lower part of the spine is suggested to increase the vertical apparent mass at the seat at the principal resonance frequency. Similar

representation of contact between the body and a backrest can be found in other dynamic models (e.g., Cho and Yoon, 2001; Liang and Chiang, 2008).

2.4.4 Finite element model

Finite element models of the human body can be developed based on detailed anthropometric information and human anatomy, and they can represent the human biodynamic responses including apparent mass and body transmissibilities (e.g., Kitazaki and Griffin, 1997; Zheng *et al.*, 2012; Liu *et al.*, 2012). Finite elements models can predict the motion of body segments and force distributions at the interfaces of the body and a seat and so as to study the internal forces associated with spinal injury (e.g., Pankoke *et al.*, 1998; Hinz *et al.*, 2002 and 2007; Wang *et al.*, 2010). Such models represent the anatomy of body with a skeletal structure and soft tissues at required regions. The finite element models usually comprise a large number of elements connected by nodes, and they are generally complex and computational costly.

A finite element model can be developed to improve understanding of the moving mechanisms of the human body when exposed to whole-body vibration (e.g., Kitazaki and Griffin, 1997; Zheng *et al.*, 2012). A passive sagittal symmetric finite element model of the upper body with beam, spring and mass elements representing the spine, viscera, head, pelvis and buttocks has been developed to perform modal analysis of the human body (Kitazaki and Griffin, 1997, Figure 2.28). This model can predict the apparent mass and body transmissibility with various postural conditions. The mode shapes of the seated human body predicted by the finite element model are in good agreement with the measured mode shapes (see Section 2.3.6; Kitazaki and Griffin, 1998). Seven mode shapes have been extracted at frequencies less than 10 Hz. The principal resonance in the vertical apparent mass at the seat around 5 Hz is found to be related to the pelvic rotation due to deformation of tissue beneath and it appeared as the fourth calculated mode shape. The principal resonance frequency has been found to decrease from ‘erect’ to ‘slouched’ sitting posture, possibly due to the increasing contact area between buttocks and seat, and the decrease in the axial stiffness of buttocks tissues. This model cannot estimate the muscle forces and spinal forces because it lacks representation of muscles.

There are some commercial finite element models of the human body developed with different applications, such as the MADYMO model (e.g., Verver *et al.* 2003), LS-Dyna Hybrid III (e.g., Mohan *et al.*, 2007) and CASIMIR (e.g., Siefert *et al.*, 2008). These models were used in the car industry to analyse the response of the human body to car crash. The MADYMO model and CASIMIR model have been further developed to represent the dynamic response of the human body and predict the forces in the spine (e.g., Verver *et al.*, 2003).The LS-Dyna Hybrid III model is generally used to represent the human body exposed to mechanical shocks of high magnitude that occur for a short period (e.g., 80 ms) without reflecting the human body biodynamic response (e.g., Mohan *et al.*, 2007).

Several other finite element models have been developed to predict the spinal loads in the human body exposed to vertical whole-body vibration (e.g., Pankoke *et al.*, 1998 and 2000; Bazrgari *et al.*, 2008). Such models are complex in structure and require validation for the development process as

well as the prediction of spinal forces. The advantages and limitations of such models are described and discussed in Section 2.6.3.

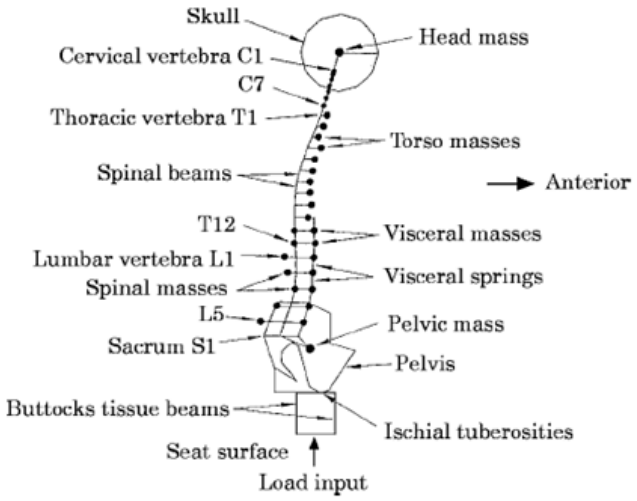

Figure 2.28 The two-dimensional finite element model of human body in the normal upright sitting posture (Kitazaki and Griffin, 1997).

2.5 Lumbar spine anatomy

2.5.1 Anatomy of lumbar spine

The human vertebral column is a complex structure consisting of vertebrae bodies, intervertebral discs, articular facet joints, ligaments and tendons (Figure 2.29) where the muscles are connected to provide flexibility of spine motion (e.g., flexion, tension, rotation). The whole spine column can be divided into three major regions from head to pelvis: cervical spine, thoracic spine and lumbar spine. Understanding the anatomy structure of the spine would help to study the spinal risks of human body exposed to whole-body vibration. The following review of spinal anatomy is based on the studies of Bogduk (1997) and the review in Kitazaki (1994). More details are described in the above studies.

The lumbar spine is typically comprised of five vertebrae (L1 to L5) increasing in size and mass from the first (L1) to the fifth (L5), interconnected with deformable intervertebral discs, and surrounded by ligaments. The lumbar vertebrae are the largest and strongest column. The vertebral bodies have a similar structure, comprised of two principal parts: the anterior vertebral body, and the posterior vertebral arch with processes (Figure 2.29a). A vertebral body consists mostly of spongy bone covered by a thin layer of cortical bone (Pang, 2005). The posterior vertebral arch consists of laminae, articular processes, spinous processes and transverse processes, which provide points of attachment for ligaments. The main functions of the vertebral column are supporting the body in the upright posture, allowing body movements and protecting the spinal cord.

The main function of the intervertebral disc is to allow movement between vertebral bodies and to transmit loads between vertebral bodies (Bogduk, 1997). The movements include flexion, extension, lateral flexion and axial rotation (cited from Kitazaki, 1994). Each intervertebral disc comprises of three basic parts: a central nucleus pulposus, a peripheral annulus fibrosis surrounding it and two vertebral endplates (Figure 2.29b). The endplates are two layers of cartilage of 0.6-1.0 mm in thickness covering the area on the vertebral body encircled by the ring apophysis (Bogduk, 1997). The vertebrae endplates are strongly bound to the intervertebral disc (annulus fibrosis) but weakly attached to the vertebral bodies. They can be torn in certain forms of spinal trauma (Bogduk, 1997). As a result, many models have been designed to predict the spinal loads at the vertebral endplates (e.g., Seidel *et al.*, 1998).The intervertebral disc contains collagen fibres with elastic properties and stretches like springs (Bogduk, 1997). Therefore, the connections between the adjacent vertebrae have been modelled by springs.

A leaning forward sitting posture applies torque to the intervertebral disc and may cause the intervertebral disc to distort. The measurements of the spinal forces (Section 2.6.2.1) or predictions of spinal forces (Section 2.6.3) usually neglect the torque applied to the disc, probably underestimating the spinal loads in the real human body (Seidel *et al.*, 1997).

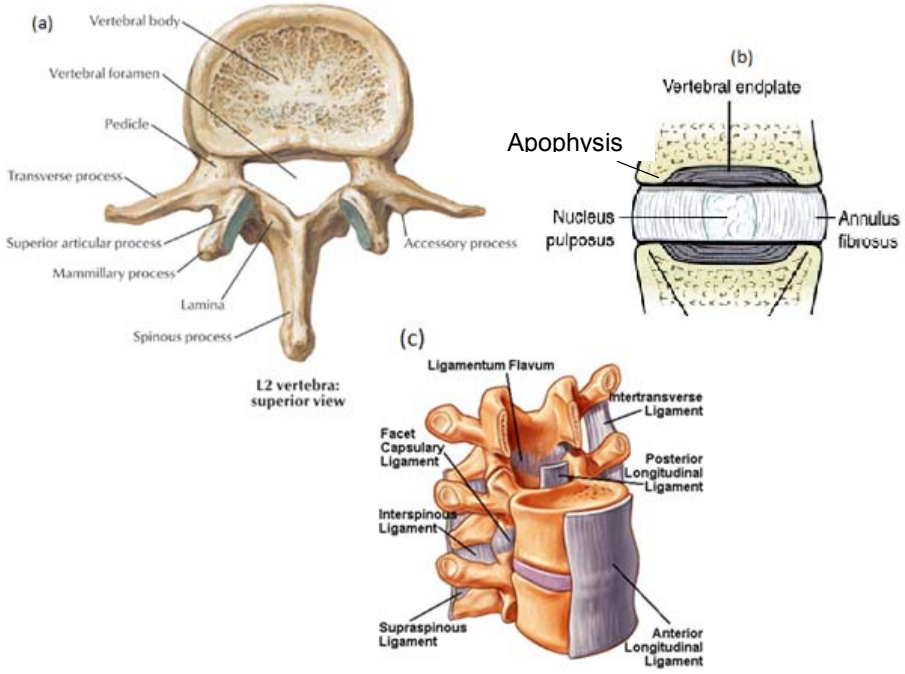

Figure 2.29 Anatomical structure of the lumbar spine segments, including: (a) vertebral body, (b) intervertebral disc and (c) ligaments (from Eidelson, available online).

The pair of the inferior articular facets of a vertebra forms articular facet joints with the corresponding pair of the superior articular facets of the next inferior vertebra. In flexion-extension, lateral flexion and axial rotation, the facing articular facets slide over each other in the direction determined by the facet orientation which determines the direction of the relative motion of the

adjacent vertebral bodies and sometimes the locking position of motion. The articular facets in the lumbar regions are not involved in weight bearing in the normal posture (Kitazaki, 1994).

The typical group of main ligaments which connect adjacent vertebrae through the cervical and thoraco-lumbar regions includes the anterior and posterior longitudinal ligaments, a pair of the capsular ligaments, a pair of the ligament flava, interspinous and supraspinous ligaments and a pair of the intertransverse ligaments (Figure 2.29c). These ligaments normally have a high elastic stiffness and have the function of connecting the vertebral bodies and protecting the spinal cord. The ligaments can resist the motions of typical vertebral bodies. For example, the twisting, forward, lateral and backward bending motions of the L5 vertebra are resisted by the iliolumbar ligament (Bogduk, 1997). More detailed information about the lumbar spine anatomy is provided by Bogduk (1997).

2.5.2 Muscles in the lumbar region

The muscles in the back are connected to the spinal column via tendons providing stability and enabling motions of the spinal column. The following text describes three main groups of muscles controlling the movement of the body in the sagittal plane and maintaining postural stability. The muscles are psoas major, multifidus, and lumbar erector spinae.

The psoas major is a long muscle arising from the anterolateral aspect of the lumbar spine and descending over the brim of the pelvis to insert into the lesser trochanter of the femur (cited from Bogduk, 1997). The psoas major has only a small effect on the flexion and extension of the lumbar spine, but it adds a large compression loads to the lower lumbar discs due to its downward architecture. During ‘sit-ups’ activity, two psoas majors may exert a compression load on the L5/S1 disc equivalent to about 100 kg.

The multifidus is the largest and most medial of the lumbar back muscles. The fascicles of the lumbar multifidus arise from the lateral surface of the caudal edge of the spinous processes of vertebrae from L1 to L5, to areas on the iliac crests and the dorsal surface of sacrum (Macintosh and Bogduk, 1987). The principal action of the multifidus is expressed in the vertical direction, acting as a posterior sagittal rotator of the individual vertebral bodies in the lumbar spine. The multifidus increases the lumbar lordosis and adds posterior compression loads and anterior tensile loads to the lumbar vertebrae and intervertebral discs.

The lumbar erector spinae is the sum of superficial muscles at the back, and is the broadest and largest muscle group in the lower back. The erector spinae consists of two muscles: the longissimus thoracis and the iliocostalis lumborum (Bogduk, 1997). Each of the two muscles has a lumbar part and a thoracic part consisting facials arising from lumbar vertebrae body and thoracic vertebrae (or ribs), respectively. The longissimus thoracis pars lumborum and illiocostalis lumborum pars lumborum consist fascicles arising from the transverse processes of the lumbar vertebrae to the iliac spine. The longissimus thoracis pars thoracis consists of fascicles arising from the ribs and transverse processes of T1 or T2 down to T12, connecting to either the spinous process of the lumbar vertebrae or the sacrum. The iliocostalis lumborum pars thoracis consists of fascicles from the lower seven or eight ribs attached to the ilium and sacrum. The lumbar erector

spinae contributes to the lumbar lordosis. The principal function of the four muscles is to produce posterior rotation of the lumbar spine in the sagittal plane. During the contraction of the muscles, forces in the horizontal direction and vertical direction are generated, but the vertical component is predominant.

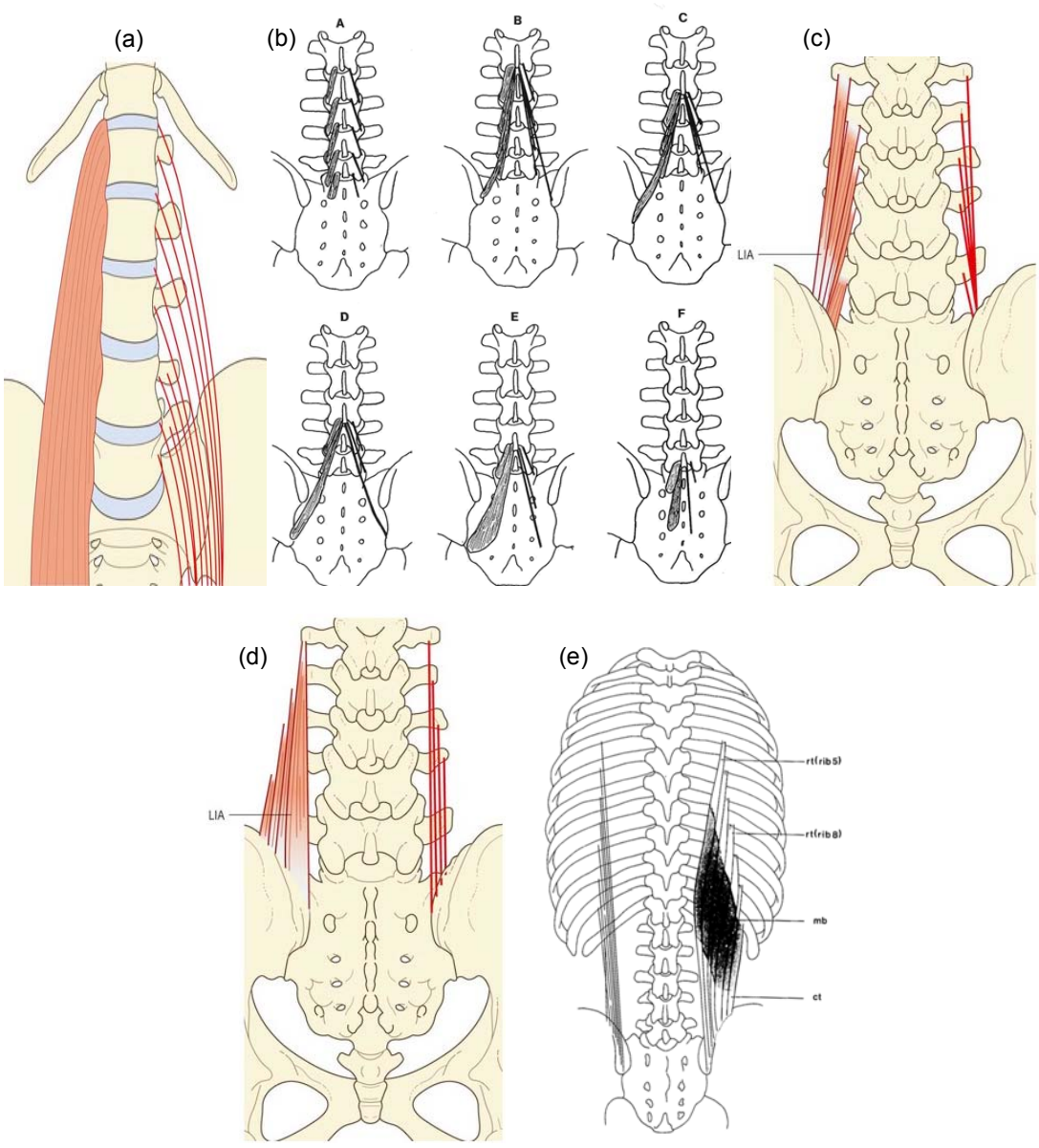

Figure 2.30 Muscles at the lumbar spine (from Bodguk, 1997) (a): Psoas major; (b): multifidus; (c): longissimus thoracis pars lumborum; (d): iliocostalis lumborum pars lumborum; (e): iliocostalis lumborum pars thoracis.

Each of the lumbar muscles is capable of several possible actions and no unique motion can be provided by one muscle. The back muscles act together with joints and ligaments against the potential displacement induced by gravity in different postures. The muscles generate forces by voluntary contraction, which provides pulling force to the attached points of the muscles. The combinations of contractions of different groups of muscles contribute to complex motions of the body. A standing posture and a sitting posture (with no support) induce similar activity of the back

muscles. Sitting with arms resting on a desk reduces the activity of back muscles (Bogduk, 1997). Sitting with a reclined backrest decreases the activity of muscles in the lumbar region (Bogduk, 1997).

During forward flexion, the muscles in the back of the thoracic region and lumbar region tense (e.g., erector spinae and multifidus), but at a certain point during forward flexion, the activity in the back msucles ceases and the vertebral column is braced by the locking of the joints and tension in the ligaments (Bogduk, 1997), but it may not occur in all subjects. Extension of the trunk from the flexed position induces high levels of back muscles activity (Bogduk, 1997). The iliocostalis and longissimus act around the thoracic part to lift the thorax by rotating it backwards. The lumbar vertebrae are rotated backwards principally by the lumbar multifidus, causing their superior surfaces to be progressively tilted upwards to support the rising thorax (Bogduk, 1997).

The downward direction of the above muscles during their action adds compression loads on the vertebrae and the intervertebral discs. Any motions involving muscle activity in the back may increase the loads acting on the intervertebral disc (Bodguk, 1997). The effect of posture and different body motions on the spinal loads will be discussed in Section 2.6.2.

A review of the architecture and function of back muscles suggest the complex nature of generating body movements, including different contributions from different muscles in a single movement. For example, the thoracic fibres of the lumbar erector spinae exert about 42% of the total compression load on the L5/S1 disc, the lumbar fibres of this muscle contribute 36%, and the multifidus contributes 22% (Bogduk, 1997). The complex nature of the muscular system suggested the complexity of modelling the effects of muscle forces producing the spinal loads. During body movements, the effects of facet joints and ligaments in the lumbar spine should be considered together with the effects of the muscles.

2.5.3 Mechanical characteristic of lumbar spine segments

The mechanical behaviour of the lumbar segments of the spine have been studied by in-vitro measurements (e.g., Berkson *et al.*, 1979; Panjabi *et al.*, 1977; Schultz *et al.*, 1979). A functional spinal unit (FSU) is usually tested during the studies. An FSU consists of two adjacent vertebrae, an intervertebral disc and the associated ligaments between them. The stiffness matrix of size 6 x 6 is used to represent the mechanical properties of an FSU, representing the translational movements (displacement) and rotational angles in all six degree-of-freedoms (e.g., Stokes *et al.*, 2002). The displacements and degrees of the FSU are measured with external loads including forces and moments in every degree-of-freedom to determine the components in the stiffness matrix.

A universal protocol for testing the properties of spinal components involves mounting the isolated specimen with fixtures supporting the specimen and providing a test motion (Figure 2.31).

The effect of a preload on the mechanical properties of lumbar motion segments has been investigated by Panjabi *et al.* (1977), in which three lumbar motion segments were studied. It was found that the spine became more flexible with preloads of forces in the lateral and anterior directions, and with moments producing lateral bending or flexion. The use of preloads tended to

increase the axial stiffness of the segment and make the segment less flexible in axial torque. Similar findings are observed in other studies (e.g., Stokes *et al.*, 2002). This suggests that the analysis of a spine that simulates the in-vivo loading condition on the spinal segments should consider the nonlinear behaviour of the segments. Otherwise, use of the stiffness data measured without preload may underestimate the behaviour of spinal segments in the in-vivo condition.

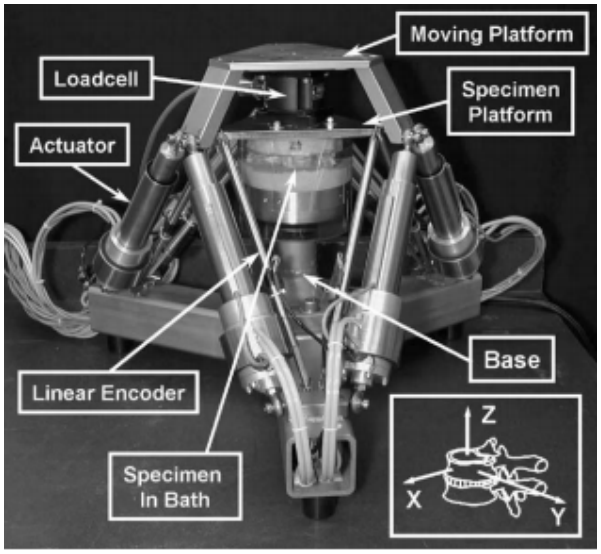

Figure 2.31 A testing rig for measuring the vertebrae body mechanical properties (Stokes *et al.*, 2002).

The mechanical properties of 42 fresh human cadaveric lumbar motion segments were tested in flexion, extension, lateral bending, torsion loads and compression and shear by systematically studies from Schultz *et al.*, (1979) and Berkson *et al.,* (1979). A compressive preload of 400 N was applied to the segments which is equivalent to the weight of the upper body supported on a vertebra (L3) of an average male adult. The relationship between applied moments and resulting rotation degrees in each testing case were recorded as curves, which would be helpful for spine modelling work. It was found that the motion segments were more flexible in shear than in compression, and the least flexible in torsion compared to bending and other motions. The mechanical behaviour of spinal segment also showed great variance among different subjects, which was mainly caused by variances in the disc area.

The in-vitro measurements of mechanical properties of spine segments may be insufficient to represent the mechanical behaviour of the entire spine system due to the absence of active muscles. The muscles have a significant effect on maintaining spine stability and will add loads to the spine segments (as discussed in Section 2.5.2). The in-vivo loads on the vertebrae are not solely the loads from the upper body due to gravity. Various finite element models have been developed based on these measured mechanical properties to study the spine behaviour in the live human body with consideration of muscles and tissues (e.g., Bazrgari *et al.*, 2008a and 2008b; Wang *et al*., 2010). These models will be reviewed in Section 2.6.3.

2.6 Forces in the lumbar spine

2.6.1 Introduction

Long term exposure to whole-body vibration may increase the risk of health, such as low back pain. Although the underlying mechanisms for this symptom remain to be identified, some researches (e.g., Ayari *et al.*, 2009) assumed that whole-body vibration induces dynamic stresses, mainly compressive, in the lumbar spine, causing micro fractures in the endplates and vertebral body, which will lead to low back pain in the long term condition. In order to give preventive advice or propose protective mechanisms, the spinal loads in lumbar spine under typical excitation are investigated. The effect of a series of factors need to be considered, including postures, support conditions and vibration magnitudes. The spinal loads can be expressed as shear forces and compressive forces and the corresponding moments acting on the intervertebral disks (Pankoke *et al.*, 2001).

Generally, the spinal forces are calculated in two parts: the static forces required to maintain a posture and the dynamic forces induced by whole-body vibration (e.g., Pankoke *et al.*, 1998; 2001). A change in posture may change the spinal curvature and results in the activation of muscles in the back to maintain such posture (Section 2.5.2). The effect of different postures (including sitting and standing postures) on static spinal loads has been measured in-vivo (e.g., Sato et al., 1999; Wilke *et al.*, 2001; Rohlmann *et al.*, 2001), which will be described in Section 2.6.2.1. The dynamic spinal loads are usually predicted from biodynamic models of the human body (e.g., Pankoke *et al.*, 1998; Fritz, 2000; Bazrgari *et al.*, 2008). The structures, the findings, and the merits of some better known models aimed at predicting spinal loads are reviewed in Section 2.6.3.

2.6.2 Spinal loads measured in experiments

2.6.2.1 In vivo spinal loads measurements

There are few in-vivo measurements of dynamic spinal loads exposed to whole-body vibration due to practical and ethical issues. The static spinal forces in the lumbar spine have been measured with either transducers inserted into the intervertebral discs or with lumbar vertebral body replacement. A summary of recent in-vivo measurements of spinal loads is listed in Table 2.1. The spinal loads have been measured in various postures in the form of force or pressure. With pressure, the spinal force can be roughly calculated by multiplying the pressure with the disc area (around 17 cm^2) obtained from CT (computer tomography) or MRI (magnetic resonance imaging) (e.g., Sato *et al.*, 1999).

With the help of spine fixation device and vertebra body replacement surgery, Rohlmann *et al.* (2001; 2008, 2011, 2012) measured the spinal loads in three patients with VBR (vertebra body replacement) at L1 level. The force transducers were implanted into the artificial vertebra. The patients were required to maintain different postures including lying, sitting and standing. The sum of shear and compressive forces in three directions were measured with each posture. It was found that the compressive spinal loads measured in an extended sitting posture were significantly lower than the loads measured in a sitting posture with upper body flexed. The reason may be due to that

sitting with upper body flexed increases the distance between the centre of gravity (COG) of the upper body and the spine, resulting in increased muscle forces required to balance the weight of the upper body. In a similar manner, an extension sitting shifts the COG of upper body posteriorly and reduces the muscle forces and the spinal loads. The significant change in the static spinal forces with flexed and extended postures may recommend an investigation into the biodynamic response and dynamic spinal loads in such postures.

The spinal loads in the lumbar spine measured with vertebra body replacement are shared by the replaced vertebra body, remaining part of the vertebra, the added bone material and the internal spinal fixation device. As a result, the force measured with vertebra body replacement only represents a part of the actual force in the spine. But these measurements can reflect the trend of spinal force changing with various factors, including backrests, inclinations of backrests, forward leaning or backward (extension and flexion) sitting, position of hands, various seat types and seat height. For example, sitting with the spine reclining posteriorly reduces the spinal loads while bent forward sitting increases the spinal load (e.g., Rohlmann *et al.*, 2008). The use of a backrest has been found to reduce the spinal loads and with increasing inclination of backrest, the spinal loads reduce gradually (Rohlmann *et al.*, 2011). Possible reasons include more support being given to the upper body from the backrest. Sitting with the arms placed on the thighs or armrests reduces the spinal loads compared to sitting with arms hanging laterally (Rohlmann *et al.*, 2011). Among these factors, contact with backrest and inclination of backrest are suggested to bring the most significant reductions of spinal force (36% compared to normal upright sitting), and hand position is also an important factor which could result in a 19% reduction of spinal force when the arms are supported on the armrest (Rohlmann *et al.*, 2011). The effects of the above factors (e.g., backrest and hands) on the static spinal loads may give hints to the total spinal loads (i.e., combined static and dynamic spinal loads) induced by whole-body vibration.

The effect of posture on the spinal loads has been further investigated with vertebral body replacement techniques and the same patients by Rohlmann *et al.* (2012) as the previous studies from the same authors. The spinal loads were measured during the processes of changing posture from lying to sitting, sitting to standing, and vice versa during the measurements. It was found that the spinal forces measured during all changes of posture were greater than the forces measured in the static standing posture. Possible reasons include the increase in the muscle activity in the body during the process of changing postures, associated with the change of the position of the centre of gravity of the upper body. Changing from sitting to standing without armrests induced the greatest maximum spinal loads among all processes of changing postures. The use of armrests was found to decrease the spinal loads significantly during the posture change. A possible explanation is that a part of the upper body weight is supported on armrests via the shoulders and arms, and the muscle activity of lumbar region reduces (see Section 2.5.2).

Apart from vertebral body replacement techniques, the spinal loads have also been measured invasively by implanting pressure transducers into the intervertebral discs directly. For example, Sato *et al.* (1999) measured the vertical and horizontal intradiscal pressures at L4-L5 of 8 healthy volunteers and 28 patients by inserting a pressure sensor with a needle (Figure 2.32) into the

intervertebral disc. The internal loads were calculated by multiplying the measured pressure by the cross section area of the vertebral disc (mean area of 17 cm^2) obtained by MRI (magnetic resonance imaging). The subjects were required to maintain eight postures during the measurement, including flexion standing, upright standing, extension standing, flexion sitting, upright sitting, extension sitting, prone lying, and lateral lying. The measured vertical spinal loads in different postures increased in the following order: prone lying: 144 N; lateral lying: 240 N; upright standing: 800 N; and upright sitting: 996 N. This study found that the spinal loads were correlated with the angle of the motion segment in various standing postures. But such correlation was not observed in various sitting postures and possible reasons may be due to the reduced angle of lumbar lordosis in a sitting posture. The reduced angle of lumbar lordosis in the sitting posture may contribute to the increased spinal loads compared with the standing posture. The lumbar lordosis may further result in variance in the activation patterns of different muscles in the lumbar in the sitting and standing postures.

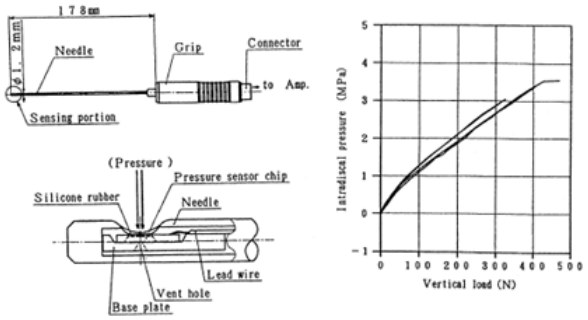

Figure 2.32 Pressure sensor used in pressure measurements in spine endplates. The specially constructed pressure-sensitive membrane at the side of its tip is inserted into the nucleus pulposus. The pressure response against the load is linear. (from Sato *et al.,* 1999).

The forces in these measurements are helpful for the calibration of biodynamic models aimed at predicting spinal loads. In order to provide a dataset of static spinal force for validation of biodynamic models, Wilke *et al.* (2001) measured the intradiscal pressure at L4-L5 intervertebral disc of a healthy volunteer. The pressure was measured by implanting a pressure transducer into the nucleus pulposus of a non-degenerated disc, as disc degeneration has an influence on static spinal force (Sato *et al.*, 1999). The subject was asked to maintain various postures during the measurement, including relaxed, flexion, extension, and rotation laterally with standing posture, and sitting with or without backrest. The positive or negative effects of posture provided by this study are similar to the results from Rohlmann *et al.* (2008). Standing with the spine in extension (with the upper body leaning backward) increased the intradiscal pressure to about 0.6 MPa, compared with a relaxed standing posture (0.5 MPa). Standing with the spine in flexion at a flexion angle of 36˚ increased the intradiscal pressure to 1.1 MPa. A forward leaning sitting posture (straight back without arm support) increased the pressure to 0.63 MPa, compared with an upright sitting posture (0.45 MPa). The pressure for an unsupported sitting posture (0.46 MPa) was close to a relaxed standing posture (0.48 MPa), which is slightly different from previous studies (e.g., Sato *et al.*, 1999). The differences between the two studies may be due to the different subjects

involved in the tests. A dynamic measurement on a pezzi-ball was carried out during jumping which resembled self-generated periodic whole-body vibration at about 1 Hz. The results showed a pressure of 0.5 MPa for upright sitting, and then the pressure cycled between 0.4 and 0.6 MPa during jumping on the ball. A flexed forward sitting posture on the ball induced a static pressure of 0.65 MPa, and the pressure varied from 0.55 to 0.75 MPa during jumping on the ball. The results indicate that the spinal loads may vary with whole-body vibration by increasing the maximum loads on the disc, and the factors affecting the static spinal loads may also affect the total spinal loads induced by whole-body vibration.

One study measured the spinal loads of patients with vertebral body replacements when exposed to vertical whole-body vibration (e.g., Rohlmann *et al.*, 2010). With increasing vibration magnitudes (from 0.25 to 1.0 m/s^2, 0.3-30 Hz), the maximum force on the artificial vertebra body increased. Contact with a vertical backrest reduced the maximum resultant force (vector sum of forces in *x*, *y* and *z* directions) by an average of 50% within five patients when compared to a relaxed sitting posture (normal upright sitting without backrest). Sitting with an inclined backrest (at 25º) further reduced the maximum resultant force. This study and a previous study (i.e., Wilke *et al.*, 2001) may indicate the importance of backrest contact in reducing spinal loads in both static and dynamic conditions. However, the measurements so far have provided limited information on the frequency dependence of dynamic spinal forces. The spinal loads measured with a vertebral body replacement device may underestimate the spinal loads or even inaccurately predict the spinal loads as it changes the mechanical properties of the vertebral body. It is desirable to have more detailed measurements about the spinal loads in the human body exposed to whole-body vibration in various postures.

2.6.2.2 Response of muscles to whole-body vibration and modelling of muscle forces

The effects of the frequency and magnitude of whole-body vibration on the EMG (i.e., electromyography) response of back muscles was investigated systematically by Robertson and Griffin (1989). The EMG signal is used to reflect the activity of muscles in the measured location. To study the effect of frequency on the EMG response, an experiment was conducted with 8 healthy male subjects without history low back pain to investigate the effect of frequency and magnitude of whole-body vibration on the EMG at back muscles (i.e., erector spinae at L3). Subjects were exposed to each of seven frequencies of sinusoidal vibration: 0.5, 1.0, 2.0, 4.0, 6.0, 8.0, and 16.0 Hz. All the stimuli had a vibration magnitude of 2.0 m/s^2 r.m.s. and a duration of at least 48 cycles of vibration. It was found that the time-history of r.m.s. of the EMG of back muscles followed the pattern of the waveform of the applied sinusoidal acceleration. However, the relationship between the excitation acceleration and the EMG depended on the frequency of excitation, particularly shown in the phase relationship between the averaged rectified EMG, averaged applied force and averaged acceleration. The EMG was found to lead the platform acceleration at frequencies of 4 Hz and below. At higher frequencies to 16 Hz, the EMG showed an increasing lag behind the acceleration.

A subsequent experiment investigated the difference between EMG response to sinusoidal and random WBV (Robertson and Griffin, 1989). It was found that the phase relationship between the

averaged EMG and the acceleration of the platform showed similar trends to both forms of excitation. The muscle activity led the platform acceleration at frequencies less than 4 Hz and showed a lag at frequencies greater than 4 Hz. However, at frequencies less than 2.5 Hz, a greater increase in EMG lead was found with random vibration than with sinusoidal vibration. An EMG lead of 180 degrees was seen at frequencies around 1 Hz with random vibration, which was considered to be possibly due to some reflex response of subjects to the onset of an unexpected fall at the top of the vibration stroke. When exposed to a random vertical vibration in a low frequency range (0.25 – 2 Hz, 1.0 m/s^2), the phase was close to that obtained with sinusoidal excitation. Exposure to a random vibration in a high frequency range (0.25 – 8 Hz, 1.0 m/s^2) induced a different phase. It was suggested that this may indicate that the higher frequency components of a broadband random vibration may cause a reduction in the muscular response to vibration of lower frequencies. The muscular response to random vibration of low frequencies may be significantly disrupted by the vibration of high frequencies and the body may be less able to maintain postural stability along spine at low frequencies.

The effect of vibration magnitude on the EMG activity of back muscle was also studied (Robertson and Griffin, 1989). The maximum EMG showed a roughly increasing trend with increasing vibration magnitude from 0.8 to 2.5 m/s^2. At all magnitudes of vibration, the greatest EMG response occurred at 4 Hz, followed by 1 Hz and 8 Hz. The trend was reversed when considering the minimum EMG of back muscles induced by various magnitudes of vibration, where 4 Hz vibration also induced the least EMG, possibly due to the relaxation of the spinal muscular during momentary motion.

A ‘build-up’ phenomenon was found in the EMG response of back muscles when exposed to shock excitation with predictable waveforms (2, 4, 8 Hz and 1, 2, 4 m/s^2 r.m.s. sinusoidal vibration with either 2.5 or 5 seconds) (Robertson and Griffin, 1989). The ‘built-up’ phenomenon referred to the increases in both phasic and tonic muscle activities over the first few cycles of the vibration duration. The tonic muscle activity is indicated by the average r.m.s. EMG produced to maintain the stability of the posture. The phasic muscle activity is indicated by the standard deviation of the averaged r.m.s. EMG, which changes during whole-body vibration. It was suggested that the predictability of the stimulus would affect the response to this type of vibration and there would be a refinement in the muscular response when the initial properties of the vibration gradually become clear. The phasic muscle activity remained approximately constant during consecutive long-periods of vibration (160 minutes) whereas the tonic muscle activity increased in amplitude during the same period of vibration. It was also noticed that the phasic muscle activity tended to be insignificant compared to the tonic muscle activity over a long duration of vibration. Possible explanations for the increase in the tonic activity include muscle fatigue and the insignificant postural change with increased exposure duration (Robertson and Griffin, 1989). The increasing tonic muscle activity may increase the spinal loads over a long-term whole-body vibration.

Table 2.1 In-vivo measurements of spinal loads

Researchers	Number of subjects	Methods and measuring location and variables	Postures	Results
Sato *et al.* (1999)	8 healthy volunteers and 28 patients	Needle shape transducer inserted into L4-L5 intervertebral disc. Vertical and horizontal intradiscal pressure measured. Disc area measured by MRI. Internal loads calculated by pressure timing area.	Flexion standing, upright standing, extension standing, flexion sitting, upright sitting, extension sitting, prone lying, and lateral lying	The spinal load varied with postures, it increased as: prone, 144 N; lateral, 240 N; upright standing, 800 N; and upright sitting 996 N. For standing posture, spinal loads were strongly related to segment angle.
Wilke *et al.* (2001)	1 healthy volunteer	A pressure transducer implanted into the nucleus pulposus of the L4-L5 intervertebral disc, intradiscal pressure measured.	Stand and sit relaxed, flexed, extended, and rotated laterally; sit with backrest; sit on a pezzi-ball;	Flexion and extension have strong influence on loads for both static and dynamic condition. With 1 Hz vibration, the time-varying forces varied between 20% of the static forces.
Rohlmann *et al.* (2008)	3 patients with vertebra body replacements (VBR)	3-axis force transducer integrated into the VBR at L1 for all the subjects. The forces reported were the sum of compressive and shear forces.	Standing, lying, sitting flexed and extend	Measured force with various postures. Extension caused less spinal loads than flexion.
Rohlmann *et al.* (2011)	5 patients with vertebra body replacements (VBR)	3-axis force transducer integrated into the VBR at L1 for four subjects and L3 for 1 subject. Compressive forces presented in the paper	Standing, flexion sitting, normal sitting, extension sitting, sitting with inclined backrest, hands on thigh, hands hanging, lying	Measured the forces with various postures; Extension cause smaller loads than flexion. Hand position has influence on internal loads.
Rohlmann *et al.* (2012)	5 patients with vertebra body replacements (VBR)	Same as the measurement in 2011.	Postural change effect: from a sitting to standing; from a flexed standing to bent forward standing, etc.	Measured the force change with posture change. A postural change induced a greater spinal load than a static posture.

As described in Section 2.5.2, the muscular system is involved in the generation of motion of the spine and the maintenance of the postural stability of the spine. The complex nature of the muscular system makes it difficult to model each group of muscles. Several primary groups of muscles in the lumbar spine have been considered in some static and biodynamic models of the human body, including erector spinae, abdominal muscles, psoas major, multifidus, quadratus lumborum and latissimus dorsi (Stokes and Gardner-Morse, 2001). For simplification, the muscle groups are usually represented by simplified sets of muscles, represented by force vectors (e.g., Barzgari *et al.*, 2008a) or linear/nonlinear springs and dampers (e.g., Stokes *et al.*, 2010). The parameters used in these models were determined either from EMG measurements (e.g., Marras and Granata, 1997), or an optimisation algorithm (e.g., Stokes and Gardner-Morse, 2001). These muscle models are complex with many assumptions and it remains to be investigated whether they are appropriate for modelling muscle behaviour in dynamic conditions.

2.6.3 Predict spinal loads by biomechanical models

The spinal loads associated with whole-body vibration are rarely measured in-vivo except for measurements with the vertebra body replacement (e.g., Rohlmann *et al.*, 2010), but biodynamic models can be developed to predict them. As described in Section 2.4, biodynamic models can be developed based on various aspects of the biodynamic responses of the human body. Simple lumped parameter models can represent both the modulus and the phase of the apparent mass of the body (e.g., Fairley and Griffin, 1989; Wei and Griffin, 1998; Qiu and Griffin, 2011b) but they do not reflect the anatomical structure of the body and so are not normally used to predict spinal forces. A single-degree-of-freedom model has been developed with the concept of dynamic response index (DRI, from Griffin, 1990). This model consists of a mass representing the upper torso and head, and a combination of a translational spring and damper representing the spine. The peak stress on the spine is calculated based on this model (Equation 2.5):

$$Peakstress \propto \omega_n^2 \delta_{max} \tag{2.5}$$

where, ω_n is the natural frequency of the single degree of freedom model, and δ_{max} is the maximum deflection. The calculation of peak stress by DRI model is convenient, but a validation of peak stress as an indicator of risk to the spine is not provided, and the effect of continuous vibration or repeated shocks is not indicated by this model.

A current standard (ISO 2631-5:2003) provides a procedure for calculating the forces in the lumbar spine with the aid of a single degree-of-freedom model based on the predicted transmissibility to the lumbar spine. The transmissibility to the lumbar spine is predicted from an artificial neural network (ANN) model. However, such a model fails to consider the effects of posture on the spinal loads and the prediction of body transmissibility is not consistent with measured responses (e.g., the predicted spine transmissibility at 0.5 Hz is 0.5 from the model, but the measured transmissibility is 1.0).

Multi-body models can reflect the anatomy of the body and represent both the apparent mass of the body and the transmissibility to specific body parts, and with suitable development they may predict spinal forces associated with vibration and shock (e.g., Fritz, 2000).

Finite element (FE) models, which can be based on anatomical measurements and material properties, are potentially capable of representing biodynamic measurements and predicting information that may be related to health and injury, including the spinal forces (e.g., Pankoke *et al.*, 1998; Ayari *et al.*, 2009; Wang *et al.*, 2010).

Many anatomical-based models have been developed to represent the human body and predict the spinal loads induced by whole-body vibration. Some of these models are summarised in Table 2.2.

There are several finite element models aimed at predicting the spinal loads of the seated human body. Some models represent the whole human body (e.g., Pankoke *et al.*, 1998), while some models only focus on the lumbar spine structure, or even a few vertebrae (e.g., Bazrgari *et al.*, 2008a). Muscle forces have an influence on the calculation of spinal loads in some finite element models. Considering the muscle forces, some models have a detailed representation of the muscular system connected to the spine (e.g., Bazrgari *et al.*, 2008a), while others linearize the muscle force or simplify the muscle forces by reducing the number of muscles integrated (e.g., Fritz, 2000). Material nonlinearity has also been considered in some models, such as the intervertebral discs, vertebrae, facets and ligaments (e.g., Bazrgari *et al.*, 2008). The body posture may affect spinal loads as a posture change will change the spine curvature (curve angle, flexion, or tension) and the muscle activity. A change in muscle activity may further change the spinal loads. A review of multi-body models and finite element models for predicting spinal forces is provided in the following sections.

2.6.3.1 The model from Fritz (2000)

Fritz (2000) presented a multi-body human model consisting of 16 rigid bodies connected by hinges (Figure 2.33). This model was used to predict the forces in the lumbar spine and investigate the relationship between the spinal force and magnitude and direction of excitation in the form of acceleration.

The mechanical behaviour of muscles in this model was simulated by 56 internal force elements in three directions. This model simulated the arms connected to the steering wheel and each arm was represented by 3 rigid bodies. In the simulation, the maximum and minimum spinal force including compressive, lateral shear and for-and-aft shear forces were calculated at the lumbar level L3-L4, and transfer functions from seat acceleration to these forces were calculated to represent the dynamic spinal forces. The simulated compressive forces were suggested to be 11% less than the actual pressure due to the lack of consideration of the torque induced by bending of the intervertebral disc. When exposed to lateral vibration, the sum of compressive and fore-and-aft shear forces at the L3/L4 disc was much less than the lateral shear forces because the lateral movements induced by lateral vibration were greater than the small movements of the bodies in the vertical direction and in the fore-and-aft direction. The expression of the dynamic spinal forces as transfer functions from acceleration at the seat to forces in the spine provides a weighting for

acceleration which might be used to assess the risk of spinal injury. However, predictions from the model lack comparisons between relevant experimental studies and the mechanisms adopted to calculate the spinal forces in this model require justification.

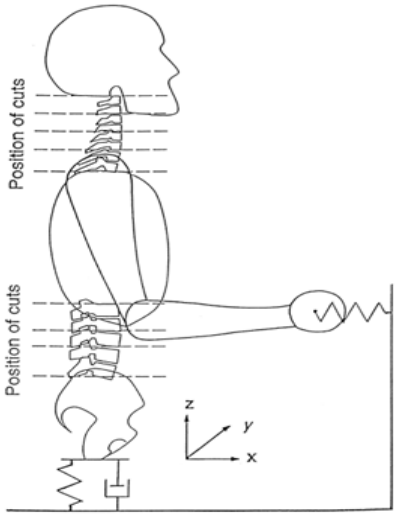

Figure 2.33 A multi-body model of the seated human body consisting of trunk, neck, head and arm. The dashed horizontal lines indicate the position of nine cuts where hinges imitate the motion segments, the connection between seat and pelvis is represented by the spine and damper in the *z*-direction (Fritz, 2000).

2.6.3.2 The model from Pankoke et al.(1998)

A 2-D finite element model of a sitting subject was developed to predict the internal spinal loads including compressive and shear force in the intervertebral disks (Pankoke *et al.,* 1998, Figure 2.34). The linear model consisted of detailed anatomical structures only in the lower lumbar spine (L3-L5), including spine segments, muscles and viscera at these locations, as low back pain was mainly reported at these locations after long-term exposure to whole-body vibration. The remaining parts of the body were modelled as rigid masses (e.g., viscera). Linear springs were used to connect the rigid bodies, representing the vertebral disks and longitudinal ligaments. The geometry, inertial properties, and mechanical properties of the lumbar spine of the model were derived from published data (e.g., Dempster and Gaughran, 1967). Some other relevant stiffness and damping parameters were determined by matching the predicted results with measured mechanical impedances and seat-to-head transmissibility. Three postures (i.e., erect, bent forward, and relaxed sitting) were considered in this study, but the results were not described. The sum of the lower back muscles forces was represented by a linear spring, and the stiffness of the spring was calculated from published data. A constant active muscle force and a constant moment on the pelvis were added to maintain the erect sitting posture. A constant force can affect the static results (e.g., spinal force) directly and also affect the dynamic results by changing the equilibrium position of the model during calculation. The model was a parametric model capable of representing the human body with different anthropometries (e.g., body height, body mass).

Table 2.2 Models aimed at predicting spinal loads.

Model	Usage	Characteristics	Verification	Shear Force calculated	Compressive force calculated
Pankoke *et al.* (1998)	Predict internal spinal loads at intervertebral discs L3/L5. Consider influence of individual properties like BH BM and postures on the spinal loads, including erect, relaxed and bent forward sitting postures.	Two dimensional linear FE model; Only anatomy in lumbar spine (L3-L5) was considered; Parametric model; Muscle forces considered, but simplified as a constant sum value obtained from related data. Lumbar spine L3-L5 modelled with material properties, other parts modelled as rigid mass.	Spinal segments validated from in vitro tests ; Complete model was verified by comparison between mechanical impedance and seat-to-head transmissibility in *x* and *z* directions; The measured and predicted force between seat and pelvis in time domain were compared.	Seidel *et al.*, (1998; 2001), Hinz *et al.*, (2002; 2007) used this model to calculate spinal loads. Hinz *et al.* calculated force at L5/S1 in relaxed posture without backrest: -60.3 - 62.1N	Hinz *et al.* calculated in relaxed posture without backrest at L5-S1: -155.6 - 150.4 N
Fritz *et al.* (2000)	Predict the spinal loads in driving posture without backrest	This model simulated the upper body, and the hand of the model was connected to the steering bar by a spring. Spine level from L1-L5, head, neck, hand, buttocks and trunk (rigid mass) were modelled.	The parameters were selected from previous papers, and the simulation results (transmissibility to head) were compared to ISO 7962.	Anterior-Posterior force at L3-L4 when exposed to 0.78 m/s^2 r.m.s. vibration at L3-L4: -3 – 31 N	Vertical direction from 0-30Hz of 0.78 m/s^2 r.m.s. at L3-L4: 425-634N
Pankoke *et al*. (2001)	Calculate spinal loads in three postures: upright sitting, bent forward, relaxed sitting;	Linear FE model simplified from Buck's model by linearization and reducing DOF at reference state; Parametric model; Muscle forces were considered only by passive properties, muscle activation was neglected. Entire body and lumbar spine L1-L5 were modelled.	Motion segments verified by measurements in mechanical properties of them under different load conditions; Dynamic behaviour verified by apparent mass and seat-to-head transmissibility	No data provided	L3-L4 Dynamic force varied from -200 to 210 N But no detailed data provided
Verver *et al.* (2003)	Calculate the spinal forces with driving posture; predict the spinal forces at all spine level	A multi-body model consists of 16 rigid bodies and detailed spine structure. The posture is driving posture and backrest is included to support the body.	Measured transmissibility to various locations on spine and head were used to verify the model.	Anterior-Posterior force at L3-L4 when exposed to 0.5-15 Hz vibration of 0.4 m/s^2 r.m.s.: Max 95N	Vertical force at L3-L4 when exposed to 0.5-15 Hz vibration of 0.4 m/s^2 r.m.s.: Max 581N

Bazrgari *et al.*, (2008a and 2008 b) (Wang *et al.,* 2010*)*	Predict spinal loads considering active muscle structures and postures' influence (sitting: 'erect', normal, and 'slouched'). The influence of excitation type and magnitude at base were predicted. Calculated the muscle force.	A 3D model with nonlinear stiffness of lumbar motion segments and buttock tissues. Complex geometry of spine and detailed muscle architecture. The active muscle force and dynamic effect of muscle force were considered. Only spine and buttocks were modelled.	Seat-to-head transmissibility and apparent mass were used to validate the model.	Wang *et al.* calculated the spinal force using this model. No data provided. Bazrgari *et al.*, 2008b calculated the response to shock of 4g at 4 Hz: Inertial force: 500 N; Muscle force: 600 N; Gravity: 150 N; Total: 1250 N;	Wang *et al.* Random vibration 1.0 m/s^2 r.m.s. force at L5/S1 in relaxed posture: 420-480 N Bazrgari *et al.*, 2008b calculated the response to shock of 4g at 4 Hz: The maximum force: Inertial force: 1400N; Muscle force: 1600N; Gravity: 400 N; Total: 3400 N;
Ayari *et al.* (2008)	Predict the relationship between mechanical stress in the vertebrae and excitation magnitude in seated posture.	The geometry of lumbar spine was carefully determined, as the material properties. A parametric linear model without muscles connected to spine. Low amplitude excitation is used in the simulation. Only the entire spine was modelled.	Validation of the whole lumbar spine was carried out by modal analysis of L4-L5 motion segments including comparison of natural frequency and mode shapes.	No data provided	Random vibration: 3.1 m/s^2 0.5-15 Hz Compressive spinal load at L3/L4 Maximum: 1030N

Models of different subjects differed in the geometry and inertial properties of the segments and also the predictions of the spinal loads. The spinal force at L3-L5 was calculated as the sum of static forces and dynamic forces. Static spinal forces were calculated from the effects of gravity and muscle forces, varying with different sitting postures. The dynamic force was predicted from the model during exposure to whole-body vibration. The total spinal forces were calculated by a superposition of the static and dynamic forces. The model was justified in the static condition and dynamic condition. The displacement and pitch angle of the lumbar spine segments (L3 to L5) predicted from the model were compared with corresponding data measured in-vitro when preloads of compression, shearing, and flexion were applied (e.g., Berkson *et al.*, 1979; Schultz *et al.*, 1979). The above process was suggested as a static verification of the model. The dynamic behaviour of the model was assessed by comparing the measured and predicted apparent mass at the seat pan and the seat-to-head transmissibility (e.g., Seidel, 1995). The model tended to underestimate the apparent mass and seat-to-head transmissibility at higher frequencies (greater than 5 Hz), possibly due to the inappropriate consideration of the muscle forces. The behaviour of a muscle would be dependent on the vibration frequencies and magnitudes, which was not represented appropriately in the model. This model was suggested to be only suitable for excitation at low frequencies, as it would underestimate the spinal loads when compared to the dynamic forces predicted by a simplistic model (e.g., Seidel *et al.*, 1998). The underestimation may be due to the linearity of the model, restrictions in modelling damping, missing dynamic muscle forces, and inappropriate modelling of buttock tissues.

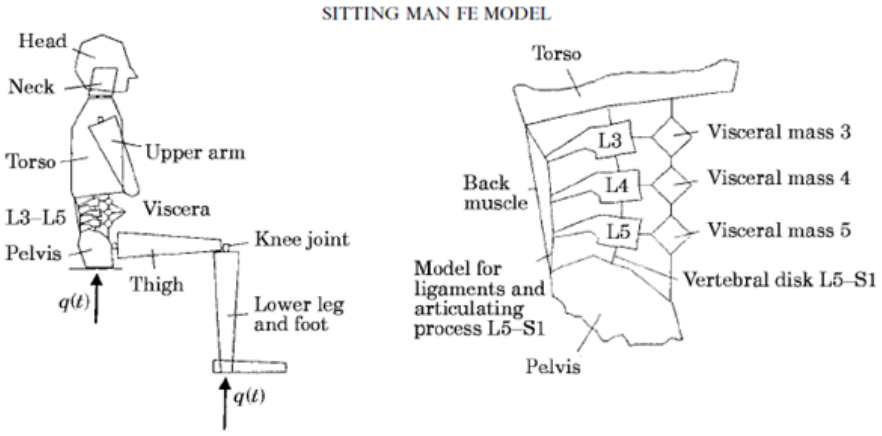

Figure 2.34 A 2 dimensional finite element model for predicting internal loads in lumbar spine L3-L5 (Pankoke *et al.*, 1998).

The same model (Pankoke *et al.*, 1998) was used to predict the spinal loads at L5/S1 in three different sitting postures (i.e., upright, erect, and bent forward) by Seidel *et al.* (2001). Static and dynamic spinal forces in the lumbar spine were calculated separately for different anthropometric parameters (body mass and body height) with three postures. It was found that reasonable variations of body mass and body height caused a considerable variation of static internal shear stress, but a minor variation of compressive stress. The dynamic compressive and shear spinal forces were expressed as transfer functions from seat acceleration to the forces at L5/S1 during

vertical vibration. It was found that the range of compressive pressure was mainly determined by the static pressure, and the dynamic pressure only contributed to a small extent, which may be because the vibration magnitude was low. An increase in the body mass and body height increased the dynamic shear pressure in the spine proportionally. The pressure was transferred into force by multiplying by the disc area. The maximum dynamic shear force occurred at a frequency around 8 to 9 Hz, while the transfer function from seat acceleration to compressive force showed two peaks at frequencies in the range 2 to 5 Hz. Considerable static and dynamic shear forces were predicted, which should be regarded as a risk factor in evaluating spinal health. Large variability was found within the static loads in different sitting postures, suggesting the importance of a postural effect on the spinal loads, although the detailed postural effect was not described in this study.

2.6.3.3 The model from Pankoke et al., (2001)

An improved finite element model was developed by Pankoke *et al.* (2001) (Figure 2.35) to calculate the internal loads in the lumbar spine. This adopted a model structure simplified from the finite element model developed by Buck and Wolfel (1998). Detailed muscle architecture was integrated, but the muscle forces were only represented by passive properties with muscle activation neglected. The muscles connected to the lumbar spine were modelled by a total of 72 linear springs. This model tended to overestimate the vertical seat-to-lumbar spine (L4) transmissibility around 5 Hz, and underestimate the mechanical impedance at frequencies greater than 6 Hz. However, the predicted spinal loads were not reviewed in this study. Observed from this study, it may suggest that a linear simplified finite-element model may predict spinal forces, but the application of this model should be restricted to a limited range of excitation intensities. A model aimed at predicting spinal loads should also consider anthropometric information, inertial information (e.g., body mass distribution), stiffness, and damping of tissues. Where some of the information is difficult to obtain (such as the stiffness and damping of body parts), the parameter identification techniques can be used to identify the parameters indirectly.

The effect of a backrest and posture (forward leaning sitting and relaxed sitting holding a steering bar) on the spinal forces at L5/S1 level (includes compressive force and shear force) was examined using the above finite element model by Pankoke *et al.* (2001) and Hinz *et al.* (2002). The model was adjusted with individual geometry data and the posture and backrest factors were also considered. The transfer functions from the vertical seat acceleration to the median predicted spinal forces were provided. The results showed that at frequencies less than 3 Hz, the compressive force in the forward leaning sitting posture was greater than in a relaxed sitting posture both with and without backrest support (note: the lumbar spine was supported with backrest in the forward leaning posture). At frequencies greater than 3 Hz, the relaxed sitting posture induced greater compressive force than a forward leaning sitting posture, irrespective with the backrest conditions. Contact with the backrest tended to decrease the peak compressive forces. Regarding the transfer function from seat acceleration (z-direction) to shear forces, the shear force was greater in the forward leaning sitting posture than the relaxed sitting posture at frequencies less than 3 Hz. The relaxed sitting posture induced greater shear force than the

forward leaning sitting posture at frequencies greater than 3 Hz.. Both the posture and the backrest affected the modulus and the frequency of the resonance in the transfer function. The static forces predicted from the model was compared to the forces measured in-vivo (e.g., Wilke *et al.*, 1999), and the model underestimated the static spinal loads. The estimation of static spinal force from the in-vivo measurement (measured in pressure) by multiplying the area of disc would overestimate the spinal forces due to the uneven pressure distribution on the intervertebral disc. The model may also underestimate the static muscle forces. For the same reasons, the dynamic forces may be underestimated by the same model.

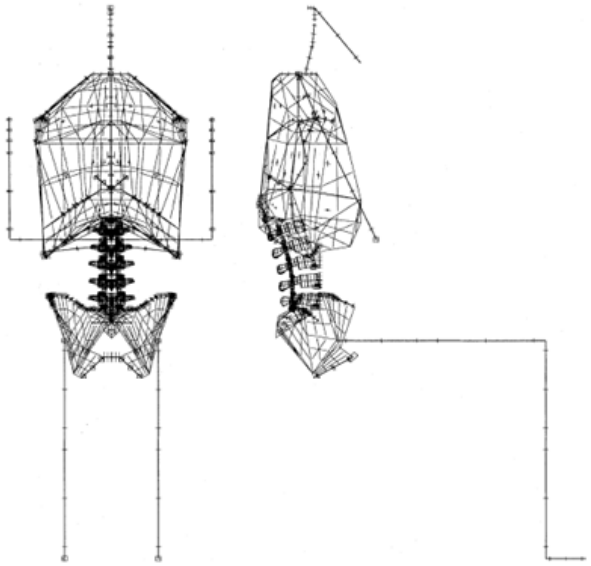

Figure 2.35 A three dimensional finite element model of seated human body with lumbar spine structure (Pankoke *et al.*, 2001).

The models described above are all linear parametric models, in which the simplification can ease computation and allow the models to be easily adjusted to an individual person. However, the two models developed by Pankoke *et al.* (1998 and 2001) neglected the active muscle force (Wang *et al.*, 2010), and the predicted spinal forces may be inaccurate. The linearity of the model may also cause an underestimation of peak forces (Seidel *et al.*, 2001).

2.6.3.4 The model from Ayari et al. (2009)

With the consideration of uneven distribution of internal loads on the intervertebral discs, Ayari *et al.* (2009) developed a 3-D parametric finite element model with detailed spine structure of a seated subject to calculate the dynamic compressive and shear forces in the lumbar spine (Figure 2.36).

This model also studied the stress/strain distribution in the lumbar spine segments to help to evaluate the health risk in the lumbar spine. The natural frequencies of the model were calibrated so that modes predicted by the model agreed with those reported in previous studies with finite elements models of the spine (e.g., Kong and Geol, 2003; Guo and Teo, 2005). The model may be over complicated to predict dynamic spinal loads, as its main purpose was to predict the dynamic

pressure distribution in vertebral segments. The model did not have integrated muscles connected to the lumbar spine, but the effect of active muscles on the internal loads exposed to whole-body vibration was considered during the determination of the damping ratios for intervertebral discs. The maximum compressive force on disk of the lumbar spine L3/L4 was greater than the forces derived from previous studies (e.g., Fritz, 2000; Verver *et al.*, 2003), possibly because the excitation was applied at the natural frequency of the spine system. The model suggested that stress was greatest at L5 and increased with increases in the vibration magnitude. The maximum spinal load induced by whole-body vibration was dependent on the frequency and magnitude of the excitation.

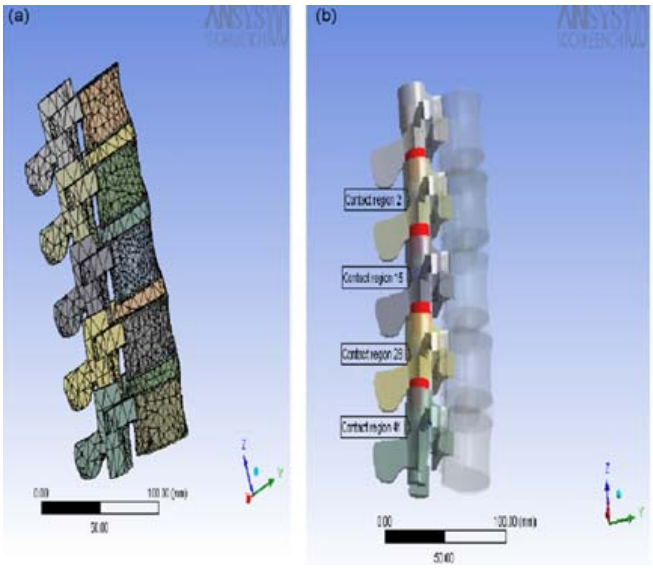

Figure 2.36 Finite element models of (a) lumbar spine and (b) contact between posterior elements (Ayari *et al.*, 2009).

2.6.3.5 The model from Verver et al. (2003)

With muscle forces incorporated into mechanical properties of joints, Verver *et al*. (2003) developed a finite element model based on the MADYMO human model (although it was stated to be multi-body model in his paper) for the seated occupant in the driving posture with backrest contact (Figure 2.37). In order to measure the pressure distribution at the buttock-seat interface and back-backrest interface, the outer surface of the human body was included in the model. All spinal and cervical vertebrae were represented by rigid bodies connected by joints. The transmissibility from seat to head, seat to neck (T1) and seat to pelvis were measured in experiments to calibrate the model. The vertical seat-to-pelvis transmissibility predicted from the model matched well with the corresponding measured response, both showing a resonance at 8 Hz. The predicted and measured vertical seat-to-T1 transmissibility contained two peaks, a peak at 6 Hz with a low magnitude and a peak at 8 Hz with a high magnitude. The vertical seat-to-head transmissibility reflected the same trend. The spinal loads at each vertebral level were also predicted. The compressive forces decreased gradually from lumbar spine to cervical spine. The maximum shear forces appeared in the lumbar spine and the lower thoracic spine. The transfer functions from seat acceleration to the dynamic spinal forces were calculated. The transfer function

of the vertical spinal force at L5/S1 showed a magnitude of 30 N*s^2/m around 0 Hz, close to the value of the mass of the body (around 30 kg) supported on the disc. The dynamic compressive forces at each lumbar intervertebral disc did not show a difference from each other when sitting with rigid seat and rigid backrest. The dynamic shear forces decreased with increasing spinal level (i.e., from L5/S1 to L1/T12) with both a rigid seat (with backrest) and a car seat (with foam seat pan and backrest). This indicates that the lumbar vertebrae moved with respect to each other in the horizontal direction during vibration. The calculated transfer functions from this study can help to calculate spinal loads and evaluate the risk to health in the spine with a typical input acceleration. One of the disadvantages of this model is that there is no representation of muscles (either passive or active) so the predicted spinal loads may be underestimated.

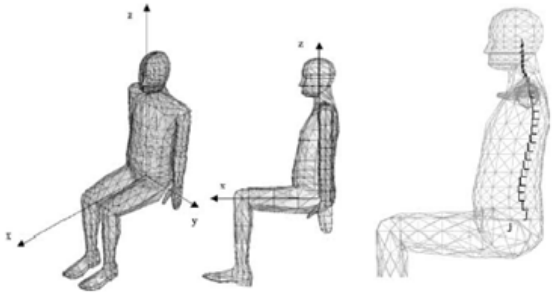

Figure 2.37 The MADYMO human model with the definition of global orientation (left) and local orientations of the vertebrae (right). (Verver *et al.*, 2003).

2.6.3.6 The model from Bazrgari et al. (2008)

With consideration of the effects of active muscle forces on spinal loads, Bazrgari *et al.* (2008a, 2008b) developed an FE model of the seated human with seven rigid bodies, representing six vertebral bodies (i.e., spinal levels of S1, L5, L4, L3, L2, L1) and the remaining body part from head to the spinal level T12 (Figure 2.38). Rotational elements were combined with deformable beams to connect these bodies. The buttocks were represented by a translational spring and damper. The detailed muscle architecture around the lumbar spine was modelled by force vectors. The mass, moment of inertia, materials stiffness, and damping coefficient of each segment were determined from previous studies (e.g., Pearsall, 1994). The beam materials had nonlinear stiffness, but the damping coefficient remained constant. The buttocks at the base was modelled by a connector element (compression only) with nonlinear stiffness defined based on previously reported data (e.g., Kitazaki and Griffin, 1997) and damping was similar to that of the lumbar segments. The muscle forces were determined with a kinematics-driven approach combined with an optimisation method (minimizing the sum of cubed muscle stress). The effects of postures (‘erect’, ‘slouched’, driving sitting posture) on spinal loads (both static and dynamic loads) were investigated, with the muscle activity varying between postures. The muscle activation increased the muscle stiffness, as well as the compressive and shear forces on the spine. The excitation at the base would also affect the muscle forces, resulting in changes in the spinal forces. A flexed (i.e., ‘slouched’) sitting posture increased the spinal loads as the inertial forces from the body mass and the muscle forces increased compared to an erect posture (maximum compressive force: flexed: 1608 N; erect: 1131

N) when exposed to whole-body vertical vibration. Reasons include the differences in the curvature of the spine, resulting in increased moment from gravity acting on L5/S1 in a flexed posture. It was also suggested that the computation of muscle forces and internal spinal loads would not be influenced by nonlinear characteristics of muscle stiffness, so during modelling, linear muscle stiffness was assumed to be sufficient.

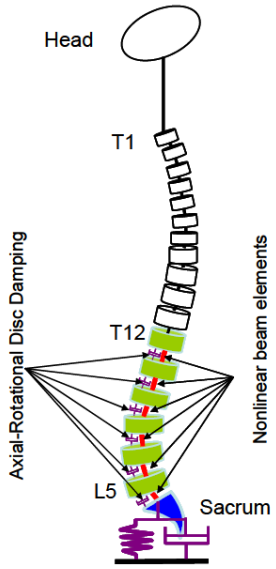

Figure 2.38 A non-linear 3-D finite element model of entire spine to calculate the spinal forces in the lumbar spine with detailed muscle architecture (Bazrgari *et al.*, 2008a).

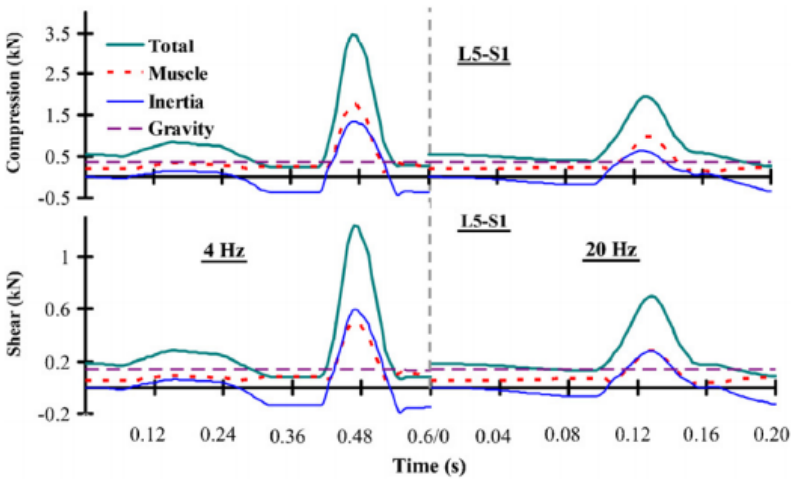

Figure 2.39 Predicted contributions of muscles, inertial and gravity in calculated spinal loads at the L5/S1 disc mid-height in local directions at excitation frequencies of 4 Hz (left) and 20 Hz (right). From Bazrgari *et al.* (2008b).

When high-magnitude vibration containing shocks (maximum 4 g, 1 g=9.8 m/s^2) of 4 Hz and 20 Hz was 'exposed' to the same model (Bazrgari *et al.*, 2008b), the muscle forces tended to contribute more than the inertial forces. An excitation of 4 Hz tended to induce greater spinal loads (both compressive and shear) than an excitation of 20 Hz (Figure 2.39). High magnitude acceleration close to the resonance frequency of the human body would increase the spinal loads as well as the risk of spinal injury by increasing muscle activity to maintain postural stability. However, the body

may not always be able to maintain equilibrium when exposed to mechanical shocks, and the motions of the body parts may greatly affect the calculation of muscle forces using the methods of this model. Similar reasons would partly result in a discrepancy between the muscle activity predicted from the model and from the measured EMG of back muscles (Robinson, 1999). Biodynamic responses of the human body exposed to high magnitude vibration and shocks are required to improve the predictions of spinal forces in such conditions.

Comparisons were made between the compressive and shear forces at L5/S1 predicted from a passive model (without muscles) and an active model (with active muscle activity) when exposed to vertical whole-body vibration by Wang *et al.* (2010). Both models were adjusted from the model developed by Bazrgari *et al.* (2008a) as introduced above. The active model showed better agreement with the mean experimental measured data in both apparent mass and seat-to-head transmissibility regarding the magnitude and phase over the frequency range 0 to 15 Hz compared to the passive model. An active model predicted greater compressive and shear forces in the spine than the passive model, suggesting a crucial role of active muscles in predictions of spinal forces.

2.7 Discussion and Conclusion

The vertical in-line apparent mass of seated people shows a principal resonance at about 5 Hz and, sometimes, a secondary resonance at around 8-10 Hz. Measurements of transmissibility along the spine help to understand the mechanisms involved in body movement during vibration and derive the modes associated with resonances in apparent mass and transmissibility. Both the overall biodynamic response (apparent mass) and the local biodynamic responses (body transmissibility) are affected by inter-subject variability (body mass, gender, and age), intra-subject variability (sitting posture, support from a backrest or footrest, and muscle tension) and vary with vibration magnitude. Modal analyses of the human body suggest the principal resonance around 5 Hz is influenced by several body modes merged together due to heavy damping in the body. The motions include the bending and pitching of the spine with axial deformation of the buttocks tissues. The secondary resonance may involve pelvis pitch and vertical motion of viscera (Section 2.3.6).

Sitting posture influences the biodynamic responses of the body (i.e., apparent mass and transmissibility) (Sections 2.2.3 and 2.3.4). Sitting posture will also affect the forces in the spine, both static forces and dynamic forces. In-vivo measurements of static spinal forces show variations with posture and effects of contact with a backrest and holding handles (Section 2.6.2.1). The variations are partially caused by changes in the muscle activity required to maintain postural stability. Support from a backrest may allow some relaxation of muscles in the back and decrease the spinal forces. Some biodynamic models predicting spinal forces have considered the effects of posture (Section 2.6.3), but the effects of backrests on spinal loads have received little attention. Biodynamic models for predicting spinal loads should reflect the overall biodynamic response (i.e., apparent mass) and also the movement of the spine (e.g., transmissibility to the spine), but the motions of the spine when sitting with a vertical backrest or an inclined backrest during vertical whole-body vibration have not been studied systematically.

The available biodynamic models for predicting spinal loads have been reviewed to understand the structure needed in such models. A representation of the spinal structure is necessary in order to predict forces at the intervertebral discs and the structure of the spine was partly represented in some models (e.g., part of the lumbar spine, in models from Pankoke *et al.,* 1998, 2001; Fritz *et al.,* 2000) and more fully represented in other models (Bazrgari *et al.,* 2008a; Verver *et al.,* 2003; Ayari *et al.,* 2008).

Previous models have found that the greatest spinal loads occurred at the lowest levels of the lumbar spine (e.g., Pankoke *et al.*, 1998; Ayari *et al.*, 2009). Some models only represented the three lowest lumbar vertebrae (i.e., L5, L4 and L3) (e.g., Pankoke *et al.*, 1998) and some other models modelled the five lumbar vertebrae (e.g., Pankoke *et al.*, 2001; Bazrgari *et al.*, 2008a). In these models (i.e., that only represent the lumbar spine) the rest of the spine (i.e., from L2 to head) is commonly represented as a rigid body. The prediction of the spinal forces in the lowest lumbar vertebrae depends on the motions of the body supported on the intervertebral disc. The representation of the remaining spine as a rigid body in these models assumes that there would be little differences in the relative motions of the spinal levels in the upper body or, if they exist, such relative motions between the spinal levels in the upper body do not affect the prediction of loads in the lumbar spine. Measurements of body transmissibilities found that differences among the vertical transmissibilities to various spinal levels in the upper body (e.g., L2, T10, T5, and T1) were small during vertical seat excitation at frequencies less than 10 Hz in the normal sitting posture (see Section 2.3.2 and Chapter 6 in Matsumoto, 1999). It seems that modelling the upper body as a rigid mass will bring only minor errors in predicting the spinal loads when exposed to vertical whole-body vibration.

The viscera in the abdomen and thorax are a large part of body mass (about 16% of the total body mass, based on the model developed by Kitazaki and Griffin, 1997). Some models have integrated the viscera into spinal segments (e.g., Bazrgari *et al.*, 2008a; Ayari *et al.*, 2009) and other models have represented the viscera as rigid masses (e.g., Pankoke *et al.*, 1998; Verver *et al.*, 2003). The viscera are not directly supported on the vertebra bodies, but surrounded by tissues. Integrating the viscera into the spinal segments may increase the mass of the body supported on the intervertebral discs and may overestimate the spinal loads. It seems to be appropriate to model the viscera as an independent mass or several masses.

A review of the muscular system (Section 2.5.2) and biodynamic models predicting spinal forces (Section 2.6.3) suggested the importance of considering muscle forces. Some models have integrated the effect of muscles into the properties of the intervertebral discs (e.g., Verver *et al.*, 2003) and other models have represented only a few of the muscles connected to the lumbar spine (e.g., Pankoke *et al.*, 2001). The muscles in most biodynamic models have been modelled as linear springs (e.g., Pankoke *et al.*, 1998 and 2001; Fritz, 2000), neglecting the active muscle forces. The EMG studies (Section 2.6.2.2) indicate that active muscle forces are evoked during whole-body vibration at low frequencies, and may contribute to the forces in the spine. However, understanding of the mechanism involved in generating active muscle forces and how to model active muscle forces requires further study.

A detailed muscle system for the lumbar spine has been represented in some models (e.g., Bazrgari *et al.*, 2008a). In these models, a force vector is used to represent a muscle fascial, with properties determined either from EMG measurements or from optimisation algorithms (e.g., least square of the summed cubic stresses from all muscles). The active muscle forces are considered in these models. But such models are very complex in structure and difficult to adapt to different postures due to the requirement to measure the response of human body and muscle activity (i.e., EMG) in each posture.

An important part of the process of developing a biodynamic model for predicting spinal loads is 'verification' or 'calibration'. Previous models have usually been verified (or calibrated) based on four principles: 1) apparent mass (e.g., Fritz, 2000; Verver *et al.*, 2003; Bazrgari *et al.*, 2008a; Wang *et al.*, 2010); 2) body transmissibility from seat to various spinal levels and head (e.g., Pankoke *et al.*, 1998; Fritz, 2000; Bazrgari *et al.*, 2008a); 3) static spinal loads measured in-vivo (e.g., Pankoke *et al.*, 2001; Hinz *et al.*, 2002); 4) mechanical properties of the spine segments (e.g., bending of the spine under preloads; Section 2.5.3) measured in-vitro (e.g., Pankoke *et al.*, 1998; Ayari *et al.*, 2009). The apparent mass has been widely used to calibrate biodynamic models, but a model with a close representation of the apparent mass may not provide a good prediction of motions of spine segments. Therefore, many biodynamic models were calibrated with body transmissibilities, particularly the vertical seat-to-head transmissibility (e.g., Pankoke *et al.*, 1998; Fritz, 2000; Bazrgari *et al.*, 2008a). But models with a good prediction of the head motions may not be able to predict appropriate motions of the lumbar spine. The head motion is relatively easy to measure compared with the motions of the lumbar spine. However, the head motion is greatly influenced by pitch motion of the head and varies with the location of measurement at the head (e.g., Paddan and Griffin, 1988; Section 2.3.2). The representation of the response of the lumbar spine to whole-body vibration is desired for models predicting spinal loads (Kitazaki and Griffin; 1998, Section 2.4.4).

In-vivo measurements can provide accurate and direct information on spinal loads and the data can assist the calibration of models for predicting spinal loads. The stiffnesses of the spinal segments in all six degrees-of-freedom obtained from in-vitro measurements (e.g., Berkson *et al.*, 1979; Panjabi *et al.*, 1977) may be different from the stiffnesses of the same spinal segments in the live body (Stokes *et al.*, 2002, Section 2.5.3), due to the absence of active muscle forces. The muscle forces add a preload to the spinal segments and this is not considered in in-vitro measurements (Section 2.5.3).

The existing models predict spinal forces in terms of maximum forces, or time-domain forces, or transfer functions from the excitation acceleration to the forces in the frequency domain. The results from different models are difficult to compare and obtain an approximate range of spinal forces, partly due to different expressions of forces and partly due to different postures and different excitations (i.e., frequencies, magnitudes) used by the model. It seems preferred to predict an appropriate range of spinal forces and investigate and understand the trends in changes of the spinal forces caused by varying posture or vibration frequency, rather than focus on predicting accurate values of spinal forces in one posture or at one frequency.

In summary, biodynamic models can be used to predict spinal forces in both compressive and shear directions. Such models should have representation of relevant parts of body anatomy, including the lumbar spine. The geometry and inertial properties of the human body can be derived from previous anthropometric measurements (e.g., NASA, 1978). Muscle forces make a significant contribution to spinal forces and their effects should be included in models predicting spinal forces. Models should also reflect appropriate biodynamic responses of the human body, including the motions of the spine. The biodynamic responses of the human body and muscle activity are affected by sitting posture and backrest contact. The effects of posture and backrests on the spinal loads exposed to whole-body vibration should be better understood. The method (e.g., structure of a model and the mechanisms for generating muscle forces) used to predict the spinal force should be justified, so as to understand the accuracy of the predictions and the limitations to the application of the model.

2.8 Research questions

In view of the current state of understanding of the biodynamic responses of the human body to vibration and how to predict of spinal forces, the research presented in this report is focused on the following questions:

(1) How does contact with a vertical or inclined backrest affect the biodynamic response (i.e., apparent mass and body transmissibilities) of the seated human body?

(2) How does sitting posture affect the biodynamic response of the seated human body?

(3) How do the spinal forces depend on the frequency of vertical vibration excitation?

(4) How does the posture of the body (including contact with a backrest) affect spinal forces and what is the underlying mechanism responsible for the effects of posture on spinal forces?

(5) To what extent does muscle activity affect spinal forces?

To answer these questions, biodynamic models have been developed in the following sections to represent the biodynamic responses of the human body. The models have been optimised using the results of new experimental studies of the apparent mass and transmissibility of the human body. The effects of posture and the effects of vertical and inclined backrests on the forces are also investigated.

Chapter 3. Apparatus and methods

3.1 Introduction

This chapter describes the apparatus and methods used in the experiments. The apparatus include transducers, vibrator and data acquisition system. The methods consist of calibration procedure of the transducers, signal processing of acquired data and methods used for correcting some raw data of the biodynamic response of body. Three experiments were conducted in this research and they were all conducted on the 1-m vertical vibrator in the main laboratory of the Human Factors Research Unit (HFRU), the Institute of Sound and Vibration Research (ISVR), University of Southampton. All experiments were approved by the Ethics Committee of the Faculty of Engineering and the Environment at the University of Southampton (approval number 14342). A summary of the experiments including title, independent variables and dependent variables are listed in Table 3.1.

Table 3.1 Summary of experiments conducted in this research

Experiment number	Title of experiment	Independent variables	Dependent variables
1	Effect of vertical and inclined backrest on the vibration transmitted to the body	Inclinations of backrest	Vertical and fore-and-aft apparent masses at the seat pan and backrest; vertical, fore-and-aft and pitch transmissibilities to pelvis, L5, L3 and T5
2	Effects of forward leaning sitting postures on the vibration transmitted to the body	Postures of normal upright sitting, anterior leaning sitting and kyphotic leaning sitting; vibration magnitude;	Vertical and fore-and-aft apparent masses at the seat pan and backrest; vertical, fore-and-aft and pitch transmissibilities to pelvis, L5, L3 and T5
3	Effects of muscle tension in the lower and upper bodies on the vibration transmitted to the body	Different amount of external force applied to the body; location of pulling force applied; vibration magnitude;	Vertical and fore-and-aft apparent masses at the seat pan and backrest; vertical, fore-and-aft and pitch transmissibilities to pelvis, L5, L3 and T5

In all three experiments, the subjects sat on a rigid seat. The directions of acceleration and forces at the human-seat pan interface and human-backrest interface followed the definition in ISO 2631-1(1997) (Figure 3.1). The vertical direction refers to *z*- direction and the fore-and-aft direction refers to *x*- direction.

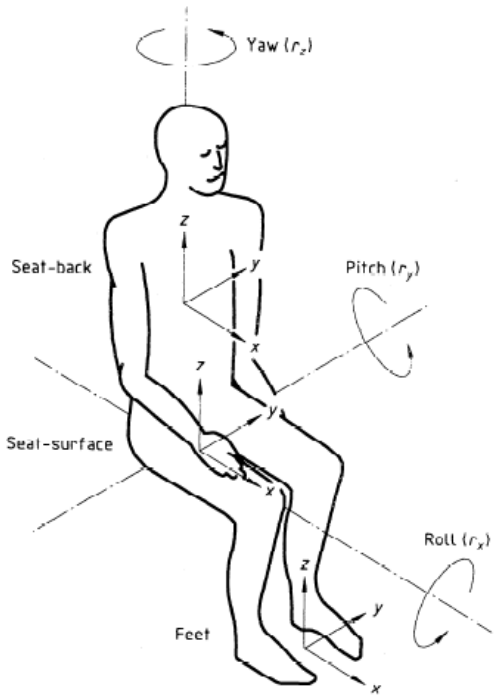

Figure 3.1 Coordinate system defined in ISO 2631-1 (1997).

3.2 Apparatus

3.2.1 Vibrator

The 1-m vertical electro-hydraulic vibrator is a product of Servotest Testing Systems Ltd., Surrey, UK. The platform of the vibrator is made of aluminium alloy and it has a surface of 1500 mm x 8900 mm and the thickness of the platform is 15 mm. The vibrator is capable of producing accelerations of $\pm$10 m/s^2 with peak-to-peak stroke of 1 m in the frequencies range 0 – 50 Hz and a dynamic load of 10 kN with a preload of 8.8 kN in the vertical direction.

3.2.2 Seat and backrest

A rigid seat made of steel was rigidly mounted on the platform with bolts (Figure 3.2). The horizontal seat pan was 500 mm above the platform (Figure 3.2) with a surface of 600 mm (width) x 400 mm (length) as shown in Figure 3.5. A safety belt with adjustable length was provided for the safety of the subjects. An emergency button was provided for the subjects to stop the vibrator when necessary during the experiment.

A rigid backrest was mounted on the platform of the vibrator to provide support to the back of the body. The backrest inclination angle can be adjusted from 0º (vertical) to 60º when it was required in the experiment. The surface of the backrest is made of plywood with a dimension of 500 mm (width) x 600 mm (height). When the backrest surface is in the vertical position, the vertical distance from the bottom edge of the backrest to the seat pan is 100 mm. The dimensions of the backrest are shown in Figure 3.3.

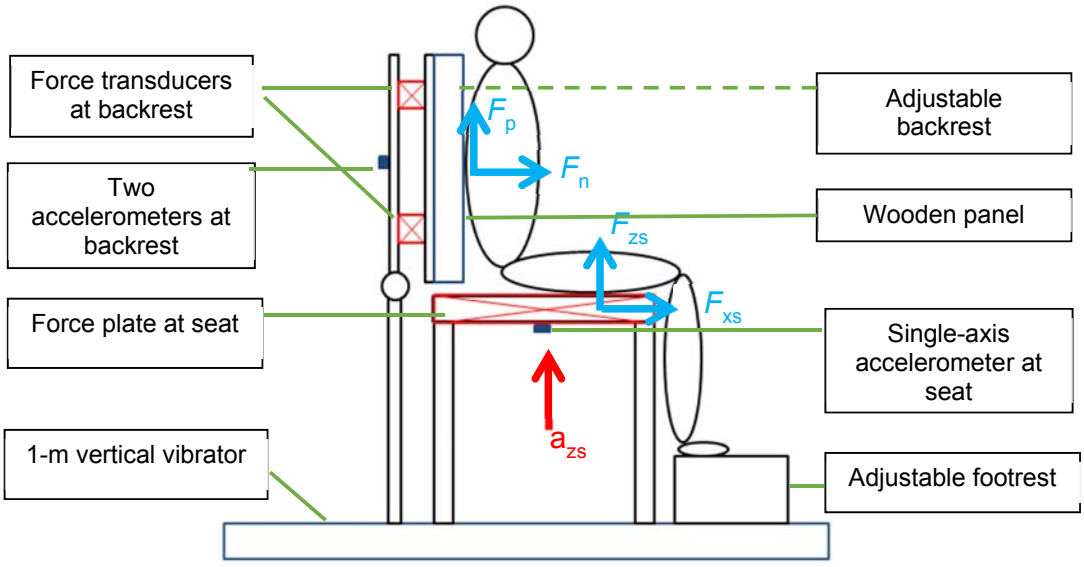

Figure 3.2 Experiment set-up with rigid seat and rigid backrest mounted on the vertical vibrator.

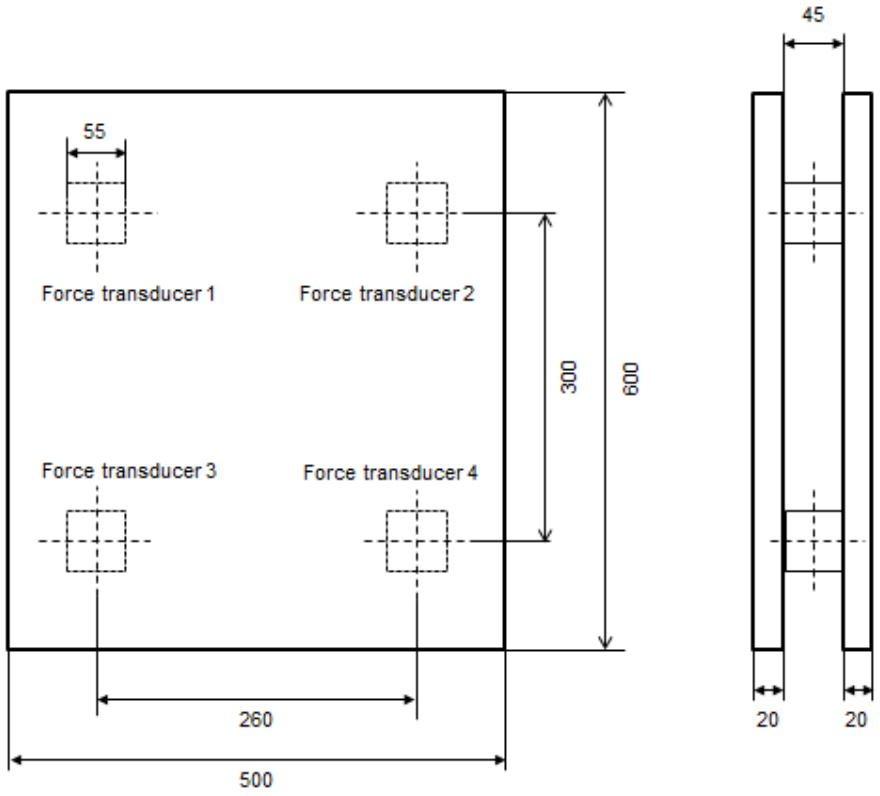

Figure 3.3 Sketch of the set-up and dimensions of the backrest surface. Four force transducers are rigidly mounted between two plywood wooden boards. The dimensions are in mm.

Two rigid wooden panels (180 mm x 600 mm) were attached firmly to the front surface of a force plate mounted on the backrest frame such that a slot of 100 mm width from the top to the bottom in the middle area of the backrest was created so as to avoid the accelerometers attached on the back of subjects contacting the backrest when sitting against the backrest. Each panel has a

dimension of 180 mm (width) x 100 mm (thickness) x 600 mm (height). The dimensions of the panels and their attachment on the backrest surface are shown in Figure 3.4.

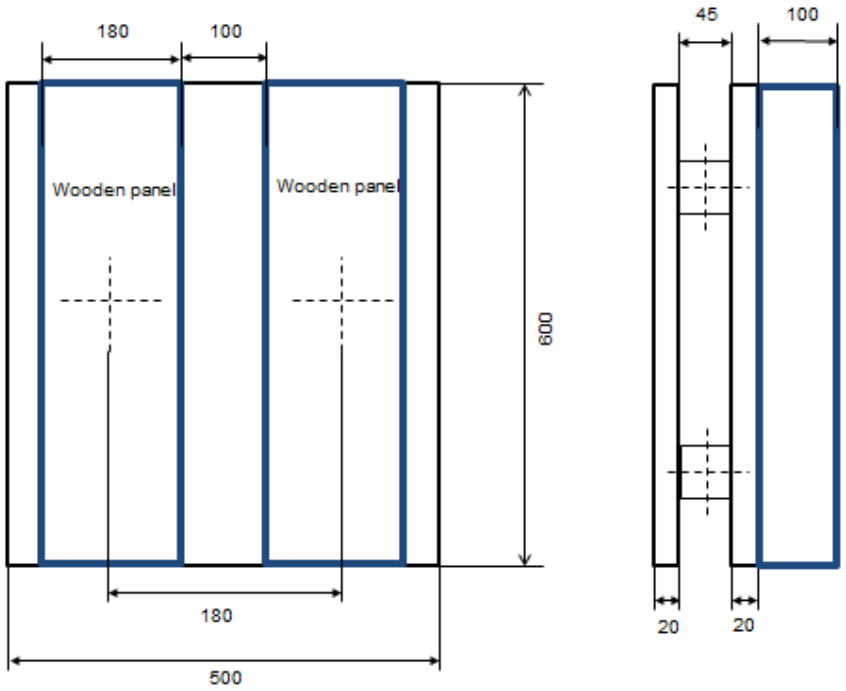

Figure 3.4 Set-up of wooden panels to form a 100-mm width slot for the accelerometers. The dimensions are in mm.

The signals to be produced by the 1-m vertical vibrator were equalised before the formal test with subjects. A random acceleration with a similar frequency content and magnitude ($a_1(t)$) to the desired signal ($a_2(t)$) was output from a computer to the vibrator. The response acceleration was measured at the centre of the surface of the force plate as ($a_3(t)$). The transfer function from the input signal ($a_1(t)$) to the response signal ($a_3(t)$) was calculated as $T(f)$. The inverse of this transfer function ($T(f)$) was applied to the desired signal ($a_2(t)$) by means of convolution to calculate the compensated input signal ($a_4(t)$). Usually, the equalisation involves several runs of the above process until the error between the r.m.s. of the input signal and the r.m.s. of the desired signals is below 5%.

The vibrator itself has a resonance frequency around 15 Hz in the fore-and-aft direction associated with its mechanical properties, and it will change with different start-up height. Based on preliminary tests, when random vibration of 0.5 m/s^2 r.m.s. and 1.0 m/s^2 r.m.s. from 0.2 -20 Hz were performed by the vibrator, the operating height of the vibrator was set-up at 300 mm level and the resonance frequency of the vibrator in the fore-and-aft direction was about 17 Hz. When the random vibration of 1.5 m/s^2 r.m.s. from 0.2 – 20 Hz was preformed, the operating height of the vibrator was set-up at 500 mm level to leave enough space (500 mm) for the downward vibration. And a resonance frequency around 15 Hz was found in the fore-and-aft cross-axis apparent mass at the seat during the experiments (e.g., Figure C1.6, Appendix C). The effect of such fore-and-aft resonance of the shaker cannot be eliminated by the equalisation of the signals produced by the shaker in the

vertical direction. The fore-and-aft apparent mass measured with 1.5 m/s^2 r.m.s. random vibration is only valid until 10 Hz.

3.2.3 Force transducers

A force plate (Kistler 9281 B) consisting of four tri-axial quartz transducers at the four corners of a rectangular welded steel frame (600 (width) mm x 400 (length) mm) was secured on the supporting surface of the seat to measure the dynamic forces in vertical and fore-and-aft directions at the seat pan interface (Figure 3.5).

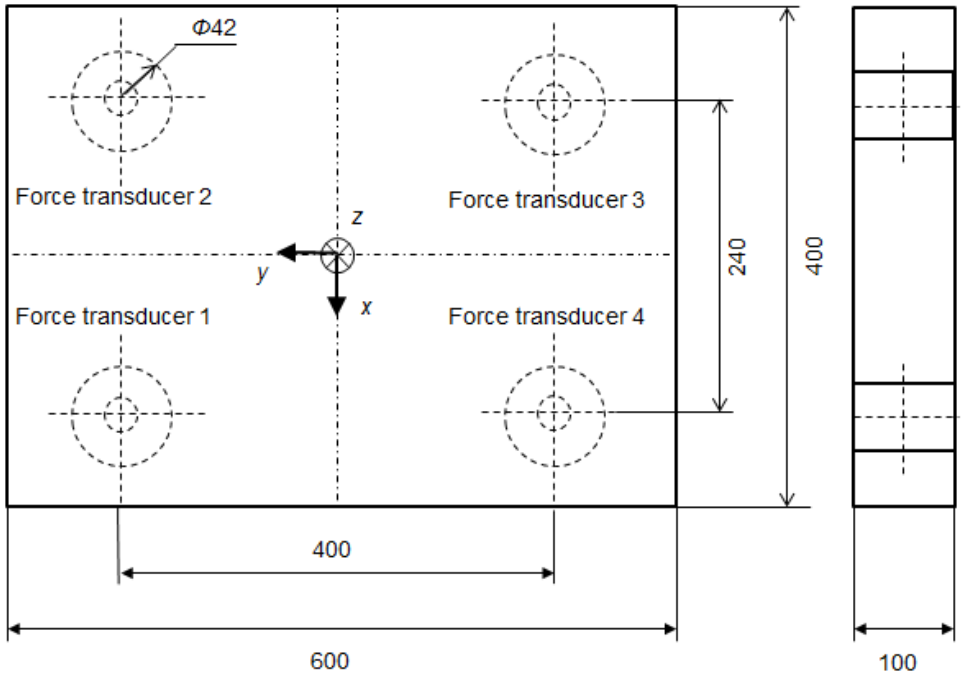

Figure 3.5 Kistler 9281 B 12 channel force platform, used as a seat pan (figure adjust from Zhen, 2014). The unit is mm.

The dimensions of this force plate are shown in Figure 3.3 and its specifications are shown in Table 3.2. The force signals from the transducers at four corners were summed to provide a single signal in the vertical and fore-and-aft directions, respectively. The signal was amplified using a Kistler 5073 charge amplifier.

The calibration of the force plate at the seat pan was performed in both vertical and fore-and-aft directions. In the vertical direction, sandbags with a known mass of 10 kg (around 98 N force) were placed on the top of the force plate. In the fore-and-aft direction, a pulley system was used to apply 49 N (5 kg weight) force to the force plate in the fore-and-aft direction. The measurement range for the force plate was applied by setting a gain in the data acquisition system to be ±2100 N for the vertical direction and ±635 N for the fore-and-aft direction. The determined measurement ranges are roughly 1.5 times above the maximum forces in the vertical and fore-and-aft directions during the measurement.

Another force plate, consisting of four tri-axial force transducers (Kistler 9602) at the four corners of a rectangular plywood frame (600 mm x 500 mm) was mounted on the backrest. The set-up of the backrest and the position of the four force transducers are shown in Figure 3.3. Each force transducer contains a steel mount with a dimension of 55 mm (length) x 55 mm (width) x 45 mm (height) and a sensor, as shown in Figures 3.3 and 3.6. The signals from the force transducers were amplified by a Kistler 5073 charger amplifier. The specifications of the Kistler 9602 force transducer are shown in Table 3.3.

Table 3.2 Specifications of Kistler 9281 B 12-channel force platform

Measuring axes	F_z	F_x, F_y
Range	-10 to 20 kN	-10 to 10 kN
Overload	-10/25 kN	-15/15 kN
Crosstalk (affection in the signal of one axis caused by another axis)		
$F_x \leftrightarrow F_y$	<±1.5%	
F_x, F_y F_z	<±1.5%	
$F_z \rightarrow F_x$, F_y	<±0.5%	
Rigidity		
x-axis (a_y=0)	≈250 N/μm	
y-axis (a_x=0)	≈400 N/μm	
z-axis (a_x=a_y=0)	≈30 N/μm	
Natural frequency		
f_n (*x*, *y*)	≈ 1000 Hz	
f_n (*z*)	≈ 1000 Hz	
Operating temperature range	0 – 60 ºC	

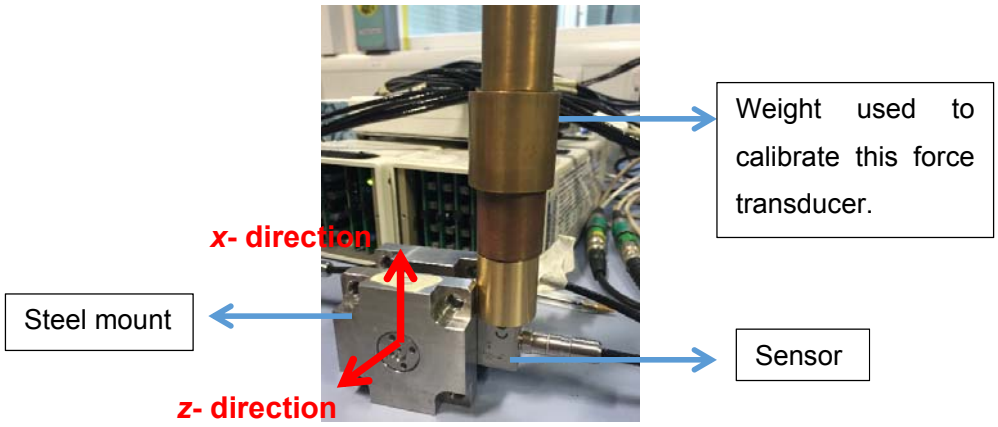

Figure 3.6 The Kistler 9602 B tri-axial force transducer installed at the force plate at the backrest at each corner.

The four force transducers mounted at the backrest were calibrated individually before the installation in both vertical and fore-and-aft directions with similar method used for force plate at the

seat pan. A mass of 10 kg was used for the calibration of the channel in the *z* direction (used to measure F_n, shown in Figures 3.1 and 3.6) and a mass of 1 kg was used for the calibration of the channel in the *x* direction (used to measure F_p shown in Figures 3.1 and 3.6). The range determined for each of the Kistler 9602 B force transducer was ±420 N in the *z*-direction and ± 340 N in the *x*-direction of the transducer. The positive direction of the force transducers in the vertical and fore-and-aft directions at backrest and seat pan followed the coordinate system defined in ISO 2631-1 (1997), shown in Figure 3.1.

Table 3.3 Some of the specifications of Kistler 9602 B tri-axial force transducer

Measuring axes	F_z	F_x, F_y
Measuring ranges		
Range I	-5.0 kN to 5.0 kN	-2.5 kN to 2.5 kN
Range II[a]	-1000 N to 1000 N	-500 N to 500 N
Preloading	25 kN	-
Overload	20%	20%
Sensitivity (nominal)		
Range I	≈1 mV/N	≈2 mV/N
Range II	≈5 mV/N	≈10 mV/N
Linearity	⩽±1.5	
Crosstalk		
$F_x \leftrightarrow F_y$	≈±5%	
$F_z \leftrightarrow F_x$, F_y	≈±3%	
Rigidity		
z-axis (a_x=a_y=0)	≈1250 N/μm	
y-axis (a_x=0) and *x*-axis (a_y=0)	≈240 N/μm	
Weight (sensor only)	≈30g	
Operating temperature range	0 – 60 ºC	

[a] Range II was used in the experiments of this study.

3.2.4 Accelerometers

Single-axial piezo-resistive accelerometers (Entran EGCSY-240D-10) were used to measure the vertical acceleration at the seat pan and vertical and fore-and-aft accelerations at the backrest frame. The Entran EGCSY-240D-10 has a sensitivity of approximately 13 mV/g with an operating range of ±10 g. Each accelerometer was calibrated to give zero reading when it was attached to a horizontal surface, and +2 g when it was inversely placed. The range determined for the single-axis accelerometers was about ± 24 m/s^2.

A total of eight tri-axial MEMS accelerometers (KXD94-2802) were mounted on the upper and bottom surfaces of four blocks made of balsa wood (Figure 3.7) to measure the body motions. Each block of balsa wood has a weight of 2 g and a dimension of 40 mm (length) x 30 mm (width) x 30mm (height). Two tri-axial accelerometers were taped on the top and bottom surfaces of the block.

KXD94-2802 transducer has a sensitivity of 200 mV/g and a range of ±10 g and the frequency range is 0 – 1000 Hz.

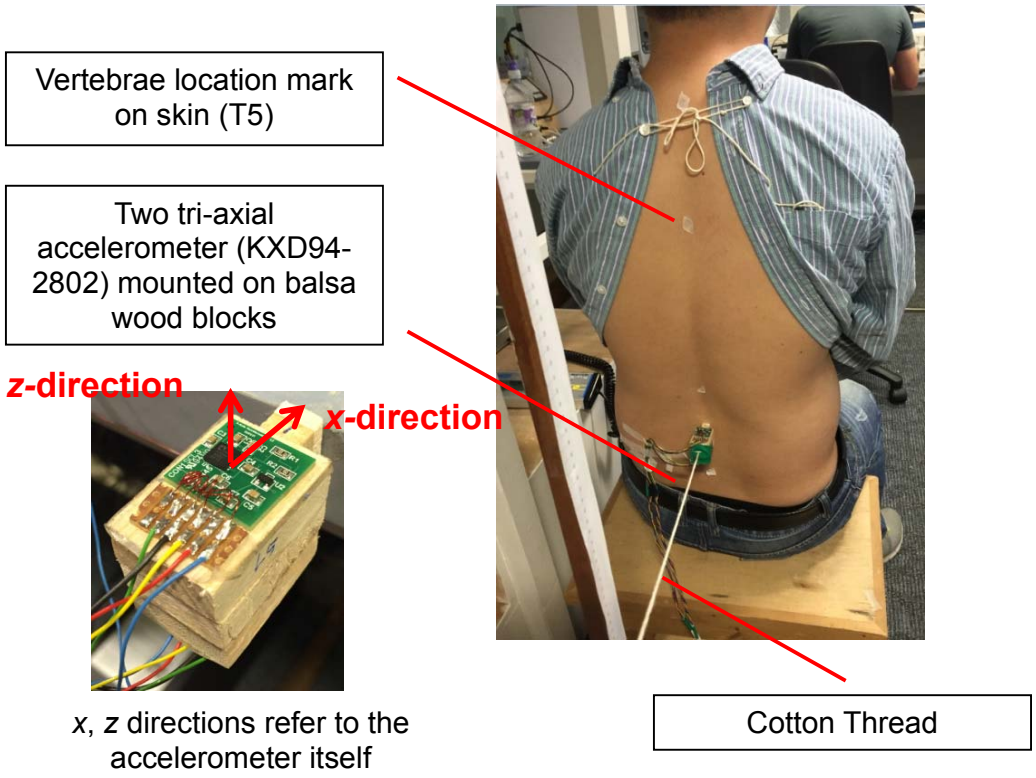

Figure 3.7 Balsa wood measuring block with accelerometers and an example of skin-tissue correction with one subject.

The tri-axial MEMS accelerometers were calibrated separately in two directions (*x*, *z*) as they were used to measure the accelerations in the *x* and *z* directions. They were calibrated to give zero readings in both vertical and fore-and-aft directions when placed on a horizontal surface. Then the vertical channel was calibrated to give +2 g reading when it was inversely placed on the horizontal surface. The horizontal channel was calibrated to give +1g reading when it was placed on a vertical surface. The ranges determined for the tri-axial accelerometers in *z*- and *x*- directions were both around ± 24 m/s^2.

Each measurement block contains two tri-axial accelerometers, and it measures two channels of *x*-direction vibration and one channel of *z*-direction vibration during the experiment (Figure 3.8 a). Before the experiment, eight tri-axial accelerometers were mounted on the top horizontal surface of the rigid seat pan to check the error of the transducers (Figure 3.8 b).

Transmissibility was calculated from the vertical acceleration at the seat pan measured by one single-axial piezo-resistive accelerometer (Entran EGCSY-240D-10) to the vertical acceleration at the seat pan measured by the *x*-axis channel of each tri-axial accelerometer at the top surface of the seat pan, giving eight vertical in-line transmissibilities (Figure 3.9 c and d). Transmissibility was calculated from the vertical acceleration at the seat pan (measured by Entran EGCSY-240D-10) to the fore-and-aft acceleration at the seat surface measured by the *z*-axis channel of each block,

giving four fore-and-aft cross-axis transmissibilities (Figure 3.9, a, b). Figure 3.8 shows the magnitude and phase of the transmissibilities. Ideally, the transmissibility should be unity and the phase should be zero (or 3.14) at all frequencies for the vertical transmissibility assuming the seat is rigid and the vibrator only produces vibration in that direction. From the results in Figure 3.9, the tri-axial accelerometers gave a transmissibility of 1.0 at frequencies 0-10 Hz. The vertical transmissibility measured by most accelerometers decreased with further increase in the frequency. At 15 Hz, the maximum error is about 3% (giving a transmissibility of 0.97). The fore-and-aft transmissibilities measured by four accelerometers were close to 0, and the phase showed values around 0. The result suggested that the 1-m vertical vibrator produces reasonably good response.

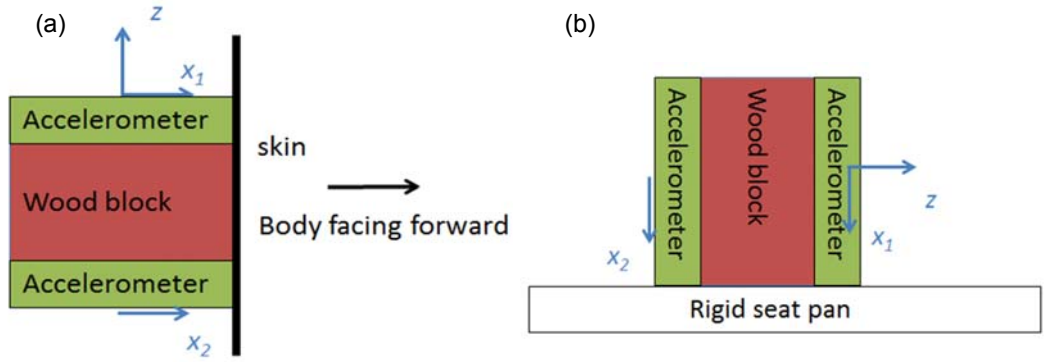

Figure 3.8 (a) Set-up of wooden blocks with accelerometers and the channels used to measure the acceleration at the body surface; (b) Position of the accelerometer during the process of checking error.

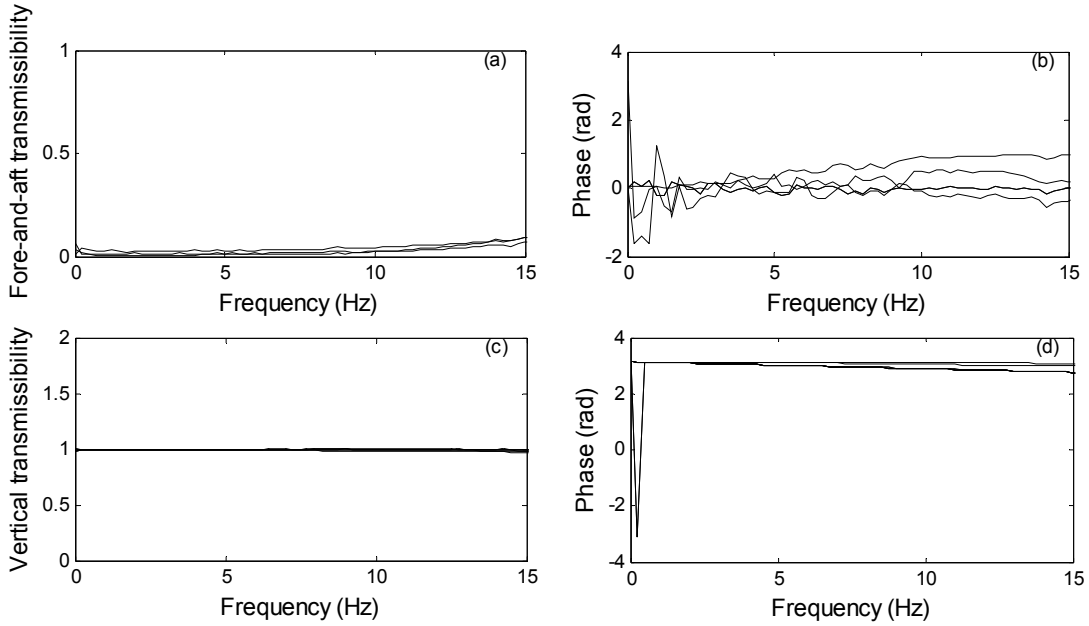

Figure 3.9 Transmissibilities and phases from the vertical seat acceleration measured with a single-axial accelerometer to the fore-and-aft acceleration measured by four tri-axial accelerometers (a, b); Transmissibilities and phases from the vertical seat acceleration to the vertical acceleration measured by eight tri-axial accelerometers (c, d).

3.2.5 Data acquisition system

The input signals (random broadband vibration) were generated using *HVLab* toolbox (version 2.0) in Matlab (R2013a, MathWorks, Massachussets, USA). The signals were generated and acquired at 256 samples/second with an anti-aliasing filter of a cut-off frequency of 100 Hz. The input and output signals were acquired and controlled by the data acquisition box NI-USB6211 16 bit. The stimuli include 60-s periods of random vertical vibration with approximately flat constant-bandwidth acceleration spectra (0.2 to 20 Hz) at three vibration magnitudes: 0.5 m/s^2, 1.0 m/s^2 and 1.5 m/s^2 r.m.s. These three signals were equalised before testing the subjects (Section 3.2.1).

3.3 Data analysis

3.3.1 Calculation of apparent mass at the seat pan

3.3.1.1 Mass cancellation at the seat pan

For the calculation of the forces at the seat and the backrest, the effect of the mass of the force plates on the measured dynamic forces was eliminated by mass cancellation in the time-domain. The acceleration time-history was multiplied by the mass of the force platform 'above' the force sensors and the resulting force subtracted from the measured force.

The detailed procedure of the mass cancellation includes the following steps:

(1). Calibrate the force transducers and accelerometers and mount them so as to measure the relevant forces and accelerations.

(2). Shake the vertical simulator without subject with random vibration used in the experiment.

(3). Calculate and plot the vertical in-line apparent mass at the seat pan and pick the apparent mass (in 'kg') at 1.0 Hz as a 'known mass'.

(4). Measure the time-history of forces with subjects sitting on the force plate and subtract the value of the vertical acceleration time-history at the seat pan multiplied by the 'known mass' from the measured force time-history, resulting in the forces to be used for calculating apparent mass.

The calculated apparent mass without subjects sitting on the force plate was shown in Figure 3.10. It suggested that the rigid seat-force plate system showed a rigid behaviour over frequencies from 0 – 15 Hz with a phase close to 0. A value of 33.0 kg was taken (the magnitude at 1.0 Hz) as the 'known mass' for the mass cancellation process.

Similarly, when there is a rigid seat pan made of wood mounted on the seat (used in Chapter 9 to provide feet hanging sitting posture), the mass cancellation results is shown in Figure 3.10 (bottom row), where the whole system without subjects sitting on it showed rigidity over 0-15 Hz. A mass of 38 kg was calculated for the mass cancellation process in this experiment.

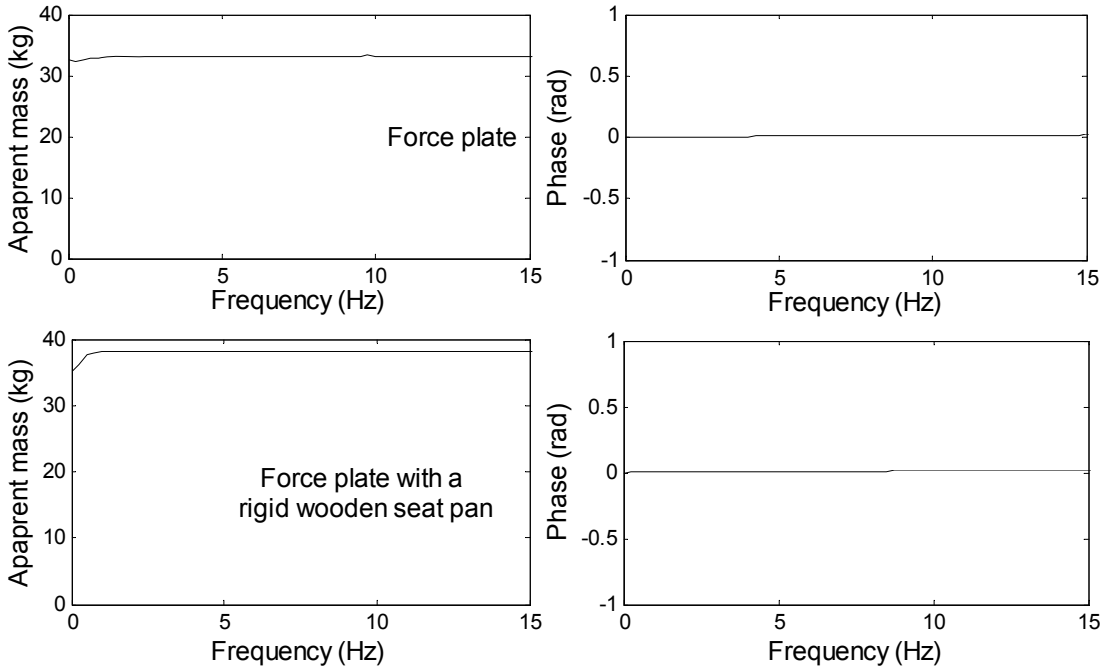

Figure 3.10 Mass cancellation: Apparent mass and phase without subjects sitting on the force plate (top row) and when there is a rigid wooden seat pan on it (bottom row). The supporting mass on the force transducers are 33 kg and 38 kg with and without a wooden seat pan.

3.3.1.2 Frequency response function

The apparent mass was calculated as the transfer function between dynamic force and acceleration using the averaged cross spectral density method (i.e., H1 estimation, Chapter 2). For the 'vertical in-line apparent mass' at the seat pan, $M_{zzs}(f)$, the measured force and acceleration were in the same direction (i.e., vertical). For the 'fore-and-aft cross-axis apparent mass' at the seat pan, $M_{xzs}(f)$, the measured fore-and-aft force was perpendicular to the acceleration (vertical) at the seat pan. The two apparent masses at the seat pan, $M_{zzs}(f)$ and $M_{xzs}(f)$, and the associated coherencies, $C_{zzs}^2(f)$ and $C_{xzs}^2(f)$, were calculated as:

$$M_{\mathrm{zzs}}(f) = \frac{G_{a_{\mathrm{zs}}F_{\mathrm{zs}}}(f)}{G_{a_{\mathrm{zs}}}(f)}, \quad C_{\mathrm{zzs}}{}^2(f) = \frac{\left|G_{a_{\mathrm{zs}}F_{\mathrm{zs}}}(f)\right|^2}{G_{a_{\mathrm{zs}}}(f)G_{F_{\mathrm{zs}}}(f)},$$

$$M_{\mathrm{xzs}}(f) = \frac{G_{a_{\mathrm{zs}}F_{\mathrm{xs}}}(f)}{G_{a_{\mathrm{zs}}}(f)}, \quad C_{\mathrm{xzs}}{}^2(f) = \frac{\left|G_{a_{\mathrm{zs}}F_{\mathrm{xs}}}(f)\right|^2}{G_{a_{\mathrm{zs}}}(f)G_{F_{\mathrm{xs}}}(f)} \tag{3.1}$$

where, $G_{a_{\mathrm{zs}}}(f)$ is the auto-spectra of the vertical acceleration at the seat pan, $a_{zs}(t)$, $G_{F_{\mathrm{zs}}}(f)$ and $G_{F_{\mathrm{xs}}}(f)$ are the auto-spectra of vertical and fore-and-aft forces measured at the seat pan, $F_{zs}(t)$ and $F_{xs}(t)$, and $G_{a_{\mathrm{zs}}F_{\mathrm{zs}}}(f)$ and $G_{a_{\mathrm{zs}}F_{\mathrm{xs}}}(f)$ are the cross-spectra between $a_{zs}(t)$ and $F_{zs}(t)$ and between $a_{zs}(t)$ and $F_{xs}(t)$.

The auto-spectra and cross-spectra of the time signals (a duration of 60 second) in this thesis were calculated either with 60 averages with an overlap of 75% (i.e., a Hamming window of 4 second) for a frequency resolution of 0.25 Hz or with 32 averages with an overlap of 75% (i.e., a Hamming window of 8 second) for a frequency resolution of 0.125 Hz.

3.3.2 Calculation of apparent mass at the backrest

3.3.2.1 Mass cancellation at the backrest

With vertical backrest, mass cancellation was performed on the dynamic forces in the fore-and-aft direction (normal to the backrest surface). With inclined backrests, mass cancellation was performed on the dynamic forces in the directions normal and parallel to the backrest surface. In the normal and the parallel directions, the time history of the acceleration was multiplied by the mass of the plate and then subtracted from the measured force time history in the same direction.

Following a similar way, the supporting mass on the force plate in the directions normal and parallel to backrest surface were determined without subjects sitting against the backrest. The backrest was inclined for 10º. The accelerometers mounted on the backrest measure the accelerations in the directions normal and parallel to the backrest surface. The in-line transfer functions from the acceleration to the measured force were calculated, as shown in Figure 3.11.

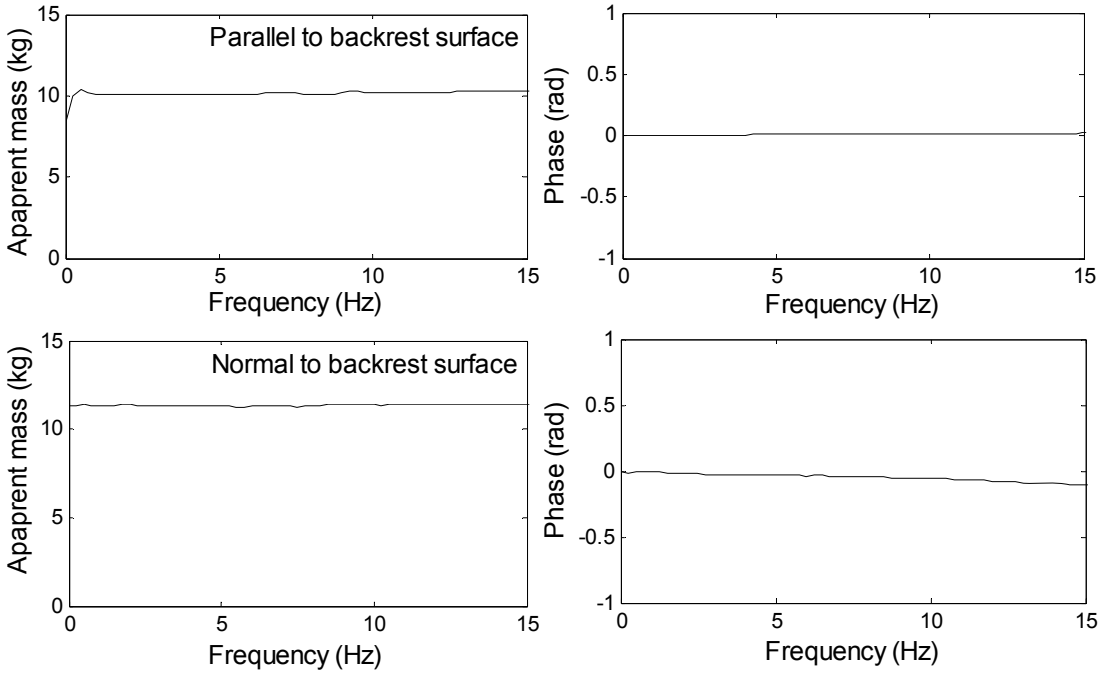

Figure 3.11 In-line apparent mass at the backrest in the direction parallel to the backrest surface (top row, showing a value of 10 kg) and in-line apparent mass at the backrest in the direction normal to the backrest surface (bottom row, showing a value of 11 kg). Phases are shown in the right column.

The bottom row in Figure 3.11 shows the mass supported on the backrest in the direction normal to the backrest. It shows a mass of 11.2 kg at 1 Hz. This value was used for the mass cancellation of the force time-history normal to the backrest (F_n).

The top row in Figure 3.11 shows the mass supported on the backrest in the direction parallel to the backrest. The mass supported is about 10 kg at 1 Hz, slightly smaller than that in the normal direction. The difference could be explained by the measurement noise when obtaining the force signal. The acceleration normal to the backrest surface may be small in value and noise would exist in the acquisition of this signal. This mass of 10 kg is used for the mass cancellation of the time-history force parallel to the backrest (F_p).

3.3.2.2 Frequency response functions

The method to calculate the apparent masses at the backrest surface was the same as calculating the apparent mass at the seat pan. The dynamic forces in directions normal to the surface of the backrest, F_n, and parallel to the surface of the backrest, F_p measured by the force plate were combined after adjusting for the inclination of the backrest, and then decomposed to obtain the forces in the vertical and fore-and-aft directions (i.e., the same coordinates used for calculating the vertical in-line and fore-and-aft cross-axis apparent mass at the seat pan). Such forces were then used to calculate the vertical in-line and fore-and-aft cross-axis apparent masses at the backrest. The details are described in Chapter 6.

When sitting against a vertical backrest or inclined backrests (e.g., Chapter 6 and Chapter 7), the seated human body were exposed to excitations from the seat pan and the backrest. The dynamic forces at the seat pan and at the backrest were contributed from both the motions from the seat pan and the backrest. The apparent masses at the seat pan and at the backrest in this sitting conditions were defined as the complex ratio from the vertical seat acceleration to the dynamic forces as described in Sections 3.3.1.2 and 3.3.2.2, in order to quantify such forces and to provide comparisons of these forces between different sitting conditions (i.e., sitting against different inclinations of backrest).

3.3.3 Calculation of transmissibility

The transmissibilities were calculated as the ratio from the acceleration at the seat to the acceleration at locations of human body. Similar to the calculation of apparent mass, the vertical and fore-and-aft transmissibility, $T_{ZZ}(f)$, $T_{XZ}(f)$, were calculated below together with the associated coherencies, $C_{Tzz}^2(f)$ and $C_{Txz}^2(f)$. T corresponds to the spinal levels, including pelvis, L5, L3 and T5.

$$T_{ZZ}(f) = \frac{G_{a_{zs}a_{tz}}(f)}{G_{a_{zs}}(f)},\ C_{Tzz}{}^2(f) = \frac{\left|G_{a_{zs}a_{tz}}(f)\right|^2}{G_{a_{zs}}(f)G_{a_{tz}}(f)}$$

$$T_{XZ}(f) = \frac{G_{a_{zs}a_{tx}}(f)}{G_{a_{zs}}(f)},\ C_{Txz}{}^2(f) = \frac{\left|G_{a_{zs}a_{tx}}(f)\right|^2}{G_{a_{zs}}(f)G_{a_{tx}}(f)} \quad (3.2)$$

where $G_{a_{zs}a_{tz}}(f)$ and $G_{a_{zs}a_{tx}}(f)$ are the cross-spectra between $a_{zs}(t)$ and $a_{tz}(t)$ and between $a_{zs}(t)$ and $a_{tx}(t)$.

The pitch motions, $\ddot{\theta}_T(t)$, at different spine levels (i.e., pelvis, L5, L3 and T5) were calculated as the ratio between the difference of the two measured fore-and-aft accelerations ($\ddot{x}_1(t)$ and $\ddot{x}_2(t)$) and the vertical distance (*d*) of the two accelerometers. The pitch transmissibility, T_{PZ}(f), was then given by the transfer function from vertical acceleration $a_{zs}(t)$ to $\ddot{\theta}_T(t)$.

$$\ddot{\theta}_T(t) = \frac{\ddot{x}_1(t) - \ddot{x}_2(t)}{d}, \quad T_{PZ}(f) = \frac{G_{a_{ZS}\theta_T}(f)}{G_{a_{ZS}}(f)} \tag{3.3}$$

where $\ddot{\theta}(t)$ is the time history of pitch angle acceleration of the corresponding vertebrae (i.e., pelvis, L5, L3 and T5). $G_{a_{zs}\theta_T}(f)$ is the cross-spectra between $a_{zs}(t)$ and $\ddot{\theta}_T(t)$.

The calculated transmissibility requires further adjustments (e.g., skin-tissue correction, angle correction) and the adjustments are detailed in the first experiment chapter (i.e., Chapter 6).

3.4 Statistical analysis

Non-parametric statistical methods were used in the analysis of data for this research with the assumption that all subjects were drawn from an unknown population. All statistical analyses were performed with Matlab (R2013a). The following text will briefly describe the statistical methods used in this research. More detailed information can be found in the reference from Siegel and Castellan (1988).

3.4.1 Friedman two-way analysis of variance

Friedman two-way analysis of variance test is used to test the null hypothesis with *k* dependent conditions drawn from same population. For example, the Friedman test can be used to examine whether a particular variable (e.g. apparent mass resonance frequency, apparent mass at resonance, parameters of fitted model) is dependent on different testing conditions (e.g. vibration magnitude, vibration waveform, direction of excitation, and posture). It means this test can investigate the effect of backrest, effect of magnitude, but it can only tell whether the variable, such as resonance or peak magnitude, are dependent on another (excitation magnitude or postures).

3.4.2 Wilcoxon matched-pairs signed ranks test

The Wilcoxon matched-pairs signed ranks test is used to determine whether two dependent (matched) conditions (samples) were different. The Wilcoxon test takes into account the direction and the magnitude of the difference between the two samples. For example, if the Friedman test found that the vibration magnitude has a significant effect on resonance frequency, the Wilcoxon test can be used to find which two vibration magnitudes have the significant difference. It means if there are three sets of variables (e.g., resonance frequency measured at three vibration magnitudes), the Wilcoxon test between each two sets (one pair) of data (so there will be three tests) can calculate the significance of each test to identify the effect of each pair of conditions on the variable.

The *p*-value indicating the significance level of the comparison between the variables conduced in the experiments in this thesis was uncorrected with number of comparisons.

3.4.3 Spearman rank-order correlation

The spearman rank-order correlation test is used to compare the ranking of data between two variables (samples) and to identify whether the two are related. For example, it can find whether there is a correlation between the resonance of vertical apparent mass and the peak resonance frequency of the cross-axis apparent mass. The correlation coefficient *r*, has a value between [-1, 1], and the closer to -1 or 1, the more related the two sets of data are. A value of 0 means no relation between the two variables. Besides, the correlation between resonance frequency of vertical (or fore-and-aft) apparent mass at the seat pan and resonance frequency of transmissibility to various location of body in different directions can be conducted to identify whether the two selected variables might have common causes.

Chapter 4. Developing a simple mathematical model of the seated human body to predict spinal forces caused by vertical vibration

4.1 Introduction

Whole-body vibration and mechanical shocks may have adverse effects on health, including increased risk of injury in the lumbar spine leading to low back pain (LBP). It is assumed that the mechanical stresses caused by vibration and shock, and impaired nutrition in the intervertebral discs, contribute to degenerative processes (e.g., International Organization for Standardization, 2003), although the underlying mechanisms remain to be identified. It is thought that the three lowest intervertebral discs in the lumbar spine are at greatest risk (Chapter 2), and that the control of loads at these locations might help to control the risks of injury. The loads on the intervertebral discs consist of shear forces, compressive forces, and moments, although the majority of studies have focused on the compressive forces.

The spinal loads can be investigated by in-vivo measurements using transducers inserted into the discs, although practical and ethical considerations mean there are few in-vivo data available. In-vivo measurements of loads in the lumbar spine have been measured using either a force transducer on an artificial vertebra implanted during the surgical replacement of a vertebral body (e.g., Rohlmann *et al.*, 2011) or a pressure transducer inserted in the nucleus pulpous of a disc (e.g., Wilke *et al.*, 2001). The spinal force may be calculated from pressure measurements and the disc area obtained from CT or MRI scans. Only a small number of subjects have been investigated with in-vivo studies, and some have had degenerated intervertebral discs likely to influence the internal loads. The loads measured with vertebral body replacements only represent part of the total spinal loads because spinal forces are shared by the remaining vertebral body, the replacement device, and the fixation device. The direct measurement of pressure tends to ignore uneven pressure distributions over the intervertebral discs.

Most in-vivo measurements have been restricted to static conditions. It has not been possible to measure the internal loads associated with the whole-body vibration and shock thought to be associated with injury. Biodynamic models, calibrated with measurements of the apparent mass and the transmissibility of the body offer a method of predicting spinal loads. To predict the internal loads at the lumbar spine, a biodynamic model should be able to reflect the overall biodynamic response (e.g., resonances as indicated by the apparent mass) and the modes of the lumbar spine associated with vibration. The measured vertical in-line apparent mass of the human body shows a clear resonance around 5 Hz (e.g., Fairley and Griffin, 1989; Qiu and Griffin, 2010). A resonance around 5 Hz has also been observed in the vertical in-line transmissibility from a seat to various locations along the spine, such as T1, T5, T12, and L3 (e.g., Kitazaki and Griffin, 1997; Matsumoto and Griffin, 2001; Zheng *et al.*, 2011a).

Three alternative types of biodynamic model are used to represent the biodynamics of the body: lumped parameter models, multi-body models, and finite element models. Simple lumped parameter models may accurately represent both the modulus and the phase of the apparent mass of the body (e.g., Fairley and Griffin, 1989; Wei and Griffin, 1998; Qiu and Griffin, 2011b) but they do not reflect the anatomical structure of the body and so are not normally used for predicting spinal forces.

Multi-body models can to some extent reflect the anatomy of the body and represent both the apparent mass of the body and the transmissibility to specific body parts, and with suitable development they may predict spinal forces associated with vibration and shock. A combined lumped parameter model and multi-body model has been used to investigate the apparent mass and body movements at the resonance frequency around 5 Hz (Matsumoto and Griffin, 2001; Figure 2.27, Chapter 2). The model comprised five rigid bodies: thighs (part 1); L4 to pelvis (part 2); T11 to L3 (part 3); viscera (part 4) and upper-body from head to T10 (part 5). Rotational joints with springs and dampers were used to connect the parts. The model was shown to reflect the vertical apparent mass and the transmissibility to the spinal levels, and predict the movement of the body at the resonance frequency of the apparent mass.

Another multi-body model was developed to represent the in-line and cross-axis biodynamic responses of the seated body to vertical vibration (Zheng *et al.,* 2011b). With rotational joints at the connections between each rigid body, the model reflected the apparent mass and the mode shapes of the body and implies that rotational elements can be used to achieve the bending of the upper-body in the sagittal plane.

Neither of the above mentioned multi-body models predicts spinal forces at the intervertebral discs, because they lack detailed representation of the spine. To predict spinal forces due to whole-body vibration, a two-dimensional multi-body model of the seated human body was developed (Fritz, 2000; Figure 2.33, Chapter 2). The model consisted of rigid body segments (head, neck, shoulder, thorax, lumbar spine, and pelvis) interconnected by joints allowing both translation and rotation. Additional force elements were used to model the muscles connected to the lumbar spine. The model, which was compared with measurements of the vertical apparent mass and vertical seat-to-head transmissibility of the body, predicted transfer functions between the input acceleration and spinal forces.

Finite element (FE) models, which can be based on anatomical measurements and material properties, are potentially capable of representing biodynamic measurements and predicting information that may be related to health and injury (e.g., Kitazaki and Griffin, 1997; Pankoke *et al.*, 1998; Wang *et al.*, 2010; Zheng *et al.,* 2012; Liu *et al.*, 2012). A two-dimensional passive finite element model of the spine, viscera, head, pelvis and buttocks was developed in the sagittal plane to predict the vibration mode shapes of the seated human body and the biodynamic responses in different postures (Kitazaki and Griffin, 1997; Figure 2.28, Chapter 2). The model divided the upper-body into several slices, with the mass and moments of inertia of the upper-body distributed at several levels along the spine. The curvature of the spine in erect, slouched, and normal postures was determined by anthropometric measurements and information provided by Privitzer

and Belytschko (1980). The stiffness and damping coefficients of the discs and buttock tissue were determined by comparing the predicted vibration mode shapes with experimental measurements obtained by the authors.

With similar techniques, Wang *et al.* (2010) used a FE model of the seated human with seven rigid bodies representing six vertebral bodies and the spine from head to T12 (Figure 2.38, Chapter 2). Rotational elements were combined with deformable beams to connect these bodies. The buttocks were represented by a set of translational springs and dampers. The model provided a reasonable representation of both the modulus and phase of the vertical in-line apparent mass at the seat pan and gave predictions of the compressive spinal forces as well as muscle forces.

A more complete anatomical representation of the whole body and the lumbar spine has been included in some FE models, with the aim of predicting spinal forces more accurately. A two-dimensional dynamic FE model consisting of rigid bodies (head, upper-body, limbs, L3-L5 vertebrae, viscera, pelvis, thighs, and legs) connected by linear springs allowing articulation and a representation of intervertebral discs and ligaments has been developed (Pankoke *et al.*, 1998; Figure 2.34, Chapter 2). The model provided reasonable representation of the mechanical impedance of the body and the seat-to-head transmissibility at low frequencies, and has been used to predict forces at intervertebral discs.

Because the human body is a complex system, and various complex factors affect the forces at the intervertebral discs (e.g., muscle activity and posture), it is not a simple task to predict the internal loads in the spine using modelling techniques. While some aspects of the model may be complex other component of the model may be relatively simple. To investigate the structure required of a simple model capable of predicting the spinal forces associated with the vertical vibration of a seated human, this study developed a multi-body model with a spinal structure for predicting the compressive spinal force at disc L5/S1.

4.2 Development of the model

4.2.1 Model description

From the literature (e.g., Pankoke *et al.*, 1998; Fritz, 2000; Matsumoto and Griffin, 2001; Wang *et al.*, 2010; Zheng *et al.*, 2011b), it seemed reasonable to treat the spine as a layered structure of rigid elements representing the vertebral bodies, and deformable elements (e.g., rotational springs and dampers) representing the intervertebral discs. Since the upper lumbar vertebrae (L1 and L2) are close to the thorax and the upper-torso and there is less bending at these levels (Panjabi *et al.*, 1980), only the three lower lumbar spinal levels (L3, L4, and L5) were modelled in this study, using rigid bodies inter-connected by rotational joints with stiffness and damping as shown in Figure 4.1. The proposed model consisted of seven parts. The parts from 1 to 7 represented the thighs, pelvis, L5, L4, L3, upper-body from head to L2, and the viscera in the abdomen, respectively.

Five linear rotational joints (r_1 to r_5) with stiffness and damping properties were used to represent the intervertebral discs (Figure 4.1). Each connection position had an eccentricity from the centre of gravity (COG) of the rigid body elements (Figure 4.1), resulting in rotational responses of the body

when exposed to vertical vibration. The viscera in the abdomen were assumed to be supported by the pelvis, and the connection was represented by the combination of a translational spring and a damper. The buttocks tissue was also represented by a combination of linear spring and damper beneath the ischial tuberosities. The vibration input was applied directly to the buttocks tissue.

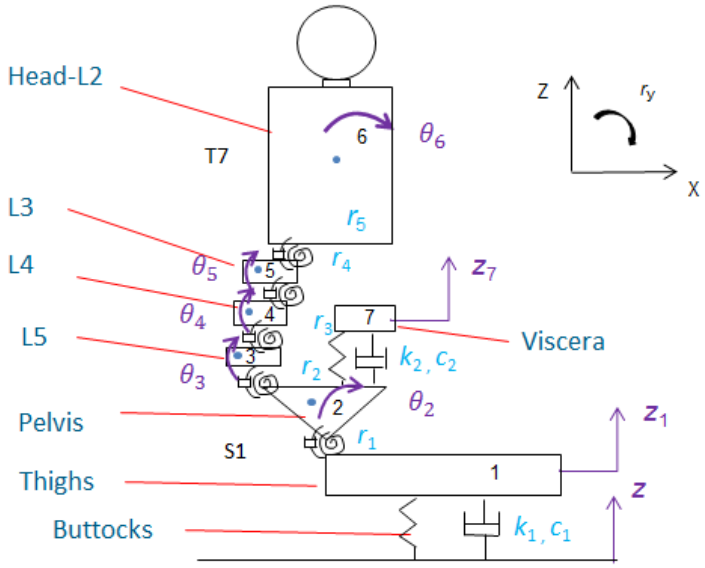

Figure 4.1 Multi-body model of the seated human body represented by seven rigid bodies connected with rotational joints, and translational springs and dampers. 1 - thighs; 2 - pelvis; 3 - L5; 4 - L4; 5 - L3; 6 - upper-body from head to L2; 7 - viscera in the abdomen. The dot in each segment represents the centre of gravity of this segment.

For simplification, the thighs and the viscera were assumed to move only in the vertical direction. It was assumed that bending movements of spine segments could be achieved by rotational movements alone and so there were no translational degrees of freedom at the joints between the spine segments. This treatment was based on the assumption that the movements of the human body at low frequencies are dominated by bending of the spine rather than axial deformation (Kitazaki and Griffin, 1997; Matsumoto and Griffin, 2001). So, in total, there were seven degrees-of-freedom in the model: two vertical and five rotational degrees-of-freedom.

4.2.2 Geometry and inertial properties

The geometry of the entire model was determined from information provided by Kitazaki and Griffin (1997), which was partly derived from direct anthropometric measurements and partly from previous studies (e.g., Privitzer and Belytschko, 1980). The data were based on a median person (i.e., 50th percentile). The coordinates for nodes representing centres of vertebral bodies along the spine from the pelvis to the head in this study corresponded to a body sitting in a normal posture (Kitazaki and Griffin, 1997).

The positions of the rotational joints were assumed to be at the midpoint of the endplates (intervertebral discs) of two adjacent vertebral bodies. The coordinates for the centre of gravity of the body segments, except for the upper-torso, viscera, and thighs, were taken from Kitazaki and Griffin (1997). It was notable that the coordinates of the nodes reflecting the geometry (i.e., spinal

curvature) were different from the nodes representing the mass of the segment in the study of Kitazaki and Griffin (1997). Since the seated body was previously represented by body slices from head to pelvis, the centre of gravity, mass, and inertial properties of the upper-torso were calculated assuming that the slices within this part (i.e., from spinal level L2 to the head) were rigidly connected. The mass and centre of gravity of the viscera were calculated in the same manner. Assuming that the centre of gravity, the mass, and the inertial properties of each body were (x_i, z_i), m_i and I_i, then the position of the centre of gravity, the mass, and the inertial properties of the upper-torso and the viscera were calculated as:

$$x = \frac{\sum_{i=1}^{i} x_i * m_i}{\sum_{i=1}^{i} m_i}, \quad z = \frac{\sum_{i=1}^{i} z_i * m_i}{\sum_{i=1}^{i} m_i}; \tag{4.1}$$

$$m = \sum_{i=1}^{i} m_i \ , \ I = \sum_{i=1}^{i} \left\{ I_i + m_i * [(x_i - x)^2 + (z_i - z)^2] \right\}; \tag{4.2}$$

The mass of the thighs was determined from the distribution of the total body mass provided by National Aeronautics and Space Administration (1978). The centre of gravity, the mass, and the inertial properties of each body segment, and the initial positions of the rotational joints at the equilibrium state of the model are shown in Table 4.1.

Table 4.1 Masses, inertial properties, and initial positions for the centres of gravity of the seven bodies and the rotational joints.

Mass / joint	Mass m_i (kg)	Moment of inertia[a] I_i (kg.m^2)	Centre of gravity of each segment (m) (x_{i0}, z_{i0}), (x_{ri0}, z_{ri0})
m_1 (thighs)	12.96	-	-
m_2 (pelvis)	10.90	9.11 x10^{-2}	(-0.0244, 0.1036)
m_3 (L5)	0.47	9.93 x10^{-4}	(-0.1476, 0.1651)
m_4 (L4)	0.56	1.43 x10^{-3}	(-0.1065, 0.2047)
m_5 (L3)	0.43	1.48 x10^{-3}	(-0.0713, 0.2451)
m_6 (head-L2)	28.88	5.98 x10^{-1}	(-0.0105, 0.6131)
m_7 (viscera)	12.80	-	(-0.0285,0.2450)
r_1[b]	-	-	(0,0)
r_2	-	-	(-0.0895, 0.1488)
r_3	-	-	(-0.0776, 0.1849)
r_4	-	-	(-0.0662, 0.2249)
r_5	-	-	(-0.0596, 0.2644)

[a] The moment of inertia was calculated around the centre of gravity of each part.
[b] r_1 represents the ischial tuberosities for which the coordinates are (0, 0), as defined in the measurements by Kitazaki and Griffin (1997).

The geometry, mass, and inertial properties should be adjusted to represent an individual subject of mass m_s. The total mass of the model was 67 kg, corresponding to a subject of 81.3 kg according to the mass distribution of the total body (considering the mass of thighs, calves and

feet; NASA, 1978), thus the scaling factors for each group of parameters were determined as: $m_s/81.3$ for mass, $(m_s/81.3)^{1/3}$ for length (assuming the density of each body part is constant), and $(m_s/81.3)^{5/3}$ for moment of inertia (Matsumoto and Griffin, 2001).

4.2.3 Equations of motion

It was assumed that all the body parts oscillate around their equilibrium positions with small displacements. The seven degree-of-freedom of this model are: z_1 and z_7, the vertical displacement of the thighs and viscera, and $\theta_2, \theta_3, \theta_4, \theta_5, \theta_6$, the absolute rotational displacements of the pelvis, the lumbar spine (at L5, L4, and L3), and the upper-body. The input was represented by displacement, z, at the buttocks tissue. The equations of motion of the model were derived using the Lagrange equation in the condition of free vibration:

$$\frac{d}{dt}\left(\frac{\partial T}{\partial \dot{q}_i}\right)+\frac{\partial D}{\partial \dot{q}_i}+\frac{\partial U}{\partial q_i}=0\ ;\ q_i=\left[z_1;\theta_2;\theta_3;\theta_4;\theta_5;\theta_6;z_7\right] \tag{4.3}$$

where T is the kinetic energy of the entire model, D is the dissipating energy related to damping, and U is the potential energy. Then T, D, and U for this model were calculated as:

$$T=\frac{1}{2}\sum_{i=1}^{7}m_i(\dot{x}_i^2+\dot{z}_i^{\,2})+\frac{1}{2}\sum_{i=2}^{6}I_i\dot{\theta}_i^{\,2}$$

$$\begin{aligned}D=&\frac{1}{2}c_1(\dot{z}_1-\dot{z})^2+\frac{1}{2}c_{r1}(\dot{\theta}_2)^2+\frac{1}{2}c_{r2}(\dot{\theta}_3-\dot{\theta}_2)^2+\frac{1}{2}c_{r3}(\dot{\theta}_4-\dot{\theta}_3)^2+\frac{1}{2}c_{r4}(\dot{\theta}_5-\dot{\theta}_4)^2\\&+\frac{1}{2}c_{r5}(\dot{\theta}_6-\dot{\theta}_5)^2+\frac{1}{2}c_2(\dot{z}_7-\dot{z}_8)^2\end{aligned}$$

$$\begin{aligned}U=&\frac{1}{2}k_1(z_1-z)^2+\frac{1}{2}k_{r1}(\theta_2)^2+\frac{1}{2}k_{r2}(\theta_3-\theta_2)^2+\frac{1}{2}k_{r3}(\theta_4-\theta_3)^2+\frac{1}{2}k_{r4}(\theta_5-\theta_4)^2\\&+\frac{1}{2}k_{r5}(\theta_6-\theta_5)^2+\frac{1}{2}k_2(z_7-z_8)^2\end{aligned} \tag{4.4}$$

where, m_i is the mass of each body part, (x_i, z_i) and $(\dot{x}_i, \dot{z}_i)$ represent the displacement and velocity of each body at the centre of gravity in the x and z directions, i = 1, 2, 3, 4, 5, 6, 7 denotes the index number of body parts. The combinations of k_1 and c_1, and k_2 and c_2, represent the stiffness and damping coefficients of the spring and damper beneath thighs and viscera, respectively, k_{ri} and c_{ri} represent the stiffness and damping coefficients of the rotational joint r_j, where j =1, 2, 3, 4, 5 denotes the index number of the rotational joint. The velocities were calculated in the matrices as:

$$\begin{bmatrix}x_2\\x_3\\x_4\\x_5\\x_6\end{bmatrix}=x_{r1}+\begin{bmatrix}h_2&0&0&0&0\\h_2+h_{r2}&h_3&0&0&0\\h_2+h_{r2}&h_3+h_{r3}&h_4&0&0\\h_2+h_{r2}&h_3+h_{r3}&h_4+h_{r4}&h_5&0\\h_2+h_{r2}&h_3+h_{r3}&h_4+h_{r4}&h_5+h_{r5}&h_6\end{bmatrix}\begin{bmatrix}\theta_2\\\theta_3\\\theta_4\\\theta_5\\\theta_6\end{bmatrix} \tag{4.5}$$

$$\begin{bmatrix} z_2 \\ z_3 \\ z_4 \\ z_5 \\ z_6 \end{bmatrix} = z_{r1} + \begin{bmatrix} l_2 & 0 & 0 & 0 & 0 \\ l_2 + l_{r2} & l_3 & 0 & 0 & 0 \\ l_2 + l_{r2} & l_3 + l_{r3} & l_4 & 0 & 0 \\ l_2 + l_{r2} & l_3 + l_{r3} & l_4 + l_{r4} & l_5 & 0 \\ l_2 + l_{r2} & l_3 + l_{r3} & l_4 + l_{r4} & l_5 + l_{r5} & i_6 \end{bmatrix} \begin{bmatrix} \theta_2 \\ \theta_3 \\ \theta_4 \\ \theta_5 \\ \theta_6 \end{bmatrix} \tag{4.6}$$

where (x_{r1}, z_{r1}) represent the movement of rotational joint r_1 in the fore-and-aft and vertical directions, respectively. As there is no horizontal degree-of-freedom at the thighs in the model, $x_{r1} = 0$, and $z_{r1} = z_1$. Parameter l_i, (i=2, 3, …, 7), represents the horizontal distance from rotational joint (i-1) to the centre-of-gravity of rigid body i. Parameter h_i, i=1,2, …, 7, represents the vertical distance from rotational joint (i-1) to the centre-of-gravity of the rigid body i. Parameter l_{ri}, i=2, 3, …, 5, represents the horizontal distance from joint i to the centre-of-gravity of rigid body i. Parameter h_{ri}, i=2, 3, …, 5, represents the vertical distance from joint i to the centre-of-gravity of rigid body i.

All the length parameters were calculated from the coordinates of the relevant points. By substituting equations (4.4), (4.5) and (4.6) into Lagrange equations (4.3), the equations of motion written in matrix form can be derived as:

$$[M][\ddot{q}] + [C][\dot{q}] + [K][q] = [F] \tag{4.7}$$

where the matrices [M], [C], and [K], are shown in Appendix D. Matrix [F] is associated with the stiffness and damping of the buttocks and the input of the system z(t):

$$[F] = [(k_1 + z(t) + c_1 + \dot{z}(t)); 0; 0; 0; 0; 0; 0] \tag{4.8}$$

Using the Laplace transform, the solution of the above equation in the frequency domain was calculated, and the vertical in-line apparent mass at the seat pan was derived as the ratio from the acceleration to the dynamic force at the human-seat interface. The dynamic force was calculated as the deformation of the spring and damper beneath the thigh.

$$M_{zzs} = \frac{L[k_1 * (z(t) - z_1(t)) + c_1 * (\dot{z}(t) - \dot{z}_1(t))]}{L[z(t)]} = \frac{(k_1 + s * c_1) * (Z(s) - Z_1(s))}{s^2 * Z(s)} \tag{4.9}$$

where the symbol 'L' indicates the Laplace transform of the time-domain variable.

Similarly, the vertical in-line transmissibility and the fore-and-aft cross-axis transmissibility to the centre of vertebral body L3 were calculated using Equations 4.10 and 4.11, respectively.

$$T_{zz\_L3} = \frac{L[z_{L3}(t)]}{L[z(t)]} = \frac{Z_1(s) + (l_2 + l_{r2}) * \theta_2(s) + (l_3 + l_{r3}) * \theta_3(s) + (l_4 + l_{r4}) * \theta_4(s) + l_5 * \theta_5(s)}{Z(s)} \tag{4.10}$$

$$T_{xz\_L3} = \frac{L[x_{L3}(t)]}{L[z(t)]} = \frac{(h_2 + h_{r2}) * \theta_2(s) + (h_3 + h_{r3}) * \theta_3(s) + (h_4 + h_{r4}) * \theta_4(s) + h_5 * \theta_5(s)}{Z(s)} \tag{4.11}$$

where $Z_1(s)$, $Z(s)$, $\theta_i(s)$ are the Laplace transforms of the displacements of each body part, and $s = j * \omega; \omega = 2\pi * f; j = \sqrt{-1}$, f is the frequency.

A detailed description of how the equations of motion were derived and how the frequency response including the apparent mass and body transmissibility were calculated are shown in Appendix D.

4.2.4 Identification of stiffness and damping parameters

The stiffness and damping parameters were determined by comparing the predicted vertical in-line apparent mass from the model, the modulus and phase of the vertical in-line transmissibility to L3, and the modulus of the fore-and-aft cross-axis transmissibility to L3, with the corresponding measured data. The measured data were from an experiment conducted with eight subjects sitting on a rigid seat with a normal upright posture (Matsumoto and Griffin, 1998). The input excitation in the vertical direction was 1.0 ms^{-2} r.m.s. random vibration (0.5 to 20 Hz). The experimental data from one individual subject (subject 3: stature 1.77 m, total weight 75 kg) were used for the model calibration.

The error function used in the model calibration was:

$$Error(\lambda) = w_1 * \sqrt{\frac{1}{N}\sum_{i=1}^{N}(\left|M_{zzs\_m}(f_i)\right| - \left|M_{zzs\_m}\ e(f_i)\right|)^2} + w_2 * \sqrt{\frac{1}{N}\sum_{i=1}^{N}(\left|T_{zz\_L3\_m}(f_i)\right| - \left|T_{zz\_L3\_m}\ e(f_i)\right|)^2} +$$
$$w_3 * \sqrt{\frac{1}{N}\sum_{i=1}^{N}(\left|T_{zz\_L3\_ph}(f_i)\right| - \left|T_{zz\_L3\_ph}\ e(f_i)\right|)^2} + w_4 * \sqrt{\frac{1}{N}\sum_{i=1}^{N}(\left|T_{xz\_L3\_m}(f_i)\right| - \left|T_{xz\_L3\_m}\ e(f_i)\right|)^2} \quad (4.11)$$

where $M_{zzs\_m}(f_i)$ and $M_{zzs\_m}\ e(f_i)$ are moduli of the predicted and measured vertical apparent mass at frequency f_i. Similarly, $T_{zz\_L3\_m}(f_i)$ and $T_{zz\_L3\_m}(f_i)$ refer to the modulus of the transmissibility in the vertical and fore-and-aft directions predicted by the model. $T_{zz\_L3\_ph}(f_i)$ is the phase of the vertical transmissibility predicted by the model. The transmissibilities $T_{zz\_L3\_m}\,e(f_i)$, $T_{zz\_L3\_ph}\,e(f_i)$, and $T_{zz\_L3\_m}\,e(f_i)$ are the moduli and phase of the corresponding measured transmissibilities, and w_1, w_2, w_3, w_4 are the weightings added to each term. The error function is a function of λ, which contains 12 variables:

$$\lambda = \left[k_1, c_1, k_{r1}, c_{r1}, k_{r2}, c_{r2}, k_{r3}, c_{r3}, k_{r4}, c_{r4}, k_{r5}, c_{r5}, k_2, c_2\right] \quad (4.12)$$

These parameters were identified through minimising the error function over the frequency range 0.5 to 20 Hz in MATLAB (version R2013a) using the optimisation algorithm Complex (Bounday, 1985) and code (Qiu and Griffin, 2011).

The optimisation results (i.e., the identified parameters) are shown in Table 4.2. The predicted apparent mass is compared with the measured apparent mass in Figure 4.3 and the predicted transmissibilities are compared with the measured transmissibilities in Figure 4.4.

Table 4.2 Stiffness and damping coefficients obtained for the model

Stiffness		Damping	
k_1	1.46x10^5 N/m	c_1	2.38x10^3 Ns/m
k_{r1}	1.00x10^3 Nm/rad	c_{r1}	4.22x10^1 Nms/rad
k_{r2}	1.66x10^3 Nm/rad	c_{r2}	1.52x10^0 Nms/rad
k_{r3}	4.91x10^3 Nm/rad	c_{r3}	4.95x10^2 Nms/rad
k_{r4}	1.08x10^3 Nm/rad	c_{r4}	4.91x10^2 Nms/rad
k_{r5}	6.76x10^2 Nm/rad	c_{r5}	4.95x10^2 Nms/rad
k_2	2.74x10^4 N/m	c_2	1.66x10^2 Ns/m

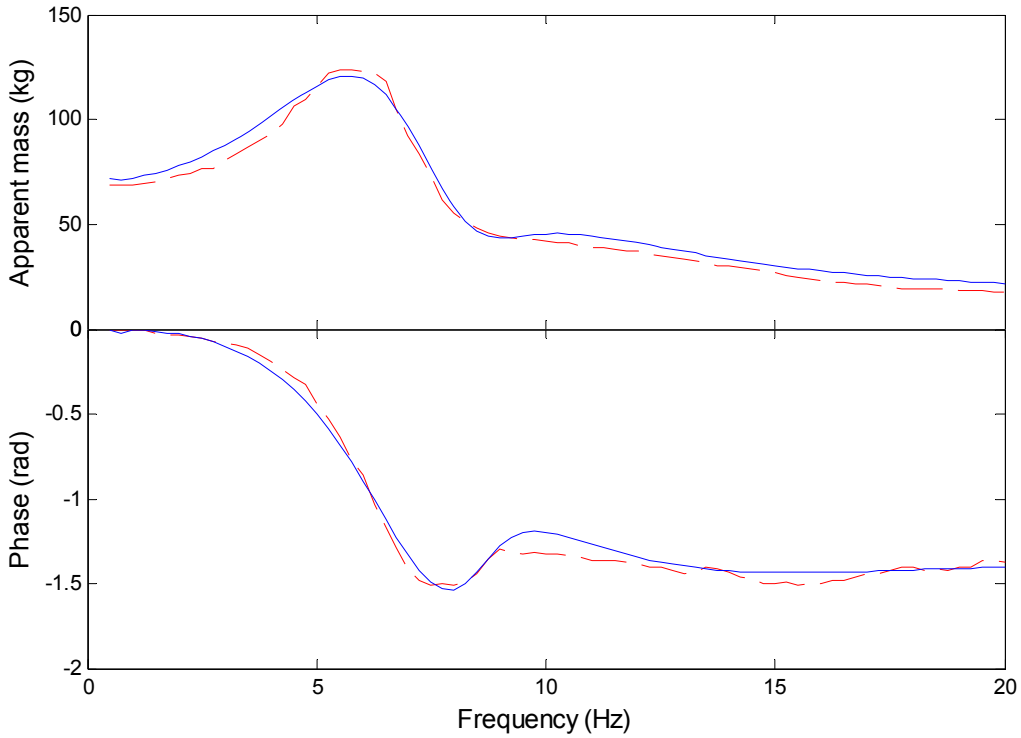

Figure 4.3 Modulus and phase of the apparent mass predicted by the model ('—') and the corresponding measured apparent mass ('– –').

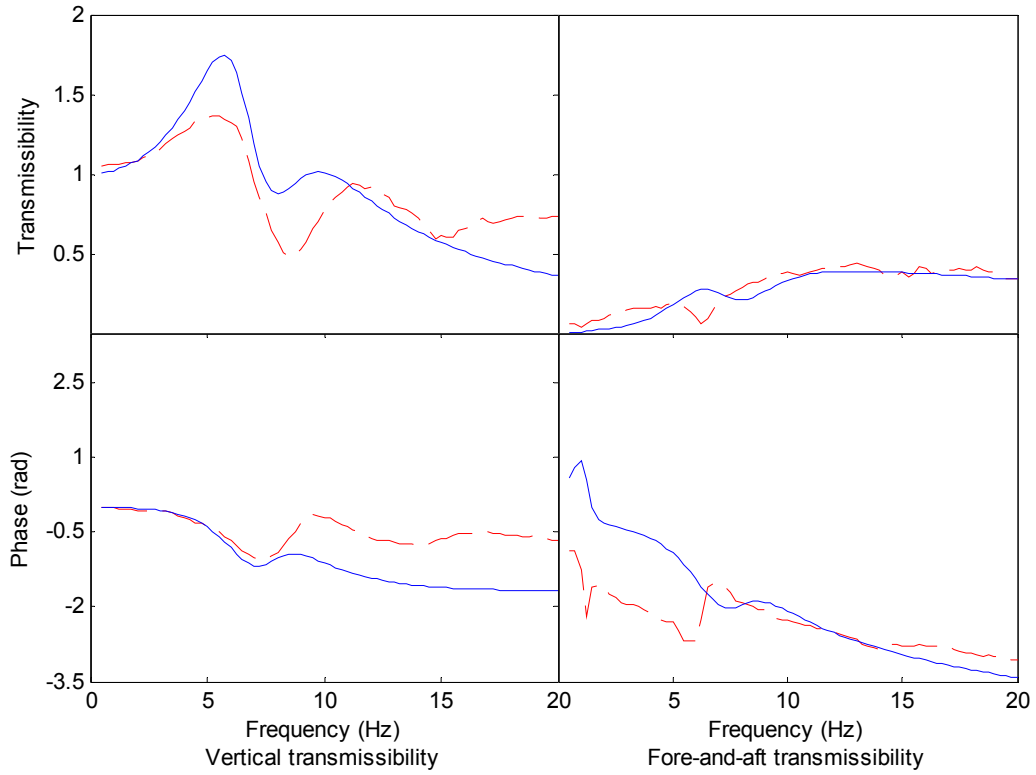

Figure 4.4 Modulus and phase of the vertical and fore-and-aft transmissibilities to L3 predicted by the model ('—') and the corresponding measured vertical and fore-and-aft transmissibilities ('– –').

As can be seen in Figures 4.3 and 4.4, the modulus and the phase of the vertical apparent mass predicted by the model are in close agreement with the measured data. The predicted vertical transmissibility to L3 shows a trend similar to the measured data, but there are some differences at the principal peak around 5 Hz. The second peak in the vertical transmissibility shows a greater disparity with the measured data. The phase of the vertical transmissibility matches reasonably well with the measured data, except at frequencies greater than 8 Hz where phase lags were observed. The modulus of the predicted fore-and-aft cross-axis transmissibility generally fits well with the measured data, but a phase lead was observed at frequencies less than 8 Hz.

4.3 Prediction of compressive force at L5/S1

The spinal forces calculated by this model were assumed to comprise a dynamic component induced by the vibration and a static part caused by the effect of gravity on the body. The static and dynamic forces were predicted at the intervertebral disc L5/S1 as this lowest spinal location was assumed to be of the greatest risk of injury during vertical whole-body vibration (e.g., Fritz, 2000). It was also assumed that all the masses above a rotational joint were supported by the joint alone, assuming the upper-body was supported only by the vertebrae of the spine.

Once the model parameters were identified, the dynamic component of the compressive force ($F_{L5/S1\_z\_d}$) at the intervertebral disc L5/S1 was predicted by calculating the vertical component of the force at rotational joint r_2. It was assumed that the vertical reacting force at the joint equals to

sum of the vertical inertial force of each components supporting on the joint. The transfer function from the vertical input acceleration to the body to the dynamic compressive force ($T_{L5/S1\_z}$) was calculated as the sum of the vertical inertia force of the segments supporting on the joint representing L5/S1. The segments include masses m_3, m_4, m_5 and m_6 (shown in Equation 4.13).

$$T_{L5/S1\_z} = \left\{ \begin{array}{l} (m_3 + m_4 + m_5 + m_6) * Z_1(s) + (m_3 + m_4 + m_5 + m_6) * (l_2 + l_{r2}) * \theta_2(s) + \\ \left[m_3 * l_3 + (l_3 + l_{r3}) * (m_4 + m_5 + m_6) \right] * \theta_3 + \left[m_4 * l_4 + (m_5 + m_6) * (l_4 + l_{r4}) \right] * \theta_4(s) + \\ \left[m_5 * l_5 + m_6 * (l_5 + l_{r5}) \right] * \theta_5(s) + m_6 * l_6 * \theta_6(s) \end{array} \right\} \Big/ Z(s) \quad (4.13)$$

For the normal sitting posture, the transfer function, $T_{L5/S1\_z}$, between the vertical acceleration at the seat and the force at L5/S1 is shown in Figure 4.5. With the predicted transfer function, a given time-history acceleration input can be applied to calculate the time-history of the spinal force, using inverse Fourier transform. Figure 4.6 shows the force time history (5 second from the 60 second signal, where the maximum force appeared at 22.5 second) predicted at L5/S1 exposed to 60-s random broadband vertical acceleration of 1.0 ms^{-2} r.m.s. with uniform distributed spectrum at the seat in a frequency range of 0.5 to 15 Hz. The result indicates how the spinal force depends on the magnitude of vibration.

The transfer function shows a clear peak around 5 Hz, and a second resonance at 8 Hz similar to the apparent mass.

The static compressive force ($F_{L5/S1\_z\_s}$) was calculated from the gravitation force on the body parts supported above rotation joint r_2:

$$F_{L5/S1\_z\_s} = (m_3 + m_4 + m_5 + m_6) * g \quad (4.14)$$

where g = 9.81 ms^{-2}, and (m_3+m_4+m_5+m_6) is the mass of the body parts supported on r_2 of the 75 kg subject represented by this model (i.e., (0.47+0.56+0.43+28.88)*75/81.3 = 27.99 kg), so, $F_{L5/S1\_z\_s}$ = 27.99 * 9.81 = 274.6 N.

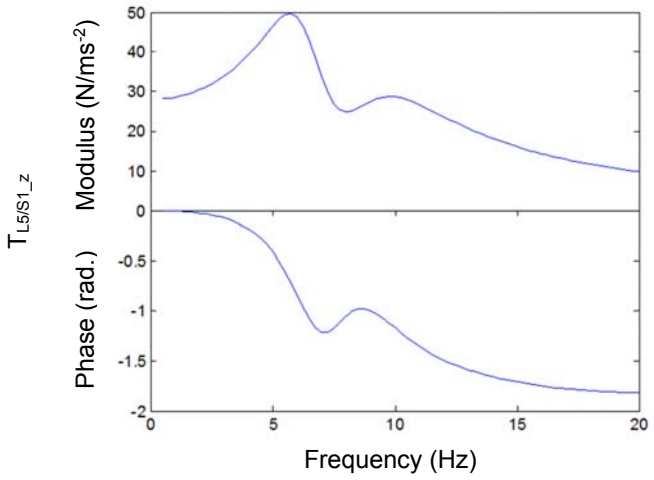

Figure 4.5 Transfer function between vertical acceleration at the seat and the vibration-induced compressive force predicted at L5/S1.

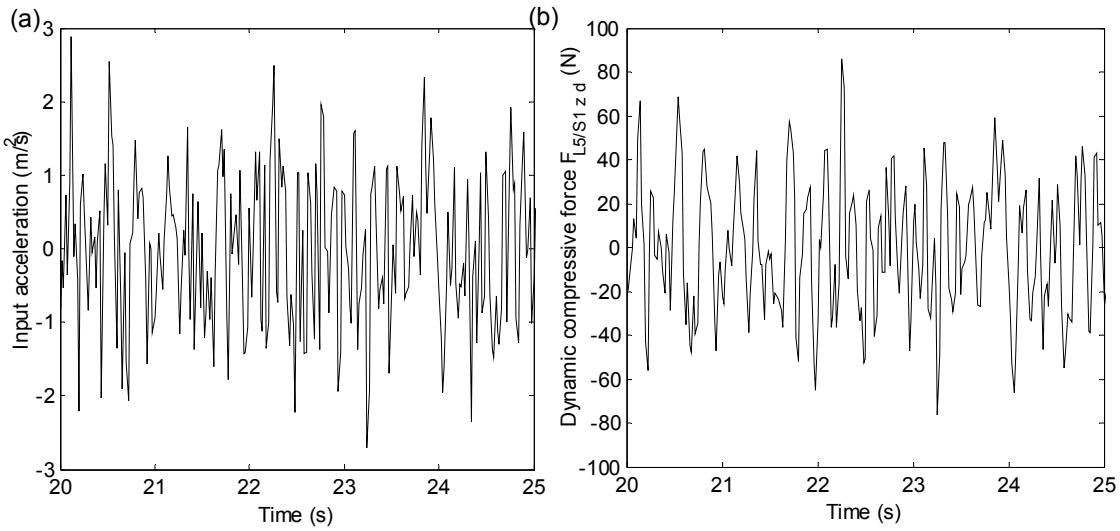

Figure 4.6 (a) 5-second example of the time-history of the vertical acceleration at the seat (1.0 ms^{-2} r.m.s. random vibration from 0.5 to 15 Hz). (b) The corresponding 5-second time-history of the dynamic compressive force.

The total compressive force was obtained as the sum of dynamic forces and the static force:

$$F_{L5/S1\_z} = F_{L5/S1\_z\_s} + F_{L5/S1\_z\_d} \quad (4.15)$$

The peak dynamic force produced by a random acceleration of 1.0 ms^{-2} r.m.s. (0.5-15 Hz) was about 80 N over 60 s, so the peak total force at L5/S1 was around 355 N. With this vibration input, the dynamic compressive force contributed about 23% to the peak total force. With an increase in the acceleration magnitude, the peak dynamic force will show proportional increases, because the model is linear. Such increase in the peak dynamic spinal force will contribute to an increase in the peak total spinal force.

4.4 Discussion

A multi-body model of the seated human body with representation of spinal anatomy has been developed to predict the loads at intervertebral discs in the lumbar region. The model predicted the apparent mass and the vertical transmissibility to the spine with a resonance around 5 Hz, consistent with experimental data. At the principal resonance, the whole-body mode was dominated by vertical and fore-and-aft motion of the pelvis with bending of the spine and no translational deformation within the spine, as suggested by Kitazaki and Griffin (1997). A second resonance at about 8 Hz in the vertical seat to L3 transmissibility may be caused by pitch motion of the pelvis and vertical motion of the viscera (Kitazaki and Griffin, 1997). It has been suggested that the motion of the pelvis is mainly influenced by deformation of the soft buttocks tissue beneath the pelvis (Matsumoto and Griffin, 2001).

It was found that the inclusion of a separate visceral mass in the model was more appropriate than distributing the visceral mass to other body parts in the model. A visceral mass supported on the pelvis seems more consistent with the real situation, as the movement of the viscera is fairly independent of the movement of the lumbar spine. The visceral mass (mass 7) was initially

considered to be distributed into various spinal levels including masses 3, 4, 5 and 6 (Figure 4.1), so as to form a six degree-of-freedom model. With the same parameters (i.e., stiffness and damping coefficients of the joints), the vertical transmissibility to L3 predicted by this six degree-of-freedom model without lumped visceral mass was compared to the corresponding transmissibilities measured and predicted by the current model (Figure 4.7). The representation of visceral mass in the multi-body model was found to decrease the peak transmissibility to L3. The involvement of viscera improved the prediction of the vertical transmissibility to the spine in the current model compared with the measured data, The above findings about the effect of visceral mass was consistent with the modelling studies from Matsumoto (1999).

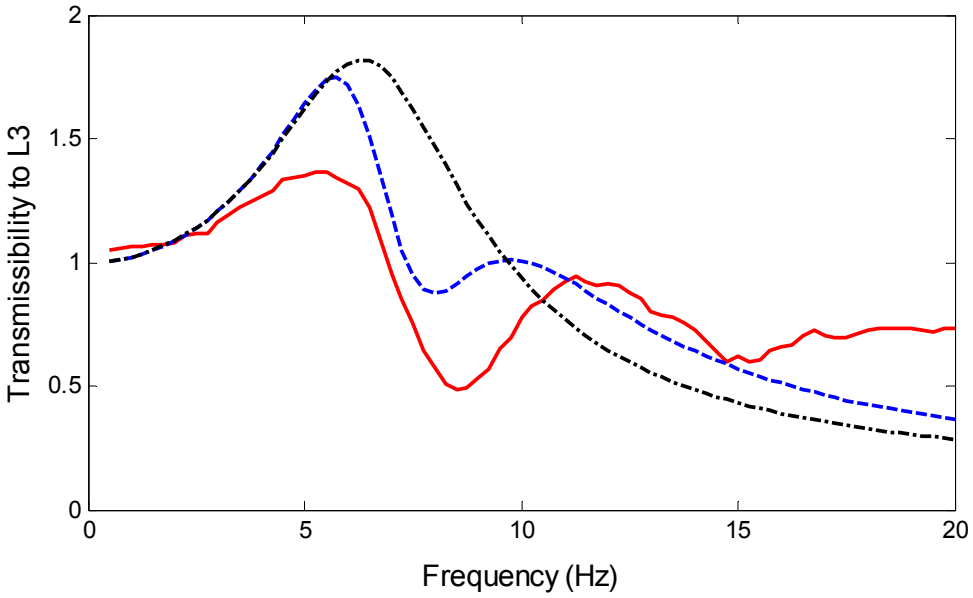

Figure 4.7 Predicted vertical transmissibility to L3 by the current 7 degree-of-freedom model ('——') and by a 6 degree-of-freedom model without visceral ('—•—'), compared with the measured vertical transmissibility to L3 ('—').

The spinal forces calculated by this model consist of both static and dynamic components. The transfer function between the dynamic spinal force and the vertical acceleration input at the seat showed a resonance around 5 Hz, which seemed to be associated with the bending of the spine as evident at the resonance of the apparent mass in a modal analysis of the response of the seated human body (Kitazaki and Griffin, 1997; Matsumoto and Griffin, 2001). The peak forces predicted with this model (355 N) were lower than those predicted by Wang *et al.* (2010) using a passive model without muscles (450 N) representing a seated human body of 75kg (same as the present study) when exposed to a similar input acceleration. The difference arises partly from Wang *et al.* (2010) distributing the visceral mass to spinal levels above the lumbar region. The visceral mass was distributed and added to different spinal levels, and the masses supporting on the L5/S1 disc was greater in the model from Wang *et al.* (2010) than the present model. The visceral (mass 7) was supported on the pelvis (mass 2) in the present study (Figure 4.1), without contributing to the calculation of spinal loads at the disc (L5/S1). It appeared that a model with the visceral mass

supported on the pelvis was more reasonable than distributing the mass to different spinal levels (as discussed in the previous paragraph).

The absence of muscles in the current model may cause underestimation of both static and dynamic spinal forces, because the spinal muscles contract, partly to support the static weight of the body and partly in response to vibration (Robertson and Griffin, 1989) and so add extra loads to the spine, which may not be negligible relative to the other sources of internal load (e.g., Wang *et al.*, 2010). A comparison between a model with active muscles and a passive model showed a 56% increase in the predicted peak compressive force with active muscles (Wang *et al.*, 2010). The force predicted with active muscles has been considered consistent with some in-vivo measurements of static spinal loads (e.g., Wilke *et al.*, 2001). Representation of muscles seems necessary in models of this type, but because muscle activity is highly dependent on sitting posture, the effect of posture should also be considered.

Posture has a large influence on spinal loads because the curvature of the spine, the centre of gravity of the body, and the muscle activity change with posture. An influence of body posture on internal loads has been reported with both in-vivo measurements of static spinal loads (e.g., Wilke *et al.*, 2001; Rohlman *et al.*, 2011) and a finite element model (e.g., Pankoke *et al.*, 1998). The current simple model is further developed in later sections to include the forces arising from muscle activity and the influence of sitting posture.

4.5 Conclusion

A multi-body model of the seated human body with seven degrees of freedom has been developed with a spinal structure appropriate for predicting the compressive forces in the lumbar spine. Seven rigid bodies connected with revolute joints and force elements were capable of reflecting vertical apparent mass. The model would need to be further developed to predict with accuracy of the vertical and fore-and-aft transmissibilities at the level of the lumbar spine under vertical excitation. The model can be developed to include representation forces from muscles so as to investigate the effect of posture on loads in the spine during exposure to whole-body vibration and mechanical shock.

Chapter 5. Biodynamic modelling of spinal forces caused by vertical vibration in three sitting postures

5.1 Introduction

Spinal loads measured in-vivo in static conditions showed that the static spinal loads varied with sitting posture (e.g., Sato *et al.*, 1999; Wilke *et al.*, 2001). In general, sitting with the body bent forward induced greater static compressive loads than sitting with the body upright or bent backward. More information about the measurements of spinal loads in-vivo has been described in Chapter 2 (Section 2.6.2.1).

In-vivo measurements of spinal loads have been restricted to static conditions, so biodynamic models, calibrated with measured apparent mass and the transmissibility of the body, have been used to predict the spinal loads associated with whole-body vibration and shock (e.g., Pankoke *et al.*, 1998; Bazrgari *et al.*, 2008). To predict the internal loads at the lumbar spine, a biodynamic model should reflect the anatomy of the body and represent both the overall biodynamic response of the body and the modes of the lumbar spine associated with vibration.

Sitting posture not only affects static spinal loads, but also affects the resonance frequency and the dynamic response at the resonance of both the apparent mass and the transmissibility of the body (e.g., Fairley and Griffin, 1989; Kitazaki and Griffin, 1998; Zheng *et al.*, 2011a). Changing from a 'slouched' sitting posture to a 'normal' sitting posture and then to an 'erect' sitting posture has been found to increase both the principal resonance frequency in the vertical apparent mass at the seat and the apparent mass at the resonance progressively (Kitazaki and Griffin, 1998). The transmissibility of the body measured in the 'normal', 'slouched' and 'erect' postures showed a similar pattern to the apparent mass, especially in the transmissibilities to the thoracic spine (e.g., T1, T6, and T11) (Kitazaki and Griffin, 1998). Apart from alterations in body geometry due to postural change (i.e., pelvis rotation and spinal curvature), it was observed that when changing from a 'slouched' posture to an 'erect' posture subjects tensed the muscles in their upper bodies (Fairley and Griffin, 1989), indicating muscle activation changes with posture.

A current standard (ISO2631-5: 2003) provides a method for predicting the forces in the spine and a method for assessing the health risk to the spine from the predicted forces. However, the effect of body posture on the spinal forces is not considered. Findings from the above studies suggest the need to investigate the effects of posture on spinal loads in dynamic conditions.

A change in posture will change the body geometry (e.g., spine curvature) and change the muscle activity used to maintain the body stability (Blüthner *et al.*, 2002). To model the effects of posture on spinal loads associated with vibration and shock, biodynamic models with representation of the muscle forces are needed. Muscle activation always adds loads to the spinal discs, due to its

architecture (see Chapter 2, Section 2.5.2). Without consideration of muscle activity the spinal forces predicted by a biodynamic model will be underestimated.

A simple multi-body model of a seated human body with lumbar representation has been developed with the capability of reflecting the vertical apparent mass and both the vertical inline transmissibility and fore-and-aft cross-axis transmissibility to the lumbar spine (Chapter 4). The compressive spinal force was predicted from the superposition of the force due to gravity acting on the body part supported on the intervertebral disc level and the inertial forces from the same body mass caused by vibration. However, without muscle representation, the predicted spinal force was underestimated compared to static measurements and the forces predicted by other models for similar conditions (e.g., Wang *et al.*, 2010).

The human muscular system is complex and the activation of muscles in both static and dynamic conditions is yet to be clarified. To predict more appropriate spinal loads associated with vibration and shock and study the effects of variations in sitting posture (i.e., erect, normal, and slouched) on the spinal forces, the simple multi-body model in Chapter 4 was further developed in this study with consideration of the forces from muscles. The advantages and disadvantages of a simple representation of the muscles in predicting spinal forces are also investigated.

5.2 Development of the model

5.2.1 Model description (geometry, mass and inertial properties)

The seven degree-of-freedom multi-body model of the seated human body developed in Chapter 4 was further developed with consideration of muscle forces. The geometry of the model in each posture was determined from the information provided by Kitazaki and Griffin (1997), partly from direct anthropometric measurements and partly derived from previous studies (e.g., Privitzer and Belytschko, 1980). The coordinates for nodes representing centres of vertebral bodies along the spine from the pelvis to the head in erect, normal, and slouched sitting postures were determined, showing different spine curvatures and pelvic rotation angles. The mass and inertial properties of the body segments in the current model were determined based on the mass distributions of a median person (i.e., 50th percentile) in different postures from the same literature. The geometry, mass, and inertial properties can be further adjusted to represent an individual subject with scaling factors correlated with the total body mass (Matsumoto and Griffin, 2001).

The initial positions of the rotational joints in the three sitting postures are shown in Table 5.1. The position of the centre of gravity, the inertial properties (including the mass) of each body segment in three sitting postures are shown in Table 5.2.

Table 5.1 Initial position for the centre of gravity of each body segment and rotational joint in three sitting postures.

Mass/joint	Centre of gravity of each segment (m) (x_{i0}, z_{i0}), (x_{ri0}, z_{ri0})		
	Erect posture	Normal posture	Slouched posture
m_1 (thighs)	-	-	-
m_2 (pelvis)	(-0.0078, 0.1061)	(-0.0244, 0.1036)	(-0.0279, 0.1026)
m_3 (L5)	(-0.1186, 0.1820)	(-0.1476, 0.1651)	(-0.1525, 0.1604)
m_4 (L4)	(-0.0701, 0.2193)	(-0.1065, 0.2047)	(-0.1128, 0.2008)
m_5 (L3)	(-0.0297, 0.2575)	(-0.0713, 0.2451)	(-0.0784, 0.2420)
m_6 (head-L2)	(0.0018, 0.6183)	(-0.0105, 0.6131)	(0.0479, 0.6082)
m_7 (viscera)	(0.0073, 0.2450)	(-0.0285, 0.2450)	(-0.0306, 0.2450)
r_1[a] (pelvis/thigh)	(0, 0)	(0, 0)	(0, 0)
r_2 (L5/S1)	(-0.0636, 0.1666)	(-0.0895, 0.1488)	(-0.0939, 0.1437)
r_3 (L4/L5)	(-0.0450, 0.2007)	(-0.0776, 0.1849)	(-0.0833, 0.1806)
r_4 (L3/L4)	(-0.0272, 0.2384)	(-0.0662, 0.2249)	(-0.0729, 0.2214)
r_5 (L2/L3)	(-0.0175, 0.2749)	(-0.0596, 0.2644)	(-0.0663, 0.2624)
[b]M_{upper}	(-0.0430, 0.5003)	(-0.0635, 0.4980)	(-0.0414, 0.5042)
[b]M_{lower}	(-0.0919, 0.1511)	(-0.1149, 0.1324)	(-0.1187, 0.1270)

[a] r_1 represents the ischial tuberosities for which the coordinates are (0, 0), as defined in measurements by Kitazaki and Griffin (1997).

[b] M_{upper} and M_{lower} refers to the connection points for muscle in present model.

Table 5.2 Mass and inertial properties for each segment in all three sitting postures.

Mass / joint	Mass m_i (kg)	Moment of inertia[a] I_i (kg.m^2)		
		Erect posture	Normal posture	Slouched posture
m_1 (thighs)	12.96	-	-	-
m_2 (pelvis)	10.90	9.11×10^{-2}	9.11×10^{-2}	9.11×10^{-2}
m_3 (L5)	0.47	9.93×10^{-4}	9.93×10^{-4}	9.93×10^{-4}
m_4 (L4)	0.56	1.43×10^{-3}	1.43×10^{-3}	1.43×10^{-3}
m_5 (L3)	0.43	1.48×10^{-3}	1.48×10^{-3}	1.48×10^{-3}
m_6 (head-L2)	28.88	5.89×10^{-1}	5.98×10^{-1}	6.17×10^{-1}
m_7 (viscera)	12.80	-	-	-

[a] The moment of inertia was calculated around the centre of gravity of each part.

5.2.2 Modelling of muscles

The muscular system is involved in the generation of motion of the spine and the maintenance of the postural stabilisation of the spine (Stokes *et al.*, 2010). The complex muscular system of the lower back consists of numerous slips of muscle connected between individual lumbar vertebrae and either the thorax, the pelvis, the sacrum, or femora (Stokes and Gardner-Morse, 1999). Generally, several primary groups of muscles have been considered in static biomechanical models of the lumbar spine, including erector spinae, abdominal muscles, psoas major, multifidus, quadratus lumborum and latissimus dorsi (Stokes and Gardner-Morse, 2001). For simplification, the muscle groups are usually modelled with simplified sets of muscles, represented by force vectors (e.g., Wang *et al.*, 2010) or linear/nonlinear springs and dampers (e.g., Stokes *et al.*, 2010). The parameters used in these models were determined either from EMG measurements (e.g., Marras and Granata, 1997), or an optimisation algorithm usually aimed at minimizing the sum of the cubic stress of all the muscle fascicles (e.g., Stokes and Gardner-Morse, 2001; Bazrgari *et al.*, 2008). These muscle models are complex with many assumptions and remain to be investigated whether they are appropriate for modelling muscle behaviour in dynamic conditions.

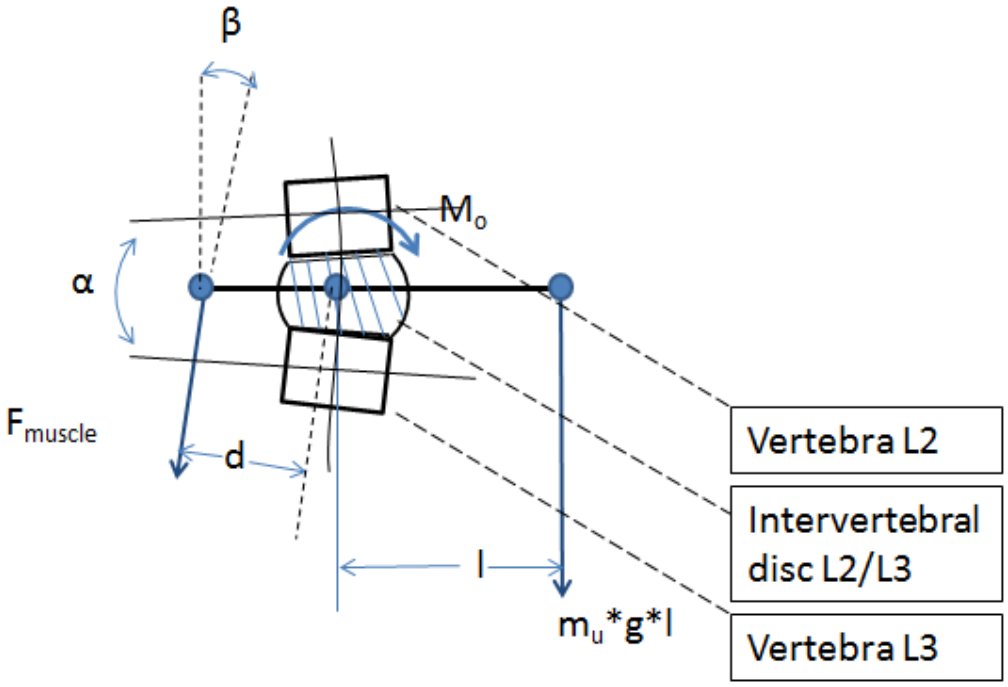

Figure 5.1 Disc angle and lever arm system used to calculate static spinal force

A major role for the muscles when sitting is to maintain the stability of the body. According to the review of the muscular system in the lumbar region in Chapter 2 (Section 2.5.2), the main group of muscles controlling postural stability in the sagittal plane connects from the thoracic spine to the pelvis (e.g., erector spinae). It seems appropriate to investigate whether the muscles can be modelled simply and effectively, for predicting spinal forces in both static and dynamic conditions when sitting in different postures. For simplicity, a linear spring was attached from the T7 spinous process to the sacrum to reflect the overall effect of muscles in the body above the seat (Figure

5.2). This spring is inclined with respect to the vertical direction, and the static and dynamic muscle forces are generated in the direction from the spinous process of T7 to the sacrum (S1) with an inclination angle β with respect to the vertical direction (Figure 5.1). The muscle force was calculated both statically and dynamically in each sitting posture, and its vertical component was further used to calculate the vertical spinal force.

.

Table 5.3 Disc angles in the lumbar spine in each of the three postures.

Disc angle (α)	Erect posture	Normal posture	Slouched posture
L2/L3	13.10º	7.76º	5.88º
L3/L4	10.87º	6.73º	5.31º
L4/L5	3.37º	2.18º	1.77º
L5/S1	-9.88º	-9.17º	-9.02º

In the static condition, the force in the element was calculated based on the moment equilibrium for the body segment. The method can be explained by a lever system model shown in Figure 5.1 with consideration of disc flexion/extension.

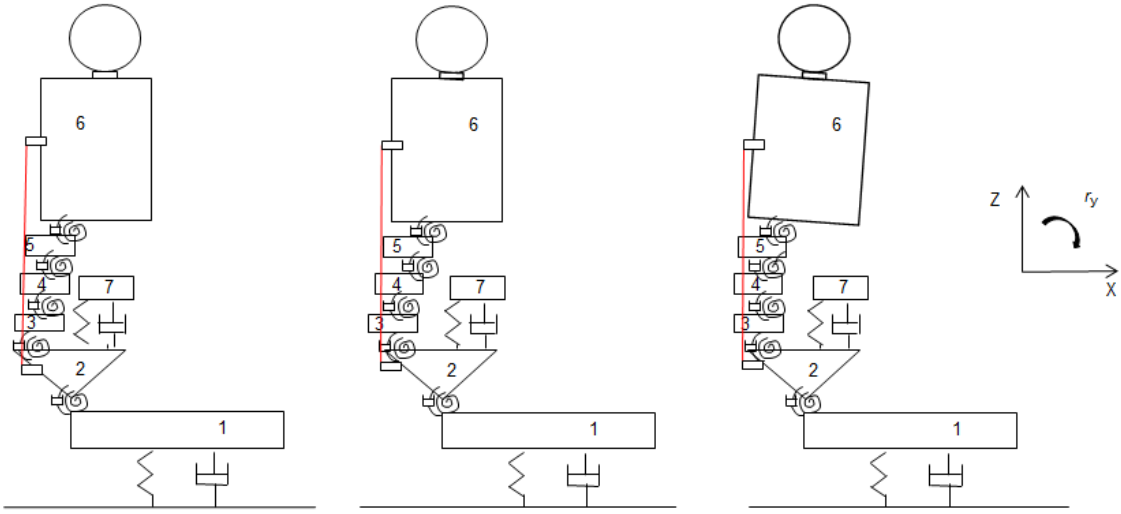

Figure 5.2 Multi-body model of the seated human body in three sitting postures: erect, normal, and slouched (from left to right). 1 - thighs; 2 - pelvis; 3 - L5; 4 - L4; 5 - L3; 6 - upper-body from head to L2; 7 - viscera in the abdomen; —— muscle connecting the T7 spinous process to the sacrum (S1).

The upper body was assumed to be in moment equilibrium around the centre of the vertebral disc (L2/L3), which means the moments generated by muscle forces ($F_{muscle} * d$) balanced the moments (M_o) generated by the non-concentric compression of the disc L2/L3 plus the moments generated by the pull of gravity on the upper body ($m*g*l$), as shown in Equation 5.1:

$$F_{muscle} * d = M_o + m * g * l \quad (5.1)$$

The moment generated by non-concentric compression of the disc was calculated as the product of rotational stiffness of the disc (k_r) and angle between the adjacent vertebra (α), expressed as:

$$M_o = k_r * \alpha \tag{5.2}$$

The inclination angle, α, of the intervertebral disc L2/L3, the horizontal distance, l, from the centre of gravity of the upper body to the disc centre, and the horizontal distance, d, from muscle force to the centre of the disc, were determined directly from the geometry of the model and varied with posture. As such, the calculation of static muscle force, F_{muscle}, also varies with posture.

The stiffness of the spring representing muscles at the back and the rotational stiffness of the L2/L3 intervertebral disc, together with other parameters in the present model (i.e., stiffness and damping for intervertebral discs and buttocks tissues) were determined by dynamic calibration as described below.

The static compressive spinal force was then calculated as the sum of the vertical component of the static muscle force (F_{muscle}) and the force arisen from the effect of gravity on the upper body (Equation 5.3). The vertical static muscle force ($F_{\text{muscle\_z}}$) was calculated as the projection of the static muscle force (F_{muscle}) considering the angle from the spinous process of T7 to sacrum (β).

$$F_{static} = F_{muscle\_z} + m * g \tag{5.3}$$

5.2.3 Equations of motion

Similar to the development of the previous model (Chapter 4), the equations of motion of the current model were derived using Lagrange equations with the assumption that all body parts oscillate around their equilibrium positions with small displacements in the condition of free vibration (Equation 5.4). Similarly, it was also assumed that the inclination angle of the spring representing the muscle force is constant (β) during the vibration (see Equation 5.7).

$$\frac{d}{dt}\left(\frac{\partial T}{\partial \dot{q}_i}\right) + \frac{\partial D}{\partial \dot{q}_i} + \frac{\partial U}{\partial q_i} = 0 \; ; \; q_i = \left[x_1; z_1; \theta_2; \theta_3; \theta_4; \theta_5; \theta_6; z_7\right] \tag{5.4}$$

where z_1 and z_7 represent the vertical displacements of the thighs and viscera, and $\theta_2, \theta_3, \theta_4, \theta_5, \theta_6$, represent the absolute rotational displacements of the pelvis, the lumbar spine (at L5, L4, and L3), and the upper-body. The kinetic energy, T, potential energy, U, and dissipation function, D, of the system were calculated as:

$$T = \frac{1}{2}\sum_{i=1}^{7} m_i(\dot{x}_i^2 + \dot{z}_i^2) + \frac{1}{2}\sum_{i=2}^{6} I_i\dot{\theta}_i^2 \tag{5.5}$$

$$\begin{aligned} D = {} & \frac{1}{2}c_1(\dot{z}_1 - \dot{z})^2 + \frac{1}{2}c_{r1}(\dot{\theta}_2)^2 + \frac{1}{2}c_{r2}(\dot{\theta}_3 - \dot{\theta}_2)^2 + \frac{1}{2}c_{r3}(\dot{\theta}_4 - \dot{\theta}_3)^2 + \frac{1}{2}c_{r4}(\dot{\theta}_5 - \dot{\theta}_4)^2 \\ & + \frac{1}{2}c_{r5}(\dot{\theta}_6 - \dot{\theta}_5)^2 + \frac{1}{2}c_2(\dot{z}_7 - \dot{z}_8)^2 \end{aligned} \tag{5.6}$$

$$U = \frac{1}{2}k_1(z_1 - z)^2 + \frac{1}{2}k_{r1}(\theta_2)^2 + \frac{1}{2}k_{r2}(\theta_3 - \theta_2)^2 + \frac{1}{2}k_{r3}(\theta_4 - \theta_3)^2 + \frac{1}{2}k_{r4}(\theta_5 - \theta_4)^2 + \frac{1}{2}k_{r5}(\theta_6 - \theta_5)^2 + \frac{1}{2}k_2(z_7 - z_8)^2 + \frac{1}{2}k_m\left[\cos\beta * (z_{T7} - z_{S1}) + \sin\beta * (x_{T7} - x_{S1})\right]^2 \quad (5.7)$$

where m_i is the mass of each body part, (x_i, z_i) and $(\dot{x}_i, \dot{z}_i)$ represent the displacement and velocity of each body at the centre of gravity in the *x* and *z* directions associated with whole-body vibration, and index *i* = 1, 2, 3, 4, 5, 6, 7 denotes the number of body parts. The combinations of k_1 and c_1, and k_2 and c_2, represent the stiffness and damping coefficients of the spring and damper beneath thighs and viscera, respectively. Parameters k_{ri} and c_{ri} represent the stiffness and damping coefficients of the rotational joints r_j, where *j* =1, 2, 3, 4, 5 denotes the number of the rotational joints. The displacements at the spinous process of T7 and the sacrum in the *x* and *z* directions are represented by (x_{T7}, z_{T7}) and (x_{S1}, z_{S1}) associated with whole-body vibration when the spring (with stiffness k_m) representing the muscles is attached. The above displacements and velocities were calculated with respect to model geometry (Chapter 4).

The responses of the above equations of motion were calculated in the frequency domain. The expressions for the vertical in-line apparent mass, the vertical in-line transmissibility, and fore-and-aft cross-axis transmissibility to the centre of vertebral body L3 followed the equations in Chapter 4 (Equations 4.7 and 4.8).

5.2.4 Calibration of models and parameters

The values for the dynamic parameters representing the rotational joints (i.e., stiffness and damping) and translational springs and dampers in each sitting posture were determined by comparing the vertical in-line apparent mass, the modulus of the vertical in-line transmissibility to L3, and the modulus of the fore-and-aft cross-axis transmissibility to L3 predicted by the model with those measured in experiments (Zheng *et al*, 2011a) via an optimisation algorithm (Bounday, 1985; Qiu and Griffin, 2011). The applied biodynamic data were median values from 12 subjects (median weight 68 kg and median stature 176 cm) measured in three sitting postures by Zheng *et al.*, (2011a) with 1.0 m/s^2 r.m.s. random vertical vibration from 0.5 to 15 Hz.

The initial values and the lower and upper bounds of the stiffness of the intervertebral disc joints were determined from published in-vitro measurements (Schultz *et al.*, 1979). The initial values and the lower and upper bounds of the remaining parameters (i.e., stiffness and damping of buttocks tissues and the viscera connection) were determined from the model developed in Chapter 4 and adjusted during the optimisation procedure.

Due to the complexity of the objective function, it could not be guaranteed that the optimisation process results in the global optimal solution. Therefore, different sets of the initial values of the optimisation parameters were tried and yielded a number of sets of model parameters during the process. To determine the best set of model parameters, the static compressive spinal force based on Equation (5.3) was calculated for each set of parameters and compared with the measured in-vivo compressive spinal force (Wilke *et al.*, 2001). The set of parameters that offered the closest

match to the measured static spinal force was adopted in the model. The calibration process described above was carried out for each sitting posture.

The model parameters identified from the above optimisation processes for each sitting posture are listed in Table 5.4. Comparisons between the predicted and measured apparent mass and transmissibilities in each sitting postures are shown in Figures 5.3 and 5.4, respectively.

As shown in Figure 5.3 and Figure 5.4, the moduli and phases of the predicted and measured vertical apparent masses match closely. The resonance frequencies of the apparent mass in the three postures showed some differences. The apparent mass at the resonance decreased in order from the erect posture to the normal posture, and to the slouched posture. A similar decreasing trend was observed in the stiffness of the buttocks tissues, k_1 (Table 5.4).

The match between the measured and predicted transmissibilities to L3 in the vertical and fore-and-aft directions was reasonable in terms of both the resonance frequencies and apparent mass at the resonance. However, in all three postures, the vertical transmissibility at resonance predicted with the model was lower than the measured transmissibility.

Table 5.4 Stiffness and damping coefficients obtained for the model in three sitting postures.

Stiffness and damping	Erect posture	Normal posture	Slouched posture
k_1 (N/m)	1.06×10^5	6.88×10^4	5.04×10^4
c_1 (Ns/m)	3.54×10^3	3.61×10^3	2.85×10^3
k_2 (N/m)	1.93×10^4	1.77×10^4	3.17×10^4
c_2 (Ns/m)	1.87×10^2	1.72×10^2	3.12×10^2
k_{r1} (Nm/rad)	1.66×10^3	1.83×10^3	4.24×10^3
c_{r1} (Nms/rad)	1.26×10^1	1.86×10^1	4.43×10^1
k_{r2} (Nm/rad)	5.80×10^1	5.80×10^1	1.72×10^2
c_{r2} (Nms/rad)	1.00×10^0	1.00×10^0	4.90×10^2
k_{r3} (Nm/rad)	1.72×10^2	5.80×10^1	5.80×10^1
c_{r3} (Nms/rad)	4.99×10^2	4.99×10^2	4.99×10^2
k_{r4} (Nm/rad)	1.72×10^2	5.80×10^1	5.80×10^1
c_{r4} (Nms/rad)	3.05×10^1	4.99×10^2	2.99×10^0
k_{r5} (Nm/rad)	1.72×10^2	5.80×10^1	5.80×10^1
c_{r5} (Nms/rad)	1.41×10^1	4.99×10^2	1.00×10^0
k_m (N/m)	2.04×10^2	1.40×10^2	3.59×10^1

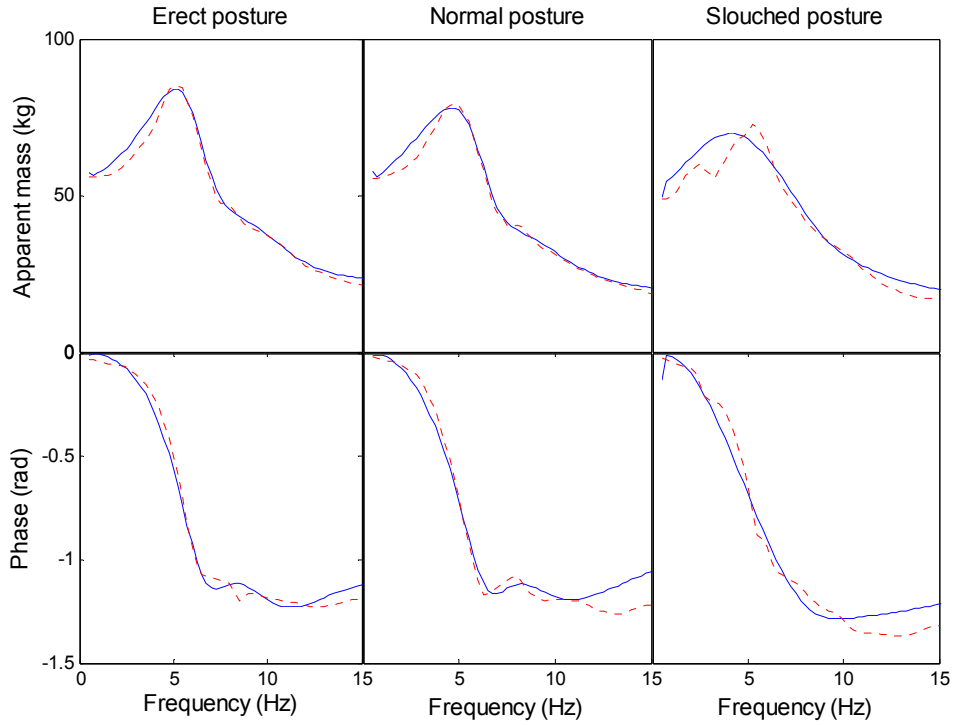

Figure 5.3 Modulus and phase of the apparent mass predicted by the model (——) and the corresponding measured apparent mass (------) in erect, normal, and slouched sitting postures.

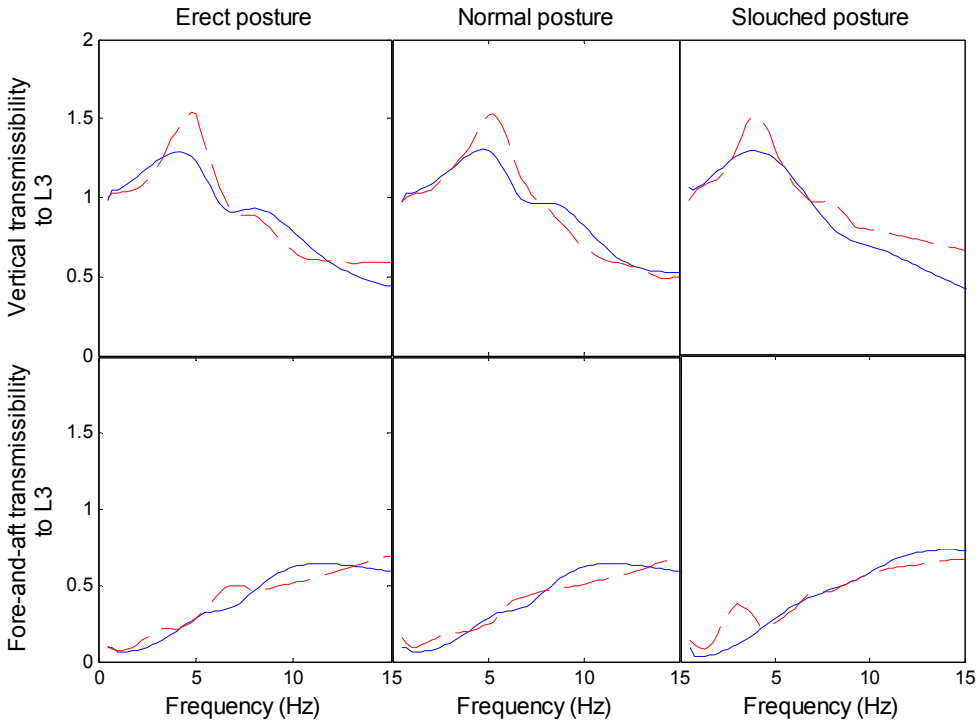

Figure 5.4 Modulus of the vertical and fore-and-aft transmissibilities to L3 predicted by the model (——) with corresponding measured vertical and fore-and-aft transmissibilities (------) in erect, normal, and slouched sitting postures.

5.3 Prediction of spinal forces

The compressive spinal forces at L5/S1 in each of the three sitting postures were calculated from the superposition of the static spinal forces (a postural-dependent constant calculated by the lever arm system illustrated in Figure 5.1) and the vertical dynamic spinal forces (the sum of the dynamic muscle force and the inertial force caused by the body mass supported on the intervertebral disc at joint r_2).

Table 5.5 Comparison between static loads predicted by the model and in-vivo measurements.

Postures	Erect posture	Normal posture	Slouched posture
Predicted in present study (L5/S1, 68 kg)	1032 N	803 N	1682 N
Measured by Wilke *et al.*, 2001 (L4/L5, 70 kg)	990 N	810 N	1620 N

With the identified model parameters, the static compressive force calculated using Equations 5.1 and 5.3 are shown in Table 5.5. The frequency-dependent transfer function, $T_{L5/S1\_z\_d}(f)$, from the vertical acceleration (input) to the dynamic compressive force (response) was computed for each posture (Figure 5.5).

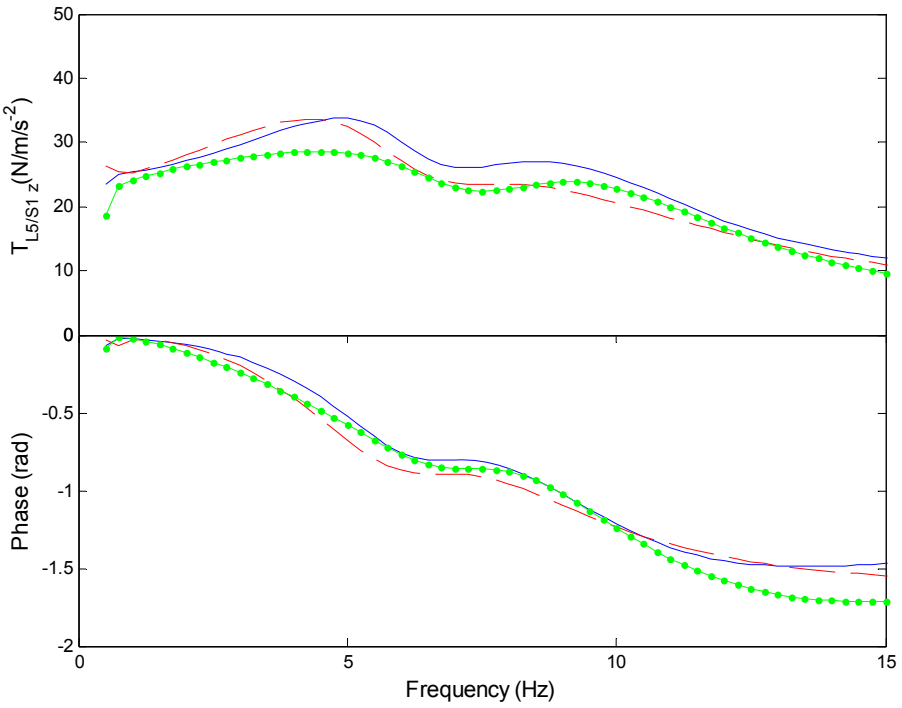

Figure 5.5 Transfer functions between vertical acceleration at the seat and the vibration-induced compressive forces at L5/S1 in three sitting postures (erect: '——'; normal: '------'; slouched: '–·–').

All three transfer functions showed a peak around 5 Hz. The transfer functions for the erect and normal sitting postures also showed a second peak around 8 Hz, similar to the resonance in the

vertical transmissibilities to L3. The static compressive spinal force at L5/S1 in the slouched posture was greater than the force in the erect and normal postures. The transfer functions from the acceleration to the dynamic spinal force in the erect posture and the normal posture showed a similar range of magnitudes over the frequency range 0 to 10 Hz, while the modulus of the transfer function for the slouched posture was less than the other two postures over the same frequency range.

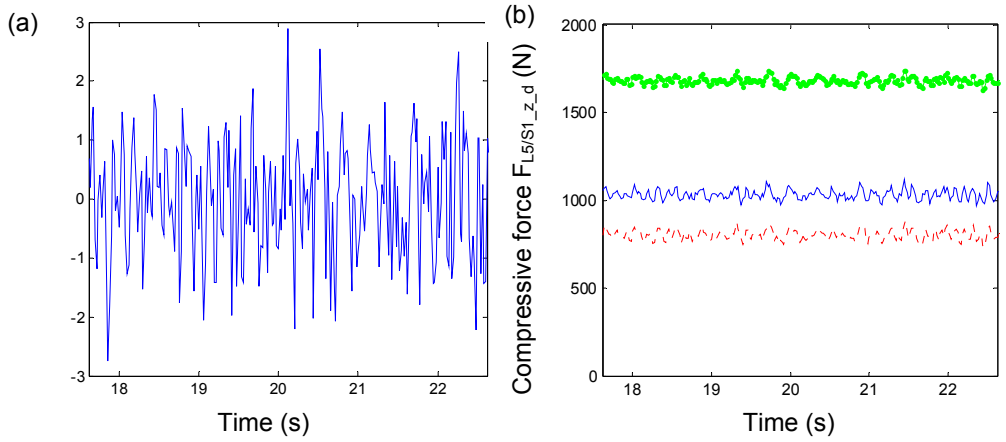

Figure 5.6 (a) Time-history of random vertical acceleration at the seat (1.0 m/s^2 r.m.s., 0.5 to 15 Hz); (b) Time-history of compressive force at L5/S1 for three postures (erect: '——'; normal: '------'; slouched: '–·–').

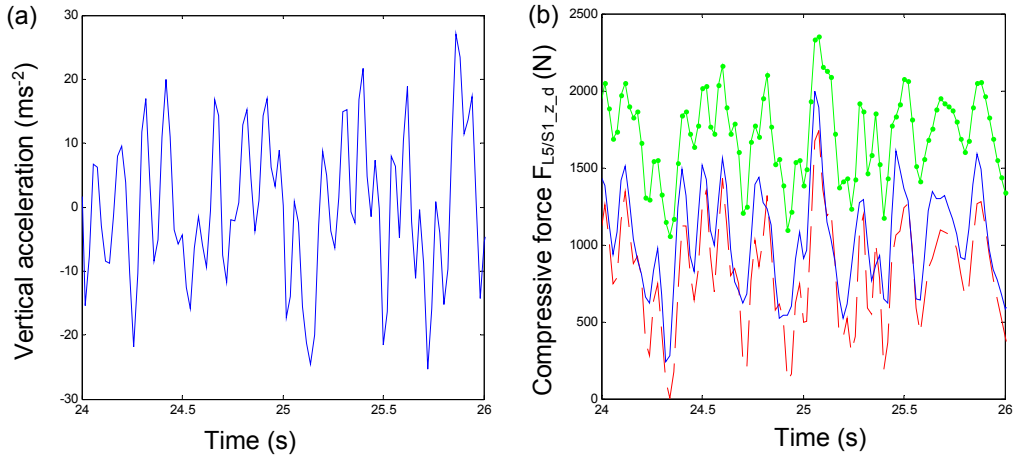

Figure 5.7 (a) Time-history of random vertical acceleration at the seat (10 m/s^2 r.m.s., 0.5 to 15 Hz); (b) Time-history of compressive force at L5/S1 for three postures (erect: '——'; normal: '------'; slouched: '–·–').

The transfer functions enable the dynamic spinal forces at L5/S1 to be calculated for a given acceleration input time history (Chapter 4). For example, with a 60-s random uniform distributed vertical acceleration of 1.0 m/s^2 r.m.s. at the seat with a flat bandwidth from 0.5 to 15 Hz, the calculated time histories of the compressive forces (static plus dynamic) at L5/S1 in the three postures are shown in Figure 5.6. It can be seen that the slouched posture caused a greater spinal force than the other two postures. This is mainly due to the increased static spinal forces while with low magnitudes of vibration the contribution of the dynamic spinal forces is relatively small. Since

the model is linear, the calculated dynamic forces will increase in proportion to the magnitude of the vibration. As shown in Figure 5.7, when the model was subjected to 60-s uniform distributed random vertical vibration of 10.0 m/s^2 r.m.s. at the seat with a flat bandwidth from 0.5 to 15 Hz, the total compressive force in each posture showed a greater variation with different static forces, due to the greater motion of upper body during the vibration. The maximum spinal force of the model in the three sitting postures when exposed to 1.0 m/s^2 r.m.s. and 10.0 m/s^2 r.m.s. vibration were shown in Table 5.6. With the greater magnitude of vibration, the slouched posture still showed the greatest compressive force, although the differences among the three postures were reduced.

Table 5.6 Predicted static, maximum dynamic, and maximum total vertical spinal force at L5/S1 when exposed to 1.0 m/s^2 r.m.s. random vertical vibration and 10.0 m/s^2 r.m.s. random vertical vibration, respectively.

Postures		Erect posture	Normal posture	Slouched posture
Predicted static force		1032 N	803 N	1682 N
Exposed to 1.0 m/s^2 r.m.s. random vertical vibration[a]	Maximum dynamic force	68 N	64 N	60 N
	Maximum total force	1100 N	867 N	1742 N
Exposed to 10.0 m/s^2 r.m.s. random vertical vibration[b]	Maximum dynamic force	736 N	692 N	633 N
	Maximum total force	1768 N	1495 N	2315 N

[a]60-s uniform distributed random vertical vibration of 1.0 m/s^2 r.m.s. from 0.5 to 15 Hz.[b]60-s uniform distributed random vertical vibration of 10.0 m/s^2 r.m.s. from 0.5 to 15 Hz

5.4 Discussion

5.4.1 Effect of posture on the predicted biodynamic response

A simple biodynamic model has been shown to be capable of predicting biodynamic responses of the human body sitting in three postures. The apparent mass was used to calibrate the model as the vibration is transmitted to the seated body directly from the seat-body interface. Most biodynamic models for predicting spinal loads seek to achieve a reasonable prediction of the apparent mass or dynamic force at the seat-body interface (e.g., Fritz, 2000; Seidel *et al.*, 2001; Wang *et al.*, 2010; Verver *et al.*, 2003). However, due to the complexity of the human body, the vibration transmitted through the body varies along the spine, as observed in the measurement of the transmissibility (e.g., Zheng *et al.*, 2011a) and indicated by modal analysis of body (e.g., Kitazaki and Griffin, 1997). The seat-to-head transmissibility was widely used in model calibration together with the apparent mass (e.g., Hinz *et al.*, 2007; Wang *et al.*, 2010), because the head motion was relatively easy to measure compared with the motion of the lumbar spine. However, the

head motion is greatly influenced by pitch motion of the head and varies with the location of measurement at the head (e.g., Paddan and Griffin, 1988). For predicting spinal loads in the lumbar region, seat-to-lumbar spine transmissibility seems more appropriate for the calibration of the model as it reflects the response of the lumbar spine to vibration, unaffected by local motion at distant body parts that do not have a significant effect on the force in the lumbar region.

Both the apparent mass and the transmissibility to L3 showed differences in the resonance frequency and the magnitude of the response at resonance among the three different sitting postures (Figures 5.3 and 5.4). The differences in apparent mass were mainly caused by changes in both geometry (i.e., changed coordinates of body segments due to changes of posture) and stiffness (mainly the stiffness of the buttocks tissues), as shown in Table 5.4. The stiffness of tissues at the buttocks decreased as the posture changed from erect to normal and then the slouched sitting posture, consistent with the modelling of Kitazaki and Griffin (1997). The decrease in the buttocks stiffness in a slouched posture might be explained by the increased contact area between the buttocks and seat pan, resulting in a decrease in the axial stiffness of the buttocks (Kitazaki and Griffin, 1997). The discrepancy in the predicted and measured responses (at the resonance frequency) in the vertical transmissibility to L3 may be due to simplification in modelling the pelvis (lack of representation of the response of the pelvis at the resonance frequency), where the body motion is dominated by pelvis motion and spine bending according to modal analysis (Kitazaki and Griffin, 1997). An alternative explanation may be that the use of joint stiffness measured in vitro for the intervertebral discs did not take into account the contribution of other muscular components (e.g., ligaments, muscles attached to the vertebral bodies). The muscle representation in the present model seems not sufficient to reflect the effect of these components in the local lumbar region, leading to an underestimate of the stiffness in the lumbar region and thus a lower response at the resonance in the vertical transmissibility to L3.

5.4.2 Modelling of muscles

The simple muscle representation in the current biodynamic model was intended to reflect the overall effect of the complex body back systems (i.e., muscles, ligaments, articular facet joints, and abdominal pressure) during sitting, not just the behaviour of an individual group of muscles (e.g., erector spinae). Representation of some local muscles in the lumbar region may improve the prediction of the motion of the lumbar spine, but the muscle system is complex and behaviour of individual elements has yet to be investigated, which limits the development of detailed muscle systems in a biodynamic model. It appears that the treatment of the muscle forces in the current simple model provided more reasonable predictions of both the static and dynamic spinal loads than the previous model without consideration of the muscle forces (Chapter 4).

The use of a lever-arm model (Figure 5.1) to estimate static compressive spinal forces at L5/S1 resulted in forces similar to in-vivo measurements of spinal loads (Equation 5.1; Table 5.5). The spinal loads measured in-vivo were expressed in terms of stress and converted into compressive spinal forces in this study by multiplying by the disc area. This may not be very accurate because this treatment assumes an even stress distribution over the intervertebral discs. In addition, differences in subject weight, stature, and posture result in different spinal forces in different

people. Although there was some inaccuracy, the static intervertebral forces predicted with the current model were appreciably greater than those solely due to the action of gravity on the body mass supported above the intervertebral disc (e.g., model developed in Chapter 4), indicating a crucial role of muscles in the generation of spinal loads, consistent with the suggestions from spine anatomy (e.g., Bugduk, 1997; see Chapter 2, Section 2.5.2).

The static compressive spinal force at L5/S1 was greater in the slouched posture than in the erect and normal postures, due to the greater horizontal distance from the centre of gravity of the upper body to the intervertebral disc, resulting in a greater muscle force in order to maintain body stability.

The dynamic muscle force arose from relative displacement between the two attachment points of the muscle in the model caused by the whole-body-vibration. The dynamic spinal loads, calculated as the superposition of the dynamic muscle force and the inertial force of the body mass supported on the disc, were predicted in terms of a frequency-dependent transfer function between the acceleration at the seat and the compressive forces at L5/S1. The transfer function in the normal sitting posture showed resonance around 5 Hz and 8 Hz, with a maximum magnitude of 40 N/ms^{-2}. Both resonances were influenced by motion of the body mass and the dynamic muscle force induced by the greater relative displacement between the attached points, consistent with the modal analysis of the response of the seated body (e.g., Kitazaki and Griffin, 1997; Matsumoto and Griffin, 2001). The differences between the acceleration to compressive force transfer functions in the three sitting postures were small, with the differences mainly due to differences in the vertical transmissibilities from the acceleration at the seat to the acceleration at the upper body.

Transfer functions between the vertical acceleration at the seat and compressive spinal forces were also predicted using biodynamic models developed by others (e.g., Fritz, 2000; Seidel *et al.*, 2001; Verver *et al.*, 2003). The transfer functions predicted in the present study, together with the transfer functions from the literature showed either one peak (e.g., Fritz, 2000; Verver *et al.*, 2003; present study) or multiple peaks (e.g., Seidel *et al.*, 2001) in the low frequency range (2.5 to 6 Hz). The peaks in all transfer functions were about 40 N/ms^{-2} to 90 N/ms^{-2}, being 2 to 3 times the modulus of the transfer function at frequencies close to 0. The spinal loads predicted from the relatively simple biodynamic model developed in this study, and also the loads predicted by some existing more complex models, showed that with lower magnitudes of vibration (e.g., around 1 m/s^2) there is a relatively small contribution to the total spinal load from the dynamic forces compared to the static load.

There are some other studies showing a crucial role for the dynamic forces from muscles when exposed to vibration with high magnitude (e.g., Bazrgari *et al.*, 2008). As reviewed in Chapter 2 (Section 2.6.3), the model developed from Bazrgari *et al.* (2008) predicted a maximum compressive spinal force at L5/S1 of 3,500 N when exposed to a sinusoidal vibration of 4 Hz at an acceleration of 4 g (g=9.81 m/s^2). The present model predicts a maximum spinal force of 2,380 N in the normal sitting posture when exposed to the same excitation (static: 810 N, dynamic: 1570 N), which is less than the predictions of the model by Bazrgari *et al.* (2008). The discrepancy between the two studies is due to the relatively small contribution of the dynamic muscle force in the present model. It is noticeable that the stiffness of the spring representing the muscles in the present model

is less (around 200 N/m) as optimised against the apparent mass and body transmissibility. It was found that muscle stiffness was insensitive to the vertical apparent mass and vertical transmissibility to L3 in the current model. The behaviour of muscles and their effects on the biodynamic response of the body should be further investigated. It is also noted that the transfer functions from the seat acceleration to the dynamic spinal force derived from the current study and other models mentioned above (e.g., Verver *et al.*, 2004; Fritz, 2000) may underestimate the dynamic muscle forces at frequencies close to 0 Hz. These transfer functions give a value (around 30 N/ms^{-2}), which is close to the mass supported on the disc (around 30 kg) at frequencies close to zero, possibly without consideration of muscle forces at these frequencies. An EMG (electromyographic) study found some phasic muscle activity (voluntarily controlled by the body) at frequencies close to 0 Hz (e.g., Robertson and Griffin, 1989).

How muscles generate forces during whole-body vibration is not fully understood. Electromyographic studies of back muscle activity indicate that the muscle force varies according to the frequency of whole-body vibration (e.g., Robertson and Griffin, 1989; Blüthner *et al.*, 2001). With whole-body vertical vibration (1.0 m/s^2 r.m.s.), Robertson and Griffin (1989) found that vibration-induced phasic muscle activity was around 20 percent of the posture-related tonic muscle activity. Blüthner *et al.* (2001) also found the muscle activity varied over the applied frequency range and between sitting postures (e.g., relaxed, erect, and forward leaning). The findings of these studies indicate that the dynamic muscle forces should be included in a model to predict spinal forces because they may influence the motion or force transmitted through the body as well as contribute to the spinal loads directly.

In the current model, the compressive force at the disc was predicted in the same direction as the excitation. However, the loads at the intervertebral discs can also include shear forces and moments, which should not be neglected when assessing the risks to the health of the intervertebral discs and adjacent tissues. It is expected that the spinal forces in other sitting postures (e.g., sitting with backrest, forward leaning sitting) may be predicted, if the model is properly adjusted (e.g., adjusting the geometry, mass and stiffness and including a representation of a backrest.

5.5 Conclusion

A multi-body model of the seated human body including a simple representation of muscle forces has been developed for erect, normal, and slouched sitting postures to predict compressive forces in the lumbar spine. The model can reflect appropriate vertical in-line apparent mass and fore-and-aft cross-axis transmissibility to the lumbar spine during vertical vibration excitation. Muscle activity, and the transmission of vibration through the body, depend on sitting posture and are prime causes of variations in spinal forces. The simple representation of the muscle forces employed in this study predicted spinal loads that appear more appropriate than the forces calculated without the inclusion of a representation of the muscles, but further investigation of spinal modelling leading to greater understanding of dynamic muscle forces is required.

Chapter 6. Effect of backrest inclination on the apparent mass at the seat and backrest and transmissibility to the spine during vertical whole-body vibration

6.1 Introduction

Drivers and passengers of many types of vehicles sit with their backs supported by backrests. Backrest support can reduce the need for muscle activity to maintain posture in static conditions (Bennett *et al.*, 1989) and stabilise the body in dynamic conditions (Oliveira *et al.*, 2001).

A backrest can modify the vibration transmitted through the body (e.g., Paddan and Griffin, 1988) and so may affect the discomfort caused by vibration (e.g., Basri and Griffin, 2013). The inclination of a seat backrest also influences the vibration transmitted to the body (e.g., Pope *et al.*, 1998) and the discomfort caused by vibration (e.g., Basri and Griffin, 2013). Compared to sitting without a backrest, the use of a backrest has been reported to reduce spinal loads during whole-body vertical vibration (0.3 to 30 Hz at 1.0 ms^{-2} r.m.s.) and inclining the backrest further reduces the spinal forces measured in-vivo with vertebral body replacements (Rohlmann *et al*., 2010).

The forces in the lumbar spine may be predicted from the sum of static spinal forces (caused by gravity) and dynamic spinal forces (induced by vibration) using simple biodynamic models (e.g., Chapters 4 and 5). Such models suggest the dynamic spinal forces depend on the vibration transmitted to the upper body. This led to the current experimental study of the effect of backrest inclination on biodynamic responses.

Compared to sitting without a backrest, a vertical backrest tends to increase the frequency of the principal resonance in the vertical apparent mass and decrease the apparent mass at the resonance (Toward and Griffin, 2009; Qiu and Griffin, 2012). This may be partly because a backrest changes the curvature of the spine and consequently the dynamic response of the body (Griffin, 1990). Increased backrest inclination tends to further increase the resonance frequency and decrease the apparent mass at the resonance (Toward and Griffin, 2009). The fore-and-aft cross-axis apparent mass is also affected by contact with a vertical backrest and the supporting conditions at the feet (Nawayseh and Griffin, 2004). When sitting with a vertical backrest, the resonance frequency in the fore-and-aft cross-axis apparent mass seems to be correlated with the resonance frequency in the vertical in-line apparent mass (e.g., Nawayseh and Griffin, 2004; Qiu and Griffin, 2012). The fore-and-aft cross-axis apparent mass at the seat has not previously been reported with an inclined backrest.

During vertical whole-body vibration, there can be considerable forces at a vertical backrest in both the vertical and fore-and-aft directions. Both the vertical in-line apparent mass and the fore-and-aft cross-axis apparent mass at a backrest were reported to have resonances around 5 Hz (e.g.,

Nawayseh and Griffin, 2004). The dynamic forces in the vertical and fore-and-aft directions have not been reported with an inclined backrest.

The effect of inclined backrests on the transmissibility of the body is not clear. Most studies of the vibration transmitted through the body have involved the measurement of head motion (e.g., Paddan and Griffin, 1988). It was found a backrest tends to increase the principal resonance frequency and peak transmissibility of the in-line vertical seat-to-head transmissibility when exposed to vertical excitation (Paddan and Griffin, 1988), possibly because of stiffening in the overall body stiffness caused by backrest contact. A study of the effect of backrest contact on pelvis rotation found that the seat-to-pelvis pitch transmissibility increased, and a clear resonance was observed at around 10 Hz when subjects sat in 'back-on' postures (Mansfield and Griffin, 2000). A more recent study found that the vertical in-line seat-to-L3 transmissibility showed a broad peak with a low magnitude and slightly increased principal resonance with vertical backrest contact, while the effect of backrest contact on fore-and-aft transmissibility to the lumbar spine was small compared to that to the thoracic spine, which was suggested to be caused by the restriction of backrest contact in the lumbar region (M-Pranesh *et al.*, 2010). However, in the results of Magnusson *et al.* (1993), backrest contact and inclination of a backrest had no significant effect on the seat-to-L3 transmissibility. There are many factors that could cause the inconsistency in the above mentioned studies, such as the characteristics of the subjects (e.g., height, age, or weight), and differences in the postures (e.g., different contact locations with the backrest, etc.

The objective of this study was to investigate how backrest inclination affects the vertical in-line apparent masses and fore-and-aft cross-axis apparent masses at the seat pan and the backrest and the overall dynamic forces applied to the seated human body during vertical whole-body vibration. The vertical in-line, fore-and-aft cross-axis, and pitch transmissibilities to various locations along the spine (L5, L3, T5 and the pelvis) were also measured together with the apparent masses to help understand the effect of backrest inclinations on the biodynamic responses. It was hypothesised that with increasing inclination of a backrest, the fore-and-aft cross-axis apparent mass at the seat pan would increase because backrest inclination introduces direct excitation to the body in the fore-and-aft direction. It was also hypothesised that contact with an inclined backrest would increase the vertical, fore-and-aft, and pitch motion of the pelvis because a part of the body mass is supported by the backrest and the body mass supported on the seat pan is reduced. The measured data were also required for the development of biodynamic models to predict the spinal forces in the seated human body exposed to vertical whole-body vibration with different backrest contact conditions.

6.2 Method

6.2.1 Apparatus

The vertical vibration was generated by a 1-m vertical vibrator. A rigid seat with an adjustable rigid backrest was mounted on the platform of the vibrator (Figure 6.1). An aluminium alloy and plywood backrest was mounted on the rigid seat so that it could be adjusted to inclinations between 0 degrees (vertical) and 60 degrees. Two rigid wooden panels were attached firmly to the front

surface of a force plate mounted on the backrest frame so as to form a sufficient slot from the top to the bottom in the middle of the backrest to avoid the accelerometers attached on the back along the spine of human body contacting the backrest when a subject sat against the backrest. When vertical, the backrest extended from 100 mm to 700 mm above the seat pan surface with an area of 600mm (height) x 500 mm (width). The subjects were asked to sit normally upright against the vertical backrest so that they were supported by either their lumbar spine or thorax. Sitting with thoracic support required the subjects to sit on the seat pan with their buttocks slightly forward from the backrest surface, whereas the pelvis was closer to the backrest surface when sitting with lumbar support.

A force plate (Kistler 9281 B) consisting of four tri-axial quartz transducers at the four corners of a rectangular welded steel frame (600 mm x 400 mm) was secured on the supporting surface of the seat to measure the dynamic forces in vertical and fore-and-aft directions at the seat pan surface. Another force plate, consisting of four tri-axial force transducers (Kistler 9602) at the four corners of a rectangular plywood frame (600 mm x 500 mm) was mounted on the backrest. The signals from the force transducers were amplified by Kistler 5073 charger amplifiers.

One single-axis piezo-resistive accelerometer (Entran EGCSY-240D-10) was mounted at the centre of the force plate on the seat pan to measure the vertical acceleration. Two single-axis piezo-resistive accelerometers (Entran EGCSY-240D-10) were mounted on the frame supporting the backrest at the location corresponding to the centre of the backrest surface so as to measure the acceleration normal to the backrest surface and parallel to the backrest surface.

The signals measured at the four corners of the force plate at the seat pan were summed to give one force signal in the vertical direction and one force signal in the fore-and-aft direction. The force signals from the each corner of the backrest in the directions normal and parallel to the backrest surface were acquired individually. All forces and acceleration signals were acquired with a 16-channel *HVLab* data acquisition system at a sampling rate of 256 samples per second via 100-Hz anti-aliasing filters.

A total of eight tri-axial accelerometers (MEMS, KXD94-2802) were mounted on the upper and lower surfaces of four blocks made from balsa wood. Each block was then taped on the subject's body surface using double-side adhesive tape to as to measure the accelerations in the vertical, fore-and-aft, and pitch directions (i.e., the mid-sagittal plane) at each of the following locations: pelvis (iliac crest), L5, L3, and T5. The pitch motion at each level was estimated from the differences in two fore-and-aft accelerations measured at the same time (described in Section 6.2.3.2), where the two accelerometers were mounted at a separation of 30 mm. The wooden block with accelerometers mounted is shown in Figure 6.2.

6.2.2 Experimental design

Twelve healthy male subjects with median age 29 years (range 22 to 34 years), median height 173.5 cm (range 160 to 184 cm), and median weight 69 kg (range 60 to 100 kg) participated in the experiment.

During the experiment subjects sat in the following conditions:

(i) upright without backrest contact (i.e., NB);

(ii) against a vertical backrest with a contact at either L2 or T5 (i.e., B_{0L2} and B_{0T5});

(iii) against the backrest inclined by 10º, 20º or 30º with a contact only at the thoracic region of the back (i.e., B_{10}, B_{20} and B_{30}).

In all six conditions, the feet were supported on an adjustable footrest to obtain average thigh contact. The hands rested on the lap.

In each condition, the subjects were exposed to 60-s periods of random vertical vibration with approximately flat constant-bandwidth acceleration spectra (0.2 to 20 Hz at 1.0 ms^{-2} r.m.s.). The experiment was approved by the Ethics Committee of the Faculty of Engineering and the Environment at the University of Southampton (approval number 14342).

The experimental set-up with an example subject sitting against the backrest reclined by 20º is shown in Figure 6.1.

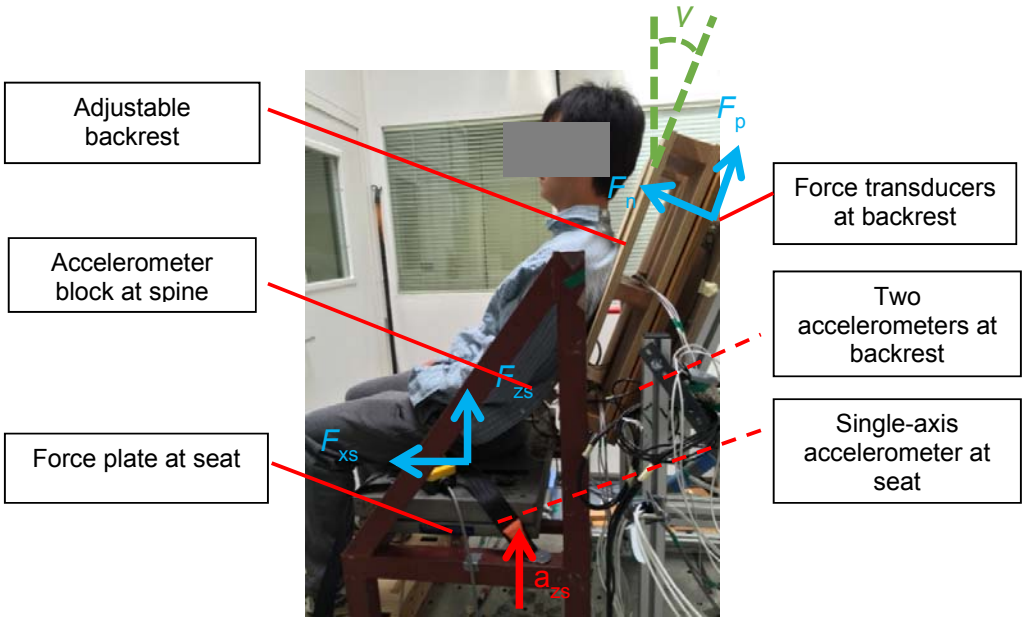

Figure 6.1 Seat on vibrator with a subject sitting against a 20º-inclined backrest. Angle γ represents the inclination angle of the backrest between the vertical direction and the backrest surface.

6.2.3 Data analysis

6.2.3.1 Mass cancellation

For the calculation of the forces at the seat and the backrest, the effects of the masses of the force plates on the measured dynamic forces were eliminated by applying mass cancellation in the time-domain. The acceleration time-history was multiplied by the mass of the force platform 'above' the force sensors and the resulting force was subtracted from the measured force. The force after subtraction in the time-history was then used to calculate the apparent mass. With inclined backrests, mass cancellation was performed on the dynamic forces in directions normal and

parallel to the backrest surface. The time history of the acceleration normal or parallel to the backrest surface was multiplied by the mass of the plate and then subtracted from the force time history measured in the same direction.

6.2.3.2 Transfer functions

Various measures of apparent mass were calculated from transfer functions between dynamic force and acceleration using the averaged cross spectral density method (60 averages using a Hamming window with an overlap of 75% for a resolution of 0.25 Hz, Chapter 3). For the 'vertical in-line apparent mass' at the seat pan, $M_{zzs}(f)$, the measured force and acceleration were in the same direction (i.e., vertical). For the 'fore-and-aft cross-axis apparent mass' at the seat pan, $M_{xzs}(f)$, the measured force was in the fore-and-aft direction and the acceleration was in the vertical direction. The two apparent masses at the seat pan, $M_{zzs}(f)$ and $M_{xzs}(f)$, and the associated coherencies, $C_{zzs}^2(f)$ and $C_{xzs}^2(f)$, were calculated as:

$$M_{zzs}(f) = \frac{G_{a_{zs}F_{zs}}(f)}{G_{a_{zs}}(f)}, \quad C_{zzs}{}^2(f) = \frac{\left|G_{a_{zs}F_{zs}}(f)\right|^2}{G_{a_{zs}}(f)G_{F_{zs}}(f)},$$

$$M_{xzs}(f) = \frac{G_{a_{zs}F_{xs}}(f)}{G_{a_{zs}}(f)}, \quad C_{xzs}{}^2(f) = \frac{\left|G_{a_{zs}F_{xs}}(f)\right|^2}{G_{a_{zs}}(f)G_{F_{xs}}(f)} \tag{6.1}$$

where, $G_{a_{zs}}(f)$ is the auto-spectra of the vertical acceleration at the seat pan, $a_{zs}(t)$, $G_{F_{zs}}(f)$ and $G_{F_{xs}}(f)$ are the auto-spectra of vertical and fore-and-aft forces measured at the seat pan, $F_{zs}(t)$ and $F_{xs}(t)$, and $G_{a_{zs}F_{zs}}(f)$ and $G_{a_{zs}F_{xs}}(f)$ are the cross-spectra between $a_{zs}(t)$ and $F_{zs}(t)$ and between $a_{zs}(t)$ and $F_{xs}(t)$.

The force transducers at the backrest measured the dynamic forces in directions normal to the surface of the backrest, F_n, and parallel to the surface of the backrest, F_p. With inclined backrests, these forces were projected so as to calculate also the forces in the vertical and fore-and-aft directions (i.e., the same coordinate system used for calculating the vertical in-line and fore-and-aft cross-axis apparent mass at the seat pan). For a backrest inclination angle α (shown in Figure 6.1), the force time histories in the vertical and fore-and-aft directions were calculated as:

$$\begin{aligned} F_{zb}(t) &= F_n(t)\sin\alpha + F_p(t)\cos\alpha \ , \\ F_{xb}(t) &= F_n(t)\cos\alpha - F_p(t)\sin\alpha \end{aligned} \tag{6.2}$$

where $F_n(t)$ and $F_p(t)$ are the force time-histories measured by the force transducers in the local coordinate system, and $F_{zb}(t)$ and $F_{xb}(t)$ are the forces projected to the vertical and fore-and-aft directions, respectively.

The vertical in-line apparent mass at the back, $M_{zzb}(f)$, was given by the transfer function between $F_{zb}(t)$ and $a_{zs}(t)$. The fore-and-aft cross-axis apparent mass at the back, $M_{xzb}(f)$, was given by the transfer function between $F_{xb}(t)$ and $a_{zs}(t)$. The two apparent masses at the back, $M_{zzb}(f)$ and $M_{xzb}(f)$, and the associated coherencies, $C_{zzb}^2(f)$, $C_{xzb}^2(f)$, were calculated as:

$$M_{zzb}(f) = \frac{G_{a_{zs}F_{zb}}(f)}{G_{a_{zs}}(f)},\ C_{zzb}{}^2(f) = \frac{\left|G_{a_{zs}F_{zb}}(f)\right|^2}{G_{a_{zs}}(f)G_{F_{zb}}(f)},$$

$$M_{xzb}(f) = \frac{G_{a_{zs}F_{xb}}(f)}{G_{a_{zs}}(f)},\ C_{xzb}{}^2(f) = \frac{\left|G_{a_{zs}F_{xb}}(f)\right|^2}{G_{a_{zs}}(f)G_{F_{xb}}(f)} \quad (6.3)$$

where $G_{F_{zb}}(f)$ and $G_{F_{xb}}(f)$ are the auto-spectra of the calculated vertical force $F_{zb}(t)$ and the calculated fore-and-aft force $F_{xb}(t)$ at the backrest; $G_{a_{zs}F_{zb}}(f)$ and $G_{a_{zs}F_{xb}}(f)$ are the cross-spectra between $a_{zs}(t)$ and $F_{zb}(t)$ and between $a_{zs}(t)$ and $F_{xb}(t)$.

As mentioned in Chapter 3, the dynamic forces at the seat pan and at the backrest in the vertical and fore-and-aft directions when sitting against backrest were contributed from the excitations from the seat pan and from the backrest. The vertical in-line apparent mass and the fore-and-aft cross-axis apparent mass at the seat pan and at the backrest defined in this Chapter were used to quantify the dynamic forces at the seat pan and at the backrest and to describe the effect of inclinations of backrest on these forces during vertical whole-body vibration.

The transmissibilities were calculated as the ratio from the amount of vibration transmitted from driving point to locations on the human body. Similar to the calculation of apparent mass, the vertical and fore-and-aft cross-axis transmissibility, $T_{ZZ}(f)$, $T_{XZ}(f)$, were calculated below together with the associated coherencies, $C_{Tzz}{}^2(f)$ and $C_{Txz}{}^2(f)$, where T corresponds to the spinal levels, including the pelvis, L5, L3 and T5.

$$T_{ZZ}(f) = \frac{G_{a_{ZS}a_{TZ}}(f)}{G_{a_{ZS}}(f)},\ C_{Tzz}{}^2(f) = \frac{\left|G_{a_{zs}a_{Tz}}(f)\right|^2}{G_{a_{zs}}(f)G_{a_{TZ}}(f)}$$

$$T_{XZ}(f) = \frac{G_{a_{ZS}a_{TX}}(f)}{G_{a_{ZS}}(f)},\ C_{Txz}{}^2(f) = \frac{\left|G_{a_{zs}a_{TX}}(f)\right|^2}{G_{a_{zs}}(f)G_{a_{TX}}(f)} \quad (6.4)$$

where $a_{TZ}(t)$ and $a_{TX}(t)$ corresponds to the vertical and fore-and-aft accelerations at different spinal levels, including the pelvis, L5, L3 and T5; $G_{a_{zs}a_{TZ}}(f)$ and $G_{a_{zs}a_{TX}}(f)$ are the cross-spectra between $a_{zs}(t)$ and $a_{TZ}(t)$ and between $a_{zs}(t)$ and $a_{TX}(t)$.

The pitch accelerations, $\ddot{\theta}_T(t)$, at the different spine levels (i.e., pelvis, L5, L3 and T5) were calculated as the ratio of the difference between two measured fore-and-aft accelerations ($\ddot{x}_1(t)$ and $\ddot{x}_2(t)$) to the (vertical) distance (d) between the two accelerometers. The pitch transmissibility, $T_{PZ}(f)$, was then given by the transfer function from the vertical acceleration $a_{zs}(t)$ to the pitch acceleration $\ddot{\theta}_T(t)$.

$$\ddot{\theta}_T(t) = \frac{\ddot{x}_1(t) - \ddot{x}_2(t)}{d},\quad T_{PZ}(f) = \frac{G_{a_{ZS}\theta_T}(f)}{G_{a_{ZS}}(f)} \quad (6.5)$$

where $G_{a_{zs}\ddot{\theta}_T}(f)$ is the cross-spectra between $a_{zs}(t)$ and $\ddot{\theta}_T(t)$.

6.2.3.3 Correction of skin-tissue effect

The motion measured on the body surface over a vertebra can be modified by the tissue and skin between the bone and the transducer (Pope *et al.*, 1986). The effect of skin and tissue on the vibration transmitted from the spinous process of vertebrae body to the skin surface in the present study was eliminated by the correction procedure introduced by Kitazaki and Griffin (1995). A single-degree-of-freedom model of the skin-tissue system is used to represent the vibration transmission from the response at a vertebra to the acceleration at the skin surface. A cotton thread was connected to each block of accelerometers. An initial force was applied to a block in the vertical or fore-and-aft direction through the thread (Figure 6.2). The free vibration response (acceleration) of the block on the skin surface at each vertebral level was measured when cutting the thread. The measurement with thread was applied to all four spinal levels in both vertical and fore-and-aft directions.

The transfer function from the seat acceleration to the acceleration at vertebrae ($T_V(f)$) was then calculated as:

$$T_V(f) = T_S(f) \times Correction\_skin(f) \tag{6.6}$$

where $T_S(f)$ is the seat to skin surface transmissibility which can be directly calculated from measured acceleration response, and *Correction_skin* (f) is the correction function defined as:

$$Correction\_skin(f) = \frac{-(f/f_0)^2 + 2*\xi*j*(f/f_0)+1}{1+2*\xi*j*(f/f_0)},\ \xi = -\frac{1-(1+\Delta f/f_0)^2}{2(1+\Delta f/f_0)} \tag{6.7}$$

The symbol f_0 is natural frequency, Δf is the half bandwidth of the FFT response of the time-history acceleration measured at skin surface, calculated as the subtraction between the frequency of half power points and the frequency of the peak (f_0). ζ is the damping ratio estimated from the frequency response of the skin-tissue system.

It has been suggested that the correction method with a single-degree-freedom model is effective at frequencies less than the estimated natural frequency of the local system (Kitazaki, 1994). It was also suggested that correction in the fore-and-aft direction is not necessary at the frequencies considered, because the stiffness of tissues in the direction normal to the skin surface was found to be much greater than the stiffness in the shear direction (Kitazaki, 1994). However, the mass of the mountings system (accelerometers and block) will affect the resonance frequency of the single degree-of-freedom system. Whether correction in the fore-and-aft direction is required depends on the natural frequency of the system in the fore-and-aft direction. A significant variability in the pitch motion of vertebrae at frequencies greater than 10 Hz was found using different sizes of balsa blocks with increasing masses from 6.3 g, 15.8 g, 25.4 g to 34.5 g (Matsumoto, 1999). It was found the measured vertical transmissibility to L3 and its corresponding phase lag increased with increasing mass and the natural frequency of the local skin-tissue system decreased with increasing mass.

In the present study, the skin-tissue correction procedure was processed in each of the three directions for every subject at every measurement location (i.e., iliac crest, L5, L3, and T5, shown in Figure 6.2). The resonance frequencies and damping ratios of 12 subjects in 3 axes at four spinal levels are shown in Appendix A.2. Generally, the resonance frequency in the *z*-direction occurred at around 15 Hz. The resonance frequency in the *x*-direction occurred at a greater frequency, around 30 Hz. The resonance frequency for the pitch direction occurred at around 20 Hz. A great variation was found in the natural frequencies within different subjects in different directions at different locations. Possible reasons could be differences in individual skin-tissue systems. The plotted correction functions show the importance of the correction procedure due to the low natural frequency of the skin-tissue system at some locations combined with some large damping ratios.

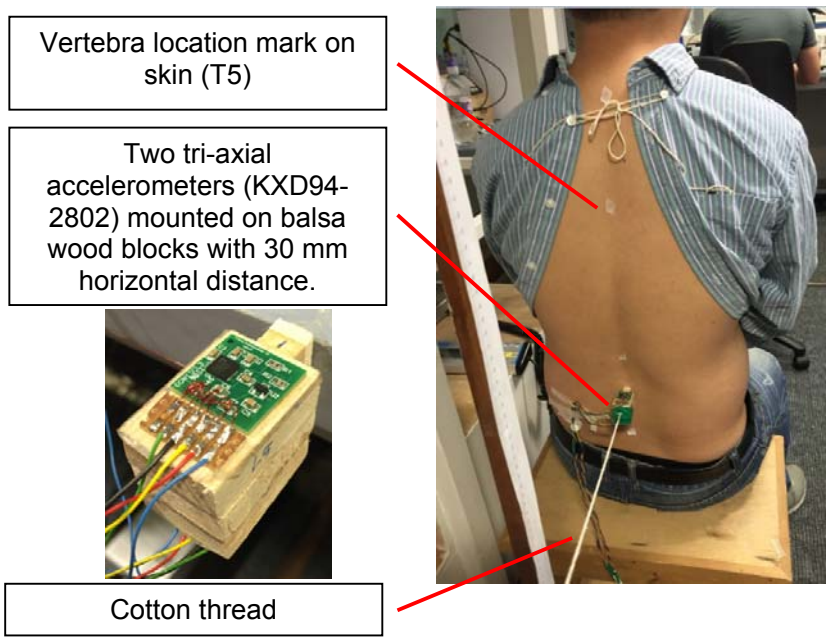

Figure 6.2 Balsa wood measuring block with accelerometers and an example of skin-tissue correction test with one subject.

An example of the effect of skin-tissue correction is shown in Figure 6.3 which shows a decrease in the vertical transmissibility to the pelvis between 6 and 15 Hz after skin-tissue correction. However, the skin-tissue correction was found to rarely affect the resonance frequency of the transmissibility.

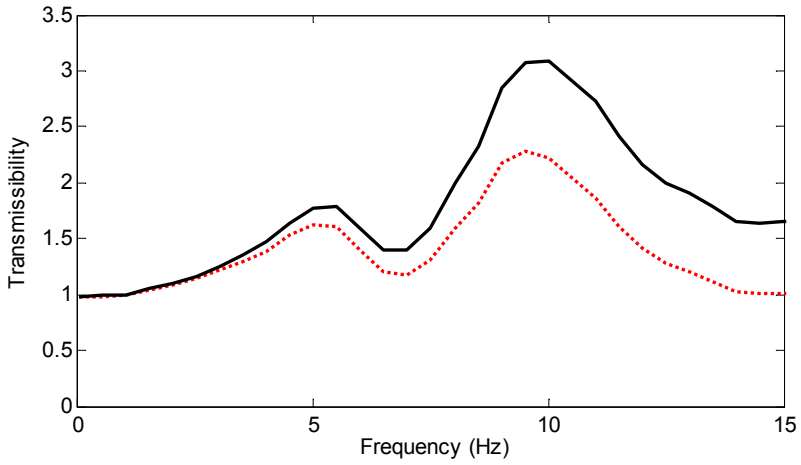

Figure 6.3 An example of the effect of skin-tissue correction on the vertical transmissibility to the pelvis (iliac crest, Subject 8). '—': measured transmissibility without correction; '···': skin-tissue corrected transmissibility.

6.2.3.4 Angle correction of spinal accelerations in vertical and fore-and-aft directions

When the blocks with accelerometers were attached on the skin surface, the accelerometers were measuring the fore-and-aft and vertical acceleration with respect to the axes parallel and normal to the skin surface, so there was an inclination between the contact surface and the *z*-axis of the global coordinate system. Angle correction was adopted to calculate the acceleration of vertebral bodies in the vertical and fore-and-aft directions following the global gravity coordinate system (Matsumoto and Griffin, 1998). The angle correction process was performed with the accelerations in vertical and fore-and-aft directions after skin-tissue correction.

The inclined angle of the skin surface with respect to the vertical direction was defined as φ, which could be calculated approximately from the vertical and fore-and-aft transmissibilities at 0.5 Hz ($T_{VXZ}(f)$ and $T_{VZZ}(f)$) with the following expression in every backrest testing condition of each subject:

$$\varphi = \arctan\left(\frac{T_{VXZ\ 0.5Hz}}{T_{VZZ\ 0.5Hz}}\right) \tag{6.8}$$

With the inclined angle defined, the transmissibilities to the spine in the vertical and fore-and-aft directions ($T_{ZZ}(f)$ and $T_{XZ}(f)$) were corrected as:

$$\begin{aligned} T_{ZZ}(f) &= T_{VXZ}(f)\sin\varphi + T_{VZZ}(f)\cos\varphi; \\ T_{XZ}(f) &= T_{VXZ}(f)\cos\varphi - T_{VZZ}(f)\sin\varphi; \end{aligned} \tag{6.9}$$

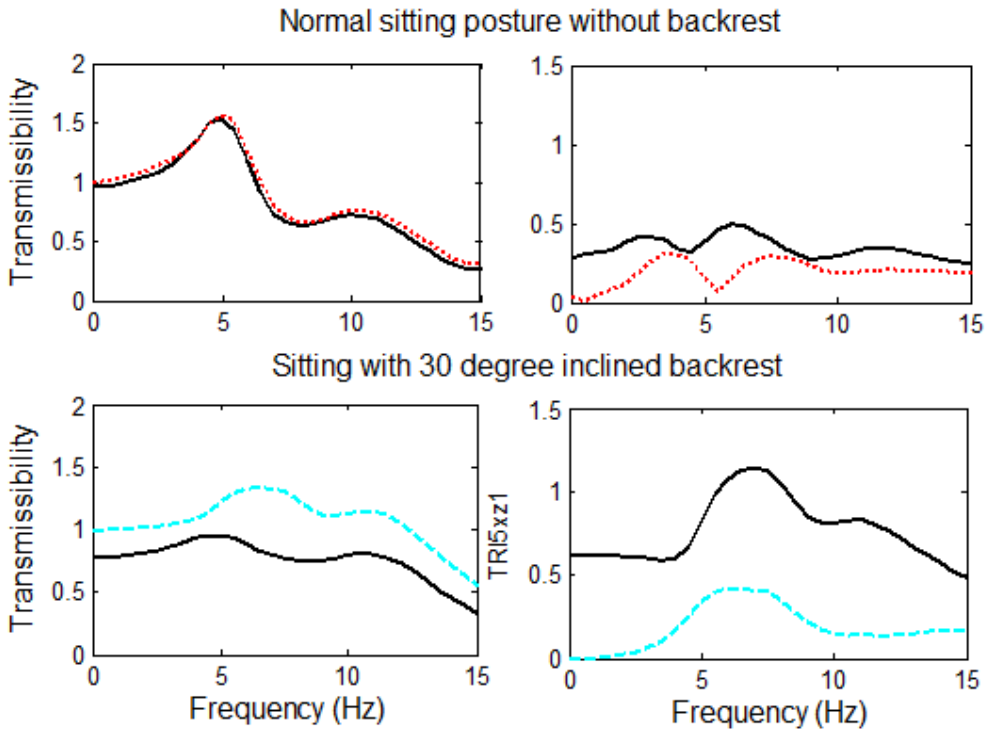

Figure 6.4 Effect of angle correction on the vertical (left column) and fore-and-aft (right column) transmissibilities to L5 in two postures. Top row: normal sitting posture without backrest; Bottom row: sitting with 30º-inclined backrest. '—': measured transmissibility without angle correction; '⋯': angle corrected transmissibility.

As expected, the angle correction process was most significant when sitting with inclined backrests. Two examples comparing the vertical and fore-and-aft transmissibilities to the lumbar spine at L5 before and after the angle correction in a normal sitting posture without backrest and with a 30º-inclined backrest are shown in Figure 6.4. It can be observed that the correction was more effective for sitting with the inclined backrest because of the greater initial inclined angle between the body surface and the vertical direction (gravity). The correction ensured the fore-and-aft transmissibility was close to zero and the vertical transmissibility was close to 1.0 at frequencies close to zero Hz, following the assumption that the body mainly moves vertically as a rigid body at very low frequencies when exposed to vertical whole-body vibration. It was found the correction reduced the fore-and-aft transmissibility at frequencies close to 0 Hz (i.e., 0-5 Hz).

The pitch motions of vertebrae have been found to result in up to 20% difference in the transmissibility to the vertebral bodies compared to the transmissibility to the spinous processes around 5 Hz (Matsumoto, 1998). However, in the current study, the transmissibility obtained at the spinous process was not further adjusted into the transmissibility to the centre of vertebral body.

6.2.3.5 Statistical analysis

Non-parametric statistical tests (Friedman two-way analysis of variance for *k*-related samples and Wilcoxon matched-pairs signed-ranks test for two-related samples) were used. The Spearman rank order correlation was employed to investigate associations between variables.

6.3 Results

6.3.1 Apparent mass at the seat pan

6.3.1.1 Vertical in-line apparent mass

The vertical in-line apparent mass at the seat pan in the upright sitting posture showed a principal resonance at about 5 Hz. Some subjects also showed a secondary resonance around 8 to 10 Hz (Figure 6.5). These findings are consistent with previous studies (e.g., Fairley and Griffin, 1989; Kitazaki, 1994; Matsumoto and Griffin, 1998; Qiu and Griffin, 2010).

The vertical apparent mass at the principal resonance frequency and at frequencies less than the principal resonance frequency showed great inter-subject variability. The phase of the vertical apparent mass at the seat pan also showed great inter-subject variability at frequencies greater than 5 Hz. The coherency function showed values close to 1.0 starting from low frequencies (0.5 Hz) for all subjects. Details about the inter-subject variability in the vertical in-line apparent mass measured at the seat pan when sitting against different backrest conditions are shown in Table A5.1 in Appendix A.5.

The median vertical apparent masses of the 12 subjects (calculated at each frequency) in each of the six sitting conditions (without backrest and with the vertical backrest at L2 or T5 or the backrest inclined by 10°, 20° and 30°) are compared in Figure 6.6.

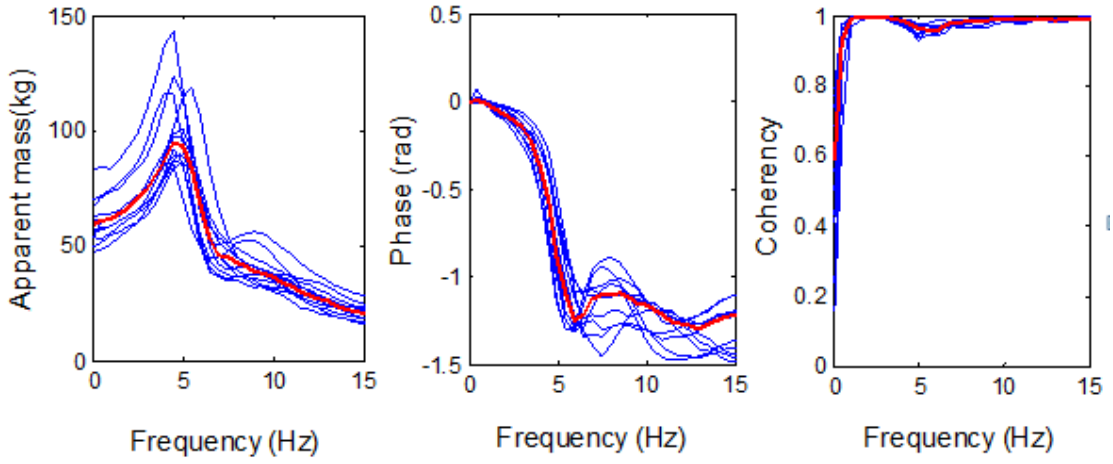

Figure 6.5 Vertical in-line apparent mass at the seat pan in the normal upright sitting posture. Twelve individual subjects: ('—'); Median of 12 subjects: ('—'). From left to right: modulus, phase, and coherency.

With the addition of the vertical backrest at T5, the vertical in-line apparent mass reduced at the 5-Hz resonance (p=0.012, Friedman). Similarly, with increasing inclination of the backrest (B_{0T5}, B_{10}, B_{20} and B_{30}), the vertical in-line apparent mass reduced at the resonance frequency (p<0.0001, Friedman) and at lower frequencies. The resonance frequency appeared to increase with increasing backrest inclination (from B_{0T5} toB_{10}, B_{20} and B_{30}), but the change was not statistically significant (p=0.122, Friedman). However, the resonance frequency in the vertical apparent mass

with the 30º backrest inclination was significantly greater than the resonance frequency for the remaining backrest conditions (p<0.05, Wilcoxon).

Changing the location of contact with a vertical backrest from L2 (B_{0L2}) to T5 (B_{0T5}) did not change significantly the resonance frequency or the apparent mass at the resonance in the vertical in-line apparent mass at the seat pan (p>0.05, Wilcoxon). The results of the Wilcoxon matched-pairs signed ranks test for changes in the resonance frequency and the apparent mass at the resonance are summarised in Table 6.1.

Table 6.1 Statistical significance of the effect of backrest inclination on the resonance frequency and the associated modulus of the vertical apparent mass at the seat pan (Wilcoxon matched-pairs signed ranks test).

Resonance frequency of vertical apparent mass at the seat pan						
	NB	B_{0L2}	B_{0T5}	B_{10}	B_{20}	B_{30}
NB	-	ns	ns	ns	ns	*
B_{0L2}		-	ns	ns	ns	*
B_{0T5}			-	ns	ns	*
B_{10}				-	ns	**
B_{20}					-	*
B_{30}						-

Vertical apparent mass at the seat pan at the resonance frequency						
	NB	B_{0L2}	B_{0T5}	B_{10}	B_{20}	B_{30}
NB	-	*	*	**	**	**
B_{0L2}		-	ns	*	**	**
B_{0T5}			-	**	**	**
B_{10}				-	**	**
B_{20}					-	**
B_{30}						-

ns: not significant; * $p \leqslant 0.05$; ** $p \leqslant 0.01$. Details of the statistics (i.e., p-value) are show in Appendix A.6.

With the backrest inclined to 20 and 30 degrees, a broad peak was observed at the primary resonance of the median vertical apparent mass (Figure 6.6), and the apparent masses from 6 of the 12 subjects showed two peaks in a frequency range of 5 to 7.5 Hz. With increasing inclination of the backrest, the magnitude of the peak at the higher frequency tended to be greater than the magnitude of the peak at the lower frequency, especially when the backrest was inclined to 30º.

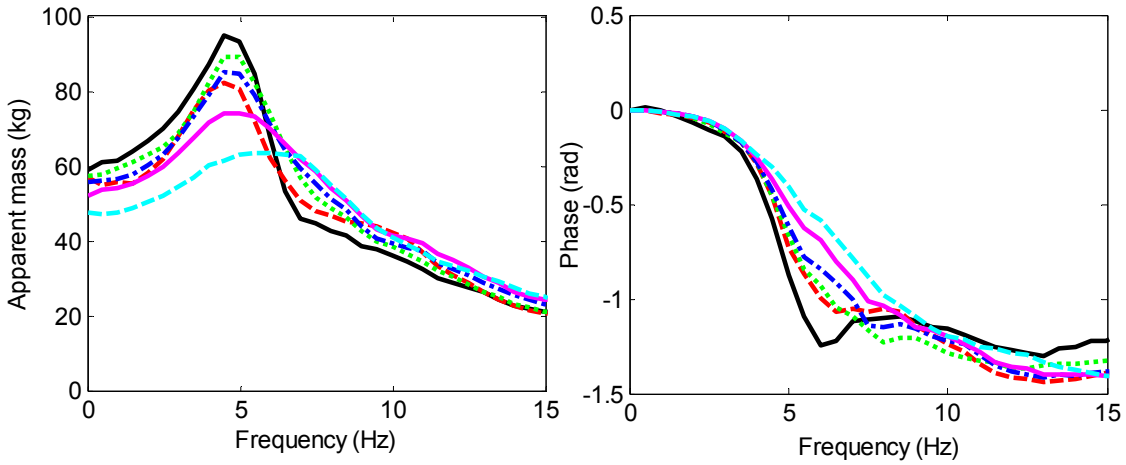

Figure 6.6 Vertical in-line apparent mass at the seat pan in different sitting conditions: normal upright sitting posture NB ('——'); vertical backrest contact at L2, B_{0L2} ('------'); vertical backrest contact at T5, B_{0T5} ('……'); 10º-inclined backrest, B_{10} ('–·–'); 20º-inclined backrest, B_{20} ('——'); 30º-inclined backrest, B_{30} ('------'). Left: modulus; right: phase. Median values from 12 subjects.

6.3.1.2 *Fore-and-aft cross-axis apparent mass*

The fore-and-aft cross-axis apparent mass of the individual subjects when sitting without backrest contact showed a principal resonance at around 5 Hz (Figure 6.7), similar to the resonance frequency in the vertical in-line apparent mass at the seat pan. Details about the inter-subject variability in the fore-and-aft cross-axis apparent mass measured at the seat pan when sitting against different backrest conditions are shown in Table A5.2 in Appendix A.5.

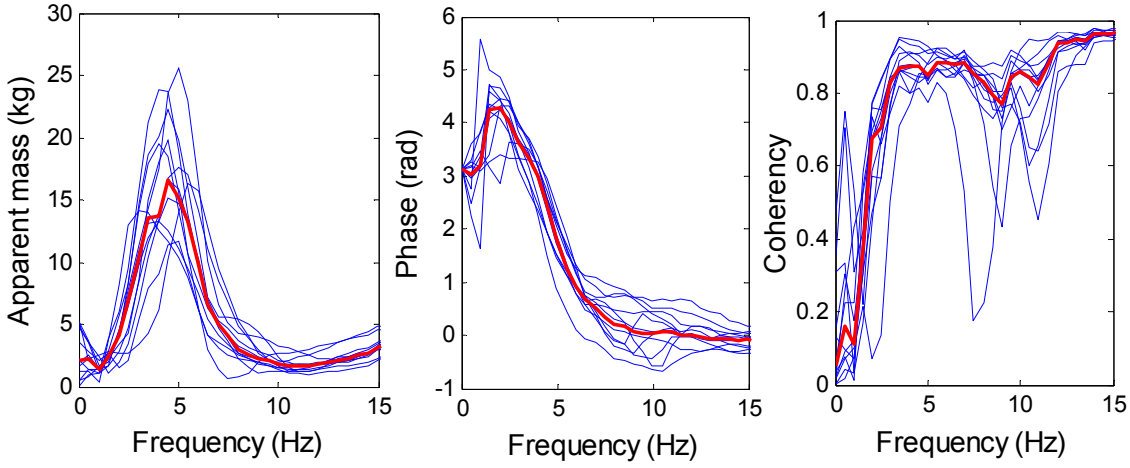

Figure 6.7 Fore-and-aft cross-axis apparent masses at the seat pan of 12 individual subjects in normal upright sitting posture. Individual subjects: ('—'); Median of 12 subjects: ('—').

For the median apparent mass of 12 subjects (Figure 6.8), with the vertical backrest at either L2 or T5 there was no significant change in either the resonance frequency (p>0.05, Wilcoxon) or the modulus of the fore-and-aft cross-axis apparent mass at the resonance (p>0.05, Wilcoxon).

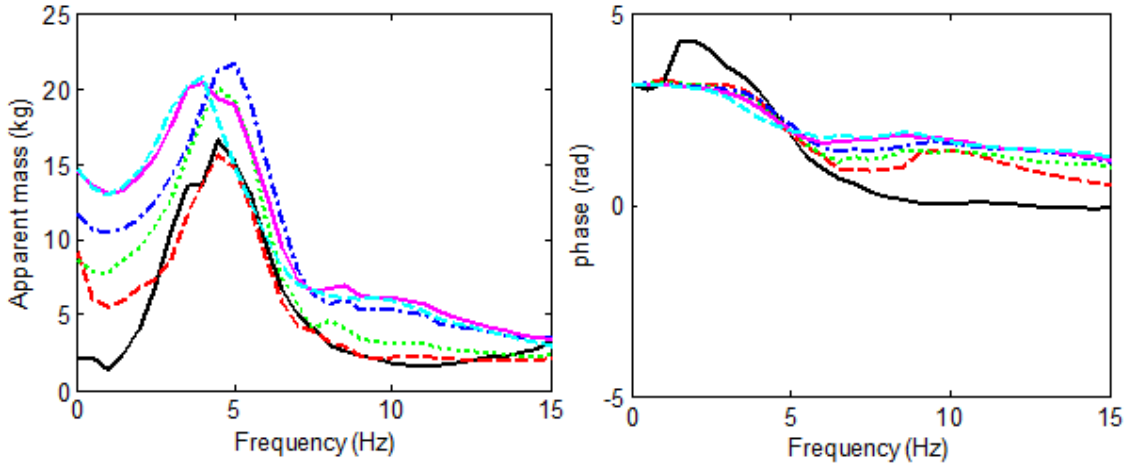

Figure 6.8 Fore-and-aft cross-axis apparent mass at the seat pan in different sitting conditions: normal upright sitting posture NB ('——'); vertical backrest contact at L2, B_{0L2} ('------'); vertical backrest contact at T5, B_{0T5} ('.....'); 10°-inclined backrest, B_{10} ('–·–'); 20°-inclined backrest, B_{20} ('— —'); 30°-inclined backrest, B_{30} ('------'). Left: modulus; right: phase. Median values from 12 subjects.

Table 6.2 Statistical significance of the effects of backrest inclination on the resonance frequency and the associated modulus of the fore-and-aft cross-axis apparent mass at the seat pan (Wilcoxon matched-pairs signed ranks test).

Resonance frequency of fore-and-aft apparent mass at the seat pan						
	NB	B_{0L2}	B_{0T5}	B_{10}	B_{20}	B_{30}
NB	-	ns	ns	ns	ns	*
B_{0L2}		-	ns	ns	*	**
B_{0T5}			-	ns	*	**
B_{10}				-	*	**
B_{20}					-	**
B_{30}						-

Fore-and-aft apparent mass at the seat pan at the resonance frequency						
	NB	B_{0L2}	B_{0T5}	B_{10}	B_{20}	B_{30}
NB	-	ns	ns	*	ns	ns
B_{0L2}		-	ns	**	ns	ns
B_{0T5}			-	*	ns	ns
B_{10}				-	ns	ns
B_{20}					-	ns
B_{30}						-

ns: not significant; * $p \leqslant 0.05$; ** $p \leqslant 0.01$. Details of the statistics (i.e., *p*-value) are show in Appendix A.6.

Comparing the fore-and-aft cross-axis apparent masses measured at the seat pan with the vertical apparent mass at the backrest at T5 and the apparent mass with three inclined backrests (i.e., B_{10}, B_{20} and B_{30}), there was a statistically significant change in the principal resonance frequency ($p<0.001$, Friedman). The resonance frequency of the fore-and-aft apparent mass at the seat pan decreased from 10º-inclined backrest to 20º-inclined backrest ($p=0.013$, Wilcoxon; Table 6.2, Figure 6.8). However, the modulus of the fore-and-aft cross-axis apparent mass at the resonance did not differ between the vertical backrest at T5 and the three inclined backrest ($p=0.134$, Friedman).

More detailed results of the statistical analysis on the differences in the resonance frequency and the associated modulus of the fore-and-aft cross-axis apparent mass are shown in Table 6.2.

The fore-and-aft cross-axis apparent mass at the seat pan increased at frequencies less than the resonance frequency when there was backrest contact at T5 ($p=0.002$, Wilcoxon; analysed at 2.5 Hz), and increased further with increasing inclination of the backrest ($p=0.001$, Friedman; analysed at 2.5 Hz; Figure 6.8).

6.3.2 Apparent mass at the backrest

6.3.2.1 Vertical in-line apparent mass

The vertical in-line apparent mass at the backrest showed a resonance in the frequency range 4 to 5.5 Hz (Figure 6.9). Details about the inter-subject variability in the vertical in-line apparent mass measured at the backrest when sitting against different backrest conditions are shown in Table A5.3 in Appendix A.5.

The resonance frequency of the vertical in-line apparent mass at the backrest measured with lumbar support (at L2) was similar to the resonance frequency of the vertical apparent mass at the backrest with thoracic support (at T5) ($p>0.05$, Wilcoxon), although the modulus of the apparent mass at the resonance was greater with contact at T5 than with contact at L2 ($p=0.009$, Wilcoxon).

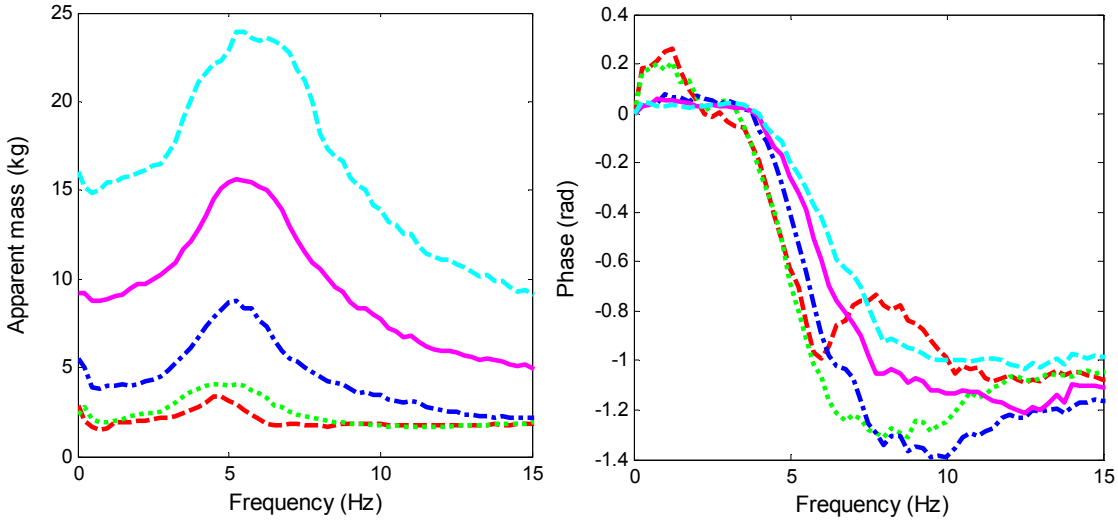

Figure 6.9 Vertical in-line apparent mass at the backrest in different sitting conditions: contact with vertical backrest at L2, B_{0L2} ('------'); contact with vertical backrest at T5, B_{0T5} ('……'); contact with 10º-inclined backrest, B_{10} ('–·–'); contact with 20º-inclined backrest, B_{20} ('——'); contact with 30º-inclined backrest, B_{30} ('------'). Left: modulus; right: phase. Median values from 12 subjects.

Both the resonance frequencies and the associated moduli of the in-line apparent masses measured at the backrest with five different backrest conditions (i.e., B_{0L2}, B_{0T5}, B_{10}, B_{20} and B_{30}) showed statistically significant differences (resonance frequencies of vertical apparent mass at the backrest: p=0.006, Friedman; apparent mass at the resonance: p<0.001, Friedman). The resonance frequency of the apparent mass at the backrest measured with the vertical backrest providing supported at T5 increased significantly compared to each of the three inclined backrest conditions (p<0.05, Wilcoxon). However, over the three inclined backrest conditions (10º, 20º and 30º inclinations of the backrest) there was no significant difference in the resonance frequencies of the vertical in-line apparent mass at the backrest (p=0.146, Friedman).

With increasing inclinations of the backrest, the vertical in-line apparent mass at the backrest tended to increase at all frequencies (0 – 15 Hz) (Figure 6.9).

6.3.2.2 Fore-and-aft cross-axis apparent mass

In all backrest conditions, the median fore-and-aft cross-axis apparent mass at the back showed a peak around 5 Hz (Figure 6.10). Details about the inter-subject variability in the vertical in-line apparent mass measured at the backrest when sitting against different backrest conditions are shown in Table A5.4 in Appendix A.5.

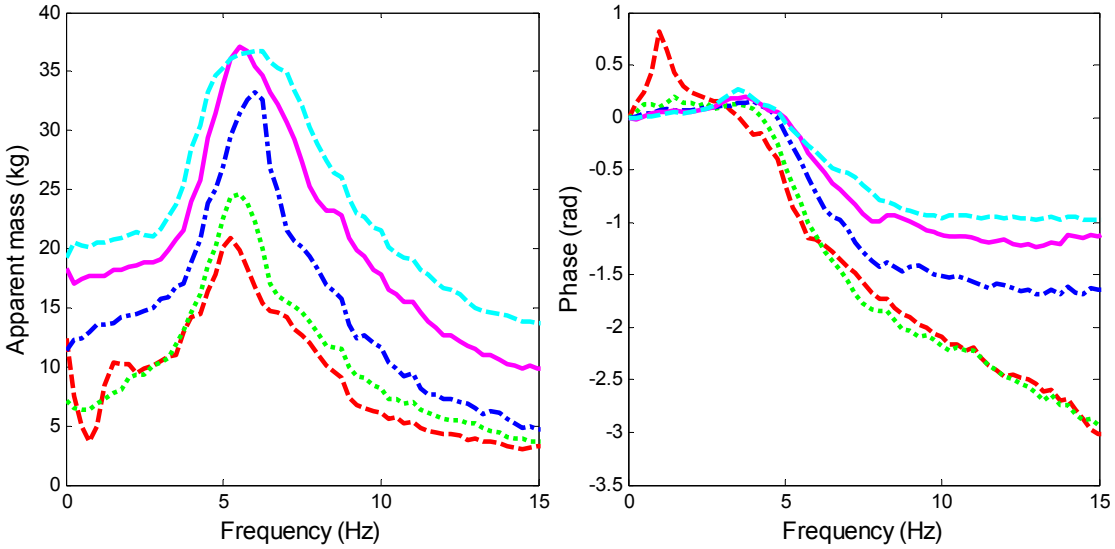

Figure 6.10 Fore-and-aft cross-axis apparent mass at the backrest in different sitting conditions: vertical backrest contact at L2, B_{0L2} ('------'); vertical backrest contact at T5, B_{0T5} ('.....'); contact with 10º-inclined backrest, B_{10} ('–·–'); 20º-inclined backrest, B_{20} ('——'); 30º-inclined backrest, B_{30} ('------'). Left: modulus; right: phase. Median values from 12 subjects.

When contact with the vertical backrest changed from L2 to T5, the fore-and-aft cross-axis apparent mass at the back at resonance increased (p=0.035, Wilcoxon), while the resonance frequency did not change (p=0.098, Wilcoxon).

There was a change in the resonance frequency among the contact conditions with vertical backrest at T5 and with the three inclined backrests (p=0.009, Friedman). The apparent mass increased at all frequencies as the backrest inclination increased.

6.3.3 Translational transmissibilities to the spine

6.3.3.1 Vertical in-line transmissibilities to spine

Transmissibilities from vertical acceleration at the seat to vertical accelerations at various spinal levels (i.e., pelvis (iliac crest), L5, L3 and T5) of 12 subjects in the normal upright sitting posture are shown in Figure 6.11.

A resonance at around 4-5 Hz was observed in the vertical transmissibilities to all locations along the spine, and a secondary resonance at around 8-10 Hz was seen for vertical transmissibilities to the pelvis, L5 and L3. Relatively greater inter-subject variability was observed for all transmissibilities at frequencies 5-15 Hz than at lower frequencies (Figure 6.11). The inter-subject variability shown at higher frequencies tended to become less apparent at the higher spine levels (i.e., L3 and T5). The vertical transmissibility at resonance tended to decrease with increasing spinal level from iliac crest to T5 (1.7 at iliac crest and 1.35 at T5; median transmissibilities).

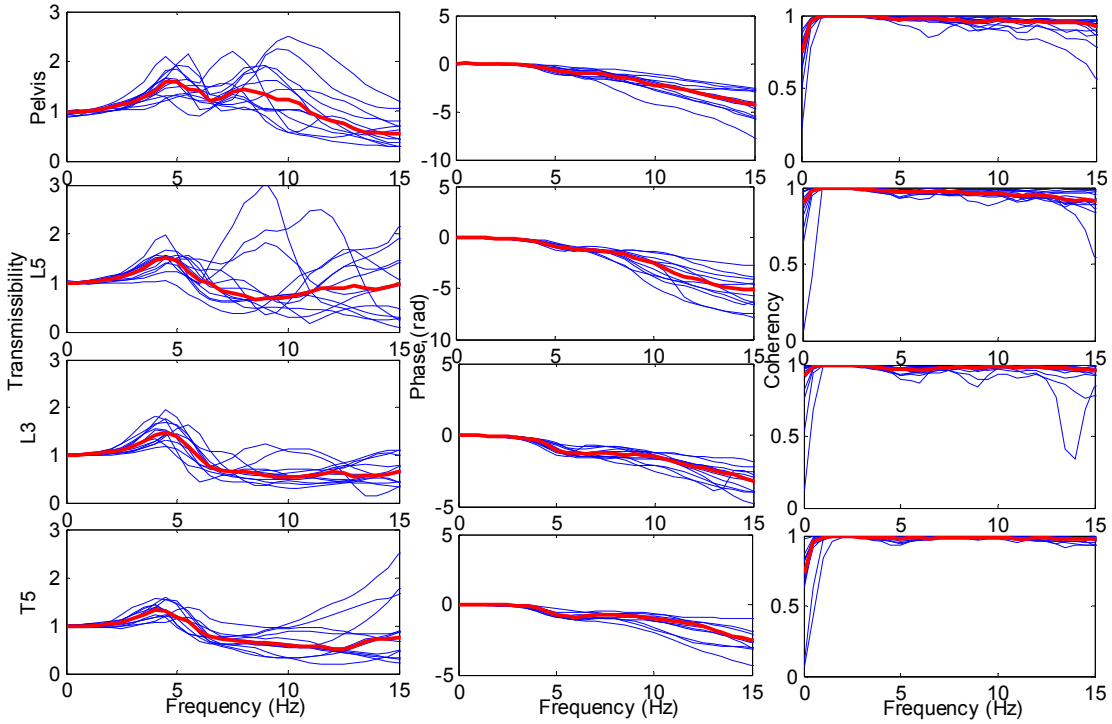

Figure 6.11 Vertical in-line transmissibilities to various spinal levels in the normal upright sitting posture without backrest of 12 individual subjects. From top row to bottom row: transmissibility to pelvis, L5, L3 and T5. Individual subject: ('—'); Median of 12 subjects: ('—'). In one row, from left to right: modulus, phase and coherency.

The median vertical transmissibilities to various spinal levels of 12 subjects in different backrest conditions (NB, B_{0L2}, B_{0T5}, B_{10}, B_{20}, and B_{30} backrest contact) are shown in Figure 6.12. The resonance frequency of the median vertical transmissibility to the pelvis (at around 5 Hz) showed no significant difference between with no backrest (NB) and with backrest contact at L2 (B_{0L2}) (p=0.504, Wilcoxon) and between NB and B_{0T5} (p=0.119, Wilcoxon). With increasing inclination of the backrest (B_{10}, B_{20} and B_{30}), the principal resonance frequency of the vertical transmissibility to the pelvis also showed no significant change (p=0.507, Friedman). The vertical transmissibility to the pelvis tended to increase at the resonance frequencies with increasing inclination of the backrest but the increase was not statistically significant (p=0.125, Friedman).

When sitting with either the vertical backrest at T5 (B_{0T5}) or inclined backrests, the resonance frequencies in the vertical transmissibility to L5 (at around 5 Hz) increased, compared to sitting without backrest (NB and B_{0T5}, p=0.008, Wilcoxon; NB and B_{10}, p=0.001, Wilcoxon; NB and B_{20}, p=0.004, Wilcoxon; NB and B_{30}, p=0.006, Wilcoxon). A similar result was observed for the vertical transmissibility to L3. The vertical transmissibility to the lumbar spine (at both L5 and L3) tended to increase at frequencies 6-10 Hz either with the vertical or inclined backrests compared to the normal upright sitting posture as shown in the median data.

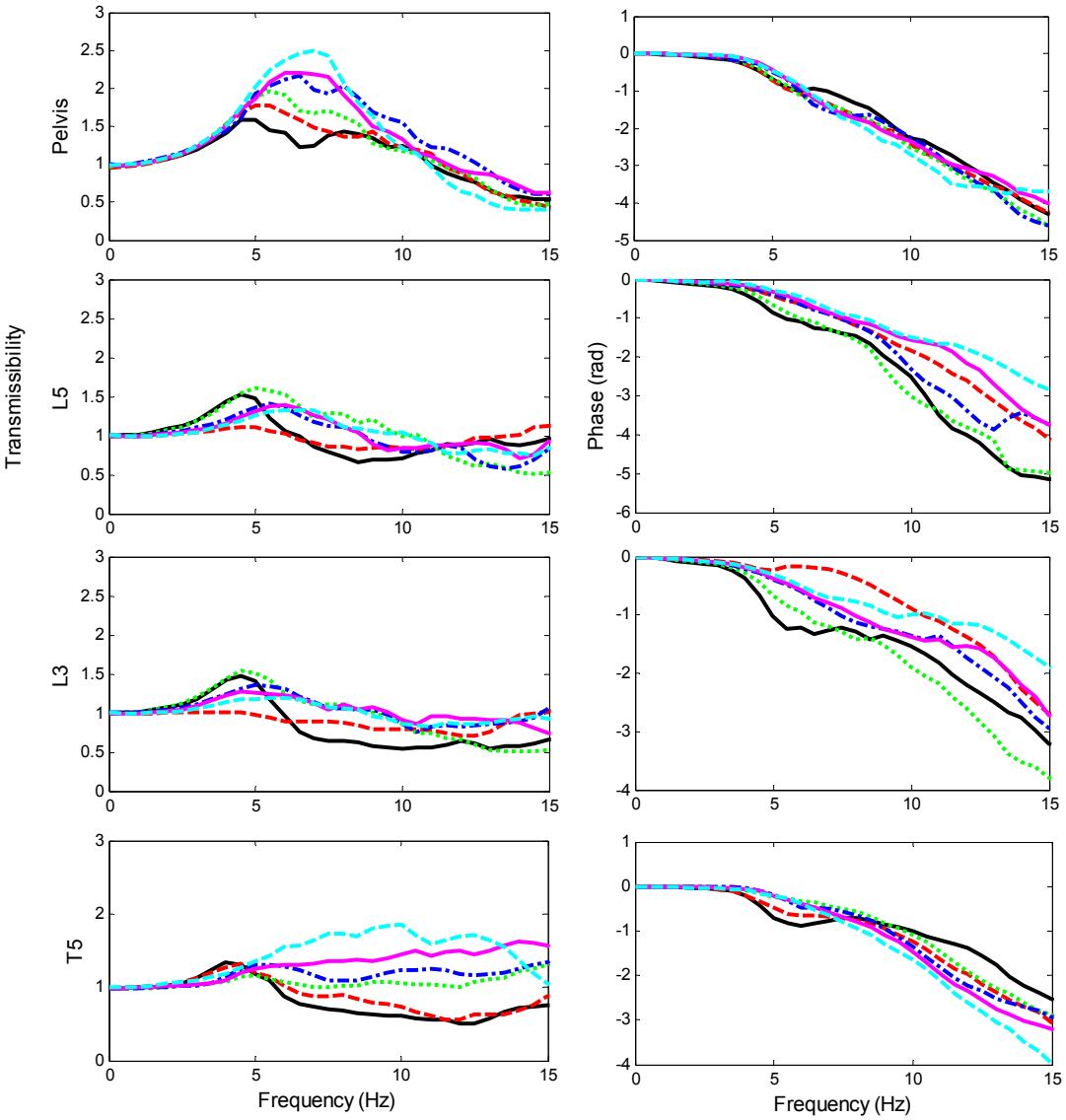

Figure 6.12 Vertical in-line transmissibilities to various spinal levels in different sitting conditions: in normal upright sitting posture NB ('——'); with vertical backrest contact at L2, B_{0L2} ('------'); with vertical backrest contact at T5, B_{0T5} ('.....'); in contact with 10º-inclined backrest, B_{10} ('–·–'); in contact with 20º-inclined backrest, B_{20} ('——'); in contact with 30º-inclined backrest, B_{30} ('------'). Left: modulus; right: phase. From top row to bottom row: transmissibility to pelvis, L5, L3 and T5. Median values from 12 subjects.

The transmissibility to the thoracic spine (T5) increased at frequencies between 5-15 Hz when introducing backrest contact. With increasing inclination of the backrest, the vertical transmissibility to T5 increased at frequencies in the range 5 – 15 Hz (p < 0.05, Friedman). The resonance frequency of the vertical transmissibility to T5 increased slightly from normal upright sitting posture to sitting with either vertical or inclined backrests (p=0.001, Friedman).

6.3.3.2 Fore-and-aft cross-axis transmissibilities to spine

The individual fore-and-aft cross-axis transmissibility from vertical acceleration at the seat to fore-and-aft acceleration at various spine levels (i.e., iliac crest, L5, L3 and T5) of 12 subjects in the normal upright sitting posture are shown in Figure 6.13, together with the median data.

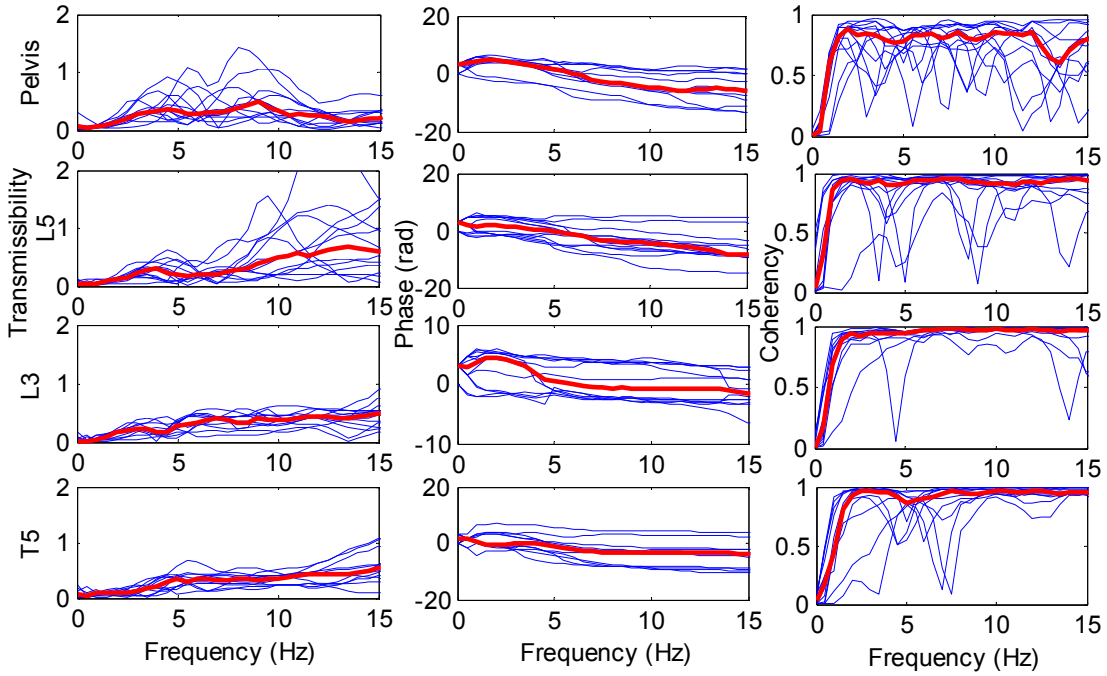

Figure 6.13 Fore-and-aft cross-axis transmissibilities to various spinal levels in normal upright sitting posture without backrest contact of 12 individual subjects. From top row to bottom row: transmissibility to pelvis, L5, L3 and T5. Individual subject: ('—'); Median of 12 subjects: ('—'). In one row, from left to right: modulus, phase and coherency.

The median fore-and-aft transmissibility to all spinal levels varied from 0 to 1 between 0 and 15 Hz (Figure 6.13). The individual transmissibilities to the pelvis, L3, and T5 varied between 0 and 1.5. Greater inter-subject variability was observed for the fore-and-aft cross-axis transmissibility to the pelvis and lower lumber spine (L5), compared to the transmissibility to L3 and T5. The transmissibility to the lower body (i.e., pelvis, L5, and L3) showed a resonance at frequency lower than 5 Hz, and the transmissibility to the pelvis and L5 showed a secondary resonance between 5 and 15 Hz. The transmissibility to T5 showed a resonance around 5 Hz, which was higher than those in the transmissibilities to the lower body. The coherencies for all transmissibilities were low at frequencies less than 3 Hz, but increased with increasing frequency.

The median fore-and-aft cross-axis transmissibilities to four spinal levels in six backrest contact conditions are shown in Figure 6.14. With vertical backrest contact, the resonance frequency of the fore-and-aft cross-axis transmissibilities to the lower body (i.e., pelvis, L5 and L3) was about 6 Hz, greater than the resonance frequency with no backrest contact (at about 3 Hz). With vertical backrest, the transmissibility to all spinal levels increased over the frequency range 5-15 Hz.

With increasing inclination of the backrest from 10º to 30º, the transmissibility to the upper body (T5) tended to increase at frequencies greater than the resonance frequency, while the trend for the transmissibility to the lower body (i.e., pelvis, L5, and L3) was less clear. The transmissibility to L5 and T5 increased significantly from the posture with no backrest to sitting with either the vertical backrest or any inclined backrests at frequencies greater than 5 Hz, particularly for the transmissibility to T5. With increasing inclination of the backrest from 10º to 30º, the resonance

frequency in the fore-and-aft cross-axis transmissibility to T5 (between 8-10 Hz) increased (p=0.004, Friedman). For all six sitting conditions, apart from a first peak occurring at around 3.5 - 5 Hz, a secondary resonance was observed for the transmissibilities to the pelvis and the lumbar spine. The secondary resonance for the transmissibility to pelvis was around 8 Hz and the secondary resonance of the transmissibilities to L5 and L3 were around 10 Hz and 13 Hz, respectively.

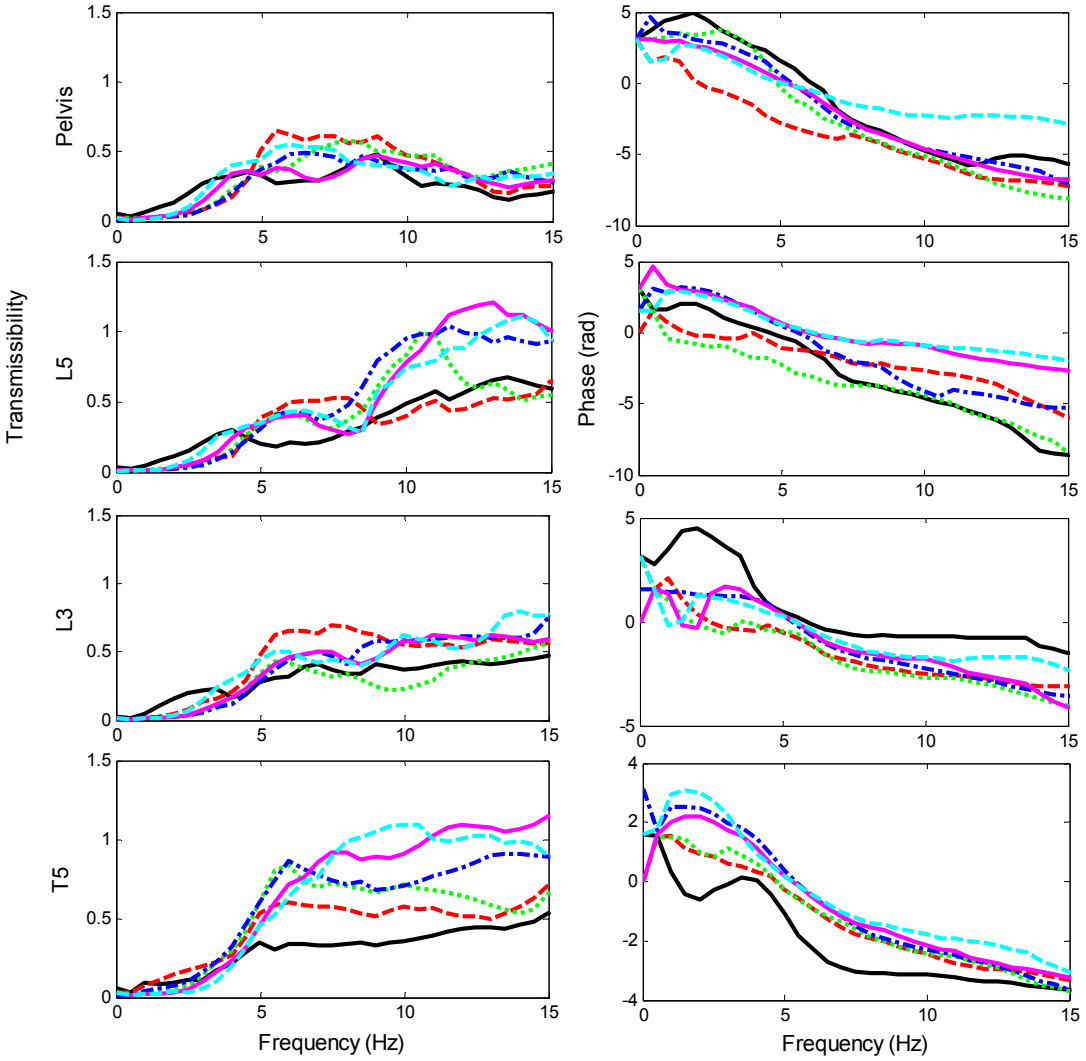

Figure 6.14 Fore-and-aft cross-axis transmissibilities to various spinal levels in different sitting conditions: normal upright sitting posture NB ('——'); vertical backrest contact at L2, B_{0L2} ('------'); vertical backrest contact at T5, B_{0T5} ('……'); contact with 10º-inclined backrest, B_{10} ('–·–'); 20º-inclined backrest, B_{20} ('——'); 30º-inclined backrest, B_{30} ('------'). Left: modulus; right: phase. From top row to bottom row: transmissibility to pelvis, L5, L3 and T5. Median values from 12 subjects.

6.3.3.3 Pitch transmissibilities to the spine

The pitch transmissibilities to each location are shown in Figure 6.15. The pitch transmissibility is deemed to be reliable only at frequencies less than 10 Hz, because a resonance around 10 Hz was observed when estimating the skin-tissue effect in the pitch direction for some subjects.

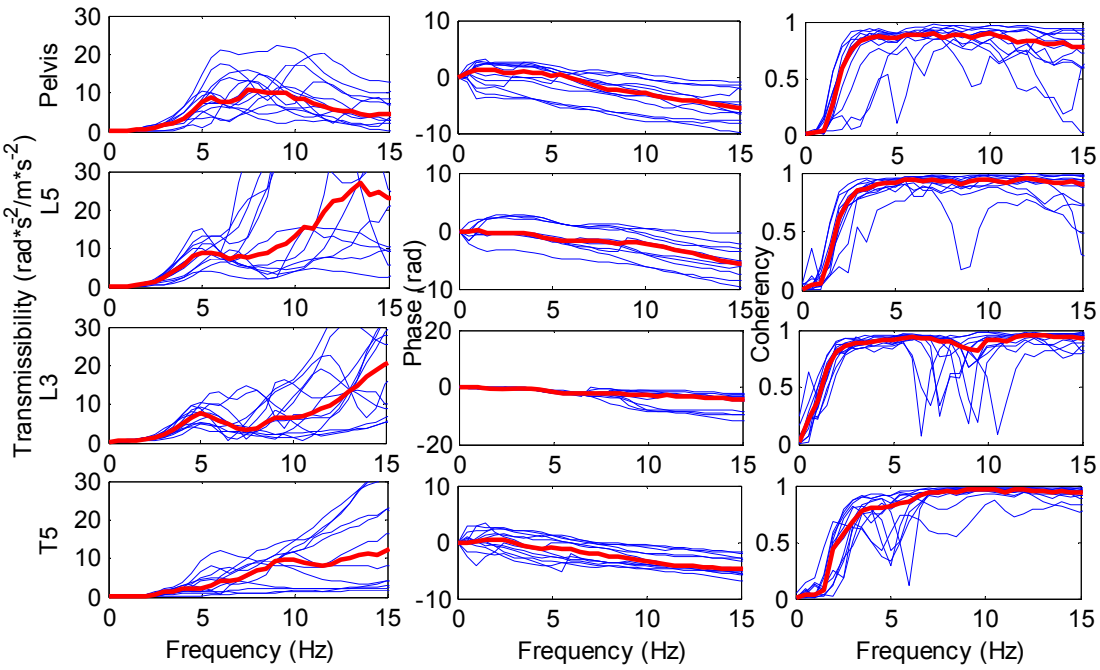

Figure 6.15 Pitch transmissibilities to various spinal levels in the normal upright sitting posture for 12 individual subjects. From top row to bottom row: transmissibility to pelvis, L5, L3 and T5. Individual subject: ('—'); Median of 12 subjects: ('—'). In one row, from left to right: modulus, phase and coherency.

At all spinal levels, the inter-subject variability in the pitch transmissibility was large at the higher frequencies (i.e., 5 - 10 Hz). The coherencies of the four transmissibilities were low at frequencies less than 2.5 Hz. All the transmissibilities were low at frequencies less than 3 Hz but increased with increasing frequency. The pitch transmissibility to the pelvis, L5, and L3 showed a resonance around 5-6 Hz, and the transmissibility to T5 showed a resonance with lower transmissibility at a lower frequency around 4 Hz. A secondary resonance at about 8 Hz was observed in the pitch transmissibility to the pelvis of some subjects. The pitch transmissibility to T5 showed another resonance at a frequency around 6 - 8 Hz for 8 of 12 subjects. The transmissibility around 5 Hz tended to decrease as the measurement location moved from the pelvis to the lumbar spine (L5 and L3), and to the thoracic spine (T5).

The pitch transmissibility to the pelvis, L3, and T5 varies between 0 and 20 in the frequency range 0-10 Hz, which is consistent with the measurements of Matsumoto and Griffin (1998). However, the pitch transmissibility to L3 for some subjects reached a value greater than 30 at around 10 Hz for some subjects.

The median pitch transmissibilities to four spinal levels with vertical and inclined backrests are shown in Figure 6.16. With either vertical or inclined backrests (10º, 20º, 30º) with support in the thoracic region, the pitch transmissibility to the pelvis increased at frequencies greater than the resonance around 5 Hz. With either a 10º-inclined backrest or a 20º- inclined backrest, the resonance frequency of the pitch transmissibility to L5 moved up to 6 - 8 Hz compared to no backrest contact. With vertical or inclined backrest contact, the resonance in the pitch

transmissibility to L3 at around 5 Hz became less distinct, but the peak at frequencies greater than 8 Hz increased with increasing inclination of the backrest.

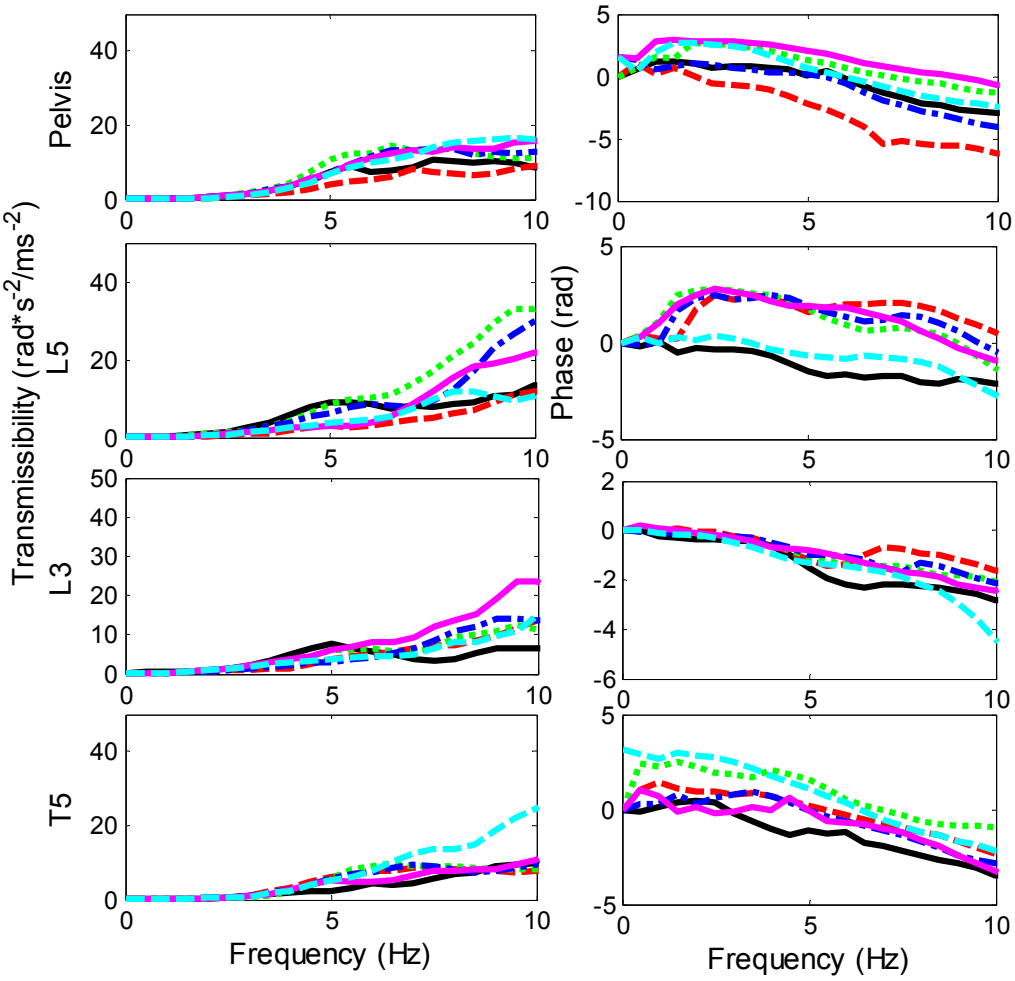

Figure 6.16 Pitch transmissibilities to various spinal levels in different sitting conditions: normal upright sitting posture NB ('——'); vertical backrest contact at L2, B_{0L2} ('------'); vertical backrest contact at T5, B_{0T5} ('……'); contact with 10º-inclined backrest, B_{10} ('–·–'); 20º-inclined backrest, B_{20} ('——'); 30º-inclined backrest, B_{30} ('------'). Left: modulus; right: phase. From top row to bottom row: transmissibility to pelvis, L5, L3 and T5. Median values from 12 subjects.

6.4 Discussion

6.4.1 Apparent mass at the seat measured in the normal upright sitting posture without backrest contact

The measured vertical in-line apparent mass at the seat in a normal upright sitting posture was consistent with previous studies (e.g., Fairley and Griffin, 1989). The principal resonance observed at about 5 Hz in all subjects was associated with vertical and fore-and-aft motion of the pelvis and bending of the spine with shear and axial deformation of buttocks tissues in accord with modal analysis and previous experimental findings (Kitazaki and Griffin, 1997; Matsumoto and Griffin, 1998). A secondary resonance at around 8 Hz was observed for the majority of subjects (8 of 12 subjects), which might be caused by pitch motion of the pelvis and vertical movement of viscera (Kitazaki and Griffin, 1997).

Inter-subject variability in the vertical apparent mass was mainly due to differences in the sitting masses of the subjects (Fairley and Griffin, 1989) and evident as the apparent mass at frequency close to zero (e.g. 0.5 Hz) in the vertical apparent mass.

6.4.2 Effect of vertical and inclined backrests on the vertical in-line apparent mass at the seat pan

An increase in the resonance frequency of the vertical in-line apparent mass at the seat pan has been reported when the back is supported by a vertical backrest (Nawayseh and Griffin, 2004), with the resonance frequency increasing further if the backrest is inclined (Toward and Griffin, 2009). In the present study, a similar increasing trend in the resonance frequency of the vertical in-line apparent mass at seat pan was observed, although a statistically significant difference was only found with a 30º-inclined backrest.

As the backrest inclination increased, the vertical apparent mass measured at the seat pan decreased at the resonance (around 5 Hz) and at lower frequencies, presumably because more of the body weight was supported by the backrest.

With increasing backrest inclination, the peak in the vertical apparent mass around the resonance broadened. With the backrest inclined to 20º or 30º, some subjects exhibited two peaks at frequencies around the resonance (in the range 4 to 8 Hz). According to a modal analysis of the human body in an upright sitting posture without backrest (e.g., Kitazaki and Griffin, 1997; Matsumoto and Griffin, 2001), the resonance frequency (around 5 Hz) arises from several body modes that are merged due to heavy damping of the body. The modes include pitch motion of the pelvis with bending of the spine combined with shear and axial deformation of buttocks tissues. The two peaks observed in the present study indicate that two or more body modes were excited in the range of 4 to 8 Hz and that increasing the inclination of the backrest tended to separate the two modes.

6.4.3 Effect of vertical and inclined backrests on fore-and-aft cross-axis apparent mass at the seat pan

When sitting without a backrest, the principal resonance in the fore-and-aft cross-axis apparent mass at the seat pan was correlated with the resonance frequency in the vertical in-line apparent mass (p<0.001, Spearman). This is consistent with the findings of some previous studies (Nawayseh and Griffin, 2004; Qiu and Griffin, 2012), and suggests that when sitting without a backrest the resonances evident in the vertical in-line apparent mass and the fore-and-aft cross-axis apparent mass have a common cause.

When sitting with a vertical backrest and supported at either L2 or T5 (B_{0L2} and B_{0T5}), the resonance frequencies in the vertical in-line apparent mass and the fore-and-aft cross-axis apparent mass were also correlated (B_{0L2}, p=0.012; B_{0T5}, p=0.003; Spearman). However, with the backrest inclined (B_{10}, B_{20} and B_{30}), the correlation was no longer statistically significant (p>0.05, Spearman). The resonance tended to be at a lower frequency in the fore-and-aft cross-axis apparent mass than in the vertical in-line apparent mass, especially when the backrest was inclined

by 20º and 30º (at 20º, 4 Hz in the fore-and-aft cross-axis and 5 Hz in the vertical in-line apparent mass; at 30º, 4 Hz in the fore-and-aft cross-axis and 5.5 Hz in the vertical in-line apparent mass; Figures 6.4 and 6.6). The absence of the correlation when the backrest was inclined indicates that different body motions may have contributed to the resonances in the fore-and-aft cross-axis apparent mass and the vertical in-line apparent mass.

6.4.4 Vertical in-line apparent mass and fore-and-aft cross-axis apparent mass at the back

When contact with the vertical backrest changed from L2 (B_{0L2}) to T5 (B_{0T5}), both the vertical in-line apparent mass and the fore-and-aft cross-axis apparent mass at the backrest increased at the resonance frequency. The resonance in the fore-and-aft cross-axis apparent mass at the back may be influenced by motions of head-neck system and fore-and-aft motion of the spine (Nawayseh and Griffin, 2004). The increased fore-and-aft cross-axis apparent mass at the backrest at resonance could be caused by increased motion of the thoracic spine with the back support in the thoracic region (i.e., B_{0T2}), as observed from the corresponding vertical and fore-and-aft transmissibilities to T5 (Figures 6.12 and 6.14).

With increasing inclination of the backrest, the vertical in-line apparent mass and the fore-and-aft cross-axis apparent masses at the back increased. The increase in both apparent masses at low frequencies indicates that more mass was supported on the backrest as the backrest inclination increased. The fore-and-aft cross-axis apparent mass at the back tended to be greater than the vertical in-line apparent mass at the back, presumable due to the greater relative motion in the fore-and-aft direction between the body and the backrest than in the vertical direction during vibration. At the resonance, with increasing inclination of the backrest (from B_{0T5} to B_{30}) the median fore-and-aft cross-axis apparent mass at the backrest increased from 22 to 40 kg whereas the median vertical in-line apparent mass at the backrest increased from 4 to 12 kg (Figures 6.7 and 6.8).

6.4.5 Dynamic forces experienced by the seated body in vertical and fore-and-aft directions

The measurements allow the calculation of how the sum of the vertical in-line (and fore-and-aft cross-axis) forces at the seat and the backrest vary according to the nature of the backrest. The transfer functions between the vertical seat acceleration and the sum of the forces at the seat pan and the backrest in the vertical and fore-and-aft directions were calculated, in the frequency domain for each subject to give the ‘overall vertical in-line apparent mass’ and the ‘overall fore-and-aft cross-axis apparent mass’ (Figure 6.17).

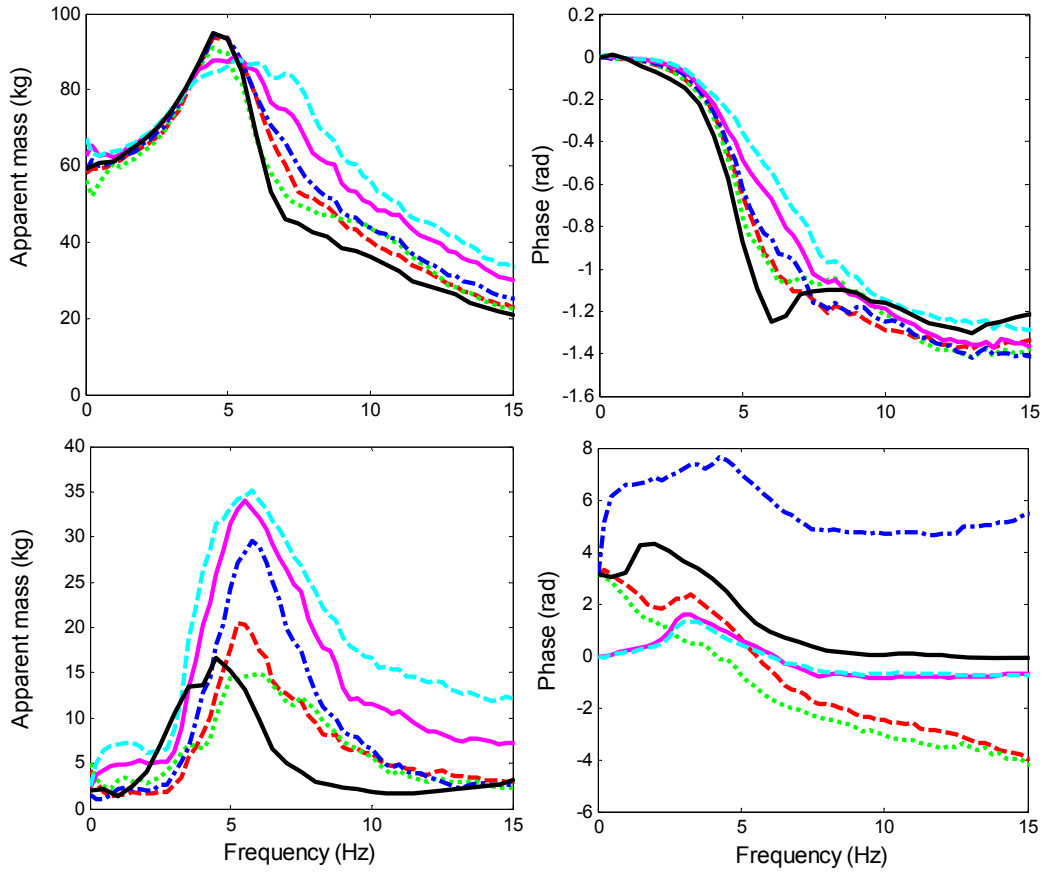

Figure 6.17 Overall vertical in-line apparent mass (top row) and overall fore-and-aft cross-axis apparent mass (bottom row) in different sitting conditions: normal upright sitting posture NB ('——'); vertical backrest contact at L2, B_{0L2} ('------'); vertical backrest contact at T5, B_{0T5} ('……'); contact with 10º inclined-backrest, B_{10} ('–·–'); 20º-inclined backrest, B_{20} ('——'); 30º-inclined backrest, B_{30} ('------'). Left: modulus; right: phase. Median values from 12 subjects.

No difference was reported in the apparent mass at 0.78 Hz calculated from the seat acceleration and the sum of vertical forces in the frequency domain (at the seat pan and backrest) when sitting with and without a backrest (Nawayseh and Griffin, 2004). In the present study, irrespective of the backrest condition, the overall vertical apparent mass at very low frequencies (e.g., 0.5 Hz) was close to the static mass when sitting with no backrest (Figure 6.17). The slight differences between the vertical apparent mass at low frequencies and the static mass could be due to variations in the support from the footrest when the backrest condition varied. With increasing inclination of the backrest the overall vertical in-line dynamic forces showed no significant change at frequencies up to 5 Hz but increased at higher frequencies in the range 6 to 15 Hz (p<0.001, Friedman). With increasing inclination of the backrest, the overall fore-and-aft cross-axis dynamic forces increased in the frequency range 5 to 15 Hz (p<0.001, Friedman).

6.4.6 Transmissibilities to the spine

The data correction method may not be effective at frequencies greater than the natural frequency of the local tissue-accelerometer system (Kitazaki and Griffin, 1995). Hence, the transmissibility data may only be valid up to 10 Hz. In a previous study (e.g., Matsumoto and Griffin, 1998), the vertical and fore-and-aft transmissibility to the centre of a vertebral body was estimated by

eliminating the effect of pitch motion from the corrected transmissibility (after skin-tissue correction) at the spinous processes. It was reported that a 20% reduction appeared at the vertical transmissibility to the vertebral body centre at the resonance frequency and at frequencies greater than the resonance (5 - 10 Hz) after eliminating the effect of pitch motion, compared to the corresponding transmissibility to the spinous processes at the same spinal level without eliminating the effect of pitch motion. The elimination of the effect of pitch motion requires the estimation of the distance from the spinous process to the vertebrae body centre, which would have varied between subjects and is difficult to measure.

In the current study, the measured transmissibility at the skin over the vertebrae body was only corrected to the spinous process, because one of the main purposes of the study was to investigate the correlation between the resonance frequency of the apparent mass and the resonance frequency of the transmissibilities to the spine in different directions and an at different locations.

The fore-and-aft and vertical transmissibilities to the lumbar spine and the pelvis measured in this study were consistent with the previous measurements (up to 10 Hz, e.g., Matsumoto and Griffin, 1998; Mansfield and Griffin, 2000). The pitch transmissibilities to all spinal levels also showed similar trends in the range up to 10 Hz with previous studies (e.g., Matsumoto and Griffin, 1998). The pitch transmissibility to L3 at 10 Hz was greater than in previous results (e.g., Matsumoto and Griffin, 1998). The differences may be due to inter-subject variability and the size or mass of the accelerometers used in two studies.

In the normal upright sitting posture without backrest contact, the pitch transmissibilities to the pelvis and the lumbar spine (i.e., L5 and L3) all showed a resonance at around 5 Hz, which was close to the resonance frequency of vertical apparent masses of the seated subjects. This resonance has been observed in some previous studies (e.g. Mansfield and Griffin, 2002), suggesting the pitch motion would also contribute to the principal resonance frequency in the apparent mass at the seat.

6.4.7 Effect of backrest and backrest inclination on body transmissibility

In the present study, with a vertical backrest or backrests of increasing inclination, the resonance frequency in the vertical transmissibility to the pelvis tended to increase, and the transmissibility at frequencies greater than the primary resonance increased. Similarly, the resonance frequency of the vertical transmissibility to the lumbar spine (L5 and L3) increased with increasing backrest inclination, but the transmissibility at resonance tended to decrease. The increase in the resonance frequency of the transmissibility to the lumbar spine may be caused by an increase in the stiffness of the lumbar spine region due to direct contact with the backrest at the thoracic level. A decrease in the vertical transmissibility at the resonance could arise from the backrest reducing the bending motion of the spine at the resonance frequency because of the constraint applied by the backrest.

With increasing inclination of the backrest, the weight supported on the pelvis reduced, which would be expected to result in an increase in the resonance frequency of the vertical

transmissibility to pelvis. The enhancement in the fore-and-aft motion of the pelvis with inclined backrests was less significant compared to the increased vertical motion.

For the pitch transmissibility to the pelvis, the median transmissibility exhibited a resonance around 5 Hz and another resonance at around 8 Hz when sitting in the normal upright sitting posture. With the vertical backrest providing support at T5, the corresponding resonance frequencies in the pelvis pitch transmissibility increased to 8 Hz and 10 Hz. The increasing trend in the resonance frequency of the pitch transmissibility to the pelvis seems different from the median data reported by Mansfield and Griffin (2002). Their results showed a decrease in the resonance frequency from 14 Hz to 10 Hz from no backrest to a 'back-on' posture, although 'not significant differences' were stated in their study. The body modes contributing to the resonance at 8-10 Hz in the current study would be different from the body modes contributing to the resonance at 10-14 Hz in the study from Mansfield and Griffin (2002).The differences between the two studies could also be due to a difference in the sitting postures adopted and the different subjects involved.

Regarding the effect of the location of backrest support on the transmissibility, with local support at the thoracic spine, the motions of the thoracic spine in both vertical and fore-and-aft directions were reduced, as shown in the significant reductions in transmissibility to T5 in both directions (Figures 6.12 and 6.14). For example, in the B_{0T5} posture, the median vertical transmissibility to T5 was around 1.1 at the resonance frequency of 5 Hz, while in normal upright sitting posture the corresponding transmissibility was about 1.5. A similar restriction of lumbar motion was observed when contact with the vertical backrest occurred at the lumbar spine (i.e., B_{0L2}). For some subjects, as the measurement location at T5 was coincident with the contact location against backrest (T5), the vertical transmissibility to T5 was around 1.0 until 6 Hz or 7 Hz because the skin and tissue at the T5 level contacted directly with the backrest and presumably moved rigidly with the backrest at these frequencies. However, the vertebral body would move in a different manner as it would move separately from the skin and tissue at this spinal level. The blocks measuring the transmissibilities were attached on the skin surface, which limits the measurement of the motions of the vertebrae bodies.

With increasing inclination of the backrest (from 10º to 30º), the resonance frequency in the fore-and-aft transmissibility to the pelvis tended to decrease (p=0.061, Friedman), and no significant difference was found from the resonance frequency of the fore-and-aft transmissibility to the lumbar region. In contrast, the resonance frequency of the fore-and-aft transmissibility to T5 tended to increase when the backrest inclination increased from 10º to 30º (p=0.004, Friedman), probably due to direct excitation in the fore-and-aft direction from the backrest and also from part of the body mass supported on the backrest.

6.4.8 Correlations between spine transmissibilities and the vertical in-line apparent mass at the seat pan

With increasing inclination of the backrest, the resonance frequency of the vertical apparent mass at the seat pan showed an increasing trend. Two peaks were observed in the vertical apparent mass at the seat pan at frequencies around 4-8 Hz with the inclined backrests, corresponding to

the principal resonance (around 5 Hz) observed in the vertical apparent mass at the seat with no backrest (as mentioned in Section 6.4.2).

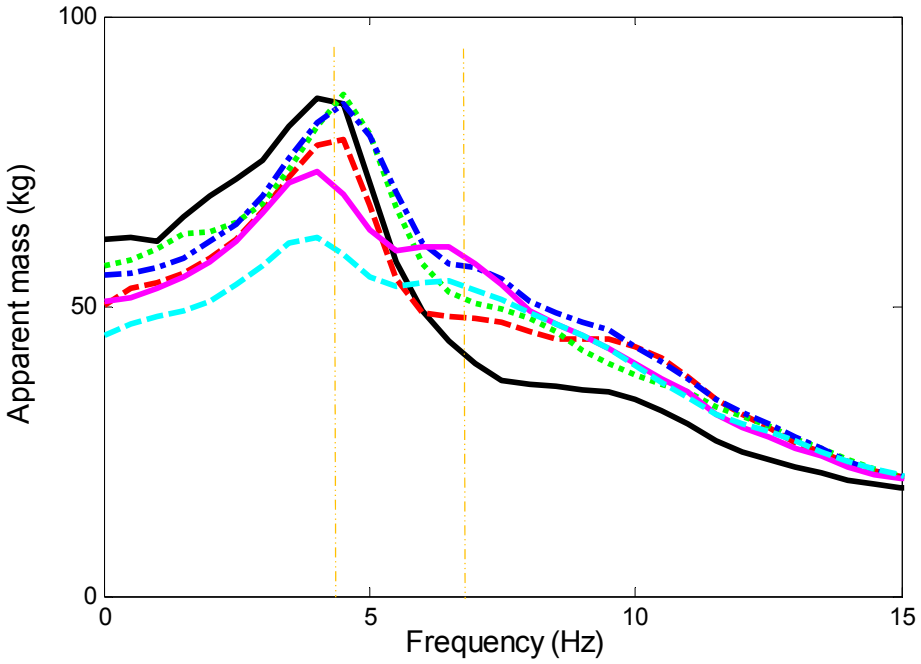

Figure 6.18 Vertical apparent mass at the seat pan for subject 6 in six backrest contact conditions. Line style of each backrest condition follows the Figure 6.17. Two peaks can be observed in the apparent mass measured with B_{20} and B_{30} conditions at 4 Hz and 6.5 Hz.

The two peaks suggest that two or more body modes were excited in the range of 4 to 8 Hz and that increasing the inclination of the backrest separated the two modes (e.g., Figure 6.18, for an individual subject), and that the two peaks might arise from motions of different body parts. Correlations between resonance frequencies of the vertical apparent mass at the seat and the resonance frequencies of the vertical body transmissibilities were conducted. The principal resonance frequencies of the vertical apparent mass at the seat pan of individual subjects in the normal upright sitting posture and when sitting with vertical backrest contact (i.e., B_{0L2}, B_{0T5}) are highlighted in Table 6.3. When contacting the inclined backrests (B_{10}, B_{20} and B_{30}), some subjects showed two peaks within the 4 to 8 Hz range. For subjects showing only one peak within the 4 to 8 Hz range, only one peak is highlighted in Table 6.3. The principal resonance frequencies (i.e., the resonance frequencies with the greatest transmissibility) of the vertical transmissibility to each spinal level for 12 subjects (shown in Appendix A.1) were used in the Spearman correlation tests. For the subjects not showing a resonance frequency in the vertical transmissibility to spinal locations, the data were removed. The Spearman correlation tests results are shown in Table 6.4.

In the normal upright sitting posture without backrest contact, the resonance frequency of the vertical apparent mass at the seat pan was correlated with the resonance frequency of the vertical transmissibility to the lumbar spine (L5 and L3) and the thoracic spine (T5). Similar results were found by Zheng (2012), where the principal resonance frequency of the vertical apparent mass at

the seat pan measured with vertical random vibration at 1.0 m/s^2 r.m.s. was correlated with the resonance frequency of the vertical transmissibility to L3, T5 and T1.

Table 6.3 Resonance frequencies of the vertical apparent mass at the seat pan measured without a backrest and with vertical and inclined backrests.

Resonance frequencies of the vertical apparent mass at the seat pan								
Posture	NB	B_{0L2}	B_{0T5}	B_{10}	B_{20}		B_{30}	
Sub 1	5	4.5	5	5.75	**4.5**	*6.25*	*3.5*	**6.75**
Sub 2	4.25	4.25	4.25	4.5	4.5	-	**4**	*7*
Sub 3	4.5	4	4.25	4.5	4.5	-	*3.5*	**5.5**
Sub 5	4.5	4.75	4.5	6.25	**5.25**	*7*	7	-
Sub 6	4.25	4.25	4.5	4.5	**4**	*6.5*	**3.75**	*6.5*
Sub 7	5.5	5.5	5.25	5.25	6	-	*5*	**7.5**
Sub 8	5	4.5	5.25	5.25	5.75	-	*5.25*	**7.75**
Sub 9	4.75	5.25	4.5	4.75	*4.5*	**6.25**	7.75	-
Sub 10	4.5	4.5	5	4.5	4.5	-	5.5	-
Sub 11	4.5	4.75	5	4.75	5.5	-	5.75	-
Sub 12	5	4.5	4.5	4.5	4.5	-	**4**	*5.25*
Sub 13	4.75	5	5.25	4.5	4.5	-	5.25	-

The numbers in **bold** indicate the peak with greater magnitude;
The numbers in *italic* indicate the peak with smaller magnitude.

Table 6.4 Correlation (Spearman test) between the principal resonance frequency of the vertical apparent mass at the seat pan and the principal resonance frequencies of the vertical transmissibilities measured with different backrest contact conditions.

	Postures	NB	B_{0L2}	B_{0T5}	B_{10}	B_{20}	B_{30}
Pelvis	Correlation coefficient (r)	0.333	0.428	0.317	0.604	0.533	0.555
	p value	0.291	0.166	0.315	0.038*	0.074	0.061
L5	Correlation coefficient (r)	0.863	0.790	0.653	0.803	0.014	0.444
	p value	0.003*	0.020*	0.057	0.003*	0.965	0.149
L3	Correlation coefficient (r)	0.887	0.215	0.333	0.739	0.324	0.010
	p value	0.001*	0.502	0.291	0.023*	0.304	0.705
T5	Correlation coefficient (r)	0.634	0.707	0.435	0.578	0.573	0.694
	p value	0.036*	0.015*	0.181	0.063	0.084	0.038*

* Statistically significant, $p<0.05$.

With the vertical backrest providing lumbar support (B_{0L2}), the principal resonance frequency of the vertical apparent mass at the seat pan was correlated with the principal resonance frequencies of the vertical transmissibilities to the lower lumbar spine (L5) and the thoracic spine (T5). With vertical backrest contact providing support at the thoracic level, there was no significant correlation between the resonance frequencies of transmissibility and apparent mass.

With the 10º-inclined backrest (B_{10}), there was a significant correlation between the resonance frequencies of the vertical transmissibilities to the lower body (including pelvis, L5 and L3) and the principal resonance frequency of the vertical in-line apparent mass at the seat pan. With 20º-inclined backrest, there was no significant correlation between the principal resonance of the vertical in-line apparent mass at the seat pan and the vertical transmissibilities to the spine. With

the 30º-inclined backrest, a significant correlation (p=0.038) was found between the principal resonance frequencies of the vertical in-line apparent mass at the seat pan and the vertical transmissibility to T5.

The insignificant correlations found with the 20º-inclined backrest might be due to some subjects showing two peaks within the frequency range 4 – 8 Hz or a broad peak over this frequency range. With the 20º-inclined backrest, the majority of the subjects showed a resonance at around 4.5 Hz with greater vertical apparent mass at the seat pan compared to another resonance at around 6 Hz. The frequency of the first peak at around 4.5 Hz was used in the correlation with the resonance frequencies in the transmissibilities. However, with 30º-inclined backrest, most subjects showed a greater apparent mass at the second resonance, hence the frequency of the second resonance for most subjects was used in the correlation with the resonance frequencies in the body transmissibilities. The peaks at different frequencies would be associated with different body modes. In order to obtain more reasonable results, the resonances in the subjects could be roughly grouped into the first resonance (i.e., at the lower frequency) and the second resonance (i.e., at the higher frequency) from 3.5 Hz to 8 Hz, irrespective of the magnitudes. For subjects only showing one peak within the frequency range, the same resonance frequency was used in both groups.

In order to understand the mechanism behind the resonances in the vertical apparent mass and find the relationship between spine motion and the resonance in the apparent mass, an additional statistical test was carried out to find the correlations of the first and the second resonance frequencies of the vertical apparent mass at the seat pan with the resonance frequency of the vertical transmissibility to the spine with 20º- and 30º- inclined backrests. The results of the correlation are shown in Table 6.6, and the first and second resonance frequencies of vertical apparent mass at the seat pan are listed in Table 6.5.

Table 6.5 First and second resonance frequencies of vertical in-line apparent mass at the seat pan at 4-8 Hz with 20º-inclined and 30º-inclined backrests.

Inclination of backrest	B_{20}		B_{30}	
Resonances in the range 4 to 8 Hz for the vertical in-line apparent mass at the seat pan	First resonance frequency (Hz)	Second resonance frequency (Hz)	First resonance frequency (Hz)	Second resonance frequency (Hz)
	4.50	6.25	3.50	6.75
	4.50	4.50	4.00	7.00
	4.50	4.50	3.50	5.50
	5.25	7.00	7.00	7.00
	4.00	6.50	3.75	6.50
	6.00	6.00	5.00	7.50
	5.75	5.75	5.25	7.75
	4.50	6.25	7.75	7.75
	4.50	4.50	5.50	5.50
	5.50	5.50	4.75	5.75
	4.50	4.50	4.00	5.25
	4.50	4.50	5.25	5.25

From Table 6.6, for the subjects showing two peaks in 4 – 8 Hz range with the 20º-inclined backrest (B_{20}), the first peak (around 4.5 Hz) in the vertical apparent mass at the seat pan was

correlated with the resonance frequency of the vertical transmissibility to the pelvis (p=0.0207, Spearman), while the second peak (around 6 Hz) in the vertical apparent mass at seat pan was correlated with the resonance frequency in the vertical transmissibility to the thoracic spine T5 (p=0.0251, Spearman). Similarly, for the subjects showing two peaks with the 30º-inclined backrest (B_{30}), a significant correlation was found between the second resonance frequency (around 6.5 Hz) in the vertical apparent mass at the seat pan and the resonance frequency in the vertical transmissibility to the thoracic spine T5 (p=0.0409, Spearman).

Table 6.6 The Spearman rank correlations between the first or second resonance frequency of vertical in-line apparent mass at the seat pan and the vertical transmissibility to the spine with 20º-inclined and 30º-inclined backrests.

B_{20}					
	location	pelvis	L5	L3	T5
First resonance	Correlation coefficient (r)	0.655	0.135	0.339	0
	p value	0.021*	0.676	0.281	1
Second resonance	Correlation coefficient (r)	0.177	-0.195	0.168	0.697
	p value	0.582	0.544	0.602	0.025*
B30					
	location	pelvis	L5	L3	T5
First resonance	Correlation coefficient (r)	0.006	-0.107	0.412	0.435
	p value	0.986	0.741	0.183	0.242
Second resonance	Correlation coefficient (r)	0.176	0.029	0.520	0.687
	p value	0.584	0.928	0.083	0.041*

* Statistically significant, p<0.05.

With the inclination of the backrest increased from 20º to 30º, the first resonance frequency in the vertical apparent mass at the seat pan tended not to change (p=0.878, Wilcoxon). However, the second resonance frequency in the vertical apparent mass at the seat pan increased (p=0.002, Wilcoxon).

The inclined backrest contact tended to separate two body modes that contribute to the principal resonance at around 5 Hz shown with no backrest contact, resulting in a broad peak or two peaks in the range 4 - 8 Hz. The vertical motion of pelvis might contribute to a body mode at about 4.5 Hz, while vertical motion of the thoracic spine (i.e., T5) might contribute to another body mode at about 6 Hz. Motions of other body parts may contribute to the above two resonances. With the inclined backrest, the second mode with vertical motion of the thoracic spine occurred at a higher frequency, resulting in the separation of the two peaks or a broad peak as described above.

6.5 Conclusion

Contact with an inclined backrest reduces the mass of the body supported on the seat pan but increases the fore-and-aft dynamic shearing force between body and the seat pan. The presence

of an inclined backrest alters the body motions and resonance frequencies in the vertical in-line apparent mass and the fore-and-aft cross-axis apparent mass measured at the seat pan.

When there is no backrest or a vertical backrest, the resonance frequency in the fore-and-aft cross-axis apparent mass at the seat pan is correlated with the resonance frequency in the vertical in-line apparent mass at the seat pan. However, the two resonance frequencies became less correlated with increasing inclination of the backrest, suggesting different body modes may contribute to the vertical in-line apparent mass and the fore-and-aft cross-axis apparent mass when the backrest is inclined. More work is required to find the body modes contributing to the resonance in the fore-and-aft cross-axis apparent mass at the seat pan.

An inclined backrest increases the mass of the upper body supported on the backrest and increases the fore-and-aft cross-axis apparent masses at both the seat pan and the backrest. The vertical motions of the pelvis, lumbar spine, and thoracic spine tend to be increased by the use of a backrest in the higher frequency range (6- 15 Hz). The use of a vertical backrest or an inclined backrest tends to have small influence on the fore-and-aft motion of the lower body (pelvis and lumbar region), but increases the motion of the thoracic spine.

An inclined backrest appears to separate two of the body modes thought to contribute to the principal resonance around 5 Hz in the vertical apparent mass at the seat pan when sitting with no backrest, resulting in a broad peak or even two peaks in the 4-8 Hz frequency range. This phenomenon may arise from changes in the vertical motions of the pelvis and the vertical motions of the thoracic spine caused by contact with an inclined backrest. With increasing inclination of a backrest, a body mode with vertical motion of the thoracic spine may become apparent at a higher frequency (in the range 5 to 8 Hz), increasing the resonance frequency in the vertical in-line apparent mass at the seat pan.

Chapter 7. Modelling of effect of backrest on spinal forces with vertical whole-body vibration

7.1 Introduction

Drivers and passengers of various types of vehicle sit with their backs supported by backrests. As discussed in the previous chapter (Chapter 6), a backrest can decrease the back muscle tension and keep the body stable during driving.

A backrest can affect the vibration transmitted through the body (e.g., Paddan and Griffin, 1988) and so affect the spinal forces at the vertebral body according to studies of biodynamic modelling (see Chapter 5). The inclination of a seat backrest also influences the vibration transmitted to the body (e.g., Pope *et al.*, 1998; Chapter 6). As reported in Chapter 6, the use of a vertical backrest tended to decrease the principal resonance frequency of the vertical apparent mass measured at the seat pan while an inclined backrest further increased the resonance frequency and decreased the apparent mass at the resonance. The overall dynamic forces on the body (i.e., the sum of forces at the seat and backrest in the vertical and fore-and-aft directions) increased when sitting with either a vertical backrest or an inclined backrest.

From in-vivo measurements of spinal forces, the use of a backrest has been reported to reduce spinal loads during whole-body vertical vibration (0.3 to 30 Hz at 1.0 ms^{-2} r.m.s.) and inclining the backrest further reduces the spinal forces measured in-vivo with vertebral body replacements compared to sitting without a backrest (Rohlmann *et al*., 2010).

One of the current standards (i.e., ISO2631-5:2003) is designed to predict risks to the health of the lumbar spine associated with high-magnitude vibration containing shocks through evaluation of the vibration transmitted to the lumbar spine. However, the model in this standard seems to predict inaccurate seat-to-spine transmissibility, and is incapable of reflecting the effects of posture on risks to health. Various multi-body models and finite element models have been developed for the purpose of predicting more accurate spinal loads and investigating factors affecting spinal loads (e.g., Pankoke *et al.*, 1998; Fritz, 2000; Wang *et al.*, 2010; Hinz *et al.*, 2007). However, the spinal forces of the seated human body predicted by these models with similar excitation are very different and there is little data to support the predicted spinal forces. These models are either complex in structure or incapable of reflecting the effects of backrests and posture on the spinal forces.

Based on the modelling studies in Chapter 4 and Chapter 5, the forces in the lumbar spine can be predicted from the sum of static spinal forces (caused by gravity) and dynamic spinal forces (induced by vibration) using simple biodynamic models. Such models suggest the dynamic spinal forces depend on the vibration transmitted to the upper body. The models developed in Chapters 4 and 5 lack representation of forces at the seat pan in the fore-and-aft direction, which makes the model unable to reflect the effect of a backrest on the fore-and-aft apparent mass. To predict the effect of vertical and inclined backrests on the spinal forces, those models should be adjusted to

include representation of backrest contact and to reflect the fore-and-aft dynamic forces between the body and the seat.

Some biodynamic models have been developed to represent the response of the human body sitting on the seat with a backrest (e.g., Cho *et al.*, 2001; Zheng *et al.*, 2011; Qiu and Griffin, 2011). The contact between the body and a backrest in the multi-body model developed by Zheng *et al.* (2011) was modelled as vertical pair and horizontal pairs of translational springs and dampers to represent the vertical and horizontal forces provided by the backrest. The predicted apparent masses at the backrest in the vertical and the fore-and-aft directions matched the corresponding apparent masses measured by Nawayseh and Griffin (2004). A similar approach was adopted by a 9 degree-of-freedom multi-body model of a human-seat system (Cho and Yong, 2001) to predict the seat-to-head transmissibility. With finite element methods, both the backrest cushion and human tissues were modelled with continuum materials to represent the contact between the back and the backrest (e.g., Pankoke *et al.*, 2008, Casimir model). In the current study, the multi-body technique was employed; the contact between the body and the backrest is modelled as vertical and horizontal pairs of springs and dampers.

The objective of this study was to develop a multi-body model of the human body sitting against a vertical backrest and inclined backrests to investigate the effects of contact with vertical and inclined backrests on the spinal forces when during vertical whole-body vibration. The multi-body model was based on the model of the effects of posture and muscle forces developed in Chapter 5.

7.2 Model development

7.2.1 Model description

A seven degree-of-freedom multi-body model with representation of back muscles of the seated human body in the sagittal plane was developed with the capability of reflecting both the overall biodynamic response and the lumbar spine motion at L3 when exposed to vertical vibration (Chapters 4 and 5). The directions *x* and *z* followed the definitions in the ISO standard (ISO2631-1: 1997). Adjustments were made to this model to include fore-and-aft and vertical springs and dampers at the backrest and a spring and damper in the fore-and-aft direction at the thighs (Figure 7.1). There were seven rigid body segments of the seated human body in this model: the upper body from head to L2, three lumbar vertebrae from L3 to L5, the pelvis, the thighs, and the viscera in the abdomen. Translational and rotational joints with stiffness and damping coefficients were used to connect the rigid bodies as described in Chapter 5.

Contact of the body with a vertical backrest was modelled by a translational spring and damper in parallel in the vertical direction combined with a translational spring and damper in parallel in the fore-and-aft direction (Figure 7.1). Both pairs of spring and damper were connected with a rigid surface and the connection was simplified to one point at either the L2 or T5 spinal level depending on the support posture adopted by the subjects. With inclined backrests (at 10º, 20º and 30º), the upper body was supported at the thorax (T5). The stiffness and damping coefficients of the corresponding elements differed between the vertical backrest and the inclined backrest, and were determined during calibration of the model.

The geometry of the model with vertical and inclined backrests was adjusted from the model with a normal upright sitting posture developed in Chapter 5. It was assumed that spinal curvature did not differ when sitting with a vertical backrest with lumbar support (L2) and sitting in a normal posture without a backrest. Hence, the spinal curvature in the normal upright sitting posture was also used when sitting against a vertical backrest with support at L2. When sitting against a vertical backrest with support at T5, the pelvis rotated at the iliac tuberosities towards the backrest by 10 degrees (Zheng *et al.*, 2011), while the spinal curvature from the lumbar spine to the head was the same as that in the normal upright sitting posture. When representing the human body sitting with inclined backrests with support at T5, the body segments above the pelvis were then reclined from the pelvis (i.e., joint r_1, Figure 7.1 b) by the angle of the inclination of the backrest to connect with the inclined backrest (Figure 7.1, b).

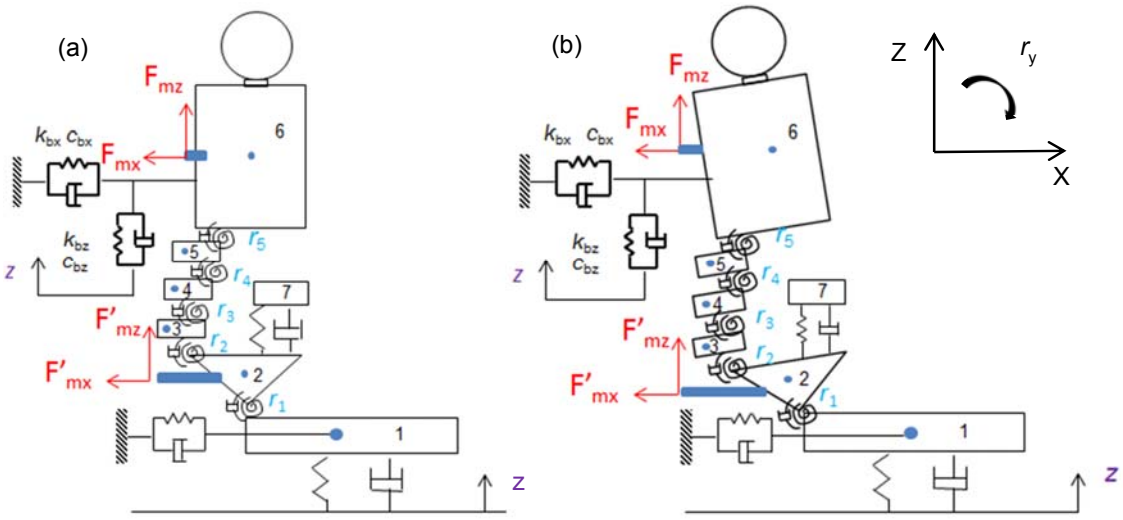

Figure 7.1 Multi-body model of the human body sitting with a vertical backrest (a) and with 10º-inclined backrest (b). 1 - thighs; 2 - pelvis; 3 - L5; 4 - L4; 5 - L3; 6 - upper-body from head to L2; 7 - viscera in the abdomen; r_1 to r_5 represent the joints from pelvis/thigh to L2/L3. Force vectors F_{mx} and F_{mz} were used to represent the muscle forces applied to the T7 spinous process. The force vectors F'_{mx} and F'_{mz} were the muscle forces acting on the sacrum (S1).

The mass and inertial properties of the body segments in the current model followed the mass distribution of the model in a normal upright sitting posture (Chapter 5) for a median person (i.e., 50th percentile), adjusted in dimension to represent an individual subject (Matsumoto and Griffin, 2001). An individual subject with a weight of 69 kg and a height of 168 cm was modelled in the current study with the biodynamic responses (apparent mass and transmissibilities to the spine) of this subject as measured in the experiment. The coordinates of key points representing centres of vertebral bodies along the spine from the pelvis to the head and the initial positions of the rotational joints are listed in Table 7.1. The coordinates of those key points in the normal sitting posture were derived from the model in Chapter4 and 5, which were from the studies by Kitazaki and Griffin (1997). The coordinates of the key points in other sitting conditions were derived from adjustments as discussed in the previous two paragraphs. The mass and inertial properties for each segment of the subject sitting against a vertical or inclined backrest are same as when sitting in the normal

posture, as shown in Table 5.2 in Chapter 5. They were also derived from previous studies (e.g., Kitazaki and Griffin, 1997; Matsumoto and Griffin, 2002; see Chapter 5).

Table 7.1 Initial positions for the centre of gravity of each body segment and rotational joints for the subject sitting against a vertical backrest and inclined backrests

Mass/joint	Centre of gravity of each segment (x_{i0}, z_{i0}) and coordinates of the joints (x_{ri0}, z_{ri0})					
	Normal posture (NB)	B0L2	B0T5	B10	B20	B30
m_1 (thighs)	-	-	-	-	-	-
m_2 (pelvis)	(-0.0244, 0.1036)	(-0.0244, 0.1036)	(-0.0420, 0.0977)	(-0.0630, 0.0760)	(-0.0752, 0.0639)	(-0.0852, 0.0498)
m_3 (L5)	(-0.1476, 0.1651)	(-0.1476, 0.1651)	(-0.1720, 0.1473)	(-0.1950, 0.1152)	(-0.2120, 0.0796)	(-0.2226, 0.0416)
m_4 (L4)	(-0.1065, 0.2047)	(-0.1065, 0.2047)	(-0.1310, 0.1869)	(-0.1614, 0.1613)	(-0.1870, 0.1308)	(-0.2069, 0.0963)
m_5 (L3)	(-0.0713, 0.2451)	(-0.0713, 0.2451)	(-0.0958, 0.2273)	(-0.1338, 0.2072)	(-0.1677, 0.1808)	(-0.1966, 0.1489)
m_6 (head-L2)	(-0.0105, 0.6131)	(-0.0105, 0.6131)	(-0.0350, 0.5953)	(-0.1378, 0.5802)	(-0.2365, 0.5474)	(-0.3279, 0.4981)
m_7 (viscera)	(-0.0285, 0.2450)	(-0.0285, 0.2450)	(-0.0530, 0.2272)	(-0.0916, 0.2145)	(-0.1275, 0.1954)	(-0.1595, 0.1703)
r_1[a] (pelvis/thigh)	(0, 0)	(0, 0)	(0,0)	(0,0)	(0,0)	(0,0)
r_2 (L5/S1)	(-0.0895, 0.1488)	(-0.0895, 0.1488)	(-0.1140, 0.1309)	(-0.1350, 0.1092)	(-0.1519, 0.0841)	(-0.1642, 0.0564)
r_3 (L4/L5)	(-0.0776, 0.1849)	(-0.0776, 0.1849)	(-0.1021, 0.1671)	(-0.1296, 0.1468)	(-0.1531, 0.1221)	(-0.1720, 0.0936)
r_4 (L3/L4)	(-0.0662, 0.2249)	(-0.0662, 0.2249)	(-0.0906, 0.2071)	(-0.1252, 0.1882)	(-0.1560, 0.1636)	(-0.1820, 0.1340)
r_5 (L2/L3)	(-0.0596, 0.2644)	(-0.0596, 0.2644)	(-0.0841, 0.2466)	(-0.1256, 0.2282)	(-0.1633, 0.2029)	(-0.1961, 0.1715)
[b]*Muscle_T7*	(-0.1135, 0.4980)	(-0.1135, 0.4980)	(-0.1379, 0.4802)	(-0.2192, 0.4489)	(-0.2938, 0.4040)	(-0.3595, 0.3469)
[b]*Muscle_S1*	(-0.1449, 0.1324)	(-0.1449, 0.1324)	(-0.1657, 0.1052)	(-0.1814, 0.0748)	(-0.1917, 0.0422)	(-0.1961, 0.0083)
[c]Backrest contact	-	(-0.1303, 0.2837)	(-0.1253, 0.5329)	(-0.2160, 0.5030)	(-0.3000, 0.4579)	(-0.3750, 0.3988)

[a] r_1 represents the ischial tuberosities for which the coordinates are (0, 0), as defined in measurements by Kitazaki and Griffin (1997).
[b] *Muscle_T7* and *Muscle_S1* refer to the locations for muscle forces (i.e., T7 and S1) in the present model.
[c] Backrest contact refers to the contact position between backrest and body, either at L2 or T5.

7.2.2 Modelling of muscles

In the current model, the effects of muscles were represented by force vectors. When exposed to vertical whole-body vibration, there will be relative motion between the upper body and the pelvis in the vertical and fore-and-aft directions as indicated from the transmissibilities of the spine. The

muscles in the human body tense involuntarily or voluntarily when the relative motions between the upper body and pelvis occur, and muscle forces are generated in both the vertical and the fore-and-aft directions to maintain postural stability. The complex muscular system of the lower back consists of numerous muscle fascicles connected between the lumbar vertebrae, thoracic vertebrae, the pelvis, the sacrum, and femora (Stokes and Gardner-Morse, 1999), as described in Chapter 5. For simplification, it was assumed the effects of muscles on the movement of the body above the seat could be represented as two force vectors (F_{mx} and F_{mz}) acting in the fore-and-aft and vertical directions on the spinous process of T7 in the upper body. The corresponding reacting force vectors (F_{mx}' and F_{mz}') were applied in the fore-and-aft and the vertical directions to the spinous process of S1 in the pelvis. These reacting forces at the S1 equalled the forces F_{mx} and F_{mz} acting at T7, but in the opposite direction.

With the vertical backrest, the static vertical and fore-and-aft supporting forces (F_{bx} and F_{bz}) at the backrest were derived from the previously measured vertical and fore-and-aft apparent masses at frequencies close to 0 Hz (0.5 Hz) in Chapter 6. Similarly, with inclined backrests (10º, 20º and 30º), the static vertical and fore-and-aft supporting forces at the backrest were derived from Chapter 6, and they are shown in Table 7.2.

Table 7.2 Static forces between backrest and back in the vertical and the fore-and-aft directions when sitting against vertical and inclined backrests.

Direction/sitting conditions	Static forces (N) between back and backrest in fore-and-aft and vertical directions				
	B_{0L2}	B_{0T5}	B_{10}	B_{20}	B_{30}
fore-and-aft (F_{bx})	9	42	106	164	184
vertical (F_{bz})	16	27	50	102	162

A lever-arm system in a form similar to the lever-arm system in Chapter 5 was developed to calculate the static muscle forces in the vertical and fore-and-aft directions (i.e., F_{mx} and F_{mz}), as shown in Figure 7.2, b. The horizontal or vertical distances from the locations of the forces from the backrest (F_{bx} and F_{bz}), muscles (F_{mx} and F_{mz}) and the effect of gravity on the mass of the body supported on the disc L2/L3 (m_u*g) to the centre of the intervertebral disc were calculated as d_{bx}, d_{bz}, d_{mx}, d_{mz}, and l. where m_u is the mass of the body supporting on the intervertebral disc L2/L3, g is the acceleration of gravity which equals to 9.81 m/s^2.

To calculate the static muscle forces and the spinal forces without vibration exposure, the upper body was assumed to be in moment equilibrium around the centre of the vertebral disc (L2/L3), which means the moments generated by the muscle forces (F_{mx} * d_{mx}+ F_{mz} * d_{mz}) balanced the moments (M_o) generated by non-concentric compression of the spinal disc plus moments generated by the pull of gravity on the upper body (m_u*g*l) as well as the moments generated by backrest support (F_{bx} * d_{bx}+ F_{bz} * d_{bz}), as shown in Equation 7.1:

$$F_{mx} * d_{mx} + F_{mz} * d_{mz} = M_o + m_u * g * l + F_{bx} * d_{bx} + F_{bz} * d_{bz} \quad (7.1)$$

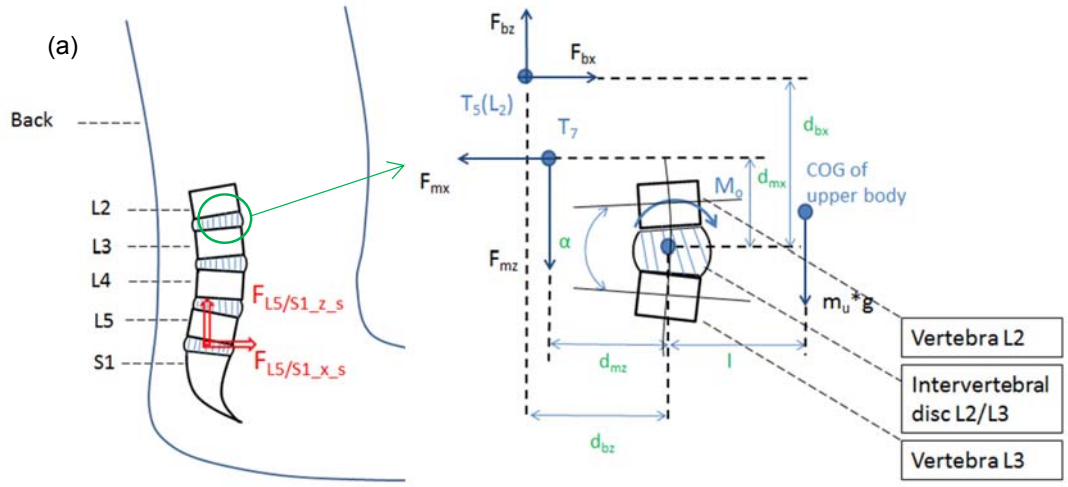

Figure 7.2 The lever-arm system (b) used for calculating the static spinal force (i.e., $F_{L5/S1\_z\_s}$ and $F_{L5/S1\_x\_s}$) at L5/S1 (i.e., joint r_2) The force vectors, positions of each force vector and the vertical or horizontal distance between each force vector to the centre of the rotational joint (r_5, L2/L3) are shown in the figure. The positive direction of each force was as shown in the figure.

The moment generated by the non-concentric compression of the spinal disc L2/L3 was calculated as the product of rotational stiffness of the disc (k_r) and the angle between the adjacent vertebrae (α), expressed as:

$$M_o = k_r * \alpha \quad (7.2)$$

In the static condition, it was assumed that the moment generated by non-concentric compression of the L2/L3 intervertebral disc was the same when sitting in the normal upright posture and when sitting with vertical or inclined backrests as the same spinal curvature was used. The horizontal distance, l, from the centre of gravity of the upper body to the centre of the disc, and the horizontal and vertical distances (d_{mz} and d_{mx}) from the vertical and the fore-and-aft muscle forces to the centre of the disc, were determined directly from the geometry of the model, and varied with the sitting condition. The horizontal and vertical distances (d_{bz} and d_{bx}) from the static vertical and fore-and-aft forces at the backrest to the centre of the L2/L3 disc were also calculated in the model based on the contact point between body and backrest. Therefore, the static muscle forces, F_{mx} and F_{mz}, varied with the inclination angle of the backrest. In the calculation it was assumed that the vector sum of the static muscle forces at T7 in the fore-and-aft and the vertical directions (i.e., F_{mx} and F_{mz}) was in the direction from the spinous process of T7 to the spinous process of S1. This assumption made the calculation of the spinal forces in the vertical and the fore-and-aft directions possible and unique.

The rotational stiffness of the L2/L3 intervertebral disc (i.e., r_5), together with remaining parameters in the present model (i.e., stiffness and damping of intervertebral discs, parameters related to the

dynamic model of muscles and buttocks tissues) were determined through the dynamic calibration of the model described in the next step (Section 7.3.1).

With the static vertical muscle force and static fore-and-aft muscle force calculated, the static vertical spinal force and static fore-and-aft spinal force at the lowest spinal level L5/S1 (i.e., joint r_2) were calculated as the sum of the static muscle force and the force due to gravity of the body mass supported on the intervertebral disc L5/S1:

$$F_{L5/S1\_z\_s} = F_{mz} + m * g - F_{bz} \tag{7.3}$$

$$F_{L5/S1\_x\_s\_} = F_{mx} - F_{bx} \tag{7.4}$$

where m is the sum of the masses of the body segments 3, 4 ,5 and 6, as shown in Figure 7.1.

For dynamic conditions, only the muscle forces associated with the passive properties of the muscles were modelled, which represented the necessary muscle forces in the body to maintain the sitting posture. The forces generated by voluntarily tensing of the muscles in the body were not considered. The muscle force in either the fore-and-aft (x) or the vertical (z) direction is assumed to depend on the properties of a spring and a damper, so the muscle force was calculated by a stiffness multiplied by the relative displacement plus a damping coefficient multiplied by the relative velocity, between the connected points in each direction:

$$F_{mx} = k_{mx}(x_{t7} - x_{s1}) + c_{mx}(\dot{x}_{t7} - \dot{x}_{s1}) \tag{7.5}$$

$$F_{mz} = k_{mz}(z_{t7} - z_{s1}) + c_{mz}(\dot{z}_{t7} - \dot{z}_{s1}) \tag{7.6}$$

The stiffness and damping coefficients (k_{mx}, k_{mz}, c_{mx}, c_{mz}) were determined in the calibration process by comparing the apparent mass and body transmissibilities predicted by the model to those measured in the experiments described in Chapter 6. (x_{t7}, z_{t7}) and (x_{s1}, z_{s1}) represent the displacements at the spinous process of T7 and the sacrum (S1) in the x and z directions (Figure 7.1) associated with whole-body vibration. Muscle activity can affect the biodynamic response of the human body (i.e., apparent mass and transmissibilities), both suggested in the current study (Chapters 6, 8 and 9) and from other studies (e.g., Matsumoto and Griffin, 2002; Huang and Griffin, 2008). The apparent masses at the seat and at the backrest at the principal resonance frequencies and the fore-and-aft transmissibility to the spine (i.e., to L3 and T5) at the resonance frequencies predicted by the current model were found to be sensitive to the stiffness and/or the damping coefficients representing the muscle forces (details are presented in Section 7.5.3).

7.2.3 Equations of motion

In a similar way described in Chapter 5, the equations of motion of the current model with backrest contact were derived using the Lagrange equation, together with the expressions of muscle forces (Equations 7.5 and 7.6). It was assumed that all body parts oscillate around the equilibrium positions with small displacements in the condition of free vibration:

$$\frac{d}{dt}\left(\frac{\partial T}{\partial \dot{q}_i}\right) + \frac{\partial D}{\partial \dot{q}_i} + \frac{\partial U}{\partial q_i} = 0 \; ; \; q_i = \left[x_1; z_1; \theta_2; \theta_3; \theta_4; \theta_5; \theta_6; z_7\right] \tag{7.7}$$

The kinetic energy, T, potential energy, U, and dissipation function, D, of the system were calculated as:

$$T = \frac{1}{2}\sum_{i=1}^{7} m_{\mathrm{i}}(\dot{x}_{\mathrm{i}}^2 + \dot{z}_{\mathrm{i}}^2) + \frac{1}{2}\sum_{i=2}^{6} I_{\mathrm{i}}\dot{\theta}_{\mathrm{i}}^2 \tag{7.8}$$

$$D = \frac{1}{2}c_1(\dot{z}_1 - \dot{z})^2 + \frac{1}{2}c_{1x}(x_1)^2 + \frac{1}{2}c_{\mathrm{r1}}(\dot{\theta}_2)^2 + \frac{1}{2}c_{\mathrm{r2}}(\dot{\theta}_3 - \dot{\theta}_2)^2 + \frac{1}{2}c_{\mathrm{r3}}(\dot{\theta}_4 - \dot{\theta}_3)^2 + \frac{1}{2}c_{\mathrm{r4}}(\dot{\theta}_5 - \dot{\theta}_4)^2$$
$$+ \frac{1}{2}c_{\mathrm{r5}}(\dot{\theta}_6 - \dot{\theta}_5)^2 + \frac{1}{2}c_2(\dot{z}_7 - \dot{z}_8)^2 + \frac{1}{2}c_{bx}(\dot{x}_b)^2 + \frac{1}{2}c_{bz}(\dot{z}_b - \dot{z})^2 + \frac{1}{2}c_{\mathrm{mz}}(\dot{z}_{t7} - \dot{z}_s)^2 + \frac{1}{2}c_{\mathrm{mx}}(\dot{x}_{t7} - \dot{x}_s)^2 \tag{7.9}$$

$$U = \frac{1}{2}k_1(z_1 - z)^2 + \frac{1}{2}k_{1x}(x_1)^2 + \frac{1}{2}k_{\mathrm{r1}}(\theta_2)^2 + \frac{1}{2}k_{\mathrm{r2}}(\theta_3 - \theta_2)^2 + \frac{1}{2}k_{\mathrm{r3}}(\theta_4 - \theta_3)^2 + \frac{1}{2}k_{\mathrm{r4}}(\theta_5 - \theta_4)^2 + \frac{1}{2}k_{\mathrm{r5}}(\theta_6 - \theta_5)^2$$
$$+ \frac{1}{2}k_2(z_7 - z_8)^2 + \frac{1}{2}k_{\mathrm{mz}}(z_{t7} - z_s)^2 + \frac{1}{2}k_{\mathrm{mx}}(x_{t7} - x_s)^2 + \frac{1}{2}k_{bx}(x_b)^2 + \frac{1}{2}k_{bz}(z_b - z)^2 \tag{7.10}$$

where (x_{b}, z_{b}) represent the displacements of the backrest contact location (i.e., L2 or T5 depending on the backrest conditions) in the x and z directions. Parameters (k_{bx}, k_{bz}) and (c_{bx}, c_{bz}) represent the stiffness and damping of the contact between the body and backrest in the x and z directions, respectively, while $k_{1\mathrm{x}}$ and $c_{1\mathrm{x}}$ represent the stiffness and damping of the connection between the thigh and seat in the fore-and-aft direction. The definitions of independent coordinates (i.e., the degrees of freedom and centres of gravity of each body segment) and the symbols of stiffness and damping connecting the body segments were the same as those adopted in the model described in Chapter 5.

7.3 Optimisation of model parameters and prediction of transmissibilities to spine

7.3.1 Optimisation of model parameters with apparent mass

The parameters of the rotational joints (i.e., stiffness and damping) and translational springs and dampers with vertical and inclined backrests were determined by minimising the error between the biodynamic responses predicted by the model and measured in experiment from an individual subject (Subject 7, Chapter 6, measured with 1.0 ms^{-2} r.m.s. random vertical vibration from 0.2 to 20 Hz). The error function involved the modulus of the vertical in-line and fore-and-aft cross-axis apparent masses at the seat pan and backrest in the frequency range 0.5 to 15 Hz (Equation 7.11). The error function was minimised using COMPLEX optimisation algorithm (Bounday, 1985) and code (Qiu and Griffin, 2011). The vertical and the fore-and-aft transmissibilities to L3 and T5 were also predicted by the model and compared with those measured from experiment.

$$Error(\lambda) = w_1 * \sqrt{\frac{1}{N}\sum_{i=1}^{N}(\left|M_{\mathrm{zzs\_m}}(f_{\mathrm{i}})\right| - \left|M_{\mathrm{zz\_s\_m}}\ e(f_{\mathrm{i}})\right|)^2} + w_2 * \sqrt{\frac{1}{N}\sum_{i=1}^{N}(\left|M_{\mathrm{zzb\_m}}(f_{\mathrm{i}})\right| - \left|M_{\mathrm{zzb\_m}}\ e(f_{\mathrm{i}})\right|)^2} +$$
$$w_3 * \sqrt{\frac{1}{N}\sum_{i=1}^{N}(\left|M_{\mathrm{xzs\_m}}(f_{\mathrm{i}})\right| - \left|M_{\mathrm{xzs\_m}}\ e(f_{\mathrm{i}})\right|)^2} + w_4 * \sqrt{\frac{1}{N}\sum_{i=1}^{N}(\left|M_{\mathrm{xzb\_m}}(f_{\mathrm{i}})\right| - \left|M_{\mathrm{xzb\_m}}\ e(f_{\mathrm{i}})\right|)^2} \tag{7.11}$$

where $M_{zzs\_m}(f_i)$ and $M_{xzs\_m}(f_i)$ are the moduli (in the unit of kg) of the predicted vertical in-line and fore-and-aft cross-axis apparent masses at the seat pan, respectively. M_{zzs_m} e(f_i) and M_{xzs_m} e(f_i) are the moduli (in the units of kg) of the corresponding apparent masses at the seat pan measured in the experiment (Chapter 6). Similarly, $M_{zzb\_m}(f_i)$ and $M_{xzs\_m}(f_i)$ are the moduli (in the units of kg) of the predicted vertical in-line and fore-and-aft cross-axis apparent masses at the backrest, respectively. M_{zzb_m} e(f_i) and M_{xzs_m} e(f_i) are the moduli (in the units of kg) of the corresponding apparent masses at the backrest measured in Chapter 6. w_1, w_2, w_3, w_4 are the weightings added to each term. The values for the weightings are: w_1=0.5, w_2=2, w_3=2, w_4=2. They were set by running several iterations of the optimisation function.

The initial values of the stiffness and damping parameters for the fore-and-aft elements connecting the body and seat were chosen from the model developed by Nawayseh and Griffin (2009). The initial values of the stiffness and damping at the backrest contact were based on the model by Zheng *et al.*, (2011). The initial values of the stiffness and damping parameters for the remaining rotational joints and translational joints were determined following the procedure in a previous model of human body in the normal sitting posture (Chapter 5), partly from in-vitro measurements of mechanical properties of vertebral body (e.g., Schultz *et al.*, 1979) and partly from relevant modelling work in Chapter 5. The initial values of the above parameters were the same in all sitting conditions (i.e., normal, sitting with vertical backrests, sitting with inclined backrests) and they are listed in Table 7.3.

The ranges (i.e., upper and lower boundaries) of the values of the stiffness and damping parameters were determined partly based on the studies in Chapter 5 and some previous modelling studies, and partly based on some experience during the optimisation. One experience was that the principal resonance frequency (4 – 8 Hz) of the vertical in-line apparent mass and fore-and-aft cross-axis apparent mass are sensitive to the stiffness parameters k_1 and k_{1x}, respectively. The lower boundary and the upper boundary for stiffness k_1 and k_{1x} were firstly calculated roughly using $k = \omega^2 * m$, where ω is natural frequency and m is the mass of the seated body. Considering the values of the parameters used in the studies from Wei and Griffin (1998) and Matsumoto and Griffin (2002), the lower and upper boundaries for such parameters were determined. Similarly, the lower and upper boundaries for the stiffness representing the backrest contact were determined based on the natural frequencies of the vertical and fore-and-aft apparent masses at the backrest.

The lower and upper boundaries for the stiffness of the rotational joints (i.e., k_{r1}, k_{r2}, k_{r3}, k_{r4}, k_{r5},) representing the intervertebral discs were also determined from in-vitro measurements (e.g., Schultz *et al.*, 1979) as mentioned in Chapter 5.

The lower and upper boundaries of the damping parameters of the rotational and translational joints were partly determined from the studies in Chapter 5, and partly determined by several iterations of the optimisation function in order to give a close match to the modulus of the apparent masses at the set pan and backrest in the vertical and fore-and-aft directions.

The lower and upper boundaries of stiffness and damping related to the muscle forces (i.e., k_{mx}, k_{mz}, $c_{mx,}$ c_{mz}) were determined by running several iterations of the optimisation function to give an appropriate value of the transfer function between the vertical spinal force and the vertical acceleration at the seat. One criterion is described in the next paragraph.

There would be several sets of parameters obtained from the optimisation process and sometimes it would be difficult to determine which set of parameters gives the global minimum error. The modulus of the transfer function between the dynamic vertical spinal force and the vertical acceleration at the seat at frequencies close to 0 Hz can be used to calculate the static spinal force. One criterion is to select the set of parameter giving a modulus of the above transfer function at frequencies close to 0 Hz (at 0.5 Hz) which can predict the static vertical spinal force close to the prediction from the lever-arm model.

The upper boundary and lower boundary of the stiffness and damping parameters are shown in Table 7.3.

Table 7.3 Initial values of the stiffness and damping parameters in the model and the lower and upper boundaries of them.

Stiffness and damping	Lower boundary	Upper boundary	Initial value
k_1 (N/m)	50000	200000	120000
c_1 (Ns/m)	500	5000	1700
k_2 (N/m)	0	50000	20000
c_2 (Ns/m)	0	5000	180
k_{r1} (Nm/rad)	58	174	58
c_{r1} (Nms/rad)	0	2000	10
k_{r2} (Nm/rad)	58	174	58
c_{r2} (Nms/rad)	0	2000	13
k_{r3} (Nm/rad)	58	174	58
c_{r3} (Nms/rad)	0	2000	20
k_{r4} (Nm/rad)	58	174	58
c_{r4} (Nms/rad)	0	2000	300
k_{r5} (Nm/rad)	58	174	58
c_{r5} (Nms/rad)	0	2000	100
k_{1x} (N/m)	1	100000	50000
c_{1x} (Ns/m)	1	5000	3000
k_{mz} (N/m)	0	500000	350000
k_{mx} (N/m)	0	500000	110000

c_{mz}(Ns/m)	0	10000	500
c_{mx}(Ns/m)	0	10000	500
Sitting with backrest			
k_{bx} (N/m)	1	150000	4000
c_{bx} (Ns/m)	1	1000	300
k_{bz} (N/m)	1	150000	4000
c_{bz} (Ns/m)	1	1000	88

The model parameters identified from the above optimisation procedure with vertical and inclined backrests are shown in Table 7.4. Comparisons between the vertical in-line apparent mass and fore-and-aft cross-axis apparent mass measured at the seat pan and at the backrest and predicted by the model in each sitting condition after model calibration are shown in Figures 7.3 to 7.10.

Table 7.4 Stiffness and damping coefficients obtained for the model when sitting in normal upright posture (NB), with vertical backrests (B_{0T5} and B_{0L2}) and with inclined backrests (B_{10}, B_{20} and B_{30}).

Stiffness and damping	Normal (NB)	B_{0L2}	B_{0T5}	B_{10}	B_{20}	B_{30}
k_1 (N/m)	118555	161054	160596	172753	137110	166023
c_1 (Ns/m)	1732	1001	538	535	1379	955
k_2 (N/m)	21859	21992	28492	35659	24159	49610
c_2 (Ns/m)	165	261	744	202	4988	320
k_{r1} (Nm/rad)	174	59	58	65	58	377
c_{r1} (Nms/rad)	0	9	1	5	6	11
k_{r2} (Nm/rad)	174	60	58	155	158	69
c_{r2} (Nms/rad)	500	3	14	1	448	857
k_{r3} (Nm/rad)	174	58	58	58	66	118
c_{r3} (Nms/rad)	79	8	1	1	2	1
k_{r4} (Nm/rad)	58	118	174	58	87	81
c_{r4} (Nms/rad)	500	963	1000	28	1973	430
k_{r5} (Nm/rad)	58	174	159	65	152	67
c_{r5}	45	998	1	840	999	999

(Nms/rad)						
k_{1x} (N/m)	75802	19036	14925	16760	71387	69142
c_{1x} (Ns/m)	5000	97	697	735	4702	4900
k_{mz} (N/m)	220994	108896	168759	312543	498467	497256
k_{mx} (N/m)	118132	4984	92381	27583	51153	39601
c_{mz}(Ns/m)	0	1	2200	9999	3798	9999
c_{mx}(Ns/m)	940	734	1	424	1887	2491
k_{bx} (N/m)	-	36454	18602	77007	99229	112472
c_{bx} (Ns/m)	-	28	770	621	319	476
k_{bz} (N/m)	-	1	1270	533	14963	27220
c_{bz} (Ns/m)	-	89	123	304	367	517

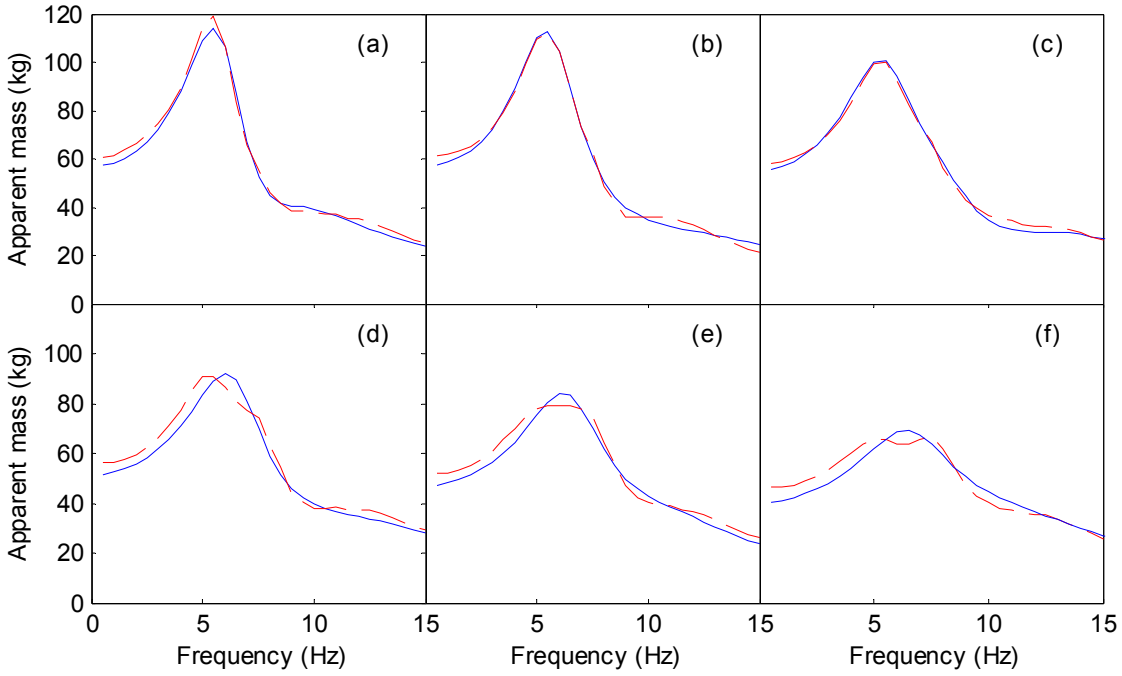

Figure 7.3 Modulus of the vertical in-line apparent mass at the seat pan in (a) normal sitting posture (NB), (b) with vertical backrest at L2 (B_{0L2}), (c) with vertical backrest at T5 (B_{0T5}), (d) with 10°-inclined backrest (B_{10}), (e) with 20°-inclined backrest (B_{20}), (f) with 30°-inclined backrest (B_{30}). '- -': experimental data; '——': predicted from model.

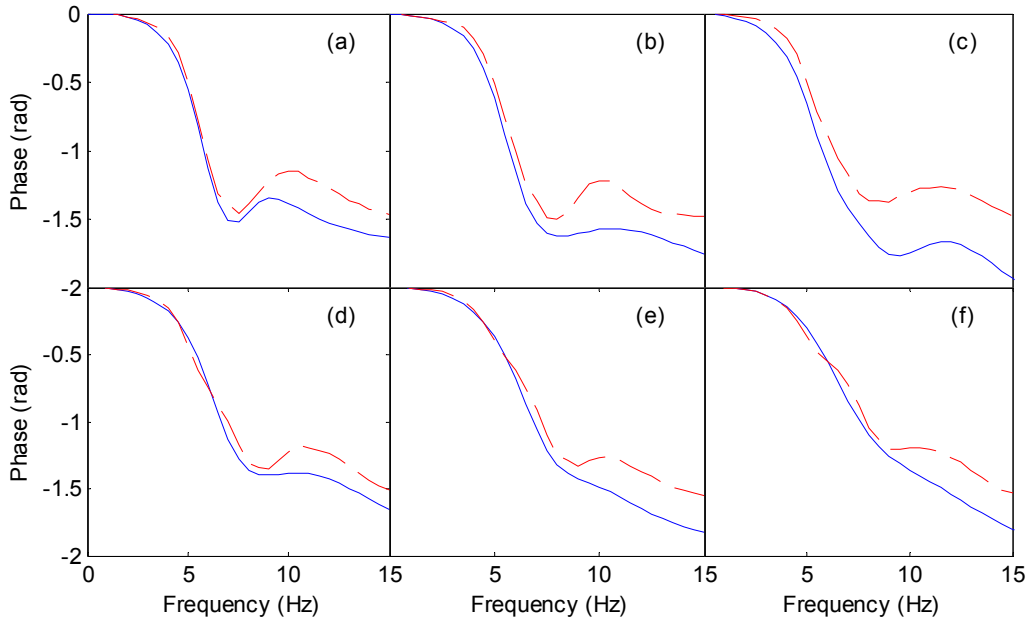

Figure 7.4 Phase of the vertical in-line apparent mass at the seat pan in (a) normal sitting posture (NB), (b) with vertical backrest at L2 (B_{0L2}), (c) with vertical backrest at T5 (B_{0T5}), (d) with 10º-inclined backrest (B_{10}), (e) with 20º-inclined backrest (B_{20}), (f) with 30º-inclined backrest (B_{30}). '- -': experimental data; '——': predicted from model.

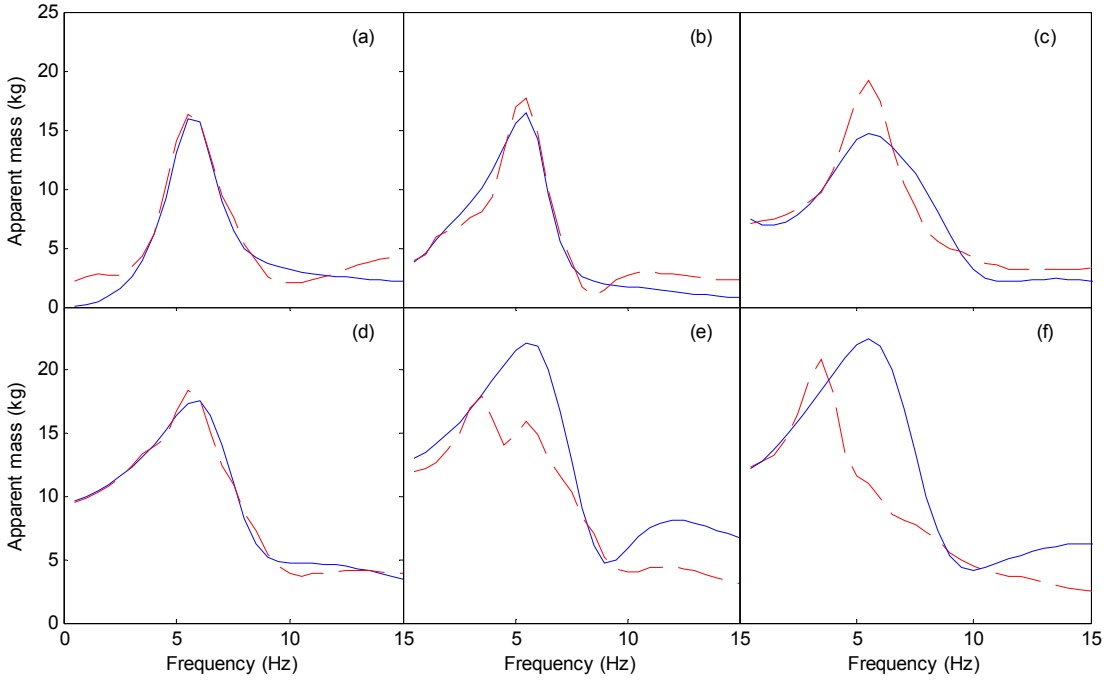

Figure 7.5 Modulus of the fore-and-aft cross-axis apparent mass at the seat pan in (a) normal sitting posture (NB), (b) with vertical backrest at L2 (B_{0L2}), (c) with vertical backrest at T5 (B_{0T5}), (d) with 10º-inclined backrest (B_{10}), (e) with 20º-inclined backrest (B_{20}), (f) with 30º-inclined backrest (B_{30}). '- -': experimental data; '——': predicted from model.

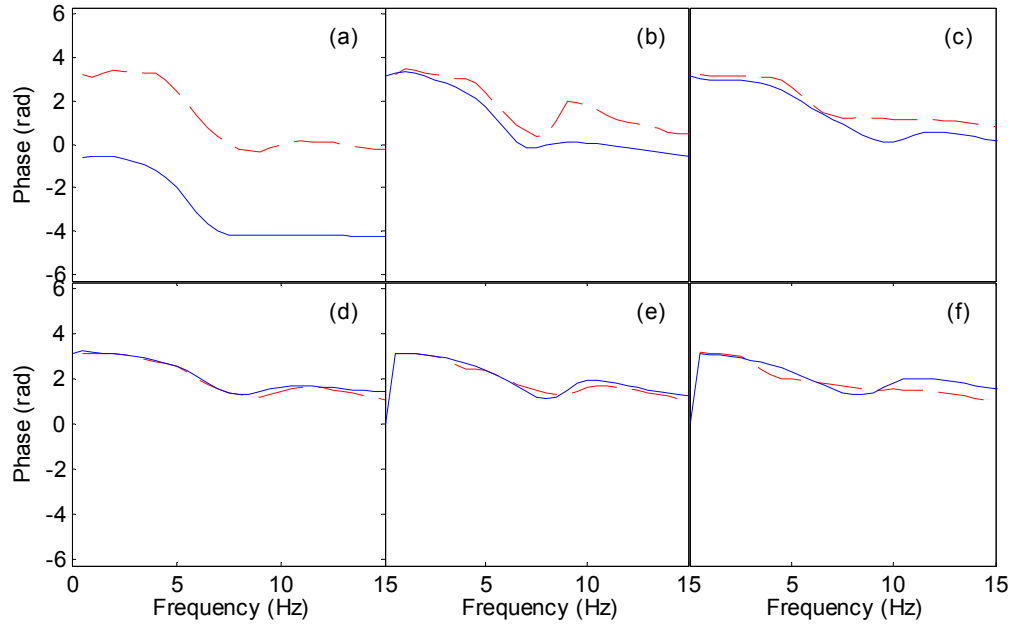

Figure 7.6 Phase of the fore-and-aft cross-axis apparent mass at the seat pan in (a) normal sitting posture (NB), (b) with vertical backrest at L2 (B_{0L2}), (c) with vertical backrest at T5 (B_{0T5}), (d) with 10º-inclined backrest (B_{10}), (e) with 20º-inclined backrest (B_{20}), (f) with 30º-inclined backrest (B_{30}). '- -': experimental data; '——': predicted from model.

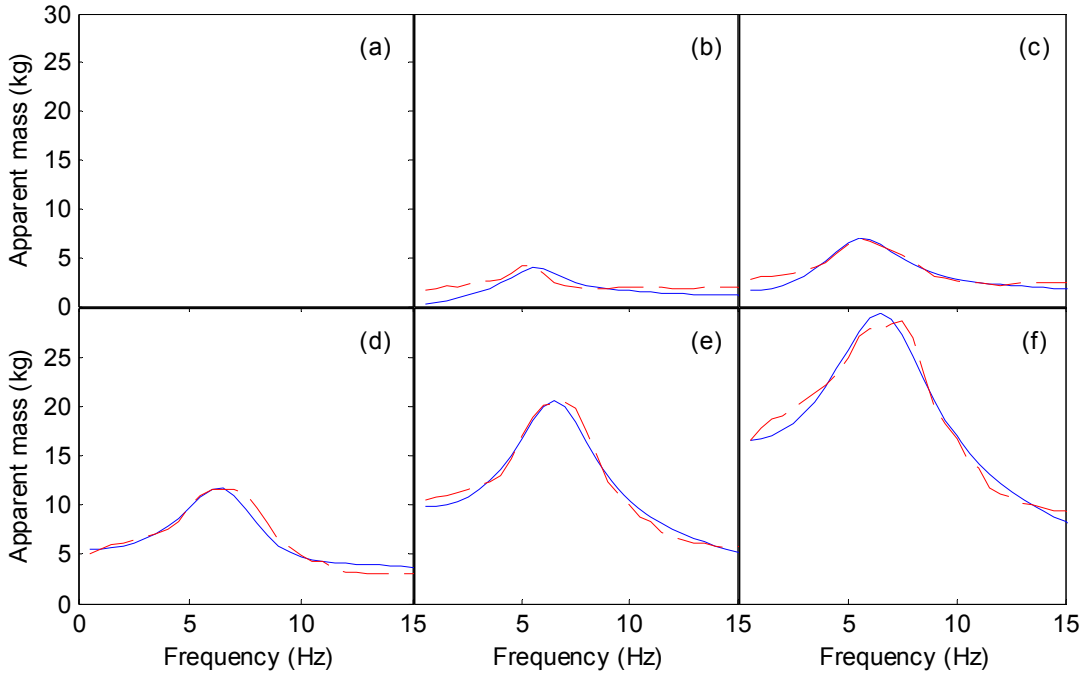

Figure 7.7 Modulus of the vertical in-line apparent mass at the back in (a) normal sitting posture (NB), (b) with vertical backrest at L2 (B_{0L2}), (c) with vertical backrest at T5 (B_{0T5}), (d) with 10º-inclined backrest (B_{10}), (e) with 20º-inclined backrest (B_{20}), (f) with 30º-inclined backrest (B_{30}). '- -': experimental data; '——': predicted from model.

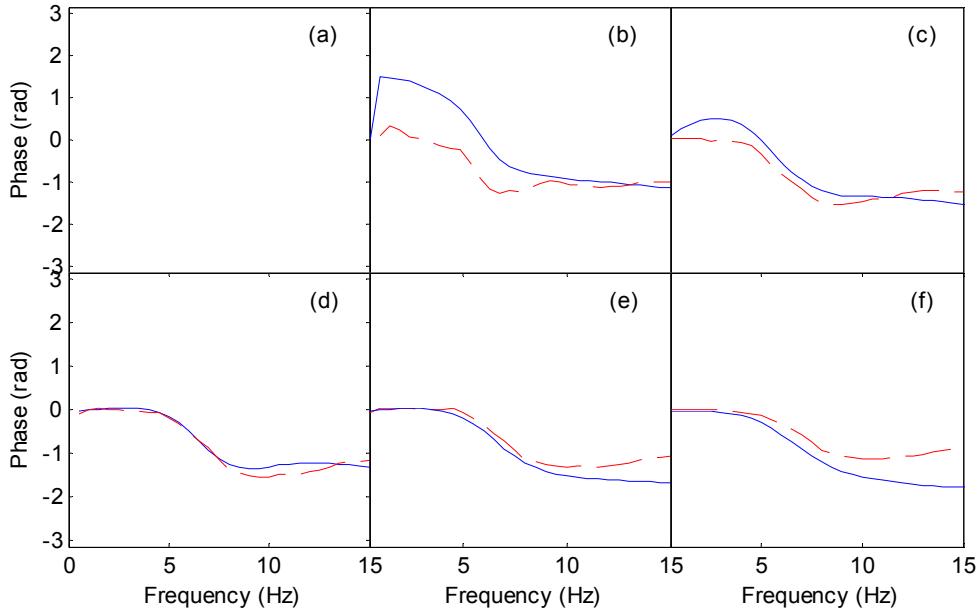

Figure 7.8 Phase of the vertical in-line apparent mass at the back in (a) normal sitting posture (NB), (b) with vertical backrest at L2 (B_{0L2}), (c) with vertical backrest at T5 (B_{0T5}), (d) with 10º-inclined backrest (B_{10}), (e) with 20º-inclined backrest (B_{20}), (f) with 30º-inclined backrest (B_{30}). '- -': experimental data; '——': predicted from model.

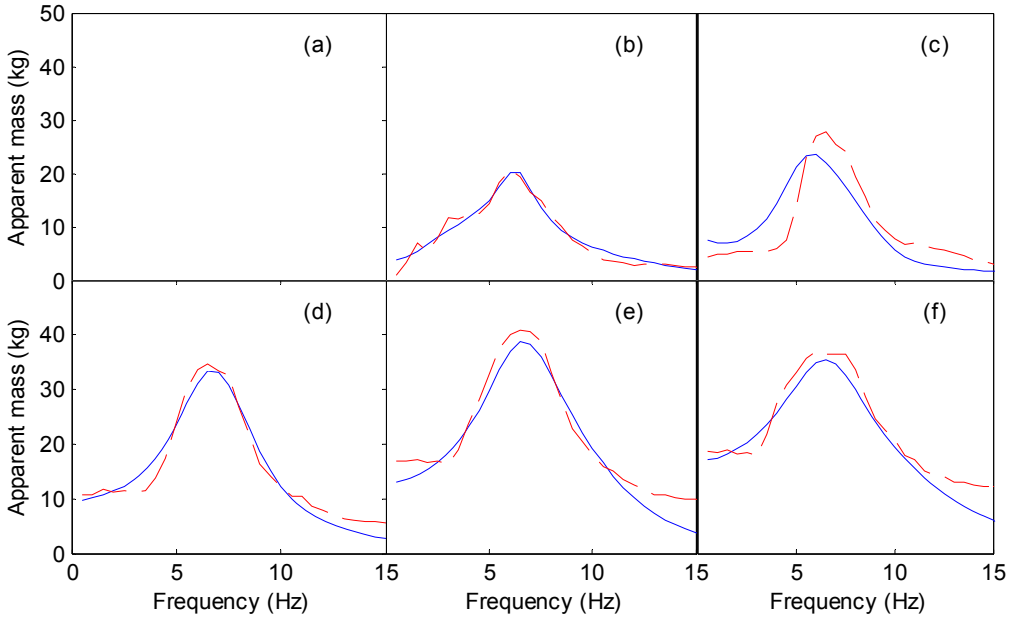

Figure 7.9 Modulus of the fore-and-aft cross-axis apparent mass at the back in (a) normal sitting posture (NB), (b) with vertical backrest at L2 (B_{0L2}), (c) with vertical backrest at T5 (B_{0T5}), (d) with 10º-inclined backrest (B_{10}), (e) with 20º-inclined backrest (B_{20}), (f) with 30º-inclined backrest (B_{30}). '- -': experimental data; '——': predicted from model.

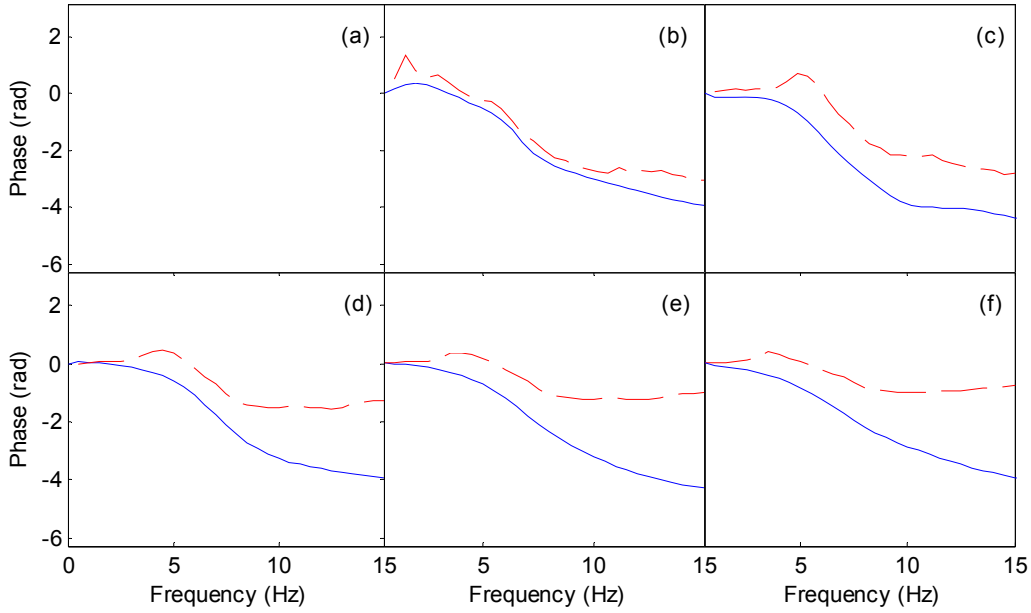

Figure 7.10 Phase of the fore-and-aft cross-axis apparent mass at the back in (a) normal sitting posture (NB), (b) with vertical backrest at L2 (B_{0L2}), (c) with vertical backrest at T5 (B_{0T5}), (d) with 10 -inclined backrest (B_{10}), (e) with 20º-inclined backrest (B_{20}), (f) with 30º-inclined backrest (B_{30}). '- -': experimental data; '——': predicted from model.

The moduli and phases of the predicted and measured vertical in-line apparent masses at the seat, the fore-and-aft cross-axis apparent mass at the seat, the vertical in-line apparent mass at the back and the fore-and-aft cross-axis apparent mass at the back in every backrest condition matched (Figures 7.3 – 7.10), except for the prediction of the fore-and-aft cross-axis apparent mass at the seat pan when with 20˚ and 30˚ backrests. The model overestimated the fore-and-aft cross-axis apparent mass at frequencies 5 to 10 Hz in B_{20} and B_{30} conditions (Figure 5). The resonance frequency of the vertical in-line apparent mass at the seat pan increased and the apparent mass at the resonance decreased with increasing inclinations of the backrest. However, there were some discrepancies in the phases of the vertical in-line and fore-and-aft cross-axis apparent masses at the back and such discrepancies will be discussed in Section 7.5.1.

7.3.2 Predictions of transmissibilities to spine

With the stiffness and damping coefficients obtained from the calibration of the model, the vertical and the fore-and-aft transmissibilities to the lumbar spine (L3) and thoracic spine (T5) were predicted and compared with the corresponding measured transmissibilities from the experiment (Figures 7.11 to 7.18).

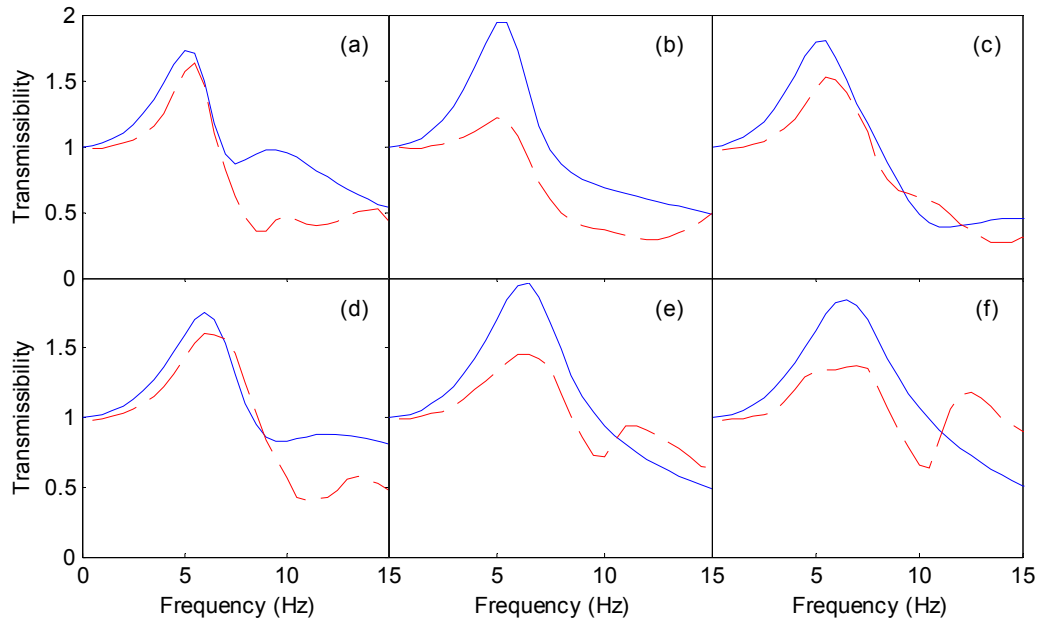

Figure 7.11 Modulus of the vertical in-line transmissibility to L3 in (a) normal sitting posture (NB), (b) with vertical backrest at L2 (B_{0L2}), (c) with vertical backrest at T5 (B_{0T5}), (d) with 10º-inclined backrest (B_{10}), (e) with 20º-inclined backrest (B_{20}), (f) with 30º-inclined backrest (B_{30}). '- -': experimental data; '——': predicted from model.

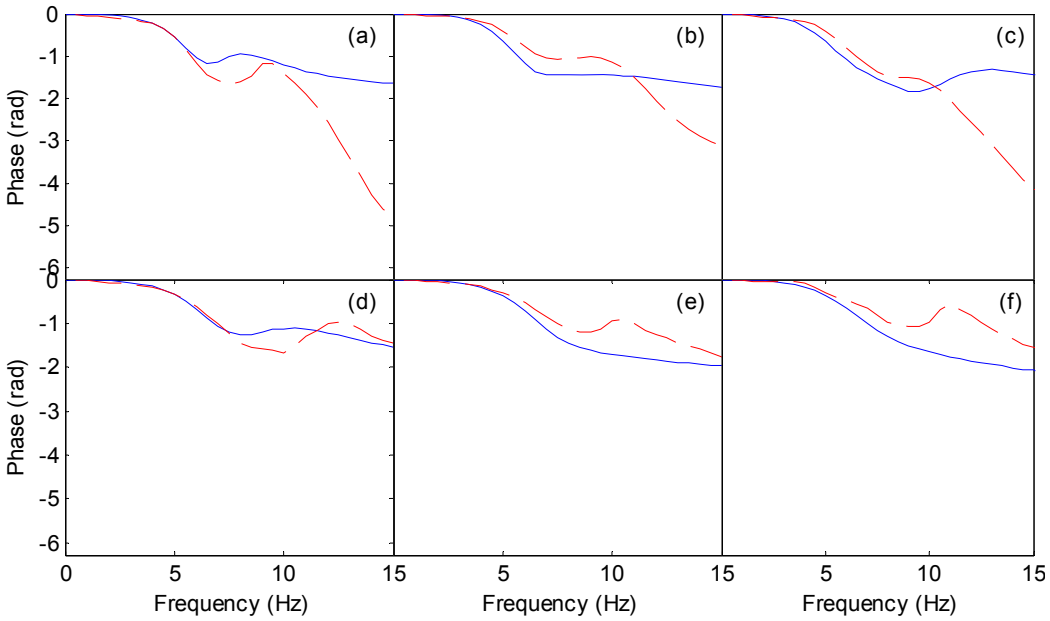

Figure 7.12 Phase of the vertical in-line transmissibility to L3 in (a) normal sitting posture (NB), (b) with vertical backrest at L2 (B_{0L2}), (c) with vertical backrest at T5 (B_{0T5}), (d) with 10º-inclined backrest (B_{10}), (e) with 20º-inclined backrest (B_{20}), (f) with 30º-inclined backrest (B_{30}). '- -': experimental data; '——': predicted from model.

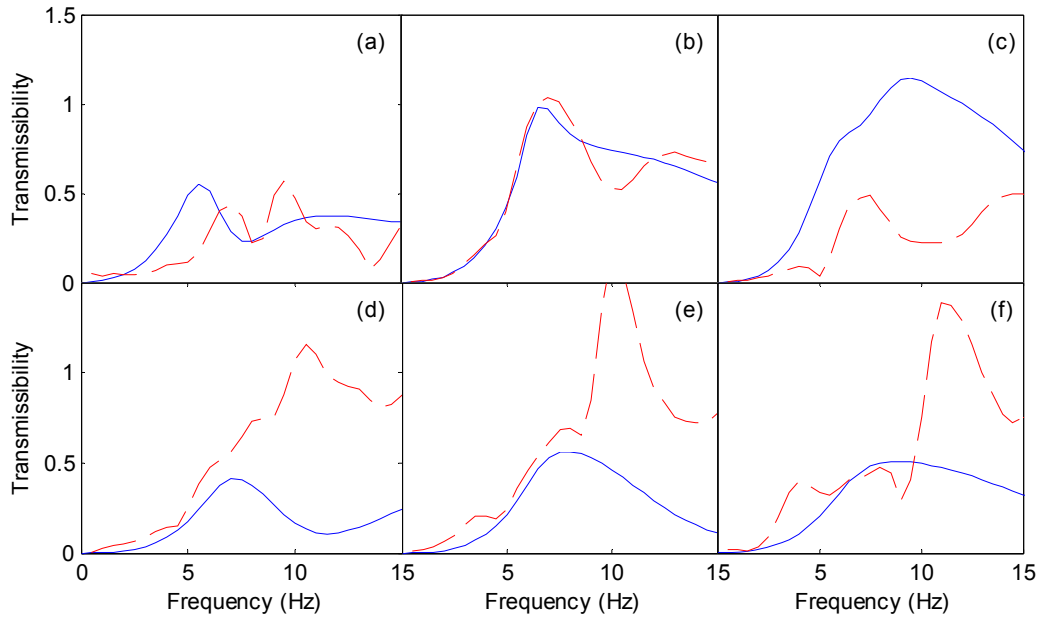

Figure 7.13 Modulus of the fore-and-aft cross-axis transmissibility to L3 in (a) normal sitting posture (NB), (b) with vertical backrest at L2 (B_{0L2}), (c) with vertical backrest at T5 (B_{0T5}), (d) with 10º-inclined backrest (B_{10}), (e) with 20º-inclined backrest (B_{20}), (f) with 30º-inclined backrest (B_{30}). '- -': experimental data; '——': predicted from model.

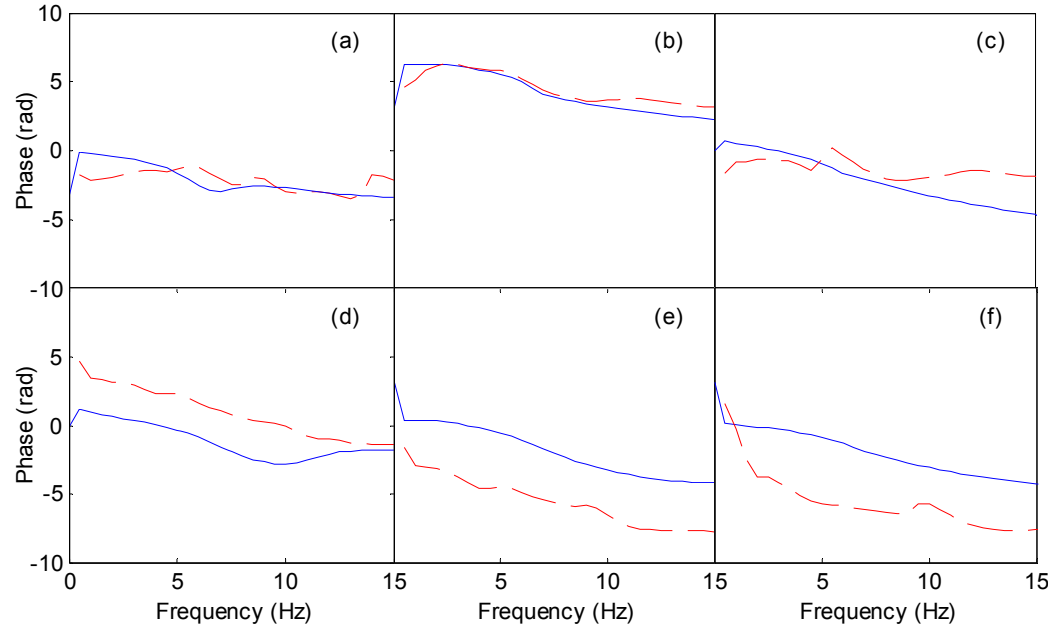

Figure 7.14 Phase of the fore-and-aft cross-axis transmissibility to L3 in (a) normal sitting posture (NB), (b) with vertical backrest at L2 (B_{0L2}), (c) with vertical backrest at T5 (B_{0T5}), (d) with 10º-inclined backrest (B_{10}), (e) with 20º-inclined backrest (B_{20}), (f) with 30º-inclined backrest (B_{30}). '- -': experimental data; '——': predicted from model.

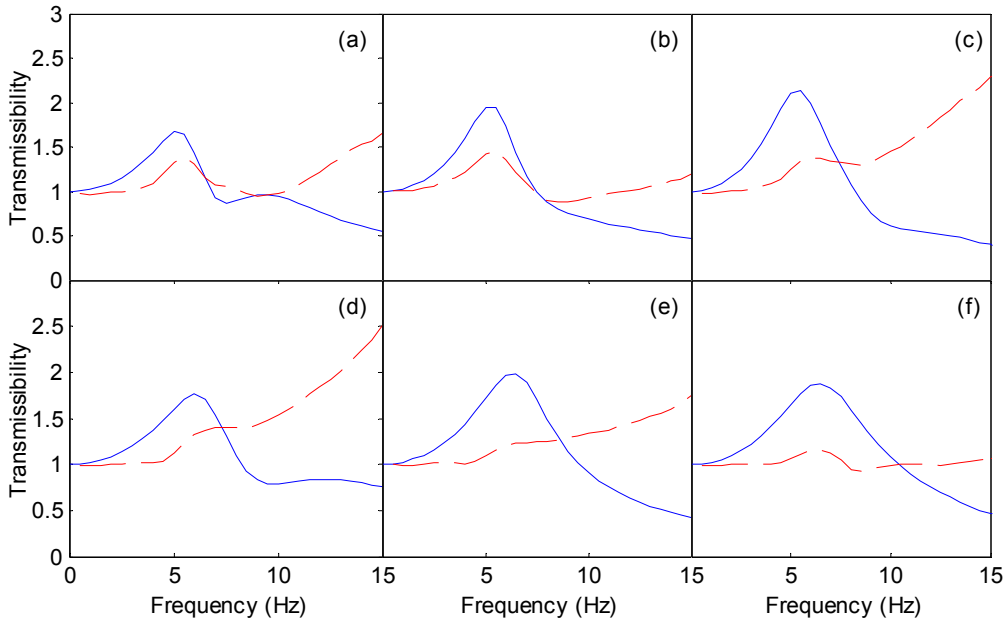

Figure 7.15 Modulus of the vertical in-line transmissibility to T5 in (a) normal sitting posture (NB), (b) with vertical backrest at L2 (B_{0L2}), (c) with vertical backrest at T5 (B_{0T5}), (d) with 10º-inclined backrest (B_{10}), (e) with 20º-inclined backrest (B_{20}), (f) with 30º-inclined backrest (B_{30}). '- -': experimental data; '——': predicted from model.

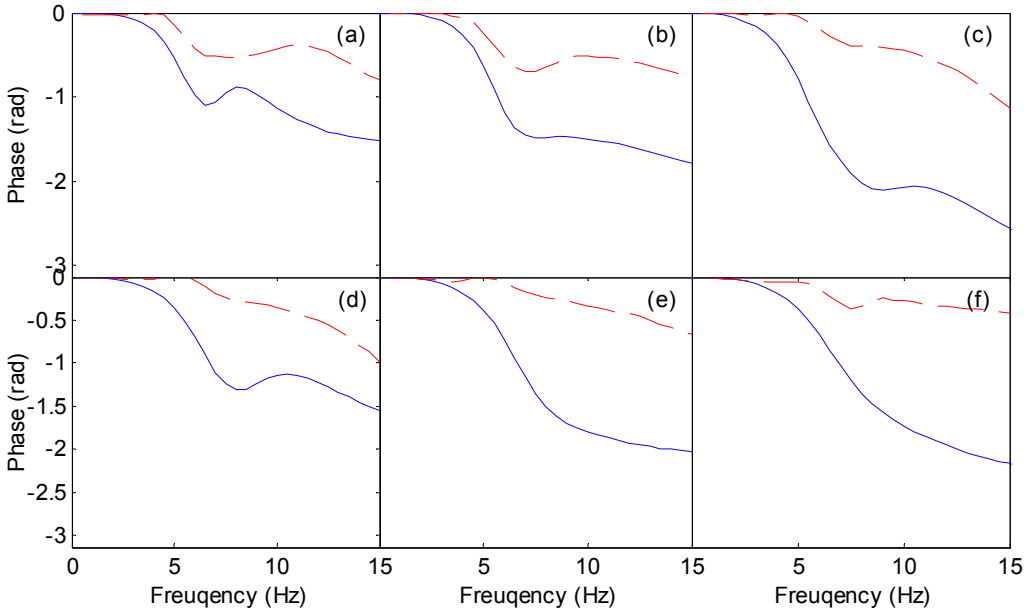

Figure 7.16 Phase of the vertical in-line transmissibility to T5 in (a) normal sitting posture (NB), (b) with vertical backrest at L2 (B_{0L2}), (c) with vertical backrest at T5 (B_{0T5}), (d) with 10º-inclined backrest (B_{10}), (e) with 20º-inclined backrest (B_{20}), (f) with 30º-inclined backrest (B_{30}). '- -': experimental data; '——': predicted from model.

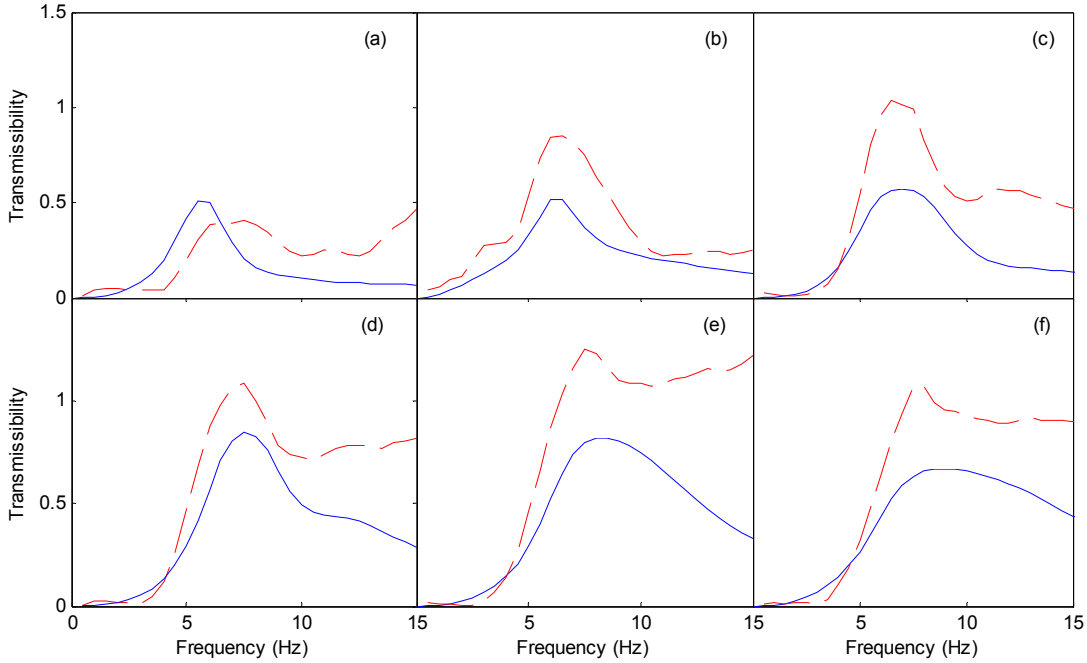

Figure 7.17 Modulus of fore-and-aft cross-axis transmissibilities to T5 in (a) normal sitting posture (NB), (b) with vertical backrest at L2 (B_{0L2}), (c) with vertical backrest at T5 (B_{0T5}), (d) with 10º-inclined backrest (B_{10}), (e) with 20º-inclined backrest (B_{20}), (f) with 30º-inclined backrest (B_{30}). '- -': experimental data; '——': predicted from model.

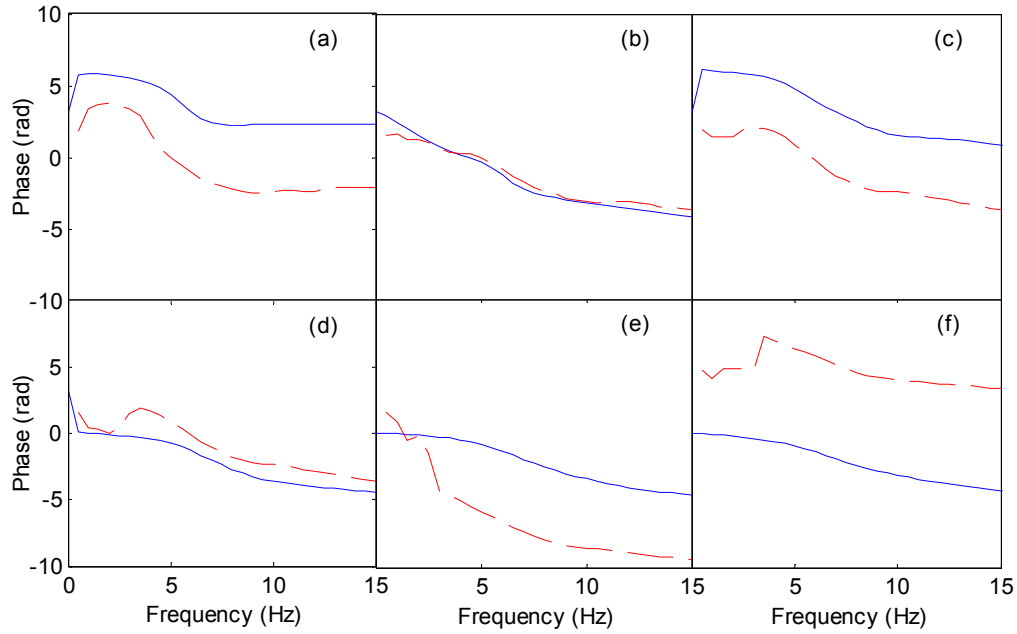

Figure 7.18 Phase of fore-and-aft cross-axis transmissibilities to T5 in (a) normal sitting posture (NB), (b) with vertical backrest at L2 (B_{0L2}), (c) with vertical backrest at T5 (B_{0T5}), (d) with 10º-inclined backrest (B_{10}), (e) with 20º-inclined backrest (B_{20}), (f) with 30º-inclined backrest (B_{30}). '- -': experimental data; '——': predicted from model.

The modulus and phase of the predicted vertical in-line transmissibility to the lumbar spine (L3) showed similar trends with the measured transmissibility in terms of resonance frequencies and phase at frequencies less than 10 Hz (Figures 7.11 and 7.12). The fore-and-aft cross-axis transmissibility to L3 appeared to be underestimated by the model at frequencies greater than 7 Hz when with inclined backrests (Figure 7.13). There were important differences in the vertical transmissibilities to T5 between the prediction of the model and measurements (Figure 7.15, d, e, f). The phase lags in the vertical transmissibility to T5 in all six sitting conditions predicted by the model with were greater than the corresponding measured data overall the frequencies 0 to 15 Hz (Figure 7.16). The modulus of the fore-and-aft transmissibility to T5 predicted tended to be underestimated by the model at the resonance frequency (5 to 8 Hz) when compared to the measured transmissibility (Figure 7.17).

7.4 Predictions of spinal forces at L5/S1 with vertical and inclined backrests

The static and dynamic spinal forces in either the vertical or the fore-and-aft directions were calculated separately at intervertebral disc L5/S1, which is the lowest spinal level assumed to be of the greatest risk of health during vertical whole-body vibration (Chapter 4). The static spinal forces were calculated in the static condition without vibration exposure and the dynamic spinal forces were calculated as variation of the force on the basis of the static spinal forces induced by the vertical whole-body vibration. The time-history of the spinal force acting on the intervertebral disc during vibration was the sum of the static spinal force and the dynamic spinal force. The calculations of the static and dynamic spinal forces are introduced below.

7.4.1 Calculation of the static spinal force with vertical and inclined backrests

The static muscle forces in the vertical and the fore-and-aft directions were calculated at the L5/S1 level based on the lever-arm system (Figure 7.2) involving the gravity of the body mass supported on the L5/S1 disc and the supporting forces from the backrest in the vertical and the fore-and-aft directions (Equations 7.2, 7.3 and 7.4). The static spinal forces at the L5/S1 intervertebral discs in the vertical direction ($F_{L5/S1\_z\_s}$) and the fore-and-aft direction ($F_{L5/S1\_x\_s}$) in the normal sitting posture (NB), with vertical backrests at L2 (B_{0L2}) and T5 (B_{0T5}), and with inclined backrests at T5 (B_{10}, B_{20} and B_{30}) are shown in Table 7.5.

With the vertical backrest supported at L2 (B_{0L2}), both the static muscle forces and the static spinal forces in the vertical and the fore-and-aft directions were close to those in the normal upright sitting posture without backrest (NB), respectively. With the vertical backrest supported at T5, the static vertical muscle force increased and the static vertical spinal force increased by about 30% compared to the normal upright sitting posture (NB). A 10º-inclined backrest increased the vertical spinal force at L5/S1 by 50% compared to the normal sitting posture (i.e., NB). A 20º-inclined backrest further increased the static vertical spinal force by 16% compared to a 10º-inclined backrest. A 30º-inclined backrest decreased the vertical spinal force by about 10% compared to a 20º-inclined backrest. Among all the sitting conditions, a 20º-inclined backrest resulted in the greatest static vertical spinal force.

Table 7.5 Prediction of muscle force and static spinal forces in the vertical and the fore-and-aft directions in different sitting conditions: normal upright posture (NB), with vertical backrests (B_{0T5} and B_{0L2}), and with inclined backrests (B_{10}, B_{20} and B_{30}).

Predicted static spinal forces (N) at L5/S1 in the vertical direction of Subject 7 of 69 kg						
	NB	B_{0L2}	B_{0T5}	B_{10}	B_{20}	B_{30}
F_{mz} (N)	264	290	465	537	623	612
$F_{L5/S1\_z\_s}$ (N)	514	524	688	737	771	701

Predicted static spinal forces (N) at L5/S1 in the fore-and-aft direction of Subject 7 of 69 kg						
	NB	B_{0L2}	B_{0T5}	B_{10}	B_{20}	B_{30}
F_{mx} (N)	23	25	35	-54	-173	-293
$F_{L5/S1\_x\_s}$ (N)	23	16	-7	-160	-338	-476

[a] '-' indicates the direction of the fore-and-aft spinal force is opposite to the positive direction defined in Figure 7.2, which is towards the back in the sagittal plane.

In the normal upright sitting posture without backrest, the spinal force in the fore-and-aft direction was solely contributed by the fore-and-aft muscle force with a small amount (23 N). With the vertical backrest supported either at L2 or at T5, the fore-and-aft muscle force increased slightly (B_{0L2}: 25 N; B_{0T5}: 35 N). Since the fore-and-aft backrest supporting force from the vertical backrests increased (Table 7.2), the calculated fore-and-aft spinal force at L5/S1 decreased. With increasing inclinations of backrest, the fore-and-aft muscle force increased significantly, resulting in a significant increase in the fore-and-aft spinal force. With inclined backrest, the direction of the fore-and-aft force changed to '-*x*' direction in the sagittal plane. The 30º-inclined backrest induced the greatest static fore-and-aft spinal force among all six sitting conditions, which was about 20-foldmore than the static fore-and-aft force in the normal upright sitting posture.

7.4.2 Calculation of the dynamic spinal force with vertical and inclined backrests

Similar to the static conditions, the dynamic spinal forces were calculated as the sum of the vertical dynamic muscle force, backrest supporting force and the inertial force of the body mass supported on the L5/S1 intervertebral disc induced by vibration in both the vertical and the fore-and-aft directions. The contributions from the muscle forces, backrest supporting forces and the inertial forces to the static spinal forces were described by Equations 7.3 and 7.4. The relationships between the above static forces are the same in the dynamic condition. Since the current model was linear, both the vertical and the fore-and-aft dynamic spinal forces in each sitting condition were evaluated in the frequency domain as transfer functions from the vertical input acceleration ($a_z(t)$) to either the dynamic vertical spinal force ($F_{L5/S1\_z\_d}(t)$) or dynamic fore-and-aft spinal force ($F_{L5/S1\_x\_d}(t)$), as shown in Equations 7.12 and 7.13.

$$T_{L5/S1\_Z}(f) = \frac{L\left[F_{L5/S1\_z\_d}(t)\right]}{L\left[a_z(t)\right]} = \frac{L\left[F_{inertial\ \_z}(t) - F_{b\_z}(t) - F_{muscle\ \ force\ \_z}(t)\right]}{L\left[a_z(t)\right]} \quad (7.12)$$

$$T_{L5/S1\_x}(f) = \frac{L\left[F_{L5/S1\_x\_d}(t)\right]}{L\left[a_z(t)\right]} = \frac{L\left[F_{inertial\ \_x}(t) - F_{b\_x}(t) - F_{muscle\ \ force\ \_x}(t)\right]}{L\left[a_z(t)\right]} \quad (7.13)$$

where the symbol '*L*' indicates the Laplace transform of the time-domain variable. Following the algorithm of Laplace transform, the above transfer functions from the vertical acceleration at the seat to the dynamic spinal forces ($T_{L5/S1\_z}(f)$, and $T_{L5/S1\_x}(f)$) were calculated as the sum of the transfer functions (i.e., complex values with real and imaginary parts) from the vertical acceleration at the seat to the muscles forces ($T_{muscle\_force\_Z}(f)$ and $T_{muscle\_force\_X}(f)$), the backrest supporting forces (vertical in-line and fore-and-aft cross-axis apparent masses at the backrest: $M_{bzz}(f)$ and $M_{bxz}(f)$), and the inertial forces ($T_{inertial\_force\_Z}(f)$ and $T_{inertial\_force\_X}(f)$) (Equations 7.12 to 7.15).

$$T_{L5/S1\_Z}(f) = T_{inertial\ \ force\ \_Z}(f) - M_{bzz}(f) - T_{muscle\ \ force\ \_Z}(f) \quad (7.14)$$

$$T_{L5/S1\_X}(f) = T_{inertial\ \ force\ \_x}(f) - M_{bxz}(f) - T_{muscle\ \ force\ \_x}(f) \quad (7.15)$$

The calculation of the above equations followed the directions defined in Figure 7.1. The vertical in-line and the fore-and-aft cross-axis apparent masses at the backrest were shown in Figures 7.7 - 7.10. The modulus and phase of the transfer functions between the vertical seat acceleration and the dynamic muscles forces in the vertical and the fore-and-aft directions are shown in Figure 7.19 and Figure 7.20, respectively.

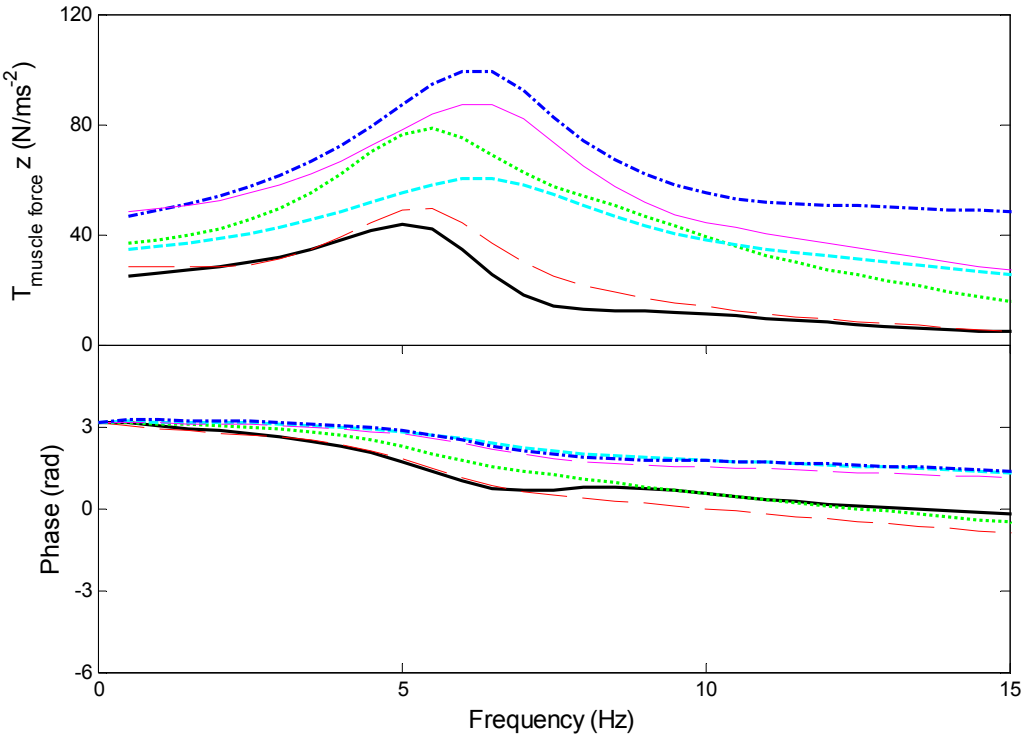

Figure 7.19 Transfer functions from vertical acceleration at the seat to the dynamic vertical muscle force in different sitting conditions: normal upright sitting posture NB ('——'); vertical backrest contact at L2, B_{0L2} ('------'); vertical backrest contact at T5, B_{0T5} ('……'); contact with 10º-inclined backrest, B_{10} ('–·–'); 20º-inclined backrest, B_{20} ('——'); 30º-inclined backrest, B_{30} ('------').

The transfer function between the vertical seat acceleration and the dynamic vertical muscle force showed a resonance at 5 to 7 Hz (Figure 7.19) with a modulus around 40 N/ms^{-2} to 100 N/ms^{-2}.

The resonance frequencies are similar to the resonance frequencies of the vertical apparent mass at the seat pan in each sitting condition (Figure 7.3). Sitting with 10º-inclined backrest induced the greatest maximum dynamic vertical muscle force (at 6 Hz) among all sitting conditions, where the maximum modulus (100 N/ms^{-2}) of the transfer function is 2.5-fold greater than the maximum modulus (40 N/ms^{-2}) of the corresponding transfer function in the normal sitting posture. In all the sitting conditions, the phase of the transfer function showed a starting value of 3.14 rad at 0 Hz.

The transfer function between the vertical seat acceleration and the dynamic fore-and-aft muscle forces showed moduli less than 40 N/ms^{-2} and resonance frequencies between 5 and 10 Hz in different sitting conditions. The transfer function between the vertical seat acceleration and the dynamic fore-and-aft muscle forces with vertical backrest (B_{0L2} and B_{0T5}) showed a phase starting from 3.14 rad, while the phase of the transfer functions in other conditions started from 0 at 0 Hz (Figure 7.20). The difference in the phase of the transfer functions at 0 Hz was associated with the body motions when sitting against backrests of different inclinations (discussed in Section 7.5.2).

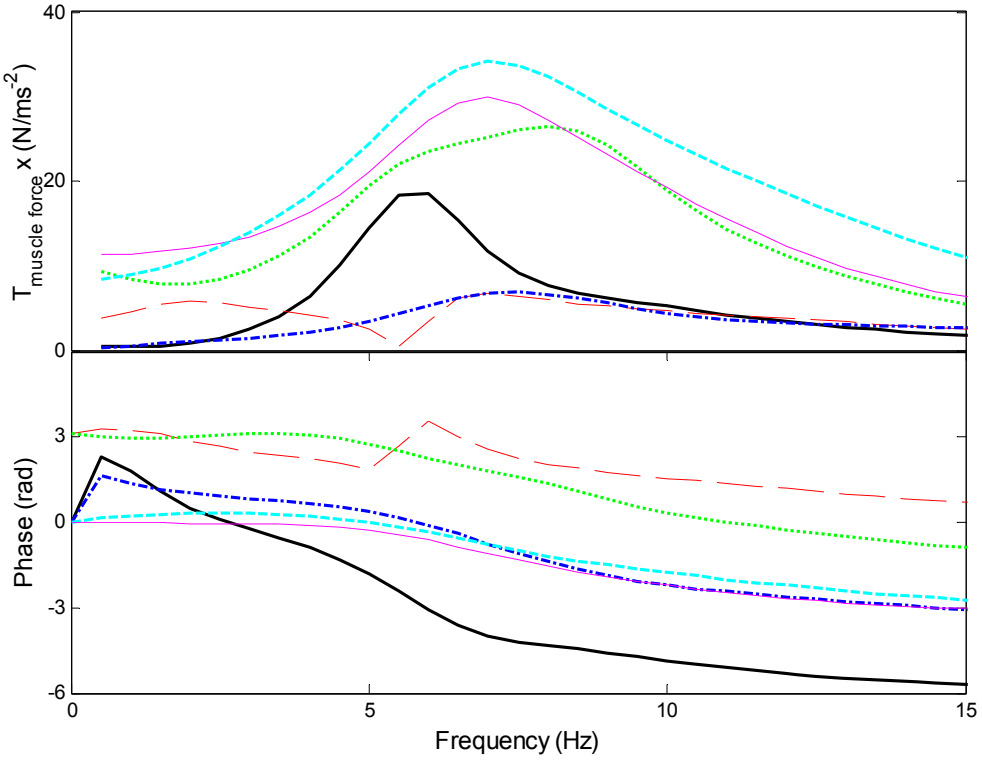

Figure 7.20 Transfer functions from vertical acceleration at the seat to the dynamic fore-and-aft muscle force at L5/S1 in different sitting conditions: normal upright sitting posture NB ('——'); vertical backrest contact at L2, B_{0L2} ('- - - -'); vertical backrest contact at T5, B_{0T5} ('.....'); contact with 10º-inclined backrest, B_{10} ('-·-·-'); 20º-inclined backrest, B_{20} ('——'); 30º-inclined backrest, B_{30} ('- - - -').

The modulus and phase of the transfer functions between the vertical seat acceleration and the vertical and the fore-and-aft inertial forces of the masses supported on L5/S1 intervertebral disc are shown in Figure 7.21 and Figure 7.22, respectively.

The transfer function between the vertical seat acceleration and the vertical inertial force in every backrest condition showed a similar pattern to the vertical in-line apparent mass at the seat pan, regarding the resonance frequency and shape of the modulus (Figure 7.21). The model of the human body sitting with vertical backrest at the thoracic support (B_{0T5}) predicted a greatest modulus (57 N/ms^{-2}) of the transfer function between the vertical seat acceleration and the vertical inertial force at the resonance frequency (6 Hz). The normal sitting posture induced a modulus (42 N/ms^{-2}) of the transfer function at the resonance frequency (5 Hz) slightly less than in the other sitting conditions. Sitting with the inclined backrest tended to increase the predicted vertical inertial forces in the range 0 to 8 Hz, compared with the normal upright sitting posture.

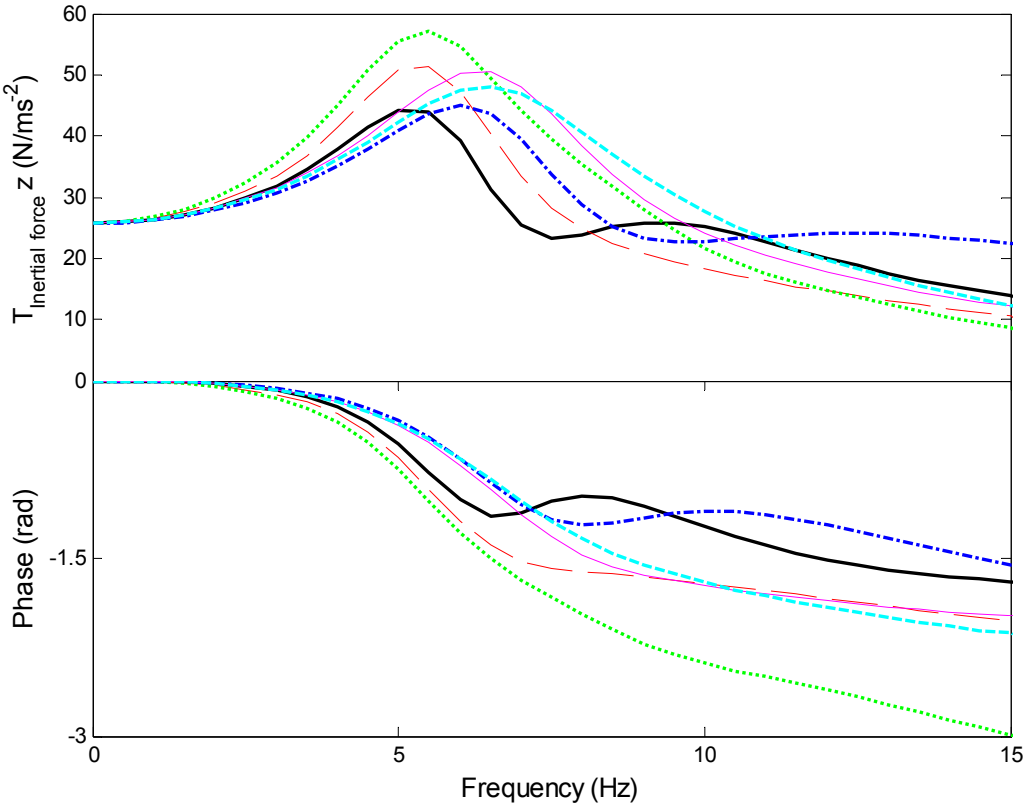

Figure 7.21 Transfer functions from vertical acceleration at the seat to vertical inertial force induced by the vertical motions of body masses supported on L5/S1 in different sitting conditions: normal upright sitting posture NB ('——'); vertical backrest contact at L2, B_{0L2} ('------'); vertical backrest contact at T5, B_{0T5} ('.....'); contact with 10º-inclined backrest, B_{10} ('–·–'); 20º-inclined backrest, B_{20} ('——'); 30º-inclined backrest, B_{30} ('------').

The transfer function between the vertical seat acceleration and the dynamic fore-and-aft inertial force showed resonance frequencies around 5 to 10 Hz, with a modulus around 13 N/ms^{-2} to 23 N/ms^{-2} at the resonance. Sitting in the B_{0T5} and inclined backrests would increase the fore-and-aft inertial force at frequencies greater than 5 Hz (Figure 7.22).

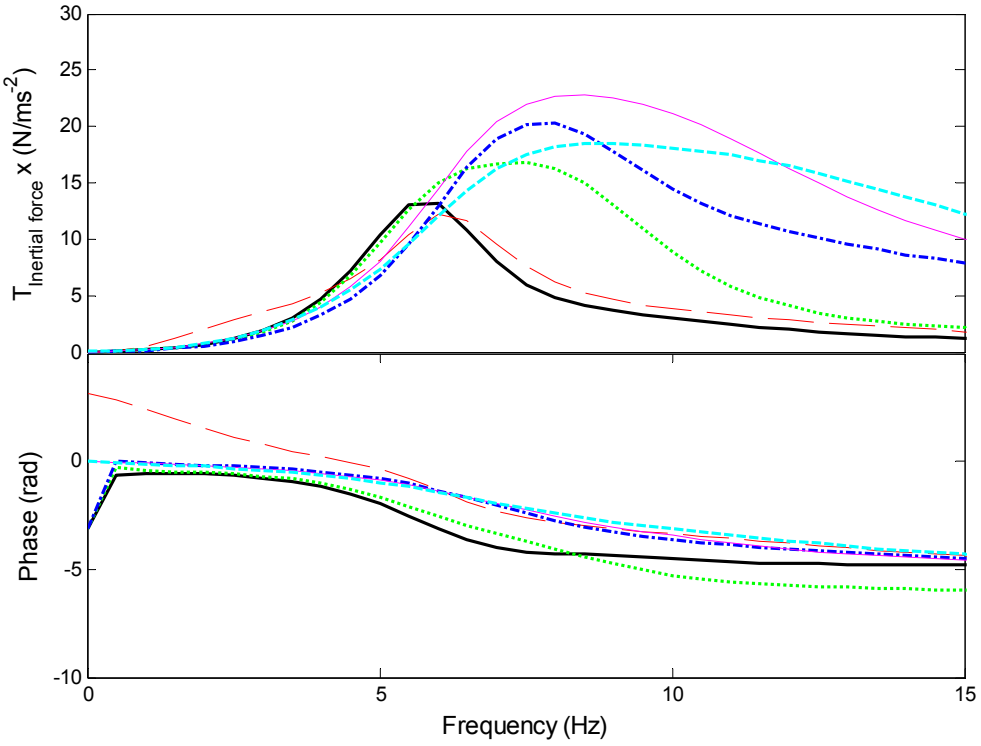

Figure 7.22 Transfer functions from vertical acceleration at the seat to fore-and-aft inertial force induced by the fore-and-aft motions of body masses supported on L5/S1 in different sitting conditions: normal upright sitting posture NB ('——'); vertical backrest contact at L2, B_{0L2} ('------'); vertical backrest contact at T5, B_{0T5} ('……'); contact with 10º-inclined backrest, B_{10} ('–·–'); 20º-inclined backrest, B_{20} ('——'); 30º-inclined backrest, B_{30} ('------').

According to Equations 7.14 and 7.15, the transfer function between the vertical seat acceleration and the dynamic spinal force was calculated as the sum of the transfer functions (i.e., complex value with real and imaginary parts) between the vertical seat acceleration and the inertial force, backrest supporting force, and dynamic muscle force in either the vertical direction or the fore-and-aft direction. The modulus and the phase of the transfer functions between the vertical seat acceleration and the dynamic spinal forces in the vertical and the fore-and-aft directions in six sitting conditions were shown in Figure 7.23 and Figure 7.24, respectively.

The transfer functions between the vertical acceleration at seat and the dynamic vertical spinal force in all the sitting conditions showed a resonance at 4 – 7 Hz close to the resonance frequencies of the vertical apparent mass at the seat pan in each sitting condition (Figures 7.3 and 7.19), and the modulus at the resonance varied from 80 N/ms^{-2} (B_{30}) to 130 N/ms^{-2} (B_{10}) (Figure 7.23). The modulus of the dynamic vertical spinal forces (transfer function) at frequencies close to 0 Hz in all sitting conditions showed a value close to the value of the static vertical spinal force dividing by the gravity (g=9.81 m/s^2), expect for the B_{30} condition.

With the vertical backrest supported at either lumbar (B_{0L2}) or thoracic (B_{0T5}) and 10˚ and 20˚ inclined backrests supported at thoracic (B_{10} and B_{20}), the dynamic vertical spinal forces increased significantly over 0 - 15 Hz, compared to the normal upright sitting posture (NB). With inclinations of

the backrest increasing from 10º to 30º with the thoracic support, the dynamic vertical spinal force at frequencies in the range 0-15 Hz decreased continuously.

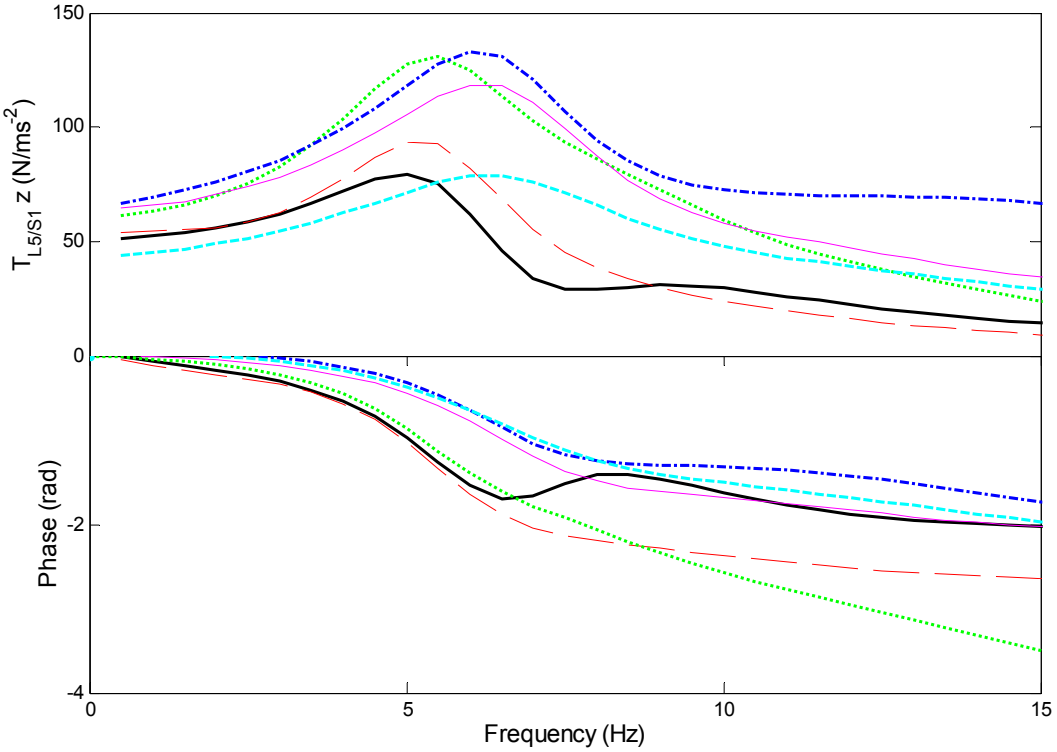

Figure 7.23 Transfer functions from vertical acceleration at the seat to the vibration induced vertical spinal force at L5/S1 in different sitting conditions: normal upright sitting posture NB ('——'); vertical backrest contact at L2, B_{0L2} ('------'); vertical backrest contact at T5, B_{0T5} ('……'); contact with 10º-inclined backrest, B_{10} ('–·–'); 20º-inclined backrest, B_{20} ('——'); 30º-inclined backrest, B_{30} ('------').

The transfer functions between the vertical acceleration at seat and the dynamic fore-and-aft spinal force at L5/S1 in all sitting conditions (Figure 7.24) showed a resonance at around 6 – 8 Hz and the modulus at the resonance varied between 5.5 N/ms^{-2} (NB) and 50 N/ms^{-2} (B_{30}). The effect of the vertical or inclined backrests on the dynamic fore-and-aft spinal forces followed a trend similar to its effect on the static fore-and-aft spinal force. The normal upright sitting posture and sitting with vertical backrest at lumbar supported tended to give the lowest dynamic fore-and-aft spinal forces among all six sitting conditions. With the vertical backrest supported at thoracic (B_{0T5}), the modulus of the transfer function between the vertical seat acceleration and the dynamic fore-and-aft spinal force increased slightly over 0 – 15 Hz with a peak modulus of 12 N/ms^{-2}, compared to no backrest sitting (i.e., NB) and sitting with vertical backrest at lumbar support (i.e., B_{0L2}). With increasing inclinations of backrest at thoracic support, the dynamic fore-and-aft spinal forces increased gradually over 0 to 15 Hz, but the difference between the dynamic fore-and-aft force in the B_{20} and B_{30} conditions were small.

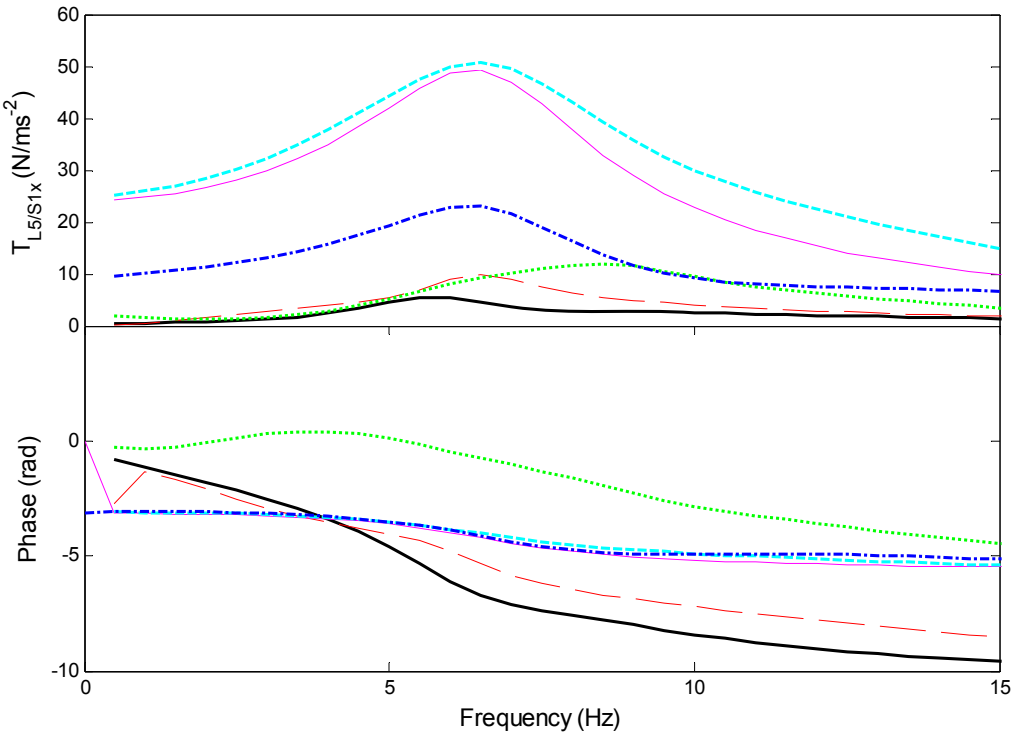

Figure 7.24 Transfer functions from the vertical acceleration at the seat to the vibration induced fore-and-aft spinal force at L5/S1 in different sitting conditions: normal upright sitting posture NB ('——'); vertical backrest contact at L2, B_{0L2} ('------'); vertical backrest contact at T5, B_{0T5} ('……'); contact with 10º-inclined backrest, B_{10} ('–·–'); 20º-inclined backrest, B_{20} ('——'); 30º-inclined backrest, B_{30} ('------').

7.5 Discussion

7.5.1 Muscle model

The model described in Chapter 5 modelled the muscle at the back as a linear spring attached from the T7 spinous process to the sacrum (S1) to reflect the overall effect of muscles on the upper body (Figure 5.1, Section 5.2.2). Such a muscle model only allows the muscle force along the direction from T7 to S1 during vibration. To generate the equations of motion, the motions of the two connecting points (T7 and S1) were projected onto this direction and it was assumed that the angle of this direction (T7 to S1) only varied by a small amount during vibration. However, the initial angle was very small (about 5 degrees) and the variation of the inclination angle (i.e., β, shown in Equation 5.7, Chapter 5) of the muscle (from T7 to S1) was greater than 5 degrees during vibration. The equations of motion (Equation 5.7, Chapter 5) can only be solved in the time-domain with consideration of the positions of the connecting point (i.e., T7 and S1) in the time-history during vibration, making the model nonlinear. The angle defining of this direction therefore cannot be simplified as a constant and time-varying values of the angle should be considered when solving the equations of motion..

The current study modelled the dynamic muscle force in both the vertical and the fore-and-aft directions with stiffness and damping coefficients. The vertical and the fore-and-aft dynamic muscle forces were generated during vibration due to the relative motions and velocities between the connecting points of the muscle (spinous process of T7 and S1). The damping coefficient was considered because the human body is a heavily damped system and the muscular system would contribute to the body damping. The passive properties of muscle forces including stiffness and damping were modelled in other studies investigating human body movements (e.g., hill-type muscle model: Winters and Woo, 1990; Nigg and Liu, 1999).

The parameters of the muscles (i.e., stiffness and damping) were determined by an optimisation process with reference to the measured biodynamic responses (i.e., apparent masses at the seat pan and backrest) of the human body together with other parameters in the model (Section 7.3.1). The modulus of the transfer function between the vertical seat acceleration and the spinal forces around 0 Hz in the normal upright sitting posture and with vertical or inclined backrests were selected to be a target during the optimisation process (Section 7.3.1). The body would move rigidly at very low frequency with little relative motions inside the body. At frequencies close to 0 Hz, the fore-and-aft transmissibilities to the spine predicted from the model were close to 0 and the vertical body transmissibilities were close to 1. When exposed to vertical acceleration at the seat with magnitude of a_z at very low frequencies (close to 0 Hz), the predictions of dynamic muscle forces, backrest supporting forces, inertial forces and the resulting dynamic spinal forces in both the vertical and the fore-and-aft directions should be close to the corresponding static forces predicted from the lever-arm system, but with the gravity (g) changed to (g+a_z). It is then suggested that the predictions of dynamic spinal force at frequencies close to 0 Hz should be close to the predictions of static spinal force. The above consistence has usually been neglected in previous models.

In the models similar to the current model, the position of the muscle vectors will affect the predictions of muscle forces in both static and dynamic conditions. The torques applied at the intervertebral disc (L2/L3) generated from the muscle forces depend on the locations of the muscles. The attached points for the muscles were selected at the spinous process of T7 and S1, partly because they were the attached points of muscles in the muscular system, and partly determined from the preliminary adjustments of the model against the appropriate range of static spinal forces from in-vivo measurements of Wilke *et al.* (2001).

7.5.2 Parameters in the model

The sensitivity of the frequency of the principal resonances in the vertical and fore-and-aft apparent masses at the seat pan (M_{zzs}, M_{xzs}) and apparent masses at the backrest (M_{zzb}, M_{xzb}) to each stiffness and damping coefficient in the model of the B_{10} condition was examined (Table 7.6). The effect of each parameter on the corresponding apparent masses at the resonance frequencies was also examined (Table 7.6). During the sensitivity analysis, the frequencies and magnitudes of the apparent masses were tabulated with $\pm$30% changes in each parameter in the model from the initial values (shown in Table 7.4).

The effects of ±30% changes in each parameter in the model of the B_{10} condition on the frequency of the principal resonance in the vertical and fore-and-aft transmissibilities to L3 (T_{zz_L3}, T_{xz_L3}) and to T5 (T_{zz_T5}, T_{xz_T5}), and the corresponding transmissibilities at the above resonance frequencies were examined and are shown in Table 7.7.

With the current set of values of the parameters in the model, it is clear that the frequency of the principal resonance in the vertical in-line apparent mass at the seat is sensitive to the stiffness and damping of the vertical elements of the buttocks (i.e., k_1 and c_1), the stiffness of the vertical backrest contact (i.e., k_{bx}), the damping of the fore-and-aft buttocks element (i.e., c_{1x}), and the rotational stiffness of the joint r_2 (i.e., k_{r2}). The vertical buttocks elements supported most of the weight of the seated body, and changes in the vertical stiffness of the buttocks affects the principal resonance frequency of the vertical apparent mass at the seat pan (e.g., Matsumoto and Griffin, 2001; Zheng *et al.*, 2012).

The frequency of the principal resonance in the fore-and-aft cross-axis apparent mass at the seat pan in the current model of the B_{10} condition was sensitive to the vertical stiffness of the buttocks (i.e., k_1), the rotational stiffness of joint r_2 (i.e., k_{r2}), and the fore-and-aft stiffness of the backrest contact (i.e., k_{bx}). The fore-and-aft apparent mass at the principal resonance was sensitive to the vertical and fore-and-aft stiffness of the buttocks tissues (i.e., k_1, k_{1x}), the damping of the joint connecting the pelvis and the thighs (i.e., c_{r1}), the rotational stiffness of the L5/S1 joint (i.e., k_{r2}), and the stiffness and damping of the muscle elements (i.e., k_{mx}, k_{mz}, c_{mx}, c_{mz}).

Both the vertical in-line apparent mass and the fore-and-aft cross-axis apparent mass at the seat pan at the principal resonance frequency were sensitive to the stiffness or damping of the pelvis joint (i.e., r_1) or lumbar spine joint (i.e., r_2), implying that rotational motion of the pelvis and bending of the lumbar spine contribute to these apparent masses at the resonance, consistent from studies of the modes of vibration of the human body (e.g., Kitazaki and Griffin, 1997; Matsumoto and Griffin, 2001).

The frequency of the principal resonance in the vertical in-line apparent mass at the backrest was sensitive to the vertical stiffness of the buttocks (i.e., k_1), the stiffness (i.e., k_2) of the elements supporting the visceral on the pelvis, the stiffness of the rotational joint r_2 (i.e., k_{r2}), and the fore-and-aft stiffness of the backrest contact (i.e., k_{bx}). The vertical inline apparent mass at the backrest at the principal resonance frequency was sensitive to the damping of the rotational joints r_1 and r_2, and the stiffness and damping of parameters of the muscle elements (i.e., k_{mx}, k_{mz}, c_{mx}, c_{mz}).

The frequency of the principal resonance in the fore-and-aft cross-axis apparent mass at the backrest was sensitive to k_1, k_2, c_{1x} and k_{bx}. The fore-and-aft cross-axis apparent mass at the backrest at the resonance frequency was sensitive to the visceral elements (i.e., k_2 and c_2), k_{r2}, k_{1x}, c_{bx} and c_{bz}.

Table 7.6 Resonance frequencies (Hz) and magnitudes (kg) of the calculated vertical in-line apparent mass and fore-and-aft cross-axis apparent masses at the seat pan and at the backrest with ±30% changes in each model parameter in the model of the B_{10} condition. The initial values of the parameters in the model are adopted from Table 7.4.

Parameters	Initial values	AM_{zzs}				AM_{xzs}				AM_{zzb}				AM_{xzb}			
		frequency (Hz)		magnitude (kg)		frequency (Hz)		magnitude (kg)		frequency (Hz)		magnitude (kg)		frequency (Hz)		magnitude (kg)	
		-30%	30%	-30%	30%	-30%	30%	-30%	30%	-30%	30%	-30%	30%	-30%	30%	-30%	30%
k_1 (N/m)	172753	5.0	5.4	*91.8**	*81.4*	4.8	5.0	18.4	16.2	*5.4*	*6.1*	*14.8*	*11.2*	*6.0*	*6.6*	28.1	29.2
c_1 (Ns/m)	535	5.4	5.2	*87.2*	*84.6*	5.1	5.0	17.3	16.8	5.9	5.8	12.7	12.4	6.5	6.4	30.2	28.5
k_2 (N/m)	35659	5.1	5.3	87.4	84.4	4.9	5.0	17.5	16.8	*5.5*	*6.0*	12.4	12.5	*6.0*	*6.6*	*27.4*	*29.8*
c_2 (Ns/m)	202	5.4	5.2	86.7	85.0	5.0	5.0	17.2	17.0	5.9	5.8	12.8	12.4	6.5	6.4	*30.1*	*28.7*
k_{r1} (Nm/rad)	65	5.3	5.3	85.1	86.7	5.0	5.0	17.1	17.1	5.8	5.9	12.4	12.7	6.4	6.4	29.3	29.4
c_{r1} (Nms/rad)	5	5.2	5.4	86.0	85.8	5.0	5.0	*17.8*	*16.5*	5.8	5.9	*12.8*	*12.3*	6.4	6.5	30.0	28.7
k_{r2} (Nm/rad)	155	*5.1*	*5.4*	*82.4*	*88.2*	*4.8*	*5.1*	16.8	17.2	*5.7*	*6.0*	12.4	12.6	6.4	6.5	*28.0*	*30.1*
c_{r2}(Nms/rad)	1	5.3	5.3	86.4	85.4	5.0	5.0	17.3	16.9	5.8	5.9	*12.7*	*12.4*	6.4	6.4	29.8	28.9
k_{r3} (Nm/rad)	58	5.3	5.3	86.1	85.6	5.0	5.0	17.2	17.1	5.8	5.9	12.6	12.5	6.4	6.4	29.5	29.2
c_{r3} (Nms/rad)	1	5.3	5.3	86.0	85.7	5.0	5.0	17.1	17.1	5.9	5.8	12.6	12.6	6.4	6.4	29.4	29.2
k_{r4} (Nm/rad)	58	5.3	5.3	85.8	85.9	5.0	5.0	17.1	17.1	5.9	5.8	12.5	12.6	6.4	6.4	29.3	29.3
c_{r4} (Nms/rad)	28	5.2	5.3	84.7	86.5	5.0	5.0	*16.9*	*17.2*	5.8	5.9	12.5	12.6	6.4	6.4	28.8	29.6

k_{r5} (Nm/rad)	65	5.3	5.3	85.9	85.9	5.0	5.0	17.1	17.1	5.9	5.9	12.6	12.6	6.4	6.4	29.3	29.3
c_{r5} (Nms/rad)	840	5.3	5.3	85.8	85.9	5.0	5.0	17.1	17.1	5.8	5.9	12.5	12.6	6.4	6.4	29.3	29.4
k_{1x} (N/m)	16760	5.4	5.2	85.3	87.0	5.0	5.1	*15.9*	*18.3*	6.0	5.8	*12.3*	*12.9*	6.4	6.4	*30.5*	*28.5*
c_{1x} (Ns/m)	735	*5.0*	*5.4*	*83.1*	*88.0*	4.9	5.1	17.2	17.3	5.7	5.9	12.4	12.7	*6.7*	*6.3*	*26.9*	*31.3*
k_{mz} (N/m)	312543	5.2	5.4	*82.2*	*88.8*	4.9	5.1	*16.3*	*17.7*	5.9	5.9	*12.0*	*12.9*	6.5	6.4	28.0	30.7
k_{mx} (N/m)	27583	5.3	5.3	85.2	86.6	4.9	5.1	*17.3*	*16.8*	5.9	5.8	*12.3*	*12.8*	6.4	6.4	29.6	28.8
c_{mz} (Ns/m)	9999	5.2	5.4	87.5	85.5	4.9	5.1	*17.6*	*16.9*	*5.7*	*6.0*	*13.1*	*12.3*	6.2	6.5	28.9	30.0
c_{mx} (Ns/m)	424	5.2	5.3	85.4	86.3	5.0	5.0	*17.7*	*16.6*	5.8	5.9	12.6	12.5	6.5	6.4	30.3	28.4
k_{bx} (N/m)	77007	*5.0*	*5.5*	83.6	86.7	*4.6*	*5.2*	*15.2*	*18.1*	*5.5*	*6.0*	12.5	12.4	*5.8*	*6.7*	27.0	28.8
c_{bx} (Ns/m)	621	5.3	5.3	86.6	85.3	5.0	5.0	17.3	17.0	5.9	5.8	12.8	12.4	6.6	6.3	*32.7*	*26.9*
k_{bz} (N/m)	533	5.3	5.3	85.8	85.9	5.0	5.0	17.1	17.1	5.8	5.9	12.5	12.6	6.4	6.4	29.3	29.3
c_{bz} (Ns/m)	304	5.3	5.3	*91.8*	*80.8*	5.1	4.9	*18.7*	*15.8*	5.8	5.9	*9.6*	*15.1*	6.3	6.5	*31.7*	*27.3*
Initial values	-	5.3		85.9		5		17.1		5.9		12.6		6.4		29.3	

*Numbers in iliac indicate changing the values of each parameter alters the response with a change greater than 10% when compared with the initial values.

Table 7.7 Resonance frequencies (Hz) and magnitudes of the calculated vertical in-line transmissibilities and fore-and-aft cross-axis transmissibilities to L3 and T5 with ±30% changes in each model parameter in the model of the B_{10} condition. The initial value of each parameter is shown in Table 7.6.

Parameters	TR_{zz_L3}				TR_{xz_L3}				TR_{zz_T5}				TR_{xz_T5}			
	frequency (Hz)		magnitude		frequency (Hz)		magnitude		frequency (Hz)		magnitude		frequency (Hz)		magnitude	
	-30%	30%	-30%	30%	-30%	30%	-30%	30%	-30%	30%	-30%	30%	-30%	30%	-30%	30%
k_1 (N/m)	4.9	5.3	1.82	1.60	6.6	7.0	0.37	0.40	4.9	5.3	1.82	1.61	7.3	7.6	0.60	0.71
c_1 (Ns/m)	5.2	5.1	1.71	1.67	6.9	6.9	0.41	0.39	5.2	5.1	1.72	1.67	7.5	7.5	0.71	0.67
k_2 (N/m)	*4.9**	*5.3*	1.66	1.70	*6.4*	*7.1*	0.35	0.41	*4.9*	*5.3*	1.66	1.71	*7.0*	*7.8*	*0.56*	*0.75*
c_2 (Ns/m)	5.2	5.1	1.70	1.68	6.9	6.9	0.41	0.39	5.2	5.1	1.71	1.68	7.5	7.5	0.71	0.67
k_{r1} (Nm/rad)	5.2	5.2	1.67	1.71	6.9	6.9	0.40	0.40	5.2	5.2	1.68	1.71	7.5	7.5	0.69	0.69
c_{r1} (Nms/rad)	5.1	5.2	1.71	1.67	6.8	6.9	0.41	0.39	5.1	5.2	1.72	1.68	7.5	7.5	0.70	0.68
k_{r2} (Nm/rad)	*5.0*	*5.3*	1.65	1.71	6.8	6.9	*0.35*	*0.43*	5.0	5.3	1.65	1.72	7.5	7.5	0.66	0.71
c_{r2} (Nms/rad)	5.2	5.2	1.71	1.68	6.9	6.9	0.40	0.40	5.2	5.2	1.71	1.68	7.5	7.5	0.70	0.68
k_{r3} (Nm/rad)	5.2	5.2	1.70	1.68	6.9	6.9	0.39	0.40	5.2	5.2	1.70	1.69	7.5	7.5	0.69	0.69
c_{r3} (Nms/rad)	5.2	5.2	1.69	1.69	6.9	6.9	0.40	0.40	5.2	5.2	1.70	1.69	7.5	7.5	0.69	0.68
k_{r4} (Nm/rad)	5.2	5.2	1.69	1.69	6.9	6.9	0.40	0.40	5.2	5.2	1.69	1.70	7.5	7.5	0.69	0.69
c_{r4} (Nms/rad)	5.1	5.2	1.67	1.70	6.8	6.9	0.38	0.41	5.1	5.2	1.68	1.71	7.5	7.5	0.68	0.69
k_{r5} (Nm/rad)	5.2	5.2	1.69	1.69	6.9	6.9	0.40	0.40	5.2	5.2	1.70	1.70	7.5	7.5	0.69	0.69
c_{r5} (Nms/rad)	5.2	5.2	1.69	1.69	6.9	6.9	0.40	0.40	5.2	5.2	1.69	1.70	7.5	7.5	0.69	0.69

k_{1x} (N/m)	5.3	5.1	1.66	1.73	6.7	7.0	*0.45*	*0.35*	5.3	5.1	1.66	1.74	7.5	7.5	0.71	0.67
c_{1x} (Ns/m)	*4.9*	*5.3*	1.66	1.72	6.8	6.9	0.41	0.41	*4.9*	*5.3*	1.67	1.73	7.6	7.5	0.66	0.71
k_{mz} (N/m)	5.1	5.3	*1.62*	*1.74*	*7.1*	*6.7*	*0.38*	*0.42*	5.1	5.3	1.63	1.75	7.6	7.5	0.67	0.71
k_{mx} (N/m)	5.2	5.2	1.67	1.71	6.8	6.9	0.42	0.38	5.2	5.2	1.67	1.72	7.5	7.5	0.69	0.68
c_{mz} (Ns/m)	5.1	5.3	*1.74*	*1.67*	6.7	6.9	*0.48*	*0.35*	5.1	5.3	1.74	1.68	7.4	7.5	*0.65*	*0.72*
c_{mx} (Ns/m)	5.2	5.2	1.69	1.69	6.9	6.9	0.41	0.39	5.1	5.2	1.69	1.70	7.6	7.4	0.72	0.66
k_{bx} (N/m)	*4.9*	*5.3*	1.67	1.69	*6.3*	*7.2*	*0.32*	*0.42*	4.9	5.3	1.68	1.69	*6.9*	*8.1*	*0.72*	*0.60*
c_{bx} (Ns/m)	5.2	5.1	1.71	1.68	7.0	6.8	*0.48*	*0.34*	5.2	5.1	1.71	1.68	7.6	7.4	*0.83*	*0.59*
k_{bz} (N/m)	5.2	5.2	1.69	1.69	6.9	6.9	0.40	0.40	5.2	5.2	1.69	1.70	7.5	7.5	0.69	0.69
c_{bz} (Ns/m)	5.2	5.2	*1.78*	*1.61*	6.8	6.9	0.41	0.39	5.2	5.2	*1.79*	*1.62*	7.4	7.6	*0.72*	*0.66*
Initial values	5.2		1.90		6.9		0.40		5.2		1.70		7.5		0.69	

*Numbers in iliac indicate changing the values of each parameter alters the response with a change greater than 10% when compared with the initial values.

The vertical in-line transmissibilities and the fore-and-aft cross-axis transmissibilities to L3 and T5 at the principal resonance frequencies were sensitive to the damping and stiffness of the muscle elements (i.e., k_{mz}, k_{mx} and c_{mz}), and the stiffness and damping of the backrest elements (e.g., k_{bx}, c_{bx}, c_{bz}). The muscles may control the pitch motions of the lumbar spine, which appear to contribute to the fore-and-aft motions of the buttocks (e.g., Zheng *et al.*, 2012).

In the current model (i.e., the B10 condition), neither the resonance frequency of the vertical in-line apparent mass and fore-and-aft cross-axis apparent mass at seat or at the backrest, nor the apparent mass (including vertical and fore-and-aft apparent masses at the seat pan and at the backrest) or transmissibility (in both vertical and fore-and-aft directions) to L3 or T5 at the resonance frequency were sensitive to the stiffness and damping of the rotational joints r_3, r_4 and r_5. More details of the sensitivity analysis can be found in Tables 7.6 and 7.7.

From the above findings, it is indicated that the optimisation of the apparent mass and body transmissibilities described in Section 7.2.2 was able to determine the values of the parameters of the buttocks elements, visceral elements, and the parameters for the rotational joints r_1 and r_2. The optimisation process can also help to determine the stiffness and damping parameters of the muscles.

The optimised values of the stiffness and damping coefficients (k_1, c_1) representing the buttock tissues beneath the thighs, and the stiffness and damping coefficients (k_2, c_2) connecting the viscera in the current model in the normal sitting posture (Table 7.4) are close to the values of the relevant parameters in the model developed by Matsumoto and Griffin (2001).

The stiffness and damping coefficients of some of the rotational joints (i.e., r_3, r_4 and r_5) in the current model showed low sensitivities to the resonance frequencies and magnitudes at the resonance frequencies of the apparent mass and body transmissibilities. Compared with the model of a similar structure of the spine developed by Matsumoto and Griffin (2001), the values of the rotational joints connecting the segments of the upper body exhibited greater values of stiffness (stiffness: 899 to 1210 Nm/rad) than the current model (58 to 155 Nm/rad). The lower values of the stiffness of the rotational joints in the current model arose because of their boundary values. The boundaries of the rotational stiffness were determined based on in-vitro studies (e.g., Schultz *et al.*, 1979; mentioned in Section 7.3.1). Due to the complexity of the live human body, and probably the absence of representation of some body structures (e.g., detailed representation of muscles and ligaments) in the current model, the values of the stiffness and damping of the rotational joints can be further explored.

7.5.3 Predictions of biodynamic response from the model

The simple multi-body model was capable of predicting reasonable overall dynamic responses and motions at lumbar and thoracic spine in all six sitting conditions (NB, B_{0L2}, B_{0T5}, B_{10}, B_{20} and B_{30}) (Sections 7.3.1 and 7.3.2). However, there were some discrepancies between the predicted and measured biodynamic responses in the phase or modulus of the apparent mass and transmissibilities to spine. The following text will discuss such discrepancies.

The phase of the vertical in-line apparent mass at the seat pan predicted by the model in all sitting conditions tended to have greater lags than the corresponding measured phase at frequencies greater than 8 Hz (Figure 7.4). One possible reason may be that the damping coefficient of the buttock tissues (c_1) is lower than the real values. The phase of the vertical apparent mass at the seat pan was not included in the error function. Alternatively, the error function could involve the apparent mass and transmissibilities in complex numbers (e.g., Matsumoto and Griffin, 2001) so that no weightings are required for the modulus and phase in the error function.

In the normal upright sitting posture, the phase of the fore-and-aft cross-axis apparent mass at the seat pan predicted from the model started at 0, while the phase of the measured fore-and-aft apparent mass at the seat started from 3.14 rad. The reason would be that the individual subject during the measurement would lean the upper body forward (the positive direction of the *x*-axis) at the beginning of the exposure, resulting in a backward acceleration ('-*x*') of the upper body and a backward ('-*x*') force at the human-seat interface. The above explanation about the body movements in the normal sitting posture is supported in a later chapter (Chapter 8) studying the effect of leaning forward sitting postures on the biodynamic response of the human body. The current multi-body model in the normal upright sitting posture does not reflect such a mechanism.

The predicted apparent masses at the back in both vertical and fore-and-aft directions matched the measured apparent masses (Section 7.3.1). But there were some differences between the predicted and measured phases in the fore-and-aft cross-axis apparent mass at the backrest, probably due to the underestimation of the damping coefficient of the elements representing the back-backrest contact (i.e., c_{bx}).

There was discrepancy in the modulus of the vertical in-line transmissibility to T5 in sitting with inclined backrest posture. The measured vertical transmissibility to T5 showed a value close to 1 at frequencies in the range 0-15 Hz (Figure 7.15). The causes would be that the accelerometers attached at the skin measured the accelerations at the skin surface instead of the acceleration at the vertebra body and the motions of the skin would be restricted by contacting with the backrest. As a result, the vertebrae body of T5 would move but the skin surface at T5 spinal level would not move. The model predicted the motion to the vertebrae body of T5 instead of the motions at the skin surface of this spinal level. Similar reasons would contribute to the differences between the predicted and measured vertical transmissibilities to L3 when sitting with vertical backrest at lumbar support (B_{0L2}) (Figure 7.11, b).

There were significant discrepancies between the phases of the predicted and measured vertical in-line transmissibilities and the fore-and-aft cross-axis transmissibilities to the lumbar (L3) and thoracic spine (T5) in all sitting conditions (Figures 7.12, 7.14, 7.16 and 7.18). There would be several reasons for these discrepancies. During the measurements of transmissibilities to spine, the fore-and-aft motions at the spine (i.e., lumbar spine and thoracic spine) tended to be small, especially when sitting with backrest, and there would be unavoidable disturbance from the measurement equipment itself. Possible causes include the set-up of the equipment and natural frequency of the accelerometer-skin system. The multi-body models developed in the present study may also have used inaccurate damping coefficients of the rotational joints connecting the

vertebrae. It is noticed that the resonance frequencies and the moduli of the apparent masses at the seat and at the backrest, and the resonance frequencies and the moduli of the transmissibilities to L3 and T5 at the resonance frequency were not sensitive to the values of the damping of the joints representing the intervertebral discs (e.g., c_{r4}, c_{r5}) in the model of the B_{10} condition (Tables 7.6 and 7.7; Section 7.5.2). However, these damping parameters may affect the phases of the transmissibilities to the spine, as discussed above.

The biodynamic models should reflect appropriate phases of the biodynamic responses. The phase of the apparent mass and the body transmissibilities at frequencies close to 0 Hz can tell whether the body moves in a correct way. The body would behave rigidly when exposed to vibration of very low frequency. When sitting with inclined backrest and exposed to vertical whole-body vibration, the phase of the fore-and-aft apparent mass should start from 3.14 rad, because a backward shear force is generated from the seat to balance the forward supporting force from the backrest.

7.5.4 Effects of vertical and inclined backrest on the static spinal forces

A lever-arm system was used to calculate the static spinal forces in every backrest condition (Figure 7.2) based on the assumption that the body is in an equilibrium state when in a static sitting posture. Force vectors in the vertical and the fore-and-aft directions were used to represent the overall effect of the muscular system in the body above the seat, including muscles, ligaments, articular facet joints and abdominal pressure, acting on the body above the seat during sitting. The compressive forces at the L4/L5 intervertebral disc of one subject (70 kg) sitting in different conditions were estimated from the pressure measured by Wilke *et al.* (2001) multiplied by the disc area of 18 cm^2 (obtained from Sato *et al.*, 1999) (Table 7.8). The predicted static vertical spinal force at L5/S1 in the current study (normal posture: 513 N) appeared smaller than the compressive forces (during relaxed sitting: 792 N) estimated from Wilke *et al.* (2001). Due to the uneven distribution of stress in the intervertebral disc, the estimation of spinal force from the measured pressure may not accurately reflect the spinal force. The predicted spinal force may be in an appropriate range.

Table 7.8 The in-vivo measurement of pressure at L4/L5 intervertebral disc of a 70 kg subject sitting in relaxed erect posture without backrest and with backrest from Wilke *et al.* (2001).

Postures	Relaxed erect sitting without backrest	Relaxed erect sitting with backrest (slightly inclined) hands and arms supported on the armchair
Pressure at L4/L5	0.44 MPa	0.33 MPa
Compressive force multiplied by disc area of 18 cm^2	792 N	594 N

In the present study, the static spinal force in the vertical direction was found to increase with vertical or inclined backrests at thoracic spine T5 (Table 7.5). With the vertical backrest supported at T5, the backrest supporting forces in the vertical and the fore-and-aft directions increased

compared to sitting with the vertical backrest supported at L2. The reasons include the mass supported on the backrest with a lumbar support being less than that with a thoracic support, because the pelvis tends to rotate forward with a thoracic support. Sitting with a vertical backrest at the lumbar support makes the contact point closer to the L5/S1 disc than sitting with a thoracic support, resulting in less torque generated from the backrest support force at the intervertebral disc (L2/L3). Therefore, less vertical muscle force is required to balance the torque, resulting in less vertical spinal force at intervertebral disc L5/S1 (see Equation 7.3).

Compared with a vertical backrest providing support in the thoracic region (e.g., at T5), the 10º-inclined and 20º-inclined backrests providing only support at T5 increased the body mass supported on the backrest. The vertical force at the backrest contact increased (Table 7.2) and the torque generated from the supporting force from the backrest against the intervertebral disc (L2/L3) increased, contributing to a further increase in the vertical muscle forces in order to maintain the stability of the lumbar spine and an increase in the vertical spinal force. It is noticed that the centre of gravity of the upper body may move towards the backrest in the sagittal plane (see Figure 7.2) when sitting with inclined backrests, and the direction of the torque at the L2/L3 disc generated from the gravity force becomes opposite to the torque generated from the backrest supporting forces (Figure 7.2). With the backrest further inclined to 30º with thoracic support, the torque generated by the act of gravity on the body supported at L5/S1 increases due to the increase in the horizontal distance from the L2/L3 intervertebral disc to the centre of gravity of the body mass supported at the disc. Then the static vertical spinal force at L5/S1 decreases compared to the condition with a 20º-inclined backrest (Equation 7.3). The static vertical force may further decrease with further increases in the backrest inclination from 30º when the backrest provides only thoracic support.

With increasing inclination of the backrest from 0º to 30º, the body mass supported on the backrest increased, increasing the fore-and-aft force at the backrest contact and increasing the fore-and-aft spinal force at the intervertebral disc L5/S1. The extent of the increase in the static fore-and-aft spinal force was greater than the extent of the increase in the static vertical spinal force. This is consistent with the observation that when the body lies on an inclined backrest supported at the thoracic spine, the muscles around the lumbar region feel tensed.

The in-vivo measurements from Wilke *et al.*, (2001) show a decrease in the vertical spinal force when sitting with a slightly inclined backrest. Possible reasons may be the support of the hands and arms on the armrest in the in-vivo study with full backrest contact.

When people sit against a vertical backrest with full back support for both the thoracic spine and the lumbar spine, the sum of the backrest supporting force can be simplified as a vertical force and a fore-and-aft force applied in the middle part of the whole spine (i.e., the higher lumbar region, L2), assuming even distribution of force over the contact area. Contact with a full backrest becomes similar to the situation when sitting with a vertical backrest with only lumbar support. Spinal forces in the vertical and the fore-and-aft directions are reduced with full back support compared to only thoracic support. When inclining a backrest with full back support, the backrest supporting forces may increase. As the torque from the backrest supporting force is opposite to the torque from the

action of gravity on the body masses, the resulting torque from the backrest supporting force and the action of gravity at the lumbar spine may decrease continuously with increasing inclination, resulting in a decrease in the muscle forces in the vertical and fore-and-aft directions and, a decrease in the predicted spinal forces. Such a decrease in the static spinal forces is consistent with in-vivo measurements of spinal force (Wilke *et al.*, 2001; Rohlmann *et al.*, 2010).

7.5.5 Effects of vertical and inclined backrests on the dynamic spinal forces

In the normal upright sitting posture without backrest, the present model predicted a similar range of dynamic vertical spinal forces compared to the predictions from some other models (e.g., Wang *et al.*, 2010). For example, the finite element model of a seated human body (around 75 kg) developed by Wang *et al.* (2010) with consideration of active muscle force predicted a compressive force at L5/S1 varying around 550 N (450 N – 700 N) when exposed to random vibration of 1 m/s^2 r.m.s. at frequencies in the range 0.5 to 15 Hz. The current model predicted a similar range of vertical forces at L5/S1 with the same exposure in the normal upright sitting posture (360 N – 660 N).

Transfer functions from the vertical acceleration at the seat to the dynamic spinal forces in the vertical and fore-and-aft directions have been calculated with models of human body sitting without backrest in some studies (e.g., Verver *et al.*, 2003; Fritz, 2000). In these studies, the modulus of the transfer functions representing the dynamic vertical forces started from around 30 N/ms^{-2} at 0 Hz. The modulus is close to the value of the mass of the upper body (30 kg) supported on the intervertebral disc at L5/S1. It indicated that there would be no muscle forces at very low frequency in these models and using these transfer functions would underestimate the spinal loads at very low frequencies.

The predictions from the present model suggested that the contributions of dynamic vertical muscle force to the dynamic vertical spinal force would be as important as the vertical inertial force during whole-body vibration in all sitting conditions. This is consistent with the prediction of spinal force by Bazrgari *et al.* (2008) with a finite element model exposed to vibration of high magnitude (peak magnitude around 40 m/s^2). They predicted greater muscle forces than the inertial forces (see the review in Chapter 2).

Sitting with vertical backrests (B_{0L2} and B_{0T5}) and 10˚- and 20˚-inclined backrests providing only thoracic support (B_{10} and B_{20}) increased the dynamic vertical spinal forces at frequencies in the range 0 to 15 Hz significantly when compared to the normal upright sitting posture (NB). The increase may be due to the significant increase in the vertical dynamic muscle forces between different sitting conditions as the differences in the inertial forces were small (Figures 7.19 and 7.21). The dynamic vertical muscle force tended to change in a similar pattern to the static vertical muscle force in different backrest conditions (discussed in Section 7.5.3). The increase in the dynamic muscle force would probably due to the increase in the phasic muscle activity (variation of tonic muscle activity induced by vibration, see Chapter 2). Studies of EMG at the back muscles from Robertson and Griffin (1989) found that increased tonic muscle activity can induce an increase in the phasic muscle activity. The tonic muscle activity required to maintain the posture

stability increased with increase in the inclinations of backrest (Table 7.5). With the inclination of the backrest increased from 10˚ to 30˚, the dynamic fore-and-aft spinal forces increased, due to the increase in the dynamic muscle force and dynamic force at the backrest contact in the fore-and-aft direction (Figures 7.20 and 7.9).

7.5.6 Some limitations of current model to vibration with high magnitude

The multi-body model works around its equilibrium position during vibration. It was assumed the equilibrium position would not be affected by changes in the vibration magnitude. This appears to be a limitation of the current model. When exposed to vibration of high magnitude the equilibrium position of human body may be altered due to nonlinearity of the body system. The stiffness and damping properties of the overall body may change with vibration magnitude (e.g., Huang and Griffin, 2006). The current linear model is incapable of reflecting this nonlinearity and may give incorrect prediction of the biodynamic response when exposed to vibration of high magnitude.

The current model of the dynamic muscle force as a passive system may only reflect part of the muscle behaviour in real conditions. With increasing vibration magnitude at low frequencies, the body may maintain the same sitting posture by voluntarily tensing the muscles in the body. The EMG study found the muscle activity leads the vertical acceleration excitation in phase at low frequencies less than 3 Hz during random vertical whole-body vibration (Robertson and Griffin, 1989), which may be due to voluntary control of the muscles. Such voluntary tensing of the muscles can be represented by an increase in the stiffness of the spring representing the muscles. The present linear model cannot reflect this increase in the stiffness of the muscles, possibly resulting in the prediction of inappropriate motions of the body and an underestimation of spinal forces at low frequencies. The current multi-body model may be improved with improved knowledge about the voluntary control of the muscles.

7.6 Conclusion

The total forces in the spine at L5/S1 in the vertical and fore-and-aft directions can be calculated by summing the static and dynamic spinal forces in each direction.

A lever-arm model can predict the static spinal forces in the vertical and the fore-and-aft directions with different backrest conditions in order to maintain the stability of the posture. Contacting a vertical backrest or a 10˚-inclined or 20˚-inclined backrest with support only at T5 provides supporting forces from the backrest that generate additional torques at the intervertebral discs in the lumbar spine. Increasing forces are therefore generated by muscles in the lumbar spine and these increase the static vertical and fore-and-aft spinal forces at L5/S1 compared to the forces during normal sitting without a backrest. Compared with a vertical backrest providing support at T5, a vertical backrest providing support at L2 decreases the vertical distance between the lumbar intervertebral disc L2/L3 and the supporting forces from the backrest, resulting in less torque at the disc L2/L3, so less muscle force is required to maintain the stability of the lumbar spine and there is less static spinal forces in the vertical and the fore-and-aft directions. Compared to a 20º-inclined backrest with support only at T5, a 30˚-inclined backrest with support at T5 decreases the

horizontal distance between the disc and the centre of gravity of the upper body, resulting in an increase in the static vertical spinal force and a decrease in the static fore-and-aft spinal force.

Multi-body models of the seated human body with representation of muscles and backrest contact can predict appropriate apparent masses and transmissibilities to the spine in different sitting conditions, including normal sitting without backrest, sitting with a vertical backrest, and sitting with inclined backrests. The models developed in the current study can predict reasonable dynamic spinal forces at L5/S1 in the vertical and fore-and-aft directions during vertical whole-body vibration in different sitting conditions.

The transfer functions between the vertical seat acceleration and the dynamic spinal force predicted by the model show resonance at frequencies in the range 4 to 8 Hz, with the frequency increasing with increasing inclination of a backrest providing only thoracic support, similar to the effect of backrest inclination on the vertical apparent mass at the seat. Vertical and inclined backrests affect the dynamic spinal forces in a way similar to their effect on the static spinal forces. A 20º-inclined backrest providing only thoracic support increases the dynamic spinal forces in the vertical and the fore-and-aft directions, due to the increase in the dynamic forces at the backrest contact and the increased motions of the spine in both directions. Further increases in the inclinations of the backrest providing only thoracic support increase the dynamic forces at the backrest contact but may decrease the dynamic vertical spinal forces.

The spinal forces predicted from the modulus of the transfer function between the dynamic spinal force and the vertical acceleration at the seat at frequencies close to 0 Hz (e.g., at 0.5 Hz) should be close to the static spinal force predicted from a lever-arm system, as required to maintain the stability of the posture.

Chapter 8. Effect of forward leaning sitting postures on the apparent mass at the seat and the vibration transmitted to the spine exposed to vertical whole-body vibration

8.1 Introduction

A forward leaning sitting posture is commonly seen when riding a motor-bike or a high speed marine craft. Compared to sitting in a normal upright posture, leaning forward is expected to induce greater compressive forces in the lumbar spine (as measured in-vivo by Wilke *et al.*, 2001). A forward leaning sitting posture will increase the distance between the centre of gravity of the upper body (i.e., the body parts above the waist, including the thoracic and head-neck regions) and the intervertebral discs, resulting in increased muscle activity to maintain body posture. The increased muscle activity will further increase spinal loads in static conditions, consistent with the measured increase in compressive forces when sitting with a forward leaning sitting posture and this may be expected to increase the risks of spinal injury.

Biodynamic studies (e.g., Kitazaki and Griffin, 1998; Zheng *et al.*, 2011) found that the overall biodynamic response of the body (i.e., apparent mass) and the local body movements of the body (i.e., transmissibilities to various body locations) are dependent on body sitting posture. For example, an 'erect' sitting posture tended to increase the resonance frequency of the vertical apparent mass compared to a 'normal' sitting posture and a 'slouched sitting posture' tended to decrease the resonance frequency of vertical apparent mass compared to a 'normal' sitting posture. From a slouched sitting posture to a normal sitting posture, then to an erect sitting posture, the resonance frequency of the vertical transmissibility to various spinal levels also increased (Kitazaki, 1994). The changes in the apparent mass and body transmissibilities may be partially due to changes in body stiffness arising from variations in muscle tension between postures and partially due to the change of body geometry (i.e., spinal curvature).

Studies have been conducted with 'anterior leaning' sitting posture and kyphotic sitting posture (e.g., Mansfield and Griffin, 2002). It was found that the 'anterior leaning' and kyphotic sitting postures do not significantly affect the resonance frequency of the vertical apparent mass at the seat pan compared to normal upright sitting posture when exposed to 1.0 m/s^2 r.m.s. random vibration. Compared to a normal sitting posture, an 'anterior leaning' sitting posture greatly increases the muscle activity in the thoracic, lumbar, and pelvis regions and moves the centre of gravity of the upper body forward. A kyphotic sitting posture induces less muscle activity and a slightly different spinal curvature. The increase of muscle activity in the upper body in the 'anterior leaning' sitting posture had no significant effect on the resonance frequency of the vertical apparent mass at the seat. This finding makes it difficult to separate the effect of muscle activity and body geometry on the resonance frequency of the vertical apparent mass at the seat pan in a forward

leaning sitting posture. Greater understanding of the effects of muscle activity and body geometry on the vertical apparent mass at the seat pan is desirable.

It becomes interesting to study the biodynamic response of the human body in a forward leaning sitting posture, as this posture involves greater muscle activity in the back and also changes the body geometry. Some previous studies have varied muscle tension in the upper body with 'upper body tensed' postures (e.g., Fairley and Griffin, 1989; Huang and Griffin, 2006) and concluded that tensing back muscles can increase the principal resonance frequency of the vertical apparent mass at the seat. However, such studies probably also increased tension in other areas of the body, including the pelvis as well as the back (lumbar and thoracic regions), which makes it difficult to identify the relative contribution from muscles in the back (e.g., erector spinae) and the pelvis region (e.g., gluteal muscles).

In the present study, the effect of two kinds of forward leaning sitting posture (i.e., 'anterior leaning' and 'kyphotic leaning' sitting postures) on the biodynamic responses (i.e., apparent mass and body transmissibilities) are investigated. In the 'anterior leaning' sitting posture, 'the spine was straight but leaning 30º forward from the iliac tuberosities'. In the 'kyphotic leaning' sitting posture, 'the spine was kyphotic while leaning 30º forward from the iliac tuberosities. The full instructions for maintaining the two postures are provided in Section 8.2.2. Compared with normal upright sitting, the centre of gravity of the upper body was further forward in both postures, but the spinal curvature differed between the two postures. The tissues in the pelvis region were expected to be compressed to a similar status in both forward leaning postures, due to the similar position of the centre of gravity of the body above the seat. The tension of back muscles (i.e., in the lumbar and thoracic region) tends to be greater in an 'anterior leaning' posture than in a 'kyphotic leaning' posture, because the muscles in the thoracic region are relaxed in the 'kyphotic leaning' sitting posture. By comparing the biodynamic response measured in the 'kyphotic leaning' and 'anterior leaning' sitting postures, how muscle activity in the upper body affects the resonance frequency of the vertical apparent mass at the seat pan could be investigated.

The objective of this study was to investigate the effect of body geometry and muscle activity on the vertical in-line and fore-and-aft cross-axis apparent mass at the seat pan. It was hypothesised that an increase in muscle activity in the upper body (i.e., thoracic region) would increase the resonance frequency of the vertical apparent mass at the seat pan. It was also hypothesised that leaning the upper body forward with 'anterior leaning' or 'kyphotic leaning' sitting postures would increase the fore-and-aft motion of the pelvis and also the fore-and-aft dynamic forces at the seat pan. The vertical, fore-and-aft, and pitch transmissibilities to various spinal levels were measured to help explain how the body moves in both forward leaning postures. The measured data were also required for the development biodynamic models of the response of the seated human body to vertical whole-body vibration and the prediction of spinal forces in forward leaning sitting postures.

8.2 Methods

8.2.1 Apparatus

Vertical vibration was generated by a 1-m stroke vertical vibrator. A rigid seat without backrest was mounted on the platform of the vibrator (Figure 8.1). The horizontal seat pan was 500 mm above the platform of the vibrator. A footrest was provided on the vibrator platform to ensure the top surfaces of the thighs of the subjects were parallel to the seat pan. The lower legs were vertically supported on the footrest. The distance between the inner surface of the calves (close to the edge of the seat pan) and the edge of the seat pan was about 5 cm. The above sitting posture has been referred to as an 'average thigh contact' by Nawayseh and Griffin (2004).

The dynamic forces (in fore-and-aft and vertical directions) at the human-seat interface were measured by a force plate (Kistler 9281 B). The vertical acceleration at the seat pan was measured by accelerometer (Entran EGCSY-240D-10). The fore-and-aft, vertical and pitch motions at skin surface at each of the spine levels iliac crest (pelvis), L5, L3 and T5 were measured with blocks of tri-axial accelerometers (MEMS, KXD94-2802).

The set-up of the force transducers and accelerometers (including locations and mounting) and the acquisition of the signals followed the methods in Chapter 6.

8.2.2 Experimental design

Twelve healthy male subjects with median age 29 years (range 22 to 34 years), median height 173.5 cm (range 160 to 184 cm) and median weight 69 kg (range 60 to 100 kg) participated in the experiment.

During the experiment the subjects sat in the following postures, starting from the 'normal' upright sitting posture followed by either 'kyphotic leaning' (KL) or 'anterior leaning' (AL) sitting postures in a random order.

In the normal upright sitting posture, subjects sat with their upper body in a comfortable upright position. In the 'anterior leaning' sitting posture, subjects sat first with their lumbar spine and pelvis rotated forward and thoracic spine rotated backward (i.e., erect spine), then they were asked to lean their spine forward 30º by rotation about the ischial tuberosities. In the 'kyphotic leaning' sitting posture, the subjects sat first with their pelvis and lumbar spine rotated backward and the thoracic spine rotated forward with their muscles relaxed in the upper body (i.e., kyphotic spine), then they were asked to lean their kyphotic spine forward 30º by rotation about the ischial tuberosities.

In all three conditions, the feet were supported on an adjustable footrest to make the top surfaces of the thighs parallel to the seat pan and the lower legs vertical and supported on the footrest (see Section 8.2.1). The hands rested on the lap, but all the subjects were asked to relax the muscles in the hands and arms so they were not using their hands or arms to support the upper body.

In each posture, the subjects were exposed to 60-s periods of random vertical vibration with approximately flat constant-bandwidth acceleration spectra (0.2 to 20 Hz) at three vibration

magnitudes: 0.5, 1.0, and 1.5 ms^{-2} r.m.s. In each sitting posture the three magnitudes were presented to subjects in random order.

The experiment was approved by the Ethics Committee of the Faculty of Engineering and the Environment at the University of Southampton (approval number 14342).

The experimental set-up and an example of one subject sitting in 'anterior leaning' posture is shown in Figure 8.1.

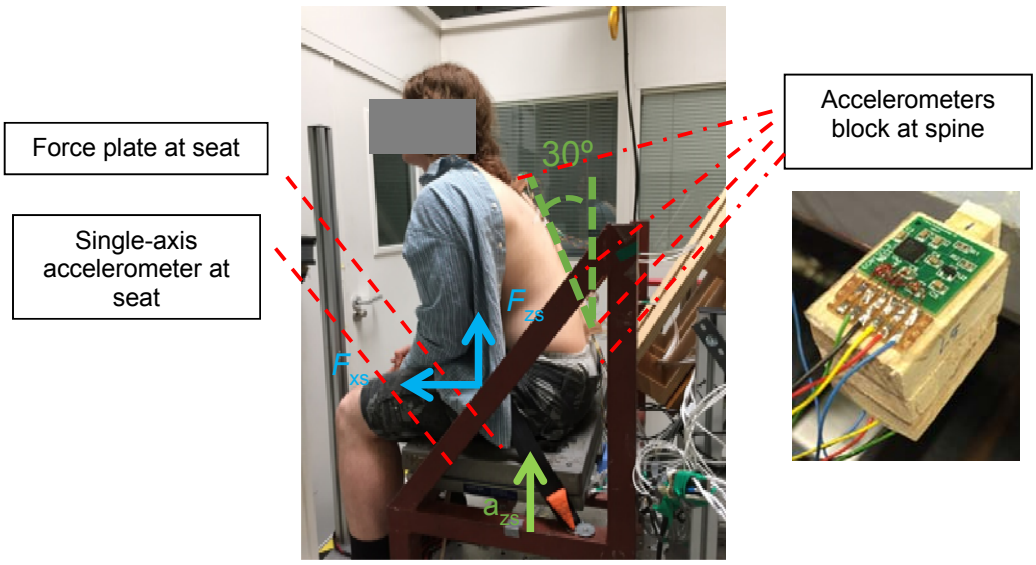

Figure 8.1 Experiment set-up with one subject sitting in 'anterior leaning' posture.

8.2.3 Data analysis

8.2.3.1 Mass cancellation

For the calculation of the forces at the seat, the effect of the mass of the force plates on the measured dynamic forces was eliminated by mass cancellation in the time-domain. The acceleration time-history was multiplied by the mass of the force platform 'above' the force sensors (33 kg) and the resulting force was subtracted from the measured force. Details are provided in Chapter 3.

8.2.3.2 Transfer functions

Following the same procedure shown in Chapter 6, the in-line vertical apparent mass and the fore-and-aft cross-axis apparent mass at the seat pan and the in-line vertical transmissibilities and fore-and-aft cross-axis transmissibilities and pitch transmissibilities to the various spinal levels (i.e., pelvis, L5, L3 and T5) were calculated using the cross spectral density method based on the measured time-history data, together with the coherence functions.

A frequency resolution of 0.25 Hz was used to calculate the transfer functions (60 averages using a Hamming window with an overlap of 75% based on H1 estimation, Chapter 3), including the apparent mass and transmissibilities to the spine. This resolution was sufficient to find the

differences between the resonance frequencies of the apparent mass and transmissibilities to the spine measured with different sitting postures (Sections 8.3.1 and 8.3.3). However, the vertical apparent masses at the seat pan were reanalysed with a resolution of 0.125 Hz to perform statistical analysis of the nonlinearity (i.e., the reduction of resonance frequencies of the vertical apparent mass at the seat pan with increasing vibration magnitude from 0.5 m/s^2 to 1.5 m/s^2; Section 8.3.2).

8.2.3.3 Correction of transmissibility data

The transmissibility to each of the three directions measured at the skin-surface was then corrected by the skin-tissue correction function in the frequency domain in each direction to obtain the estimated transmissibility to the vertebral body at every spinal level (Equation 8.1).

$$T_{vertebral\ \ body}(f) = T_{skin}(f) \times Correction\ \_\ skin(f) \tag{8.1}$$

The skin-tissue correction method was introduced by Kitazaki and Griffin (1995) and it was described in detail in Chapter 6. The natural frequencies and damping ratios of the local skin-tissue system in each of the testing postures were measured directly before the exposure, using the same method as in Chapter 6. The transmissibilities obtained at the vertebral body in the vertical and fore-and-aft directions were further adjusted into the vertical and horizontal directions according to the earth-based coordinates system in the frequency domain. The ratio from the vertical transmissibility at 0.5 Hz to the fore-and-aft transmissibility at 0.5 Hz determined the inclination angle (α) between skin surface and the vertical direction as it was assumed that the body moves rigidly at 0.5 Hz. The vertical and fore-and-aft transmissibilities to the pelvis in the 'anterior leaning' sitting posture before angle correction are shown in Figure B2 in Appendix B. The coherency functions of the vertical and fore-and-aft transmissibilities at around 0.5 Hz show values close to 1.0. The high coherencies indicate the body motions at 0.5 Hz are mainly induced by the vertical acceleration at the seat. The angle (φ) was then used to calculate the corrected vertical and fore-and-aft transmissibility ($T_{ZZ\_a}(f)$, $T_{XZ\_a}(f)$) in the frequency domain:

$$\begin{aligned} T_{zz\_a}(f) &= T_{xz}(f)\sin\varphi + T_{zz}(f)\cos\varphi; \\ T_{xz\_a}(f) &= T_{xz}(f)\cos\varphi - T_{zz}(f)\sin\varphi; \end{aligned} \tag{8.2}$$

Details about the angle correction method can be found in Chapter 6.

8.2.3.4 Statistical analysis

Non-parametric statistical tests (Friedman two-way analysis of variance for *k*-related samples and Wilcoxon matched-pairs signed-ranks test for two-related samples) were used. The Spearman rank order correlation was employed in to investigate associations between variables.

8.3 Results

8.3.1 Apparent mass at the seat pan in normal, 'kyphotic leaning', and 'anterior leaning' postures

8.3.1.1 Vertical in-line apparent mass

The vertical in-line apparent masses of the 12 individual subjects in a normal upright sitting posture exposed to 1.0 m/s^2 r.m.s. vibration showed a principal resonance at around 5 Hz (Figure 8.2). A secondary resonance at around 8-10 Hz was observed for some subjects, consistent with previous studies (e.g., Fairley and Griffin, 1989). As found in studies in Chapter 6, the apparent mass showed large inter-subject variability in the low frequency range 0.5 – 5 Hz, related with the body mass of each subject. Details about the inter-subject variability in the vertical in-line apparent mass measured at the seat pan in three sitting postures when exposed to 0.5 m/s^2, 1.0 m/s^2, and 1.5 m/s^2 r.m.s. vibration are shown in Tables B.1 to B.3 in Appendix B.

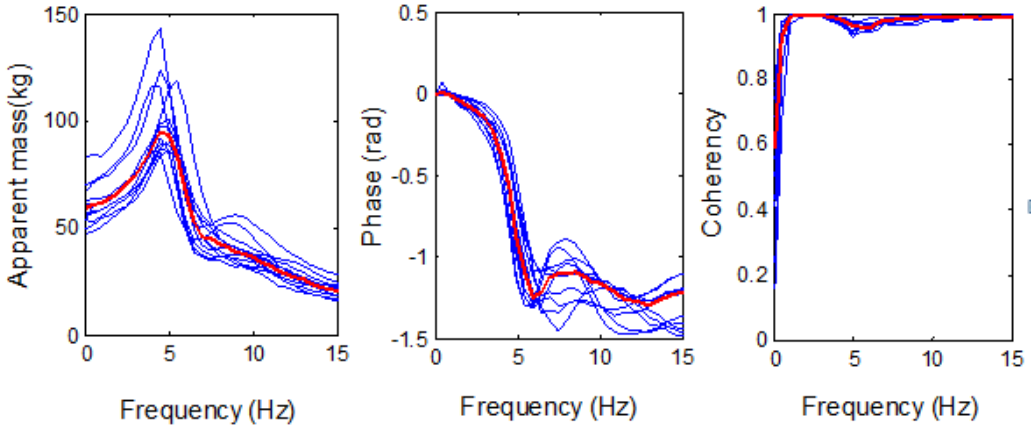

Figure 8.2 Vertical in-line apparent masses at the seat pan in normal upright sitting posture for 12 individual subjects when exposed to 1.0 m/s^2 r.m.s. vibration. Individual subjects: ('—'); median of 12 subjects: ('—'). In one row, from left to right: modulus, phase and coherency.

The vertical in-line apparent masses of the 12 individual subjects in a 'kyphotic leaning' sitting posture exposed to 1.0 m/s^2 r.m.s. vibration showed a principal resonance at around 5 Hz, close to that in the normal upright sitting posture. The majority subjects (10 of 12) also showed another resonance at a lower frequency around 2.5 Hz with a smaller magnitude (Figure 8.3).

The median vertical apparent masses of the 12 subjects in the 'normal upright', 'kyphotic leaning' and 'anterior leaning' sitting postures when exposed to 1.0 m/s^2 r.m.s. vibration are compared in Figure 8.5.

The vertical in-line apparent masses of the 12 individual subjects in an 'anterior leaning' sitting posture exposed to 1.0 m/s^2 r.m.s. vibration also showed a principal resonance at around 5 Hz, close to those in the above two sitting postures. Similar to sitting in a 'kyphotic leaning' posture, the majority of the subjects (11 of 12) also showed a resonance at a lower frequency (2.5 Hz) (shown in Figure 8.4).

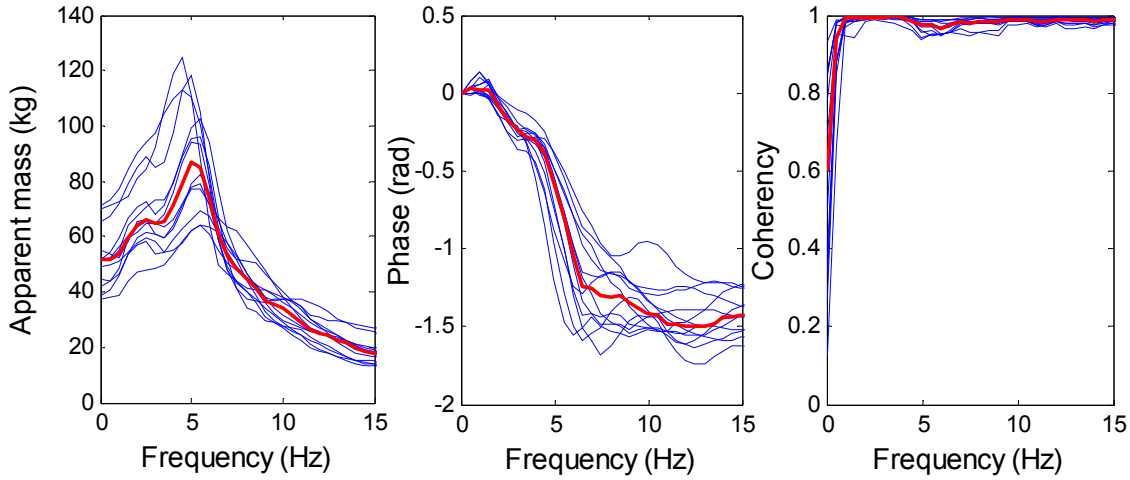

Figure 8.3 Vertical in-line apparent masses at the seat pan in a 'kyphotic leaning' sitting posture for 12 individual subjects when exposed to 1.0 m/s^2 r.m.s. vibration. Individual subjects: ('—'); median of 12 subjects: ('—'). In one row, from left to right: modulus, phase and coherency.

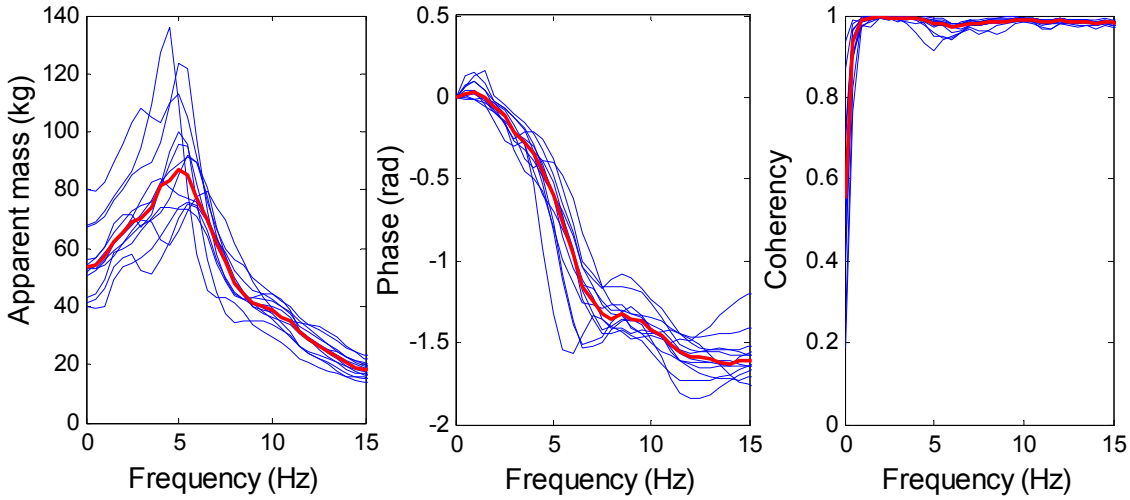

Figure 8.4 Vertical in-line apparent masses at the seat pan in an 'anterior leaning' sitting posture for 12 individual subjects when exposed to 1.0 m/s^2 r.m.s. vibration. Individual subjects: ('—'); median of 12 subjects: ('—'). In one row, from left to right: modulus, phase and coherency.

With the upper body leaning forward with either a kyphotic spine (i.e., 'kyphotic leaning') or an erect spine (i.e., 'anterior leaning'), the principal resonance frequency of the vertical apparent mass at the seat increased significantly (normal posture compared with 'kyphotic leaning' posture, p=0.039, Wilcoxon, Table 8.1; normal posture compared with 'anterior leaning' posture, p=0.002, Wilcoxon, Table 8.1). The median resonance frequency of the vertical apparent mass at the seat pan increased from 4.75 Hz in the normal sitting posture to 5.25 Hz in the 'kyphotic leaning' posture, and to 5.625 Hz in the 'anterior leaning' sitting posture. The apparent mass at the resonance frequency decreased from the normal sitting posture to the 'kyphotic leaning' sitting posture (p=0.012, Wilcoxon). However, the apparent mass at the resonance frequency in the 'anterior leaning' sitting posture showed no significant difference compared to that in the normal upright

sitting posture (p=0.176, Wilcoxon).The 'anterior leaning' posture significantly increased the resonance frequency of the vertical apparent mass at the seat pan compared to the 'kyphotic leaning' sitting posture (p=0.023, Wilcoxon, Table 8.1), and there was a corresponding increase in the apparent mass at the resonance (p=0.077, Wilcoxon, Table 8.1).

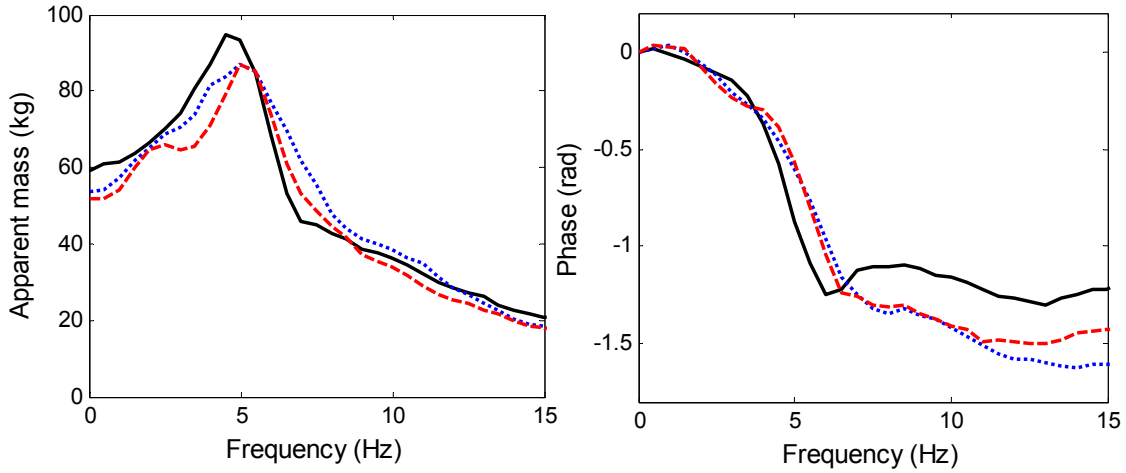

Figure 8.5 Vertical in-line apparent mass at the seat pan in different sitting postures when exposed to 1.0 m/s^2 r.m.s. vibration: normal upright sitting posture, normal ('——'); 'kyphotic leaning' posture, KL ('------'); 'anterior leaning' posture, AL ('.....'); Left: modulus; right: phase. Median values from 12 subjects.

When exposed to 0.5 m/s^2 r.m.s. vibration or 1.5 m/s^2 r.m.s. vibration over the same frequency range (0.2 - 20 Hz), the median vertical in-line apparent mass at the seat pan measured in the three sitting postures (normal upright, 'kyphotic leaning' and 'anterior leaning') are shown in Figures 8.6 and 8.7, respectively. Similar to the findings with 1.0 ms^{-2} r.m.s., a resonance was observed at a frequency (2.5 Hz) lower than the principal resonance frequency with in both 'kyphotic leaning' and 'anterior leaning' sitting postures with the majority subjects. With the higher vibration magnitude (i.e., 1.5 m/s^2 r.m.s.), the number of subjects showing a resonance at the lower frequency tended to decrease (i.e., at 0.5 m/s^2 r.m.s., 12 of 12 subjects; at 1.5 m/s^2 r.m.s., 10 of 12 subjects).

Table 8.1 Statistical significance of the effects of forward leaning sitting postures on the resonance frequency in the vertical apparent mass at the seat pan and the modulus of the apparent mass at resonance measured with 1.0 m/s^2 r.m.s. vibration. Wilcoxon matched-pairs signed ranks test.

Resonance frequency of vertical apparent mass at the seat pan			
	Normal	KL	AL
Normal	-	* ↑ (KL)	** ↑ (AL)
KL		-	* ↑ (AL)
AL			-

Vertical apparent mass at the seat pan at the resonance frequency			
	Normal	KL	AL
Normal	-	* ↓ (KL)	ns
KL		-	ns
AL			-

ns: not significant; * p≤0.05; ** p≤0.01. The arrow indicates increase or decrease of the variables in the brackets compared to the variable in the same row. Details of the statistics (i.e., p-value) are show in Appendix B.

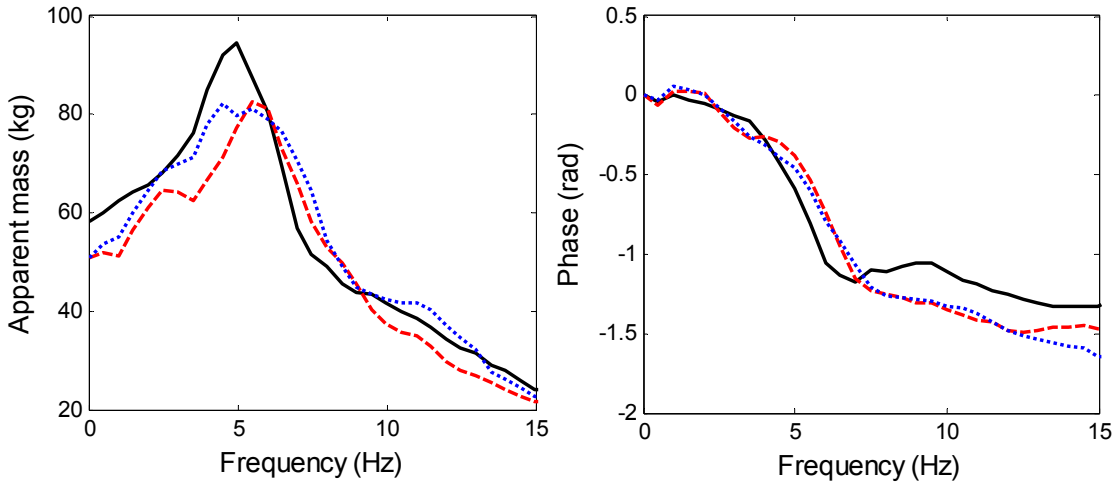

Figure 8.6 Vertical in-line apparent mass at the seat pan in different sitting postures when exposed to 0.5 m/s^2 r.m.s. vibration: normal upright sitting posture, normal ('——'); 'kyphotic leaning' posture, KL ('------'); 'anterior leaning' posture, AL ('……'); Left: modulus; right: phase. Median values from 12 subjects.

Table 8.2 Statistical significance of the effects of forward leaning postures on the resonance frequency in the vertical apparent mass at the seat pan and the modulus of the apparent mass at resonance measured with 0.5 m/s^2 r.m.s. vibration. Wilcoxon matched-pairs signed ranks test.

Resonance frequency of vertical apparent mass at the seat pan			
	Normal	KL	AL
Normal	-	** ↑(KL)	** ↑(AL)
KL		-	ns
AL			-

Vertical apparent mass at the seat pan at the resonance frequency			
	Normal	KL	AL
Normal	-	* ↓(KL)	* ↓(AL)
KL		-	ns
AL			-

ns: not significant; * $p \leq 0.05$; ** $p \leq 0.01$. The arrow indicates increase or decrease of the variables in the brackets compared to the variable in the left column of the same row. Details of the statistics (i.e., p-value) are show in Appendix B.

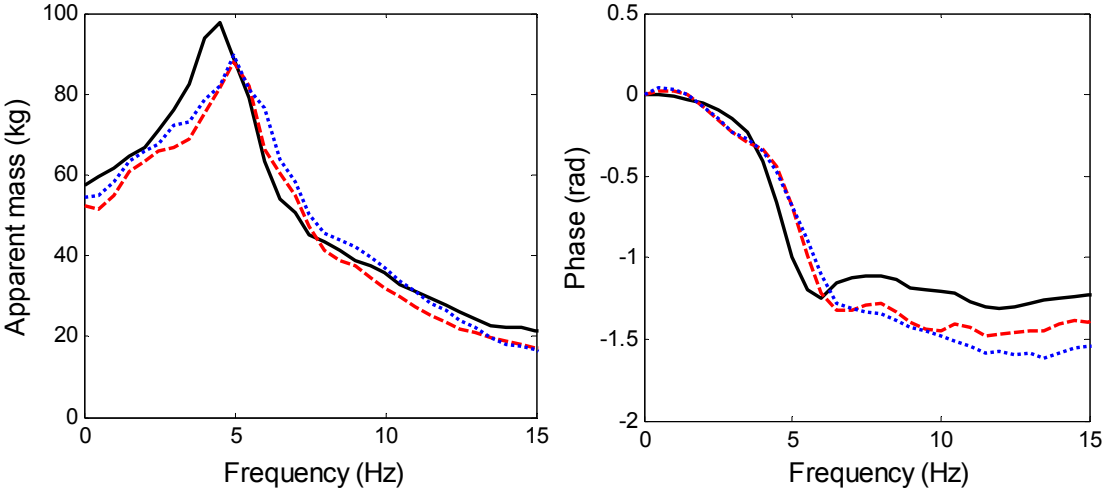

Figure 8.7 Vertical in-line apparent mass at the seat pan in different sitting postures when exposed to 1.5 m/s^2 r.m.s. vibration: normal upright sitting posture, normal ('——'); 'kyphotic leaning' posture, KL ('------'); 'anterior leaning' posture, AL ('……'); Left: modulus; right: phase. Median values from 12 subjects.

Table 8.3 Statistical significance of the effects of forward leaning sitting postures on the resonance frequency in the vertical apparent mass at the seat pan and the modulus of the apparent mass at resonance measured with 1.5 m/s^2 r.m.s. vibration. Wilcoxon matched-pairs signed ranks test.

Resonance frequency of vertical apparent mass at the seat pan			
	Normal	KL	AL
Normal	-	** ↑ (KL)	** ↑ (AL)
KL		-	ns
AL			-

Vertical apparent mass at the seat pan at the resonance frequency			
	Normal	KL	AL
Normal	-	**↓ (KL)	* ↓ (AL)
KL		-	ns
AL			-

ns: not significant; * $p \leq 0.05$; ** $p \leq 0.01$. The arrow indicates increase or decrease of the variables in the brackets compared to the variable in the left column of the same row. Details of the statistics (i.e., *p*-value) are show in Appendix B.

Similar to the situation with 1.0 m/s^2 r.m.s., both forward leaning postures (i.e., KL and AL) caused significantly decreases of the apparent mass at the resonance frequency with both 0.5 and 1.5 m/s^2 r.m.s. vibration magnitudes (p=0.021 and 0.027, Wilcoxon, Table 8.2). In both cases, the resonance frequency of the vertical apparent mass at the seat significantly increased from that with a normal upright sitting posture to either the 'kyphotic leaning' sitting posture (0.5 m/s^2 r.m.s.: p=0.003, Wilcoxon, Table 8.2; 1.5 m/s^2 r.m.s.: p=0.002, Wilcoxon, Table 8.3) or the 'anterior leaning' sitting posture (0.5 m/s^2 r.m.s.: p=0.003, Wilcoxon, Table 8.2; 1.5 m/s^2 r.m.s.: p=0.008, Wilcoxon, Table 8.3).

When exposed to 0.5 m/s^2 r.m.s. vibration, the resonance frequency showed no significant difference between the 'kyphotic leaning' and the 'anterior leaning' sitting postures (p=0.676, Wilcoxon, Table 8.2), although the median data showed an increase from 5.75 Hz to 6.125 Hz. When exposed to 1.5 m/s^2 r.m.s. vibration, the resonance frequency also showed no significant difference between the 'kyphotic leaning' and the 'anterior leaning' sitting postures (p=0.469, Wilcoxon, Table 8.3), as both resonance occurred at 5.25 Hz in the median apparent mass. There was no significant difference between the apparent masses at the resonance frequency in the 'kyphotic leaning' and the 'anterior leaning' sitting postures when exposed to either 0.5 m/s^2 r.m.s. (p=0.791, Wilcoxon, Table 8.2) or 1.0 m/s^2 r.m.s. vibration (p=0.380, Wilcoxon, Table 8.3).

8.3.1.2 Fore-and-aft cross-axis apparent mass

The fore-and-aft cross-axis apparent masses of the individual subjects in 'normal', 'kyphotic leaning', and 'anterior leaning' sitting postures when exposed to 1.0 m/s^2 r.m.s. vibration are shown in Figures 8.8, 8.9 and 8.10, respectively. The resonance frequency in the fore-and-aft cross-axis apparent mass in the normal upright sitting posture occurred at around 5 Hz, similar to the resonance frequency in the vertical apparent mass at the seat (Figure 8.2). While in the 'kyphotic leaning' sitting posture, the fore-and-aft apparent masses of most subjects showed a principal resonance at around 4 Hz, lower than the corresponding resonance frequency in vertical apparent mass in the same posture (Figure 8.3 and 8.9). Some subjects showed a principal resonance at frequencies greater than 5 Hz (Figure 8.9). The fore-and-aft apparent mass in the 'anterior leaning' sitting posture showed large inter-subject variability, the principal resonance frequency occurred at 4 - 7 Hz (Figure 8.10). Apart from the resonance at around 5 Hz, the fore-and-aft apparent mass showed resonances at lower frequencies in both forward leaning sitting postures ('AL' and 'KL'),

one at around 1.5 Hz and another at around 3 Hz. The peak at around 1.5 Hz was also seen in subjects sitting in the normal upright posture. Details about the inter-subject variability in the fore-and-aft cross-axis apparent mass measured at the seat pan in three sitting postures when exposed to 0.5 m/s^2, 1.0 m/s^2, and 1.5 m/s^2 r.m.s. vibration are shown in Tables B.4 to B.6 in Appendix B.

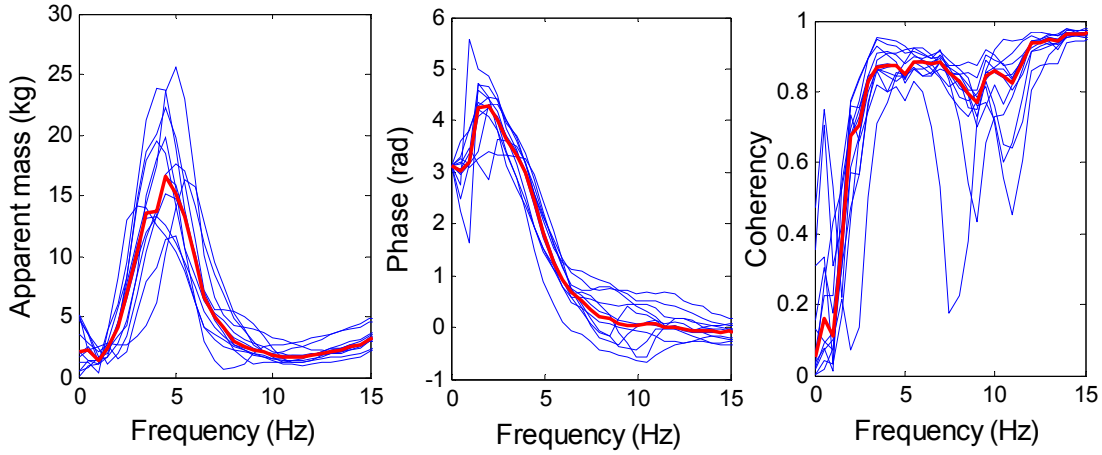

Figure 8.8 Fore-and-aft cross-axis apparent masses at the seat pan in the normal upright sitting posture for 12 individual subjects when exposed to 1.0 m/s^2 r.m.s. vibration. Individual subjects: ('—'); Median of 12 subjects: ('—'). In one row, from left to right: modulus, phase and coherency.

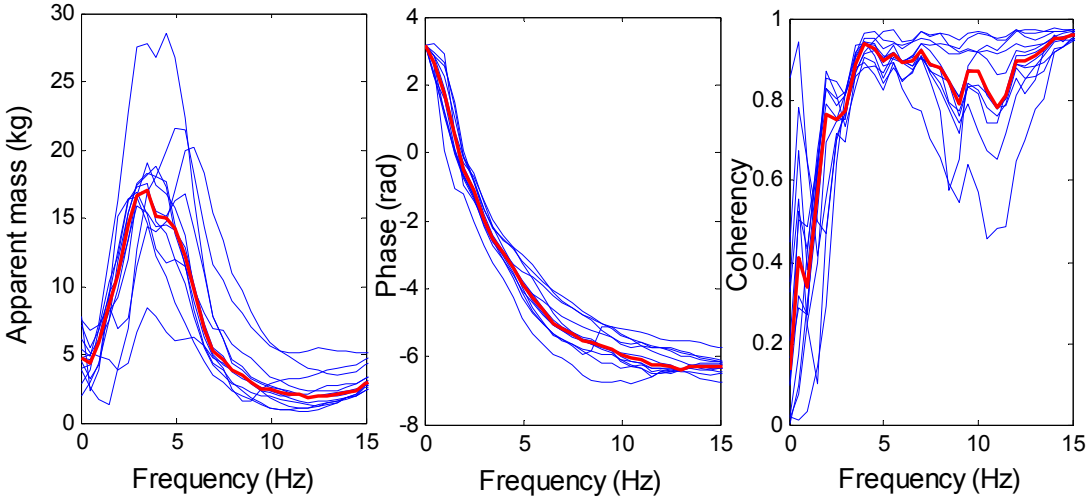

Figure 8.9 Fore-and-aft cross-axis apparent masses at the seat pan in the 'kyphotic leaning' sitting posture for 12 individual subjects when exposed to 1.0 m/s^2 r.m.s. vibration. Individual subjects: ('—'); Median of 12 subjects: ('—'). In one row, from left to right: modulus, phase and coherency.

The median fore-and-aft cross-axis apparent mass at the seat pan for the 12 subjects in three sitting postures (i.e., normal, KL and AL) when exposed to 1.0 m/s^2 r.m.s. vibration are shown in Figure 8.11. In the 'kyphotic leaning' sitting posture, the principal resonance frequency (defined as the frequency of the peak with greatest magnitude) in the fore-and-aft cross-axis apparent mass tended to decrease compared with the normal sitting posture, although the decrease was not statistically significant (p=0.065, Wilcoxon). The same conditions apply to the 'anterior leaning' sitting posture and the normal upright sitting posture (p=0.328, Wilcoxon). There was also no

significant difference between the resonance frequency in the 'kyphotic leaning' and the 'anterior leaning' sitting postures (p=0.345, Wilcoxon, Table 8.4).

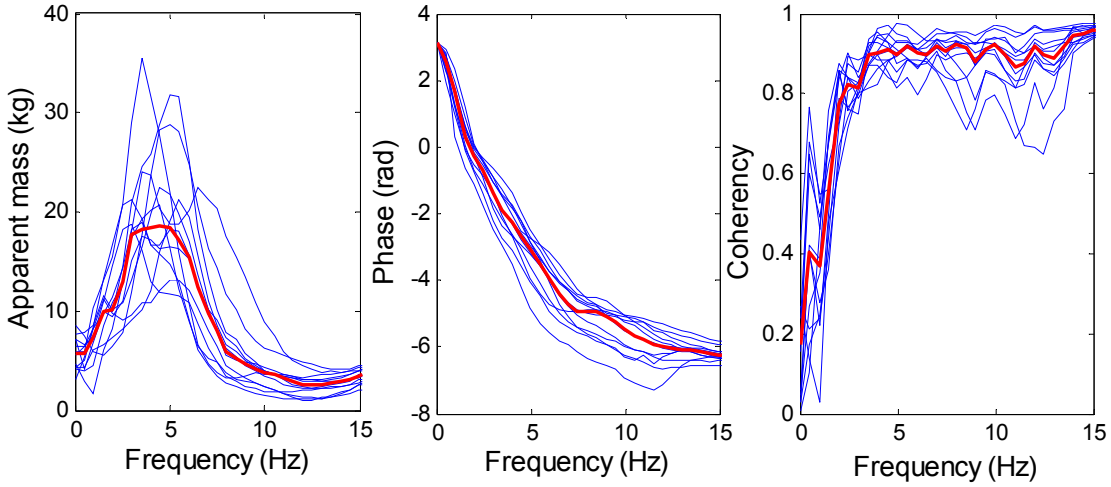

Figure 8.10 Fore-and-aft cross-axis apparent masses at the seat pan in the 'anterior leaning' sitting posture for 12 individual subjects when exposed to 1.0 m/s^2 r.m.s. vibration. Individual subjects: ('—'); Median of 12 subjects: ('—'). In one row, from left to right: modulus, phase and coherency.

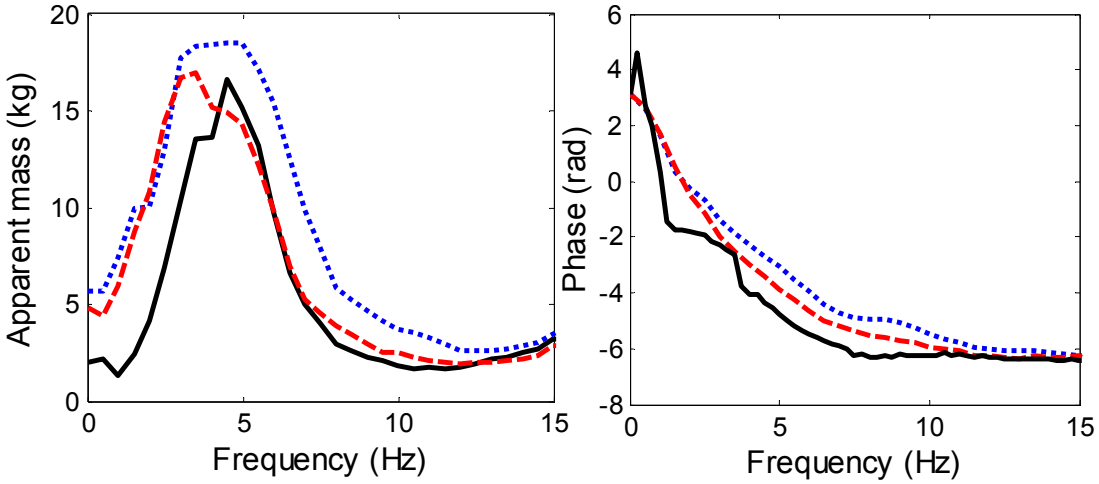

Figure 8.11 Fore-and-aft cross-axis apparent mass at the seat pan in different sitting postures when exposed to 1.0 m/s^2 r.m.s. vibration: normal upright sitting posture, normal ('——'); 'kyphotic leaning' posture, KL ('------'); 'anterior leaning' posture, AL ('.....'); Left: modulus; right: phase. Median values from 12 subjects.

The fore-and-aft cross-axis apparent mass at the principal resonance frequency showed no significant difference from the normal to the 'kyphotic leaning' sitting postures (p=0.470, Wilcoxon, Table 8.4). The fore-and-aft cross-axis apparent mass in the 'anterior leaning' sitting posture increased significantly (p=0.007, Wilcoxon, Table 8.4) compared with normal upright sitting posture. The 'anterior leaning' sitting posture also induced greater fore-and-aft apparent mass at the principal resonance than the 'kyphotic leaning' sitting posture (p=0.001, Wilcoxon, Table 8.4).

When exposed to 0.5 m/s^2 r.m.s. and 1.0 m/s^2 r.m.s. vibration, the fore-and-aft cross-axis apparent mass at the seat showed similar trends as with 1.0 m/s^2 r.m.s. vibration regarding the effect of forward leaning postures (Figures 8.12 and 8.13). The resonance frequency in the fore-and-aft apparent mass decreased significantly from the 'normal' sitting posture to the 'kyphotic leaning'

sitting posture (p=0.027, Wilcoxon, Table 8.5) with 0.5 m/s^2 r.m.s. vibration, and tended to decrease with 1.5 m/s^2 r.m.s. vibration (p=0.070, Wilcoxon, Table 8.6). The fore-and-aft cross-axis apparent mass at the resonance increased significantly from the normal sitting posture to the 'anterior leaning' sitting posture (0.5 m/s^2 r.m.s.: p=0.009, Wilcoxon; 1.5 m/s^2 r.m.s.: p=0.021, Wilcoxon). More detailed statistical analysis of the effects of the forward leaning sitting postures with 0.5 and 1.0 m/s^2 r.m.s. vibration can be found in Tables 8.5 and 8.6, respectively.

Table 8.4 Statistical significance of the effects of forward leaning sitting postures on the principal resonance frequency of the fore-and-aft cross-axis apparent mass at the seat pan and the modulus of the apparent mass at principal resonance measured with 1.0 m/s^2 r.m.s. Wilcoxon matched-pairs signed ranks test.

Principal resonance frequency of fore-and-aft cross-axis apparent mass at the seat pan			
	Normal	KL	AL
Normal	-	ns	ns
KL		-	ns
AL			-

Fore-and-aft cross-axis apparent mass at the seat pan at the principal resonance frequency			
	Normal	KL	AL
Normal	-	ns	** ↑ (AL)
KL		-	** ↑ (AL)
AL			-

ns: not significant; * p≤0.05; ** p≤0.01. The arrow indicates increase or decrease of the variables in the brackets compared to the variable in the left column of the same row. Details of the statistics (i.e., p-value) are show in Appendix B.

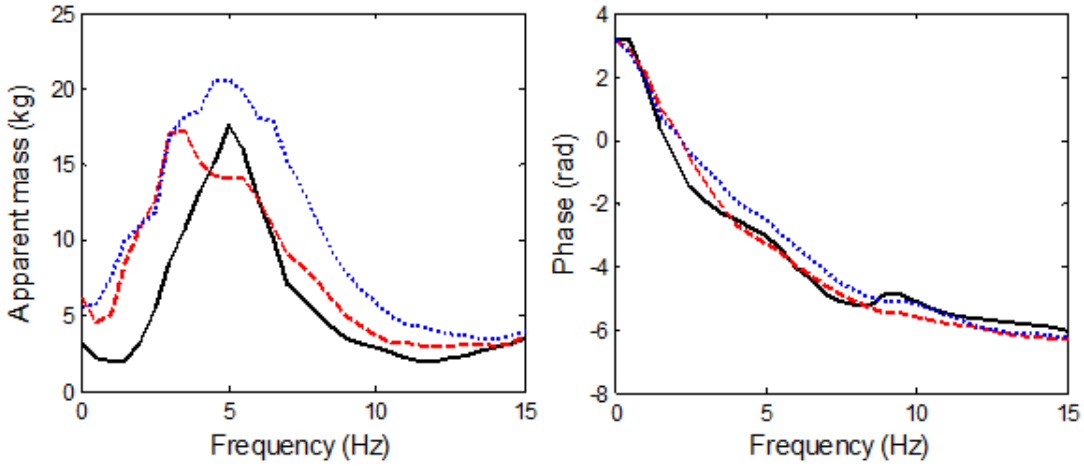

Figure 8.12 Fore-and-aft cross-axis apparent mass at the seat pan in different sitting postures when exposed to 0.5 m/s^2 r.m.s. vibration: normal upright sitting posture, normal ('——'); 'kyphotic leaning' posture, KL ('------'); 'anterior leaning' posture, AL ('.....'); Left: modulus; right: phase. Median values from 12 subjects.

Table 8.5 Statistical significance of the effects of forward leaning sitting postures on the principal resonance frequency in the fore-and-aft cross-axis apparent mass at the seat pan and the modulus of the apparent mass at principal resonance measured with 0.5 m/s^2 r.m.s. Wilcoxon matched-pairs signed ranks test.

Principal resonance frequency of fore-and-aft cross-axis apparent mass at the seat pan			
	Normal	KL	AL
Normal	-	*↓(KL)	ns
KL		-	ns
AL			-

Fore-and-aft cross-axis apparent mass at the seat pan at the principal resonance frequency			
	Normal	KL	AL
Normal	-	ns	** ↑ (AL)
KL		-	** ↑(AL)
AL			-

ns: not significant; * $p \leq 0.05$; ** $p \leq 0.01$. The arrow indicates increase or decrease of the variables in the brackets compared to the variable in the left column of the same row. Details of the statistics (i.e., *p*-value) are show in Appendix B.

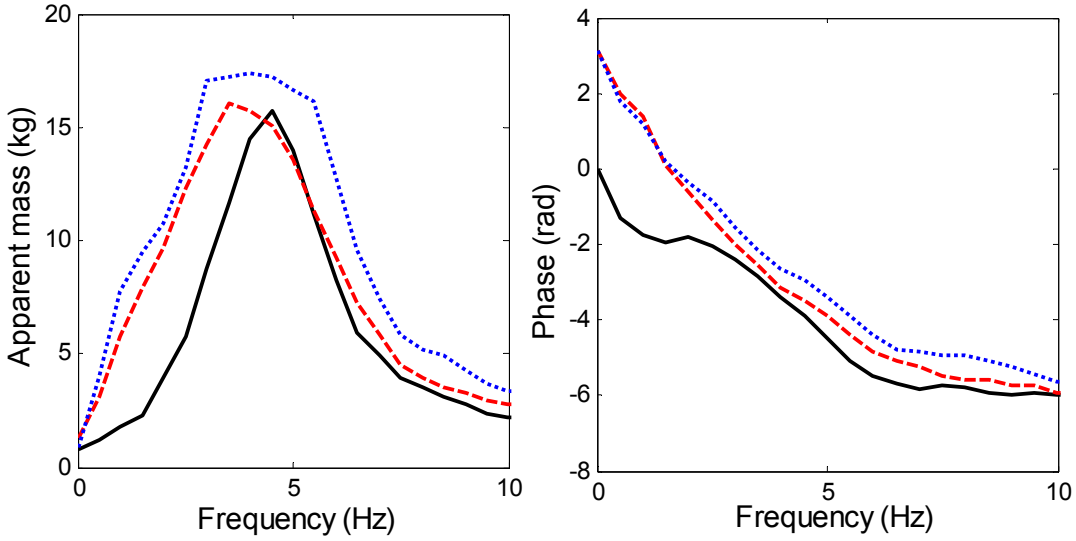

Figure 8.13 Fore-and-aft cross-axis apparent mass at the seat pan in different sitting postures when exposed to 1.5 m/s^2 r.m.s. vibration: normal upright sitting posture, normal ('——'); 'kyphotic leaning' posture, KL ('------'); 'anterior leaning' posture, AL ('.....'); Left: modulus; right: phase. Median values from 12 subjects.

Table 8.6 Statistical significance of the effects of forward leaning sitting postures on the principal resonance frequency in the fore-and-aft cross-axis apparent mass at the seat pan and the modulus of the apparent mass at principal resonance measured with 1.5 m/s^2 r.m.s. Wilcoxon matched-pairs signed ranks test.

Principal resonance frequency of fore-and-aft cross-axis apparent mass at the seat pan			
	Normal	KL	AL
Normal	-	ns	ns
KL		-	ns
AL			-

Fore-and-aft cross-axis apparent mass at the seat pan at the principal resonance frequency			
	Normal	KL	AL
Normal	-	ns	* ↑ (AL)
KL		-	** ↑ (AL)
AL			-

ns: not significant; * $p \leq 0.05$; ** $p \leq 0.01$. The arrow indicates increase or decrease of the variables in the brackets compared to the variable in the left column of the same row. Details of the statistics (i.e., *p*-value) are show in Appendix B.

8.3.2 Effect of forward leaning sitting postures on the nonlinearity in the vertical in-line apparent mass

The effects of vibration magnitude (i.e., 0.5, 1.0 and 1.5 m/s^2 r.m.s.) on the apparent mass in different sitting postures are shown in figures below (i.e., Figure 8.14: normal; Figure 8.15: 'kyphotic leaning'; Figure 8.16: 'anterior leaning').

The principal resonance frequencies in the vertical apparent mass at the seat pan decreased from low magnitude excitation (0.5 m/s^2 r.m.s.) to high magnitude excitation (1.5 m/s^2 r.m.s.) in all three sitting postures (median of 12 subjects, Table 8.7). For the median apparent mass, the 'anterior leaning' sitting posture showed the greatest decrease in the principal resonance frequency (i.e., 0.875 Hz) from 0.5 m/s^2 r.m.s. vibration to 1.0 m/s^2 r.m.s. vibration, compared to 0.5 Hz decrease in both 'normal' and 'kyphotic leaning' sitting postures. The corresponding apparent mass at the principal resonance showed a slight increase with increasing vibration magnitudes. The nonlinear behaviour of seated human body observed in all three sitting postures was consistent with previous studies (e.g., Mansfield and Griffin, 2002).

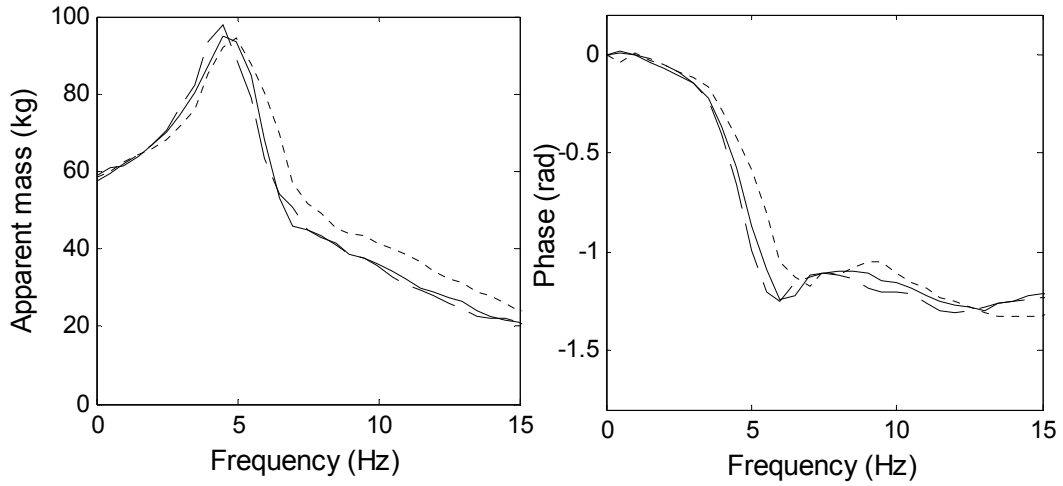

Figure 8.14 Effect of vibration magnitude on the vertical in-line apparent mass at the seat pan in the normal upright sitting posture: 0.5 m/s^2 r.m.s. ('**……**'); 1.0 m/s^2 r.m.s. ('**——**'); 1.5 m/s^2 r.m.s. ('**- - - - -**'); Left: modulus; right: phase. Median values from 12 subjects.

Table 8.7 Effect of vibration magnitude (0.5, 1.0 and 1.5 m/s^2 r.m.s.) on the principal resonance frequencies of vertical apparent mass at the seat in normal, 'kyphotic leaning' (KL) and 'anterior leaning' (AL) sitting postures. Medians of 12 subjects.

Median principal resonance of vertical apparent mass at the seat (Hz) of 12 subjects.			
	Normal	KL	AL
0.5 m/s^2	5	5.750	6.125
1.0 m/s^2	4.750	5.250	5.625
1.5 m/s^2	4.500	5.250	5.250

Median vertical apparent mass at the seat at the principal resonance (kg) of 12 subjects.			
	Normal	KL	AL
0.5 m/s^2	97.330	86.270	89.180
1.0 m/s^2	97.525	91.135	94.155
1.5 m/s^2	102.450	92.930	95.420

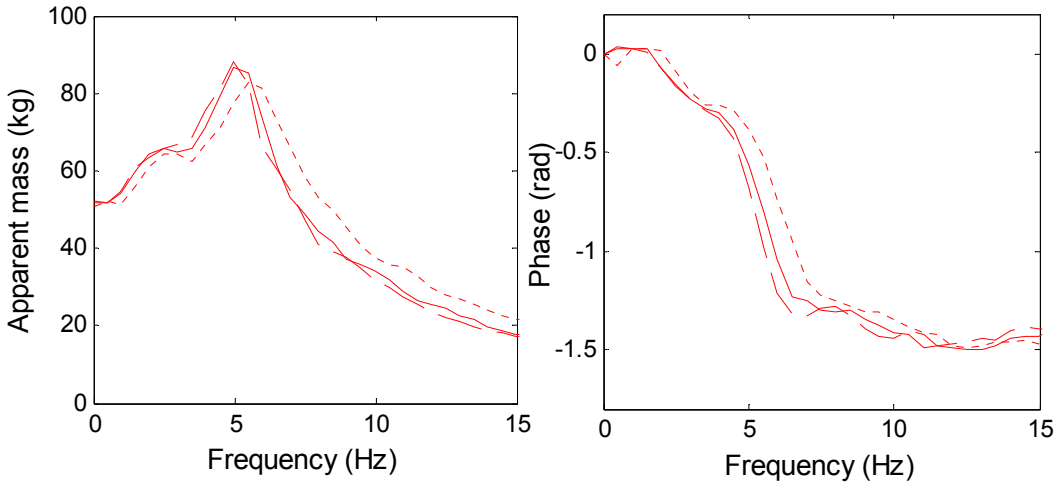

Figure 8.15 Effect of vibration magnitude on the vertical in-line apparent mass at the seat pan in the 'kyphotic leaning' sitting posture: 0.5 m/s^2 r.m.s. ('……'); 1.0 m/s^2 r.m.s. ('——'); 1.5 m/s^2 r.m.s. ('------'); Left: modulus; right: phase. Median values from 12 subjects.

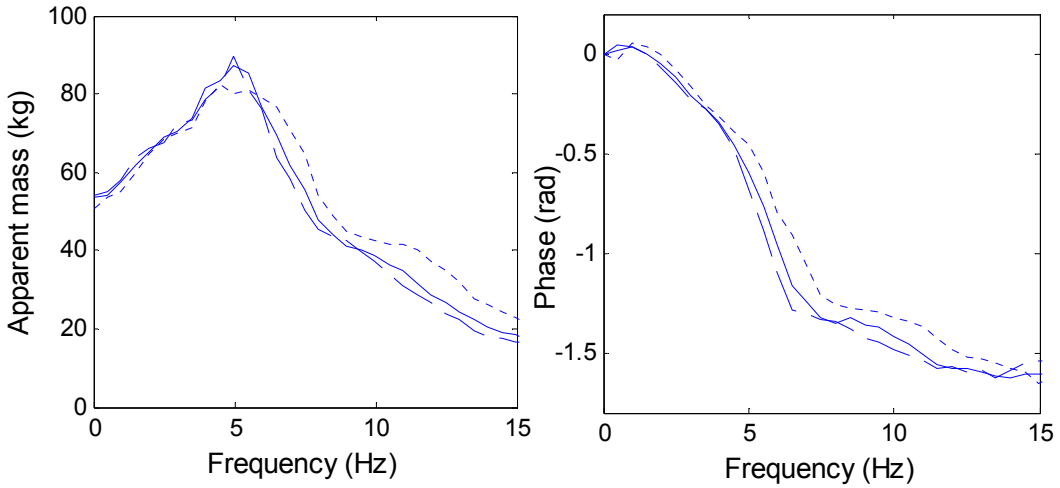

Figure 8.16 Effect of vibration magnitudes on the vertical in-line apparent mass at the seat pan in the 'anterior leaning' sitting posture: 0.5 m/s^2 r.m.s. ('……'); 1.0 m/s^2 r.m.s. ('——'); 1.5 m/s^2 r.m.s. ('------'); Left: modulus; right: phase. Median values from 12 subjects.

Between the principal resonance frequencies of the vertical apparent masses of individual subjects in all three sitting postures there was a significant decrease from 0.5 m/s^2 r.m.s. to 1.0 m/s^2 r.m.s. (p<0.05, Wilcoxon, Table 8.8). However, a significant decrease in resonance frequency from 1.0 m/s^2 r.m.s. to 1.5 m/s^2 r.m.s. was only found in the 'anterior leaning' sitting posture (p<0.001, Wilcoxon, Table 8.8).

The peak at the lower frequency (about 2.5 Hz) in the vertical apparent mass at the seat pan also showed a decreasing trend with increasing vibration magnitude in the 'kyphotic leaning' and the 'anterior leaning' sitting postures, but the change was less distinct than the change in the frequency of the principal resonance. Table 8.9 shows the number of subjects showing a peak at the lower frequency measured with all three vibration magnitudes and the statistical test of the effect of vibration magnitude on the frequency of the peak in the 'kyphotic leaning' and the 'anterior leaning'

sitting postures. In the 'kyphotic leaning' sitting posture, the frequency of the peak at the lower frequency showed no significant difference with increasing vibration magnitude (p=0.319, Friedman). In the 'anterior leaning' sitting posture, the frequency of the peak at the lower frequency decreased significantly with increasing vibration magnitude (p<0.001, Friedman). More detailed statistical results can be found in Table 8.9.

Table 8.8 Statistical significance of the changes in the principal resonance frequencies with three vibration magnitudes in each of the three sitting postures: 'normal', 'kyphotic leaning' (KL) and 'anterior leaning' (AL). Top: Friedman two-way analysis of variance for k-related samples. Bottom: Wilcoxon matched-pairs signed ranks test.

Friedman test of principal resonance frequencies at three vibration magnitudes: 0.5, 1.0 and 1.5 m/s^2 r.m.s.			
Postures	Normal	KL	AL
p	**	**	**

Wilcoxon test of principal resonance frequency of vertical apparent mass at the seat at three vibration magnitudes: 0.5, 1.0 and 1.5 m/s^2 r.m.s.												
Normal					KL					AL		
	0.5	1	1.5			0.5	1	1.5			0.5	1	1.5
0.5	-	*↓(1)	**↓(1.5)		0.5	-	**↓(1)	**↓(1.5)		0.5	-	**↓(1)	**↓(1.5)
1		-	ns		1		-	ns		1		-	**↓(1.5)
1.5			-		1.5			-		1.5			-

ns: not significant; * p≤0.05; ** p≤0.01. The arrow indicates increase or decrease of the variables in the brackets compared to the variable in the left column the same row. Details of the statistics (i.e., p-value) are show in Appendix B.

Table 8.9 Statistical significance of the changes in the frequencies of the peak occurring at a lower frequency with three vibration magnitudes in the 'kyphotic leaning' (KL) and the 'anterior leaning' (AL) sitting postures. Wilcoxon matched-pairs signed ranks test.

Friedman test of frequency of fist peak in three vibration magnitudes: 0.5, 1.0 and 1.5 m/s^2 r.m.s.		
Postures	KL	AL
p	ns	**
Number of subjects showing the first peak	7	9

Wilcoxon test of principal resonance frequency of vertical apparent mass at the seat in three vibration magnitudes: 0.5, 1.0 and 1.5 m/s^2 r.m.s. in 'anterior leaning' sitting posture			
	0.5	1	1.5
0.5	-	**↓(1)	**↓(1.5)
1		-	*↓(1.5)
1.5			-

ns: not significant; * p≤0.05; ** p≤0.01. The arrow indicates increase or decrease of the variables in the brackets compared to the variable in the left column of the same row. Details of the statistics (i.e., p-value) are show in Appendix B.

8.3.3 Transmissibility to the spine

The vertical, fore-and-aft, and pitch transmissibilities to the pelvis, lumbar spine, and thoracic spine were measured together with the apparent mass. In this section, only the transmissibilities measured with 1.0 m/s^2 are presented with the aim of understanding the body motion in the forward leaning sitting postures.

8.3.3.1 Vertical in-line transmissibility to the spine

The median vertical transmissibilities to various spinal levels (i.e., pelvis, L5, L3 and T5) of 12 subjects are shown in Figure 8.17.

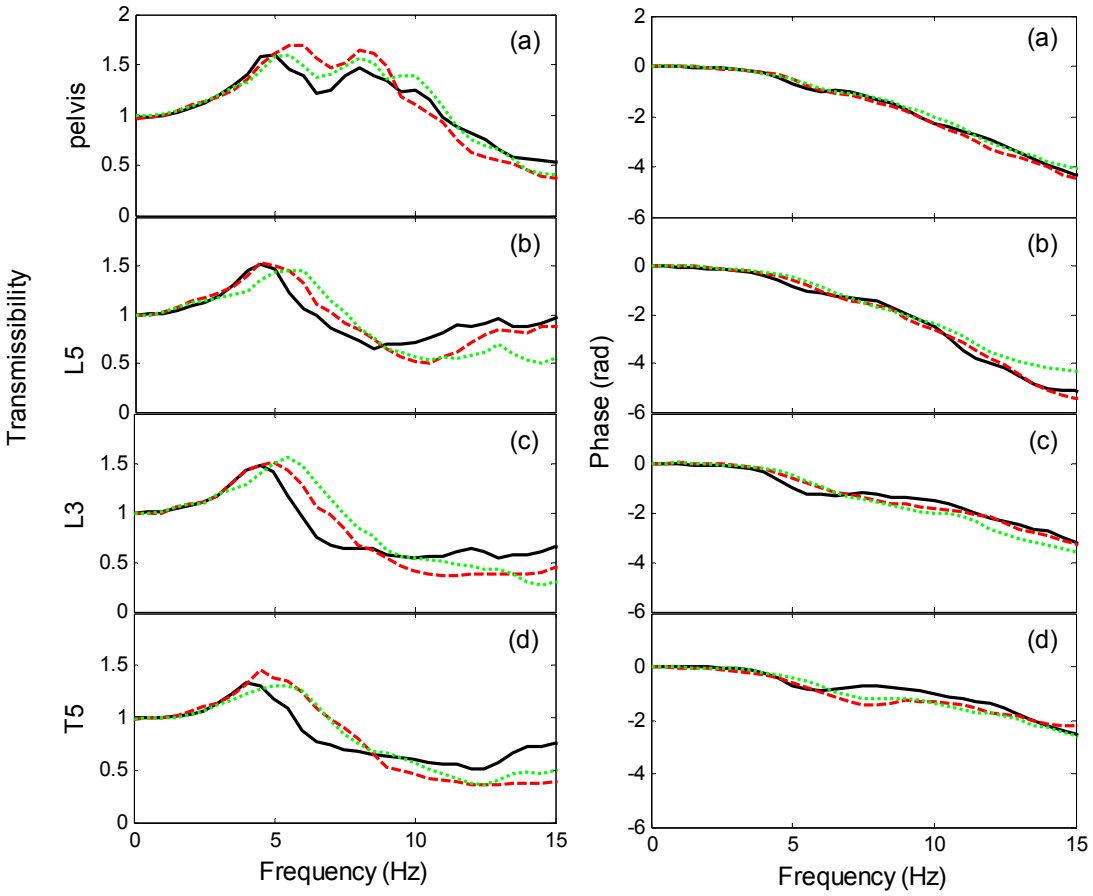

Figure 8.17 Median transmissibilities from seat acceleration to vertical acceleration of the spine for subjects sitting in three different postures: '—', normal; '- -', 'kyphotic leaning'; '…', 'anterior leaning'. Medians of 12 subjects.

The resonance frequency of the vertical transmissibility to pelvis and the transmissibility at the resonance frequency increased in the 'kyphotic leaning' sitting posture compared to the normal sitting posture (p<0.05, Wilcoxon, Table 8.10). The resonance frequency of the vertical transmissibility to the pelvis in the 'anterior leaning' sitting posture was significantly lower than in the 'kyphotic leaning' posture (p=0.039, Wilcoxon). The resonance frequency of the vertical

transmissibility to the lumbar spine (L5 and L3) increased significantly from the normal sitting posture to the 'kyphotic leaning' sitting posture, then to the 'anterior leaning' sitting posture (p<0.05, Wilcoxon, Table 8.10). The vertical transmissibility to both L5 and L3 at the resonance frequency increased in the 'anterior leaning' sitting posture (p<0.05, Wilcoxon) compared to the normal upright sitting posture.

The resonance frequencies in the vertical transmissibility to the thoracic spine (T5) increased in both the 'kyphotic leaning' posture and the 'anterior leaning' sitting posture (p<0.05, Wilcoxon, Table 8.10), compared to the 'normal' sitting posture. However, there was no significant change in the vertical transmissibility to T5 at the resonance frequency in any of the three sitting postures (p>0.05, Wilcoxon, Table 8.10).

Table 8.10 Statistical significance of the effects of the forward leaning sitting postures on the resonance frequency in the vertical transmissibility to the spine and the transmissibility at resonance measured with 1.0 m/s^2 r.m.s. vibration. Wilcoxon matched-pairs signed ranks test.

Pelvis	Resonance frequency				Transmissibility at resonance			
	Normal	KL	AL			Normal	KL	AL
Normal	\	0.029*↑(KL)	0.184		Normal	\	0.027*↑(KL)	0.274
KL		\	0.039*↓(AL)		KL		\	0.380
AL			\		AL			\

L5	Resonance frequency				Transmissibility at resonance			
	Normal	KL	AL			Normal	KL	AL
Normal	\	0.031*↑(KL)	0.005**↑(AL)		Normal	\	0.151	0.064↑(AL)
KL		\	0.078		KL		\	0.519
AL			\		AL			\

L3	Resonance frequency				Transmissibility at resonance			
	Normal	KL	AL			Normal	KL	AL
Normal	\	0.022*↑(KL)	0.002**↑(AL)		Normal	\	0.424	0.064↑(AL)
KL		\	0.016*↑(AL)		KL		\	0.151
AL			\		AL			\

T5	Resonance frequency				Transmissibility at resonance			
	Normal	KL	AL			Normal	KL	AL
Normal	\	0.008**↑(KL)	0.011*↑(AL)		Normal	\	0.092	0.110
KL		\	0.234		KL		\	0.622
AL			\		AL			\

ns: not significant; * p≤0.05; ** p≤0.01. The arrow indicates increase or decrease of the variables in the brackets compared to the variable in the left column of the same row.

8.3.3.2 Fore-and-aft cross-axis transmissibility to the spine

In the two forward leaning sitting postures, the fore-and-aft transmissibilities to all spinal locations tended to increase at low frequencies (up to 8 Hz) compared to the 'normal' sitting posture. The fore-and-aft transmissibility to the pelvis, L5, and L3 showed a resonance at around 3.5 Hz, and the fore-and-aft transmissibility to T5 showed a resonance at around 5 Hz in the normal sitting posture. Both 'kyphotic leaning' and 'anterior leaning' sitting postures tended decrease the resonance frequency and increase the transmissibility at resonance to all spinal levels, although no significant differences were found in the resonance frequency of the fore-and-aft transmissibilities measured between the three sitting postures (Table 8.11). The transmissibility at the resonance frequency increased significantly in both the 'kyphotic leaning' and the 'anterior leaning' sitting postures compared to the 'normal' sitting posture (p<0.05, Wilcoxon, Table 8.11) The fore-and-aft transmissibility to T5 showed a clear peak at around 3 Hz in the 'kyphotic leaning' and the 'anterior leaning' sitting postures, while the peak was not observed in the normal sitting posture (Figure 8.18).

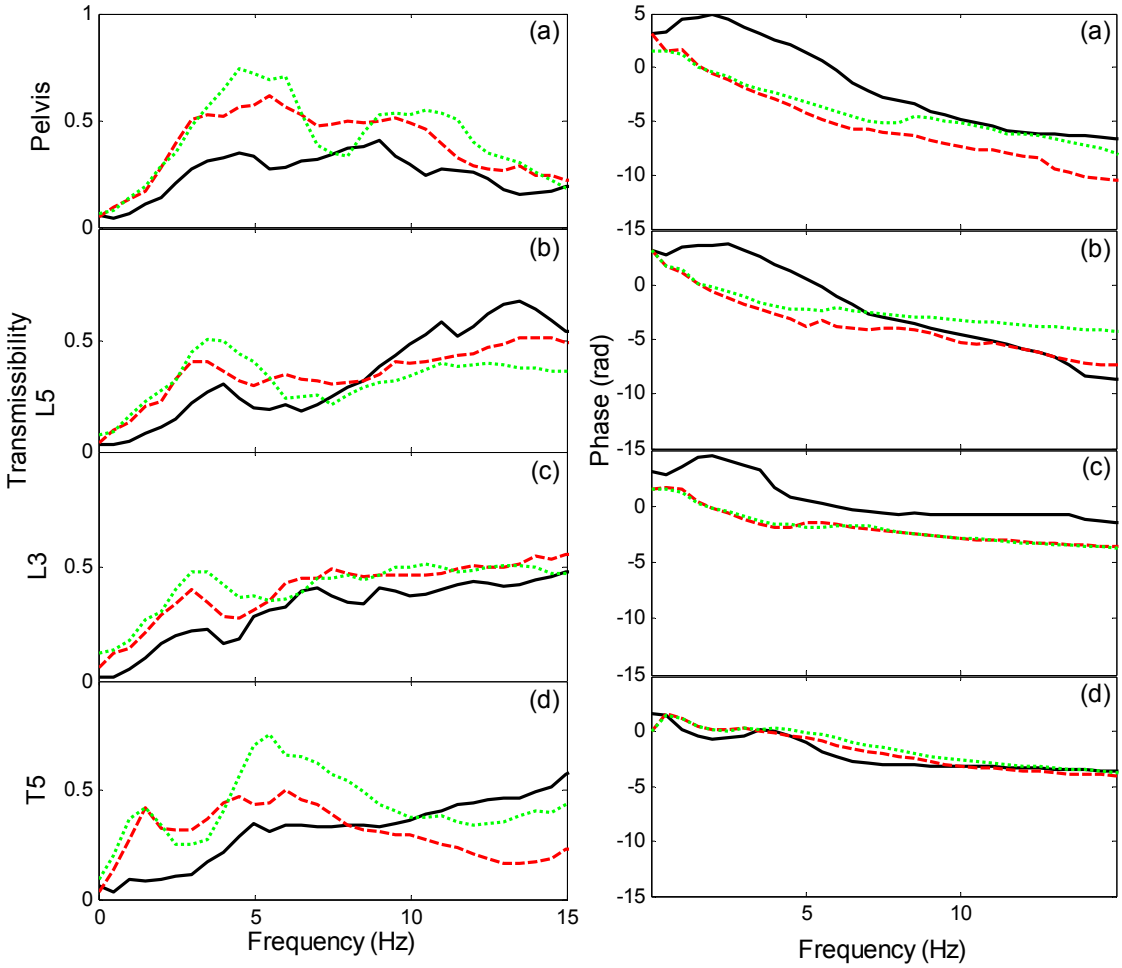

Figure 8.18 Median transmissibilities from seat acceleration to fore-and-aft acceleration of the spine for subjects sitting in three different postures: '—', normal; '- -', 'kyphotic leaning'; '...', 'anterior leaning'. Medians of 12 subjects.

Table 8.11 Statistical significance of the effects of forward leaning sitting postures on the resonance frequency of the fore-and-aft transmissibility to spine and the transmissibility at resonance measured with 1.0 m/s^2 r.m.s. vibration. Wilcoxon matched-pairs signed ranks test.

Pelvis	Resonance frequency				Transmissibility at resonance			
	Normal	KL	AL			Normal	KL	AL
Normal	\	0.945	0.455		Normal	\	0.301	0.005**↑(AL)
KL		\	0.684		KL		\	0.016*↑(AL)
AL			\		AL			\

L5	Resonance frequency				Transmissibility at resonance			
	Normal	KL	AL			Normal	KL	AL
Normal	\	0.425	0.313		Normal	\	0.009**↑(KL)	0.002**↑(AL)
KL		\	0.930		KL		\	0.151
AL			\		AL			\

L3	Resonance frequency				Transmissibility at resonance			
	Normal	KL	AL			Normal	KL	AL
Normal	\	0.016*↑(KL)	0.102		Normal	\	0.034*↑(KL)	0.003**↑(AL)
KL		\	0.031*↑(AL)		KL		\	0.043*↑(AL)
AL			\		AL			\

T5	Resonance frequency				Transmissibility at resonance			
	Normal	KL	AL			Normal	KL	AL
Normal	\	0.397	1		Normal	\	0.130	0.002**↑(AL)
KL		\	0.422		KL		\	0.176
AL			\		AL			\

ns: not significant; * $p \leq 0.05$; ** $p \leq 0.01$. The arrow indicates increase or decrease of the variables in the brackets compared to the variable in the left column of the same row

8.3.3.3 Pitch transmissibility to the spine

The median transmissibilities from vertical seat acceleration to the pitch acceleration at various spinal vertebrae are shown in Figure 8.19. In all three sitting postures, the pitch transmissibilities to L5, L3 and T5 showed an increasing trend over frequencies, while the pitch transmissibility to the pelvis showed a principal peak at frequencies less than 10 Hz. In general, there were no significant differences in the pitch transmissibility to the various spinal levels within the three sitting postures at frequencies less than 10 Hz. It is difficult to use statistical techniques to analysis the trend of changes in the pitch transmissibilities in three sitting postures because the resonance shown by one subject in one posture did not appear in other postures of the same subject and some resonance shown by one subject did not appear in the transmissibility measured in other subjects. The majority subjects had a principal resonance at frequencies greater than 10 Hz, but the pitch transmissibilities were only considered reliable at frequencies less than 10 Hz due to the limitation of equipment (as stated in Chapter 6). The majority subjects also showed a resonance at frequencies around 4.5 to 7 Hz with a transmissibility usually less 10 (rad*s^2/m).

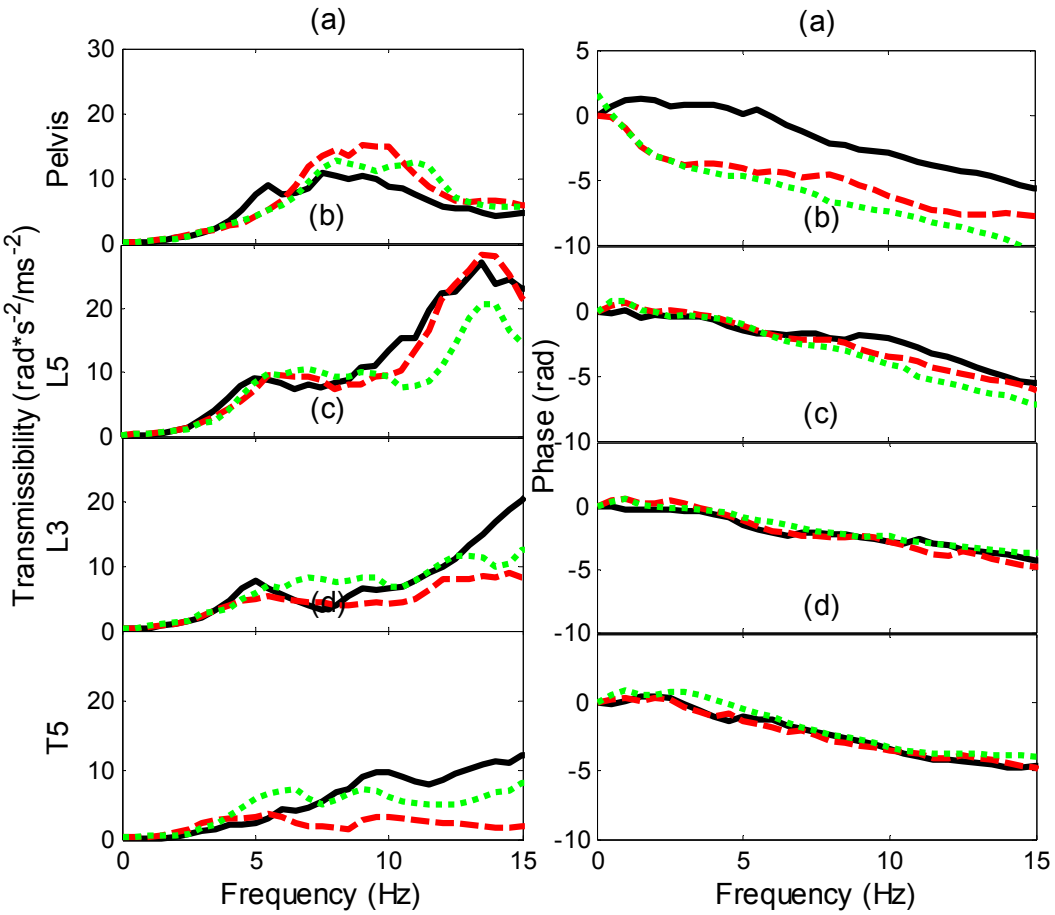

Figure 8.19 Median transmissibilities from vertical seat acceleration to pitch acceleration of the spine for subjects sitting in three different postures: '—', normal; '- -', 'kyphotic leaning'; '...', 'anterior leaning'. Medians of 12 subjects.

The subjects showing a clear resonance frequency in the pitch transmissibility at around 5 Hz to all spinal levels were selected to conduct statistical analysis. It was found that there were no significant differences in the resonance frequency of the pitch transmissibility to the pelvis (around 5 Hz) in the three different postures (p=0.764, Friedman). Similarly, no significant differences were found in the resonance frequency (around 5 Hz) of the pitch transmissibilities to the other spinal levels in the three sitting postures (L5: p=0.951, Friedman; L3: p=0.214, Friedman; T5: p=0.629, Friedman). No significant differences were found in the pitch transmissibility to the pelvis or to L5 at the resonance around 5 Hz (pelvis: p=0.651, Friedman; L5: p=0.368, Friedman) within the three sitting postures. The pitch transmissibilities to L3 and to T5 at the resonance frequency (around 5 Hz) in the 'anterior leaning' sitting posture were greater than that in either 'kyphotic leaning' and normal sitting postures (p<0.05 for all pairs of comparison, Wilcoxon). Some subjects showed a clear peak in the pitch transmissibility at frequencies around 2.5 Hz in the 'kyphotic leaning' and 'anterior leaning' sitting postures, which might be related with the resonance at around 2.5 Hz observed in the vertical apparent mass at the seat pan in the same postures.

8.4 Discussion

8.4.1 Effect of forward leaning sitting postures on the vertical in-line apparent mass at the seat pan

The resonance frequency in the vertical in-line apparent mass at the seat pan increased when the upper body was leaning forward with either a kyphotic spine ('kyphotic leaning') or an erect spine ('anterior leaning'). From 'kyphotic leaning' to 'anterior leaning', there was a significant increase in the resonance frequency of the vertical apparent mass with 1.0 m/s^2 r.m.s. vibration (Table 8.1).

It appeared that some subjects may have adopted incorrect forward leaning sitting postures during the experiment, which would impede the testing of the hypothesis. Maintaining a forward leaning posture required effort during the experiment, especially with a high vibration magnitude (i.e., 1.5 m/s^2 r.m.s.). During the experiment, a few subjects may have supported their upper body on the thighs via the hands on lap when sitting in the 'kyphotic leaning' posture, because they felt more relaxed (although they were asked not to do so), and this increased the mass supported on the footrest and reduced the mass on the seat. In the 'anterior leaning' posture, the subjects were asked to maintain a 30º forward leaning, but they may not have supported the body mass on the thighs through the hands because the whole body was more tensed, so that more mass was supported on the seat compared to the 'kyphotic leaning' posture. Some subjects tended to leaning forward less when exposed to vibration with the higher magnitude (i.e., 1.5 m/s^2 r.m.s.) to feel more 'safe' and 'comfortable' as they were required to tense the muscles around the pelvis and in the back (e.g., erector spinae) in the 'anterior leaning' sitting posture. The above factors were difficult to monitor during the experiment and they may have contributed to the trends in the resonance frequency measured in the two forward leaning postures (KL and AL) for some subjects and explain their trends being opposite to the majority of subjects. By analysing the individual data after removing some odd data (large reductions in the static sitting masses in the two forward leaning sitting postures compared to the normal sitting posture), the vertical apparent masses of three subjects (Subjects 1, 5, 12) with the three vibration magnitudes were removed from the statistical analysis. The effects of the forward leaning sitting postures on the resonance frequencies in the vertical apparent mass at the seat pan were recalculated and are presented in Table 8.12.

The difference in the statistical significance before (Tables 8.1, 8.2 ,8.3) and after removing the data from three subjects (Table 8.12) appears in the significant increase in the resonance frequency of the vertical apparent mass at seat when changing from the 'kyphotic leaning' sitting posture to the 'anterior leaning' sitting posture with 0.5 m/s^2 r.m.s. vibration.

During the experiment, the subjects were asked to sit with the majority of their thighs supported on the on the seat pan, and asked not to support the body on the thighs via the hands or arms. However, it seemed unavoidable for some subjects to not push down with the hands during the 'kyphotic leaning' sitting posture because the rest of the body was relaxed, especially when the subject had been sitting for a long period. The increase in the resonance frequency of the apparent mass in the 'kyphotic leaning' posture with some vibration magnitudes could be due to the reduced mass supported on the seat pan as the body leaning forward in a relaxed posture with the feet

supporting a part of the body mass. The effect of the change of the muscle activity on the principal resonance frequency of vertical apparent mass at the seat pan from the normal sitting posture to the 'kyphotic leaning' would be masked by the decrease of the mass supporting on the seat pan. However, when exposed to 1.0 m/s^2 r.m.s. vibration, there was no significant difference between the resonance frequency in the 'kyphotic leaning' and the normal sitting postures, which might be because some subjects controlled their posture as this would be the first session during the experiment and there was no significant change in the body mass supported on the seat pan between normal and 'kyphotic leaning' sitting postures. This might indicate that solely a change of upper body geometry (i.e., centre of gravity of the upper body) may have a limited influence on the principal resonance frequency in the vertical apparent mass measured at the seat. The study of Mansfield and Griffin (2002) also suggested that the changes in apparent mass and transmissibility caused by changes in vibration magnitude were greater than the changes caused by postural changes.

Table 8.12 Statistical significance of the effects of forward leaning sitting postures on the resonance frequency in the vertical apparent mass at the seat pan with 0.5, 1.0 and 1.5 m/s^2 r.m.s. of 9 subjects. Wilcoxon matched-pairs signed ranks test.

Resonance frequency of vertical apparent mass at the seat pan with 0.5 m/s^2 r.m.s.			
	Normal	KL	AL
Normal	-	0.023*↑ (KL)	0.008**↑ (AL)
KL		-	0.031* ↑ (AL)
AL			-

Resonance frequency of vertical apparent mass at the seat pan with 1.0 m/s^2 r.m.s.			
	Normal	KL	AL
Normal	-	0.188	0.008**↑ (AL)
KL		-	0.016* ↑ (AL)
AL			-

Resonance frequency of vertical apparent mass at the seat pan with 1.5 m/s^2 r.m.s.			
	Normal	KL	AL
Normal	-	0.016*↑ (KL)	0.016*↑ (AL)
KL		-	0.125
AL			-

ns: not significant; * $p \leq 0.05$; ** $p \leq 0.01$. The arrow indicates increase or decrease of the variables in the brackets compared to the variable in the same row

In the 'anterior leaning' sitting posture, the centre of gravity of the upper body was controlled to be more or less the same as in the 'kyphotic leaning' posture, and the rotation of pelvis was also similar to the 'kyphotic leaning' sitting posture (slight greater in AL than KL due to the kyphotic spine in KL posture). The compression of the tissues around the pelvis and the tension of muscles around the pelvis (e.g., gluteal muscles, which is responsible for pelvis tilt) were expected to be similar in both forward leaning postures. However, to maintain the 'anterior leaning' posture the

muscles in the back (i.e., lumbar and thoracic region) needed to tense, especially the muscles in the thoracic region. A significant increase in the resonance frequency of the vertical apparent mass at the seat pan from the 'kyphotic leaning' posture to the 'anterior leaning' posture with both 0.5 and 1.0 m/s^2 r.m.s. vibration magnitudes (Table 8.12) was found in the present study. This suggests that increased muscle activity in the upper body may increase the overall body stiffness, resulting in an increase in the resonance frequency of the vertical apparent mass at the seat. The increase in muscle activity mainly involves tonic muscle activity required to maintain posture.

At low frequencies (close to 0 Hz), the median apparent mass in both 'kyphotic leaning' and 'anterior leaning' postures reduced by around 8 kg (from a median sitting mass of 58 kg) when exposed to 1.0 m/s^2 r.m.s. vibration. This could be due to increased weight supported at the feet in order to maintain the upper body leaning forward sitting posture. Based on a single degree-of-freedom model, with the sitting mass decreased to 86% (calculated as 50/58), the resonance frequency of such model would increase by around 7% ($f_2 = f_1 * \sqrt{m_1 / m_2}$). Therefore, the resonance frequency would change from 4.75 Hz in the normal sitting posture (with 1.0 m/s^2 r.m.s. vibration) to 5.12 Hz in the 'kyphotic leaning' sitting posture, which is close to the resonance frequency of median vertical apparent mass of the 12 subjects in the 'kyphotic leaning' posture (5.25 Hz). The increase in the resonance frequency of the vertical apparent mass from 'normal' to 'kyphotic leaning' sitting postures may be caused by the decrease in the mass supported on the seat pan. However, tension in the buttocks tissues and other muscles would also tend to increase the resonance frequency in the 'kyphotic leaning' sitting posture.

8.4.2 Effect of forward leaning sitting postures on the fore-and-aft cross-axis apparent mass at the seat pan

The resonance frequency of the median fore-and-aft cross-axis apparent mass was lower in the 'kyphotic leaning' sitting posture than in the normal upright sitting posture (Figure 8.14), but no statistically differences were found between the individual principal resonance frequency of the fore-and-aft apparent masses in these two postures (Figure 8.11). The inconsistency could be due to the multiple peaks in the fore-and-aft cross-axis apparent mass at the seat. In the 'kyphotic leaning' sitting posture, some subjects showed one peak at a low frequency with the greatest magnitude (e.g., 2.75 Hz, Subject 5 in the 'kyphotic leaning' posture), but some other subjects showed a peak with greatest magnitude at a higher frequency (e.g., 5.75 Hz, Subject 6 in the 'anterior leaning' posture). The peaks at different frequencies may be associated with different body modes. The peak occurring at a lower frequency (around 2.5 Hz) in the fore-and-aft apparent mass would be associated with the greater anterior-posterior motion of the head and pelvis in phase, caused by bending of the entire spine (Kitazaki and Griffin, 1998). The peak occurring at a greater frequency (around 5 Hz) would be associated with the vertical and shear motions of the buttock tissues, as suggested from the modal analysis from Kitazaki and Griffin (1997 and 1998). The peaks at similar frequencies (around 3 Hz and around 5 Hz) were also observed in the fore-and-aft in-line apparent mass when exposed to fore-and-aft whole-body vibration (Nawayseh and Griffin, 2005), where three vibration modes were found in the fore-and-aft apparent mass at around

1, 1-3 and 3-5 Hz. Sitting in a 'kyphotic leaning' posture could excite and enhance the above vibration mode at a lower frequency in some subjects, resulting in a greater peak in the fore-and-aft apparent mass at a lower frequency (around 2.5 Hz) than at a higher frequency (around 5 Hz),

Sitting in the 'anterior leaning' posture would also excite and enhance the vibration mode at a lower frequency in the fore-and-aft apparent mass, similar to the condition with the 'kyphotic leaning' posture. Besides, fore-and-aft motion of both the pelvis and the lumbar spine increased (Figure 8.18) compared to the 'kyphotic leaning' and normal sitting postures, contributing to the increase in the fore-and-aft apparent mass at the resonance at a higher frequency (around 5 Hz). In the 'anterior leaning' sitting posture, the peak at the higher frequency (around 5 Hz) was of the greatest magnitude for the majority subjects.

The fore-and-aft cross-axis apparent mass at all frequencies (in the range 0 – 15 Hz) was found to be greater in the 'anterior leaning' posture than in the other two postures (see Figure 8.11). Possible reasons would be due to the greater shear motions at the ischial tuberosity (Figure 8.18) caused by greater pitch motions of the entire spine in the 'anterior leaning' sitting posture (Figure 8.19).

It is noticeable that the phase of the fore-and-aft cross-axis apparent mass at the seat pan in each of the three sitting postures started from 3.14 rad at frequencies close to zero (0.5 Hz) when exposed to 1.0 m/s^2 r.m.s. and 0.5 m/s^2 r.m.s. vibration. If the body were rigid, the fore-and-aft cross-axis apparent mass at 0 Hz would be zero. When exposed to vibration, the initial posture would determine the direction of the fore-and-aft dynamic force at very low frequencies (i.e., less than 0.5 Hz). In a forward leaning sitting posture, when vertical acceleration is applied to the seat, the inertial mass (e.g., upper body) would cause the upper body to leaning forward more (forward displacement), resulting in backward acceleration of the centre of mass of the upper body and a corresponding backward force at the body-seat interface, giving a phase of 3.14 rad. Note that the direction of displacement is opposite to the direction of acceleration with sinusoidal motion. In the normal upright sitting posture, voluntary or involuntary movements of the body in response to the motion would affect the initial phase of the fore-and-aft cross-axis apparent mass at the seat pan. For example, if a subject sat with a slightly kyphotic spine, the body would move forward more without voluntary control of the body, resulting in a phase start at 3.14 rad, similar to the forward leaning sitting postures. Alternatively, the upper body would move backwards voluntarily to maintain the normal upright sitting posture at the initial moment of excitation, resulting in a positive fore-and-aft force at the human-seat interface (i.e., backward displacement). Such positive fore-and-aft force would cause the initial phase (at around 0.5 Hz) to start at 0 rad (Figure 8.8 and Appendix B, Figure B1).

It is also noticeable that when exposed to 1.5 m/s^2 r.m.s. vibration, the fore-and-aft cross-axis apparent mass at the seat increased as the frequency increased from 10 Hz to 15 Hz. The reason would be that the vibrator had a resonance around 13 Hz with the operating height used to generate the 1.5 m/s^2 r.m.s. vibration (Appendix B, Figure B1), while with 0.5 and 1.0 m/s^2 r.m.s. random vibration, a lower operating height was used and the resonance of the vibrator occurred at

a frequency greater than 15 Hz. As a results, the fore-and-aft cross-axis apparent mass at the seat pan when exposed to 1.5 m/s^2 r.m.s. was only valid within 0-10 Hz.

8.4.3 Effect of forward leaning sitting postures on the non-linearity of the seated human body

The nonlinear behaviour of the human body (i.e., decreasing principal resonance frequency with increasing vibration magnitude) was found in the normal posture, the 'kyphotic leaning' posture, and the 'anterior leaning' posture. The decrease in the resonance frequency was greater when the vibration magnitude changed from 0.5 to 1.0 m/s^2 r.m.s. than when the magnitude changed from 1.0 to 1.5 m/s^2 r.m.s., consistent with Mansfield and Griffin (2002).

The median resonance frequencies in the vertical apparent mass in the 'anterior leaning' posture decreased from 6.25 Hz with 0.5 m/s^2 r.m.s. to 5.25 Hz with 1.5 m/s^2 r.m.s. This decrease in the 'anterior leaning' sitting posture was greater than the decrease in the normal sitting posture (from 5 Hz to 4.5 Hz when the vibration magnitude increased from 0.5 to 1.5 m/s^2 r.m.s.). This might be caused by greater tension of the muscles in the upper body (e.g., erector spinae muscles). The muscle activity around the pelvis (e.g., gluteal muscles) was also expected to be increased in the 'anterior leaning' sitting posture compared to the normal sitting posture. However, any such increase in muscle tension around the pelvis did not produce a reduction in the nonlinearity, which seems inconsistent with the findings of Matsumoto and Griffin (2002). They suggested that tensing the abdominal muscles and the buttocks tended to decrease the reduction in the resonance frequency with increasing vibration magnitude (Matsumoto and Griffin, 2002). Possible reasons would be due to different groups of muscles tensed in the present study and the study of Matsumoto and Griffin (2002). The muscles controlling pelvis rotation were tensed in the present study, including the gluteal muscles. However, in the experiment of Matsumoto and Griffin (2002), the subjects were asked to voluntary tense muscles in the buttocks and the subjects may have only tensed the muscles in the thighs (e.g., biceps femoris). Tension in thigh muscles might contribute to the nonlinearity (e.g., Liu *et al.*, 2015).

While in the 'kyphotic leaning' sitting posture, the median resonance frequencies in the vertical apparent mass decreased from 5.75 Hz to 5.25 Hz with the vibration magnitude increasing from 0.5 to 1.5 m/s^2 r.m.s., similar to the decrease in the normal sitting posture. The tension of the muscles in the upper body in the 'kyphotic leaning' posture was similar to that in the 'normal' sitting posture, and so expected to result in a similar nonlinearity in the 'kyphotic leaning' and 'normal' postures. As a result, it might be speculated that muscle activity in the upper body makes a significant contribution to the nonlinearity in the body.

A peak in the vertical in-line apparent mass occurred at frequencies (about 2.5 Hz) lower than the principal resonance in both the 'kyphotic leaning' and the 'anterior leaning' sitting postures of the majority subjects with all three vibration magnitudes. This is probably because a vibration mode of the upper body occurred at that frequency and was only excited in the forward leaning postures. The vibration mode consists of the fore-and-aft motion of the head and pelvis in phase caused by bending of spine (Kitazaki and Griffin, 1997), same as the causes for the lower peak in the fore-

and-aft apparent mass discussed in Section 8.4.2. The body transmissibility data in the present study show that the vertical transmissibility to the thoracic spine (i.e., T5) and the fore-and-aft transmissibility to the lumbar spine (L5 and L3) and the thoracic spine (T5) had a peak at around 2.5 Hz, similar to the first peak shown in the vertical apparent mass in the forward leaning postures. This suggests the first peak in the vertical apparent mass at around 2.5 Hz is associated with the vertical and fore-and-aft motions of the thoracic spine and also the fore-and-aft motions of the lumbar spine in the forward leaning sitting postures.

The frequency of the first peak in the vertical in-line apparent mass in the 'anterior leaning' sitting posture decreased with increasing vibration magnitude, but there was no significant decrease in the 'kyphotic leaning' sitting posture. Possible causes would be that the tension of the muscles in the upper body differed between the two forward leaning postures. In the 'anterior leaning' sitting posture, the tonic activity of muscles at the back (e.g., erector spinae) may have been greater than in the 'kyphotic leaning' sitting posture, and this may have increased the pitch motion of the upper body in the 'anterior leaning' sitting posture (pitch transmissibilities to T5; Figure 8.19). The decreasing frequency for the first peak with 'anterior leaning' may be due to the same cause as the decreasing frequency of the principal resonance, possibly due to the dynamic properties of buttocks tissues or the tension of muscles (e.g., Matsumoto and Griffin, 2001; Huang and Griffin, 2006). In the 'kyphotic leaning' sitting posture, the muscles in the upper back (e.g., erector spinae) were in a relaxed state with little tonic muscle activity, although there may have been some voluntary or involuntary muscle activity, especially at the lower frequencies. Voluntary muscular activity can reduce the nonlinearity in the apparent mass (Huang and Griffin, 2006), and it is conceivable that such voluntary motions may occur in the 'kyphotic leaning' sitting postures so as to reduce the nonlinearity.

8.4.4 Effect of forward leaning sitting postures on body transmissibility

The resonance frequency in the vertical transmissibility to the spine (i.e., to the pelvis, L3 and T5), and the transmissibility at resonance, were greater in both 'kyphotic leaning' and 'anterior leaning' sitting postures, than in the normal sitting posture (Figure 8.17). The increase in the vertical transmissibilities to the spine would presumably be due to a forward leaning posture increasing the horizontal distance between the centre of gravity of the upper body and the driving point between the pelvis and the seat pan, resulting in greater pitch motion of the pelvis at some frequencies (Figure 8.19). The increase in pitch motion in the leaning forward postures (i.e., 'kyphotic leaning' and 'anterior leaning' sitting postures) would increase both the vertical and the fore-and-aft motion at various spinal levels. The increase of the resonance frequency of the vertical transmissibilities to the pelvis and the lumbar spine (i.e., L3 and L5) could be due to increased compression of tissues and increased tension of muscles around the pelvis region or the muscles at lumbar spine and thoracic spine with the upper body leaning forward in the 'kyphotic leaning' and 'anterior leaning' sitting postures. With increasing tension of muscles in the upper body, the resonance frequency of the vertical transmissibility to L3 and T5 increased from the 'kyphotic leaning' sitting posture to the 'anterior leaning' sitting posture.

The fore-and-aft transmissibilities to the pelvis, lumbar spine, and thoracic spine increased in the 'kyphotic leaning' and 'anterior leaning' sitting postures at frequencies less than 8 Hz compared to the normal sitting posture (Figure 8.18). The increase in fore-and-aft transmissibilities to the spine in the two frequency ranges 0-5 Hz and 5-8 Hz may be due to different reasons. Increased pitch motion of the pelvis with the upper body leaning forward would increase the fore-and-aft transmissibilities to the spine at frequencies in the range 5-8 Hz. At frequencies less than 5 Hz there were only marginal differences between the three sitting postures in the pitch transmissibility to each spine level (i.e., pelvis, L5, L3 and T5) (Figure 8.19). The increase in fore-and-aft transmissibilities to the spine at frequencies less than 5 Hz with the upper body leaning forward may be due to the excitation of two body modes occurring at 2.2 Hz (second mode) and 3.4 Hz (third mode), as suggested by Kitazaki and Griffin (1998). The two body modes correspond to the first and second modes of a beam with both ends free, both associated with fore-and-aft motions of the pelvis and the spine. When the upper body leans forward in the 'kyphotic leaning' and 'anterior leaning' sitting postures these modes increase the motion of the pelvis and the spine at frequencies less than 5 Hz. The same body modes also contribute to a resonance around 2.5 Hz in the vertical in-line apparent mass measured at the seat (Section 8.4.3).

In all three sitting postures, pitch transmissibility to all spinal levels increased with increasing frequency up to around 10 Hz. The pitch transmissibility to the pelvis in all three sitting postures showed a resonance around 8-10 Hz, consistent with modal analysis of the human body (Kitazaki and Griffin, 1998). Rotational modes of the pelvis were found at the sixth mode (at about 8.1 Hz) and at the seventh mode (around 8.7 Hz) in the modal analysis of Kitazaki and Griffin (1998). The pitch transmissibilities to the pelvis and lumbar spine at frequencies less than 5 Hz showed little difference among the three sitting postures (normal, 'KL' and 'AL'). In all three sitting postures, the pitch transmissibility to L5 was greater than the pitch transmissibility to other locations (e.g., L3 and T5; Figure 8.19), suggesting relative motion between locations along the spine. Such relative motions between body segments include bending of the lumbar spine and pitching of the pelvis, which would contribute to the principal resonance frequency of the vertical apparent mass at the seat pan (Matsumoto, 1999).

8.4.5 Correlations between the transmissibility to different spinal levels and the vertical apparent mass at the seat pan

The vertical apparent mass at the seat pan in the 'kyphotic leaning' sitting posture and the 'anterior leaning' sitting posture showed evidence of a resonance at around 3 Hz, lower than the principal resonance in the vertical apparent mass around 5 Hz. For the subjects showing this peak at a low frequency around 3 Hz, the corresponding fore-and-aft transmissibility to the lumbar spine at L5 and L3 showed peaks at similar frequencies, indicating the possible cause for the peak in the vertical apparent mass at the seat pan at this low frequency. A correlation test showed that there was a significant correlation between the frequencies of the peaks at around 3 Hz in the fore-and-aft transmissibility to L5 and L3 and the corresponding peaks in the vertical apparent mass at the seat pan when sitting in the 'anterior leaning' posture ($p<0.05$, Spearman, Table 8.13), but no significant correlations in the 'kyphotic leaning' posture ($p>0.05$, Spearman, Table 8.13). Neither

the vertical transmissibilities to any spinal level nor the fore-and-aft transmissibilities to the pelvis or T5 showed peaks at around 3 Hz in the majority of subjects in either the 'kyphotic leaning' or the 'anterior leaning' sitting postures (3/12 subjects showed peaks at around 3 Hz in these vertical and fore-and-aft transmissibilities), which differs from the situation in the vertical apparent mass at the seat pan (9/12 subjects showed peaks at around 3 Hz in the vertical apparent mass).

Table 8.13 Correlation (Spearman test) between the frequency of the peaks in the vertical apparent mass at the seat pan at around 3 Hz and the frequency of the peaks in the fore-and-aft transmissibilities to the lumbar spine at around 3 Hz.

	Postures	KL	AL
Fore-and-aft transmissibility to L5	Correlation coefficient (r)	0.525	0.647
	p value	0.147	0.059
Fore-and-aft transmissibility to L3	Correlation coefficient (r)	0.037	0.700
	p value	0.925	0.036*

ns: not significant; * $p \leq 0.05$; ** $p \leq 0.01$.

The correlation analysis in Chapter 6 found that the principal resonance frequency in the vertical apparent mass at the seat pan in the normal sitting posture was correlated with the principal resonance frequencies in the vertical transmissibilities to L5, L3 and T5. Similarly, in the 'anterior leaning' sitting postures, the principal resonance frequency in the vertical apparent mass at the seat pan was correlated with the vertical transmissibility to L5, L3 and T5 ($p<0.05$, Spearman, Table 8.14). However, in the 'kyphotic leaning' sitting posture, the principal resonance in the vertical apparent mass was only correlated with the vertical transmissibility to T5 ($p<0.05$, Spearman, Table 8.14).

Table 8.14 Correlation (Spearman test) between the principal resonance frequency of the vertical apparent mass at the seat pan and the resonance frequency of the vertical transmissibilities measured in different sitting postures

	Postures	KL	AL
Pelvis	Correlation coefficient (r)	0.374	0.235
	p value	0.231	0.462
L5	Correlation coefficient (r)	-0.111	0.631
	p value	0.730	0.028*
L3	Correlation coefficient (r)	0.253	0.888
	p value	0.427	**
T5	Correlation coefficient (r)	0.615	0.869
	p value	0.033*	**

ns: not significant; * $p \leq 0.05$; ** $p \leq 0.01$.

The differences in the correlations between the resonance in the vertical apparent mass and the body transmissibilities in the 'kyphotic leaning' and 'anterior leaning' sitting postures may be due to greater body damping in the 'kyphotic leaning' sitting posture. The increased body damping might

merge the vibration modes from different body parts together. The damping of the human body arises from the material properties of the tissues, which absorb energy during whole-body vibration. The damping may be related to the muscle tension at some body locations. In the ‘kyphotic leaning’ and ‘anterior leaning’ sitting postures, the tension of muscles in the buttocks are similar, but the muscles in the lumbar and thoracic spine tensed more in the ‘anterior leaning’ sitting posture, which would affect the transmissibilities to the lumbar spine and the thoracic spine.

8.5 Conclusions

Leaning the upper body forward in an ‘anterior leaning’ posture increases tension in muscles of the back, which is likely to increase the overall body stiffness and increase the frequency of the principal resonance in the vertical apparent mass of the body measured at the seat pan. Moderate changes of the geometry of the upper body without tensing the muscles in the back of a seated person (i.e., without moving the centre of gravity of the upper body) have only a limited influence on the principal resonance frequency in the vertical apparent mass measured at the seat.

With the upper body leaning forward in either a ‘kyphotic leaning’ sitting posture or an ‘anterior leaning’ sitting posture, a body mode around 2.5 Hz is excited and contributes to a resonance around 2.5 Hz in the vertical apparent mass at the seat pan. This body mode consists of fore-and-aft and vertical motions of the lumbar and thoracic spine.

Pitch motions of the lumbar spine and the upper body increase when sitting with the upper body leaning forward, probably due to the increased horizontal distance of the centre of gravity from contact between body and the location of support at the seat pan. The increased pitch motion of the pelvis and the spine may increase the dynamic fore-and-aft force at the seat pan.

The measurements of apparent mass and transmissibilities to the body from this study will be used to optimise the dynamic model of the body so as to predict the effect of posture on spinal forces (see Chapter 10).

Chapter 9. Effect of muscle activity on biodynamic response of the human body when exposed to vertical whole-body vibration

9.1 Introduction

Tensing the muscles in the body affects the biodynamic response of the human body (e.g., Fairley and Griffin, 1989; Huang and Griffin, 2006). Tensing the muscles to move from a 'slouched' sitting posture to an 'erect' sitting posture may increase the resonance frequency in the vertical apparent mass measured at the seat pan (e.g., Fairley and Griffin, 1989; Kitazaki and Griffin, 1998). From a slouched sitting posture to a normal sitting posture, then to an erect sitting posture, the resonance frequency of the vertical transmissibility to various spinal levels also increased (Kitazaki, 1994). Sitting in an 'anterior leaning' posture or a 'kyphotic' posture did not seem to alter the principal resonance frequency from that in a normal sitting posture during exposure to random vertical vibration of 1.0 m/s^2 r.m.s. (Mansfield and Griffin, 2002), even though the 'anterior leaning' sitting posture involved more muscle tension in the back than the normal sitting posture. However, in the study reported in Chapter 8, the tensing of muscles in the back in an 'anterior leaning' sitting posture appeared to contribute to an increase in the principal resonance frequency of the vertical apparent mass at the seat pan compared with a 'kyphotic leaning' sitting posture. The relative influence of muscle tension in the upper and lower body (lower lumbar spine and around the pelvis) on the principal resonance frequency remains to be investigated.

It has been suggested that muscle activity may contribute to the nonlinearity in the dynamic responses of the seated human body exposed to vertical whole-body vibration (seen as a decrease in the resonance frequency in the vertical apparent mass with increasing magnitude of vibration). For example, tensing the abdominal muscles and tensing the buttock tissues reduced the nonlinearity, while tensing the muscles in the upper body showed only a marginal influence on the nonlinearity (e.g., Matsumoto and Griffin, 2002). An increase in the phasic muscle activity caused by voluntary periodic movements of the upper body reduced the nonlinearity in the vertical apparent mass of sitting subjects (Huang and Griffin, 2006).

In reported studies of the effects of muscle activity on the biodynamic responses it may have been difficult for the subjects to maintain a constant muscle tension during exposure to vibration. Individual subjects may also have differed in their ability to control particular groups of muscles by a particular amount of tension (Matsumoto and Griffin, 2002). A quantitative relationship between the amount of muscle tension and changes in the apparent mass measured at the seat remains to be found. Further studies are required to substantiate previous findings and improve understanding of the influence of muscle activity on biodynamic responses.

The objective of this study was to investigate the effect of tensing different groups of muscle on the vertical in-line apparent mass and the fore-and-aft cross-axis apparent mass at the seat pan. The groups of muscles studied include muscles in the upper body (e.g., erector spinae in the thoracic

region: longissimus thoracis pars thoracis and iliocostalis lumborum pars thoracis) and muscles in the lower body (e.g., psoas major, gluteal muscles in the lower lumbar and pelvis region).

To increase the tension of the muscles in specific regions, an external force was applied to either the upper body or the lower body (i.e., iliac crest). This method of applying an external force was used by Robertson and Griffin (1989) to investigate the effect of loading conditions on muscle fatigue during exposure to whole-body vibration. Such external force can increase the tonic muscle activity in the erector spinae, as shown by electromyography (EMG) measurements. In the current study, a spring balance was used to apply external forces to the body.

Biodynamic models of the seated human body have been developed to investigate the mechanisms associated with the principal resonance frequency of the vertical apparent mass measured at the seat pan (e.g., Kitazaki and Griffin, 1997; Matsumoto and Griffin, 2001). Such models suggest that increasing the stiffness of the buttocks tissues will increase the resonance frequency, while increasing the stiffness of the joints connecting the segments of the upper body have no effect on the resonance frequency.

It was hypothesised that an increase in muscle activity in the back or around the pelvis would increase the frequency of the principal resonance in the vertical apparent mass at the seat. It was also hypothesised that tensing the muscles around the pelvis would produce a greater increase in the principal resonance frequency than tensing the muscles in the upper body.

9.2 Methods

9.2.1 Apparatus

Vertical vibration was generated by a 1-m stroke vertical vibrator. A rigid seat without backrest was mounted on the platform of the vibrator (Figure 9.1). The horizontal steel seat pan was 500 mm above the platform of the vibrator. A rigid flat wooden seat pan was rigidly mounted 200 mm above the steel seat pan. The subjects were asked to sit on the wooden seat pan with their feet hanging. The horizontal distance between the rear surface of the calves and the front edge of the wooden seat pan was about 5 cm, so that the calves did not touch the seat pan during vibration.

The dynamic forces (in the fore-and-aft and vertical directions) at the human-seat interface were measured by a force plate (Kistler 9281 B) mount on the seat pan. The vertical acceleration at the seat pan was measured by an accelerometer (Entran EGCSY-240D-10) placed at the centre of the seat pan.

The signals were acquired with a 16-channel *HVLab* data acquisition system at a sampling rate of 256 samples per second via 100-Hz anti-aliasing filters.

A spring balance with a range of 0-15 kg was used to apply fore-and-aft external force to either the thoracic region (at T5) or the iliac crest. An inextensible belt with a buckle was tied loosely around the body, and the spring balance was fastened to the belt (Figure 9.1). The other end of the spring balance was fixed loosely around a rigid pillar rigidly secured on the platform in front of the seat. The horizontal distance between the rigid pillar and the front of the seat pan was about 250 mm. The pillar was on the centre-line of the seat pan (Figure 9.1).

9.2.2 Experimental design

Twelve healthy male subjects with median age 29 years (range 22 to 34 years), median stature 173.5 cm (range 160 to 184 cm) and median weight 69 kg (range 60 to 100 kg) participated in the experiment.

During the experiment the subjects sat upright in six conditions in the following order:

(iv) normal upright sitting with feet hanging (i.e., normal);
(v) upright sitting with 50 N force applied to pelvis (i.e., FP);
(vi) upright sitting with 50 N force applied to upper body at T5 (i.e., FU);
(vii) upright sitting with 100 N force applied to pelvis (i.e., 2FP);
(viii) upright sitting with 100 N force applied to upper body at T5 (i.e., 2FU);
(ix) upright sitting with upper body voluntarily tensed (i.e., UT).

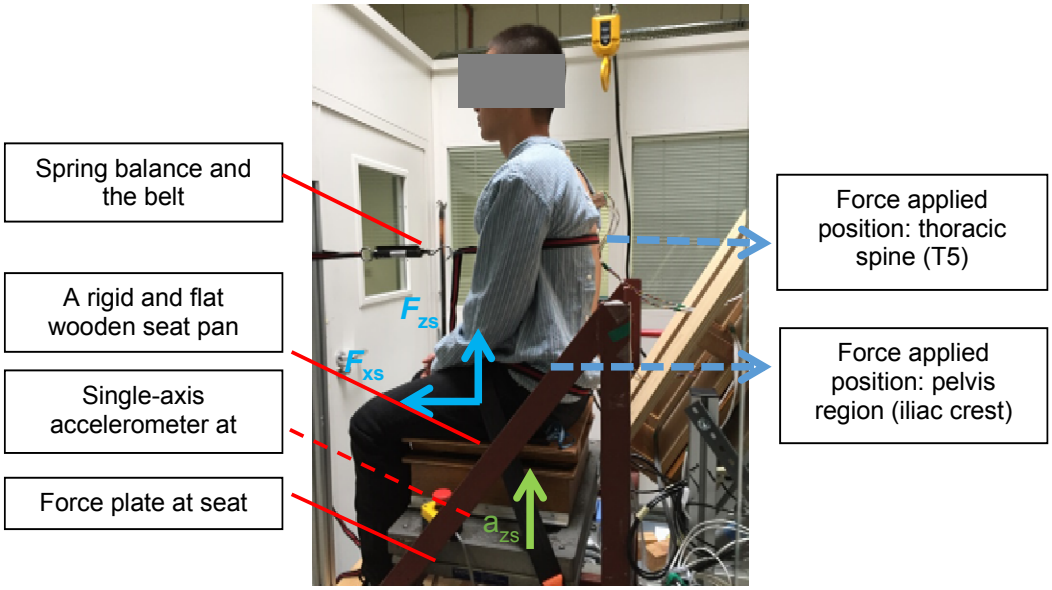

Figure 9.1 Experiment set-up with one subject sitting upright with 50 N force applied to the thoracic region.

Subjects were required to keep an upright sitting posture in all conditions. An external force was applied to either the pelvis or the upper body (around T5). In the conditions 'FU' and '2FU', a belt was worn by the subjects at the level of T5. By adjusting the length of the belt while pulling the spring balance, a fore-and-aft force (of 50 N or 100 N) was applied to the upper body (at T5). The buttocks and thighs of the seated subjects were maintained in the same position when the force was applied.

In the conditions 'FP' and '2FP', a belt was worn by the subjects at the iliac crest. As when applying forces to the upper body, 50 N or 100 N force was applied to the iliac crest. The subjects were asked to relax the muscles in their upper body during the vibration exposure.

In the condition 'UT', the subjects were required to voluntarily tense the muscles in their upper body by holding their breath (i.e., slow exhaling-inhaling to assist maintenance of muscle tension). A

similar posture has been used in previous studies (e.g., Fairley and Griffin, 1989; Huang and Griffin, 2006).

In each condition, the subjects were exposed to 60-s periods of random vertical vibration with an approximately flat constant-bandwidth acceleration spectrum (0.2 to 20 Hz) at 1.0 m/s^2 r.m.s.

The experiment was approved by the Ethics Committee of the Faculty of Engineering and the Environment at the University of Southampton (approval number 14342).

The experimental set-up and an example of one subject sitting upright with 50 N force applied to the upper body (i.e., FU) are shown in Figure 9.1.

9.2.3 Data analysis

9.2.3.1 Mass cancellation

For the calculation of the forces at the seat, the effect of the mass of the top surface of the force plate and the wooden seat pan mounted on the force plate on the measured dynamic force was eliminated by mass cancellation in the time-domain. The vertical acceleration time-history was multiplied by the mass of the force platform and wooden seat pan 'above' the force sensors (38 kg) and the resulting force was subtracted from the measured vertical force. Details are provided in Chapter 3.

9.2.3.2 Transfer functions

Following the same procedure in Chapter 6, the vertical in-line apparent mass ($M_{zzs}(f)$) and the fore-and-aft cross-axis apparent mass ($M_{xzs}(f)$) at the seat pan were calculated using the cross spectral density method (60 averages using a Hamming window with an overlap of 75% for a frequency resolution of 0.25 Hz, H1 estimation, Chapter 3) based on the measured time-history data, together with the coherence functions.

A frequency resolution of 0.125 Hz (32 averages using a Hamming window with an overlap of 75%, H1 estimation Chapter 3) was used to calculate the vertical in-line and fore-and-aft cross-axis apparent masses at the seat pan.

9.2.3.3 Statistical analysis

Non-parametric statistical tests (Friedman two-way analysis of variance for *k*-related samples and Wilcoxon matched-pairs signed-ranks test for two-related samples) were used. The Spearman rank order correlation was employed in to investigate associations between variables.

9.3 Results

9.3.1 Effect of muscle tension on the vertical in-line apparent mass at the seat pan when exposed to 1.0 m/s^2 r.m.s. vertical whole-body vibration

The vertical in-line apparent masses of subjects sitting in the upright posture with feet hanging when exposed to 1.0 m/s^2 r.m.s. vibration showed principal resonances around 4.5 Hz (Figure 9.2).

A few subjects showed secondary resonances around 8 Hz. The apparent mass at a frequency close to zero (i.e., 0.5 Hz) was assumed to represent the sitting mass of each subject. The vertical apparent masses measured at the seat pan for individual subjects in all six sitting conditions (with 1.0 m/s^2 r.m.s.) are shown in Appendix C.1. Details about the inter-subject variability in the vertical in-line apparent mass measured at the seat pan in all six sitting conditions when exposed to 1.0 m/s^2 r.m.s. vibration are shown in Table C3.1 in Appendix C.3.

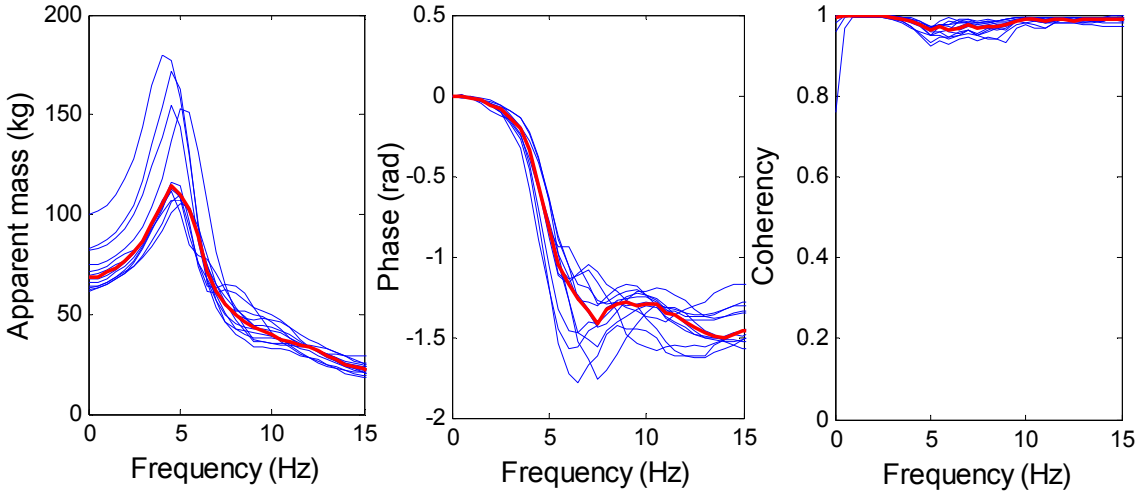

Figure 9.2 Vertical in-line apparent masses at the seat pan in the normal upright sitting posture for 12 individual subjects when exposed to 1.0 m/s^2 r.m.s. vertical vibration. Individual subjects: ('—'); Median of 12 subjects: ('—'). In one row, from left to right: modulus, phase and coherency.

The median vertical in-line apparent masses of the 12 subjects in each of the six sitting conditions (sitting upright without force applied and with force applied to the thoracic spine and pelvis) are shown in Figure 9.3.

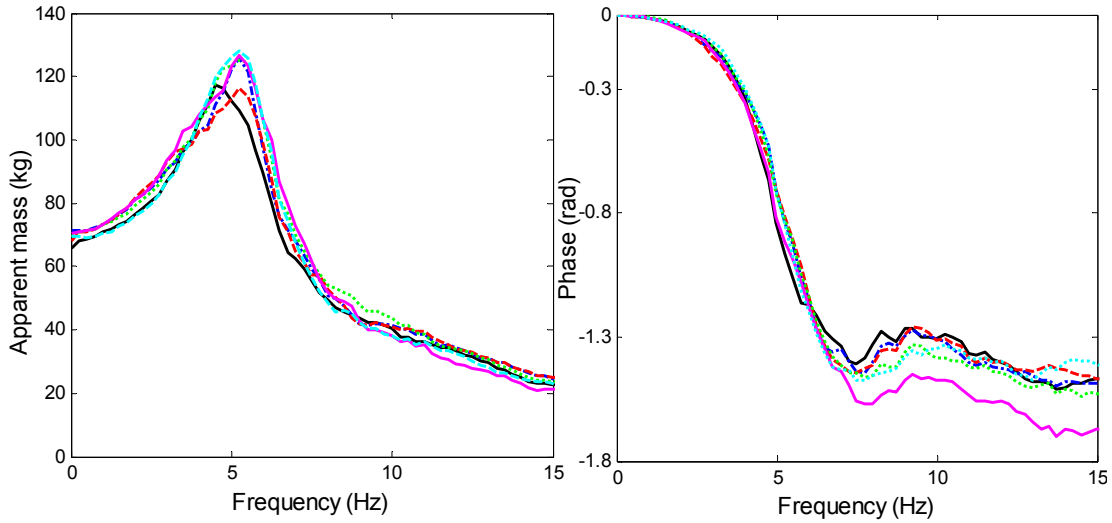

Figure 9.3 Vertical in-line apparent mass at the seat pan in different sitting conditions when exposed to 1.0 m/s^2 r.m.s. vibration: normal upright sitting posture: normal ('——'); with 50 N force applied to pelvis: FP ('--•--•--'); with 100 N force applied to pelvis: 2FP ('------'); with 50 N force applied to upper body T5: FU ('·····'); with 100 N force applied to upper body T5: 2FU ('—'); upright

sitting with upper body voluntarily tensed: UT ('– – –'). Left: modulus; right: phase. Median values from 12 subjects.

There were significant differences in the principal resonance frequency of the apparent mass over the six conditions (p=0.048, Friedman). With 50-N force applied to the pelvis (i.e., FP), the resonance frequency in the vertical apparent mass increased to around 5 Hz from around 4.5 Hz in the normal upright sitting posture (p=0.043, Wilcoxon). However, there was no significant difference between the resonance frequency obtained with 50-N and 100-N forces applied to pelvis (FP and 2FP: p=0.820, Wilcoxon). With 50-N or 100-N forces applied to the upper body (i.e., FU and 2FU), the principal resonance frequency of the vertical apparent mass tended to increase by a similar amount (about 0.75 Hz) from that in the normal sitting posture, although a statistically significant difference was only found between the normal sitting posture and '2FU' (p=0.050, Wilcoxon). There was no significant difference in the resonance frequency of the vertical apparent mass between the two different forces applied to the upper body (i.e., comparison of FU and 2FU: p=0.844, Wilcoxon).

Table 9.1 Statistical significances of the effects of muscle tension and applied forces on the principal resonance frequency in the vertical apparent mass at the seat pan and the modulus of the apparent mass at resonance. Wilcoxon matched-pairs signed ranks test.

Resonance frequency of the vertical apparent mass at the seat pan						
	Normal	FP	2FP	FU	2FU	UT
Normal	-	*↑(FP)	ns	ns	*↑(2FU)	**↑ (UT)
FP		-	ns	ns	ns	ns
2FP			-	ns	ns	ns
FU				-	ns	ns
2FU					-	ns
UT						-

Vertical apparent mass at the seat pan at the resonance frequency						
	Normal	FP	2FP	FU	2FU	UT
Normal	-	ns	ns	ns	ns	ns
FP		-	**↓ (2FP)	ns	ns	ns
2FP			-	*↑ (FU)	* ↑ (2FU)	* ↑ (UT)
FU				-	ns	ns
2FU					-	ns
UT						-

ns: not significant; * p≤0.05; ** p≤0.01. The arrow indicates increase or decrease of the variable in the column compared to the variable in the same row. Details about the statistics (i.e., p-value) are shown in Appendix C.4.

Tensing the upper body voluntarily (i.e., UT) increased the principal resonance frequency in the vertical apparent mass at the seat by around 0.615 Hz (in median data) compared to the normal upright sitting posture (p=0.005, Wilcoxon), similar to the increase when 50 N force was applied to the pelvis (FP) or to the upper body (FU). No significant difference was found between the principal resonance frequencies of the vertical apparent mass measured with the upper body voluntarily tensed (i.e., UT) and any condition with force applied (i.e., comparison of FP, 2FP, FU and 2FU; p>0.05, Wilcoxon, for all conditions; Table 9.1).

The vertical in-line apparent mass at the principal resonance frequency showed statistically significant differences over the six conditions (p=0.001, Friedman). With 100-N force applied to the

pelvis region (i.e., 2FP), the vertical apparent mass at the principal resonance was less than in the normal sitting posture (p=0.064, Wilcoxon; Table 9.1). The apparent mass at the resonance decreased with increasing force applied at the pelvis (i.e., compare FP to 2FP: p<0.001, Wilcoxon). The apparent mass at the principal resonance frequency further increased with force applied to the upper body (i.e., FU and 2FU) or with the upper body voluntarily tensed (i.e., UT) (p<0.05, Wilcoxon; Table 9.1). No significant difference was found in either the frequency of the principal resonance or the apparent mass at the principal resonance between the two conditions with force applied to the upper body (i.e., FU and 2FU) or the upper body tensed (UT) (p>0.05, Wilcoxon, Table 9.1).

9.3.2 Effect of muscle tension on the fore-and-aft cross-axis apparent mass at the seat pan when exposed to 1.0 m/s^2 r.m.s. vertical whole-body vibration

The fore-and-aft cross-axis apparent masses at the seat pan for 12 subjects sitting in the normal upright posture showed a principal resonance around 5 Hz (Figure 9.4), similar to the principal resonance frequency in the vertical in-line apparent mass at the seat. Large inter-subject variability was found in the fore-and-aft cross-axis apparent mass at the resonance frequency (around 5 Hz). The fore-and-aft cross-axis apparent masses at seat pan for individual subjects in all six sitting conditions (with 1.0 m/s^2) are shown in Appendix C.1. Details about the inter-subject variability in the fore-and-aft cross-axis apparent mass measured at the seat pan in all six sitting conditions when exposed to 1.0 m/s^2 r.m.s. vibration are shown in Table C3.2 in Appendix C.3.

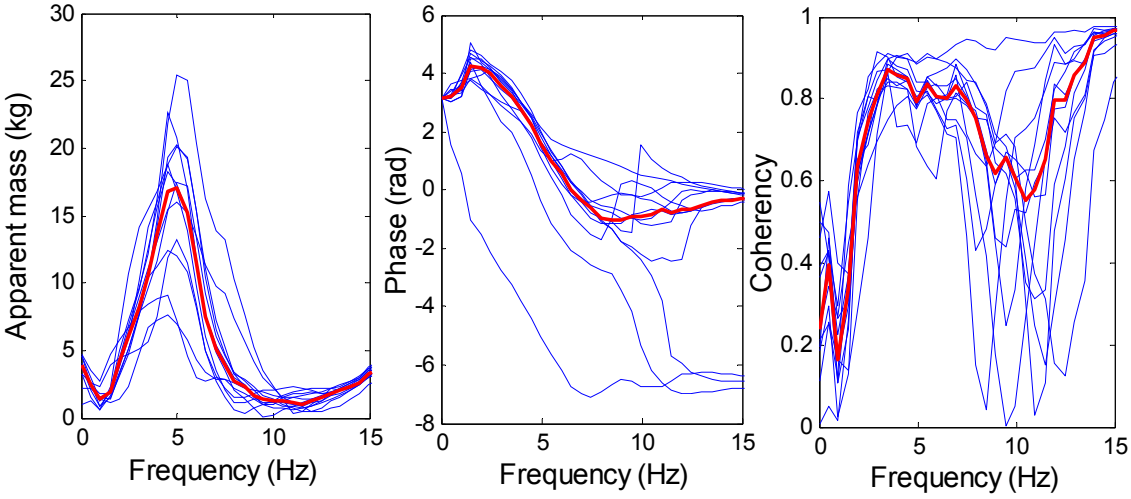

Figure 9.4 Fore-and-aft cross-axis apparent mass at the seat pan in the normal upright sitting posture for 12 individual subjects exposed to 1.0 m/s^2 r.m.s. vibration. Individual subjects: ('—'); Median of 12 subjects: ('—'). In one row, from left to right: modulus, phase and coherency.

The median fore-and-aft cross-axis apparent mass at the seat pan for the 12 subjects in all six sitting conditions (i.e., normal, FU, FP, 2FU, 2FP and UT) when exposed to 1.0 m/s^2 r.m.s. vibration are shown in Figure 9.5. Within all six conditions, the fore-and-aft cross-axis apparent mass at the seat pan showed a similar principal resonance frequency around 5 Hz (p=0.129, Friedman; Figure 9.5).

With 100-N force applied either to the pelvis (2FP) or to the upper body (2FU), the principal resonance frequency increased slightly (about 0.5 Hz in the median apparent mass) from the normal sitting posture (Table 9.2). The influence of applied force or tensing the muscles in the upper body tended to have a more significant effect on the fore-and-aft cross-axis apparent mass at the resonance frequency (p<0.01, Friedman) than on the resonance frequency. Compared to either the normal or the UT postures, the apparent mass at the resonance frequency increased with each of the four conditions with force applied (FU, 2FU, FP and 2FP; p<0.05, Wilcoxon, Table 9.2). With increasing force (50 N to 100 N) applied to the pelvis or the upper body, the fore-and-aft cross-axis apparent mass at the resonance frequency increased slightly (p<0.05, Wilcoxon, Table 9.2). No significant difference was found in the apparent mass at the resonance frequency between the normal sitting posture and the upper body tensed sitting posture (p>0.05, Wilcoxon, Table 9.2).

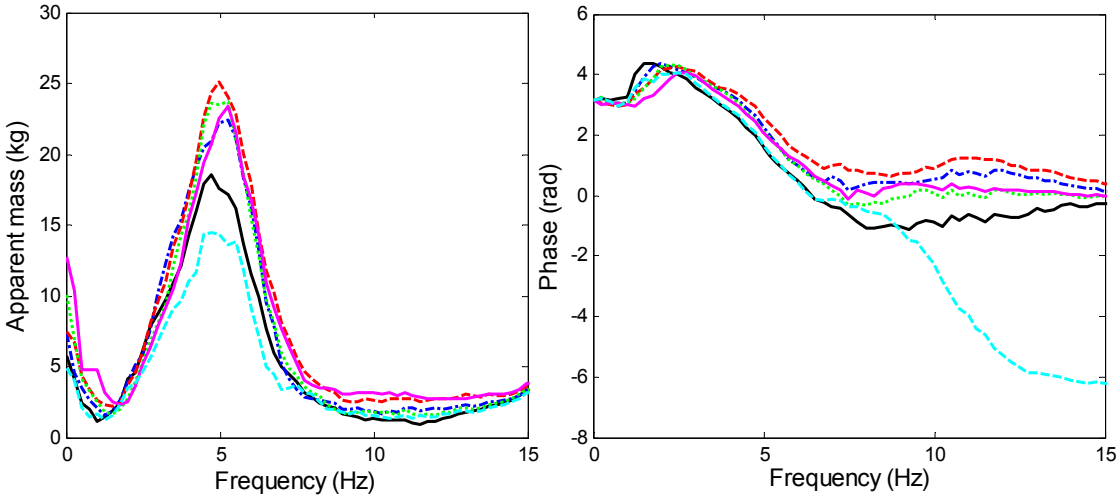

Figure 9.5 Fore-and-aft cross-axis apparent mass at the seat pan in different sitting conditions when exposed to 1.0 m/s^2 r.m.s. vibration: normal upright sitting posture: normal ('——'); with 50 N force applied to pelvis: FP ('--•--•--'); with 100 N force applied to pelvis: 2FP ('------'); with 50 N force applied to upper body T5: FU ('·····'); with 100 N force applied to upper body T5: 2FU ('—'); upright sitting with upper body voluntarily tensed: UT ('– – –'). Left: modulus; right: phase. Median values from 12 subjects.

Table 9.2 Statistical significances of the effects of muscle tension and applied forces on the resonance frequency in the fore-and-aft apparent mass at the seat pan and the modulus of the apparent mass at the resonance. Wilcoxon matched-pairs signed ranks test.

Resonance frequency of fore-and-aft apparent mass at the seat pan						
	normal	FP	2FP	FU	2FU	UT
normal	-	ns	**↑ (2FP)	ns	ns	ns
FP		-	ns	ns	ns	ns
2FP			-	ns	ns	ns
FU				-	ns	ns
2FU					-	ns
UT						-

Fore-and-aft apparent mass at the seat pan at the resonance frequency						
	normal	FP	2FP	FU	2FU	UT
normal	-	*↑ (FP)	**↑ (2FP)	*↑ (FU)	**↑ (2FU)	ns
FP		-	**↑ (2FP)	ns	ns	**↓ (UT)
2FP			-	ns	ns	**↓ (UT)
FU				-	*↑ (2FU)	**↓ (UT)
2FU					-	**↓ (UT)
UT						-

ns: not significant; * $p \leq 0.05$; ** $p \leq 0.01$. The arrow indicates increase or decrease of the variables in the column compared to the variable in the same row. Details about the statistics (i.e., *p*-value) are shown in Appendix C.4.

9.3.3 Effect of muscle tension on the nonlinearity in the vertical in-line apparent mass at the seat pan

The effect of vibration magnitude (i.e., 0.5, 1.0 and 1.5 m/s^2 r.m.s.) on the vertical in-line apparent mass at the seat pan in the six sitting conditions (i.e., normal, FP, 2FP, FU, 2FU and UT) are shown in Figure 9.6.

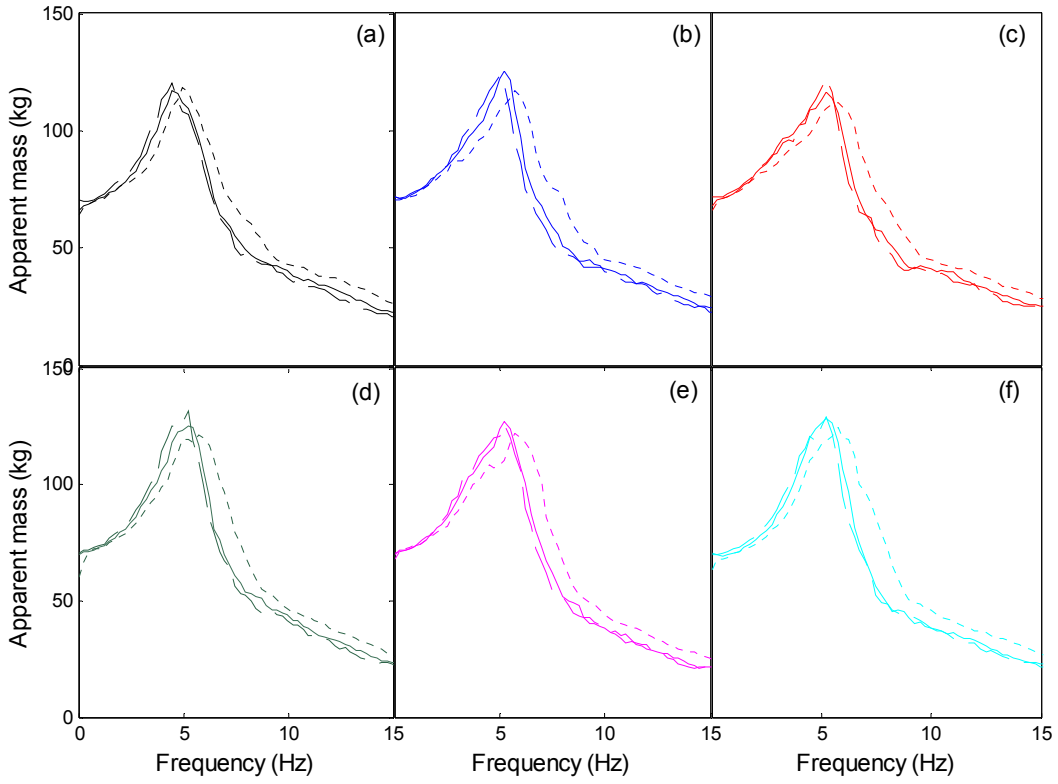

Figure 9.6 Effect of vibration magnitude on the vertical in-line apparent mass at the seat pan in six sitting conditions with three vibration magnitudes: 0.5 m/s^2 r.m.s. ('**.....**'); 1.0 m/s^2 r.m.s. ('**——**'); 1.5 m/s^2 r.m.s. ('**------**'); (a) normal; (b) FP; (c) 2FP; (d) FU; (e) 2FU; (f) UT. Median values from 12 subjects.

The principal resonance frequency in the vertical apparent mass at the seat pan decreased with increasing vibration magnitude in all six sitting conditions (p<0.05, Friedman, for all six conditions). It is noticeable that as the vibration magnitude increased from 1.0 m/s^2 r.m.s. to 1.5 m/s^2 r.m.s., there was no significant change in the resonance frequency in the vertical apparent mass in any of the six sitting conditions (p>0.05, Wilcoxon), except for the condition with 50 N force applied at the pelvis (i.e., FP) where a decrease was found (p=0.031, Wilcoxon, Table 9.3).

The median apparent mass in the normal and upper body tensed (i.e., UT) postures both showed a decrease of 0.5 Hz in the principal resonance frequency from 0.5 m/s^2 r.m.s. vibration to 1.0 m/s^2 r.m.s. vibration, consistent with previous studies (Matsumoto and Griffin, 2002). With 50 N or 100 N forces applied to the upper body (i.e., FU and 2FU), the principal resonance frequency decreased by about 0.5 Hz and 0.625 Hz, close to the decrease in the normal and upper body tensed sitting postures. With either 50 N or 100 N force applied to the pelvis (i.e., FP and 2FP), the principal resonance frequency decreased by about 1 Hz, which was greater than in any of the four other sitting conditions (normal, UT, FU and 2FU).

Table 9.3 Statistical significances of the effects of vibration magnitude on the principal resonance frequency in the vertical in-line apparent mass over three vibration magnitudes in each of the six sitting conditions: (a) normal; (b) FP; (c) 2FP; (d) FU; (e) 2FU; (f) UT. Wilcoxon matched-pairs signed ranks test.

vibration magnitudes	0.5[a]	1.0[a]	1.5[a]		0.5	1.0	1.5
(a) normal upright sitting				(b) FP			
0.5	-	0.006**[b]	0.002**	0.5	-	0.006**	0.001**
1.0		-	0.406	1.0		-	0.031*
(c) 2FP				(d) FU			
0.5	-	0.006**	0.002**	0.5	-	0.006**	0.001**
1.0		-	0.125	1.0		-	0.148
(e) 2FU				(f) UT			
0.5	-	0.001**	0.001**	0.5	-	0.031*	0.024*
1.0		-	0.070	1.0		-	0.242

[a] 0.5, 1.0 and 1.5 refer to vibration magnitudes (m/s^2 r.m.s.).
[b] refers to significance level (p) value; * p≤0.05; ** p≤0.01

Table 9.4 Principal resonance frequency in the median vertical in-line apparent mass with three vibration magnitudes in each of the six sitting conditions and the decrease in the frequency of the resonance as the magnitude increased from 0.5 m/s^2 r.m.s. to 1.5 m/s^2 r.m.s. in each sitting condition.

Median principal resonance frequency (Hz) of the vertical apparent mass with three vibration magnitudes in all six sitting conditions				
Sitting postures	vibration magnitudes			Decrease in the frequency (Hz) from 0.5 m/s^2 r.m.s. to 1.5 m/s^2 r.m.s. vibration
	0.5 m/s^2	1.0 m/s^2	1.5 m/s^2	
normal	5	4.500	4.500	0.5
FP	5.750	5.125	4.750	1.0
2FP	5.750	5.125	4.750	1.0
FU	5.625	5.125	5.125	0.5
2FU	5.750	5.250	5.125	0.625
UT	5.625	5.125	5.125	0.5

The decreases in the principal resonance frequency in the vertical in-line apparent mass at the seat of individual subjects in all six sitting conditions are shown in Table 9.5. No statistically significant difference was found in the decrease of the principal resonance frequency by comparing any pair of the six sitting conditions (p>0.05, Wilcoxon, Table 9.6). This shows that force applied to the body (either the pelvis or the upper body) had little or no effect on the nonlinear behaviour of seated subjects.

Table 9.5 Decrease in the principal resonance frequency of the vertical in-line apparent mass at the seat pan for individual subjects from 0.5 m/s^2 r.m.s. to 1.5 m/s^2 r.m.s. vibration in six sitting conditions.

Decreased principal resonance frequency of the vertical apparent mass from 0.5 m/s^2 r.m.s. to 1.5 m/s^2 r.m.s. vibration.						
	normal	FP	2FP	FU	2FU	UT
Sub1	0.75	0.50	0.50	0.50	0.50	0.0
Sub2	0.50	0.50	0.50	0.75	0.75	-0.25
Sub3	0.50	0.25	0.25	0.5	0.75	0.25
Sub5	0.50	1.25	0.50	0.5	1.25	0.50
Sub6	0.75	0.0	0.0	-0.25	-0.25	0.50
Sub7	0.50	0.75	1.75	0.50	0.75	0.75
Sub8	-0.25	1.00	1.25	0.25	2.00	1.50
Sub9	0.50	0.75	0.0	1.00	1.25	2.00
Sub10	0.50	0.75	0.50	0.75	0.50	0.75
Sub11	0.50	0.75	0.75	0.50	0.50	1.00
Sub12	0.50	0.75	1.50	0.50	0.50	0.75
Sub13	0	0.50	0.50	0.50	0.50	-0.75

Table 9.6 Statistical significances of the effects of muscle tension on the decreases in the principal resonance frequency in the vertical in-line apparent mass at the seat pan. Wilcoxon matched-pairs signed ranks test.

Wilcoxon test of the decrease in the principal resonance frequencies of vertical apparent mass in each pair of sitting conditions					
	FP	2FP	FU	2FU	UT
normal	0.191[a]	0.375	0.516	0.168	0.828
FP	-	0.906	0.258	0.383	0.680
2FP		-	0.516	0.754	0.492
FU			-	0.156	0.725
2FU				-	0.425
UT					-

[a] refers to significance level (p) value; * p≤0.05; ** p≤0.01

9.4 Discussion

9.4.1 Method of using a spring balance to provide fore-and-aft external force to the body

A spring balance was used to apply 50-N or 100-N static forces to the upper body or to the pelvis (i.e., iliac crest) to increase the activity of muscles in specific body regions. A belt with a spring

balance is not by itself expected to affect the principal resonance of the vertical in-line apparent mass at the seat around 5 Hz. An eight degree-of-freedom model of a subject of 69 kg in the normal sitting posture has been developed in Chapter 7. A spring (k_s) of stiffness 1250 N/m (i.e., 6 cm for 10 kg pulling force) was added to connect the upper body to a rigid surface (Figure 9.7) to represent the external force applied conditions studied in the present study. The remaining parameters in the model were not changed (Chapter 7). No difference was found between the vertical in-line apparent masses at the seat pan predicted with and without adding a fore-and-aft spring (k_s), and adding a fore-and-aft spring slightly decreased the predicted fore-and-aft cross-axis apparent mass at the seat (Figure 9.8). The model calculated the biodynamic response (e.g., apparent mass) from the equilibrium position and assumed no changes in the parameters in the model, which may not be the case in the real human. Adding an external force will alter the muscle activity in the body, so that some values of the parameters in the model, such as the stiffness of the muscles or the stiffness of the joints interconnecting the body segments, will change, and causes alternations in the biodynamic responses.

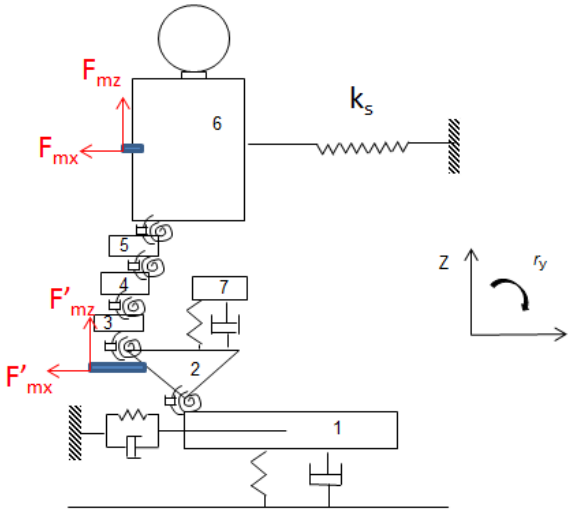

Figure 9.7 Eight degree-of-freedoms multi-body model developed in Chapter 7 with adding a spring (k_s) to T5 in the fore-and-aft direction. The remaining parameters are the same as the model in the normal sitting posture in Chapter 7.

The activity of the muscles of the back of a seated human body exposed to whole-body vibration can be subdivided as 'tonic muscle activity' and 'phasic muscle activity'. The tonic muscle activity is defined as the average r.m.s. of the EMG produced to maintain the stability of posture, while the phasic muscle activity is defined as the standard deviation of the averaged r.m.s. of the EMG, which varies during each cycle of vibration (Robertson and Griffin, 1989). The increase in muscle activity when applying an external force to the body, or by voluntarily tensing the muscles in the body, is associated with an increase in the tonic muscle activity generated to maintain a stable posture.

With forces applied to the pelvis (i.e., FP and 2FP), the tonic activity of the muscles around the pelvis (e.g., gluteal muscles) and in the lower lumbar region (e.g., psoas major) are assumed to have increased in order to maintain the upright sitting posture. Subjects were asked to maintain a

relaxed upper body, so that some muscles in the lumbar region (e.g., erector spinae in the lumbar region) and in the upper body (e.g., erector spinae in the thoracic region) are assumed to have been relaxed.

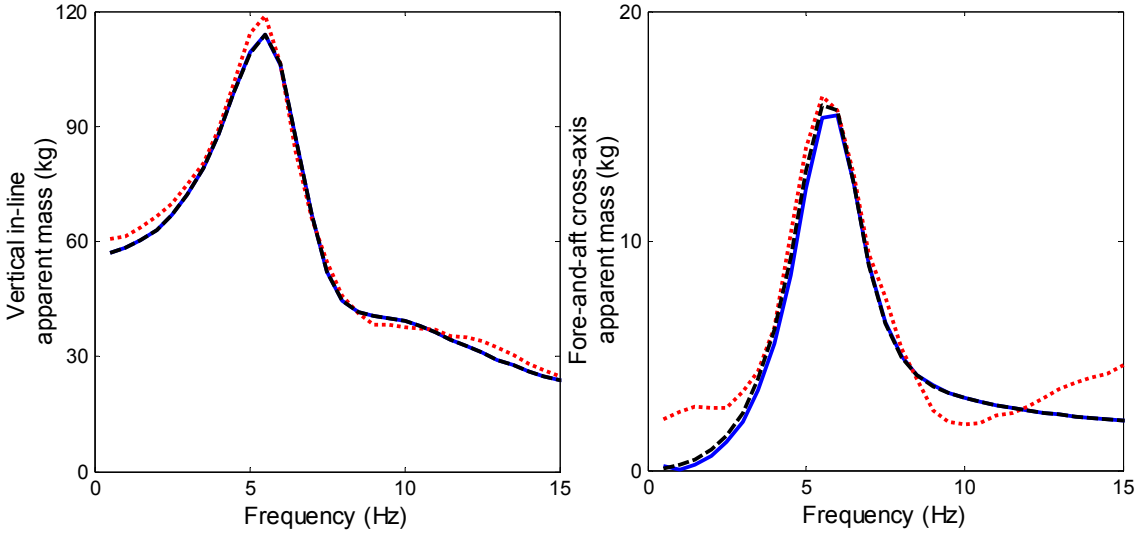

Figure 9.8 Vertical in-line apparent mass and fore-and-aft cross-axis apparent mass at the seat pan. Prediction from the multi-body model developed in Chapter 7 in the normal sitting posture ('---'); Same model with a spring (k_s) pulling the upper body at T5 in the fore-and-aft direction with stiffness of 1250 N/m ('—'); The corresponding measured apparent masses at the seat pan from Chapter 7: '...'.

With forces applied to the upper body (i.e., FU and 2FU), the tonic activity of the muscles in the upper body (e.g., erector spinae in the thoracic region: longissimus thoracis pars thoracis and illiocostalis lumborum pars thoracis) and the muscles in the lower body, including the lumbar region (e.g., erector spinae in the lumbar region: longissimus thoracis pars lumborum and illiocostalis lumborum pars lumborum, multifidus, psoas major) and around the pelvis (e.g., gluteal muscles) will have increased.

Applying force to the upper body (i.e., FU and 2FU) is expected to have increased activity in the muscles in the lumbar region and around the pelvis more than when applying the same amount of force to the pelvis (i.e., FP and 2FP), because an additional torque is applied to the lumbar and the pelvis region with fore-and-aft forces applied to the upper body.

Static friction forces between the buttocks and the seat pan are induced in the fore-and-aft direction to balance the fore-and-aft external forces applied to the body. The static friction forces are generated due to friction at the contact between the body (e.g., pelvis and thighs) and the seat. When the amount of force is too large to be pulled against by the seated human body, the subject cannot keep a stable posture during vibration, and the entire body may be pulled to rotate forward, affecting the vertical apparent mass at the seat pan (An example is given in the later text.).

When exposed to 1.0 m/s^2 r.m.s. vibration, one subject (Sub 6, 68 kg) showed a principal resonance around 3.5 Hz with 100 N force applied to the upper body (i.e., 2FU), and a resonance around 4 Hz with 100 N force applied to the pelvis (i.e., 2FP), both resonances occurred at a lower

frequency than the principal resonance in the normal posture, which was around 4.5 Hz. The remaining subjects showed an increase in the resonance frequency with force applied at the upper body. The reduction in the frequency of the principal resonance in the vertical apparent mass at the seat pan in Subject 6 may be due to the applied force being too large and the entire body tending to be pulled to rotate forward around the contact point between the thigh and seat pan. The contact area between the buttocks and seat decreased, resulting in a decrease in the stiffness at the buttocks region and a decrease in the frequency of the principal resonance in the vertical apparent mass at the seat (Kitazaki and Griffin, 1997).

With external force applied to the body, it was noticed that some subjects adjusted their spinal curvature slightly in the lumbar spine to lean the body backward, so that the centre of gravity of the upper body moved backward. The torque generated from gravity then increased so as to balance the torque from the external force applied at the pelvis, and the activity of the muscles in the back would have reduced. This situation is similar to that reported by Robertson and Griffin (1989): some subjects may lean backward and the harness worn by the subject to apply external force to the upper body may act to some degree as a backrest, possibly causing a reduction in muscle activity. To what extent this phenomenon affects the apparent mass requires further investigation.

9.4.2 Effect of muscle tension on the vertical in-line apparent mass at the seat pan

With forces applied to the pelvis and the upper body, the majority of subjects showed an increase in the frequency of the principal resonance in the vertical in-line apparent mass at the seat (Figure 9.3; Table 9.1), presumably due to an increase in the tension of the muscles in the upper body or the lower body (i.e., lower lumbar and pelvis region) causing an increase in the overall body stiffness. With 1.0 m/s^2 r.m.s. vibration, the extent of the increase in the principal resonance frequency in the median vertical in-line apparent mass from normal upright sitting posture to any of the other five sitting conditions was similar (about 0.625 Hz, see Section 9.3.1). No significant differences in the frequency of the principal resonance in the vertical apparent mass at the seat were found between any of the applied force conditions (Table 9.1). As discussed in Section 9.4.1, the muscles in the lower body (lower lumbar and pelvis region) were tensed when forces were applied to the upper body (i.e., FU and 2FU) or to the pelvis (i.e., FP and 2FP), and the muscles in the upper body were further tensed when force was applied to the upper body (i.e., FU and 2FU). This suggests that tensing the muscles in the upper body may not have a significant effect on the frequency of the principal resonance in the vertical in-line apparent mass at the seat. Alternatively, if tensing the muscles in the upper body increased the principal resonance frequency, any such increase was insignificant relative to the increase in the resonance frequency produced by tensing muscles around the pelvis. Tensing the muscles around the pelvis may increase the stiffness of the buttocks tissues, resulting in the vibration mode involving motion of the buttocks (i.e., vertical and shear motion) occurring at a higher frequency than without tensing of the muscles around the pelvis. Such a mode of vibration may contribute to the principal resonance in the vertical apparent mass at the seat pan. Both Kitazaki and Griffin (1997) and Matsumoto and Griffin (2001) suggested that a body mode involving vertical and shear motions of the buttocks tissues may contribute to the principal resonance around 5 Hz. Tensing the muscles in the upper body may increase the

stiffness of the upper body but not increase the frequency of the principal resonance in the vertical apparent mass as much as tensing the buttocks tissues (Kitazaki and Griffin, 1997). Similar results were obtained by Matsumoto and Griffin (2001) with the use of multi-body models, and it was found that increasing the vertical stiffness of the buttocks tissues produced a greater increase in the frequency of the principal resonance in the vertical apparent mass than increasing the rotational stiffness of the joint connecting the upper body and the lumbar spine.

When the force applied to the pelvis increased from 50 N (i.e., FP) to 100 N (i.e., 2FP), tonic activity of the muscles around the pelvis further increased. However, with increased tonic muscle activity around the pelvis the principal resonance frequency did not increase further (Table 9.1, Section 9.3.1). A possible explanation may be that there is a limit to the contribution from muscle tension increasing the overall body stiffness so as to increase the frequency of the principal resonance in the vertical apparent mass at the seat pan. When the increase in muscle activity exceeds a certain amount, the body stiffness may not be further increased. An alternative explanation would be that the increase in muscle activity around the pelvis from 'FP' to '2FP' was less significant than from the normal sitting posture to 'FP' due to a nonlinear relationship between the amount of force applied to the body and the increase in the muscle activity. From the subjective responses of the subjects it was noticed that they required less effort to balance an applied force of 50 N than an applied force of 100 N, irrespective of the location of the applied force (i.e., iliac crest or T5). In the EMG studies of Robertson and Griffin (1989), an approximately linear relationship was found between the force applied (from 2.0 to 12.5 kg masses via a pulley system and the amplitude of the evoked muscle activity. The hypothesis that there is a limit to the effect of the increase in the muscle activity on the overall body stiffness seems more likely.

9.4.3 Effect of muscle tension on the fore-and-aft cross-axis apparent mass at the seat

Applying external forces to the body (around the pelvis and to the upper body), or sitting with the upper body voluntarily tensed (i.e., UT), had an insignificant effect on the frequency of the principal resonance in the fore-and-aft cross-axis apparent mass around 5 Hz (Table 9.2). The muscle tension seems to be insignificant in affecting the frequency of the principal resonance in the fore-and-aft apparent mass at the seat, which is consistent with the suggestions of Matsumoto and Griffin (2002). Compared to the normal upright sitting posture, the fore-and-aft cross-axis apparent mass at the resonance frequency around 5 Hz increased with forces applied to the pelvis or the upper body (i.e., FP, 2FP, FU and 2FU). According to the modal analysis of the seated human body from Kitazaki and Griffin (1997 and 1998), the principal resonance in the fore-and-aft apparent mass at the seat involves bending motion of spine, with vertical and fore-and-aft motions of the pelvis. With force applied to the body, the fore-and-aft motions of the pelvis and also the upper body increased (shown by the transmissibility in Figure C2.2 in Appendix C.2), contributing to the increase in the fore-and-aft apparent mass at the resonance frequency. The median fore-and-aft cross-axis transmissibilities to the pelvis and the lumbar spine (L5 and L3) and the thoracic spine (T5) showed an increase with 100-N force applied to the pelvis and the upper body (i.e., 2FP and 2FU) at frequencies from 3.5 Hz to 6 Hz with a resonance frequency around 4 to 5 Hz. A fore-

and-aft force applied to the body seems to excite the vibration modes of the seated human body associated with fore-and-aft motions of the pelvis and the lumbar spine, such as the second, third, and fourth modes reported by Kitazaki and Griffin (1998), contributing to the increase in the fore-and-aft apparent mass at the resonance frequency.

In the upper body tensed sitting posture (i.e., UT), the fore-and-aft cross-axis apparent mass at the principal resonance (around 5 Hz) of 8 of 12 subjects decreased by a range of 20% to 60% compared to the normal upright sitting posture, although no statistically significant difference was found. The above trend was opposite to the conditions when 100-N force was applied to the body (i.e., 2FU and 2FP). The fore-and-aft transmissibility to the pelvis and the lumbar spine (i.e., L5 and L3) showed a decrease in the upper body tensed posture (i.e., UT) compared to the normal sitting posture (Figure C2.2 in Appendix C.2). Possible reasons include that the subjects may reduce fore-and-aft motions of their pelvis and spine by tensing the body voluntarily in the upper body tensed posture (i.e., UT). Alternatively, the damping coefficients of the body may increase with voluntary tension of the muscles, causing a decrease in the fore-and-aft cross-axis apparent mass at the resonance, as suggested from a combined experiment and modelling study by Huang and Griffin (2006).

Applying external forces to the body (FU, 2FU, FP and 2FP) tended to have less effect on the frequency of the principal resonance in the fore-and-aft apparent mass at the seat than on the frequency of the principal resonance in the vertical apparent mass at the seat. The frequency of the principal resonances in the fore-and-aft apparent mass and vertical apparent mass of individual subject exposed to 1.0 m/s^2 r.m.s. vibration in all six sitting conditions were compared. Significant difference was found in the normal sitting posture (p=0.05, Wilcoxon), but any of the five remaining conditions showed no significant differences between the two resonance frequencies (p>0.05, Wilcoxon). In the normal sitting posture, there was no significant correlation between the frequencies of the principal resonance in the vertical and fore-and-aft apparent masses (p=0.104, r=0.516, Spearman). This suggests the principal resonance in the fore-and-aft cross-axis apparent mass and the vertical in-line apparent mass may arise from different body motions, consistent with some previous studies (e.g., Chapter 6; Nawayseh and Griffin, 2004). The principal resonance around 5 Hz in the vertical in-line apparent mass comes from a combination of different body modes merged together due to the heavy damping of the body (e.g., Kitazaki and Griffin, 1997, 1998). As sitting conditions change, there may be a change in the body modes excited at specific frequencies and different motions of the pelvis and spine. Altering these motions could affect the frequency of the principal resonance in the fore-and-aft cross-axis apparent mass at the seat and the corresponding apparent mass at resonance.

9.4.4 Effect of muscle tension on the nonlinearity of the seated human body

The nonlinear behaviour of the human body (referring to the decrease in the principal resonance frequency in the vertical in-line apparent mass with increase in the vibration magnitude) was observed in all six sitting conditions (normal, FP, 2FP, FU, 2FU, UT). The nonlinear behaviour in the normal upright sitting posture and in the upper body tensed posture (i.e., UT) was consistent with previous studies (e.g., Matsumoto and Griffin, 2002; Huang and Griffin, 2006).

No statistically significant difference was found in the amount of decrease in the resonance frequency of the vertical in-line apparent mass with increase in the vibration magnitude in any of the six sitting conditions (Table 9.6). A previous study (Matsumoto and Griffin, 2002) suggested that tensing the muscles or tissues in the buttocks or at the abdomen would significantly reduce the nonlinearity compared to a normal upright sitting posture. The differences between the findings of the effect of muscle tension on the nonlinearity in the present study and the study from Matsumoto and Griffin (2002) may be due to the differences in the subjects used in the two studies. Individual subjects may have differed in their ability to control particular groups of muscles to a particular amount of tension in two studies. The vibration magnitudes used in the two studies were also different: the study from Matsumoto and Griffin (2002) used a low vibration magnitude (0.35 m/s^2 r.m.s.) and the decrease in the principal resonance frequency may be more distinct with low vibration magnitudes than the current study. In many studies it is preferred to use a logarithmic scale of vibration magnitudes to investigate the nonlinearity (e.g., Matsumoto and Griffin, 2002; Huang and Griffin, 2006) rather than the linear change in the current study.

There are some studies suggesting that the nonlinear behaviour of the body may not be contributed from the changes of the tonic muscle activity with different vibration magnitudes (Huang, 2008). The increase in the muscle activity by applying external forces to the body or by voluntarily tensing the muscles in the body in the present study is associated with an increase in the tonic muscle activity, which was generated to maintain a stable posture. The tonic muscle activity seems not to change with vibration magnitude according to EMG studies (e.g., Robertson and Griffin, 1989), so that it will not affect the overall body stiffness. Robertson and Griffin (1989) found that the tonic activity of the erector spinae in the back tended to be similar when the vibration magnitude (sinusoidal vibration) increased from 0.8 m/s^2 to 2.5 m/s^2 over the frequency range 1 to 32 Hz. Tonic muscle activity may not be a cause of the nonlinearity (Huang, 2008), and tensing the muscles in the human body with different tonic muscle activity by applying external forces may not affect the nonlinearity of the body.

9.5 Conclusion

Applying external forces to the lower body (in the area of the lower lumbar spine, pelvis, and thighs) or the upper body can tense the muscles in these areas. Increased tension of muscles in either the lower body or the upper body increases the frequency of the principal resonance in the vertical in-line apparent mass at the seat, which is likely due to an increase in overall body stiffness.

The tensing of the muscles in the upper body results in smaller increases in the frequency of the principal resonance in the vertical in-line apparent mass than tensing the muscles in the lower body.

Tensing the muscles in the upper body and around the pelvis has little or no effect on the frequency of the principal resonance in the fore-and-aft cross-axis apparent mass at the seat. Different body motions may contribute to the principal resonances in the vertical in-line apparent mass and the fore-and-aft cross-axis apparent mass.

Chapter 10. Modelling of the effect of forward leaning sitting postures on the spinal forces

10.1 Introduction

A 'kyphotic leaning' and an 'anterior leaning' sitting posture increased the resonance frequency of the vertical in-line apparent mass at the seat pan compared to a normal sitting posture (Chapter 8). In-vivo measurements of the static spinal force found that a forward leaning sitting posture induced greater compressive spinal force than a normal sitting posture (Wilke *et al.*, 2001). It is therefore interesting to study the spinal forces in the forward leaning sitting posture when the body is exposed to vertical whole-body vibration.

The forces in the lumbar spine can be predicted from the sum of static spinal forces (caused by gravity) and dynamic spinal forces (induced by vertical vibration) using a simple multi-body model (Chapters 5 and 7). Such models calculate the static spinal force arising from both the muscle force required to maintain body posture and the force due to the gravity acting on the body mass supported on the intervertebral disc. The dynamic spinal forces were calculated from the inertial forces due to vibration transmitted to the upper body and the muscle forces arising from relative movements within the body during the vibration. In both the static and dynamic conditions, only the 'passive' muscle force was modelled in the current study, which represents the necessary forces from the muscle to maintain the stability of the posture without and with vibration. The forces generated from the voluntarily tensing of the muscles were not modelled (see Chapter 7). Forward leaning sitting postures ('kyphotic leaning' and 'anterior leaning') increase the horizontal distance between the centre of gravity of the upper body and the L5/S1 intervertebral disc. This results in static muscle activity in the body being increased relative to a 'normal' sitting posture, including the muscles in the thoracic, lumbar and pelvis regions (Chapter 8). A forward leaning posture also affects the dynamic spinal forces during vibration due to alteration of the vibration transmitted to the upper body (see Chapter 8, Section 8.3.3).

This chapter investigates how static and dynamic spinal forces at the L5/S1 intervertebral disc may be affected by 'kyphotic leaning' and 'anterior leaning' sitting postures compared to a normal sitting posture. The multi-body models developed in Chapter 7 are assumed to be capable of predicting biodynamic responses (i.e., apparent mass and body transmissibilities) and dynamic forces in the spine. The model developed in Chapter 7 will be adjusted to suit the forward leaning postures with model parameters (e.g., stiffness and damping and also spinal curvature) adjusted to predict spinal forces at L5/S1 in 'kyphotic leaning' and 'anterior leaning' sitting postures.

10.2 Method

10.2.1 Model description

An eight degree-of-freedom model with muscular system was developed in Chapter 7 to represent the human body sitting with and without a backrest. The model was capable of reflecting the effects of the backrest on the vertical and fore-and-aft apparent masses at the seat pan and the motions of the lumbar spine and the thoracic spine. In this Chapter, the same model is adjusted to the 'kyphotic leaning' sitting posture and the 'anterior leaning' sitting posture by leaning forward by 30º a kyphotic spine and an erect spine around the joint connecting the pelvis and thigh (i.e. joint r_1, Figure 10.1), respectively.

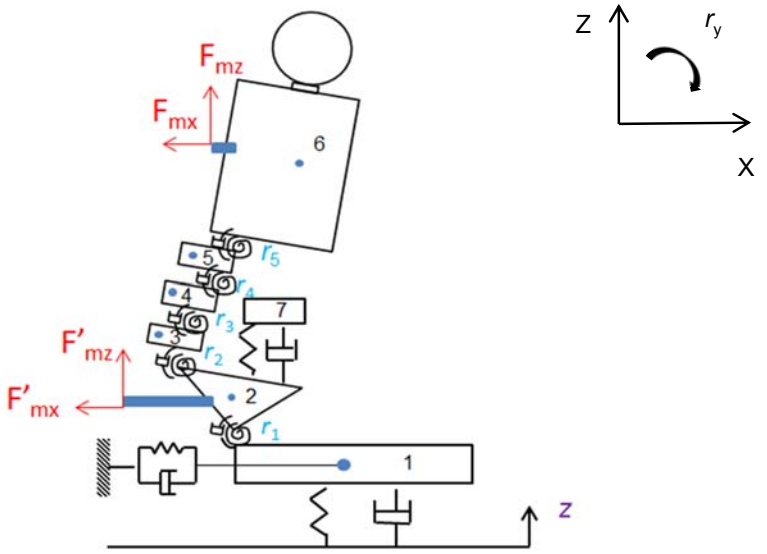

Figure 10.1 Model in the 'anterior leaning' sitting posture:1 - thighs; 2 - pelvis; 3 - L5; 4 - L4; 5 - L3; 6 - upper-body from head to L2; 7 - viscera in the abdomen; '—' Force vectors F_{mx} and F_{mz} were used to represent the muscle forces applied to the T7 spinous process. r_1 to r_5 represent the joint pelvis/thigh to L2/L3. The force vectors F'_{mx} and F'_{mz} were the muscle forces acting on the sacrum (S1).

The coordinates of the key points representing centres of vertebra bodies and the initial positions of the rotational joints in the kyphotic posture (modelled as a slouched posture) and the erect sitting posture were those defined in Chapter 5. The coordinates of the nodes representing the centre of gravity of the body segments and the rotational joints in the 'kyphotic leaning' and 'anterior leaning' sitting postures are derived by forward rotating the coordinates of the key points of the body segments and joints supported on joint r_1 by 30º in the kyphotic and erect sitting postures, respectively. The coordinates of those key points are listed in Table 10.1. The muscle forces were modelled as force vectors in the vertical and the fore-and-aft directions in both static and dynamic conditions as described in Chapter 7. The mass and inertial properties in the 'anterior leaning' and the 'kyphotic leaning' sitting postures followed the distribution in the normal sitting posture of an individual subject of 69 kg, as shown in Table 5.1 in Chapter 5.. The model in the 'anterior leaning' sitting posture is shown in Figure 10.1.

Table 10.1 Initial position for the centre of gravity of each body segment and rotational joints for a subject sitting in the 'kyphotic leaning' and the 'anterior leaning' postures.

Mass/joint	Centre of gravity of each segment(x_{i0}, z_{i0}), and coordinates of the joints (x_{ri0}, z_{ri0})	
	Kyphotic leaning (KL)	Anterior leaning (AL)
m_1 (thighs)	-	-
m_2 (pelvis)	(0.0271, 0.1029)	(0.0307, 0.1019)
m_3 (L5)	(-0.0519, 0.2152)	(-0.0452, 0.2168)
m_4 (L4)	(0.0027, 0.2303)	(0.0101, 0.2305)
m_5 (L3)	(0.0532, 0.2488)	(0.0608, 0.2479)
m_6 (head-L2)	(0.3456, 0.5028)	(0.2975, 0.5362)
m_7 (viscera)	(0.0924, 0.2261)	(0.0978, 0.2264)
r_1[a] (pelvis/thigh)	(0, 0)	(0, 0)
r_2 (L5/S1)	(-0.0095, 0.1714)	(-0.0032, 0.1736)
r_3 (L4/L5)	(0.0182, 0.1980)	(0.0252, 0.1990)
r_4 (L3/L4)	(0.0476, 0.2282)	(0.0551, 0.2278)
r_5 (L2/L3)	(0.0738, 0.2604)	(0.0806, 0.2588)
[b]*Muscle_T7*	(0.1730, 0.4823)	(0.1507, 0.4880)
[b]*Muscle_S1*	(-0.0653, 0.1843)	(-0.0593, 0.1871)

[a] r_1 represents the ischial tuberosities for which the coordinates are (0, 0), as defined in measurements by Kitazaki and Griffin (1997).

[b] *Muscle_T7* and *Muscle_S1* refers to the locations for muscle forces (i.e., T7 and S1) in the present model.

The calculation of spinal forces at the intervertebral disc L5/S1 (i.e., joint r_2) in the static and dynamic conditions followed the methods in Chapter 7, assuming the upper body is in moment equilibrium around the L2/L3 joint (i.e., joint r_5). The lever-arm system was used to calculate the static muscle forces required to maintain both sitting postures.

$$F_{mx} * d_{mx} + F_{mz} * d_{mz} = M + m * g * l \tag{10.1}$$

The definitions of the symbols (i.e., F_{mx}, d_{mx}, F_{mz}, d_{mz}, F_{mx}, M, m, g, l) follow the description in Chapter 7 (Section 7.2.2).

The moment (M_o) due to the non-concentric compression of the L2/L3 intervertebral disc in the 'anterior leaning' sitting posture was assumed to be the same as the moment calculated for the 'erect' sitting posture (Chapter 5), and the corresponding moment for the 'kyphotic leaning' posture was assumed to be the same as the moment calculated for the 'slouched' sitting posture (Chapter 5). The reasons for such assumptions are due to the same spinal curvatures from the pelvis to the

head between 'kyphotic leaning' and 'slouched' sitting postures, between 'anterior leaning' and 'erect' sitting postures as modelled in the current study.

In the dynamic condition, the force vectors of the muscle forces in the vertical and the fore-and-aft directions (i.e., F_{mx} and F_{mz}) were represented in a same way as described in Chapter 7:

$$F_{mx} = k_{mx}(x_{t7} - x_{s1}) + c_{mx}(\dot{x}_{t7} - \dot{x}_{s1}) \tag{10.2}$$

$$F_{mz} = k_{mz}(z_{t7} - z_{s1}) + c_{mz}(\dot{z}_{t7} - \dot{z}_{s1}) \tag{10.3}$$

where k_{mx}, k_{mz}, c_{mx}, c_{mz} are the stiffness and damping coefficients related to the forces from muscle. (x_{t7}, z_{t7}) and (x_{s1}, z_{s1}) represent the displacements at the spinous process of T7 and the sacrum (S1) in the x and z directions (Figure 7.1) associated with whole-body vibration. The above expressions (Equations 10.2 and 10.3) were used in deriving the equations of motion, same as the Equations 7.5 and 7.6 in Chapter 7.

10.2.2 Equations of motion

The equations of motion of the model of the human body in the 'kyphotic leaning' and 'anterior leaning' sitting postures were the same as those of the previous model of a normal upright sitting posture (Chapter 7), with the assumption that all body parts oscillate around the equilibrium positions with small displacements in the condition of free vibration:

$$\frac{d}{dt}\left(\frac{\partial T}{\partial \dot{q}_i}\right) + \frac{\partial D}{\partial \dot{q}_i} + \frac{\partial U}{\partial q_i} = 0\ ;\ q_i = \left[x_1; z_1; \theta_2; \theta_3; \theta_4; \theta_5; \theta_6; z_7\right] \tag{10.4}$$

The kinetic energy, T, potential energy, U, and dissipation function, D, of the system were calculated as:

$$T = \frac{1}{2}\sum_{i=1}^{7} m_i(\dot{x}_i^2 + \dot{z}_i^2) + \frac{1}{2}\sum_{i=2}^{6} I_i\dot{\theta}_i^2 \tag{10.5}$$

$$\begin{aligned} D = {} & \frac{1}{2}c_1(\dot{z}_1 - \dot{z})^2 + \frac{1}{2}c_{1x}(x_1)^2 + \frac{1}{2}c_{r1}(\dot{\theta}_2)^2 + \frac{1}{2}c_{r2}(\dot{\theta}_3 - \dot{\theta}_2)^2 + \frac{1}{2}c_{r3}(\dot{\theta}_4 - \dot{\theta}_3)^2 + \frac{1}{2}c_{r4}(\dot{\theta}_5 - \dot{\theta}_4)^2 \\ & + \frac{1}{2}c_{r5}(\dot{\theta}_6 - \dot{\theta}_5)^2 + \frac{1}{2}c_2(\dot{z}_7 - \dot{z}_8)^2 + \frac{1}{2}c_{mz}(\dot{z}_{T7} - \dot{z}_{s1})^2 + \frac{1}{2}c_{mx}(\dot{x}_{T7} - \dot{x}_{S1})^2 \end{aligned} \tag{10.6}$$

$$\begin{aligned} U = {} & \frac{1}{2}k_1(z_1 - z)^2 + \frac{1}{2}k_{1x}(x_1)^2 + \frac{1}{2}k_{r1}(\theta_2)^2 + \frac{1}{2}k_{r2}(\theta_3 - \theta_2)^2 + \frac{1}{2}k_{r3}(\theta_4 - \theta_3)^2 + \frac{1}{2}k_{r4}(\theta_5 - \theta_4)^2 + \frac{1}{2}k_{r5}(\theta_6 - \theta_5)^2 \\ & + \frac{1}{2}k_2(z_7 - z_8)^2 + \frac{1}{2}k_{mz}(z_{T7} - z_{S1})^2 + \frac{1}{2}k_{mx}(x_{T7} - x_{S1})^2 \end{aligned} \tag{10.7}$$

Where the definitions of independent coordinates (i.e., the degrees of freedom and centres of gravity of each body segment) and the symbols of stiffness and damping coefficients of the joints connecting the body segments are the same as those described in Chapter 7 (the model with muscles in the normal sitting posture).

10.3 Optimisation of model parameters and prediction of transmissibilities to spine

10.3.1 Optimisation of model parameters with apparent mass

The parameters of the rotational joints (i.e., stiffness and damping) and translational springs and dampers in the two forward leaning sitting postures (i.e., KL and AL) were determined by minimising the error between the biodynamic responses predicted by the model and measured in an experiment with an individual subject (Subject 7, Chapter 8, measured with 1.0 m/s^2 r.m.s. random vertical vibration from 0.2 to 20 Hz). The error function involved the modulus and phase of both the vertical in-line and fore-and-aft cross-axis apparent masses at the seat pan in the frequencies 0.5 to 15 Hz. The error function is shown in Equation 10.8.

$$Error(\lambda) = w_1 * \sqrt{\frac{1}{N}\sum_{i=1}^{N}(\left|M_{zzs\_m}(f_i)\right| - \left|M_{zzs\_m}\, e(f_i)\right|)^2} + w_2 * \sqrt{\frac{1}{N}\sum_{i=1}^{N}(\left|M_{zzs\_ph}(f_i)\right| - \left|M_{zzs\_ph}\, e(f_i)\right|)^2} + w_3 * \sqrt{\frac{1}{N}\sum_{i=1}^{N}(\left|M_{xzs\_m}(f_i)\right| - \left|M_{xzs\_m}\, e(f_i)\right|)^2} + w_4 * \sqrt{\frac{1}{N}\sum_{i=1}^{N}(\left|M_{xzs\_ph}(f_i)\right| - \left|M_{xzs\_ph}\, e(f_i)\right|)^2} \quad (10.8)$$

where $M_{zzs\_m}(f_i)$ and $M_{zzs\_m}\,e(f_i)$ are moduli (in kg) of the predicted and measured vertical apparent mass at the seat pan at frequency f_i. $M_{zzs\_ph}(f_i)$ and $M_{zzs\_ph}\,e(f_i)$ are phases (in rad) of the predicted and measured vertical apparent mass at the seat pan at frequency f_i. Similarly, $M_{xzs\_m}(f_i)$ and $M_{xzs\_ph}(f_i)$, $M_{xzs\_m}\,e(f_i)$ and $M_{xzs\_ph}\,e(f_i)$ refer to the moduli (in kg) and phases (in rad) of the predicted and measured fore-and-aft cross-axis apparent mass at the seat pan. w_1, w_2, w_3, w_4 are the weightings added to each term. The values for the weightings are: w_1=0.5, w_2=1, w_3=0.5, w_4=1. They were set by running several iterations of the optimisation function.

An optimisation algorithm 'Complex' (Bounday, 1985) and code (Qiu and Griffin, 2011) were used to minimise the error function (Equation 10.8). The initial values of stiffness and damping coefficient and the lower and upper boundaries of these values during the optimisation process were the same as those applied when modelling the normal upright sitting posture in Chapter 7 (Table 7.3).

Comparisons between the vertical in-line apparent mass and the fore-and-aft cross-axis apparent mass measured at the seat pan and predicted by the model in both sitting postures after model calibration are shown in Figures 10.2 and 10.3. The vertical inline and the fore-and-aft cross-axis apparent masses in the normal sitting posture predicted in Chapter 7 are also shown in Figures 10.2 and 10.3.

Table 10.2 Stiffness and damping coefficients obtained for the model when sitting in the 'kyphotic leaning' sitting posture (KL) and the 'anterior leaning' sitting posture (AL).

Stiffness and damping	Kyphotic leaning (KL)	Anterior leaning (AL)
k_1 (N/m)	112234	114047
c_1 (Ns/m)	1402	1463
k_2 (N/m)	23080	27051

c_2 (Ns/m)	208	163
k_{r1} (Nm/rad)	149	58
c_{r1} (Nms/rad)	999	16
k_{r2} (Nm/rad)	58	58
c_{r2} (Nms/rad)	999	9
k_{r3} (Nm/rad)	58	58
c_{r3} (Nms/rad)	1	11
k_{r4} (Nm/rad)	58	174
c_{r4} (Nms/rad)	3	746
k_{r5} (Nm/rad)	58	58
c_{r5} (Nms/rad)	2	4
k_{1x} (N/m)	21674	50567
c_{1x} (Ns/m)	315	495
k_{mz} (N/m)	50000	50000
k_{mx} (N/m)	50000	238584
c_{mz} (Ns/m)	1	3794
c_{mx} (Ns/m)	1947	980

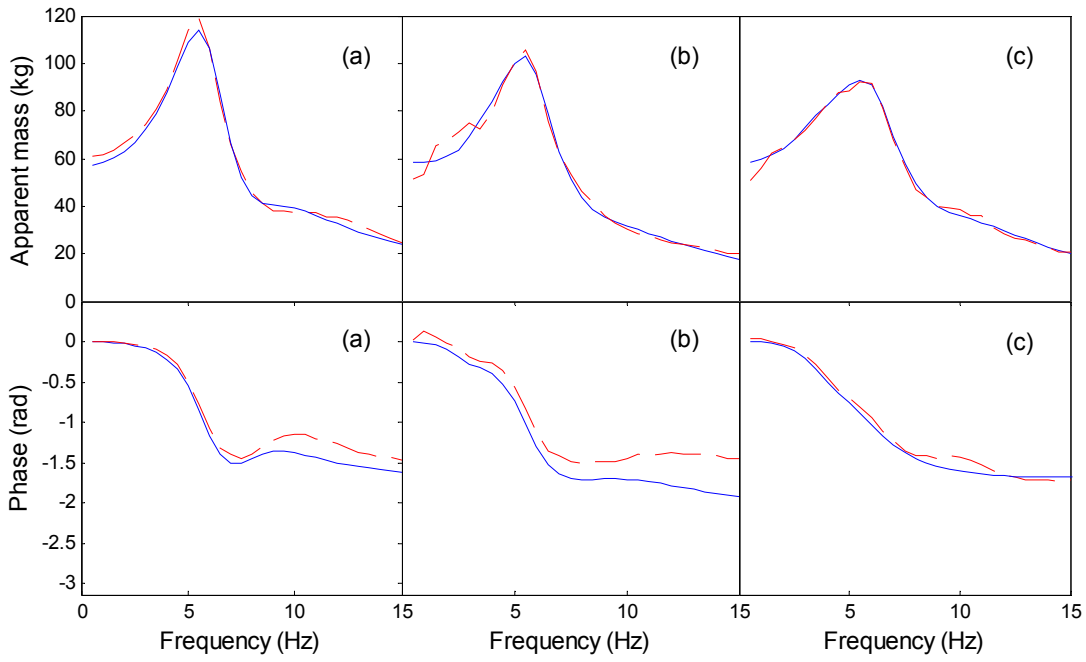

Figure 10.2 The vertical in-line apparent mass at the seat pan predicted with the model ('——') and measured from experiment ('- -') in three sitting postures: (a) normal; (b) KL; (c) AL; Top row: modulus; Bottom row: phase.

The moduli and phases of the predicted and measured vertical in-line apparent mass at the seat pan and the fore-and-aft cross-axis apparent mass at the seat pan in each sitting posture matched

(Figures 10.2 and 10.3). With the upper-body leaning forward in either the 'kyphotic leaning' or the 'anterior leaning' sitting posture, the resonance frequency of the vertical apparent mass at the seat pan increased. In the normal sitting posture, the phase of the fore-and-aft cross-axis apparent mass predicted from the model starts at 0 rad while the phase of the measured fore-and-aft apparent mass starts at 3.14 rad. The difference is due to the motions of the body at the beginning of the exposure to vibration in the experiment, as discussed in Chapter 8. In the 'kyphotic leaning' and the 'anterior leaning' sitting postures, the phase of the predicted fore-and-aft cross-axis apparent mass led the phase of the measured fore-and-aft apparent mass, the causes will be discussed later (see Section 10.5.3).

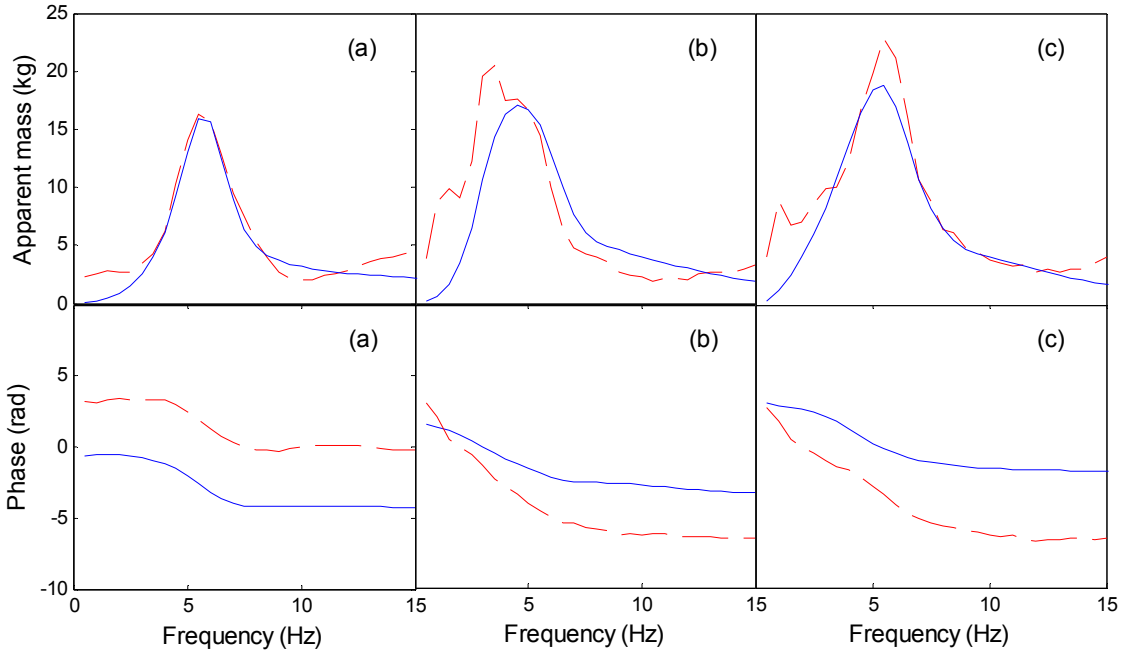

Figure 10.3 The fore-and-aft cross-axis apparent mass at the seat pan predicted with the model ('——') and measured from experiment ('- -') in three sitting postures: (a) normal (b) KL (c) AL; Top row: modulus; Bottom row: phase.

10.3.2 Predictions of body transmissibilities

With the calibrated model, the vertical in-line and the fore-and-aft cross-axis transmissibilities to the lumbar spine (L3) and thoracic spine (T5) were predicted and compared with the corresponding measured transmissibilities as measured in Chapter 8 (Figures 10.4 to 10.7). The vertical transmissibility to L3 predicted by the models in the 'kyphotic leaning' and the 'anterior leaning' sitting postures tended to be overestimated at frequencies greater than 7 Hz compared to the measured transmissibility. Both the vertical and the fore-and-aft transmissibility to T5 predicted with the model fitted the measured transmissibilities, but there were some differences shown at the resonance frequency and transmissibility at the resonance frequency in the 'kyphotic leaning' and 'anterior leaning' sitting postures (Figures 10.6 and 10.7).

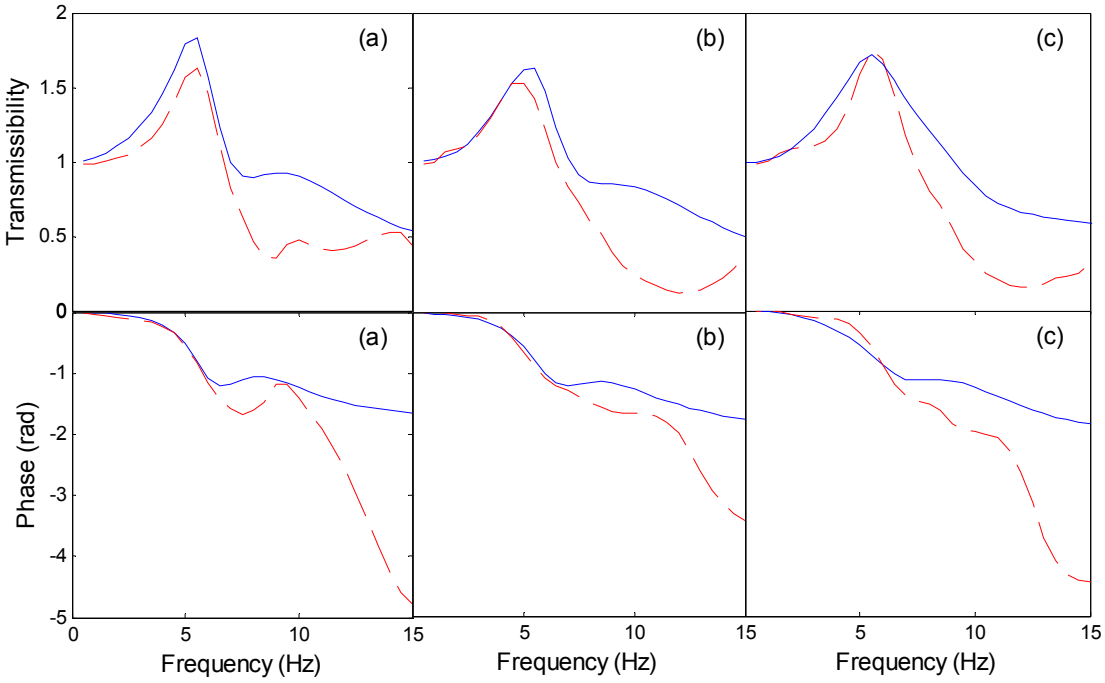

Figure 10.4 The vertical in-line transmissibility to L3 predicted with the model ('——') and measured from experiment ('- -') in three sitting postures: (a) normal (b) KL (c) AL; Top row: modulus; Bottom row: phase.

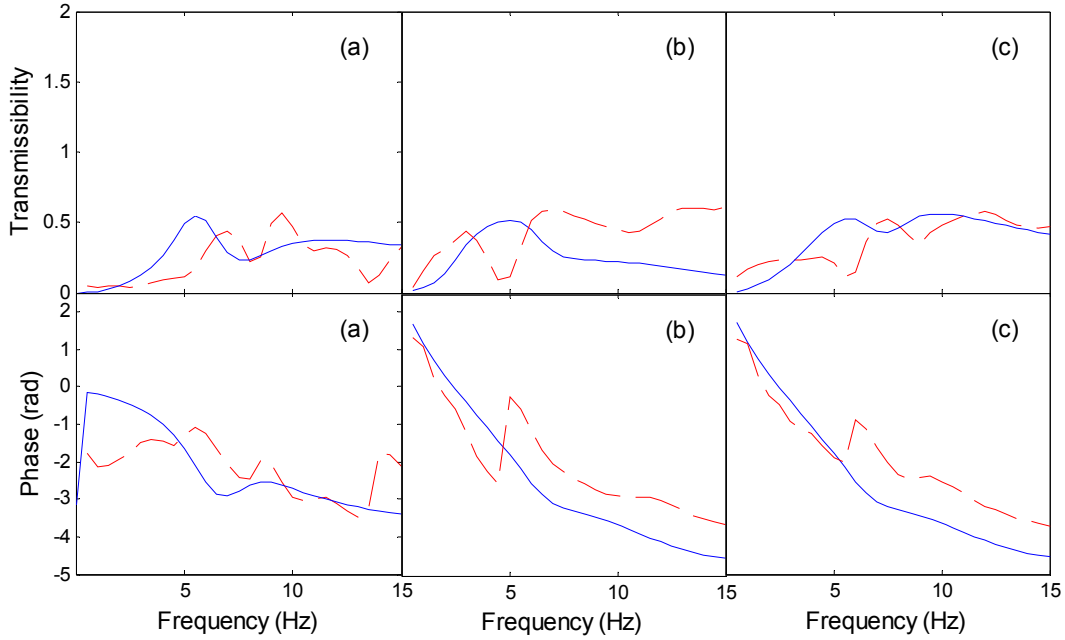

Figure 10.5 The fore-and-aft cross-axis transmissibility to L3 predicted with the model ('——') and measured from experiment ('- -') in three sitting postures: (a) normal (b) KL (c) AL; Top row: modulus; Bottom row: phase.

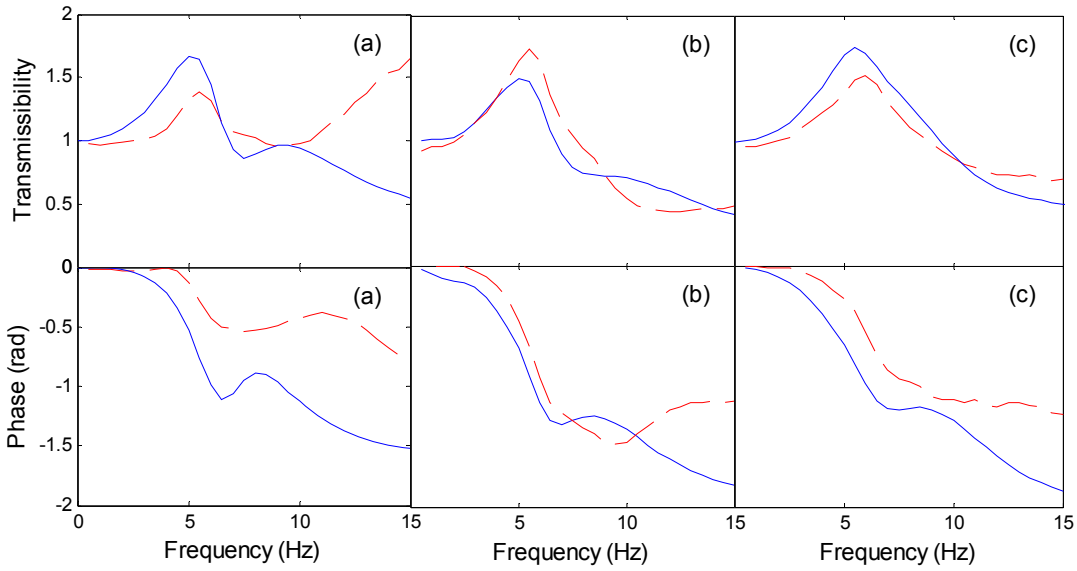

Figure 10.6 The vertical in-line transmissibility to T5 predicted with the model ('——') and measured from experiment ('- -') in three sitting postures: (a) normal (b) KL (c) AL; Top row: modulus; Bottom row: phase.

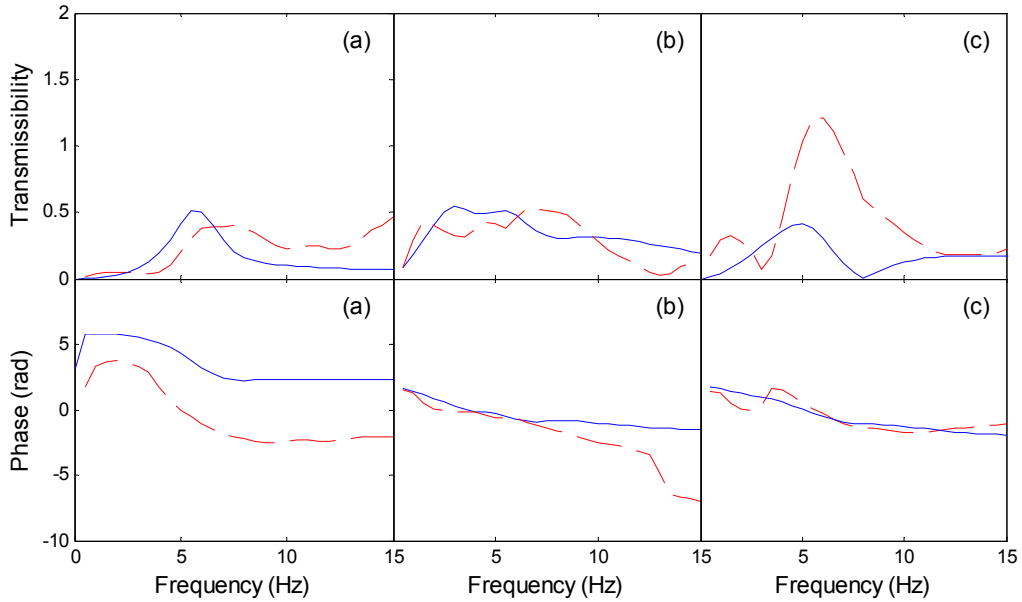

Figure 10.7 The fore-and-aft cross-axis transmissibility to T5 predicted with the model ('——') and measured from experiment ('- -') in three sitting postures: (a) normal (b) KL (c) AL; Top row: modulus; Bottom row: phase.

10.4 Predictions of static and dynamic spinal forces at L5/S1

10.4.1 Static spinal forces in 'kyphotic leaning' and 'anterior leaning' sitting postures

Based on the lever-arm system, the muscle forces required to maintain the body stability in the vertical and the fore-and-aft directions (F_{mx} and F_{mz}) were calculated. The static vertical spinal force at L5/S1 ($F_{L5/S1\_z\_s}$) was then calculated as the sum of the vertical muscle force and the force due to the gravity of the body mass supported on the intervertebral disc, as discussed in Section 10.1. The static fore-and-aft spinal force at L5/S1 ($F_{L5/S1\_x\_s}$) was assumed to equal to the fore-and-aft muscle force to maintain the force balance at the disc L5/S1, as shown in the lever-arm system in Chapter 7 (Figure 7.2). The static vertical spinal force and the static fore-and-aft spinal force in each sitting posture are shown in Table 10.3.

Table 10.3 Prediction of muscle forces and static spinal forces in the vertical and the fore-and-aft directions in three sitting postures: normal sitting posture (normal), 'kyphotic leaning' (KL) sitting posture and 'anterior leaning' (AL) sitting posture.

Predicted static spinal forces (N) at L5/S1 in the vertical direction of Subject 7 of 69 kg			
	normal	Kyphotic leaning (KL)	Anterior leaning (AL)
F_{mz} (N)	264	945	691
$F_{L5/S1\_z\_s}$ (N)	513	1195	941

Predicted static spinal forces (N) at L5/S1 in the fore-and-aft direction of Subject 7 of 69 kg			
	normal	Kyphotic leaning (KL)	Anterior leaning (AL)
F_{mx} (N)	23	756	482
$F_{L5/S1\_x\_s}$ (N)	23	756	482

When sitting in the 'kyphotic leaning' posture, both the vertical and the fore-and-aft muscle forces increased compared to a normal sitting posture. The static vertical spinal force at L5/S1 increased to become twice as much as that in the normal sitting posture, while the fore-and-aft spinal force increased about 35-fold. When sitting in the 'anterior leaning' posture, both the static vertical spinal force and the static fore-and-aft spinal forces increased compared to the normal sitting posture, but both forces were smaller than those in the 'kyphotic leaning' sitting posture (Table 10.3).

10.4.2 Dynamic spinal forces in the 'kyphotic leaning' and the 'anterior leaning' sitting postures

The dynamic spinal force at L5/S1 was calculated as the vector sum of the dynamic muscle force and the inertial forces from the body mass supported on the L5/S1 disc during vibration in both the vertical and the fore-and-aft directions (Chapter 7).

Following the same method used in Chapter 7, transfer function representing the dynamic spinal forces in the vertical and the fore-and-aft directions ($T_{L5/S1\_z}(f)$, and $T_{L5/S1\_x}(f)$) were calculated as

the sum of the transfer functions (i.e., complex value including the real and imaginary parts) from vertical seat acceleration to the muscle forces ($T_{muscle\_force\_Z}(f)$ and $T_{muscle\_force\_X}(f)$) and the inertial forces ($T_{inertial\_force\_Z}(f)$ and $T_{inertial\_force\_X}(f)$).

$$T_{L5/S1\_Z}(f) = T_{inertial\ \ force\ \_Z}(f) - T_{muscle\ \ force\ \_Z}(f) \tag{10.9}$$

$$T_{L5/S1\_X}(f) = T_{inertial\ \ force\ \_X}(f) - T_{muscle\ \ force\ \_X}(f) \tag{10.10}$$

The modulus and phase of the transfer functions from the vertical seat acceleration to the vertical and fore-and-aft inertial forces of the masses supported on L5/S1 intervertebral disc are shown in Figure 10.8 and Figure 10.9, respectively.

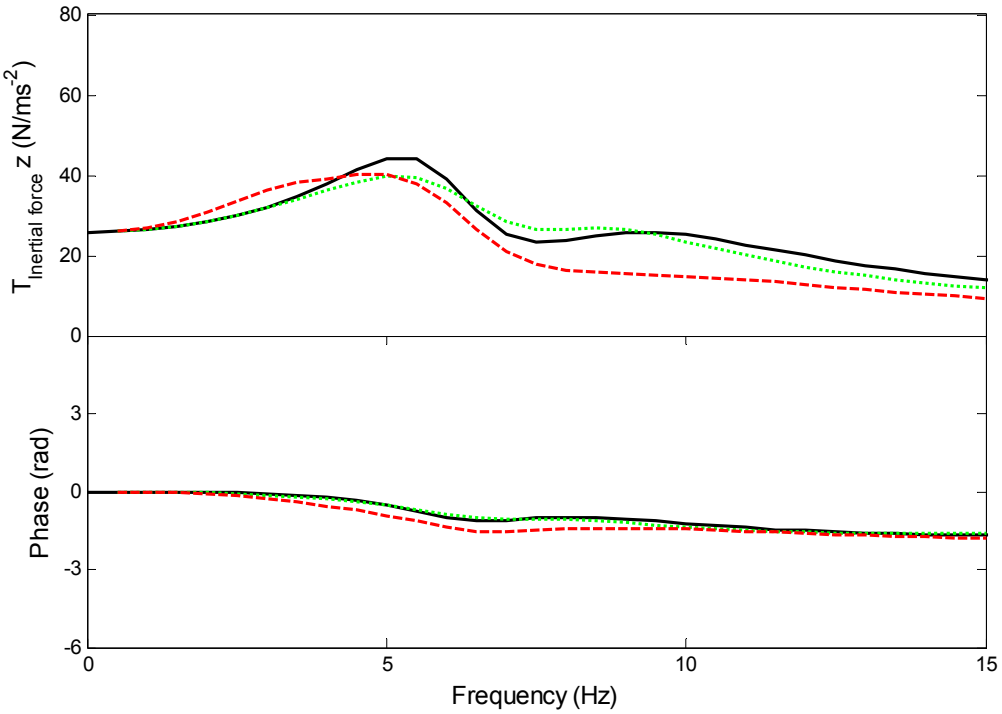

Figure 10.8 Transfer functions from vertical acceleration at the seat to vertical inertial force induced by the vertical motions of body masses supported on L5/S1 in three sitting postures: normal sitting posture (normal) ('——'); 'kyphotic leaning' sitting posture (KL) ('------'); 'anterior leaning' sitting posture (AL) ('……').

The transfer functions between the vertical acceleration at the seat and the vertical inertial force in each of the three sitting postures showed a resonance around 5 Hz. The vertical inertial forces in the 'kyphotic leaning' and 'anterior leaning' sitting postures were similar, and the moduli of the transfer function were smaller than the normal sitting posture at 5 Hz.

The 'kyphotic leaning' and the 'anterior leaning' sitting postures induced greater fore-and-aft inertial forces than the normal sitting posture at frequencies less than 5 Hz. The differences between the fore-and-aft inertial forces in the three postures at frequencies greater than 5 Hz were small. It is noticeable that the phases of the transfer function between vertical seat acceleration and the fore-and-aft inertial forces in the 'kyphotic leaning' and 'anterior leaning' sitting postures tended to start

from 3.14 rad (at 0.5 Hz), while the corresponding phase in the normal sitting posture started from 0 rad at 0.5 Hz.

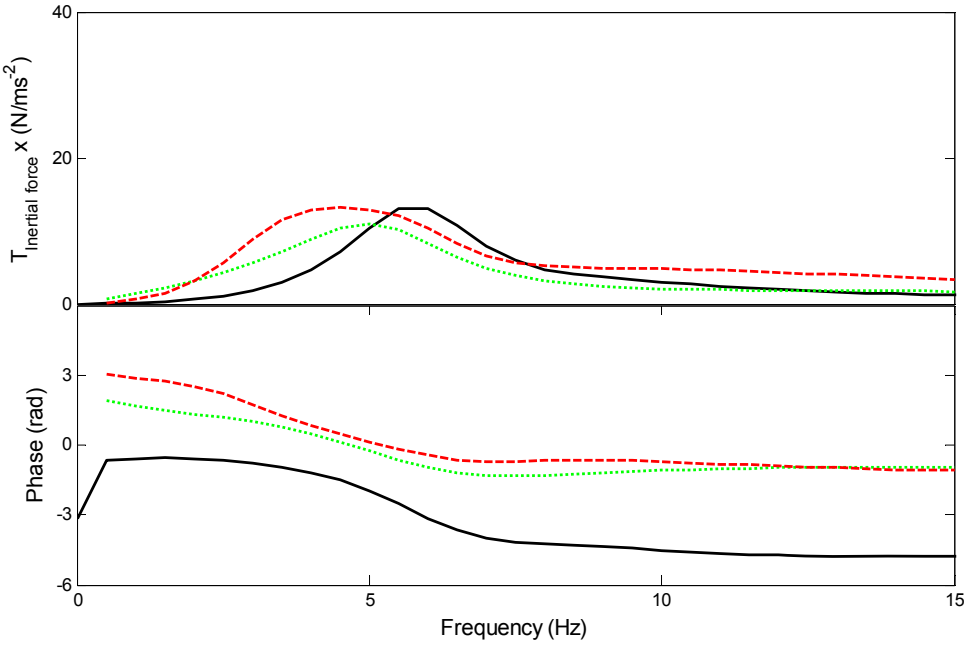

Figure 10.9 Transfer functions from vertical acceleration at the seat to fore-and-aft inertial force induced by the fore-and-aft motions of body masses supported on L5/S1 in three sitting postures: normal sitting posture (normal) ('——'); 'kyphotic leaning' sitting posture (KL) ('------'); 'anterior leaning' sitting posture (AL) ('……').

The moduli and phases of the transfer functions between vertical seat acceleration and the dynamic muscle forces in the vertical and the fore-and-aft directions are shown in Figure 10.10 and Figure 10.11, respectively. The transfer function between the vertical seat acceleration and the dynamic vertical muscle forces in the 'kyphotic leaning' and 'anterior leaning' sitting postures both had a phase started from 0 rad (at 0.5 Hz), and the forces were lower than the vertical muscle force in the normal sitting posture. The phase of the transfer function between the vertical muscle force and vertical seat acceleration in the normal sitting posture started from 3.14 rad.

The 'kyphotic leaning' sitting posture induced greater fore-and-aft muscle force than the 'anterior leaning' sitting posture and the normal sitting posture. The transfer function between the vertical seat acceleration and the fore-and-aft muscle forces in the 'kyphotic leaning' sitting posture showed a resonance around 3.5 Hz with a magnitude around 50 N/ms^{-2} (Figure 10.11). The dynamic fore-and-aft muscle force in the 'anterior leaning' sitting posture at frequencies less than 5 Hz was greater than the force in the normal posture, but the moduli of the transfer functions in both postures were less than 20 N/ms^{-2} at frequencies less than 15 Hz.

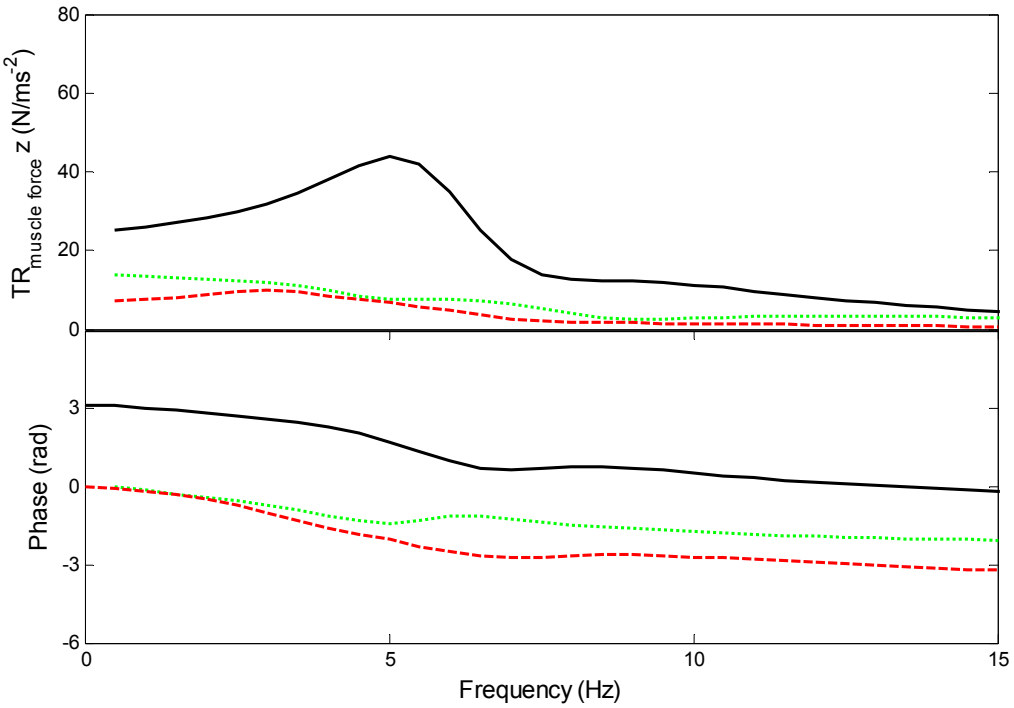

Figure 10.10 Transfer functions from vertical acceleration at the seat to the dynamic vertical muscle force in three sitting postures: normal sitting posture (normal) ('——'); 'kyphotic leaning' sitting posture (KL) ('------'); 'anterior leaning' sitting posture (AL) ('……').

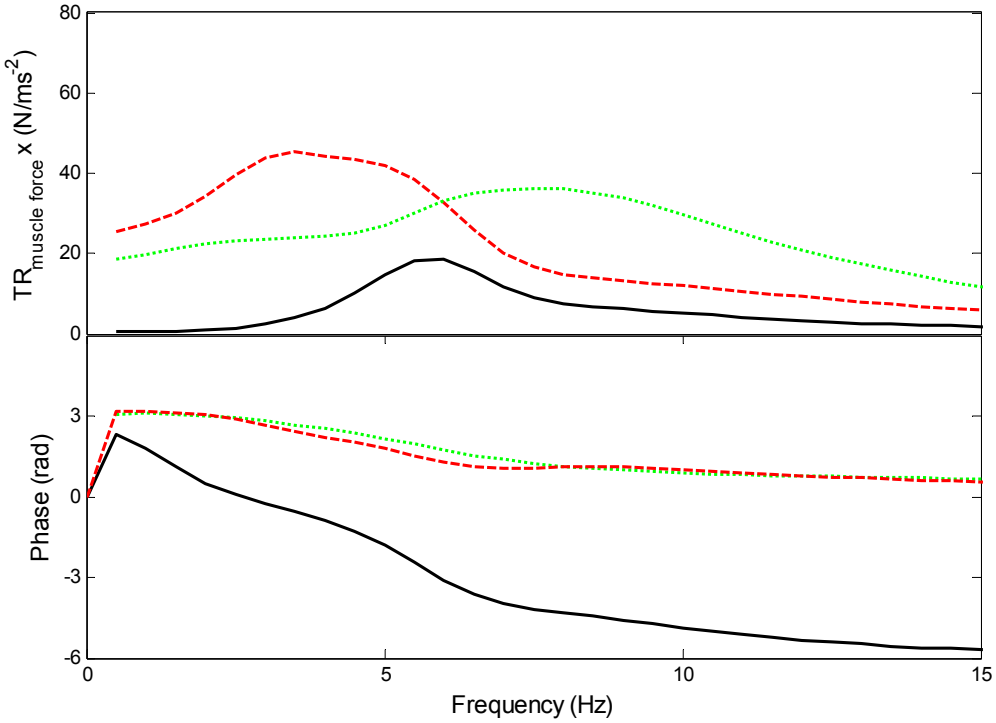

Figure 10.11 Transfer functions from vertical acceleration at the seat to the dynamic fore-and-aft muscle force in three sitting postures: normal sitting posture (normal) ('——'); 'kyphotic leaning' sitting posture (KL) ('------'); 'anterior leaning' sitting posture (AL) ('……').

According to Equation 10.9, the transfer function (i.e., complex value) between the vertical seat acceleration and vertical inertial force (Figure 10.9) was added to the transfer function (i.e., complex value) between the vertical seat acceleration and the dynamic vertical muscle force (Figure 10.10) to obtain the transfer function between the vertical seat acceleration to the dynamic vertical spinal force. The transfer function from vertical seat acceleration to the dynamic fore-and-aft spinal force was obtained in a similar way (Equation 10.10). The moduli and phases of the transfer functions between the vertical seat acceleration and the dynamic spinal forces in the vertical and fore-and-aft directions in the three sitting postures are shown in Figure 10.12 and Figure 10.13, respectively.

The transfer function between the vertical seat acceleration and the dynamic vertical spinal force in the three sitting postures all showed a resonance around 5 Hz. The vertical dynamic spinal force in the 'kyphotic leaning' and the 'anterior leaning' sitting postures were similar, but both of them were less than the dynamic vertical spinal force in the normal sitting posture at 0 to15 Hz (i.e., the maximum modulus of the corresponding transfer function: KL: 40 N/ms^{-2}; AL: 35 N/ms^{-2}; normal: 80 N/ms^{-2}). A maximum of reduction in the dynamic spinal force was about 50% around 5 Hz in the 'anterior leaning' sitting posture.

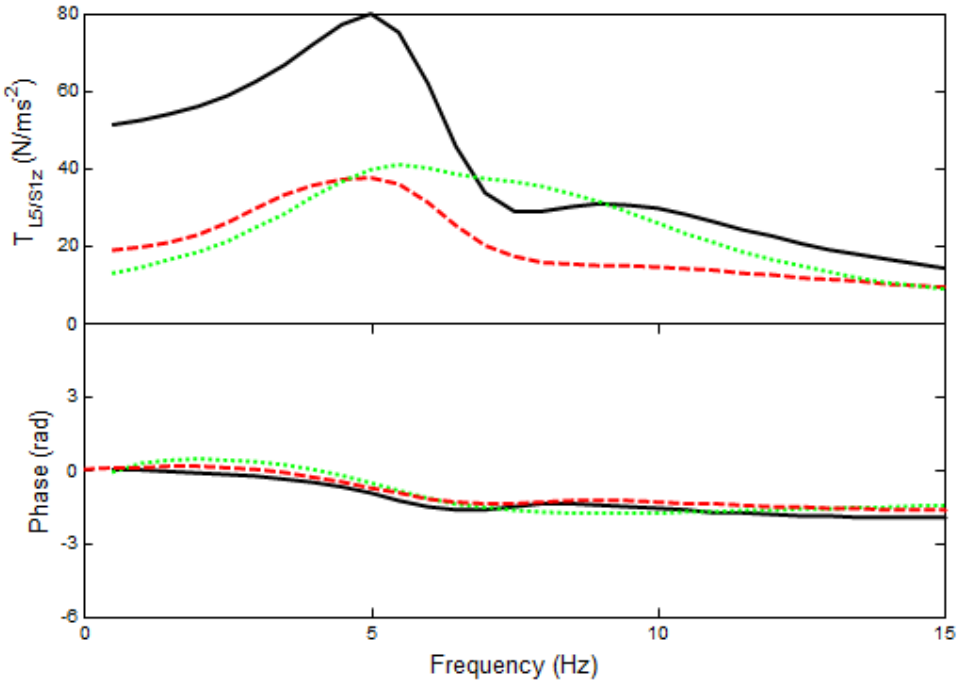

Figure 10.12 Transfer functions from vertical acceleration at the seat to the vibration induced vertical spinal force at L5/S1 in three sitting postures: normal sitting posture (normal) ('——'); 'kyphotic leaning' sitting posture (KL) ('------'); 'anterior leaning' sitting posture (AL) ('……').

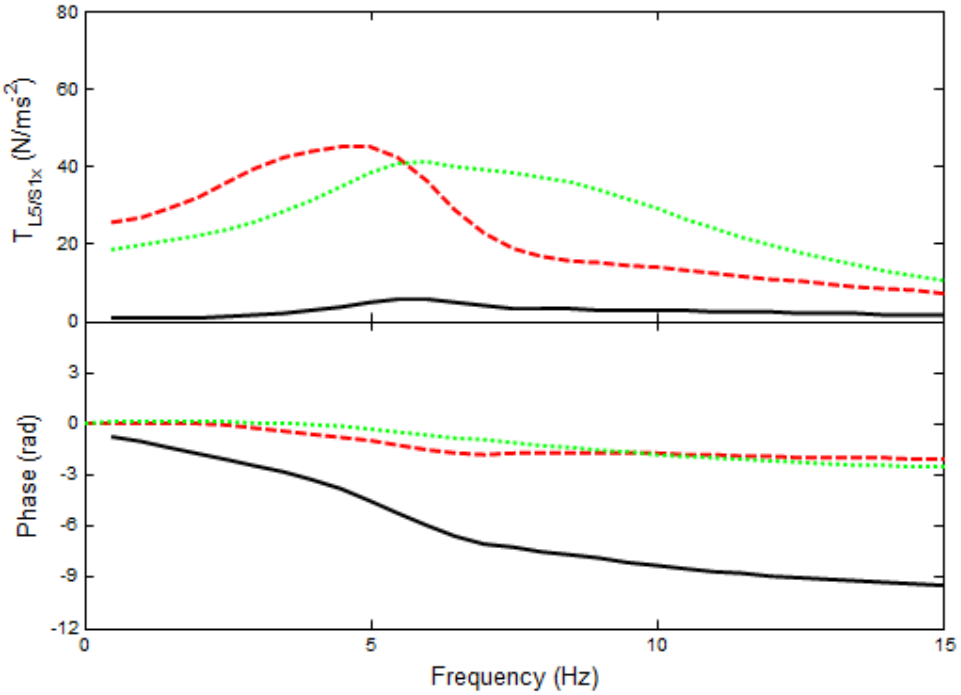

Figure 10.13 Transfer functions from vertical acceleration at the seat to the vibration induced dynamic fore-and-aft spinal force at L5/S1 in three sitting postures: normal sitting posture (NB) ('——'); 'kyphotic leaning' sitting posture (KL) ('------'); 'anterior leaning' sitting posture (AL) ('……').

The transfer function between the vertical seat acceleration and the dynamic fore-and-aft spinal force in the normal sitting posture showed a resonance around 5.5 Hz with a magnitude of 5 N/ms^{-2}, which was much smaller than the dynamic vertical force at the same frequency (80 N/ms^{-2}). In the 'kyphotic leaning' and 'anterior leaning 'sitting postures, the transfer function between the vertical seat acceleration and the dynamic fore-and-aft spinal forces both showed a resonance around 5 Hz with magnitudes of about 50 N/ms^{-2} ('kyphotic leaning') and 40 N/ms^{-2} ('anterior leaning'), respectively. The dynamic fore-and-aft forces in the 'kyphotic leaning' and 'anterior leaning' sitting postures were greater than the dynamic fore-and-aft force in the normal sitting posture at frequencies less than 10 Hz.

10.5 Discussion

10.5.1 Static spinal force

The use of a lever-arm system predicted an amount of vertical and fore-and-aft static spinal forces in three sitting postures (Table 10.3) close to the forces from in-vivo measurements (e.g., Sato *et al.*, 1999; Wilke *et al.,* 2001). The compressive pressure at L3/L4 of a subject (70 kg) sitting in different postures were measured by Wilke *et al.* (2001), including bent forward sitting postures with and without the elbows supported on the thigh and flexed actively forward sitting posture (muscle tensed in the back) (Table 10.4). With an average disc area of 18 cm^2 from the anthropometric measurement (Sato *et al.*, 1999), the compressive spinal forces were calculated by multiplying the disc area with the compressive pressure, as shown in Table 10.4.

Table 10.4 In-vivo measured compressive forces at L4/L5 measured from Wilke *et al.* (2001) of a subject (70 kg) sitting in different postures, including the normal upright and bent forward sitting postures.

Postures	Normal upright	Erect bent forward	Flexed forward with elbows on thigh	Flexed actively forward
Measured compressive spinal pressure at L4/L5	0.45 MPa	0.63 MPa	0.43 MPa	0.9 MPa
Converted compressive spinal force at L4/L5	810 N	1134 N	774 N	1620 N

In the normal sitting posture, the predicted static vertical spinal force was 513 N, while the measured was 810 N. In the 'kyphotic leaning' sitting posture, the model predicted a vertical spinal force of 1195 N, corresponding to the measured force of 1620 N in a flexed actively forward sitting posture, which is similar to the 'kyphotic leaning' sitting posture with the hands not supported on the thigh used in the experiment. The static vertical spinal force predicted in the 'anterior leaning' sitting posture was 941 N, close to the measured force in the erect bent forward sitting posture (1134 N). The discrepancy found in the predicted and measured spinal forces was partly due to the differences in the subjects (e.g., stature and weight), and partly due to some inaccuracy in estimating the spinal force from the measured pressure, as the stress was assumed to unevenly distribute over the intervertebral discs (Chapters 5 and 7). Although there were some deviations, the use of a lever-arm system in the present study predicted reasonable amount of static spinal forces in each sitting posture.

The present study also predicted an increase in the vertical spinal forces with body leaning forward (i.e., 'kyphotic leaning' and 'anterior leaning'), consistent with the data from the in-vivo measurements (Table 10.4). The reasons may be partly due to the increased horizontal distance between the intervertebral disc (L5/S1) and the centre of gravity of the body mass supported on the disc in the forward leaning postures (i.e., 'KL' and 'AL'), resulting in an increase in the torques applied on the intervertebral disc from the force due to gravity. Both forward leaning sitting postures also induced greater static fore-and-aft spinal forces than the normal sitting posture, as the muscles in the back generates downward forces with both vertical and fore-and-aft components (see Chapter 2, Section 2.5.3).

The static spinal forces in the vertical and the fore-and-aft directions in the 'anterior leaning' sitting posture were smaller than those in the 'kyphotic leaning' sitting posture (Table 10.3). This may be due to the difference in the spinal curvature in the two postures, resulting in different positions of the centre of gravity of the upper body. The horizontal distance from the centre of gravity of upper body to the intervertebral disc (L5/S1) in the 'anterior leaning' sitting posture was smaller than in the 'kyphotic leaning' sitting posture. As a result, less force was required from the muscles to maintain the 'anterior leaning' sitting posture (Table 10.3). With a view into the muscular system in the human body, more muscle forces may generate in the back in the 'anterior leaning' sitting posture than in the 'kyphotic leaning' sitting posture. The 'kyphotic leaning' sitting posture may induce forces generated from the ligaments or joints to support the upper body. As the representation of the muscle in the current model considered the overall effect from the muscular

system, including the muscle, ligaments, and joints, the involvement of different muscular components in the two postures cannot be reflected.

10.5.2 Dynamic vertical spinal force

As discussed in Chapter 7, the models aimed at predicting spinal forces should predict reasonable dynamic spinal force at the frequency close to 0 Hz to be consistent with the static spinal forces in both the vertical and the fore-and-aft directions. It appeared, however, that the current models for the 'anterior leaning' and 'kyphotic leaning' sitting postures could not fully reflect this characteristic (see Table 10.3 and Figure 10.12).

The dynamic vertical spinal forces at the frequencies close to zero (i.e., 0.5 Hz) were predicted as 20 N/ms^{-2} (equivalent to 194 N in the static condition) for the 'kyphotic leaning' sitting posture and 10 N/ms^{-2} (equivalent to 98 N in the static condition) for the 'anterior leaning' sitting posture, respectively (Figure 10.12). The static vertical spinal forces calculated from the lever-arm system in the 'kyphotic leaning' and 'anterior leaning' sitting postures are 1195 N and 941 N, respectively (Table 10.3). The dynamic vertical spinal forces at frequencies close to zero appeared to be underestimated at frequencies close to zero (e.g., 0.5 to 1 Hz) when compared to the static spinal forces (Table 10.3). Similar situation was noticed and discussed in Chapter 7.

The underestimation of the muscle forces is associated with the model structure and values of the parameters in the model. The present model was adapted to the 'anterior leaning' sitting posture and 'kyphotic leaning' sitting posture by rotating the mass above the joint connecting the pelvis and thigh (i.e., joint r_1) forward by 30 degrees from the erect spine and kyphotic spine (Figure 10.1). The position of the spinal process of T7 lied forward beyond the position of the joint of L5/S1, as shown in Table 10.1 (i.e., the x- coordinate of T7 is greater than the x- coordinate of joint r_2). When the model was exposed to the vertical whole-body vibration, the upper body (mass m_6) started to move or lean further forward (in +x direction, supported by the measured apparent masses and body transmissibilities, as discussed in Chapter 8). This resulted in a backward (-x) acceleration of the centre of mass of the upper body (the direction of the displacement is in opposite direction to that of the acceleration assuming sinusoidal motion) and a backward force (-x) at the body-seat interface, giving a starting phase of 3.14 rad (at frequency close to zero) in both the fore-and-aft cross-axis apparent mass (Figure 10.3; also discussed in Chapter 8) and the fore-and-aft cross-axis transmissibility to T5 (Figure 10.7). At the same time, the upper body mass moved downward (-z), resulting in an upward acceleration (+z) of the upper body (m_6), giving a phase of 0 rad in the vertical in-line transmissibility to T5 (Figure 10.6). In the present model, the vertical dynamic muscle force was represented by a stiffness coefficient timing the relative displacement between the connected points (T7 and S1) and a damping coefficient timing the relative velocity between the connected points in the vertical direction (Equation 10.5). As a result, the downward motion of the upper body shortened the distance between T7 and S1 and gave a upward (+z) dynamic vertical muscle force applied to the upper body (m_6), giving a starting phase of 0 rad in the transfer function from the vertical seat acceleration to the dynamic vertical muscle force (Figure 10.10). The transfer function from the vertical acceleration at the seat to the dynamic vertical inertial force also showed a starting phase of 0 rad (Figure 10.8). According to Equation 10.9, the resulted transfer function

from the seat acceleration to the dynamic vertical spinal force showed a small amount of modulus at frequencies close to 0 Hz (Figure 10.12).

10.5.3 Dynamic fore-and-aft spinal force

Leaning the upper body forward also induced a greater amount of fore-and-aft dynamic spinal forces than a normal sitting posture. The 'kyphotic leaning' and the 'anterior leaning' sitting postures both induced greater fore-and-aft motions of the upper body (Figure 10.7) than the normal sitting posture, resulting in greater relatively motions between the muscle attachment points (T7 and S1) in the fore-and-aft direction during whole-body vibration. The predicted dynamic fore-and-aft muscle force and dynamic fore-and-aft spinal force at the frequency close to zero in the current model were also smaller than the corresponding static forces (Table 10.3 and Figure 10.13). This may be partly due to similar reasons to that discussed for the vertical spinal forces, and partly due to the parameters of the current model not being globally optimised. With different values of the model parameters the model may give different vibration modes. During the calibration of the model, there may be several sets of model parameters that can all provide reasonable apparent masses and body transmissibilities matching with the corresponding measured data. But not all sets of model parameters can reflect the physical meanings of the biodynamic system and different sets of model parameters will result in different predictions of dynamic spinal forces.

There are several strategies for determining the parameters in the current model, as discussed in Chapter 7 (Section 7.3.1). The initial values and ranges of the parameters of stiffness and damping coefficients in the current model followed the model described in Chapter 7. They were determined based on previous studies, including modelling studies (e.g., Kitazaki and Griffin, 1997; Matsumoto and Griffin, 2001), and in-vitro measurements of the spinal segments (e.g., Schultz *et al.*, 1979).

A sensitivity analysis has been conducted for the set of parameters in the current model in the 'anterior leaning' sitting posture. The effect of $\pm$30% change of the values of each parameter in the model on the principal resonance frequencies of the vertical and fore-and-aft apparent masses (M_{zzs} and M_{xzs}) at the seat pan and the corresponding apparent masses at the principal resonance frequencies was examined (Table 10.5). The above effect on the principal resonance frequencies of the vertical and fore-and-aft transmissibilities to L3 and T5, and the corresponding transmissibilities at the resonance frequencies were also examined (Table 10.6).

From the results shown in Table 10.5, the frequency of the principal resonance in the vertical in-line apparent mass at the seat was sensitive to the vertical stiffness of the buttocks elements (i.e., k_1) and the vertical stiffness of the element connecting the viscera and the pelvis (i.e., k_2). The vertical apparent mass at the resonance frequency was sensitive to the stiffness and damping of the vertical buttocks elements (i.e., k_1 and c_1), and the stiffness and damping of the elements connecting the viscera and pelvis (i.e., k_2 and c_2).

The fore-and-aft cross-axis apparent mass at the seat pan was sensitive to the fore-and-aft element of the buttocks. The principal resonance frequency of the fore-and-aft apparent mass at the seat pan was sensitive to k_1, k_2 and k_{1x}, The fore-and-aft cross-axis apparent mass at the resonance frequency was sensitive to c_1, k_{1x} and c_{1x}.

Table 10.5 Resonance frequencies (Hz) and magnitudes (kg) of the calculated vertical in-line apparent mass and fore-and-aft cross-axis apparent mass at the seat pan with ±30% changes in each model parameter in the model of the 'AL' sitting posture. The initial values of the parameters in the model are adopted from Table 10.2.

Parameters	Initial values	AM_{zzs}				AM_{xzs}			
		frequency (Hz)		magnitude (kg)		frequency (Hz)		magnitude (kg)	
		-30%	30%	-30%	30%	-30%	30%	-30%	30%
k_1 (N/m)	114047	*5.2**	*6.3*	*112.52*	*131.41*	*5.3*	*6.2*	*21.56*	*25.40*
c_1 (Ns/m)	1463	5.9	5.8	*155.50*	*109.78*	5.9	5.8	*30.21*	*21.34*
k_2 (N/m)	27051	*5.4*	*6.1*	*118.07*	*128.25*	*5.4*	*6.0*	*24.61*	*23.47*
c_2 (Ns/m)	163	5.9	5.8	*132.14*	*122.69*	5.9	5.8	*26.41*	*23.22*
k_{r1} (Nm/rad)	58	5.8	5.8	126.82	126.80	5.8	5.8	24.58	24.71
c_{r1} (Nms/rad)	16	5.8	5.8	126.32	127.24	5.9	5.8	25.77	23.71
k_{r2} (Nm/rad)	58	5.8	5.8	126.82	126.80	5.8	5.8	24.59	24.70
c_{r2} (Nms/rad)	9	5.8	5.8	126.67	126.91	5.9	5.8	25.11	24.34
k_{r3} (Nm/rad)	58	5.8	5.8	126.81	126.81	5.8	5.8	24.63	24.66
c_{r3} (Nms/rad)	11	5.8	5.8	126.69	126.88	5.8	5.8	24.88	24.51
k_{r4} (Nm/rad)	174	5.8	5.8	126.81	126.81	5.8	5.8	24.65	24.65
c_{r4} (Nms/rad)	746	5.8	5.8	126.81	126.81	5.8	5.8	24.65	24.65
k_{r5} (Nm/rad)	58	5.8	5.8	126.80	126.81	5.8	5.8	24.66	24.63
c_{r5} (Nms/rad)	4	5.8	5.8	126.82	126.80	5.8	5.8	24.71	24.59
k_{1x} (N/m)	50567	5.8	5.9	124.29	127.15	*5.6*	*6.0*	*18.55*	*27.96*
c_{1x} (Ns/m)	495	5.8	5.8	128.51	125.53	5.8	5.8	*27.57*	*22.58*
k_{mz} (N/m)	50000	5.8	5.8	126.73	126.90	5.8	5.8	24.67	24.60
k_{mx} (N/m)	238584	5.8	5.8	127.82	126.09	5.8	5.9	25.55	24.39
c_{mz} (Ns/m)	3794	5.8	5.8	126.61	126.97	5.8	5.8	25.40	24.09
c_{mx} (Ns/m)	980	5.8	5.8	126.98	126.63	5.8	5.8	24.51	24.77
Initial values	-	5.8		126.81		5.8		24.65	

*Numbers in iliac indicate changing the values of each parameter alters the response with a change greater than 10% when compared with the initial values.

Table 10.6 Resonance frequencies (Hz) and magnitudes of the calculated vertical in-line transmissibiliteis and fore-and-aft cross-axis transmissibilities to L3 and T5 with ±30% changes in each model parameter in the model of the 'AL' sitting posture. The initial value of each parameter is shown in Table 10.2.

Parameters	TR_{zz_L3}				TR_{xz_L3}				TR_{zz_T5}				TR_{xz_T5}			
	frequency (Hz)		magnitude		frequency (Hz)		magnitude		frequency (Hz)		magnitude		frequency (Hz)		magnitude	
	-30%	30%	-30%	30%	-30%	30%	-30%	30%	-30%	30%	-30%	30%	-30%	30%	-30%	30%
k_1 (N/m)	*5.0**	*6.1*	*1.79*	*1.90*	*5.3*	*6.2*	*0.58*	*0.69*	*5.0*	*6.1*	*1.80*	*1.93*	*5.0*	*5.9*	*0.48*	*0.47*
c_1 (Ns/m)	*5.8*	*5.5*	*2.30*	*1.66*	5.9	5.8	*0.82*	*0.58*	5.8	5.6	*2.34*	*1.68*	*5.7*	*5.3*	*0.59*	*0.44*
k_2 (N/m)	*5.2*	*5.9*	*1.76*	*1.96*	*5.4*	*6.1*	0.64	0.66	*5.2*	*5.9*	*1.77*	*2.00*	*5.2*	*5.6*	*0.53*	*0.45*
c_2 (Ns/m)	5.7	5.7	*1.94*	*1.87*	5.9	5.8	*0.70*	*0.64*	5.7	5.7	1.97	1.90	5.6	5.4	*0.52*	*0.47*
k_{r1} (Nm/rad)	5.7	5.7	1.90	1.90	5.9	5.9	0.66	0.67	5.7	5.7	1.93	1.93	5.5	5.5	0.49	0.50
c_{r1} (Nms/rad)	5.7	5.7	1.90	1.90	5.9	5.9	0.68	0.65	5.7	5.7	1.92	1.93	5.6	5.5	0.51	0.48
k_{r2} (Nm/rad)	5.7	5.7	1.90	1.90	5.9	5.9	0.66	0.67	5.7	5.7	1.93	1.93	5.5	5.5	0.49	0.50
c_{r2} (Nms/rad)	5.7	5.7	1.90	1.90	5.9	5.8	0.67	0.66	5.7	5.7	1.93	1.93	5.5	5.5	0.50	0.49
k_{r3} (Nm/rad)	5.7	5.7	1.90	1.90	5.9	5.9	0.66	0.67	5.7	5.7	1.93	1.93	5.5	5.5	0.49	0.49
c_{r3} (Nms/rad)	5.7	5.7	1.90	1.90	5.9	5.9	0.67	0.66	5.7	5.7	1.93	1.93	5.5	5.5	0.50	0.49
k_{r4} (Nm/rad)	5.7	5.7	1.90	1.90	5.9	5.9	0.67	0.67	5.7	5.7	1.93	1.93	5.5	5.5	0.49	0.49
c_{r4} (Nms/rad)	5.7	5.7	1.90	1.90	5.9	5.9	0.67	0.67	5.7	5.7	1.93	1.93	5.5	5.5	0.49	0.49
k_{r5} (Nm/rad)	5.7	5.7	1.90	1.90	5.9	5.9	0.66	0.67	5.7	5.7	1.93	1.93	5.5	5.5	0.49	0.49
c_{r5} (Nms/rad)	5.7	5.7	1.90	1.90	5.9	5.8	0.67	0.66	5.7	5.7	1.93	1.93	5.5	5.5	0.49	0.49
k_{1x} (N/m)	5.6	5.7	*1.86*	*1.93*	*5.7*	*6.0*	*0.52*	*0.75*	5.6	5.8	1.90	1.94	*4.9*	*5.8*	*0.34*	*0.60*
c_{1x} (Ns/m)	5.7	5.7	1.90	1.90	5.8	5.9	*0.72*	*0.63*	5.7	5.7	1.94	1.92	5.5	5.6	*0.53*	*0.47*
k_{mz} (N/m)	5.7	5.7	1.89	1.91	5.9	5.9	0.67	0.66	5.7	5.7	1.92	1.93	5.5	5.5	0.49	0.49
k_{mx} (N/m)	5.7	5.7	1.90	1.90	5.9	5.8	*0.76*	*0.62*	5.7	5.7	1.94	1.92	5.4	5.6	0.50	0.50
c_{mz} (Ns/m)	5.7	5.7	1.90	1.90	5.8	5.9	0.67	0.66	5.7	5.7	1.93	1.93	5.5	5.5	0.51	0.48
c_{mx} (Ns/m)	5.7	5.7	1.90	1.90	5.9	5.9	0.67	0.66	5.7	5.7	1.93	1.92	5.5	5.5	0.49	0.50
Initial values	5.7		1.90		5.9		0.67		5.7		1.93		5.5		0.49	

*Numbers in iliac indicate changing the values of each parameter alters the response with a change greater than 10% when compared with the initial values.

From the sensitivity analysis of the parameters on the body transmissibilities in Table 10.6, the frequencies of the principal resonances in the vertical in-line transmissibilities and fore-and-aft cross-axis transmissibilities to L3 and T5 were sensitive to the parameters of the vertical and fore-and-aft elements of the buttocks and, sometimes, the stiffness or damping of the translational element connecting the viscera and the pelvis.

The fore-and-aft transmissibilities to L3 and T5 at the principal resonance frequencies were sensitive to the fore-and-aft stiffness of the muscle force (i.e., k_{mx}). However, neither the resonance frequency nor the magnitude at the resonance frequency of the biodynamic response (i.e., apparent mass and body transmissibiliteis) were sensitive to the vertical stiffness and damping of the muscle force (i.e., k_{mz} and c_{mz}). The above responses were not sensitive to the parameters of the rotational joints connecting the body segments (i.e., k_{r1}, c_{r1}, k_{r2}, c_{r2}, k_{r3}, c_{r3}, k_{r4}, c_{r4}, k_{r5}, c_{r5}). Detailed results can be found in Table 10.6.

Based on the above discussion, the values of the parameters of the buttocks elements and viscera elements can be optimised. The optimised values of the stiffness and damping coefficients (k_1, c_1) representing the buttocks beneath the thighs, and the stiffness and damping coefficients (k_2, c_2) connecting the viscera in the current model in the 'anterior leaning' and 'kyphotic leaning' sitting postures are close to the relevant parameters in the model developed by Matsumoto and Griffin (2001).

It is noticed that the values of some parameters (e.g., k_{r1}, c_{r1}, c_{1x}, k_{mz}, k_{mx}, c_{mz}) in the 'kyphotic leaning' sitting posture reached the limit of the boundaries set for the optimisation process. Similarly, the stiffness and damping parameters related to the muscle forces (i.e., k_{mz}, k_{mx}) reached the limit during the optimisation process. One criterion for selecting parameters of the model is to select the set of parameters giving a modulus of the above transfer function at frequencies close to 0 Hz (at 0.5 Hz) which can predict the static vertical spinal force close to the prediction from the lever-arm model (Chapter 7, Section 7.3.1). As discussed in the above sections (Sections 10.5.2 and 10.5.3), the structure of the current model in the forward leaning sitting postures (i.e., 'kyphotic leaning' and 'anterior leaning') cannot satisfy the above criterion, although the predictions of biodynamic responses matched the measured responses (Sections 10.3.1 and 10.3.2). It seems more necessary to improve the structure of the current model than focus on the values of the parameters of the current model.

10.5.4 Modelling of muscles

In human body, erector spinae is one of the main groups of muscle in the back, and it lies at the back via tendons connecting with various points along spine. With the body leaning forward, the muscles deform into curved shapes and great forces are generated from the back muscles. The current simplified muscle model could not fully reflect such mechanisms.

Sitting with upper body leaning forward tilts the pelvis forward and tenses the muscles (e.g., psoas major muscles, Chapter 2, Section 2.5.3) that control the tilting of the pelvis. The psoas major connects from the lumbar to the sacrum, and it may contribute to a large amount of compressive

forces to the disc L5/S1 (Bogduk, 1997). The current model considered the effect of such muscles by merging them into the spinal discs without considering the loads it may induce.

The lack of representation of the psoas major muscles and the oversimplified representation of muscles in the back may underestimate the dynamic muscle forces and the spinal forces in the forward leaning sitting postures during vertical whole-body vibration. More studies about the muscle behaviour and the role of the detailed muscular system on the spinal forces during vibration are required so as to improve modelling of the muscles and accuracy of the predicted spinal forces.

10.6 Conclusion

The models developed from Chapter 7 for the 'kyphotic leaning' and 'anterior leaning' postures are capable of predicting vertical in-line apparent mass and fore-and-aft cross-axis apparent mass at the seat pan as well as motions of the lumbar spine and the thoracic spine during vertical whole-body vibration.

The use of a lever-arm system can predict appropriate static spinal forces used to maintain the body posture. Transfer functions between the vertical seat acceleration and the dynamic spinal forces have been calculated to describe the frequency-dependent spinal forces caused by vertical vibration. Leaning the upper body forward in either the 'kyphotic leaning' or the 'anterior leaning' sitting postures increases the distance from the intervertebral disc L5/S1 to the centre of gravity of the body mass supported on the disc, resulting in a significant increase in the static spinal forces in the vertical and fore-and-aft directions. Similarly, leaning the upper body forward in either 'kyphotic leaning' or 'anterior leaning' sitting postures induces a significant amount of dynamic fore-and-aft spinal force due to the increasing fore-and-aft motions of the upper body.

The current multi-body models in the 'kyphotic leaning' or 'anterior leaning' sitting postures may underestimate the dynamic spinal forces at frequencies close to 0 Hz in the vertical and the fore-and-aft directions, due to the current method of representing forces from muscles in the model. A model that can predict appropriate biodynamic response may not predict reasonable spinal forces. Further investigations of the modelling of muscles in the forward leaning postures are required.

Chapter 11. General discussion

11.1 Introduction

The main objective of this entire study was to advance the understanding of the forces in the spine of the seated human body when exposed to vertical whole-body vibration. Multi-body models have been developed to predict the spinal forces in different sitting postures when exposed to vertical whole-body vibration (Chapters 4, 5, 7 and 10). This chapter discusses the main questions that were formulated after a review of previous relevant studies (Chapter 2): 1) how does contact with a vertical or inclined backrest affect the biodynamic response of the seated human body, 2) how does sitting posture affect the biodynamic response of the seated human body, 3) how do the spinal forces depend on the frequency of vertical vibration, 4) how does sitting posture affect spinal forces and by what underlying mechanism, and 5) to what extent does muscle activity affect spinal forces.

Biodynamic responses (i.e., apparent masses and body transmissibilities) were measured in various sitting postures and backrest conditions (Chapters 6, 8 and 9) to advance the understanding of the moving mechanisms of the human body.

11.2 Effect of posture and backrest contact on the biodynamic response of the human body

11.2.1 Mechanism of the effects of posture and backrest contact on biodynamic responses

When exposed to vertical whole-body vibration, the apparent mass and transmissibility of the human body, including the resonance frequencies in the vertical in-line apparent mass at the seat, varied with sitting posture and backrest contacts (Chapter 6 and 8). Several different mechanisms may be responsible for the changes in apparent mass and transmissibilities with sitting posture, including: 1) parts of the body mass may be supported at locations other than the seat pan; 2) changes in muscle tension and body stiffness; 3) excitation of different body modes. These mechanisms are discussed in sequence below.

Body support may share a part of the body masses and reduce the amount of mass supported on the seat pan. Contact with an inclined backrest reduces the mass of the body supported on the seat pan but increases the fore-and-aft dynamic shearing force between the body and the seat pan. An inclined backrest increases the mass of the upper body supported on the backrest and increases the fore-and-aft cross-axis apparent masses at both the seat pan and the backrest (Chapter 6). Leaning the body forward with hands resting on the thighs may result in part of the mass of the upper body being supported on the feet (‘kyphotic leaning’ sitting posture of some subjects, Chapter 8). The above changes cause the body mass supported on the seat pan to decrease, and a corresponding increase in the principal resonance frequency in the vertical apparent mass.

Sitting with different postures may alter the tension of muscles in the body, causing alterations in the resonance frequencies in the apparent mass or body transmissibilities. Leaning the upper body forward in an 'anterior leaning' sitting posture increases the tension of the muscles in the back, which is likely to increase the overall body stiffness so as to increase the principal resonance frequency of the vertical apparent mass at the seat pan (Chapter 8). The increase in the principal resonance frequency has also been observed with an upper body tensed sitting posture in previous studies (e.g., Fairley and Griffin, 1989; Huang and Griffin, 2006). The experiment in Chapter 9 further found that tension of muscles in the lower body and tension of muscles in the upper body may both induce an increase in the principal resonance frequency of the vertical apparent mass at the seat pan, and tensing the muscles around the pelvis may be more responsible for increasing the principal resonance frequency than tensing the muscles in the upper body. Such results were consistent with the modelling studies showing that the axial stiffness of the buttocks was more sensitive to the principal resonance frequency around 5 Hz than the rotational stiffness of the 'joint' connecting the upper body and the lumbar spine (e.g., Kitazaki and Griffin, 1997; Matsumoto and Griffin, 2001).

A change in sitting posture or body contact (e.g., backrest) may also alter some of the vibration modes of the seated human body, and so alter the biodynamic responses. Previous studies have investigated the vibration modes of the seated human body (e.g., Kitazaki and Griffin, 1997 and 1998; Matsumoto and Griffin, 2001) and suggested that the principal resonance frequency of the vertical apparent mass around 5 Hz involved several body modes merged together due to the heavy damping of the body (Chapter 2, Section 2.3.6). Kitazaki and Griffin (1998) suggested the fourth (4.9 Hz) and fifth body modes (5.6 Hz) may contribute to the principal resonance frequency, consisting of an entire body mode including the bending of the spine, vertical motions of viscera and vertical and shear deformations of the buttocks tissues. Matsumoto and Griffin (2001) suggested that the resonance of the apparent mass around 5 Hz may be attributed to a vibration mode consisting of vertical motion of the pelvis and legs and a pitch motion of the pelvis. Significant correlations have been found between the principal resonance frequency of the vertical apparent mass at the seat pan and each of the resonance frequencies in the vertical transmissibilities to the pelvis, lumbar spine, and thoracic spine in a normal sitting posture (Chapter 6), consistent with the fourth and fifth body modes from Kitazaki and Griffin (1998).

An inclined backrest appears to separate two of the body modes thought to contribute to the principal resonance around 5 Hz in the vertical apparent mass at the seat pan when sitting with no backrest, resulting in a broad peak or even two peaks over the frequency range 4 - 8 Hz (Chapter 6).

Sitting with the upper body leaning forward may excite vibration modes of the seated human body at frequencies less than 5 Hz (second and third modes reported by Kitazaki and Griffin, 1998), resulting in a resonance at 2.5 Hz in the vertical apparent mass at the seat pan. Such body modes also increase the fore-and-aft motions of the pelvis and the spine at frequencies less than 5 Hz (Chapter 8).

Altering the sitting posture may also affect the resonance frequency of the fore-and-aft cross-axis apparent mass at the seat pan in a way different from its effect on the resonance frequency in the vertical in-line apparent mass at the seat pan (Chapter 6 and 9). When there is no backrest or a vertical backrest, the resonance frequency in the fore-and-aft cross-axis apparent mass at the seat pan was correlated with the resonance frequency in the vertical apparent mass at the seat pan (Chapter 6), consistent with some previous studies (e.g., Qiu and Griffin, 2010; Zhou, 2016). However, the two resonance frequencies became less correlated with increasing inclination of the backrest (Chapter 6) and in a normal sitting posture with feet hanging (Chapter 9). This may suggest that different body modes are contributing to the resonances in the vertical in-line apparent mass and the fore-and-aft cross-axis apparent mass when sitting with the backrest is inclined or in a feet hanging posture or, possibly, other postures. It was observed in the experiment described in Chapter 8 that some individual subjects showed a principal resonance frequency in the fore-and-aft apparent mass around 3 Hz, but a principal resonance around 5 Hz in the vertical apparent mass at the seat pan in the 'kyphotic leaning' sitting posture (e.g., Subject 1 and 7). The second and third modes of the body associated with fore-and-aft motions of the pelvis and spine (Kitazaki and Griffin, 1998) may be excited in the 'kyphotic leaning' sitting posture and contribute to the differences in the resonance frequencies in the fore-and-aft and vertical apparent masses.

11.2.2 Effect of posture on the nonlinearity

The decrease in the principal resonance frequency in the vertical apparent mass at the seat pan with increasing vibration magnitude (referred to as a 'nonlinearity') has been found in all the studied postures (i.e., normal sitting with and without feet hanging, 'anterior leaning', and 'kyphotic leaning' sitting postures), consistent with previous studies involving similar postures (e.g., Matsumoto and Griffin, 2002; Mansfield and Griffin, 2002; Huang and Griffin, 2006). Tensing the muscles around the pelvis in a 'kyphotic leaning' sitting posture and in an 'anterior leaning' sitting posture seemed not to result in a reduction in the nonlinearity (Chapter 8, Section 8.4.3). Tensing the muscles around the pelvis by applying external forces to the pelvis also had an insignificant influence on the nonlinearity (Chapter 9, Section 9.4.3). The above findings in this study may seem to be inconsistent with the findings by Matsumoto and Griffin (2002). They suggested that tensing the abdominal muscles and the buttocks tended to decrease the reduction in the resonance frequency with increasing vibration magnitude (Matsumoto and Griffin, 2002). Differences in the findings in the two studies may be due to differences in the subjects. The ability to control a group of muscles at a certain amount of tension will differ between subjects, especially during a vibration exposure of 60 seconds.

Increasing the tension of muscles in the upper body with external forces applied to the body and sitting with the muscles in the upper body voluntarily tensed also brought no significant change in the extent of the nonlinearity compared to sitting in a normal posture without force applied (Chapter 9, Section 9.4.3). The above findings are consistent with some previous studies adopting an upper body tensed sitting posture (e.g., Matsumoto and Griffin, 2002; Huang and Griffin, 2006).

In a summary, the present studies suggest that muscle activity may have an insignificant influence on the nonlinearity of the seated human body. The muscle activity involved in the different sitting

postures and different sitting conditions studied in the presented study involved a change in the tonic muscle activity, which is generated to maintain postural stability. Previous EMG studies (e.g., Robertson and Griffin, 1989) found that the tonic activity of the erector spinae in the back tended to be similar when the vibration magnitude (sinusoidal vibration) increased from 0.8 m/s^2 to 2.5 m/s^2 over the frequency range 1 - 32 Hz. Therefore, the alteration in the overall stiffness of the body with an increase in the vibration magnitude may not be due to changes in the tonic muscle activity in the body, as suggested by Huang (2008).

Involuntary phasic muscle activity (i.e., variations of muscle activity due to whole-body vibration) could be responsible for part of the nonlinearity (Huang, 2008), as it changes with vibration magnitude (Robertson and Griffin, 1989). The first peak in the vertical apparent mass at the seat pan in the 'kyphotic leaning' sitting posture showed a non-statistically significant decrease in frequency with increasing vibration magnitude (Chapter 8, Section 8.4.3). Possible causes include voluntary motions of the upper body occurring at frequencies less than 3 Hz in the 'kyphotic leaning' sitting posture, and the voluntary muscular activity reducing the nonlinearity (Huang and Griffin, 2006).

11.3 Effect of sitting posture and backrest contact on vertical and fore-and-aft spinal forces

11.3.1 Static spinal forces

A lever-arm system has been used to predict the static spinal forces of the seated human body when sitting in the normal sitting posture (Chapters 4, 5, and 7), sitting with vertical and inclined backrests (Chapter 7), and in two forward leaning sitting postures ('kyphotic leaning' and 'anterior leaning', Chapter 10). The static muscle force can contribute much to the static vertical spinal force and, in some postures, the vertical static force from the muscles is greater than the force arising from gravity acting on the body mass supported by the spinal disc (Table 11.1). The static fore-and-aft spinal forces when sitting in the normal posture and forward leaning posture (KL and AL) are arise solely from the static fore-and-aft component of muscle force. When sitting against backrest, the supporting force from the backrest contributes to the fore-and-aft spinal force.

Without backrest support, the fore-and-aft and vertical spinal forces depend on the distance between the centre of gravity of the upper body and the L5/S1 intervertebral disc. With the greatest distance, the forward leaning sitting postures induce the greatest vertical and fore-and-aft static spinal forces (Chapter 10).

With backrest support, the contact point between the body and backrest may affect the static spinal force. Sitting with a vertical backrest at the lumbar support induced less vertical spinal force than sitting with a vertical backrest at the thoracic support (Chapter 7). The reasons include that the mass supported on the backrest with a lumbar support is less than with a thoracic support, because the pelvis tends to rotate forward with a thoracic support. Sitting with a vertical backrest at the lumbar support makes the contact point closer to the L5/S1 disc than sitting with a thoracic support, resulting in less torque generated from the backrest support force at the intervertebral disc

(L5/S1). Therefore, less vertical muscle force is required to balance the torque, resulting in less vertical spinal force.

Table 11.1 Prediction of muscle force and static spinal forces in the vertical and fore-and-aft directions in different sitting conditions for an individual subject: normal posture (NB), with vertical backrests (B_{0T5} and B_{0L2}), with inclined backrests (B_{10}, B_{20} and B_{30}) and in the 'kyphotic leaning' (KL) and 'anterior leaning' (AL) sitting postures.

Predicted static muscle force (N) and spinal force (N) at L5/S1 in the vertical direction of subject 7 of 69 kg								
	NB	B_{0L2}	B_{0T5}	B_{10}	B_{20}	B_{30}	KL	AL
F_{mz} (N)	264	290	465	537	623	612	945	691
$F_{L5/S1\_z\_s}$ (N)	514	524	688	737	771	701	1195	941
Force due to gravity (N)	250							

Predicted static spinal forces (N) at L5/S1 in the fore-and-aft direction of subject 7 of 69 kg[a]								
	NB	B_{0L2}	B_{0T5}	B_{10}	B_{20}	B_{30}	KL	AL
F_{mx} (N)	23	25	35	-54	-173	-293	756	482
$F_{L5/S1\_x\_s}$ (N)	23	16	-7b	-160	-338	-476	756	482

[a] The static fore-and-aft force due to the body mass supporting on the disc is zero.

[b] '-' indicates the direction of the horizontal spinal force is towards the back '-*x*' according to the axes in the sagittal plane.

11.3.2 Dynamic spinal forces

The dynamic spinal forces in each sitting condition were calculated as the sum of the dynamic muscle forces and the inertial forces associated with the vertical and fore-and-aft motions of the upper body exposed to vertical whole-body vibration. The dynamic muscle forces were represented by transfer functions between vertical acceleration at the seat to the forces in the spine.

One of the main suggestions from the current study is that the predicted dynamic spinal force should be consistent with the static spinal force in all sitting postures (Chapter 7). The body moves rigidly at very low frequencies with little relative motion inside the body. When exposed to vertical acceleration at the seat pan with a magnitude a_z at very low frequencies (close to 0 Hz), the prediction of dynamic muscle forces, backrest supporting forces (if there are any), inertial forces, and the resulting dynamic spinal forces in both the vertical and the fore-and-aft directions should be close to that predicted from the lever arm system used to calculate the static spinal force, but with the gravity (g) changed to ($g+a_z$). Expressed simply, if the static spinal force has a value of 513 N (i.e., in a normal sitting posture), the corresponding dynamic spinal force should have a value of 51 N/ms^{-2} at frequencies close to 0 Hz (Figure 11.1). The above assumption may be limited to a restricted range of vibration magnitudes, possibly less than 1 g (g=9.81 m/s^2) at which the body is able to move rigidly at frequencies close to zero (discussed in Section 11.5). The need for consistency between the prediction of forces (e.g., spinal forces, supporting forces from backrest) from the multi-body model at frequencies close to 0 Hz and the forces measured in static condition

could be used to calibrate the biodynamic models. The apparent masses at the seat pan and the backrest at frequencies close to 0 Hz represent the part of the body mass supported at the seat pan and backrest. The predictions of apparent mass from biodynamic models should give an appropriate value of the magnitude of the apparent mass close to 0 Hz so as to predict appropriate spinal forces. Biodynamic models predicting spinal forces should predict compressive and shear forces similar to the measured forces when there is no vibration. The effects of posture on the static spinal forces found by in-vivo measurements should also be reflected by the biodynamic models (as discussed in Section 11.5).

The current multi-body model is able to predict appropriate vertical and fore-and-aft dynamic spinal forces in the normal sitting posture, sitting with vertical and inclined backrests (Chapter 7), satisfying the need for 'consistency' in the model at low frequencies mentioned above. However, the dynamic spinal forces predicted in the 'kyphotic leaning' and 'anterior leaning' sitting postures tended to be underestimated, due to underestimation of the dynamic muscle forces (Chapter 10, Section 10.4.2).

Sitting with vertical and inclined backrests altered the dynamic spinal forces (vertical and fore-and-aft) in a similar manner to their effect on the static spinal forces. Similar to the static condition, sitting with an inclined backrest or sitting with the upper body leaning forward (Chapter 10) increased the fore-and-aft dynamic spinal force so that it was comparable to the vertical dynamic spinal force. For example, sitting with 30º inclined backrest (B_{30}) induced a dynamic fore-and-aft force with a modulus of 50 N/ms^{-2} at 7 Hz (i.e., the principal resonance frequency; Figure 11.2) and the vertical dynamic force had a modulus of 75 N/ms^{-2} at 7 Hz. A 'kyphotic leaning' sitting posture induced a dynamic fore-and-aft spinal force with a modulus of 50 N/ms^{-2} at 5 Hz. The appreciable fore-and-aft spinal forces in such postures arise from the fore-and-aft motions of the body (both the pelvis and the upper body).

11.4 The applicability of the current model

The lever-arm system developed in the current study to predict static spinal force seems to work well, with the vertical static spinal force in every sitting posture matching the compressive force measured in-vivo (e.g., Wilke *et al.*, 2001), both in terms of values and trends with changing sitting posture. A similar lever-arm system has been used in previous studies to calculate forces in the spine (e.g., Seidel *et al.*, 1986; Bogduk, 1997; Seidel *et al.*, 1997). Robertson adopted the lever-arm model developed from Seidel *et al.*, (1986) to calculate the compressive spinal force during vertical whole-body vibration. An EMG-force relationship was assumed to calculate muscle forces and forces from ligaments were also calculated. However, such models have assumed the whole-body is rigid which is not the case as is evident in the body transmissibilities. The development of such a lever-arm system requires consideration of body anatomy, such as the determination of the centre of gravity of body segments, the attachment locations of the muscles, lever arms of force vectors, etc. The determination of the model structure is partly based on human anatomy, and partly from assumptions (e.g., position of muscle vectors, Chapter 5 and 7), which may be an uncertainty in both the current models and other lever-arm models (e.g., Seidel *et al.*, 2001). The

lever-arm system is useful in predicting the static spinal force, but may need further adjustment to predict the dynamic spinal force.

The transfer functions from vertical acceleration at the seat to the dynamic vertical spinal forces in a normal sitting posture or a driving posture have also been derived in previous studies (e.g., Fritz, 2000; Seidel *et al.*, 2001; Verver *et al.*, 2003; Hinz *et al.*, 2007), as shown in Figure 11.1.

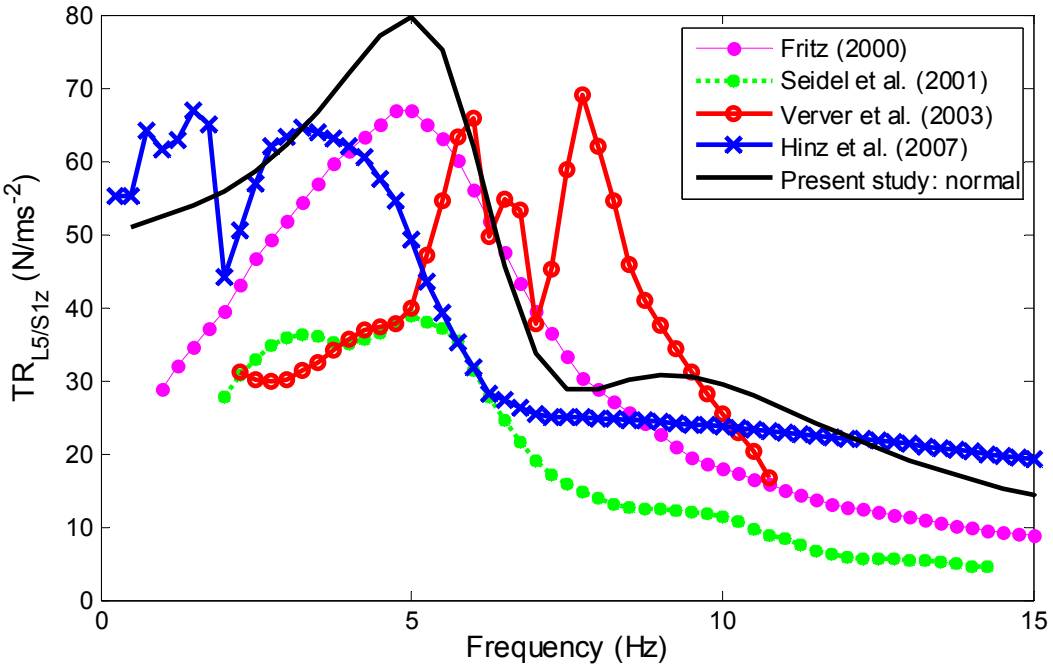

Figure 11.1 Transfer functions from vertical acceleration at the seat to vibration induced vertical spinal force at L5/S1 in the normal sitting posture (or a driving posture) in different studies: Present study, normal ('——'); from Fritz (2000), normal ('–·–'); from Seidel *et al.*, (2001), driving ('···◇···'); from Verver *et al.*, (2003), normal ('-o-'); from Hinz *et al.* (2007), driving ('-x-').

The shapes of the transfer functions have varied between different studies, due to the different methods of predicting spinal force and differences in the subjects (e.g., body mass and sitting posture). The transfer functions predicted in some studies (e.g., Fritz, 2000; Seidel *et al.*, 2001; Verver *et al.*, 2003) showed a dynamic spinal force with a modulus of 30 N/ms^{-2} at frequencies close to 0 Hz, which is similar to the body mass supported on the disc (around 30 kg) in the normal sitting posture (Figure 11.1). There may be some muscle activity at such low frequencies (e.g., Robertson and Griffin, 1989; Blüthner *et al.*, 2002), so transfer functions with the modulus starting from about 30 N/ms^{-2} may underestimate the vertical dynamic spinal forces. The above mentioned consistence between the dynamic spinal force and static spinal force should be represented in such biodynamic models. The current multi-body model for the normal sitting posture and sitting with backrest conditions showed such consistence. It was noticed that the transfer function from the vertical acceleration at the seat to the compressive spinal force derived from Hinz *et al.* (2007) showed a modulus of around 60 N/ms^{-2} at frequencies close to 0 Hz, suggesting the muscles forces may contribute to this amount of dynamic force at such low frequencies. However, the multi-peak phenomenon shown in the transfer function from this model seems to lack an explanation, although it was explained by the authors to be due to the inclination of the vertebral disc so that the

fore-and-aft body motions would contribute to the compressive forces. This model from Hinz *et al.* (2007) is currently proposed for use in a new version of ISO 2631-5.

There are some other studies indicating the crucial role of dynamic muscle forces when exposed to vibration with a high magnitude (e.g., Bazrgari *et al.*, 2008). As reviewed in Chapter 2 (Section 2.6.3), the model developed from Bazrgari *et al.*(2008) predicted a maximum compressive spinal force at L5/S1 of 3,500 N when exposed to a sinusoidal vibration of 4 Hz with the maximum acceleration of 4 g (g=9.81 m/s^2). The present model (Chapter 7) in the normal sitting posture has a dynamic force with a modulus of 75 N/ms^{-2} at 4 Hz, giving a maximum vertical spinal force at L5/S1 of 3453 N (static: 513 N; dynamic: 75*4*9.8 = 2940 N). The prediction from the present study is similar to the predictions from Bazrgari *et al.* (2008). The model developed by Bazrgari *et al.* (2008) has detailed representation of the muscle architecture. It may suggest that in some ways the simple representation of muscle forces in the current study can predict appropriate muscle forces and spinal forces in the normal sitting posture when exposed to vertical whole-body vibration.

Some studies have also predicted the dynamic fore-and-aft spinal forces in a normal or driving sitting posture (e.g., Fritz, 2000; Seidel *et al.*, 2001; Verver *et al.*, 2003), as shown in Figure 11.2. The transfer functions for the fore-and-aft spinal forces in the normal sitting posture in different studies show a small range of forces (less than 10 N/ms^{-2}), except for the study of Fritz (2000). The results from the current study show a resonance frequency around 6 Hz, similar to the transfer function obtained by Verver *et al.* (2003). The fore-and-aft spinal force should also be consistent with the prediction of static fore-and-aft spinal force. When sitting with an inclined backrest (Figure 11.2), or with the upper body leaning forward, there will be significant dynamic fore-and-aft spinal force, which should be taken into account when assessing risk to the health of the spine (Seidel *et al.*, 1997 and 2001).

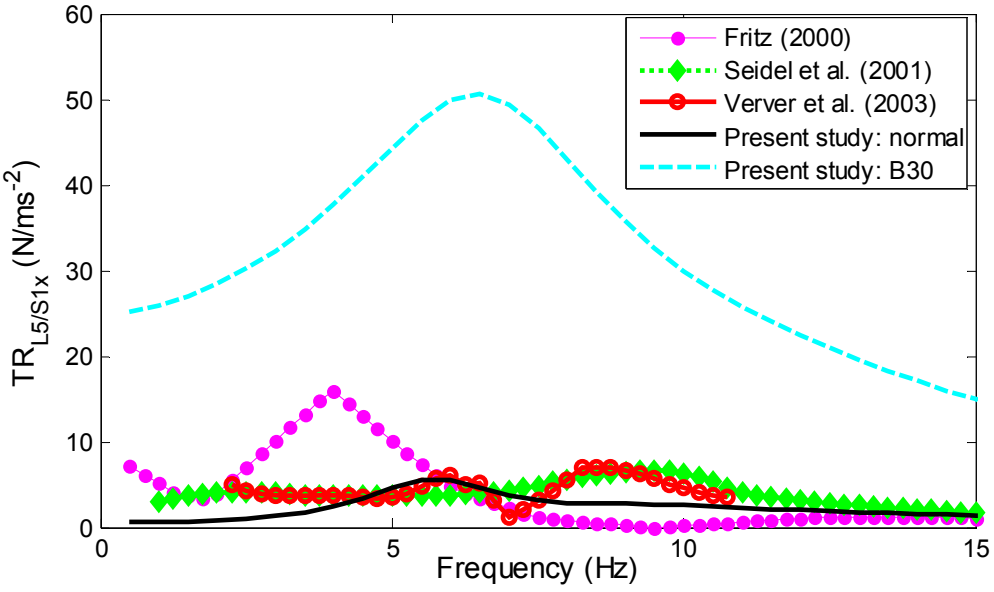

Figure 11.2 Transfer functions from vertical acceleration at the seat to vibration induced fore-and-aft spinal force at L5/S1 in the normal sitting posture (or a driving posture) in different studies:

Present study, normal ('——'); Present study, B_{30} ('- - -'); from Fritz (2000), normal ('–·–'); from Seidel *et al.*, (2001), driving ('···◇···'); from Verver *et al.*, (2003), normal ('-o-').

11.5 Limitations of the current modelling method

The current multi-body model can predict appropriate biodynamic responses, but has inevitable uncertainties in predicting muscle forces during exposure to vertical whole-body vibration (Chapter 7 and Chapter 10). Although the suggestion that the dynamic spinal forces should be consistent with the static spinal forces (Chapter 7) may help the prediction of dynamic spinal forces, the current model may not be able to maintain such consistence in some sitting postures (e.g., 'kyphotic leaning' and 'anterior leaning' sitting postures; Chapter 10). Possible reasons may be due to the modelling of the muscle forces in dynamic conditions.

The largest uncertainty in the current model lies in the modelling of muscle forces, both statically and dynamically. The muscle forces form a main component of the spinal loads, either with or without whole-body vibration, as discussed above. As assumed in previous biomechanical models (e.g., Seidel *et al.*, 1997; Bazrgari *et al.*, 2008), the muscular system provides the forces to keep the body in force and moment equilibrium. But some groups of muscles may generate more force than required to maintain body stability and are therefore balanced by other groups of muscles (e.g., Seidel *et al.*, 1997). An increase in force from any group of muscles will tend to increase the spinal forces.

The summation of all back muscles to form a single representation of muscle force (as a force vector) is a gross simplification of the complicated anatomy of the body. Such simplification in the model may be appropriate in the normal sitting posture or with vertical and inclined backrests, but not in the forward leaning sitting postures (see Chapter 10). With the upper body leaning forward, the attachment points of the muscle vectors move forward and the upper body moves downward, causing muscles forces in the upward direction at frequencies close to 0 Hz and resulting in an underestimation of the dynamic spinal forces. Possible solutions include involvement of a more detailed representation of the muscular system (see Chapter 10, Section 10.4.2), as suggested by EMG findings of differences between different groups of muscles during whole-body vibration (e.g., Blüthner *et al.*, 2002).

The current model of the dynamic muscle force as a passive system may partly reflect the muscle behaviour in real conditions. With increasing vibration magnitude at low frequencies, the body may maintain the same sitting posture by voluntarily tensing the muscles in the body, which could be represented by an increase in the stiffness of the spring representing the muscles. However, the present linear model cannot reflect this increase in the stiffness of the muscle, possibly resulting in the prediction of inappropriate motions of the body and an underestimation of spinal forces at low frequencies.

The calculation of spinal forces in the current model neglect the torque applied to the intervertebral discs. In reality there is non-concentric compression of a spinal disc, as suggested by Seidel *et al.*, (1997) with their lever-arm model. The extent of the underestimation of spinal loads due to lack of

consideration of torque may depend on the sitting posture, and would be most significant in the forward leaning sitting posture.

The current model also neglects the nonlinearity in the human response to vertical whole-body vibration (Section 11.2.2). In the normal sitting posture with high magnitude vibration (i.e., maximum 4 g sinusoidal vibration of 4 Hz; Section 11.4) the model predicts similar maximum vertical spinal forces to the model developed by Bazrgari *et al.* (2008). But whether the values and trends of the transfer function representing the dynamic spinal forces derived from the present studies are really applicable to high magnitude vibration remains to be studied. There is little understanding of the biodynamic responses of the human body and muscle behaviour when exposed to vibration of such high magnitude. Greater knowledge of muscle behaviour and the role of the muscular system in contributing to the spinal loads during vibration is desired.

A model for predicting spinal forces may need to have its application limited to a restricted range of vibration magnitudes. Both the biodynamic response (e.g., Matsumoto and Griffin, 1998; Huang and Griffin, 2006; Chapter 8 and 9; discussed in Section 11.2.2) and the muscle activity (e.g., Robertson and Griffin, 1989) change with increasing vibration magnitude and these changes are sufficient to affect the dynamic spinal forces. The limit of the vibration magnitude that the current model can be applied to is unknown, but less than ±1 g. Patelli (2016) found that with an upward shock of 1 g at frequencies less than 4 Hz, the seated human body may leave the seat and then subsequently impact with the seat. The current models do not reflect such mechanisms.

Figure 11.1 and Figure 11.2 show that the prediction of spinal forces has varied greatly in different studies. There is currently no criterion for deciding whether a model is an adequate representation or whether spinal forces are adequately predicted. One possible reason is the absence of suitable in-vivo measurement of spinal forces when exposed to whole-body vibration. The prediction of spinal forces is dependent on many various assumptions, the modelling method, the subjects to be modelled, and other factors as discussed above. Models for predicting spinal forces should represent known information as much as possible, including the body movements, muscular responses, and measurements of static spinal forces. A reflection of the effect of posture on the above responses is also desired (Kitazaki and Griffin, 1998). The effect of posture on the biodynamic responses and spinal forces may be associated with changes of muscle activity, motions of body segments, and stiffness of the buttocks tissues. The reasonable reflection of the effect of posture may suggest the model has a proper structure that is able to reflect appropriate mechanisms related to body movements and spinal forces. The model developed in the current study is able to predict the effect of variations in posture and backrest contact on the biodynamic responses and spinal forces when exposed to vertical whole-body vibration, but it may require further development of the muscular system so as to predict the effect of forward leaning sitting postures on the spinal forces.

Chapter 12. Conclusions and recommendations

12.1 Conclusions

The following conclusions are made against the 'research questions' put forward at the end of Chapter 2.

Sitting against a backrest affects the apparent mass and transmissibility of the seated human body when exposed to vertical whole-body vibration:

- Increasing the inclination of a backrest increases the mass of the upper body supported on the backrest and increases the vertical in-line apparent mass and the fore-and-aft cross-axis apparent mass at the backrest.
- Compared with a normal sitting posture without backrest, a vertical or an inclined backrest tends to increase the vertical motions of the pelvis, lumbar spine, and thoracic spine at frequencies in the range 6 to 15 Hz.
- The presence of an inclined backrest can separate vibration modes of the body that contribute to the principal resonance in the vertical in-line apparent mass at the seat pan around 5 Hz when sitting with no backrest, resulting in a broader peak or even two peaks in the vertical apparent mass at the seat pan at frequencies in the range 4 to 8 Hz.
- The presence of a vertical or an inclined backrest increases the fore-and-aft cross-axis apparent mass measured at the seat pan at frequencies in the range 1 to 15 Hz.

Changing posture can alter muscle tension in the body and the excitation of body modes, and alter the resonance frequencies in the apparent mass and transmissibility of the body:

- Leaning the upper body forward in an 'anterior leaning' sitting posture increases the tension of muscles in the back, and is likely to increase the overall body stiffness and increase the principal resonance frequency in the vertical apparent mass measured at the seat pan.
- Sitting in a kyphotic leaning' sitting posture or an 'anterior leaning' sitting posture during vertical vibration increases the fore-and-aft motions of the pelvis and spine at frequencies less than 5 Hz, and may induce a resonance in the vertical apparent mass at the seat pan around 2.5 Hz.

The forces in the spine in the vertical and fore-and-aft directions at the L5/S1 intervertebral disc can be calculated by summing the static and dynamic spinal forces in each direction. A lever-arm system can be developed based on the moment equilibrium of the lumbar intervertebral disc. It can be used to predict the static spinal forces of subjects sitting with various backrest conditions (both vertical and inclined backrests) and sitting in forward leaning postures in order to maintain the stability of the posture. Multi-body models that include the structure of the lumbar spine and muscle forces may be used to predict how the apparent mass and transmissibility of the body and forces in the spine depend on sitting condition during whole-body vertical vibration. The following

conclusions are made regarding how the predicted spinal forces depend on the frequency of vertical vibration:

- Transfer functions between vertical acceleration at the seat pan and vertical and fore-and-aft spinal forces show resonance at frequencies in the range 4 to 8 Hz, similar to the principal resonances in the vertical in-line apparent mass and the fore-and-aft cross-axis apparent mass.
- The spinal forces in both vertical and fore-and-aft directions predicted from the moduli of the transfer functions between vertical acceleration at the seat pan and dynamic spinal forces at frequencies close to 0 Hz should be close to the static spinal forces predicted with the lever-arm system to maintain the stability of the posture.

Varying sitting posture or backrest contact alters the distance between the L5/S1 intervertebral disc and the centre of gravity of the part of the body supported on the disc, so as to affect the static muscle force required to maintain posture. Motions of the spine and pelvis differ between different sitting postures and backrest conditions, resulting in different dynamic muscle forces during vertical vibration. Consequently, both the static and the dynamic spinal forces differ between sitting postures and backrest conditions:

- The predicted static and dynamic vertical spinal forces at L5/S1 are less with a vertical lumbar support than with a vertical thoracic support.
- With a backrest providing only thoracic support, increasing the inclination to 20º increases static muscle forces required to maintain the stability of the spine in both vertical and fore-and-aft directions. The predicted static spinal forces are greater when sitting with such a backrest inclined by 20˚ than when sitting in a normal posture without backrest and in all other conditions studied here with a backrest (i.e., vertical backrest providing lumbar support or thoracic support, and 10º- and 20º- inclined backrests providing only thoracic support).
- A 20º-inclined backrest providing only thoracic support also increases both vertical and fore-and-aft dynamic spinal forces during vertical vibration, due to increased dynamic force between the back and the backrest and increased motion of the spine in both directions.
- Further increases in the inclination of a backrest can decrease both the static and the dynamic spinal forces at L5/S1 due to increased support of the body mass on the backrest.
- A ‘kyphotic leaning’ sitting posture may result in the greatest static spinal force in both vertical and fore-and-aft directions at L5/S1, due to increased fore-and-aft distance between the centre of gravity of the upper body and the intervertebral disc.
- Leaning the upper body forward increases the fore-and-aft dynamic spinal force so that it may become similar in magnitude to the vertical dynamic spinal force.

Muscle activity affects the biodynamic response of the human body (i.e., apparent mass and transmissibilities) during vertical vibration of the seated body and also affects the predicted spinal forces:

- Tensing muscles in either the lower body (in the area of the lower lumbar spine, pelvis and thighs) or the upper body by applying external forces to these locations increases the principal resonance frequency in the vertical in-line apparent mass measured at the seat pan.
- Tensing the muscles in the upper body may have an insignificant effect, or at least produce a smaller increase in the principal resonance frequency than tensing the muscles in the lower body.
- In the postures studied (i.e., normal sitting without backrest, forward leaning, sitting with vertical and inclined backrests), the muscle force contributes to the spinal forces both with and without whole-body vibration.
- A representation of muscle forces is required in models predicting spinal forces.

12.2 Recommendations for future research

While these studies have explored the effects of posture on response to vertical whole-body vibration there have been no known studies of the effects of posture on human responses to mechanical shocks. It is recommended to measure the effects of variations in sitting posture on the biodynamic responses of the human body during exposure to mechanical shocks, including shocks with high magnitudes. The maximum vibration magnitude to which the current model is applicable is unknown, but possibly less than 1 g, because the body may leave the seat with shocks greater than 1 g (Patelli, 2016; Hinz *et al.*, 2007). The range of vibration magnitudes over which the current model and any other biodynamic model can be applied is uncertain. The biodynamic responses of the human body have mostly been measured with continuous random broadband vibration at magnitudes up to 2.0 m/s^2 r.m.s.

A proposed revision of ISO 2631-5:2014 employs a finite element model with a consideration of the effect of posture to evaluate the severity of vibration with peak magnitudes less than 1 g. The proposed standard also uses an artificial neural network (ANN) model to assess the severity of vibration with peak magnitudes greater than 1 g, but without considering the effect of posture. It is recommended to investigate the effects of high magnitude vibration and mechanical shocks on the prediction of spinal forces.

Some factors other than the characteristics of vibration and the posture of the body can affect the spinal forces during whole-body vibration. These factors include differences between subjects (e.g., Seidel *et al.*, 2001). It is recommended to identify the effect of the inter-subject variabilities on spinal forces and compare the size of the effect of inter-subject variability with the size of the effects of other factors including posture on the spinal forces.

It is desirable to improve the modelling of the forces from muscles with investigations of a more representative and detailed muscular system. The accuracy of models in predicting spinal forces depends on the accuracy of the modelling of the muscular system. The present model includes a simple representation of the overall forces from all back muscles and other relevant muscular elements (e.g., facet joints and ligaments). The simplification of muscles in the current model may result in an underestimation of the spinal forces when sitting in forward leaning sitting postures

during exposure to vertical whole-body vibration (Chapter 10). A more comprehensive muscular system with ligaments and muscles in different body regions has been included in some models (e.g., Hinz *et al.*, 2007; see Chapter 2). However, such models are mostly based on the response of the muscular system in static conditions. There is usually great simplification of the properties of the muscles (e.g., to linear springs) with a great reduction in the number of muscles in the models. The errors introduced by such simplifications remain to be investigated. Electromyographic studies of the responses of back muscles during whole-body vibration have shown that muscle activity varies with vibration magnitude and vibration frequency and is affected by sitting posture (e.g., Robertson and Griffin, 1989; Blüthner *et al.*, 2002). Models of the human body in static conditions have shown effects of different muscle groups in maintaining postural stability. For example, Stokes *et al.* (2011) found that the activation of abdominal muscles increased spinal stability, and the activation of abdominal muscles can affect the forces in the spine. Most existing models appear only to represent the activities of a few muscles in the body (e.g., muscles in the back) during whole-body vibration (e.g., Bazrgari *et al.*, 2008). Some models use an optimisation algorithm to determine activity in the modelled muscles during vibration (e.g., Pankoke *et al.*, 1998; Hinz *et al.*, 2007; see Chapter 2), which may be different from the true response of the muscles. With a more detailed representation of the muscular system and with a more complete representation of muscle activity during vibration, a model can improve the understanding of the relationship between the spinal forces and the activity of various groups of muscle. Such a model could also help to investigate the complexity in modelling the muscles to predict spinal force.

As recommended by Seidel *et al.* (2001), a standard such as ISO 2631-5:2003 should take into consideration the effects of posture, body contact with a seat, and fore-and-aft (shear) forces when predicting spinal forces to assess the severity of whole-body vibration. The current study found that posture and backrests can increase or decrease the spinal forces, and that some postures (e.g., sitting with an inclined backrest and sitting with the upper body leaning forward) increase the fore-and-aft spinal forces during whole-body vibration. The current standard and a proposed revision of ISO 2631-5:2003 both assume the Palmgren-Miner fatigue theory to evaluate the risks to the health of the spine, so only considering the compressive forces acting on the disc (see ISO 2631-5:2003 for details). A consideration of the damaging mechanisms associated with the shear forces acting on the disc is recommended.

The virtual absence of measurements of spinal forces in the live human body during whole-body vibration leads to difficulties in calibrating models. If the spinal forces during whole-body vibration could be measured in-vivo, the effects of vibration frequency, vibration magnitude, variations in posture, and other affecting factors the spinal forces could be studied. Studies measuring the static spinal force using the invasive methods (e.g., Kato *et al.*, 1999; Wilke *et al.*, 2001) may cause injury to the body during whole-body vibration. The spinal forces during whole-body vibration have been measured with vertebral body replacements (VBR) inserted during surgery in patients with spine problems (e.g., Rohlmann *et al.*, 2010; see Chapter 2). However, an artificial vertebra changes the structure of the spine and only measures a part of the spinal forces acting at this spinal level, and may affect the frequency-dependence of the spinal forces. In static conditions, Rohlmann *et al.* (2008) reported a compressive spinal force of 353 N for a 74 kg subject with the VBR at T12-L2,

smaller than the force (equivalent to 810 N) measured in a healthy subject of 70 kg by Wilke *et al.* (2001). It is necessary to explore whether the spinal forces of health subjects can be measured during whole-body vibration safely and reliably.

Appendix A Appendix A Effect of backrest on the biodynamic response of the human body

A.1 Resonance frequencies and magnitudes at the resonance frequency of fore-and-aft cross-axis transmissibilities to pelvis, L5, L3 and T5.

Table A1.1 First resonance of the fore-and-aft cross-axis transmissibilities to pelvis, L5, L3 and T5:

Pelvis	1st resonance											
	NB		B_{0L2}		B_{0T5}		B_{10}		B_{20}		B_{30}	
	f(Hz)	TR	f	TR	f	TR	f	TR	f	TR	f	TR
Sub1	3	0.53	8	1.17	6.5	1.06	7	1.44	6.5	1.27	6.5	0.62
Sub2	4.5	0.33	5.5	0.74	4.5	0.26	5	0.44	5.5	0.49	6.5	0.73
Sub3	5.5	1.08	8	1.17	5.5	1.53	5.5	0.82	4.5	0.52	3.5	0.54
Sub5	4.5	0.44	6	0.95	5.5	0.51	5.5	0.42	4	0.31	4	0.37
Sub6	4	0.67	4	0.12	7	0.98	7.5	0.64	4	0.49	4	0.45
Sub7	6	0.77	6	0.51	5.5	0.26	6	0.26	4	0.34	5.5	0.54
Sub8	3.5	0.40	8	1.87	5	0.21	4	0.13	8	1.02	8	1.06
Sub9	5	0.61	7	0.41	4.5	0.49	5.5	0.39	4.5	0.28	4	0.32
Sub10	3	0.31	5.5	1.85	6	2.31	9	1.35	7	1.65	5.5	1.17
Sub11	4.5	0.91	7	0.44	7	0.51	7	0.65	6	0.59	8	0.57
Sub12	3.5	0.30	5.5	0.57	10	0.91	5.5	0.39	5.5	0.72	5.5	0.64
Sub13	2.5	0.17	5.5	0.32	7.5	0.41	6	0.44	4	0.28	4	0.37

L5	1st resonance											
	NB		B_{0L2}		B_{0T5}		B_{10}		B_{20}		B_{30}	
	f(Hz)	TR	f	TR	f	TR	f	TR	f	TR	f	TR
Sub1	4	0.41	5.5	0.56	5.5	0.45	5.5	0.60	5.5	0.58	6	0.46
Sub2	4.5	0.63	5	0.68	4.5	0.60	5	0.52	6.5	0.29	6.5	0.41
Sub3	6	0.44	5.5	0.48	5.5	0.45	5.5	0.28	4.5	0.35	5.5	0.46
Sub5	3.5	0.20	6	0.71	6.5	0.76	6	0.51	12	1.48	13	2.01
Sub6	3.5	0.34	9.5	0.69	5	0.62	5.5	0.58	5.5	0.64	5.5	0.67
Sub7	7.5	0.34	7	0.66	6	0.45	8	1.36	8	1.22	4	0.40
Sub8	3.5	0.31	5	0.35	6	0.40	7.5	0.39	7.5	0.30	6.5	0.43
Sub9	5	0.46	7	0.25	5.5	0.28	5.5	0.28	5.5	0.32	5.5	0.34
Sub10	4	0.34	5.5	1.32	6	0.99	5	0.24	5	0.37	4	0.40
Sub11	4.5	0.50	5.5	0.37	7.5	1.20	4.5	0.24	5.5	0.39	5.5	0.25
Sub12	3	0.17	6	0.88	10	0.84	9	0.90	6	0.76	6	0.63
Sub13	2.5	0.16	4	0.13	9	0.31	9	1.01	5.5	0.54	6	0.63

L3	1st resonance											
	NB		B_{0L2}		B_{0T5}		B_{10}		B_{20}		B_{30}	
	f(Hz)	TR	f	TR	f	TR	f	TR	f	TR	f	TR
Sub1	2.5	0.32	8.5	0.90	6	0.91	6.5	1.01	7	0.96	7.5	0.88
Sub2	6	0.48	7	0.53	7	0.36	5.5	0.27	6.5	0.32	3.5	0.28
Sub3	6	0.46	5.5	0.63	5.5	0.51	5.5	0.29	5.5	0.53	5.5	0.51
Sub5	6	0.30	10	0.98	6.5	0.56	6.5	0.44	4	0.27	4	0.24
Sub6	3.5	0.40	7.5	0.41	5	0.26	5.5	0.32	6	0.46	5.5	0.55

Sub7	7	0.44	7	1.04	7.5	0.49	10.5	1.16	4	0.21	4	0.40
Sub8	3.5	0.33	5	0.47	8	0.31	7.5	0.91	7.5	0.68	8	0.77
Sub9	4.5	0.44	7	0.84	6	0.42	6.5	0.84	6.5	0.64	6	0.54
Sub10	2.5	0.23	5.5	1.25	6	0.75	6	0.65	6	0.61	5.5	0.50
Sub11	3.5	0.25	5.5	0.76	5.5	0.44	5.5	0.30	6	0.34	6.5	0.44
Sub12	3	0.21	3	0.15	6.5	0.53	10	1.24	9	1.08	6	0.73
Sub13	8.5	0.21	6	0.32	6	1.35	5.5	0.35	5.5	0.29	6	0.61

T5	1st resonance											
	NB		B_{0L2}		B_{0T5}		B_{10}		B_{20}		B_{30}	
	f(Hz)	TR	f	TR	f	TR	f	TR	f	TR	f	TR
Sub1	5	0.41	7.5	0.87	5.5	0.64	5.5	0.40	5	0.26	4	0.30
Sub2	4	0.21	6	0.47	5.5	1.20	5.5	1.52	6	1.34	7	1.33
Sub3	6.5	0.34	5.5	0.51	5	1.05	5.5	0.93	7	0.59	6.5	0.71
Sub5	4	0.38	5.5	0.90	5.5	1.04	6.5	0.98	8	1.15	12	2.74
Sub6	4.5	0.43	5	0.65	5.5	0.60	6	0.62	6	0.77	6	0.52
Sub7	7.5	0.41	6.5	0.85	6.5	1.04	7.5	1.09	7.5	1.25	7.5	1.07
Sub8	9	0.54	9	0.82	9	0.43	7.5	0.99	9	0.79	9.5	1.35
Sub9	5.5	0.46	6.5	0.69	6	0.83	6.5	0.77	8	1.01	8	0.96
Sub10	4.5	0.41	7.5	0.21	8	0.73	6	0.69	7.5	0.62	13	1.42
Sub11	6	0.44	5.5	0.69	6	0.98	6	1.00	6.5	0.98	6.5	0.67
Sub12	0.5	0.27	1.5	0.28	6	0.59	5.5	0.55	11.5	3.15	12.5	2.88
Sub13	5.5	0.67	6	0.57	6	0.85	6	0.86	9	1.28	9.5	1.10

Table A1.2 Second resonance of the fore-and-aft cross-axis transmissibilities to pelvis, L5, L3 and T5

Pelvis	2nd resonance											
	NB		B_{0L2}		B_{0T5}		B_{10}		B_{20}		B_{30}	
	f(Hz)	TR	f	TR	f	TR	f	TR	f	TR	f	TR
Sub1	9	1.06	8	1.17	9.5	1.28	7	1.44	6.5	1.27	12	0.31
Sub2	9.5	0.30	5.5	0.74	4.5	0.26	5	0.44	5.5	0.49	6.5	0.73
Sub3	8	1.43	8	1.17	5.5	1.53	5.5	0.82	4.5	0.52	8.5	0.83
Sub5	4.5	0.44	6	0.95	12	0.58	5.5	0.42	12	0.29	14	0.60
Sub6	9	0.51	7	0.56	7	0.98	7.5	0.64	9.5	0.21	10	0.31
Sub7	6	0.77	12	0.47	12.5	0.67	12	1.04	12.5	0.65	16	0.38
Sub8	7.5	0.73	8	1.87	8	0.98	7.5	0.83	12.5	0.92	12	1.12
Sub9	10.5	0.35	16	0.39	9.5	0.52	9.5	0.42	9.5	0.54	9.5	0.58
Sub10	9.5	0.60	9	1.45	15.5	0.39	17.5	0.36	17	0.42	8.5	1.35
Sub11	8.5	0.56	7	0.44	9.5	0.24	13.5	0.55	10	0.72	11	0.56
Sub12	6.5	0.29	9	0.53	10	0.91	9	0.50	14.5	0.25	9.5	0.40
Sub13	7	0.37	9.5	0.41	13	0.12	8.5	0.23	9	0.44	8	0.45

L5	2nd resonance											
	NB		B_{0L2}		B_{0T5}		B_{10}		B_{20}		B_{30}	
	f(Hz)	TR	f	TR	f	TR	f	TR	f	TR	f	TR
Sub1	18.5	2.06	5.5	0.56	10.5	0.90	12.5	1.10	13	1.42	13	1.30
Sub2	4.5	0.63	5	0.68	4.5	0.60	5	0.52	6.5	0.29	6.5	0.41

Sub3	9.5	1.55	14	0.83	11	1.16	10.5	1.30	11.5	1.14	5.5	0.46
Sub5	3.5	0.20	6	0.71	10	1.97	13	1.67	12	1.48	13	2.01
Sub6	9.5	0.83	9.5	0.69	17.5	0.59	11	0.94	14.5	1.30	13.5	1.04
Sub7	14.5	0.36	17.5	0.60	12	1.96	11	1.86	11	1.22	8.5	0.69
Sub8	7.5	0.29	8	0.74	13	0.17	12.5	0.20	13	0.17	15	0.18
Sub9	5	0.46	12	0.75	5.5	0.28	18.5	2.55	16.5	1.72	15	0.56
Sub10	11.5	1.21	5.5	1.32	9.5	1.80	9.5	1.71	9	1.93	9	2.40
Sub11	8	0.82	13	0.97	10	1.44	7.5	0.77	12.5	1.25	11	2.01
Sub12	6.5	0.22	18	1.23	14	0.32	9	0.90	13	2.03	10	1.38
Sub13	6.5	0.19	12	0.76	11.5	0.25	18	1.92	10.5	2.52	18.5	2.37

L3	2nd resonance											
	NB		B_{0L2}		B_{0T5}		B_{10}		B_{20}		B_{30}	
	f(Hz)	TR	f	TR	f	TR	f	TR	f	TR	f	TR
Sub1	6	0.50	8.5	0.90	6	0.91	6.5	1.01	7	0.96	7.5	0.88
Sub2	6	0.48	7	0.53	7	0.36	5.5	0.27	6.5	0.32	7	0.39
Sub3	6	0.46	5.5	0.63	5.5	0.51	5.5	0.29	5.5	0.53	5.5	0.51
Sub5	12	0.43	10	0.98	13	0.29	12.5	0.24	11	0.40	4	0.24
Sub6	11.5	0.25	7.5	0.41	10	0.62	11	1.17	11	1.10	9.5	1.88
Sub7	9.5	0.57	13	0.73	7.5	0.49	10.5	1.16	8	0.70	8	0.48
Sub8	6.5	0.56	9	0.66	8	0.31	7.5	0.91	11.5	0.77	12	0.90
Sub9	10.5	0.44	7	0.84	15	1.19	6.5	0.84	6.5	0.64	17	1.49
Sub10	6	0.44	5.5	1.25	13.5	1.13	11	0.36	12.5	0.43	16	1.32
Sub11	6	0.33	5.5	0.76	15	1.04	14.5	0.59	11	0.54	18	0.61
Sub12	8	0.56	7	0.93	10	0.68	10	1.24	16	1.18	9.5	0.78
Sub13	8.5	0.21	15	0.84	17	0.55	9.5	0.29	9	0.25	9	0.95

T5	2nd resonance											
	NB		B_{0L2}		B_{0T5}		B_{10}		B_{20}		B_{30}	
	f(Hz)	TR	f	TR	f	TR	f	TR	f	TR	f	TR
Sub1	5	0.41	7.5	0.87	5.5	0.64	5.5	0.40	5	0.26	4	0.30
Sub2	4	0.21	6	0.47	5.5	1.20	5.5	1.52	6	1.34	7	1.33
Sub3	6.5	0.34	5.5	0.51	5	1.05	5.5	0.93	7	0.59	6.5	0.71
Sub5	4	0.38	5.5	0.90	5.5	1.04	6.5	0.98	14	2.27	12	2.74
Sub6	4.5	0.43	11.5	0.93	5.5	0.60	13	0.92	6	0.77	12.5	1.14
Sub7	7.5	0.41	6.5	0.85	11.5	0.57	15	0.82	7.5	1.25	7.5	1.07
Sub8	9	0.54	9	0.82	9	0.43	7.5	0.99	9	0.79	9.5	1.35
Sub9	5.5	0.46	17	0.82	6	0.83	6.5	0.77	18	1.42	16	1.25
Sub10	15.5	1.09	7.5	0.21	8	0.73	13	0.97	13	1.37	13	1.42
Sub11	6	0.44	11	0.68	11.5	0.76	10.5	0.65	11	0.77	10	0.58
Sub12	18	1.39	6.5	0.37	13	2.28	13.5	2.35	11.5	3.15	12.5	2.88
Sub13	18.5	0.62	6	0.57	8	0.90	9	0.94	9	1.28	16.5	0.73

1. the row with symbol f(Hz) indicates the resonance frequency
2. the row with symbol TR indicates the corresponding transmissibility at the resonance frequency

A.2 Resonance frequency and damping ratio of the accelerometer block and skin-tissue system of 12 subjects

Table A2.1 Resonance frequency of the accelerometer block and skin-tissue system of 12 subjects

Resonance frequency (Hz) of skin-tissue correction system												
Location	Pelvis			L5			L3			T5		
Direction	pitch	x	z	pitch	x	z	pitch	x	z	pitch	x	z
Sub1	11.6	13.5	19.0	10.0	42.9	10.0	14.5	45.4	14.5	18.0	38.9	18.0
Sub2	33.9	31.9	17.5	33.4	37.4	16.0	36.9	41.4	16.5	28.9	29.4	16.0
Sub3	33.9	34.4	12.0	26.5	22.5	12.5	32.4	28.9	12.0	28.5	34.9	10.0
Sub5	27.5	28.9	19.0	9.5	29.4	9.5	16.5	17.5	16.5	16.0	36.9	16.0
Sub6	23.4	25.5	15.5	12.0	20.0	12.0	10.0	28.4	10.0	8.5	35.4	36.4
Sub7	28.9	40.4	19.5	13.0	41.4	13.0	12.5	42.4	12.5	15.3	28.0	38.4
Sub8	29.9	20.5	16.5	17.0	18.0	17.0	18.2	19.5	18.0	11.5	14.0	11.5
Sub9	15.0	10.0	15.0	10.0	10.5	9.5	11.5	37.5	12.0	14.0	48.4	14.0
Sub10	22.0	22.0	14.5	30.9	29.9	11.5	31.9	32.4	13.0	32.4	30.4	10.5
Sub11	28.9	30.9	13.5	17.9	28.0	9.5	30.9	15.5	12.0	24.0	24.0	10.0
Sub12	30.4	26.5	19.0	31.9	25.0	10.5	47.9	41.9	15.5	28.9	30.4	14.0
Sub13	16.5	18.5	13.0	16.5	16.5	8.0	11.5	11.0	12.0	26.0	23.0	11.0
Median	28.2	26	16	16.75	26.5	11	17.35	30.65	12.75	21	30.4	14

Table A2.2 Damping ratio of the accelerometer block and skin-tissue system of 12 subjects

Damping ratio of skin-tissue correction system												
Location	Pelvis			L5			L3			T5		
Direction	pitch	x	z	pitch	x	z	pitch	x	z	pitch	x	z
Sub1	0.32	0.57	0.22	0.22	0.22	0.30	0.19	0.39	0.20	0.22	0.37	0.22
Sub2	0.23	0.40	0.23	0.17	0.18	0.21	0.13	0.17	0.16	0.26	0.23	0.22
Sub3	0.44	0.40	0.32	0.28	0.20	0.22	0.34	0.19	0.27	0.31	0.20	0.42
Sub5	0.28	0.32	0.39	0.15	0.21	0.18	0.21	0.23	0.16	0.21	0.27	0.20
Sub6	0.38	0.40	0.28	0.26	0.31	0.16	0.22	0.21	0.24	0.34	0.26	0.23
Sub7	0.28	0.52	0.49	0.14	0.20	0.15	0.13	0.17	0.14	0.09	0.33	0.22
Sub8	0.40	0.43	0.41	0.18	0.20	0.17	0.26	0.24	0.25	0.20	0.14	0.20
Sub9	0.34	0.30	0.29	0.14	0.18	0.16	0.20	0.27	0.28	0.22	0.26	0.30
Sub10	0.30	0.26	0.35	0.25	0.28	0.16	0.18	0.16	0.20	0.32	0.27	0.24
Sub11	0.30	0.29	0.30	0.25	0.20	0.14	0.25	0.60	0.28	0.26	0.35	0.20
Sub12	0.37	0.36	0.32	0.16	0.16	0.19	0.27	0.24	0.28	0.24	0.24	0.17
Sub13	0.38	0.42	0.43	0.27	0.32	0.13	0.18	0.15	0.32	0.23	0.26	0.19
Median	0.33	0.4	0.32	0.2	0.2	0.165	0.205	0.22	0.245	0.235	0.26	0.22

A.3 Initial angle (φ) of the accelerometers block attached on spinal levels in no backrest, vertical and inclined backrests

Table A3 The initial angle (φ) of the accelerometers block attached on spinal levels in no backrest, vertical backrest and inclined backrest contact conditions

Sub 1						
	NB	B0L2	B0T5	B10	B20	B30
pelvis	21.9	5.4	17.2	24.3	28.4	31.1
L5	-32.3	25.0	31.3	42.3	48.6	52.3
L3	26.7	13.2	17.7	26.6	35.9	41.6
T5	-9.0	-26.0	-4.7	4.0	10.8	20.4

Sub 2						
	NB	B0L2	B0T5	B10	B20	B30
pelvis	8.3	7.7	28.3	38.2	39.2	40.9
L5	15.6	17.0	35.2	43.6	45.8	47.0
L3	11.2	9.2	28.7	37.2	42.0	45.2
T5	-19.6	-9.7	-5.6	8.3	17.5	26.3

Sub 3						
	NB	B0L2	B0T5	B10	B20	B30
pelvis	5.8	9.2	18.3	26.5	35.2	41.1
L5	12.3	17.8	20.6	34.3	38.3	43.1
L3	11.4	14.4	20.9	29.8	38.3	45.5
T5	-20.9	-24.2	-14.6	-11.8	-10.3	2.5

Sub 4						
	NB	B0L2	B0T5	B10	B20	B30
pelvis	5.7	-3.0	16.8	26.2	34.4	34.2
L5	31.6	28.7	38.8	49.2	49.8	52.2
L3	21.6	21.0	30.0	41.1	47.2	48.0
T5	-24.8	-15.0	-6.2	-1.8	18.9	16.7

Sub 5						
	NB	B0L2	B0T5	B10	B20	B30
pelvis	2.3	-6.6	13.6	12.5	15.8	31.7
L5	18.6	12.9	2.2	6.1	5.7	1.7
L3	18.1	-12.3	26.3	25.5	29.7	35.9
T5	-26.8	-24.4	-17.2	4.9	1.7	13.4

Sub 6						
	NB	B0L2	B0T5	B10	B20	B30
pelvis	-7.8	-8.8	6.7	19.3	26.6	28.3
L5	11.2	18.3	32.2	44.9	51.1	49.7
L3	7.2	5.0	24.3	38.2	47.5	49.7
T5	-2.1	-14.1	2.4	11.4	20.6	36.2

Sub 7						
	NB	B0L2	B0T5	B10	B20	B30
pelvis	9.0	6.5	25.9	19.7	28.2	34.6
L5	17.5	18.1	25.7	31.9	37.4	38.7
L3	9.8	10.8	30.1	27.7	37.2	44.1
T5	-18.8	-10.7	6.5	1.2	5.4	23.9

Sub 8						
	NB	B0L2	B0T5	B10	B20	B30
pelvis	6.2	3.5	29.6	21.6	31.9	36.6
L5	17.5	19.9	23.6	34.6	36.4	35.8
L3	7.7	13.1	33.6	23.9	35.6	43.8
T5	-27.9	-10.0	-9.6	-10.4	0.8	11.4

Sub 9						
	NB	B0L2	B0T5	B10	B20	B30
pelvis	6.1	6.7	14.3	17.8	24.8	32.2
L5	29.3	26.5	35.3	39.5	46.0	47.5
L3	-16.2	12.4	32.4	26.7	35.5	40.1
T5	-13.6	-10.1	12.3	5.9	16.8	31.6

Sub 10						
	NB	B0L2	B0T5	B10	B20	B30
pelvis	6.4	-7.6	2.5	11.8	19.1	25.6
L5	23.0	25.2	33.1	42.9	47.3	52.8
L3	18.6	21.4	27.4	39.5	47.1	52.3
T5	-18.5	-16.5	-9.4	-0.6	9.8	16.5

Sub 11						
	NB	B0L2	B0T5	B10	B20	B30
pelvis	-10.0	-15.4	4.4	2.4	7.0	11.9
L5	10.0	10.1	27.1	22.9	33.0	34.8
L3	4.1	6.2	16.9	15.9	26.2	31.8
T5	-11.9	-20.9	-8.0	-2.2	4.6	12.6

Sub 12						
	NB	B0L2	B0T5	B10	B20	B30
pelvis	4.4	10.1	11.3	31.0	35.5	37.4
L5	-5.5	4.1	5.3	35.9	26.6	37.8
L3	4.4	11.5	8.4	27.5	30.9	37.3
T5	-1.5	-9.5	11.4	13.0	18.3	25.5

A.4 Resonance frequencies of the seat to spine transmissibilities in the vertical direction measured without backrest and with vertical and inclined backrests

Table A4 Resonance frequencies of the seat to spine transmissibilities in the vertical direction measured without backrest and with vertical and inclined backrests

Resonance frequency of vertical **seat to pelvis** transmissibility						
Posture	NB	B_{0L2}	B_{0T5}	B_{10}	B_{20}	B_{30}
Sub 1	4.5	5.5	5.5	6	6	7.5
Sub 2	4	4	4.5	4.5	4.5	5.5
Sub 3	4.5	5.5	6	5.5	7	7.5
Sub 5	5	6	6	7.5	7	7.5
Sub 6	4.5	4.5	5	5	4.5	4.5
Sub 7	5.5	5.5	6	6	6	6
Sub 8	5.5	5	5.5	7	8	8
Sub 9	5	6	5.5	5.5	6	5.5
Sub 10	5	5.5	6	6	6	6
Sub 11	7	5	5.5	7.5	7.5	6
Sub 12	6	5.5	5.5	6	6	6
Sub 13	5.5	5	5.5	5.5	5	5.5

Resonance frequency of vertical **seat to L5** transmissibility						
Posture	NB	B_{0L2}	B_{0T5}	B_{10}	B_{20}	B_{30}
Sub 1	4.5	4	5	6	6	6.5
Sub 2	4	4	4.5	5.5	4.5	4.5
Sub 3	4.5	8	5	6	9	9.5
Sub 5	4.5	\	9.5	9.5	7	6.5
Sub 6	4.5	4.5	5	5	4.5	4
Sub 7	5.5	5.5	6	6.5	6.5	7
Sub 8	5	4.5	5	5.5	6	6.5
Sub 9	4.5	5	5	5.5	5.5	5.5
Sub 10	4.5	5	5.5	5.5	6	5.5
Sub 11	4.5	5	6	6	6	5.5
Sub 12	4.5	\	4.5	\	9	5.5
Sub 13	4.5	\	5	5	4.5	4.5

Resonance frequency of vertical **seat to L3** transmissibility						
Posture	NB	B_{0L2}	B_{0T5}	B_{10}	B_{20}	B_{30}
Sub 1	4.5	3	5	5.5	6	6.5
Sub 2	4	4	4.5	5.5	6	6
Sub 3	4	4	5	5.5	4.5	5.5
Sub 5	4.5	9	6.5	6.5	7.5	7
Sub 6	4	4	4.5	4.5	4	4
Sub 7	5.5	5	5.5	6	6.5	7
Sub 8	5	5	5.5	5.5	5	5.5
Sub 9	4.5	4.5	4.5	\	6	6
Sub 10	4	7	5.5	\	5.5	5.5
Sub 11	4.5	4.5	5	5.5	6.5	5.5
Sub 12	4.5	4	4.5	10	4	4
Sub 13	4.5	5	5	5	8	5.5

Resonance frequency of vertical **seat to T5** transmissibility						
Posture	NB	B_{0L2}	B_{0T5}	B_{10}	B_{20}	B_{30}
Sub 1	4	5	5	5.5	6	7.5
Sub 2	4	4	5.5	6	6	6.5
Sub 3	4	4	4.5	5	5.5	6
Sub 5	4.5	4.5	6	6.5	7.5	7.5
Sub 6	4	4.5	4	5	\	\
Sub 7	5.5	5.5	6	7.5	\	6.5
Sub 8	4.5	4.5	5	5.5	5.5	9
Sub 9	4.5	5	4.5	4.5	8	8
Sub 10	4	3.5	6.5	5	6	7
Sub 11	4.5	4.5	\	\	5.5	\
Sub 12	4.5	4.5	4.5	4.5	4.5	\
Sub 13	5.5	4.5	5.5	5	5.5	6

A.5 Inter-subject variability in the measured apparent masses at the seat pan and at the backrest

Tables A5.1 Inter-subject variability in the measured vertical in-line apparent mass at the seat pan at 2.5 Hz, 5 Hz, and 10 Hz, referring to Figure 6.6 in Chapter 6.

Vertical in-line apparent mass (kg) at the seat pan at 2.5 Hz						
Sitting conditions	NB	B_{0L2}	B_{0T5}	B_{10}	B_{20}	B_{30}
Median	69.93	65.06	65.08	63.18	59.48	52.10
Min	60.45	52.35	54.83	52.27	46.45	42.84
Max	98.93	94.43	91.86	90.26	86.19	75.47
Lower quartile Q1	65.30	60.15	58.86	58.82	54.72	49.87
Upper quartile Q3	75.30	76.12	75.91	71.80	64.95	61.23
Inter-quartile range (Q3-Q1)	10.00	15.98	17.05	12.98	10.23	11.36

Vertical in-line apparent mass (kg) at the seat pan at 5 Hz						
Sitting conditions	NB	B_{0L2}	B_{0T5}	B_{10}	B_{20}	B_{30}
Median	94.56	86.86	90.02	85.24	73.63	62.71
Min	71.41	67.87	68.79	65.49	57.73	50.42
Max	121.12	121.93	118.75	119.77	112.04	90.38
Lower quartile Q1	89.46	78.38	79.94	76.64	62.67	54.11
Upper quartile Q3	105.49	97.29	103.10	96.18	81.65	75.38
Inter-quartile range (Q3-Q1)	16.03	18.91	23.15	19.54	18.97	21.27

Vertical in-line apparent mass (kg) at the seat pan at 10 Hz						
Sitting conditions	NB	B_{0L2}	B_{0T5}	B_{10}	B_{20}	B_{30}
Median	36.53	42.41	38.83	39.63	41.96	41.20
Min	30.23	26.81	28.38	35.05	39.48	38.37
Max	52.56	50.85	51.23	52.99	51.44	53.25
Lower quartile Q1	33.58	37.41	34.32	38.59	40.50	40.13
Upper quartile Q3	38.92	45.69	42.04	44.40	48.11	47.77
Inter-quartile range (Q3-Q1)	5.34	8.27	7.72	5.81	7.61	7.64

Tables A5.2 Inter-subject variability in the measured fore-and-aft cross-axis apparent mass at the seat pan at 2.5 Hz, 5 Hz, and 10 Hz, referring to Figure 6.8 in Chapter 6.

Fore-and-aft cross-axis apparent mass (kg) at the seat pan at 2.5 Hz						
Sitting conditions	NB	B_{0L2}	B_{0T5}	B_{10}	B_{20}	B_{30}
Median	7.21	7.35	9.82	12.48	15.47	16.34
Min	2.52	3.40	5.34	9.78	12.74	13.22
Max	15.06	12.99	15.09	16.47	19.47	24.25
Lower quartile Q1	3.69	5.86	8.33	11.29	13.77	15.49
Upper quartile Q3	8.49	10.13	12.40	14.06	17.60	18.39
Inter-quartile range (Q3-Q1)	4.79	4.27	4.07	2.77	3.83	2.90

Fore-and-aft cross-axis apparent mass (kg) at the seat pan at 5 Hz						
Sitting conditions	NB	B_{0L2}	B_{0T5}	B_{10}	B_{20}	B_{30}
Median	16.11	16.49	19.30	22.58	19.36	14.78
Min	10.54	6.47	10.23	14.29	10.18	9.87
Max	27.79	26.98	26.30	32.62	26.74	24.08
Lower quartile Q1	13.95	14.82	16.79	18.60	15.39	11.55
Upper quartile Q3	18.79	21.31	21.56	26.73	23.31	18.66
Inter-quartile range (Q3-Q1)	4.85	6.49	4.78	8.12	7.92	7.11

Fore-and-aft cross-axis apparent mass (kg) at the seat pan at 10 Hz						
Sitting conditions	NB	B_{0L2}	B_{0T5}	B_{10}	B_{20}	B_{30}
Median	1.89	2.10	3.23	5.33	6.11	5.92
Min	1.25	0.79	1.90	3.37	3.71	4.12
Max	3.40	6.03	5.19	7.80	8.76	8.33
Lower quartile Q1	1.63	1.65	2.56	4.13	5.07	4.96
Upper quartile Q3	2.39	3.28	4.37	5.60	7.55	7.46
Inter-quartile range (Q3-Q1)	0.76	1.64	1.81	1.47	2.48	2.50

Tables A5.3 Inter-subject variability in the measured vertical in-line apparent mass at the backrest at 2.5 Hz, 5 Hz, and 10 Hz, referring to Figure 6.9 in Chapter 6.

Vertical in-line apparent mass (kg) at the backrest at 2.5 Hz						
Sitting conditions	NB	B_{0L2}	B_{0T5}	B_{10}	B_{20}	B_{30}
Median	-	2.10	2.45	4.31	9.98	16.40
Min	-	0.74	0.27	0.57	4.75	11.98
Max	-	2.50	3.43	6.41	11.57	21.23
Lower quartile Q1	-	1.60	2.20	4.10	9.23	15.08
Upper quartile Q3	-	2.25	2.83	5.12	10.64	19.56
Inter-quartile range (Q3-Q1)	-	0.65	0.63	1.02	1.41	4.48

Vertical in-line apparent mass (kg) at the backrest at 5 Hz						
Sitting conditions	NB	B_{0L2}	B_{0T5}	B_{10}	B_{20}	B_{30}
Median	-	3.15	4.02	8.71	15.46	22.91
Min	-	0.60	3.02	2.59	6.46	15.15
Max	-	4.11	6.34	10.01	17.03	32.88
Lower quartile Q1	-	2.44	3.35	7.31	13.94	21.24
Upper quartile Q3	-	3.65	5.01	8.96	16.52	25.94
Inter-quartile range (Q3-Q1)	-	1.21	1.65	1.65	2.58	4.69

Vertical in-line apparent mass (kg) at the backrest at 10 Hz						
Sitting conditions	NB	B_{0L2}	B_{0T5}	B_{10}	B_{20}	B_{30}
Median	-	1.83	1.75	3.44	7.77	13.92
Min	-	0.97	1.04	2.67	4.88	11.65
Max	-	3.57	3.73	5.96	10.16	16.65
Lower quartile Q1	-	1.38	1.56	3.04	6.60	13.65
Upper quartile Q3	-	2.55	1.86	3.71	9.32	15.08
Inter-quartile range (Q3-Q1)	-	1.18	0.30	0.66	2.72	1.43

Tables A5.4 Inter-subject variability in the measured fore-and-aft cross-axis apparent mass at the backrest at 2.5 Hz, 5 Hz, and 10 Hz, referring to Figure 6.10 in Chapter 6.

Fore-and-aft cross-axis apparent mass (kg) at the backrest at 2.5 Hz						
Sitting conditions	NB	B_{0L2}	B_{0T5}	B_{10}	B_{20}	B_{30}
Median	-	9.82	9.30	14.75	18.84	21.22
Min	-	5.82	3.49	10.58	14.85	17.82
Max	-	15.14	17.37	17.42	24.69	23.58
Lower quartile Q1	-	7.42	8.01	13.19	17.00	19.85
Upper quartile Q3	-	11.76	10.46	15.66	20.68	22.63
Inter-quartile range (Q3-Q1)	-	4.34	2.45	2.47	3.68	2.78

Fore-and-aft cross-axis apparent mass (kg) at the backrest at 5 Hz						
Sitting conditions	NB	B_{0L2}	B_{0T5}	B_{10}	B_{20}	B_{30}
Median	-	20.07	22.51	26.96	33.95	35.29
Min	-	6.61	13.93	23.56	23.16	30.24
Max	-	29.50	33.85	48.47	48.61	53.42
Lower quartile Q1	-	14.48	15.96	25.40	30.69	32.87
Upper quartile Q3	-	22.05	24.27	31.69	38.08	37.74
Inter-quartile range (Q3-Q1)	-	7.56	8.31	6.28	7.39	4.87

Fore-and-aft cross-axis apparent mass (kg) at the backrest at 10 Hz						
Sitting conditions	NB	B_{0L2}	B_{0T5}	B_{10}	B_{20}	B_{30}
Median	-	6.13	8.13	11.61	17.78	21.54
Min	-	2.10	5.15	8.69	13.09	19.11
Max	-	10.47	10.75	18.64	21.92	24.17
Lower quartile Q1	-	5.24	7.77	10.13	15.81	20.60
Upper quartile Q3	-	8.11	8.59	12.18	18.47	22.50
Inter-quartile range (Q3-Q1)	-	2.87	0.82	2.05	2.66	1.90

A.6 Details about the statistics in the Wilcoxon test in Chapter 6

Table 6.1 Statistical significance of the effect of backrest inclination on the resonance frequency and the associated modulus of the vertical apparent mass at the seat pan (Wilcoxon matched-pairs signed ranks test).

Resonance frequency of vertical apparent mass at the seat pan						
	NB	B_{0L2}	B_{0T5}	B_{10}	B_{20}	B_{30}
NB	-	0.4531	0.5547	0.3633	0.1797	0.0142
B_{0L2}		-	0.2852	0.2539	0.0625	0.0132
B_{0T5}			-	0.6563	0.4385	0.0244
B_{10}				-	0.8594	0.0078
B_{20}					-	0.0142
B_{30}						-

Vertical apparent mass at the seat pan at the resonance frequency						
	NB	B_{0L2}	B_{0T5}	B_{10}	B_{20}	B_{30}
NB	-	0.0049	0.0122	0.0010	0.0005	0.0005
B_{0L2}		-	0.6772	0.0161	0.0005	0.0005
B_{0T5}			-	0.0068	0.0005	0.0005
B_{10}				-	0.0005	0.0005
B_{20}					-	0.0005
B_{30}						-

Table 6.2 Statistical significance of the effects of backrest inclination on the resonance frequency and the associated modulus of the fore-and-aft cross-axis apparent mass at the seat pan (Wilcoxon matched-pairs signed ranks test).

Resonance frequency of fore-and-aft apparent mass at the seat pan						
	NB	B_{0L2}	B_{0T5}	B_{10}	B_{20}	B_{30}
NB	-	0.6797	0.2344	0.1172	0.2031	0.0166
B_{0L2}		-	0.3125	0.3281	0.0469	0.0010
B_{0T5}			-	1.0000	0.0156	0.0005
B_{10}				-	0.0127	0.0005
B_{20}					-	0.0020
B_{30}						-

Fore-and-aft apparent mass at the seat pan at the resonance frequency						
	NB	B_{0L2}	B_{0T5}	B_{10}	B_{20}	B_{30}
NB	-	0.9697	0.2661	0.0269	0.0522	0.0522
B_{0L2}		-	0.3013	0.0024	0.0669	0.0640
B_{0T5}			-	0.0400	0.3804	0.5693
B_{10}				-	0.1748	0.2036
B_{20}					-	0.8501
B_{30}						-

Appendix B Effect of forward leaning sitting posture on the biodynamic response of human body

Table B1 The first and second resonance frequency of the fore-and-aft cross-axis apparent mass at the seat pan within the frequency range 2.5 – 7 Hz.

Vibration magnitudes: 0.5 m/s² r.m.s.						
Postures:	P0		KL		AL	
Resonances:	1st	2nd	1st	2nd	1st	2nd
Sub1	-	3.25	2.75	2.75	2.75	2.75
Sub2	-	4.5	**3.25**	5.75	3.5	**6.25**
Sub3	2.75	**4.5**	2.75	**4.5**	4	4
Sub5	-	5	3	3	3	3
Sub6	-	5	3.5	**6.5**	**5**	5.75
Sub7	2.75	**6.25**	**3.5**	5.75	3.5	**6.5**
Sub8	-	5.75	4.5	**6.25**	**3.75**	8
Sub9	5	**5.75**	**3.5**	5.75	**5**	5.75
Sub10	-	4	**3**	4.25	3.5	**5**
Sub11	-	**5**	3.5	**4.75**	3.5	**4.5**
Sub12	-	6.25	**2**	7	3.25	**5.75**
Sub13	2.5	**5**	**2.75**	5.75	3.5	**5.75**

Vibration magnitudes: 1.0 m/s² r.m.s.						
Postures:	P0		KL		AL	
Resonances:	1st	2nd	1st	2nd	1st	2nd
Sub1	-	2.75	3	3	2.75	2.75
Sub2	-	4	**3**	4.75	5.25	5.25
Sub3	-	4.5	3	3	3.5	3.5
Sub5	-	4.5	2.75	2.75	**2.75**	5.75
Sub6	-	4	3.25	**5.75**	4.5	**5**
Sub7	-	5.75	**3.25**	4.5	3	**5.75**
Sub8	-	5.25	3.75	**5.25**	**3.5**	6.5
Sub9	-	5	**3**	5.5	4.5	4.5
Sub10	-	3.75	**3**	4.75	**3.75**	5
Sub11	-	4.5	4	4	4.5	4.5
Sub12	-	4.5	**3.5**	6	3.5	**5.25**
Sub13	-	4.75	**2.75**	5.25	**3.25**	5.25

Vibration magnitudes: 1.0 m/s² r.m.s.						
Postures:	P0		KL		AL	
Resonances:	1st	2nd	1st	2nd	1st	2nd
Sub1	-	2.75	2.75	2.75	2.75	2.75
Sub2	3.5	**4.25**	3.5	**4.25**	3.5	**5.25**

Sub3	-	4.25	2.75	**4.25**	3.25	3.25
Sub5	-	4.5	2.75	2.75	2.75	2.75
Sub6	-	4.5	3.5	**5.5**	**4.25**	5.25
Sub7	-	5.25	**3.25**	4.5	5.25	5.25
Sub8	-	5.25	5.25	5.25	**3.5**	6
Sub9	-	4.5	3.5	**5.25**	4	**5.25**
Sub10	3.5	**4.5**	**2.75**	4.25	**3.5**	5.25
Sub11	3.5	**4.5**	3.5	**4.25**	3.5	**4.25**
Sub12	-	5.25	3.5	**6**	3.5	**5.25**
Sub13	-	4.5	**2.75**	5.25	**2.75**	5.25

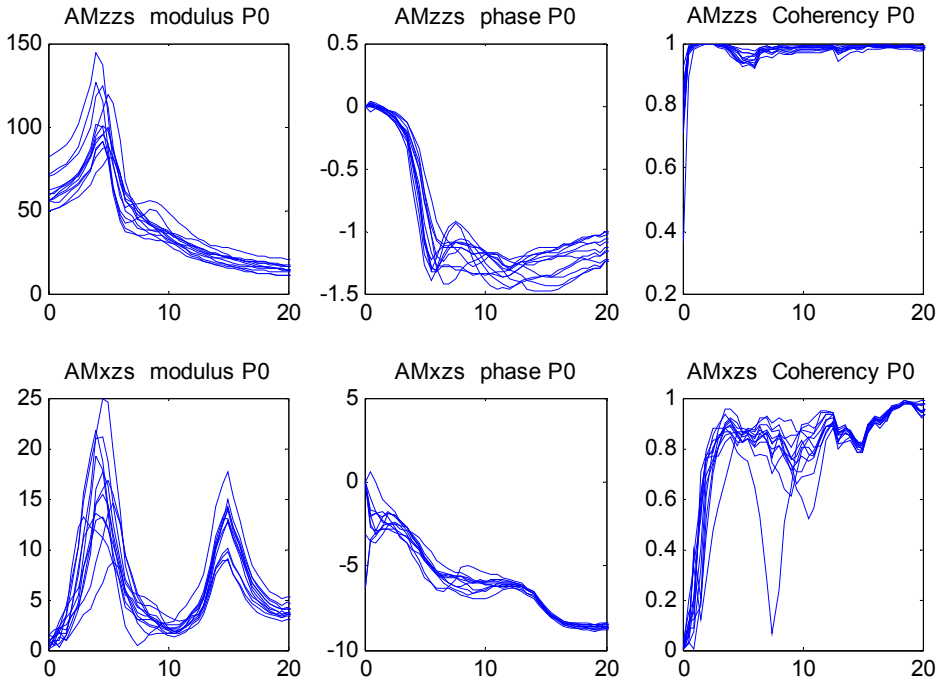

Figure B1 The vertical in-line apparent masses and fore-and-aft cross-axis apparent masses of 12 subjects in the normal upright sitting posture when exposed to 1.5 m/s^2 r.m.s. vibration. Top row: modulus, phase, and coherency of the vertical in-line apparent mass from left to right. Bottom row: modulus, phase, and coherency of the fore-and-aft cross-axis apparent mass from left to right.

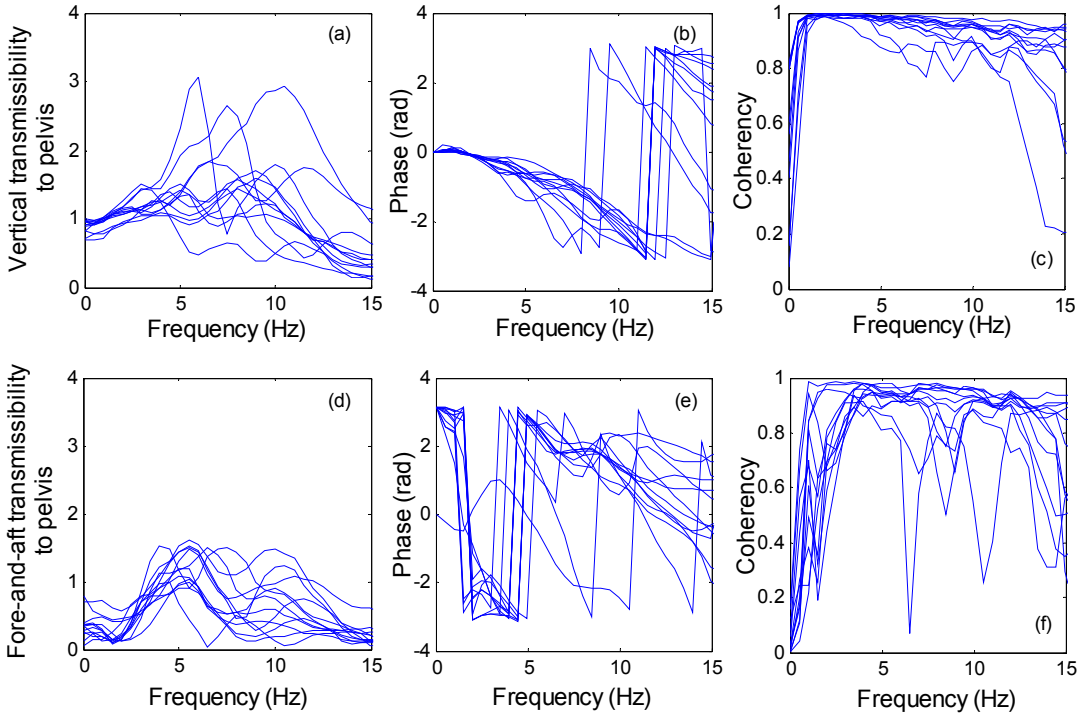

Figure B2 Vertical and fore-and-aft transmissibilities from vertical acceleration at the seat to the pelvis (measured at the iliac crest) before angle correction. (a) and (d) show the modulus; (b) and (e) show the phase; (c) and (f) show the coherency function.

Tables B.1 Inter-subject variability in the measured vertical in-line apparent mass at the seat pan at 2.5 Hz, 5 Hz, and 10 Hz exposed to 1.0 m/s^2 r.m.s. random vibration from 0.2 – 20 Hz, referring to Figure 8.5 in Chapter 8.

Vertical in-line apparent mass (kg) at the seat pan at 2.5 Hz			
Sitting conditions	Normal	KL	AL
Median	69.93	65.98	68.88
Min	60.45	47.92	54.52
Max	98.93	94.27	103.22
Lower quartile Q1	65.30	60.93	64.21
Upper quartile Q3	75.30	75.29	76.03
Inter-quartile range (Q3-Q1)	10.00	14.36	11.82

Vertical in-line apparent mass (kg) at the seat pan at 5 Hz			
Sitting conditions	Normal	KL	AL
Median	94.56	86.78	87.09
Min	71.41	62.15	66.14
Max	121.12	118.00	123.61
Lower quartile Q1	89.46	74.23	73.90
Upper quartile Q3	105.49	102.14	102.69
Inter-quartile range (Q3-Q1)	16.03	27.91	28.79

Vertical in-line apparent mass (kg) at the seat pan at 10 Hz			
Sitting conditions	Normal	KL	AL
Median	36.53	33.99	38.60
Min	30.23	26.72	29.26
Max	52.56	39.95	44.48
Lower quartile Q1	33.58	28.46	36.13
Upper quartile Q3	38.92	37.66	41.82
Inter-quartile range (Q3-Q1)	5.34	9.20	5.69

Tables B.2 Inter-subject variability in the measured vertical in-line apparent mass at the seat pan at 2.5 Hz, 5 Hz, and 10 Hz exposed to 0.5 m/s^2 r.m.s. random vibration from 0.2 – 20 Hz, referring to Figure 8.6 in Chapter 8.

Vertical in-line apparent mass (kg) at the seat pan at 2.5 Hz			
Sitting conditions	Normal	KL	AL
Median	68.02	64.45	68.51
Min	57.69	49.94	58.13
Max	95.22	93.14	98.06
Lower quartile Q1	63.94	59.97	62.05
Upper quartile Q3	72.72	73.60	74.51
Inter-quartile range (Q3-Q1)	8.79	13.63	12.45

Vertical in-line apparent mass (kg) at the seat pan at 5 Hz			
Sitting conditions	Normal	KL	AL
Median	94.63	77.44	79.85
Min	78.48	56.20	59.01
Max	141.22	124.03	136.79
Lower quartile Q1	87.36	65.25	71.63
Upper quartile Q3	105.13	93.12	95.49
Inter-quartile range (Q3-Q1)	17.77	27.87	23.86

Vertical in-line apparent mass (kg) at the seat pan at 10 Hz			
Sitting conditions	Normal	KL	AL
Median	41.61	37.42	42.41
Min	32.18	30.81	30.30
Max	55.06	53.27	52.99
Lower quartile Q1	37.29	34.53	38.37
Upper quartile Q3	43.34	43.34	46.78
Inter-quartile range (Q3-Q1)	6.05	8.81	8.41

Tables B.3 Inter-subject variability in the measured vertical in-line apparent mass at the seat pan at 2.5 Hz, 5 Hz, and 10 Hz exposed to 1.5 m/s^2 r.m.s. random vibration from 0.2 – 20 Hz, referring to Figure 8.7 in Chapter 8.

Vertical in-line apparent mass (kg) at the seat pan at 2.5 Hz			
Sitting conditions	Normal	KL	AL
Median	70.81	65.80	67.72
Min	57.59	48.70	57.06
Max	101.16	96.77	111.62
Lower quartile Q1	66.17	60.62	64.02
Upper quartile Q3	75.08	74.57	76.89
Inter-quartile range (Q3-Q1)	8.91	13.95	12.87

Vertical in-line apparent mass (kg) at the seat pan at 5 Hz			
Sitting conditions	Normal	KL	AL
Median	88.85	87.88	89.71
Min	80.84	60.85	69.81
Max	119.17	110.98	123.38
Lower quartile Q1	82.37	68.72	73.85
Upper quartile Q3	101.05	105.03	94.56
Inter-quartile range (Q3-Q1)	18.68	36.31	20.71

Vertical in-line apparent mass (kg) at the seat pan at 10 Hz			
Sitting conditions	Normal	KL	AL
Median	35.72	31.85	37.02
Min	29.56	26.32	26.46
Max	49.18	40.32	43.51
Lower quartile Q1	32.42	27.23	34.62
Upper quartile Q3	37.28	37.33	39.08
Inter-quartile range (Q3-Q1)	4.86	10.11	4.45

Tables B.4 Inter-subject variability in the measured fore-and-aft cross-axis apparent mass at the seat pan at 2.5 Hz, 5 Hz, and 10 Hz exposed to 1.0 m/s^2 r.m.s. random vibration from 0.2 – 20 Hz, referring to Figure 8.11 in Chapter 8.

Fore-and-aft cross-axis apparent mass (kg) at the seat pan at 2.5 Hz			
Sitting conditions	Normal	KL	AL
Median	7.21	14.43	12.93
Min	2.52	4.32	7.81
Max	15.06	22.75	20.90
Lower quartile Q1	3.69	10.84	10.35
Upper quartile Q3	8.49	16.26	15.46
Inter-quartile range (Q3-Q1)	4.79	5.42	5.11

Fore-and-aft cross-axis apparent mass (kg) at the seat pan at 5 Hz			
Sitting conditions	Normal	KL	AL
Median	16.11	14.29	18.46
Min	10.54	6.02	11.79
Max	27.79	26.73	31.82
Lower quartile Q1	13.95	11.94	15.96
Upper quartile Q3	18.79	16.41	21.79
Inter-quartile range (Q3-Q1)	4.85	4.48	5.84

Fore-and-aft cross-axis apparent mass (kg) at the seat pan at 10 Hz			
Sitting conditions	Normal	KL	AL
Median	1.89	2.49	3.71
Min	1.25	1.10	1.49
Max	3.40	5.86	8.98
Lower quartile Q1	1.63	1.94	2.37
Upper quartile Q3	2.39	2.94	4.09
Inter-quartile range (Q3-Q1)	0.76	1.00	1.72

Tables B.5 Inter-subject variability in the measured fore-and-aft cross-axis apparent mass at the seat pan at 2.5 Hz, 5 Hz, and 10 Hz exposed to 0.5 m/s^2 r.m.s. random vibration from 0.2 – 20 Hz, referring to Figure 8.12 in Chapter 8.

Fore-and-aft cross-axis apparent mass (kg) at the seat pan at 2.5 Hz			
Sitting conditions	Normal	KL	AL
Median	5.53	12.64	11.86
Min	2.57	6.08	6.97
Max	11.97	22.74	18.53
Lower quartile Q1	3.93	12.09	11.49
Upper quartile Q3	7.02	14.32	16.44
Inter-quartile range (Q3-Q1)	3.09	2.23	4.94

Fore-and-aft cross-axis apparent mass (kg) at the seat pan at 5 Hz			
Sitting conditions	Normal	KL	AL
Median	17.55	14.11	20.69
Min	7.03	4.78	10.96
Max	27.60	27.28	31.58
Lower quartile Q1	12.70	11.44	16.01
Upper quartile Q3	21.92	17.66	24.12
Inter-quartile range (Q3-Q1)	9.21	6.23	8.11

Fore-and-aft cross-axis apparent mass (kg) at the seat pan at 10 Hz			
Sitting conditions	Normal	KL	AL
Median	2.84	3.65	5.81
Min	1.23	2.12	1.81
Max	5.46	8.80	16.33
Lower quartile Q1	2.04	2.74	3.26
Upper quartile Q3	3.36	4.90	6.61
Inter-quartile range (Q3-Q1)	1.32	2.16	3.35

Tables B.6 Inter-subject variability in the measured fore-and-aft cross-axis apparent mass at the seat pan at 2.5 Hz, 5 Hz, and 10 Hz exposed to 1.5 m/s^2 r.m.s. random vibration from 0.2 – 20 Hz, referring to Figure 8.13 in Chapter 8.

Fore-and-aft cross-axis apparent mass (kg) at the seat pan at 2.5 Hz			
Sitting conditions	Normal	KL	AL
Median	5.75	12.30	13.24
Min	2.74	6.87	5.83
Max	12.08	18.89	29.37
Lower quartile Q1	4.40	10.71	10.84
Upper quartile Q3	8.74	14.10	16.82
Inter-quartile range (Q3-Q1)	4.33	3.39	5.98

Fore-and-aft cross-axis apparent mass (kg) at the seat pan at 5 Hz			
Sitting conditions	Normal	KL	AL
Median	13.98	13.60	16.63
Min	8.19	7.69	10.95
Max	24.61	22.84	30.99
Lower quartile Q1	12.13	11.59	12.95
Upper quartile Q3	16.45	18.41	20.55
Inter-quartile range (Q3-Q1)	4.31	6.82	7.60

Fore-and-aft cross-axis apparent mass (kg) at the seat pan at 10 Hz			
Sitting conditions	Normal	KL	AL
Median	2.19	2.82	3.38
Min	1.49	1.56	1.78
Max	3.43	5.29	7.87
Lower quartile Q1	1.95	2.22	2.78
Upper quartile Q3	2.41	3.45	4.42
Inter-quartile range (Q3-Q1)	0.46	1.24	1.65

Table 8.1 Statistical significance of the effects of forward leaning sitting postures on the resonance frequency in the vertical apparent mass at the seat pan and the modulus of the apparent mass at resonance measured with 1.0 m/s² r.m.s. vibration. Wilcoxon matched-pairs signed ranks test.

Resonance frequency of vertical apparent mass at the seat pan			
	Normal	KL	AL
Normal	-	0.0391 ↑ (KL)	0.002 ↑ (AL)
KL		-	0.0234 ↑ (AL)
AL			-

Vertical apparent mass at the seat pan at the resonance frequency			
	Normal	KL	AL
Normal	-	0.0122 ↓ (KL)	0.1763
KL		-	0.0771
AL			-

Table 8.2 Statistical significance of the effects of forward leaning postures on the resonance frequency in the vertical apparent mass at the seat pan and the modulus of the apparent mass at resonance measured with 0.5 m/s² r.m.s. vibration. Wilcoxon matched-pairs signed ranks test.

Resonance frequency of vertical apparent mass at the seat pan			
	Normal	KL	AL
Normal	-	0.0029 ↑(KL)	0.0029 ↑(AL)
KL		-	0.6758
AL			-

Vertical apparent mass at the seat pan at the resonance frequency			
	Normal	KL	AL
Normal	-	0.0210 ↓(KL)	0.0269 ↓(AL)
KL		-	0.7910
AL			-

Table 8.3 Statistical significance of the effects of forward leaning sitting postures on the resonance frequency in the vertical apparent mass at the seat pan and the modulus of the apparent mass at resonance measured with 1.5 m/s² r.m.s. vibration. Wilcoxon matched-pairs signed ranks test.

Resonance frequency of vertical apparent mass at the seat pan			
	Normal	KL	AL
Normal	-	0.0020↑ (KL)	0.0078 ↑ (AL)
KL		-	0.4688
AL			-

Vertical apparent mass at the seat pan at the resonance frequency			
	Normal	KL	AL
Normal	-	0.0015↓ (KL)	0.0425 ↓ (AL)
KL		-	0.3804
AL			-

Table 8.4 Statistical significance of the effects of forward leaning sitting postures on the principal resonance frequency of the fore-and-aft cross-axis apparent mass at the seat pan and the modulus of the apparent mass at principal resonance measured with 1.0 m/s² r.m.s. Wilcoxon matched-pairs signed ranks test.

Principal resonance frequency of fore-and-aft cross-axis apparent mass at the seat pan			
	Normal	KL	AL
Normal	-	0.0654	0.3281
KL		-	0.3447
AL			-

Fore-and-aft cross-axis apparent mass at the seat pan at the principal resonance frequency			
	Normal	KL	AL
Normal	-	0.4697	0.0068 ↑ (AL)
KL		-	0.0005 ↑ (AL)
AL			-

Table 8.5 Statistical significance of the effects of forward leaning sitting postures on the principal resonance frequency in the fore-and-aft cross-axis apparent mass at the seat pan and the modulus of the apparent mass at principal resonance measured with 0.5 m/s^2 r.m.s. Wilcoxon matched-pairs signed ranks test.

Principal resonance frequency of fore-and-aft cross-axis apparent mass at the seat pan			
	Normal	KL	AL
Normal	-	0.0273↓(KL)	0.3750
KL		-	0.1367
AL			-

Fore-and-aft cross-axis apparent mass at the seat pan at the principal resonance frequency			
	Normal	KL	AL
Normal	-	0.5186	0.0093 ↑ (AL)
KL		-	0.0024 ↑(AL)
AL			-

Table 8.6 Statistical significance of the effects of forward leaning sitting postures on the principal resonance frequency in the fore-and-aft cross-axis apparent mass at the seat pan and the modulus of the apparent mass at principal resonance measured with 1.5 m/s^2 r.m.s. Wilcoxon matched-pairs signed ranks test.

Principal resonance frequency of fore-and-aft cross-axis apparent mass at the seat pan			
	Normal	KL	AL
Normal	-	0.0703	0.1016
KL		-	0.6406
AL			-

Fore-and-aft cross-axis apparent mass at the seat pan at the principal resonance frequency			
	Normal	KL	AL
Normal	-	0.4126	0.0210 ↑ (AL)
KL		-	0.0093 ↑ (AL)
AL			-

Table 8.8 Statistical significance of the changes in the principal resonance frequencies with three vibration magnitudes in each of the three sitting postures: 'normal', 'kyphotic leaning' (KL) and 'anterior leaning' (AL). Top: Friedman two-way analysis of variance for *k*-related samples. Bottom: Wilcoxon matched-pairs signed ranks test.

Friedman test of principal resonance frequencies at three vibration magnitudes: 0.5, 1.0 and 1.5 m/s^2 r.m.s.			
Postures	Normal	KL	AL
p	0.0096	0.0001	0.0001

Wilcoxon test of principal resonance frequency of vertical apparent mass at the seat at three vibration magnitudes: 0.5, 1.0 and 1.5 m/s^2 r.m.s.												
Normal					KL					AL		
	0.5	1	1.5			0.5	1	1.5			0.5	1	1.5
0.5	-	0.0500 ↓(1)	0.0078↓(1.5)		0.5	-	0.0010 ↓(1)	0.0010↓(1.5)		0.5	-	0.0029 ↓(1)	0.0010↓(1.5)
1		-	0.3594		1		-	0.7813		1		-	0.0078↓(1.5)
1.5			-		1.5			-		1.5			-

Table 8.9 Statistical significance of the changes in the frequencies of the peak occurring at a lower frequency with three vibration magnitudes in the 'kyphotic leaning' (KL) and the 'anterior leaning' (AL) sitting postures. Wilcoxon matched-pairs signed ranks test.

Friedman test of frequency of fist peak in three vibration magnitudes: 0.5, 1.0 and 1.5 m/s^2 r.m.s.		
Postures	KL	AL
p	0.3189	0.0002
Number of subjects showing the first peak	7	9

Wilcoxon test of principal resonance frequency of vertical apparent mass at the seat in three vibration magnitudes: 0.5, 1.0 and 1.5 m/s^2 r.m.s. in 'anterior leaning' sitting posture			
	0.5	1	1.5
0.5	-	0.0039↓(1)	0.0039↓(1.5)
1		-	0.0156↓(1.5)
1.5			-

Appendix C Effect of muscle activity on the biodynamic response of the human body

C.1 Vertical and fore-and-aft apparent mass at the seat pan measured with 1.0 m/s^2 vertical whole-body vibration

Vertical apparent mass at the seat pan of individual subjects:

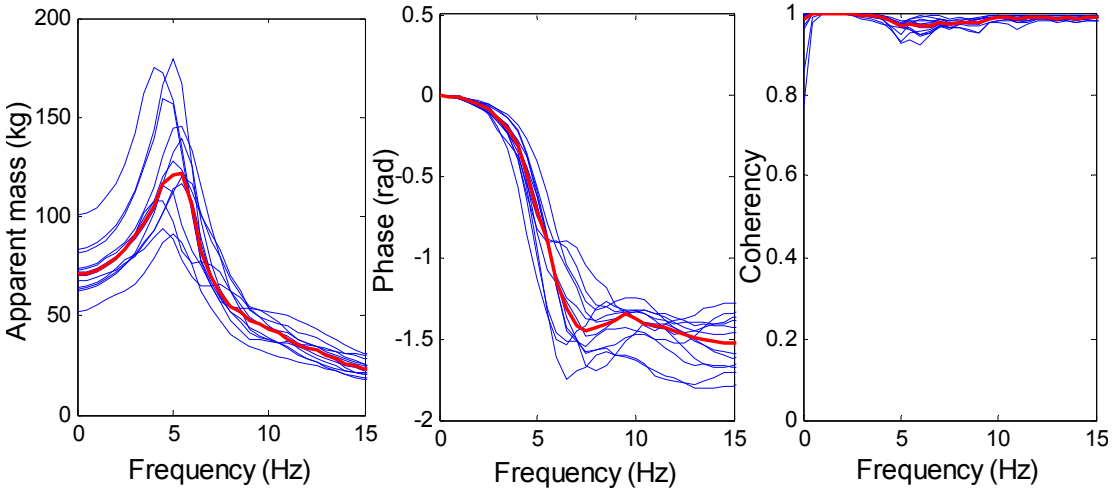

Figure C1.1 Vertical in-line apparent mass at the seat pan in normal upright sitting posture with 50 N force applied to thoracic spine (FU) of 12 individual subjects when exposed to 1.0 m/s^2 r.m.s. vibration. Individual subject: ('—'); Median of 12 subjects: ('—'). In one row, from left to right: modulus, phase and coherency.

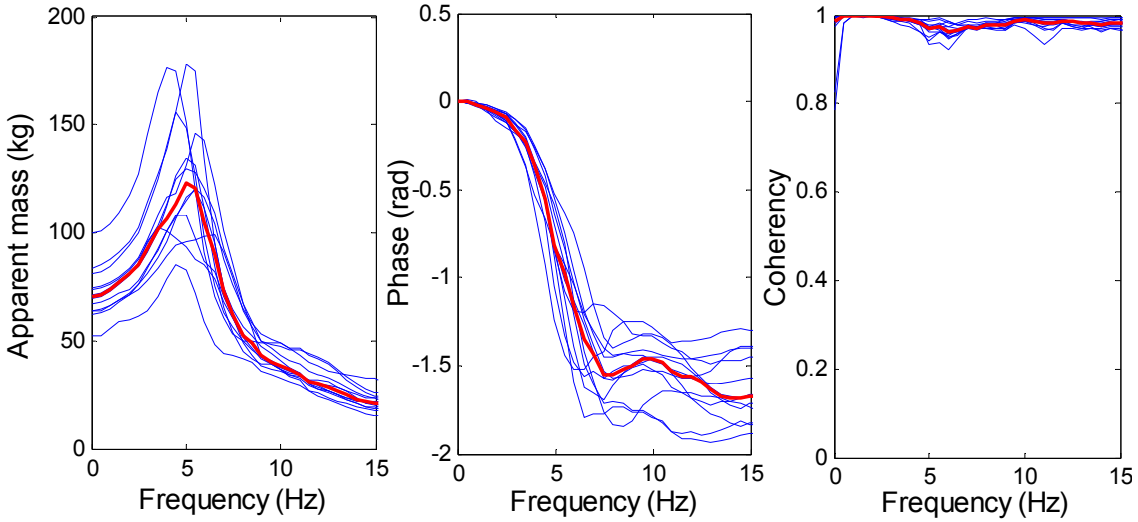

Figure C1.2 Vertical in-line apparent mass at the seat pan in normal upright sitting posture with 100 N force applied to thoracic spine (2FU) of 12 individual subjects when exposed to 1.0 m/s^2 r.m.s. vibration. Individual subject: ('—'); Median of 12 subjects: ('—'). In one row, from left to right: modulus, phase and coherency.

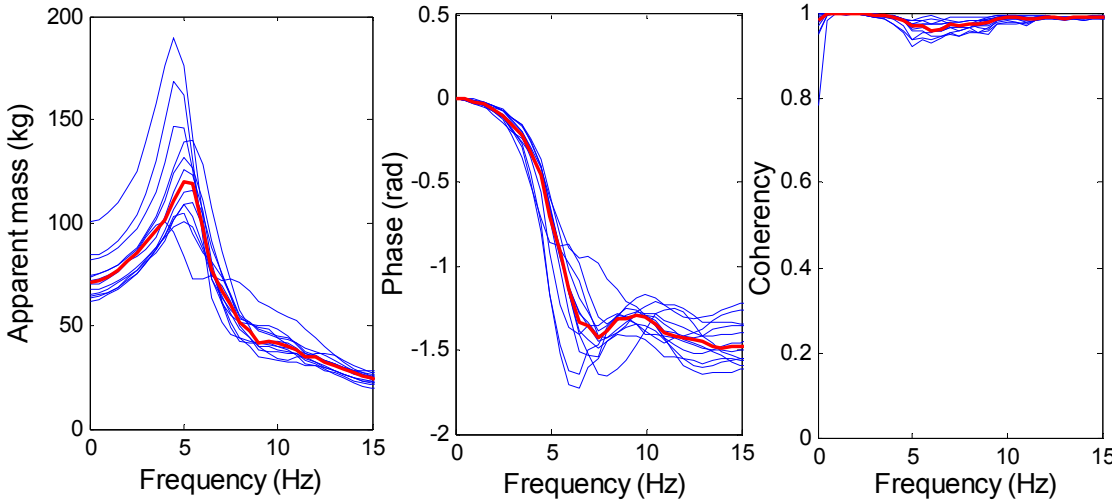

Figure C1.3 Vertical in-line apparent mass at the seat pan in normal upright sitting posture with 50 N force applied to pelvis (FP) of 12 individual subjects when exposed to 1.0 m/s^2 r.m.s. vibration. Individual subject: ('—'); Median of 12 subjects: ('—'). In one row, from left to right: modulus, phase and coherency.

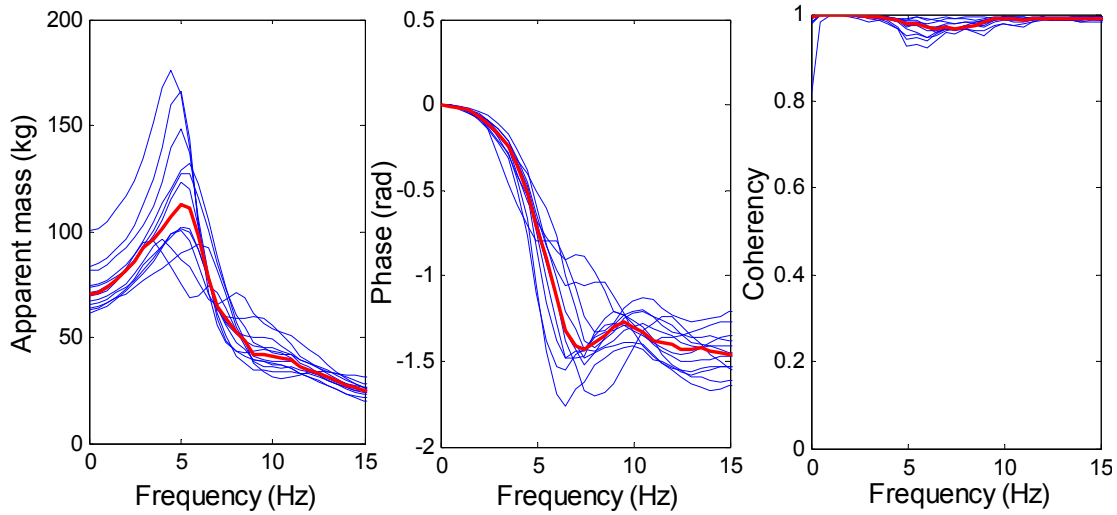

Figure C1.4 Vertical in-line apparent mass at the seat pan in normal upright sitting posture with 100 N force applied to pelvis (2FP) of 12 individual subjects when exposed to 1.0 m/s^2 r.m.s. vibration. Individual subject: ('—'); Median of 12 subjects: ('—'). In one row, from left to right: modulus, phase and coherency.

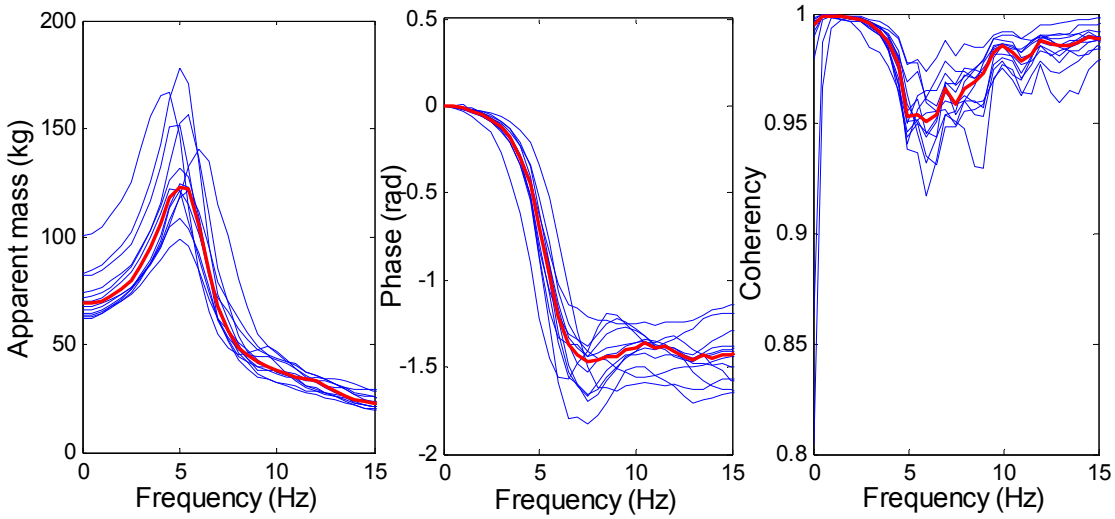

Figure C1.5 Vertical in-line apparent mass at the seat pan in normal upright sitting posture with upper body voluntary tensed (UT) of 12 individual subjects when exposed to 1.0 m/s^2 r.m.s. vibration. Individual subject: ('—'); Median of 12 subjects: ('—'). In one row, from left to right: modulus, phase and coherency.

Fore-and-aft cross-axis apparent mass at the seat

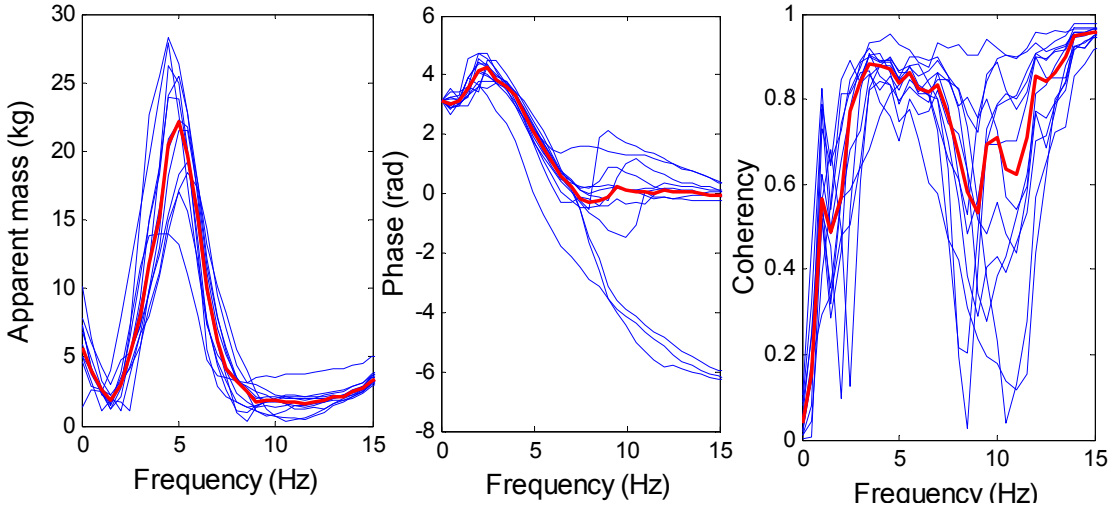

Figure C1.6 Fore-and-aft cross-axis in-line apparent mass at the seat pan in normal upright sitting posture with 50 N force applied to thoracic spine (FU) of 12 individual subjects when exposed to 1.0 m/s^2 r.m.s. vibration. Individual subject: ('—'); Median of 12 subjects: ('—'). In one row, from left to right: modulus, phase and coherency.

2FU 1.0 rms:

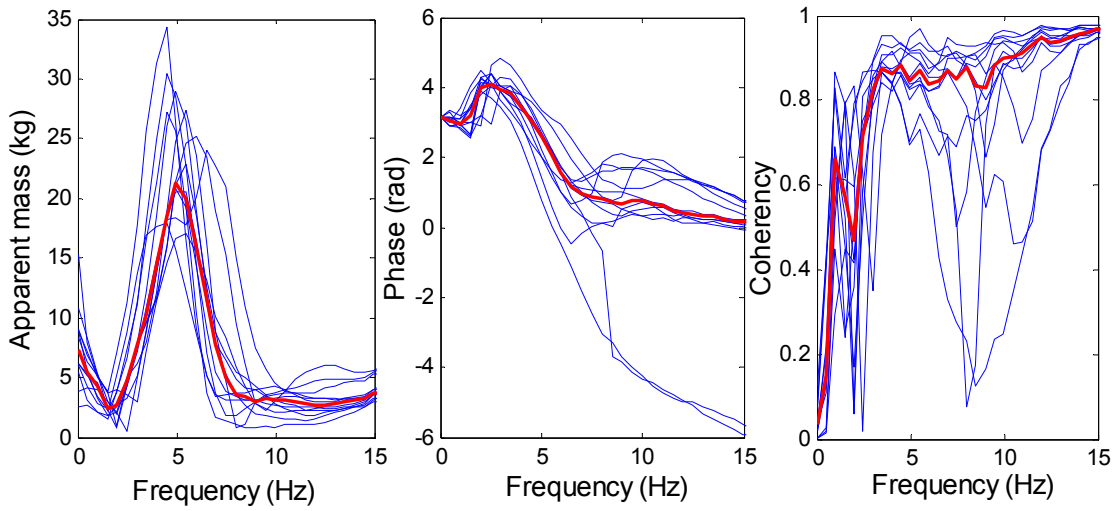

Figure C1.7 Fore-and-aft cross-axis in-line apparent mass at the seat pan in normal upright sitting posture with 100 N force (2FU) applied to thoracic spine (T5) of 12 individual subjects when exposed to 1.0 m/s^2 r.m.s. vibration. Individual subject: ('—'); Median of 12 subjects: ('—'). In one row, from left to right: modulus, phase and coherency.

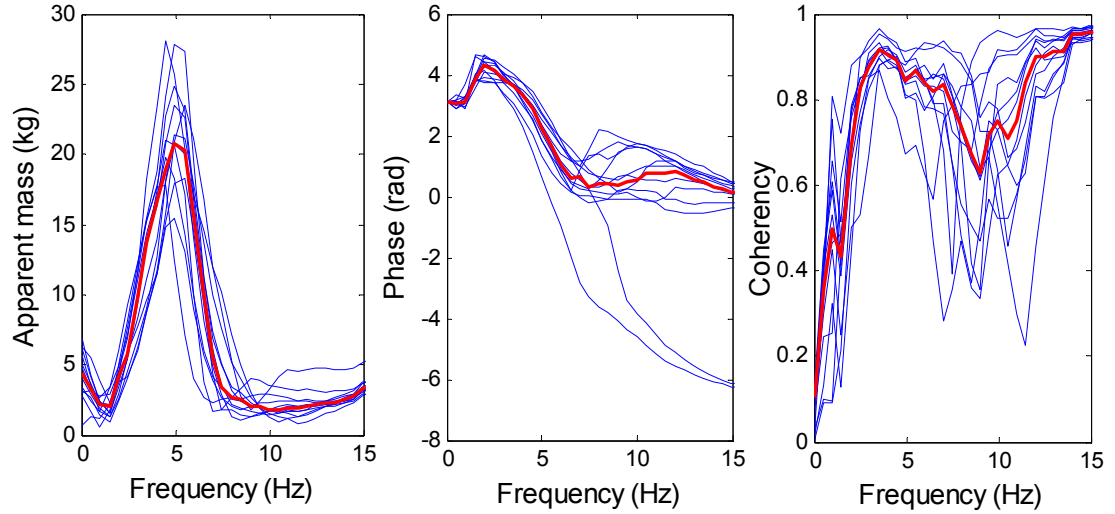

Figure C1.8 Fore-and-aft cross-axis in-line apparent mass at the seat pan in normal upright sitting posture with 50 N force applied to pelvis (FP) of 12 individual subjects when exposed to 1.0 m/s^2 r.m.s. vibration. Individual subject: ('—'); Median of 12 subjects: ('—'). In one row, from left to right: modulus, phase and coherency.

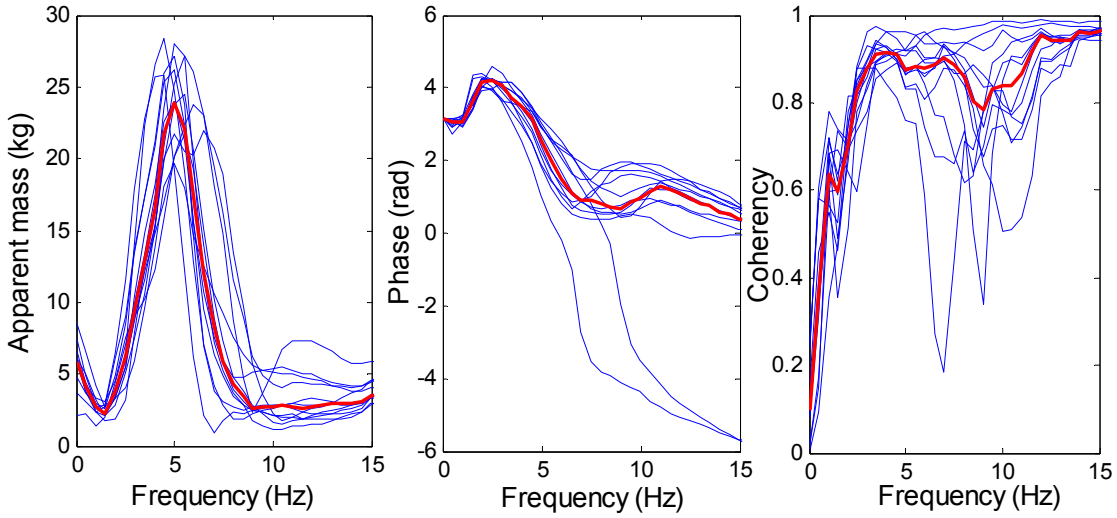

Figure C1.9 Fore-and-aft cross-axis in-line apparent mass at the seat pan in normal upright sitting posture with 100 N force applied to pelvis (2FP) of 12 individual subjects when exposed to 1.0 m/s^2 r.m.s. vibration. Individual subject: ('—'); Median of 12 subjects: ('—'). In one row, from left to right: modulus, phase and coherency.

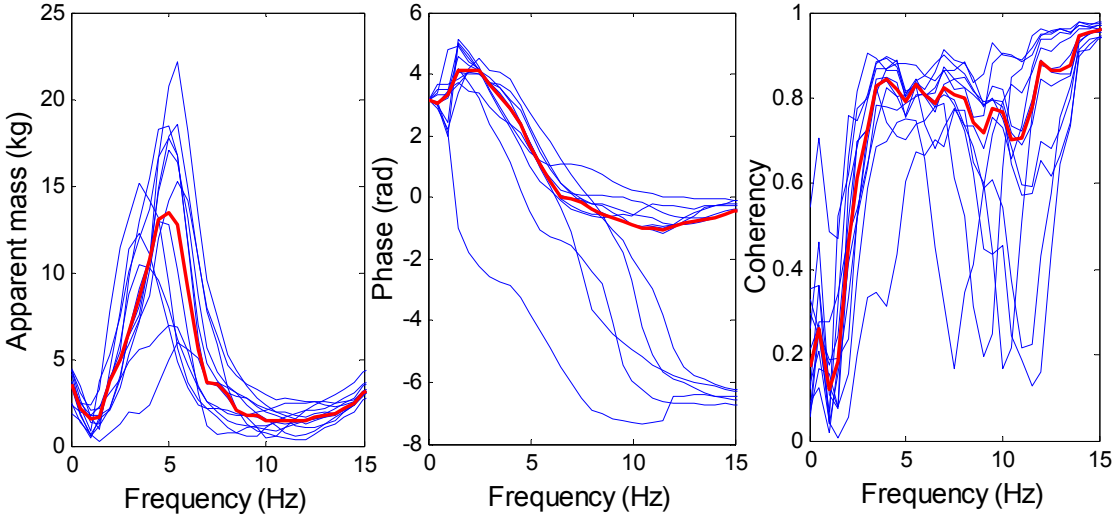

Figure C1.10 Fore-and-aft cross-axis in-line apparent mass at the seat pan in normal upright sitting with upper body voluntary tensed (UT) of 12 individual subjects when exposed to 1.0 m/s^2 r.m.s. vibration. Individual subject: ('—'); Median of 12 subjects: ('—'). In one row, from left to right: modulus, phase and coherency.

C.2 Median vertical transmissibility, fore-and-aft transmissibility and pitch transmissibility to spinal levels: pelvis, L5, L3 and T5.

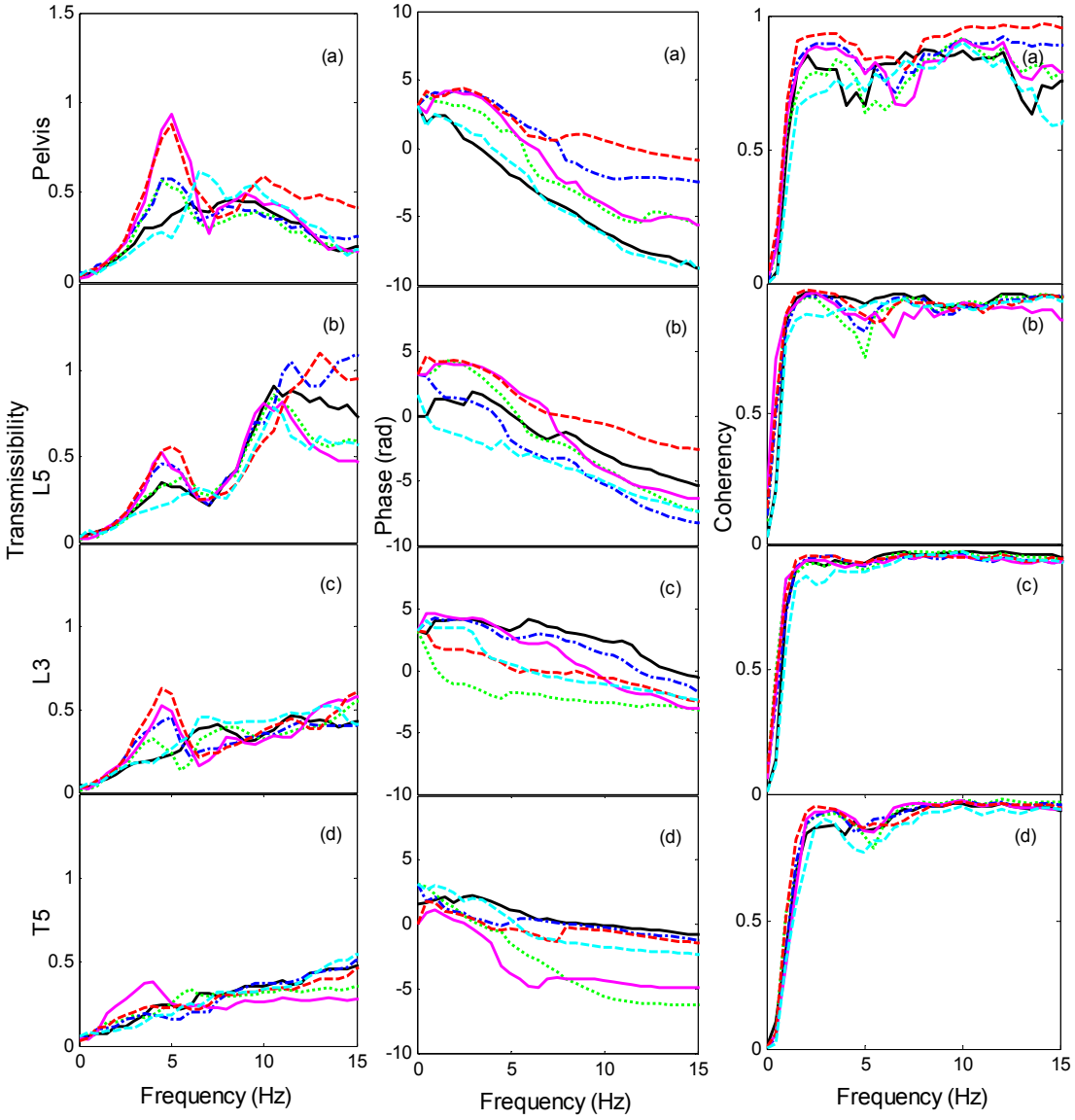

Figure C2.1 Fore-and-aft cross-axis transmissibilities to spinal levels (a: pelvis; b: L5; c: L3; d: T5) in different sitting conditions: normal upright sitting posture when exposed to 1.0 m/s^2 r.m.s. vibration: normal ('——'); FP ('--•--•--'); 2FP ('------'); FU ('·····'); 2FU ('—'); UT ('– – '). Left: modulus; middle: phase; right: coherency functions. Median values from 12 subjects.

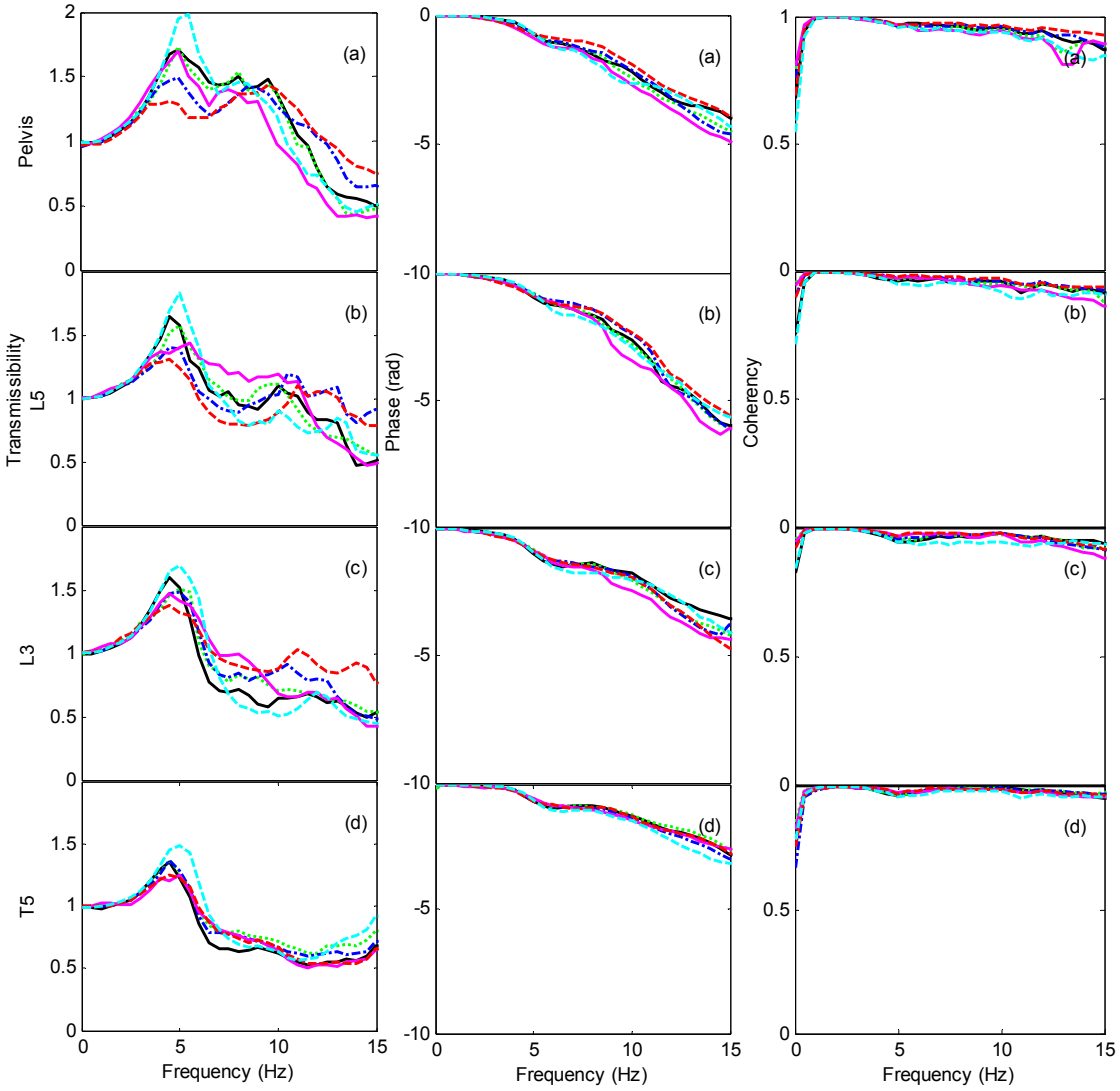

Figure C2.2 Vertical in-line transmissibilities to spinal levels (a: pelvis; b: L5; c: L3; d: T5) in different sitting conditions: normal upright sitting posture when exposed to 1.0 m/s^2 r.m.s. vibration: normal upright sitting posture: normal ('——'); with 50 N force applied to pelvis: FP ('–•–•–'); with 100 N force applied to pelvis: 2FP ('------'); with 50 N force applied to upper body T5: FU ('·····'); with 100 N force applied to upper body T5: 2FU ('—'); upright sitting with upper body voluntary tensed: UT ('– – –'). Left: modulus; right: phase. Median values from 12 subjects.

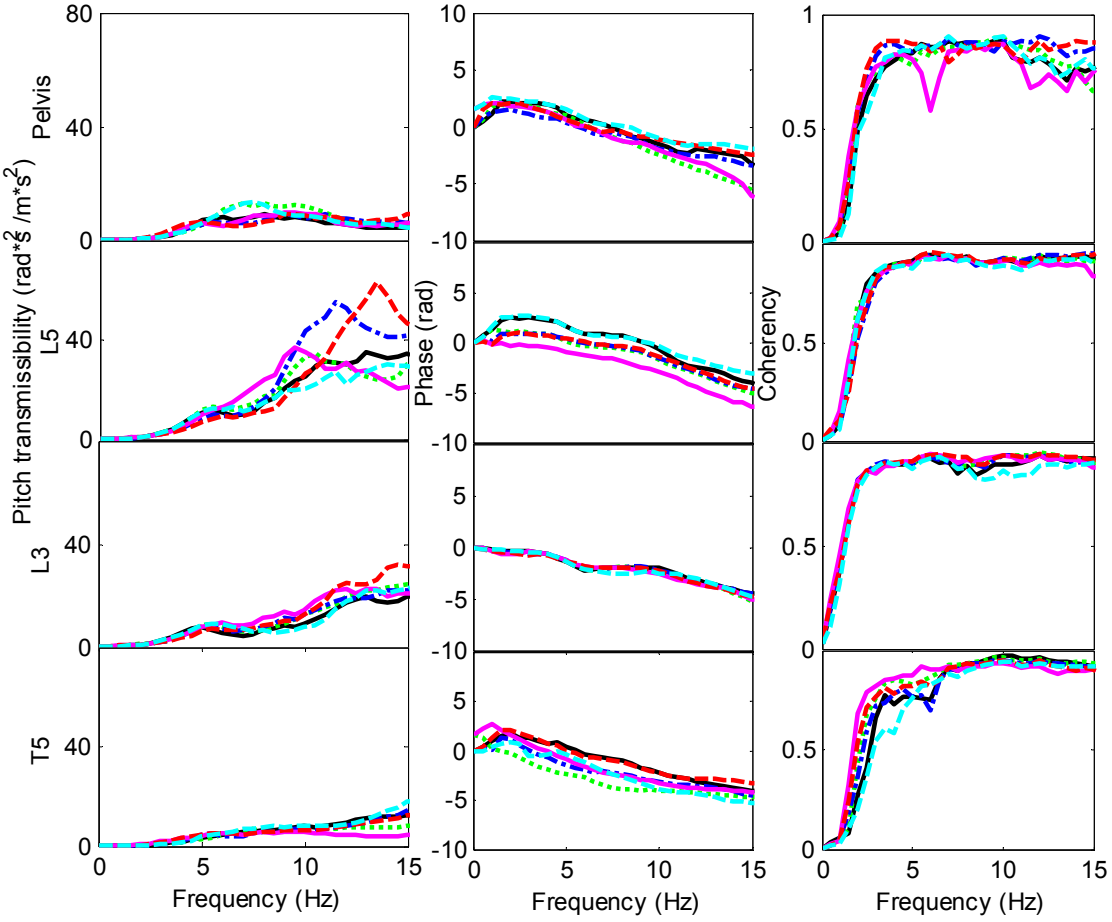

Figure C2.3 Pitch transmissibilities to spinal levels (a: pelvis; b: L5; c: L3; d: T5) in different sitting conditions: normal upright sitting posture when exposed to 1.0 m/s^2 r.m.s. vibration: normal upright sitting posture: normal ('——'); with 50 N force applied to pelvis: FP ('--•--•--'); with 100 N force applied to pelvis: 2FP ('------'); with 50 N force applied to upper body T5: FU ('·····'); with 100 N force applied to upper body T5: 2FU ('—'); upright sitting with upper body voluntary tensed: UT ('– – –'). Left: modulus; right: phase. Median values from 12 subjects.

C.3 Inter-subject variability in the measured apparent masses in six sitting conditions

Tables C3.1 Inter-subject variability in the measured vertical in-line apparent mass at the seat pan at 2.5 Hz, 5 Hz, and 10 Hz when exposed to vertical random vibration of 1.0 m/s^2 r.m.s. from 0.2 – 20 Hz, referring to Figure 9.3 in Chapter 9.

Vertical in-line apparent mass (kg) at the seat pan at 2.5 Hz						
Sitting conditions	Normal*	FU	2FU	FP	2FP	UT
Median	80.81	83.60	85.45	84.92	86.12	79.98
Min	73.80	62.57	60.98	75.21	73.52	73.07
Max	127.55	126.09	127.20	124.50	123.66	125.24
Lower quartile Q1	76.52	76.16	76.15	77.09	77.61	75.49
Upper quartile Q3	90.44	90.66	91.68	90.30	90.96	89.36
Inter-quartile range (Q3-Q1)	13.93	14.50	15.54	13.21	13.35	13.87

Vertical in-line apparent mass (kg) at the seat pan at 5 Hz						
Sitting conditions	Normal*	FU	2FU	FP	2FP	UT
Median	110.16	120.62	123.16	120.16	112.43	122.72
Min	100.90	88.24	82.88	83.31	75.28	98.52
Max	162.74	179.62	178.22	176.04	165.94	177.71
Lower quartile Q1	107.80	108.65	104.84	107.46	97.46	118.55
Upper quartile Q3	146.16	147.86	137.79	140.44	133.41	148.23
Inter-quartile range (Q3-Q1)	38.37	39.20	32.94	32.99	35.95	29.67

Vertical in-line apparent mass (kg) at the seat pan at 10 Hz						
Sitting conditions	Normal*	FU	2FU	FP	2FP	UT
Median	40.14	43.58	37.95	41.37	40.95	37.81
Min	32.82	30.87	32.20	32.89	31.49	32.61
Max	49.89	51.78	48.64	56.88	55.51	46.93
Lower quartile Q1	37.26	37.78	36.59	38.30	36.98	37.04
Upper quartile Q3	44.15	45.50	44.47	44.45	45.77	42.62
Inter-quartile range (Q3-Q1)	6.89	7.72	7.88	6.15	8.79	5.58

* referring to normal sitting posture with feet hanging

Tables C3.2 Inter-subject variability in the measured fore-and-aft cross-axis apparent mass at the seat pan at 2.5 Hz, 5 Hz, and 10 Hz when exposed to vertical random vibration of 1.0 m/s^2 r.m.s. from 0.2 – 20 Hz, referring to Figure 9.3 in Chapter 9.

Fore-and-aft cross-axis apparent mass (kg) at the seat pan at 2.5 Hz						
Sitting conditions	Normal*	FU	2FU	FP	2FP	UT
Median	6.01	5.15	4.69	5.82	6.20	4.94
Min	2.26	1.12	0.44	4.08	3.23	1.29
Max	10.73	11.48	11.22	9.28	11.60	11.47
Lower quartile Q1	5.05	4.25	4.11	5.20	5.37	3.86
Upper quartile Q3	6.77	6.48	6.76	7.24	7.78	6.31
Inter-quartile range (Q3-Q1)	1.72	2.23	2.65	2.04	2.42	2.45

Fore-and-aft cross-axis apparent mass (kg) at the seat pan at 5 Hz						
Sitting conditions	Normal*	FU	2FU	FP	2FP	UT
Median	17.04	22.20	21.29	20.81	23.86	13.48
Min	7.03	13.25	15.74	12.46	19.33	4.98
Max	25.45	26.38	29.00	27.86	28.03	20.76
Lower quartile Q1	12.92	18.04	20.00	18.20	20.14	7.67
Upper quartile Q3	20.18	24.13	25.83	23.84	25.51	17.77
Inter-quartile range (Q3-Q1)	7.25	6.09	5.83	5.64	5.38	10.10

Fore-and-aft cross-axis apparent mass (kg) at the seat pan at 10 Hz						
Sitting conditions	Normal*	FU	2FU	FP	2FP	UT
Median	1.26	1.81	3.08	1.79	2.69	1.46
Min	0.22	0.67	0.78	1.28	1.12	0.46
Max	2.38	3.52	4.64	3.49	5.41	2.96
Lower quartile Q1	1.11	1.24	2.49	1.62	2.13	0.98
Upper quartile Q3	1.78	2.00	3.62	2.45	4.53	2.08
Inter-quartile range (Q3-Q1)	0.67	0.76	1.13	0.83	2.40	1.10

* referring to normal sitting posture with feet hanging

C.4 Details about the statistics in the Wilcoxon test in Chapter 9

Table 9.1 Statistical significances of the effects of muscle tension and applied forces on the principal resonance frequency in the vertical apparent mass at the seat pan and the modulus of the apparent mass at resonance. Wilcoxon matched-pairs signed ranks test.

Resonance frequency of the vertical apparent mass at the seat pan						
	Normal	FP	2FP	FU	2FU	UT
Normal	-	0.0430↑(FP)	0.1499	0.0781	0.0501↑(2FU)	0.0049↑ (UT)
FP		-	0.8203	0.6133	0.4531	0.1328
2FP			-	0.9570	0.5313	0.5938
FU				-	0.8438	0.1016
2FU					-	0.6328
UT						-

Vertical apparent mass at the seat pan at the resonance frequency						
	Normal	FP	2FP	FU	2FU	UT
Normal	-	0.7334	0.0640	0.7910	0.9697	0.1294
FP		-	0.005↓ (2FP)	0.5830	0.5693	0.2036
2FP			-	0.0210↑ (FU)	0.0151 ↑ (2FU)	0.0342 ↑ (UT)
FU				-	0.5186	0.3394
2FU					-	0.2412
UT						-

Table 9.2 Statistical significances of the effects of muscle tension and applied forces on the resonance frequency in the fore-and-aft apparent mass at the seat pan and the modulus of the apparent mass at the resonance. Wilcoxon matched-pairs signed ranks test.

Resonance frequency of fore-and-aft apparent mass at the seat pan						
	normal	FP	2FP	FU	2FU	UT
normal	-	0.1250	0.0156↑ (2FP)	0.7578	0.0742	0.6484
FP		-	0.1250	0.6250	0.3438	0.7617
2FP			-	0.1719	1	0.2539
FU				-	0.0938	0.8164
2FU					-	0.3047
UT						-

Fore-and-aft apparent mass at the seat pan at the resonance frequency						
	normal	FP	2FP	FU	2FU	UT
normal	-	0.0210↑ (FP)	0.0005↑ (2FP)	0.0161↑ (FU)	0.0005↑ (2FU)	0.2661
FP		-	0.0171↑ (2FP)	0.8501	0.1514	0.0010↓ (UT)
2FP			-	0.1763	0.7910	0.0005↓ (UT)
FU				-	0.0425↑ (2FU)	0.0015↓ (UT)
2FU					-	0.0005↓ (UT)
UT						-

Appendix D Mathematical expression for the development of the multibody model without backrest

The 7 degree-of-freedom multibody model described in Chapter 4 with positions of centre of gravity (COG) of the body segments is shown in Figure D.1. This section described the process of deriving the equations of motion and how the equations of motion of this model were solved in the frequency domain.

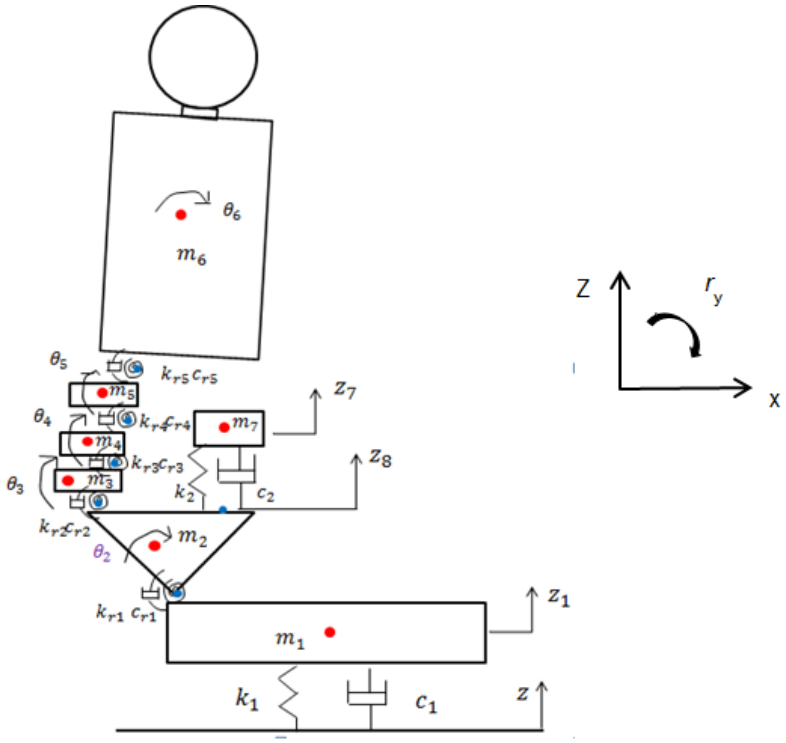

Figure D.1 Multi-body model of the seated human body represented by seven rigid bodies connected with rotational joints, and translational springs and dampers. 1 - thighs; 2 - pelvis; 3 - L5; 4 - L4; 5 - L3; 6 - upper-body from head to L2; 7 - viscera in the abdomen.

The equations of motion of the model with backrest were derived using Lagrange equations with the assumption that all body parts oscillate around their equilibrium positions with small displacements. The model (Figure 1) has seven degree-of-freedom: z_1 and z_7, the vertical displacement of the thighs and viscera, and, $\theta_2, \theta_3, \theta_4, \theta_5, \theta_6$, the absolute rotational displacements of the pelvis, the lumbar spine (at L5, L4, and L3), and the upper-body. The input was represented by displacement, z, at the buttocks tissue. The equations of motion of the model were derived using Lagrange equations:

$$\frac{d}{dt}\left(\frac{\partial T}{\partial \dot{q}}\right)+\frac{\partial D}{\partial \dot{q}}+\frac{\partial U}{\partial q}=0\ ;\ q=\left[z_1;\theta_2;\theta_3;\theta_4;\theta_5;\theta_6;z_7\right] \tag{D.1}$$

The kinetic energy, T, potential energy, U, and dissipation function, D, of the system were calculated as:

$$T = \frac{1}{2}\sum_{i=1}^{7} m_i(\dot{x}_i^2 + \dot{z}_i^2) + \frac{1}{2}\sum_{i=2}^{6} I_i\dot{\theta}_i^2 \quad \text{(D.2)}$$

$$D = \frac{1}{2}c_1(\dot{z}_1 - \dot{z})^2 + \frac{1}{2}c_{r1}(\dot{\theta}_2)^2 + \frac{1}{2}c_{r2}(\dot{\theta}_3 - \dot{\theta}_2)^2 + \frac{1}{2}c_{r3}(\dot{\theta}_4 - \dot{\theta}_3)^2 + \frac{1}{2}c_{r4}(\dot{\theta}_5 - \dot{\theta}_4)^2 + \frac{1}{2}c_{r5}(\dot{\theta}_6 - \dot{\theta}_5)^2 + \frac{1}{2}c_2(\dot{z}_7 - \dot{z}_8)^2 + \frac{1}{2}c_{bz}(\dot{z}_b - \dot{z})^2 \quad \text{(D.3)}$$

$$U = \frac{1}{2}k_1(z_1 - z)^2 + \frac{1}{2}k_{r1}(\theta_2)^2 + \frac{1}{2}k_{r2}(\theta_3 - \theta_2)^2 + \frac{1}{2}k_{r3}(\theta_4 - \theta_3)^2 + \frac{1}{2}k_{r4}(\theta_5 - \theta_4)^2 + \frac{1}{2}k_{r5}(\theta_6 - \theta_5)^2 + \frac{1}{2}k_2(z_7 - z_8)^2 + \frac{1}{2}k_{bz}(z_b - z)^2 \quad \text{(D.4)}$$

where, m_i is the mass of each body part, (x_i, z_i) and $(\dot{x}_i, \dot{z}_i)$ represent the displacement and velocity of each body at the centre of gravity in the *x* and *z* directions associated with whole-body vibration, i = 1, 2, 3, 4, 5, 6, 7 denotes the number of body parts. The combinations of k_1 and c_1, and k_2 and c_2, represent the stiffness and damping coefficients of the spring and damper beneath thighs and viscera, respectively, k_{ri} and c_{ri} represent the stiffness and damping coefficients of the rotational joint r_j, where j =1, 2, 3, 4, 5 denotes the number of the rotational joint.

As assumed that each rotational segment oscillates around its equilibrium position with small displacement, the process of the calculation of displacement was shown below:

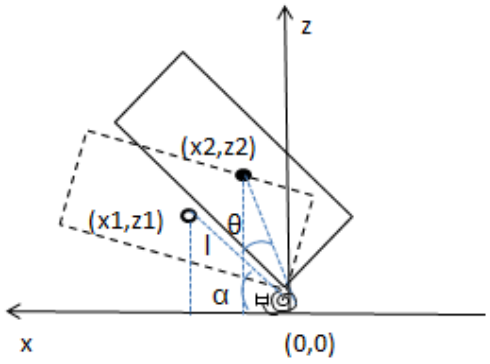

Figure D.2 Simplification in calculating the movement of the COG of body segments or point on the body.

where, (x1,z1) is the initial position, (x2,z2) is the position when the segment rotates with the angle of θ. l is the distance between the centre of gravity of this segment and the connecting point (0,0). Therefore, the horizontal displacement Δx , and vertical displacement Δz were calculated as:

$$\Delta x = x2 - x1 = l * \cos(\alpha + \theta) - l * \cos\alpha = l * [\cos\alpha * (\cos\theta - 1) - \sin a * \sin\theta] \ ;$$

$$\Delta z = z2 - z1 = l * \sin(\alpha + \theta) - l * \sin\alpha = l * [\sin\alpha * (\cos\theta - 1) + \cos\alpha * \sin\theta] \quad \text{(D.5)}$$

As the rotational angle θ is small, then $\cos\theta - 1 \approx 0$, and $\sin\theta \approx \theta$; therefore,

$$\Delta x \approx l * \sin\alpha * \theta \ ;$$

$$\Delta z \approx l * \cos\alpha * \theta \ ; \quad \text{(D.6)}$$

Following the same assumption and method, the movements (i.e., velocity) of the COG of each body segment was calculated as:

$$\begin{bmatrix} x_2 \\ x_3 \\ x_4 \\ x_5 \\ x_6 \end{bmatrix} = x_{r1} + \begin{bmatrix} h_2 & 0 & 0 & 0 & 0 \\ h_2 + h_{r2} & h_3 & 0 & 0 & 0 \\ h_2 + h_{r2} & h_3 + h_{r3} & h_4 & 0 & 0 \\ h_2 + h_{r2} & h_3 + h_{r3} & h_4 + h_{r4} & h_5 & 0 \\ h_2 + h_{r2} & h_3 + h_{r3} & h_4 + h_{r4} & h_5 + h_{r5} & h_6 \end{bmatrix} \begin{bmatrix} \theta_2 \\ \theta_3 \\ \theta_4 \\ \theta_5 \\ \theta_6 \end{bmatrix} \quad \text{(D.7)}$$

$$\begin{bmatrix} z_2 \\ z_3 \\ z_4 \\ z_5 \\ z_6 \end{bmatrix} = z_{r1} + \begin{bmatrix} l_2 & 0 & 0 & 0 & 0 \\ l_2 + l_{r2} & l_3 & 0 & 0 & 0 \\ l_2 + l_{r2} & l_3 + l_{r3} & l_4 & 0 & 0 \\ l_2 + l_{r2} & l_3 + l_{r3} & l_4 + l_{r4} & l_5 & 0 \\ l_2 + l_{r2} & l_3 + l_{r3} & l_4 + l_{r4} & l_5 + l_{r5} & i_6 \end{bmatrix} \begin{bmatrix} \theta_2 \\ \theta_3 \\ \theta_4 \\ \theta_5 \\ \theta_6 \end{bmatrix} \quad \text{(D.8)}$$

(D.7)

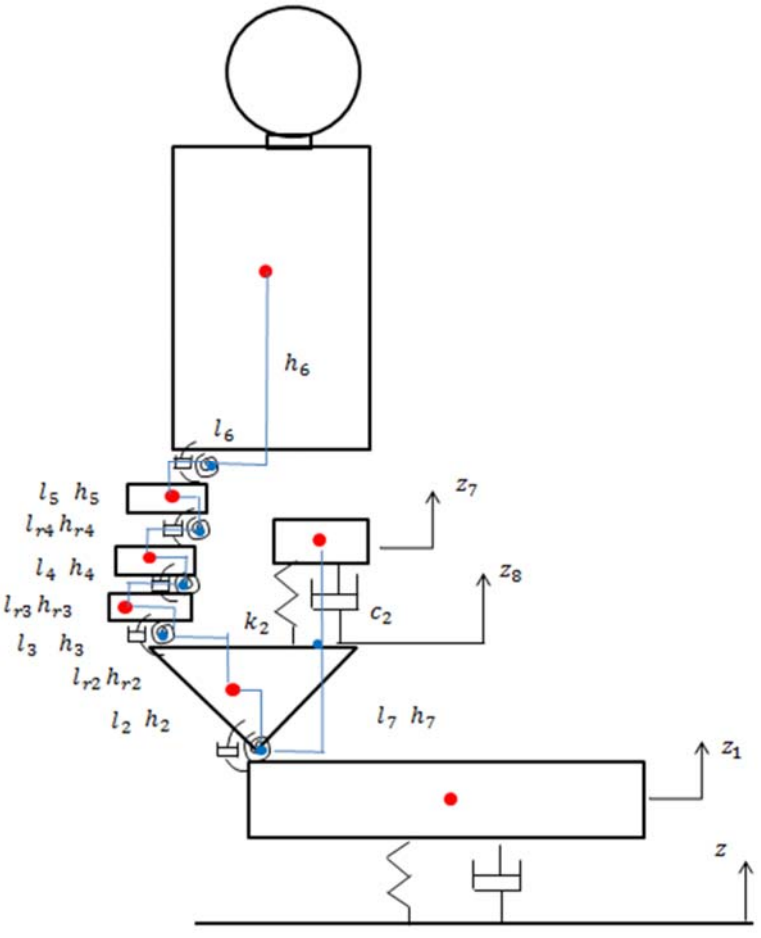

Figure D.3 The length parameters in the multi-body model.

When the centre of gravity (COG) of each segment and positions for each joints were expressed as coordinates, the length parameters can be calculated as:

l_2= $x_{r1} - x_2$; h_2= $z_2 - z_{r1}$;

l_{r2}= $x_2 - xr_2$; h_{r2}= $z_{r2} - z_2$;

l_3= $xr_2 - x_3$; h_3= $z_3 - z_{r2}$;

l_{r3}= $x_3 - x_{r3}$; h_{r3}= $z_{r3} - z_3$;

l_4= $xr_3 - x_4$; h_4= $z_4 - z_{r3}$;

l_{r4}= $x_4 - x_{r4}$; h_{r4}= $z_{r4} - z_4$;

l_5= $x_{r4} - x_5$; h_5= $z_5 - z_{r4}$;

l_{r5}= $x_5 - x_{r5}$; h_{r5}= $z_{r5} - z_5$;

l_6= $x_{r5} - x_6$; h_6= $z_6 - z_{r5}$; (D.9)

where $(\dot{x}_{r1}, \dot{z}_{r1})$ represents the movement (i.e., velocity) of rotational joint r_1 in the fore-and-aft and vertical directions, respectively. As there is no horizontal degree-of-freedom at the thighs in the model, $\dot{x}_{r1} = 0$, and $\dot{z}_{r1} = \dot{z}_1$. Parameter l_i, i=2, 3, …, 7, represents the horizontal distance from rotational joint (i-1) to the centre-of-gravity of the rigid body i. Parameter h_i, i=1,2, …, 7, represents the vertical distance from rotational joint (i-1) to the centre-of-gravity of rigid body i. Parameter l_{ri}, i=2, 3, …, 5, represents the horizontal distance from joint i to the centre-of-gravity of rigid body i. Parameter h_{ri}, i=2, 3, …, 5, represents the vertical distance from joint i to the centre-of-gravity of rigid body i.

From the kinetic matrix T, potential energy matrix U and damping matrix D, seven equations were generated to form the equations of motion. The calculation process was shown below:

The differentials of the kinetic matrix T were calculated as:

$$\frac{\partial T}{\partial \dot{z}_1} = (m_1 + m_2 + m_3 + m_4 + m_5 + m_6) * \dot{z}_1 + [m_2 * l_2 + (m_3 + m_4 + m_5 + m_6) * (l_2 + lr_2)] * \dot{\theta}_2 + [m_3 * l_3 + (m_4 + m_5 + m_6) * (l_3 + lr_3)] * \dot{\theta}_3 + [m_4 * l_4 + (m_5 + m_6) * (l_4 + lr_4)] * \dot{\theta}_4 + [m_5 * l_5 + m_6 * (l_5 + lr_5)] * \dot{\theta}_5 - m_6 * l_6 * \dot{\theta}_6; \quad \text{(D.10)}$$

$$\frac{\partial T}{\partial \dot{\theta}_2} = [m_2 * l_2 + (m_3 + m_4 + m_5 + m_6) * (l_2 + lr_2)] * \dot{z}_1 + [m_2 * (h_2)\text{^}2 + (h_2 + h_{r2})\text{^}2 * (m_3 + m_4 + m_5 + m_6) + m_2 * (l_2)\text{^}2 + (m_3 + m_4 + m_5 + m_6) * (l_2 + l_{r2})\text{^}2 + I_2] * \dot{\theta}_2 + [m_3 * (h_2 + h_{r2}) * h_3 + (h_2 + h_{r2}) * (h_3 + h_{r3}) * (m_4 + m_5 + m_6) + m_3 * (l_3) * (l_2 + l_{r2}) + (m_4 + m_5 + m_6) * (l_2 + l_{r2}) * (l_3 + l_{r3})] * \dot{\theta}_3 + [m_4 * (h_2 + h_{r2}) * h_4 + (h_2 + h_{r2}) * (h_4 + h_{r4}) * (m_5 + m_6) + m_4 * (l_4) * (l_2 + l_{r2}) + (m_5 + m_6) * (l_2 + l_{r2}) * (l_4 + l_{r4})] * \dot{\theta}_4 + [m_5 * (h_2 + h_{r2}) * h_5 + (h_2 + h_{r2}) * (h_5 + h_{r5}) * (m_6) + m_5 * (l_5) * (l_2 + l_{r2}) + (m_6) * (l_2 + l_{r2}) * (l_5 + l_{r5}) * \dot{\theta}_5 + [m_6 * (h_2 + h_{r2}) * h_6 + m_6 * (l_2 + l_{r2}) * l_6] * \dot{\theta}_6; \quad \text{(D.11)}$$

Similarly, the remaining differentials of kinetic matrix T, damping D and potential energy matrix U are derived in same manner, including: $\frac{\partial T}{\partial \dot{\theta}_3}$, $\frac{\partial T}{\partial \dot{\theta}_4}$, $\frac{\partial T}{\partial \dot{\theta}_5}$, $\frac{\partial T}{\partial \dot{\theta}_6}$, $\frac{\partial T}{\partial \dot{z}_7}$, $\frac{\partial D}{\partial \dot{z}_1}$, $\frac{\partial D}{\partial \dot{\theta}_2}$, $\frac{\partial D}{\partial \dot{\theta}_3}$, $\frac{\partial D}{\partial \dot{\theta}_4}$, $\frac{\partial D}{\partial \dot{\theta}_5}$, $\frac{\partial D}{\partial \dot{\theta}_6}$, $\frac{\partial D}{\partial \dot{z}_7}$, $\frac{\partial U}{\partial z_1}$, $\frac{\partial U}{\partial \theta_2}$, $\frac{\partial U}{\partial \theta_3}$, $\frac{\partial U}{\partial \theta_4}$, $\frac{\partial U}{\partial \theta_5}$, $\frac{\partial U}{\partial \theta_6}$, $\frac{\partial U}{\partial z_7}$.

The equations of motion were then derived as:

$$[M][\ddot{q}] + [C][\dot{q}] + [K][q] = [F] \tag{D.12}$$

With Laplace transform, the response of the above equation in the frequency domain was calculated, and the apparent mass in vertical direction, fore-and-aft and vertical transmissibility to lumbar spine (L3) are derived in the same manner as model in normal sitting posture.

The mass matrix was in the form of 7 x 7:

$$[M] = [7 \times 7]$$

where,

$M(1,1)= m_1+m_2+m_3+m_4+m_5+m_6$;
$M(1,2)= m_2*l_2+(m_3+m_4+m_5+m_6)*(l_2+l_{r2})$;
$M(1,3)= m_3*l_3+(m_4+m_5+m_6)*(l_3+l_{r3})$;
$M(1,4)= m_4*l_4+(m_5+m_6)*(l_4+l_{r4})$;
$M(1,5)= m_5*l_5+m_6*(l_5+l_{r5})$;
$M(1,6)=-m_6*l_6$;
$M(1,7)=0$;

$M(2,1)=M(1,2)$;
$M(2,2)=m_2*(h_2)^2+(h_2+h_{r2})^2*(m_3+m_4+m_5+m_6)+m_2*(l_2)^2+(m_3+m_4+m_5+m_6)*(l_2+l_{r2})^2+I_2$;
$M(2,3)=m_3*(h_2+h_{r2})*h_3+(h_2+h_{r2})*(h_3+h_{r3})*(m_4+m_5+m_6)+m_3*(l_3)*(l_2+l_{r2})+(m_4+m_5+m_6)*(l_2+l_{r2})*(l_3+l_{r3})$;
$M(2,4)=m_4*(h_2+h_{r2})*h_4+(h_2+h_{r2})*(h_4+h_{r4})*(m_5+m_6)+m_4*(l_4)*(l_2+l_{r2})+(m_5+m_6)*(l_2+l_{r2})*(l_4+l_{r4})$;
$M(2,5)=m_5*(h_2+h_{r2})*h_5+(h_2+h_{r2})*(h_5+h_{r5})*(m_6)+m_5*(l_5)*(l_2+l_{r2})+(m_6)*(l_2+l_{r2})*(l_5+l_{r5})$;
$M(2,6)=m_6*(h_2+h_{r2})*h_6+m_6*(l_2+l_{r2})*l_6$;
$M(2,7)=0$;

$M(3,1)=M(1,3)$;
$M(3,2)=M(2,3)$;
$M(3,3)=m_3*(h_3)^2+(h_3+h_{r3})^2*(m_4+m_5+m_6)+m_3*(l_3)^2+(m_4+m_5+m_6)*(l_3+l_{r3})^2+I_3$;
$M(3,4)=m_4*(h_3+h_{r3})*h_4+(h_3+h_{r3})*(h_4+h_{r4})*(m_5+m_6)+m_4*(l_4)*(l_3+l_{r3})+(m_5+m_6)*(l_3+l_{r3})*(l_4+l_{r4})$;
$M(3,5)=m_5*(h_3+h_{r3})*h_5+(h_3+h_{r3})*(h_5+h_{r5})*(m_6)+m_5*(l_5)*(l_3+l_{r3})+(m_6)*(l_3+l_{r3})*(l_5+l_{r5})$;
$M(3,6)=m_6*(h_3+h_{r3})*h_6+m_6*(l_3+l_{r3})*(l_6)$;
$M(3,7)=0$;

$M(4,1)=M(1,4)$;
$M(4,2)=M(2,4)$;
$M(4,3)=M(3,4)$;
$M(4,4)=m_4*(h_4)^2+(h_4+h_{r4})^2*(m_5+m_6)+m_4*(l_4)^2+(m_5+m_6)*(l_4+l_{r4})_2+I_4$;
$M(4,5)=m_5*(h_4+h_{r4})*h_5+(h_4+h_{r4})*(h_5+h_{r5})*(m_6)+m_5*(l_4)*(l_4+l_{r4})+(m_6)*(l_4+l_{r4})*(l_5+l_{r5})$;
$M(4,6)=m_6*(h_4+h_{r4})*h_6+m_6*(l_4+l_{r4})*(l_6)$;
$M(4,7)=0$;

$M(5,1)=M(1,5)$;
$M(5,2)=M(2,5)$;
$M(5,3)=M(3,5)$;
$M(5,4)=M(4,5)$;
$M(5,5)=m_5*(h_5)^2+(h_5+h_{r5})^2*(m_6)+m_4*(l_5)^2+(m_6)*(l_5+l_{r5})^2+I_5$;
$M(5,6)=m_6*(h_5+h_{r5})*h_6+m_6*(l_5+l_{r5})*(l_6)$;
$M(5,7)=0$;

$M(6,1)=M(1,6)$;

$M(6,2)=M(2,6)$;
$M(6,3)=M(3,6)$;
$M(6,4)=M(4,6)$;
$M(6,5)=M(5,6)$;
$M(6,6)=m_6*(h_6)^2+m_6*(l_6)^2+I_6$;
$M(6,7)=0$;

$M(7,1)=M(1,7)$;
$M(7,2)=M(2,7)$;
$M(7,3)=M(3,7)$;
$M(7,4)=M(4,7)$;
$M(7,5)=M(5,7)$;
$M(7,6)=M(6,7)$;
$M(7,7)=m_7$;

The damping matrix [*C*] is:

$$[C]=\begin{bmatrix} c1+c2 & c2*l7 & 0 & 0 & 0 & 0 & -c2 \\ c2*l7 & cr4+cr5+c2*l7^2 & -cr4 & 0 & 0 & 0 & -c2*l7 \\ 0 & -cr4 & cr3+cr4 & -cr3 & 0 & 0 & 0 \\ 0 & 0 & -cr3 & cr2+cr3 & -cr2 & 0 & 0 \\ 0 & 0 & 0 & -cr2 & cr1+cr2 & -cr1 & 0 \\ 0 & 0 & 0 & 0 & -cr1 & cr1 & 0 \\ -c2 & -c2*l7 & 0 & 0 & 0 & 0 & c2 \end{bmatrix} \quad \text{(D.13)}$$

The stiffness matrix [*K*] is:

$$[K]=\begin{bmatrix} k1+k2 & k2*l7 & 0 & 0 & 0 & 0 & -k2 \\ k2*l7 & kr4+kr5+k2*l7^2 & -kr4 & 0 & 0 & 0 & -k2*l7 \\ 0 & -kr4 & kr3+kr4 & -kr3 & 0 & 0 & 0 \\ 0 & 0 & -kr3 & kr2+kr3 & -kr2 & 0 & 0 \\ 0 & 0 & 0 & -kr2 & kr1+kr2 & -kr1 & 0 \\ 0 & 0 & 0 & 0 & -kr1 & kr1 & 0 \\ -k2 & -k2*l7 & 0 & 0 & 0 & 0 & k2 \end{bmatrix} \quad \text{(D.14)}$$

the matrix [*I*] is:

$$[F]=\begin{bmatrix} k1+c1*s \\ 0 \\ 0 \\ 0 \\ 0 \\ 0 \\ 0 \end{bmatrix} Z(s)=[\mathrm{Y}]*\mathrm{Z(s)} \quad \text{(D.15)}$$

With Laplace transform, $s=j*\omega=\omega=2\pi*f$; $j=\sqrt{-1}$, f is the frequency. The equation of motion was solved in the frequency domain:

$$\left[\ [M]\omega^2+[C]\omega*j+[K]\right]*[Q]=[Y]*Z(s);$$

$$[Q]=[Z_1;\Phi_2;\Phi_3;\Phi_4;\Phi_5;\Phi_6;Z_7;] \quad \text{(D.16)}$$

Then,

$$\frac{[Q]}{Z(s)} = \frac{[Y]}{\left[-[M]\omega^2 + [C]\omega * j + [K]\right]}; \tag{D.17}$$

With the matrix [M], [C], and [K] determined, for each frequency f_i, the transfer function from the input Z to each degree of freedom was obtained. The transfer function listed below could be calculated as a function of frequency:

$$\frac{Z_1}{Z}(f); \frac{\Phi_2}{Z}(f); \frac{\Phi_3}{Z}(f); \frac{\Phi_4}{Z}(f); \frac{\Phi_5}{Z}(f); \frac{\Phi_6}{Z}(f); \frac{Z_7}{Z}(f); \tag{D.18}$$

With these transfer functions determined, the vertical apparent mass at seat and both vertical and fore-and-aft transmissibilities to various spine levels could be calculated with expressions containing length relationships. For example, the math expressions for vertical apparent mass and vertical and fore-and-aft transmissibilities to the centre of lumbar spine L3 are listed below:

Vertical apparent mass at seat:

$$APM = \frac{(k_1 + j * 2 * \pi * f * c_1) * (Z(f) - Z_1(f))}{(j * 2 * \pi * f)^2 * Z(f)} \tag{D.19}$$

Vertical transmissibility to COG of L3:

$$TR_{L3\_v} = \frac{Z_1(f) + (l_2 + l_{r2}) * \Phi_2(f) + (l_3 + l_{r3}) * \Phi_3(f) + (l_4 + l_{r4}) * \Phi_4(f) + l_5 * \Phi_5(f)}{Z(f)} \tag{D.20}$$

Cross-axis fore-and-aft transmissibility to COG of L3:

$$TR_{L3\_f} = \frac{(h_2 + h_{r2}) * \Phi_2(s) + (h_3 + h_{r3}) * \Phi_3(s) + (h_4 + h_{r4}) * \Phi_4(s) + h_5 * \Phi_5(s)}{Z(s)} \tag{D.21}$$

List of References

Adams M, Bogduk N, Burton K and Dolan P (2006), The Biomechanics of Back Pain, 2nd ed. Edinburgh: Churchill Livingstone. p. 177-194.

Ayari H, Thomas M, Dore S and Serrus O (2009), Evaluation of lumbar vertebra injury risk to the seated human body when exposed to vertical vibration, Journal of Sound and Vibration, 321, 454-470.

Basri B and Griffin MJ (2013) Predicting discomfort from whole-body vertical vibration when sitting with an inclined backrest, Applied Ergonomics, Volume 44, Issue 3, 423-434.

Bazrgari B, Shirazi-Adl A and Kasra M (2008a), Computation of trunk muscle forces, spinal loads and stability in whole-bopdy vibration, Jounral of Sound and Vibration, 318, 1334-1347.

Bazrgari B, Shirazi-Adl A and Kasra M (2008b), Seated whole body vibrations with high-magnitude accelerations-relative roles of inertial and muscle forces, Journal of Biomechanics, Volume 41, Issue 12, Pages 2639-2646.

Bennett DL, Gillis DK, Portney LG, Romanow M and Sanchez AS (1989) Comparison of integrated electromyographic activity and lumbar curvature during standing and sitting in three chairs, Physical Therapy, 69 (11), 902-913

Berkson MH, Nachemson A and Schultz AB (1979), Mechanical properties of human lumbar spine motion segments – Part II: response in compression and shear; influence of gross morphology, Journal of Biomechanical Engineering, 101, 53-57.

Blüthner R, Seidel H and Hinz B (2001) Examination of the myoelectric activity of back muscles during random vibration – methodical approach and first results. Clinical Biomechanics, 16, Supplement No. 1, S25-S30.

Blüthner R, Seidel H and Hinz B (2002) Myoelectric response of back muscles to vertical random whole-body vibration with different magnitudes at different postures. Journal of Sound and Vibration, 253(1), 37-56.

Bluthner R, Seidel H and Hinz B (2002) Myoelectric response of back muscles to vertical random whole-body vibration with different magnitudes at different postures, Journal of Sound and Vibration, 253(1), 37-56

Boileau P-E and Rakheja S (1998) Whole-body vertical biodynamic response characteristics of the seated vehicle driver: measurement and model development, International Journal of Industrial Ergonomics, Volume 22, Issue 6, 449-472.

Bogduk N (1997) Clinical Anatomy of the Lumbar Spine and Sacrum, 3rd ed. New York: Churchill Livingstone. p.118.

Bounday BD (1985) Basic Optimisation Methods, Edward Arnold, London 1985

Bovenzi M (1996) Low back pain disorders and exposure to whole-body vibration in the workplace, Semin Perinatol, 20(1): 38-53

Bovenzi M and Zadini A (1992) Self-reported low back symptoms in urban bus drivers exposed to whole-body vibration. Spine, 17(9):1048-59

Bridger RS (2003) Introduction to Ergonomics, 2nd ed. London: Taylor & Francis. p.33.

Cho Y and Yoon YS (2001) Biomechanical model of human on seat with backrest for evaluating ride quality. International Journal of Industry Ergonomics, 27, 331-345.

Christophy M (2009) A detailed open-source musculoskeletal model of the human lumbar spine, Master thesis, University of California, Berkeley, US.

Dewangan KN, Shahmir A, Rakheja S and Marcotte P (2013) Seated body apparent mass response to vertical whole-body vibration: gender and anthropometric effects, International Journal of Industrial Ergonomics, 43, 375-391.

Eidelson SG (online) Lumbar spine: low back anatomy, available online at: http://www.spineuniverse.com/anatomy/lumbar-spine

Fairley TE and Griffin MJ (1989) The apparent mass of the seated human body: vertical vibration. Journal of Biomechanics, 22, 81-94.

Fritz M (2000) Description of the relation between the forces acting in the lumbar spine and whole-body vibrations by means of transfer functions. Clinical Biomechanics, 15, 234-240.

Griffin MJ, Lewis CH, Parsons KC and Whitham EM (1979) The biodynamic response of the seated human body and its application to standards. Presented in Models and Analogues for the evaluation of human biodynamic response, performance and protection conference, France.

Griffin M.J. (1990) Handbook of Human Vibration, London, Academic Press Limited.

Griffin M.J. (2001) The validation of biodynamic models, Clinical Biomechanics 16, Supplement No. 1 S81-S92.

Han KS, Rohlmann A, Yang SJ, Kim BS and Lim TH (2011) Spinal muscles can create compressive follower loads in the lumbar spine in a neutral standing posture. Medical Engineering & Physics, 33, 472-478.

Hinz B and Seidel H (1987), The nonlinearity of the human body's dynamic response during sinusoidal whole body vibration, Industrial Health, 25 (1987), pp. 169–181

Hinz B, Seidel H, Menzel G and Bluthner R (2002) Effects related to random whole-body vibration and posture on a suspended seat with and without backrest, Journal of Sound and Vibration, 253(1), 265-282.

Hinz B, Seidel H, Blüthner R, Menzel G, Hofmann J, Gericke L and Schust M (2007) Whole-body vibration experimental work and biodynamic modelling. VIBRISKS Annex 18 to Final Technical Report.

Huang Y and Griffin MJ (2006) Effect of voluntary periodic muscular activity on nonlinearity in the apparent mass of the seated human body during vertical random whole-body vibration, Journal of Sound and Vibration, 298, 824-840.

Huang Y (2008) Mechanism of nonlinear biodynamic response of the human body exposed to whole-body vibration, PhD thesis, University of Southampton, Southampton

International Organization for Standardization (2003) Mechanical vibration and shock- Evaluation of human exposure to whole-body vibration- Part 5: Method for evaluation of vibration containing multiple shocks, ISO 2631-5.

Jenkins GM and Watts DG (1968) Spectral analysis and its applications, Holden-Day, 1968.

Kitazaki S (1994) Modelling mechanical responses to human whole-body vibration, PhD thesis, University of Southampton, Southampton.

Kitazaki S and Griffin MJ (1997) A modal analysis of whole-body vertical vibration, using a finite element model of the human body, Journal of Sound and Vibration, 200, 83-103.

Kitazaki S and Griffin MJ (1998) Resonance behaviour of the seated human body and effects of posture, Journal of Biomechanics, 31, 143-149.

Kitazaki S and Griffin MJ (1995) A data correction method for surface measurement of vibration on the human body, Journal of Biomechanics, Vol.28, No.7, pp 885-890.

Liang CC and Chiang CF (2008) Modelling of a seated human body exposed to vertical vibrations in various automotive postures, Industrial Health, 46, 125-137.

Liu C, Qiu Y and Griffin MJ (2012) A finite element model of the vertical in-line and fore-and-aft cross-axis apparent mass and transmissibility of the human body sitting on a rigid seat and exposed to vertical vibration, 47th UK Conference on Human Response to Vibration, Southampton.

Liu C, Qiu Y and Griffin MJ (2015) Role of the thighs in the biodynamic response of the human body sitting on a rigid seat exposed to vertical vibration. Presented at the 50th UK Conference on Human Response to Vibration, Southampton.

M-Pranesh A, Rakheja S and Demont R (2010) Influence of support conditions on vertical whole-body vibration of the seated human body, Industrial Health, 48, 682-697.

Machintosh JE and Bogduk N (1987) Volvo award in basic science. The morphology of the lumbar erector spinae. Spine, 12(7), 658-668.

Marras WS and Granata KP (1997) The development of an EMG-assisted model to assess spine loading during whole-body free-dynamic lifting. J.Electromyogr. Kinesiol Vol.7, No.4, pp. 259-268

Magnusson M, Pope M, Rostedt M and Hansson T (1993), Effect of backrest inclination on the transmission of vertical vibrations through the lumbar spine, Clinical Biomechanics 8, 5–12.

Matsumoto Y and Griffin MJ (1998a) Movement of the upper-body of seated subjects exposed to vertical whole-body vibration at the principal resonance frequency, Journal of Sound and Vibration, 215 (4), 743-762.

Matsumoto Y and Griffin MJ (1998b), Dynamic response of the standing human body exposed to vertical vibration: influence of posture and vibration magnitude, Journal of Sound and Vibration, 212(1), 85-107.

Matsumoto Y (1999) Dynamic response of standing and seated persons to whole-body vibration: principal resonance of the body, PhD thesis, University of Southampton, Southampton.

Matsumoto Y and Griffin MJ (2000), Comparison of biodynamic responses in standing and seated human bodies, Journal of Sound and Vibration, 238 (4), 691-704.

Matsumoto Y and Griffin MJ (2001) Modelling the dynamic mechanisms associated with the principal resonance of the seated human body, Clinical Biomechanics, 16, 31-44.

Matsumoto Y and Griffin MJ (2002a) Effect of muscle tension on non-linearity of the apparent masses of seated subjects exposed to vertical whole-body vibration, Journal of Sound and Vibration, 253(1), 77-92.

Matsumoto Y and Griffin MJ (2002b) Nonlinear characteristics in the dynamic responses of seated subjects exposed to vertical whole-body vibration, Journal of Biomechanical Engineering, Vol. 124, 527-532.

Mansfield N.J. and Griffin M.J. (2000) Non-linearities in apparent mass and transmissibility during exposure to whole-body vertical vibration, Journal of Biomechanics 33, 933-941.

Mansfield NJ, Holmlun P and Lundstrom R (2001) Apparent mass and absorbed power during exposure to whole-body vibration and repeated shocks, Journal of Sound and Vibration, 248(3), 427-440.

Mansfield NJ and Griffin MJ (2002) Effects of posture and vibration magnitude on apparent mass and pelvis rotation during exposure to whole-body vertical vibration, Journal of Sound and Vibration, 253(1), 93-107.

Mansfield NJ (2005) Human response to vibration, CRC Press, Boca Ratton London New York Washington DC.

Mansfield NJ, Holmlund P, Lundstrom R, Lenzuni P and Nataletti P (2006), Effect of vibration magnitude, vibration spectrum and muscle tension on apparent mass and cross-axis transfer functions during whole-body vibration exposure, Journal of Biomechanics, 39, 3062-3070.

Messenger AJ and Griffin MJ (1989) Effects of anthropometric and postural vairables on the transmission of whole-body vertical vibration from seat to head, ISVR Technical Report, No 172, University of Southampton, Southampton.

McKenzie R and May S (2003) The Lumbar Spine Mechanical Diagnosis and Therapy, 2nd ed. Waikanae, New Zealand: Spinal Publications, New Zealand. p. 103-120.

Nawayseh N and Griffin MJ (2003), Non-linear dual-axis biodynamic response to vertical whole-body vibration, Journal of Sound and Vibration 268, 503–523.

Nawayseh N and Griffin MJ (2004) Tri-axial forces at the seat and backrest during whole-body vertical vibration, Journal of Sound and Vibration, 277, 309-326.

Nawayseh N and Griffin MJ (2009), A model of the vertical apparent mass and the fore-and-aft cross-axis apparent mass of the human body during vertical whole-body vibration, Journal of Sound and Vibration 319, 719–730.

National Aeronautics and Space Administration (1978) NASA Reference Publication 1024. Anthropometric source book, Volume 1: anthropometry for designers.

Nigg BM and Liu W (1999), The effect of muscle stiffness and damping on simulated impact fore peaks during running, Jounral of Biomechanics, 32, 849-856.

Oliveira CG, Simpson DM and Nadal J (2001) Lumbar back muscle activity of helicopter pilots and whole-body vibration, Journal of Biomechanics 34, 1309-1315

Paddan GS and Griffin MJ (1988) The transmission of translational seat vibration to the head – I. vertical seat vibration, Journal of Biomechanics, Vol.21. No.3, pp 191-197.

Paddan GS and Griffin MJ (1998) A review of the transmission of translational seat vibration to the head, Journal of Sound and Vibration, 215(4), 863-882.

Panjabi M and White A (1980) Basic biomechanics of the spine, Neurosurgery, Vol. 7, No. 1, 76-93

Panjabi MM, Krag MH, White AA and Southwick WO (1977), Effects of preload on load displacement curves of the lumbar spine, Orthopedic Clinics of North America 8, 181–192.

Pang TY (2005) The transmission of vibration at the lower lumbar spine due to whole-body vibration: a numerical human model study, PhD thesis, RMIT University, Australia.

Pankoke S, Buck B and Woelfel H (1998) Dynamic FE model of sitting man adjustable to body height, body mass and posture used for calculating internal forces in the lumbar vertebral disks, Journal of Sound and Vibration 215 (4), 827-839.

Pankoke S, Hofmann J and Wölfel HP (2001) Determination of vibration-related spinal loads by numerical simulation. Clinical Biomechanics 16, Supplement No.1, S45-S56

Patelli G (2016) Effects of vertical mechanical shocks and body posture on discomfort, PhD thesis, University of Southampton, Southampton.

Pope MH, Svensson M, Broman H and Andersson GBJ (1986) Mounting of the transducers in measurement of segmental motion of the spine. Journal of Biomechanics 19 (8): 675-677.

Pope MH, Wilder DG and Magnusson M (1998) Possible mechanisms of low back pain due to whole-body vibration, Journal of Sound and Vibration, 215(4), 687-697.

Privitzer E and Belytschko T (1980) Impedance of a three-dimensional head-spine model, Mathematical Modelling Vol. 1 189-209

Qiu Y and Griffin MJ (2010) Biodynamic responses of the seated human body to single-axis and dual-axis vibration, Industrial Health, 48 (5), pp. 615-627

Qiu Y and Griffin MJ (2011a) Modelling the fore-and-aft apparent mass of the human body and the transmissibility of seat backrests, Vehicle System Dynamics Vol. 49, No.5, 703-722

Qiu Y and Griffin MJ (2011b), Modelling the fore-and-aft apparent mass of the human body and the transmissibility of seat backrests, Vehicle System Dynamics, Vol. 49, No. 5, 703–722.

Qiu Y and Griffin MJ (2012) Biodynamic response of the seated human body to single-axis and dual-axis vibrations: effect of backrest and non-linearity, Indutrial Health, 50, 37-51.

Robertson CD and Griffin MJ (1989) Laboratory studies of the electromyographic response to whole-body vibration, ISVR Technical Report No 184, University of Southampton.

Robinson DG (1999) The dynamic response of the seated human to mechanical shock, PhD thesis, Simon Fraser University, Canada.

Rohlmann A, Arntz U, Graichen F and Bergmann G (2001) Loads on an internal spinal fixation device during sitting, Journal of Biomechanics, 34, 989-993.

Rohlmann A, Hinz B, Blüthner R, Graichen F and Bergmann G (2010) Loads on a spinal implant measured in vivo during whole-body vibration, Eur Spine J, 19, 1129-1135.

Rohlmann A, Graichen F, Bender A, Kayser R and Bergmann G (2008) Loads on a telemeterized vertebral body replacement measured in three patients within the first postoperative month, Clinical Biomechanics, 23, 147-158.

Rohlmann A, Hinz B, Bluthner R, Graichen F and Bergmann G (2010) Loads on a spinal implant measured in vivo during whole-body vibration, Eur Spine J, 19:1129-1135.

Rohlmann A, Zander T, Graichen F, Dreischarf M and Bergmann G (2011) Measured loads on a vertebral body replacement during sitting, The Spine Journal 11, 870-875.

Rohlmann A, Petersen R, Schwachmeyer V, Graichen F and Bergmann G (2012) Spinal loads during position changes, Clinical Biomechanics, 27, 754-758.

Sato K, Kikuchi S and Yonezawa T (1999) In vivo intradiscal pressure measurement in healthy individuals and in patients with ongoing back problems. Spine, Volume 24, Number 23, 2468-2474.

Schultz AB, Warwick DN, Berkson MH and Nachemson AL (1979) Mechanical properties of human lumbar spine motion segments – Part 1: response in flexion, extension, lateral bending, and torsion, Journal of Biomechanical Engineering, 101, 46-52.

Schuenke M, Ross LM, Schulte E, Lamperti ED and Shcumacher U (2010) General anatomy and musculoskeletal system, Thieme, New York.

Seidel H, Blüthner R, Hinz B and Schust M (1997) Stresses in the lumbar spine due to whole-body vibration containing shocks (Final Report). Dortmund/Berlin, 1997

Seidel H, Blüthner R, Hinz B and Schust M (1998) On the health risk of the lumbar spine due to whole-body vibration- theoretical approach, experimental data and evaluation of whole-body vibration, Journal of Sound and Vibration, 215(4), 723-741

Seidel H, Blüthner R and Hinz B (1986) Effects of sinusoidal whole-body vibration on the lumbar spine: the stress-strain relationship. Int. Arch. Occup. Environ. Hlth., 57, 207-223.

Seidel H, Blüthner R and Hinz B (2001) Application of finite-element models to predict forces acting on the lumbar spine during whole-body vibration. Clinical Biomechanics, 16 Supplement, No. 1, S57-S63.

Shin K and Hammond JK (2008) Fundamentals of signal process for sound and vibration engineers, John Wiley & Sons, Ltd, Chichester, England.

Stokes IAF and Gardner-Morse M (1999) Quantitative anatomy of the lumbar musculature. Journal of Biomechanics, 32, 311-316.

Stokes IAF and Gardner-Morse M (2001) Lumbar spinal muscle activation synergies predicted by multi-criteria cost function. Journal of Biomechanics, 34, 733-740.

Stokes IA, Gardner-Morse M, Churchill D and Laible JP (2002) Measurement of a spinal motion segment stiffness matrix, Journal of Biomechanics, 35, 517-521.

Stokes IAF, Gardner-Morse M and Henry SM (2010) Intra-abdominal pressure and abdominal wall muscular function: Spinal unloading mechanism. Clinical Biomechanics, 25, 859-866.

Toward MGR and Griffin MJ (2009) Apparent mass of the human body in the vertical direction: Effect of seat backrest, Journal of Sound and Vibration, 327, 657-669.

Toward M.G.R. and Griffin M.J. (2010a) Apparent mass of the human body in the vertical direction: Effect of a footrest and a steering wheel, Journal of Sound and Vibration 329, 1586–1596.

Toward M.G.R. and Griffin M.J. (2010b) A variable parameter single degree-of-freedom model for predicting the effects of sitting posture and vibration magnitude on the vertical apparent mass of the human body, Industrial Health 48, 654–662.

Toward M.G.R. and Griffin M.J. (2011) Apparent mass of the human body in the vertical direction: Inter-subject variability, Journal of Sound and Vibration 330, 827–841.

Verver MM, Hoof J, Oomens CWJ, Wouw N and Wismans JSHM (2003) Estimation of spinal loading in vertical vibrations by numerical simulation. Clinical Biomechanics, 18, 800-811.

Wang W, Rakheja S and Boileau P-E (2004) Effects of sitting postures on biodynamic response of seated occupants under vertical vibration, International Journal of Industrial Ergonomics, 34, 289-306.

Wang W, Bazrgari B, Shirazi-adl A, Rakheja S and Boileau P (2010) Biodynamic response and spinal load estimation of seated body in vibration using finite element modelling, Industrial Health, 48, 557-564.

Wei L and Griffin MJ (1998) Mathematical models of apparent mass of seated human body seated to vertical vibration, Journal of Sound and Vibration, 215 (5), 855-874.

Wilke H, Neef P, Hinz B, Seidel H and Claes L (2001) Intradiscal pressure together with anthropometric data – a data set for the validation of models, Clinical Biomechanics 16 Supplement No.1 S111-S126.

Zheng G (2011) Biodynamics of the seated human body with dual-axis excitation: nonlinearity and cross-axis coupling, PhD thesis, University of Southampton, Southampton.

Zheng G, Qiu Y and Griffin MJ (2011a) Effect of sitting posture on the transmissibility and apparent mass of the seated human body exposed to vertical vibration, The 46th UK conference on Human Response to Vibration, Buxton.

Zheng G, Qiu Y and Griffin MJ (2011b) An analytical model of the in-line and cross-axis apparent mass of the seated human body exposed to vertical vibration with and without a backrest. Journal of Sound and Vibration, 330 (26), 6509-6525.

Zheng G, Qiu Y and Griffin MJ (2012) A dynamic finite element model of the seated occupant for ride comfort analysis, Proceedings of International Symposium on Computational Modelling and Analysis of Vehicle Body Noise and Vibration, University of Sussex, 27th – 28th.